U. PORTO

FEUP **FACULDADE DE ENGENHARIA**
UNIVERSIDADE DO PORTO

CYCLIC LIQUEFACTION SUSCEPTIBILITY OF SOILS FROM FIELD AND LABORATORY TESTS

Methodologies and critical analyses

CATARINA PAISANA FERREIRA CORREIA RAMOS

Dissertation submitted to the Faculty of Engineering of the University of Porto in accordance with the requirements of the degree of Doctor in Civil Engineering

Supervisor: António Joaquim Pereira Viana da Fonseca, Ph.D.

Co-Supervisor: Matthew Richard Coop, Ph.D.

JULY 2021

Challenges are what make life interesting and

overcoming them is what makes life meaningful.

Joshua J. Marine

ABSTRACT

During the last century, earthquakes have been responsible for many human casualties and resulted in very high economic and social damage. Soil liquefaction, defined by the rapid increase in pore water pressure and consequent loss of shear strength and stiffness, is often associated to this natural disaster. The understanding of the cyclic behaviour of soils under earthquake motions requires extensive testing and advanced methods of analysis. Besides, the characterisation of liquefiable soils is essential for the calibration of advanced models and their adoption in engineering practice. The purpose of this research work was to deepen the studies in cyclic liquefaction, by improving the understanding of the cyclic liquefaction behaviour of natural soils and contributing to the identification of factors that affect the liquefaction resistance of soils.

An extensive experimental campaign was carried out in Lezíria Grande de Vila Franca de Xira and Benavente, on the left margin of the Lower Tagus River Valley, including boreholes with standard penetration tests (SPT), piezocone penetration tests (CPTu), flat dilatometer tests (DMT), and in situ measurement of shear wave velocities, as well as the collection of undisturbed samples with Mazier and the new Gel-Push samplers. The investigated experimental sites were constituted by very heterogeneous soil profiles, with interbedded sand-silt-clay layers. Despite the heterogeneity of the soil profiles, thick liquefiable sand layers were found, thus concluding that the experimental site area was prone to liquefaction. The use of different methodologies for the assessment of liquefaction susceptibility was proven to be beneficial, especially when complemented with laboratory analyses. A new chart relating LPI and LSN_{20} values was proposed to assess liquefaction severity and damage. The quality of the samples was evaluated by means of a variety of methods, and the Mazier and Gel-Push samplers proved to be competent for the majority of soil types collected.

The cyclic behaviour of the soils collected at that experimental site was investigated in the laboratory through cyclic triaxial and cyclic direct simple shear tests. The effects of various soil properties and state parameters on the cyclic liquefaction resistance and behaviour of the collected soils was evaluated. Besides, the effect of fabric was assessed by comparing the behaviour of undisturbed and reconstituted specimens. The results showed that for soils with fines content lower than 6%, the reconstituted specimen exhibited higher cyclic resistance than the undisturbed specimen, while the opposite was observed for soil with more than 6% fines content. Further analyses of results showed significant differences on the behaviour of undisturbed and reconstituted specimens, mostly justified by the influence of fabric. The undisturbed specimens exhibited a more stable behaviour, with a steady and constant increase in strains, often biased to the extension side. By contrast, the reconstituted specimens exhibited low strain development during initial loading cycles, after which the strains increase exponentially, associated with excess pore pressure, and occur to both compression and extension sides.

The liquefaction susceptibility was evaluated using an energy-based approach, considering the dissipated energy at liquefaction. The effect of several factors on the dissipated energy at liquefaction was assessed and the reconstituted and undisturbed specimens were analysed in terms of pore pressure evolution with cumulative dissipated energy per unit volume of soil up to the onset of liquefaction.

RESUMO

Durante o ultimo século, os terramotos foram responsáveis pela perda de muitas vidas e resultaram em danos económicos e sociais muito elevados. A liquefação do solo, definida pelo rápido aumento da pressão neutra e consequente perda de resistência e rigidez do solo, está frequentemente associada a esse desastre natural. A compreensão do comportamento cíclico dos solos sujeitos a forças sísmicas exige ensaios complexos e métodos de análise avançados. Para além disso, a caracterização de solos liquidificáveis é essencial para a calibração de modelos avançados e a sua utilização na prática de engenharia. O objetivo deste trabalho foi aprofundar os estudos em liquefação cíclica, melhorando a compreensão do comportamento da liquefação cíclica em solos naturais e contribuindo para a identificação de fatores que afetam a resistência dos solos à liquefação.

Uma extensa campanha experimental foi realizada na Lezíria Grande de Vila Franca de Xira e Benavente, na margem esquerda do vale inferior do rio Tejo, incluindo furos com ensaios de penetração dinâmica (SPT), ensaios com cone penetrómetro (CPTu), ensaios com dilatómetro de Marchetti (DMT) e medição de ondas de corte, assim como a recolha de amostras não perturbadas utilizando os amostradores Mazier e o novo Gel-Push. Os locais investigados são constituídos por perfis de solo bastante heterogéneos, com intercalações de areia, silte e argila. Apesar da heterogeneidade dos perfis de solo, algumas camadas de areia liquidificável foram identificadas, concluindo-se que é um local suscetível à liquefação. A utilização de diferentes metodologias para avaliação da suscetibilidade à liquefação foi benéfica, principalmente quando complementada com análises laboratoriais. Um novo gráfico que relaciona os valores de LPI e LSN_{20} foi proposto para avaliar a gravidade e danos causados pela liquefação dos solos. A qualidade das amostras foi avaliada através de diversos métodos e ambos os amostradores Mazier e Gel-Push foram competentes na recolha de amostras da maioria dos solos.

O comportamento cíclico dos solos recolhidos no referido campo experimental foi investigado em laboratório através de ensaios triaxiais cíclicos e de corte direto simples cíclicos. Os efeitos que várias propriedades do solos e parâmetros de estado têm na resistência à liquefação cíclica e comportamento dos solos recolhidos foram avaliados. Além disso, o efeito da fábrica foi analisado através da comparação do comportamento de amostras intactas e reconstituídas. Os resultados mostraram que para solos com menos de 6% de finos, a amostra reconstituída exibiu maior resistência que a amostra intacta, enquanto que o contrário foi observado para amostras com mais de 6% de finos. Uma análise mais detalhada dos resultados mostrou diferenças significativas no comportamento das amostras intactas e reconstituídas, justificadas pelo efeito da fábrica. As amostras intactas exibiram um comportamento mais estável, com um aumento constante da deformação axial, frequentemente enviesada para o lado das extensões. Por outro lado, as amostras reconstituídas exibiram baixas deformações durante os primeiros ciclos de carregamento, após os quais se verifica um aumento exponencial da deformação axial, associada ao excesso de pressão neutra, tanto em compressão como em extensão.

A suscetibilidade à liquefação foi avaliada através da abordagem energética, considerando a energia dissipada até à liquefação. O efeito de vários fatores na energia dissipada na liquefação foi avaliado e as amostras reconstituídas e intactas foram estudadas em termos da geração de poro pressão com a energia dissipada acumulada por unidade de volume de solo.

ACKNOWLEDGEMENTS

This work would not have been possible without the help and support of the following people, for whom I express my most sincere acknowledgements.

First of all, to Professor António Viana da Fonseca, who supervised this work, for the scientific support and many conversations, for being an example of perseverance and work, and for sharing his knowledge of Geotechnical Engineering in such a passionate way.

To Professor Matthew Richard Coop, who co-supervised this work and was always available to discuss my work; for all the kind words, hospitality and generosity.

To Professor Janko Logar, for allowing the possibility to go spend three weeks at University of Ljubljana; to Professor Matej Maček for his support and shared knowledge about the cyclic simple shear equipment; and to Aleš Oblak for his kindness, support, and for showing me around the beautiful country of Slovenia.

To Dr. Béatrice Baudet for her hospitality and help when I was at University College London; to Fatin Altuhafi for showing me around UCL and for keeping me company and to Abi Cartwright for the help with the Morphologi G3 equipment. When I was in London, I stayed at my friend Débora's house, and to her I express my deepest thanks, for being one of my best friends and for her kindness and generosity.

À Associação de Beneficiários da Lezíria Grande de Vila Franca de Xira, na pessoa do Engenheiro Rui Paixão, e à Câmara Municipal de Benavente, pela disponibilidade e permissão para execução dos ensaios de campo.

À equipa do LabGEO da FEUP: ao Sr. Armando Pinto por todos os ensinamentos sobre o trabalho laboratorial e sobre a vida; à Cláudia Pinto pela disponibilidade, competência e amizade; e à Daniela Coelho, por tudo o que me ensinou acerca de técnicas laboratoriais e execução de ensaios, pela companhia diária e porque, ao longo destes anos na FEUP, se tornou numa amiga verdadeira. Sem dúvida que foram essenciais nesta etapa.

À Cristiana Ferreira, pelas muitas palavras amigas e conselhos e pela disponibilidade infinita para me ajudar, e à Sara Rios, pelo exemplo de empenho e trabalho.

Aos colegas e investigadores da secção de Geotecnia do Departamento de Engenharia Civil, por toda a ajuda e disponibilidade prestadas, foi bom trabalhar ao vosso lado: Bruno Delgado, Cláudia Cordeiro, Claver Giovanni, David Besenzon, Diana Cordeiro, Fausto Molina-Gómez, Francisca Alves, José Cândido, Julieth Quintero, Rita Lamas, Rubens Alves, Sofia Saldanha.

Às minhas *girls*, Ana Pernil, Débora Reis, Joana Soares Dias, Luísa Rocha e Brigite Azevedo, por estarem sempre lá para mim, e pelos momentos de diversão, de cumplicidade e de crescimento pessoal. De sempre, para sempre.

Aos amigos e voluntários do GASPORTO, por me fazerem ver o mundo com outros olhos e me ajudarem no caminho para ser uma pessoa mais tolerante e atenta ao outro.

À minha mãe e ao meu pai, por sempre acreditarem em mim mesmo quando eu deixei de acreditar, por me mostrarem o que é o amor incondicional e por nunca me deixarem desistir. Obrigada pela educação que me deram e por estarem sempre aí para mim e para a Kika.

À minha irmã Francisca, pelo companheirismo, amor e apoio, e às minhas avós Fina e Tina, por serem os pilares da minha família e por me ensinarem tanto sobre a vida e o trabalho. Aos meus avôs António João e Luís, porque estão muitas vezes no meu pensamento como referência de pessoas exemplares.

E ao Luís, pela paciência, motivação, companhia de vida e, principalmente, pelo amor. Sou grata por te ter comigo.

Muito obrigada a todos.

Thank you all.

TABLE OF CONTENTS

Cyclic Liquefaction Susceptibility of Soils from Field and Laboratory Tests. Methodologies and critical analyses

XX

LIST OF FIGURES

LIST OF TABLES

ABBREVIATIONS AND SYMBOLS

Abbreviations

ADVDPC	Advanced Pressure/Volume Controller
AR	Aspect ratio
ASTM	American Society for Testing and Materials
BE	Bender element
BP	Back Pressure
BPT	Becker Penetration Test
CDSS	Cyclic direct simple shear test
CP	Cell Pressure
CPT	Cone Penetration Test
CPTu	Piezocone Penetration Test
CRR	Cyclic Resistance Ratio
CS	Critical State
CSL	Critical state Line
CSR	Cyclic Stress Ratio
CSSM	Critical State Soil Mechanics
CTx	Cyclic triaxial test
D&M	Dames and Moore
DMT	Flat dilatometer test
DWF	Magnitude Scaling Factor
EC	Eurocode
EILD	Earthquake induced liquefaction disasters
ENE	East-Northeast
FC	Fines Content
FCT	Fundação para a Ciência e Tecnologia
FEUP	Faculdade de Engenharia da Universidade do Porto
FLS	Flow Liquefaction Surface
GP	Gel-Push
GSD	Grain Size Distribution
JGS	Japanese Geotechnical Society
LabGEO	Laboratory of Geotechnics of FEUP
LabGeoUL	Geotechnical laboratory of University of Ljubljana
LL	Liquid Limit

LPI	Liquefaction Potential Index
LSN	Liquefaction Severity Index
LTV	Lower Tagus River Valley
LVDT	Linear Variable Differential Transformer
MFS	Maximum flooding surface
MMI	Modified Mercalli Intensity
MSF	Magnitude Scaling Factor
MSK	Medvedev-Sponheuer-Karnik scale
MT	Moist tamping
NASEM	National Academies of Sciences, Engineering, and Medicine
NCEER	National Center for Earthquake Engineering Research
NSF	National Science Foundation
OCR	Overconsolidation ratio
PEC	Pseudoenergy capacity
PGA	Peak ground acceleration
PI	Plasticity Index
PL	Air Pluviation
PVC	Polyvinyl Chloride
SA	Seismic Action
SAGI	Shape-angularity group indicator
SCPTu	Seismic piezocone penetration test
SDMT	Seismic flat dilatometer test
SDU	Sample dispersion unit
SOF	Standard Operation Procedure
SPT	Standard penetration test
SSL	Steady State Line
UCL	University College London
UL	University of Ljubljana

Symbols

$(N_1)_{60}$	normalised SPT blowcount
$(N_1)_{60cs}$	normalised SPT blowcount for equivalent clean sand
a	curve fitting parameter
A	area of the specimen

xliv

A	material coefficient used to determine G_{max}
a_g	design ground acceleration on type A ground
a_{gR}	reference peak ground acceleration on type A ground
a_{max}	peak ground acceleration
b	curve fitting parameter
B	Skempton pore pressure parameter
c	normalisation exponent that depends on the friction ratio and the tip resistance
C_C	shape coefficient
C_D	normalisation parameter of SPT blowcount to account for the borehole diameter
C_E	normalisation parameter of SPT blowcount to account for the energy transmitted to the rod train
C_{FC}	fitting parameter based on site-specific data
C_N	normalisation parameter to account for the overburden stress
C_R	normalisation parameter of SPT blowcount to account for the rod train length
c_r	cyclic triaxial to direct simple shear correction factor
CRR_{15}	CRR for failure in 15 cycles
$CRR_{7.5}$	CRR normalised to an earthquake magnitude 7.5
CRR_{ss}	cyclic resistance ratio of simple shear test
CRR_{tx}	cyclic resistance ratio of triaxial test
C_S	normalisation parameter of SPT blowcount to account for the use of split spoons
CSR_{field}	field cyclic stress ratio
CSR_{ss}	cyclic stress ratio of simple shear test
CSR_{tx}	cyclic stress ratio of triaxial test
C_U	uniformity coefficient
d	depth at the midpoint of the critical layer
D_m	initial diameter of the membrane
D_R	relative density
D_{ro}	relative density at the steady state line
D_{50}	mean grain size
e	void ratio
e_c	intergranular void ratio
$(e_c)_{eq}$	equivalent intergranular void ratio
e_{cs}	void ratio at critical state
E_D	Dilatometer Modulus
e_f	interfine void ratio

$(e_f)_{eq}$	equivalent interfine void ratio
e_L	void ratio at the end of oedometric loading
E_m	elastic modulus of the membrane
e_{min}	minimum void ratio
e_{max}	maximum void ratio
e_U	void ratio at the end of oedometric unloading
e_0	initial void ratio
$e_{0,cs}$	void ratio at critical state at zero confining stress
f	exponent function of the in situ conditions; used to determine K_σ
$F(e)$	void ratio function
FC_{est}	estimated fines content
FC_{lab}	laboratory-measured fines content
F_h	horizontal force
F_r	normalised friction ratio
f_s	sleeve friction stress
FS_{liq}	Factor of safety against liquefaction
F_v	vertical force
g	acceleration of gravity
G_{max}	small-strain shear modulus
G_s	specific weight
G_{sec}	secant shear modulus
G_0	shear modulus
H	height of the specimen
I_c	soil behaviour type index
I_D	Material Index
k	Empirical exponent of the overconsolidation ratio OCR depending on the plasticity index
K_{a1}	factor to account for the effect of ageing on V_{S1}
K_{a2}	factor to account for the effect of ageing on V_{S1}
K_c	normalisation parameter function of the soil behaviour type
K_D	Horizontal stress index
K_0	at rest earth pressure coefficient
K_α	correction factor that takes into account the initial static shear stress
K_σ	correction factor that takes into account the initial overburden pressure
LSN_{20}	Liquefaction Severity Number considering the first 20 m of depth

L_t	travel length
m	exponent used to normalise SPT blowcount or cone penetration resistance
M_{cs}	critical shear stress ratio
M_{max}	constrained modulus
M_w	moment magnitude
M_0	constrained modulus
n	exponent used to normalise cone penetration resistance
N_c	number of cycles
N_{liq}	number of cycles to trigged liquefaction
N_{SPT}	SPT blowcount
p_a	atmospheric pressure
P_L	Probability of liquefaction
p'	mean effective stress
p'_{cs}	mean effective stress at critical state
p'_0	initial mean effective stress
q	deviatoric stress
Q_{cn}	normalised cone resistance
q_c	cone resistance
$q_{c,1,mod}$	normalised cone tip resistance
q_{c1N}	normalised cone resistance
q_{c1Ncs}	normalised cone resistance for equivalent clean sand
q_t	corrected cone tip resistance
Q_{tn}	normalised cone resistance
$Q_{tn,cs}$	normalised cone resistance for equivalent clean sand
r_d	shear stress reduction coefficient
R_f	friction ratio
r_u	excess pore water pressure ratio
S	soil factor
S	elastic response spectrum parameter
S_{ij}	non-dimensional material constant reflecting the fabric and structure of the soil
S_{max}	factor that depends on the ground type
S_r	saturation degree
t_m	initial thickness of the membrane
t_t	wave travel time
u	pore water pressure

V_P	compression wave velocity
V_S	shear wave velocity
$V_{Sinsitu}$	field-measured shear wave velocity
V_{Slab}	laboratory-measured shear wave velocity
V_S^*	normalised shear wave velocity with the void ratio function
V_S^{**}	normalised shear wave velocity with the void ratio function and confining pressure
V_{S1}	normalised V_S according to the vertical effective stress
V_{S1}^*	maximum limit of V_{S1}
w	water content
W_s	dissipated energy normalised by the initial effective mean stress
$W_{s,liq}$	normalised dissipated energy at liquefaction
$W_{s,ru=0.65}$	normalised dissipated energy at $r_u=0.65$
z	depth
$(\varepsilon_v)_m$	vertical strain of the membrane
$(\varepsilon_{vol})_m$	volumetric strain of the volume enclosed by the membrane
α	ratio of the design ground acceleration on type A ground to the acceleration of gravity
α	ratio of the initial static shear by the normal effective stress action on the plane of maximum shear stress
α	angle that measures the orientation of σ_1
α	calibration parameter
β	calibration parameter
γ	shear strain
γ_{DA}	double amplitude shear strain
γ_I	importance factor
γ_{lim}	limiting shear strain
γ_{max}	maximum shear strain
γ_{SA}	single amplitude shear strain
Γ	void ratio intercept
$\Delta(N_1)_{60}$	equivalent clean sand adjustment for SPT blow count
Δe	void ratio variation
Δh	horizontal displacement
ΔH	axial displacement
Δq_{c1N}	equivalent clean sand adjustment for cone resistance
Δu	excess pore water pressure
ΔW	dissipated energy per unit volume of soil

ΔW_{liq}	dissipated energy at liquefaction
$\Delta \sigma_3$	confining pressure variation
ε_a	axial strain
$\varepsilon_{a,DA}$	double amplitude axial strain
$\varepsilon_{a,SA}$	single amplitude axial strain
ε_r	radial strain
ε_v	volumetric strain
λ	gradient/slope of the CSL
υ	Poisson's ratio
ξ_a	curve fitting parameter for curved CSL
ξ_R	relative state parameter index
ρ	soil mass density
ρ_{dmax}	maximum dry density
ρ_{dmin}	minimum dry density
σ_1	maximum principal stress
σ'_{1c}	maximum principal stress on triaxial shear stress conditions
σ'_{3c}	minimum principal stress on triaxial shear stress conditions
σ'_c	initial effective confining stress
σ'_h	effective horizontal stress
σ'_i	principal effective stresses in the wave propagation direction i
σ'_j	principal effective stresses in the wave polarisation direction j
σ_m	mean total stress
σ'_v	effective vertical stress
σ_v	total vertical stress
σ'_{v0}	initial effective vertical stress
σ_{v0}	initial total vertical stress
σ'_o	initial effective mean stress
τ	shear stress
τ_{av}	average cyclic shear stress
τ_c	seismic shear stress
τ_{cyc}	cyclic shear stress
τ_{st}	static shear stress
ϕ'_{cv}	constant volume friction angle
Φ^{-1}	inverse cumulative normal distribution function
ψ	state parameter

PART I - INTRODUCTION AND LITERATURE REVIEW

1. INTRODUCTION

1.1. PROLOGUE AND RESEARCH MOTIVATION

During the last century, earthquakes have been responsible for many human casualties and resulted in very high economic and social damage. Therefore, they are considered one of the biggest causes of death in Europe when concerning natural disasters. One of the associated phenomena is the liquefaction of soils, which can have devastating consequences, as evidenced by recent events in Japan (Boulanger, 2012) or New Zealand (Cubrinovski et al., 2011). Another example is the north of Italy, affected in May 2012 by an earthquake of moderate magnitude, about 5.9 on the Richter scale (Fioravante et al., 2013). Consequently, there has been major damage to infrastructures mainly due to liquefaction. Studies of soil identification and geotechnical characterisation were carried out and allowed to conclude that the risk had been underestimated. This highlights the importance of the identification, and characterisation of liquefiable soils and the mitigation of this risk.

In Portugal, particularly in the south-west coast, the combination of widespread Holocene alluvial sandy deposits and high seismicity of the region increases the likelihood of the occurrence of earthquake induced liquefaction disasters (EILDs). Two of the most devastating earthquakes that occurred in the south-west coast of Portugal were the 1755 Lisbon earthquake and the 1909 Benavente earthquake, responsible for the loss of many human lives and the destruction of several engineering works. This evidences the importance of the study of soils susceptible to liquefaction and their clear identification to refine methods and obtain more reliable results. Besides, the characterisation of liquefiable soils is essential for the calibration of advanced models and their adoption in engineering practice, to help prevent such disasters.

The resistance to cyclic loading of soils might be determined from field or laboratory testing. However, for an adequate interpretation of laboratory tests, the specimens have to accurately represent the in situ state, which requires the collection of high-quality samples, an expensive and difficult process. For this reason, in engineering practice, it is more common to perform field tests and use empirical correlations to assess liquefaction susceptibility or to perform tests on reconstituted specimens. Therefore, the

selection of the most appropriate field tests is essential for a correct interpretation of the soil profiles and to avoid major uncertainties related to the materials characteristics.

Laboratory tests have been carried out in granular soils either under static/monotonic loading or in cyclic loading conditions by the FEUP-CONSTRUCT research group (Viana da Fonseca et al., 2011; Soares, 2014), using the Critical State Soil Mechanics (CSSM) framework to predict liquefaction. However, some limitations were identified due to factors such as fines content, soil fabric (reproduction of the natural arrangement of the particles during preparation of the specimens), ageing (overconsolidation and cementation), and stress-path. The study of the effect of certain parameters in the cyclic behaviour of soils is fundamental to understand soil behaviour and their implications on cyclic resistance.

Moreover, the accurate determination of cyclic liquefaction resistance of the soil requires the collection of high-quality samples or the preparation of reconstituted specimens that reproduce the undisturbed behaviour. For this reason, the use of new methods to collect undisturbed samples of soil and the treatment of the results with novel approaches is important to improve the understanding of the liquefaction behaviour of sandy soils and to find correlations between undisturbed and reconstituted specimens. Furthermore, recently, the Laboratory of Geotechnics at FEUP acquired a new Cyclic Simple Shear device that allows the performance of advanced cyclic tests, thus broadening the scope of the research.

1.2. SCOPE AND OBJECTIVES

This thesis has been developed within the framework of two research projects of CONSTRUCT-GEO centre of FEUP: the National project "Liquefaction Assessment Protocols to Protect Critical Infrastructures against Earthquake Damage: LIQ2PROEARTH", funded by the Portuguese Foundation for Science and Technology (FCT); and the European project LIQUEFACT (Assessment and mitigation of liquefaction potential across Europe: a holistic approach to protect structures/infrastructures for improved resilience to earthquake-induced liquefaction disasters), funded by the European Union's Horizon 2020 research and innovation programme.

The purpose of this work is to deepen the studies in cyclic liquefaction, as it is a problem of great importance, especially when considering non-consensual factors, such as fines content, soil fabric, and stress-path. The aim of the field and laboratory tests is to improve the understanding of the cyclic liquefaction behaviour of natural soils and contribute to the identification of factors that affect the soils liquefaction resistance. The work consists of two main parts: the field investigation of the experimental site and the laboratory testing of undisturbed and reconstituted specimens.

The field investigation of the experimental site involved the following objectives:

- Definition of an adequate experimental site for the performance of field tests and collection of undisturbed samples;
- Characterisation of the experimental site soil profiles and liquefaction susceptibility assessment, by comparing and contrasting different field test techniques;
- Collection of high quality samples using the Mazier sampler, the Dames and Moore, and the new Gel-Push sampler, and report on the quality of the samples retrieved.

The laboratory testing of undisturbed and reconstituted specimens was conducted with the followings objectives:

- Characterisation of the intrinsic properties (grain size distribution curves, fines content, plasticity index, specific gravity, void ratio limits, shape parameters) of young Holocene alluvial soils present in a highly liquefiable region of Portugal;
- Definition of the critical state lines of soils collected on the pilot site;
- Evaluation of the effect of various parameters, such as confining pressure, relative density, fabric, and loading conditions, on the undrained behaviour of sands under cyclic loading;
- Identification and characterisation of the cyclic behaviour of those materials, by performing tests on undisturbed high quality samples;
- Interpretation of the cyclic tests results and study the liquefaction resistance using the energy-based approach.

1.3. THESIS ORGANISATION

The present document is organised in four parts, corresponding to the main research work phases:

I – Introduction and Literature Review

II – Field-based evaluation of LTV soils

III – Laboratory evaluation of LTV soils

IV – Summary and Conclusions

Each part is organised into Chapters that gather the information and results of each work phase. However, there is some cross-over between the parts, as for example the laboratory evaluation of shear wave velocity and sample density is used in the sample quality assessment, presented in Part II, and the CPTu data is compared with laboratory data in terms of cyclic resistance in Part III. A more detailed description of each part of the work is presented, as follows.

Part I is composed of the introduction and literature review, and incorporates the research motivation, scope and objectives of the research work. The Literature Review on soil liquefaction focuses on the main aspects of soil liquefaction, such as the mechanism of soil liquefaction, the critical state soil mechanics, and the behaviour of soils under both monotonic and cyclic loading. The liquefaction susceptibility criteria is explained in detail. Furthermore, the evaluation of liquefaction from empirical criteria, in situ tests and laboratory tests are explored. The last part of the Literature Review focuses on the knowledge on factors affecting cyclic liquefaction.

Part II corresponds to the field-based evaluation of LTV soils, outlining the experimental site characterisation, the field tests performed and the sample quality assessment. This part is divided into three Chapters:

Chapter 3 presents a detailed description of the seismicity and historical liquefaction in Portugal, and the procedure of selection of the experimental site area. Moreover, the location of field tests is presented, as well as the sampling programme for the collection of undisturbed soil samples.

Chapter 4 outlines the results of field tests and a thorough liquefaction susceptibility assessment, and some recommendations and main findings on the performance of field tests to assess liquefaction susceptibility.

The last chapter of this part, Chapter 5, presents the results of the sample quality assessment, based on visual inspection, comparison between shear wave velocity measurements, volume changes during reconsolidation and sample density. The chapter ends with recommendations and main finding for sample quality assessment.

Part III focuses on the laboratory evaluation of the behaviour of LTV soils, and it includes the following Chapters:

Chapter 6 outlines the laboratory work performed, as well as the equipment and procedures used for the performance of the tests involved in this investigation.

Chapter 7 presents an in depth characterisation of the intrinsic properties and monotonic behaviour of four case study soils collected at the experimental site.

Chapter 8 presents the results of cyclic triaxial and cyclic direct simple shear tests performed on reconstituted specimens of the case study soils, and assesses the effect of several factors on the cyclic liquefaction resistance of those soils, including state parameters (void ratio and confining pressure), frequency of loading, sample preparation technique, boundary conditions, water content, and loading conditions.

Chapter 9 aims to characterise the intrinsic properties of soils from undisturbed specimens collected at the experimental site and to compare them with benchmark soils tested by other authors.

Chapter 10 addresses the cyclic liquefaction behaviour of the undisturbed samples collected with Mazier and Gel-Push samplers, by presenting a detailed study of their liquefaction susceptibility and investigating the effect of natural fabric in liquefaction resistance. Moreover, this Chapter presents a comparison between field and laboratory data in terms of cyclic resistance and factor of safety against liquefaction.

Chapter 11 is dedicated to the evaluation of liquefaction using an energy-based approach, and focuses on the factors that affect the dissipated energy at liquefaction, the estimation of soil capacity energy, and pore pressure build-up.

Finally, Part IV (Chapter 12) presents the main conclusions and recommendations for future research work.

2. LITERATURE REVIEW ON SOIL LIQUEFACTION

2.1. LIQUEFACTION – AN INTRODUCTION

Liquefaction is one of the most intriguing and interesting themes in geotechnical earthquake engineering. Its complex concept has been intensively studied over the last half century, especially after the 1964 Niigata earthquake in Japan and the 1964 Alaska earthquake. The consequences of these earthquakes included many liquefaction-induced damages, slope failures, foundation failures and lateral spreading (Kramer, 1996).

Liquefaction is a phenomenon that occurs normally in saturated loose granular soils. It is typically associated with the increase in pore water pressure and consequent decrease of the mean effective stress, which causes the soil resistance to decrease until zero. The soil begins to behave like a liquid, not showing resistance, which can cause devastating disasters. The build-up of pore pressure is due to the non-existence of drainage in quick loadings which prevents its immediate dissipation. When the pore pressure increases enough to equal the total stress, the effective mean stress is reduced to essentially zero and liquefaction occurs. Sladen et al. (1985) defined liquefaction as *"a phenomenon wherein a mass of soil loses a large percentage of its shear resistance, when subjected to monotonic, cyclic, or shock loading, and flows in a manner resembling a liquid until the shear stresses acting on the mass are as low as the reduced shear resistance"*.

At first, liquefaction began to be studied in clean sands due to the characteristics of the soils involved in the Niigata earthquake. However, subsequent earthquakes such as the 1999 Kocaeli earthquake in Turkey, the 1999 Chi-Chi earthquake in Taiwan, and the 2011 Tohoku earthquake in Japan induced liquefaction in sands with considerable non/low plastic fines, while the 1983 Borah Peak earthquake in USA, and the 1995 Kobe earthquake in Japan incurred liquefaction in well-graded gravelly soils (Kokusho, 2017). More recent events include the 2011 Great East Japan earthquake (Boulanger, 2012), the 2010 Canterbury (Darfield) and 2011 Christchurch earthquakes in New Zealand (Cubrinovski et al., 2011), and the 2012 Emilia-Romagna earthquake (Fioravante et al., 2013), that caused multiple deaths and serious damage to buildings and infrastructures.

Liquefaction-induced instabilities can be responsible for devastating damage. The most common liquefaction failures are strongly related to shear strength loss and include flow failures and deformation failures. Flow liquefaction failures are characterised by the flow movement of a soil mass, causing huge landslides (Figure 2.1b). On the other hand, deformation failures may not involve flow and large displacements. The deformations develop slowly and are incremental, causing extensive damage, such as lateral spreading, ground tilting or differential settlements (Figure 2.1a). Fissures and scarps may form at the surface and underground liquefiable soil may erupt, forming sand boils (Figure 2.1c, d).

Figure 2.1 – Liquefaction-induced damage: a) Tilted buildings during Niigata Earthquake in 1964 (USGS, 2020a); b) Landslide caused by El Salvador earthquake in 2001 (USGS, 2020b); c) and d) liquefaction in residential areas (Cubrinovski et al., 2011)

2.2. MECHANISM OF SOIL LIQUEFACTION

As was referred above, soil liquefaction commonly refers to the build-up of excess pore water pressure in a loose saturated soil during earthquake loading, causing the loss of shear resistance. Figure 2.2 presents an illustrative scheme of the phenomenon, which is related to a loose soils tendency to reduce in volume (contract) when sheared. However, if drainage is prevented, the pore pressure increases with the shear load. When the pore pressure is enough to break the shear static stress between the particles,

the soil starts to behave like a liquid, with the particles suspended in the water and can undergo large deformations. After shearing, as the pore pressure starts to dissipate, the particles settle in the water and pore water is expelled, which can be observed in the surface as sand boils.

a)   b)   c)
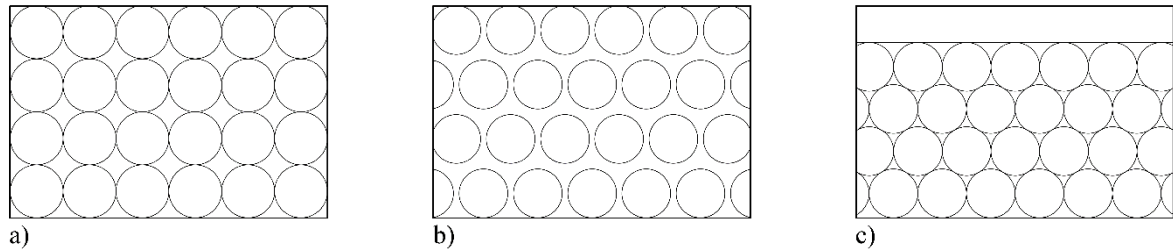
Figure 2.2 – Idealised schematic of liquefaction (NASEM, 2016)

Considering the different mechanisms of ground failure due to liquefaction, Robertson (1994) and Robertson and Fear (1995) proposed a liquefaction classification system that divided liquefaction into flow liquefaction and cyclic softening. Flow liquefaction is a strain softening response that occurs under undrained conditions, when static shear exceeds residual strength, and can be triggered by monotonic or cyclic loading. On the other hand, cyclic softening corresponds to a progressive pore pressure build-up in soils with a tendency to dilate under undrained monotonic shear, leading to the decrease in soil stiffness during cyclic loading. Cyclic softening was sub-divided into two behaviours: cyclic liquefaction and cyclic mobility. Cyclic liquefaction is characterised by zero effective stress condition and large deformations due to shear stress reversal. On the other hand, cyclic mobility occurs when there is no shear stress reversal and no zero effective stress condition is attained. Figure 2.3 presents the suggested flow chart for the evaluation of soil liquefaction.

The distinction between flow liquefaction triggered by cyclic loading and cyclic liquefaction is difficult to assess based on observed deformations, as both can cause very large deformations (Robertson and Wride, 1998). The main difference is that in cyclic liquefaction, deformations occur essentially during the cyclic loading, tending to stop after the seismic event, whereas when flow liquefaction occurs the deformations can continue after the event due to load redistribution. Examples of cyclic liquefaction were observed after the 1964 Niigata and 1995 Kobe earthquakes, in the form of lateral spreads, cracking, sand boils, and settlements, while flow liquefaction occurred, for example, in the Fort Peck Dam and the Stava tailings dam, causing major landslides (Robertson and Wride, 1998).
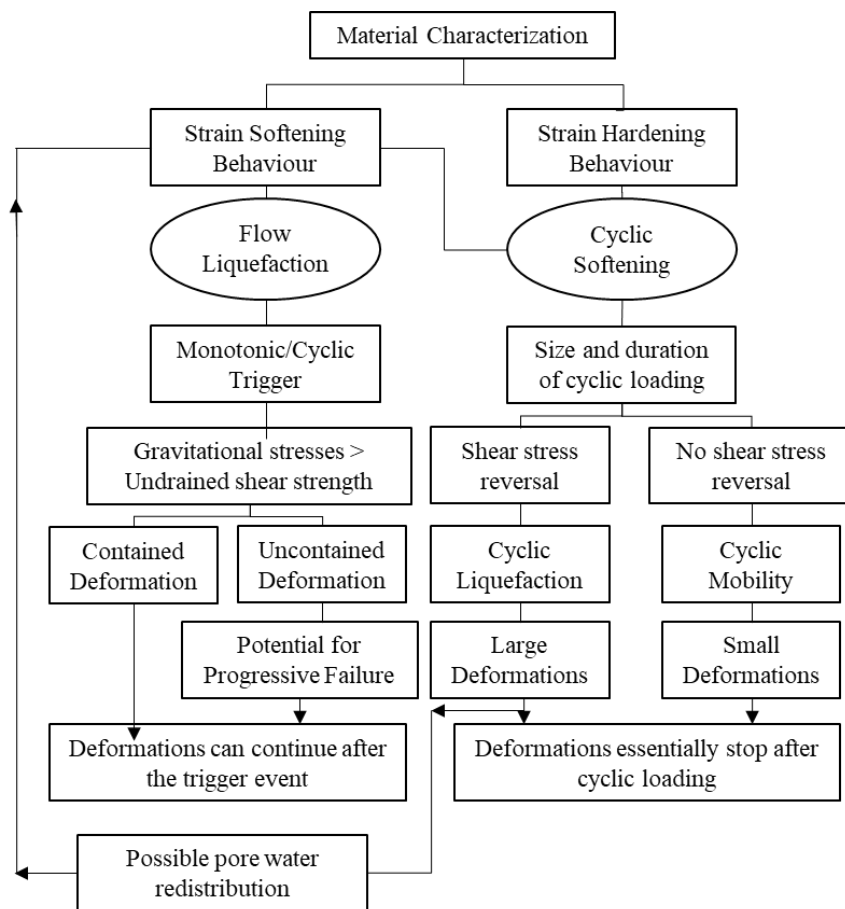
Figure 2.3 – Flow chart for liquefaction evaluation (after Robertson, 1994)

The focus of the present work is the behaviour of soils under cyclic loading. However, it is important to understand how the phenomenon develops under monotonic loads, as the study of static liquefaction has contributed to the identification of the effective stress conditions necessary for the initiation of liquefaction (Kramer, 1996). This section presents the mechanics of soil liquefaction, under both monotonic and cyclic loading. As the liquefaction assessment of sands is strongly supported by the critical state soil mechanics framework, its basic concepts are also introduced.

2.2.1. CRITICAL STATE SOIL MECHANICS

Soils experience different volume change behaviour, depending on whether their initial state is loose or dense. The tendency of soils to change volume while shearing was termed by Reynolds (1885) as dilatancy, and is a characteristic that distinguishes soils from other engineering materials (Jefferies and Been, 2016). When soils are monotonically sheared, initially loose sands tend to decrease in volume (contract), while initially dense sands tend to contract at first but then dilate (increase in volume).

Intrigued by this volume change behaviour, Casagrande (1936) performed a series of strain-controlled triaxial tests on loose and dense sand specimens, and concluded that all specimens tested at the same effective confining pressure converged to the same void ratio at large strains (Figure 2.4). This constant void ratio was termed critical void ratio, e_c, and was uniquely related to the effective confining pressure. Later, Taylor (1948) reported that the critical void ratio decreased with the increase of effective confining pressure. The relationship between the critical void ratio and mean effective stress defines the critical void ratio line, also termed critical state line (CSL), which separates loose and dense states.
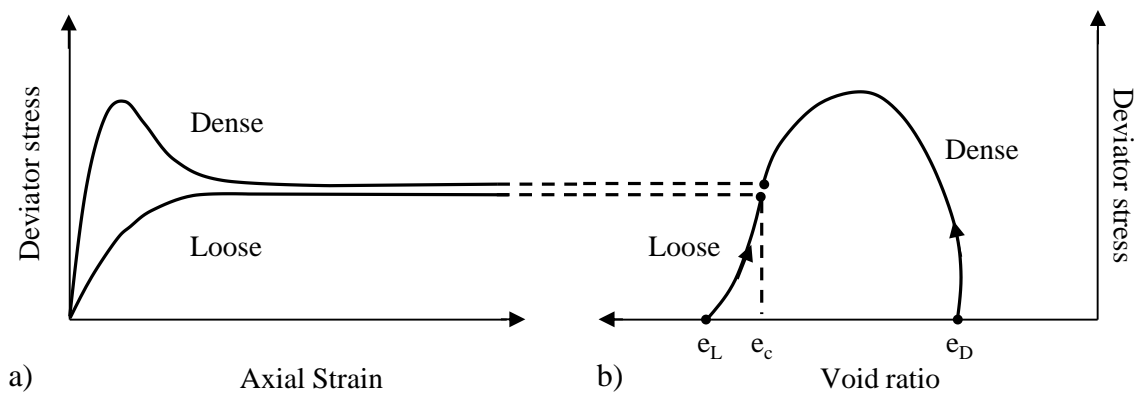
Figure 2.4 – a) Stress-strain; b) stress-void ratio curves for loose and dense sands at the same effective confining pressure sheared under drained conditions (adapted from Kramer, 1996)

The Critical State Soil Mechanics (CSSM) framework, developed by Schofield and Wroth (1968), was the first to assume density as a state variable. It describes globally the mechanical behaviour of soils, considering the volume changes during shearing. The critical state concept is based on the occurrence of an ultimate state that is reached when a soil is submitted to continuous deformation, and was defined by Roscoe et al. (1958) as the state at which *"a soil continues to deform at constant stress and constant void ratio"*, following the work of Casagrande.

A few years later, Castro (1969) performed a series of stress-controlled triaxial tests, and found that loose sands consistently resulted in liquefaction failure and landed on a steady-state line (SSL) at the end of the tests. The steady-state was defined by Poulos (1981) as *'the steady-state of deformation for any mass of particles is that state in which the mass is continuously deforming at constant volume, constant normal effective stress, constant shear stress and constant velocity'*.

There is some discussion about if the CSL and SSL are the same. However, the comparison of the two definitions presented above, by Roscoe et al. (1958) and Poulos (1981), indicates that both concepts are very similar. Therefore, in this work, it will be assumed that the two lines are the same, as proposed by Been et al. (1991) and Jefferies and Been (2016).

Figure 2.5 shows the dimensional CSL, where the black dot corresponds to the critical state, the white dots represent the projection on the three planes, the black square is the initial point before undrained shearing and the white squares are its projections.
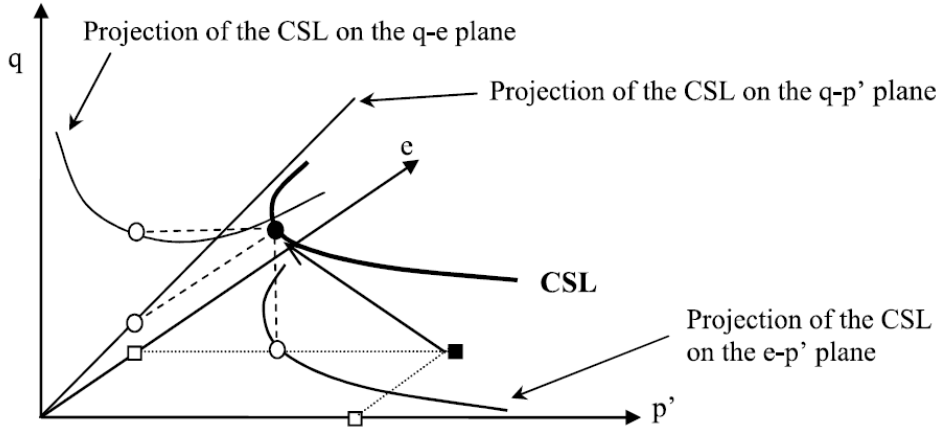
Figure 2.5 – Dimensional Critical State Line (Carrera, 2008)

Critical state lines are typically curved lines that tend to a horizontal asymptote for low pressures and become linear for high stress levels, in the e-log(p') plane (Verdugo and Ishihara, 1996; Carrera et al., 2011; Bedin et al., 2012). Li and Wang (1998) proposed equation (2.1) to compute the CSL over a wide range of pressures, where e_{cs} and p'_{cs} are the void ratio and the mean stress at critical state, respectively, $e_{0,cs}$ is the critical state void ratio for $p'= 0$ kPa, p_a is the atmospheric pressure, and λ and ξ_a are curve fitting parameters that depend on soil characteristics.

$$e_{cs} = e_{0,cs} - \lambda \left(\frac{p'_{cs}}{p_a} \right)^{\xi_a} \tag{2.1}$$

However, the critical state line is often modelled as bilinear, with one line corresponding to low pressures and other corresponding to high pressures. The equations are normally represented in the void ratio – mean stress plane as:

$$e_{cs} = \Gamma - \lambda \log(p'_{cs}) \tag{2.2}$$

where e_{cs} and p'_{cs} are the void ratio and the mean stress at critical state, respectively, and Γ and λ are intrinsic properties of the soil. Γ corresponds to the void ratio intercept, i.e., the value of the void ratio when p' equals 1 kPa (on the logarithmic scale) and λ is the gradient (i.e. slope) of the CSL.

In terms of shear stress, the critical state line is often represented by the critical shear stress ratio, M_{cs}, or the constant volume friction angle (ϕ'_{cv}), which is identical to the critical friction angle (ϕ'_{cs}). In the q–p' space, the CSL is defined as the Mohr-Coulomb failure line. The critical shear stress ratio, M_{cs}, is the slope of the line and is related to the constant volume friction angle. For triaxial compression, the CSL is defined in terms of stress invariants and the relationship between M_{cs} and ϕ'_{cs} is as follows:

$$q_{cs} = M_{cs} \times p'_{cs} \tag{2.3}$$

$$M_{cs} = \frac{6 \sin \phi'_{cs}}{3 - \sin \phi'_{cs}} \tag{2.4}$$

For specimens sheared under drained conditions, where volume change occurs, it was defined that loose specimens tend to contract, decreasing in volume, while dense specimens tend to dilate, increasing in volume. However, in tests performed with undrained shear, the specimen volume is constant. Therefore, the behaviour is expressed through the excess pore pressure. Dense specimens develop negative excess pore pressure, as they tend to dilate, while loose specimens develop positive excess pore pressure, as they tend to contract (Figure 2.6). The Critical State Line defines the ultimate state of any soil specimen at large strains, regardless of initial state or drainage conditions. Moreover, the uniqueness of the CSL is accepted by many authors (Verdugo and Ishihara, 1996; Atkinson, 2007; Carrera, 2008; Carrera et al., 2011).
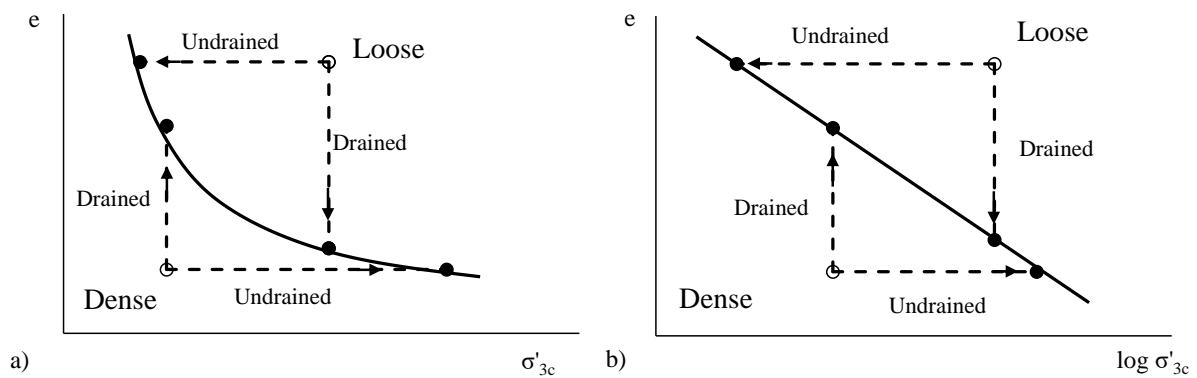
Figure 2.6 – Behaviour of loose and dense specimens under drained and undrained conditions for: a) arithmetic; b) logarithmic effective confining pressure (adapted from Krammer, 1996)

Casagrande (1936) proposed the Critical Void Ratio line (CVR; also known as CSL) as the boundary between contractive and dilative behaviour, hence separating soil according to their susceptibility to liquefy under undrained conditions. Figure 2.7 presents this consideration, where soils with initial states

above the CSL are susceptible to liquefy, while specimens initially plotted below the CSL are considered non-susceptible to liquefaction.
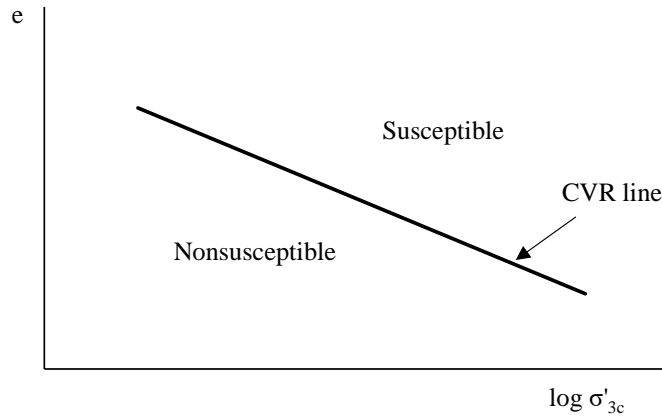
Figure 2.7 – CVR as a boundary between initial states susceptible and nonsusceptible to liquefaction (adapted from Kramer, 1996)

Taking the above into consideration, it is observed that the void ratio alone does not define the behaviour tendency of a soil specimen. The stress level, represented by the mean effective stress is also relevant, as the confining level influences the soil response. Two specimens with the same void ratio can be located on either side of the CSL, according to the stress level, hence having different behaviours. The state parameter, ψ, was first introduced by Wroth and Bassett (1965) and later named as such by Been and Jefferies (1985). It defines the position of a soil specimen in relation to the critical state line and can be defined as the distance between the current void ratio (e) and the void ratio at critical state (e_{cs}) for the current mean stress (Figure 2.8).

$$\psi = e - e_{cs}$$

(2.5)
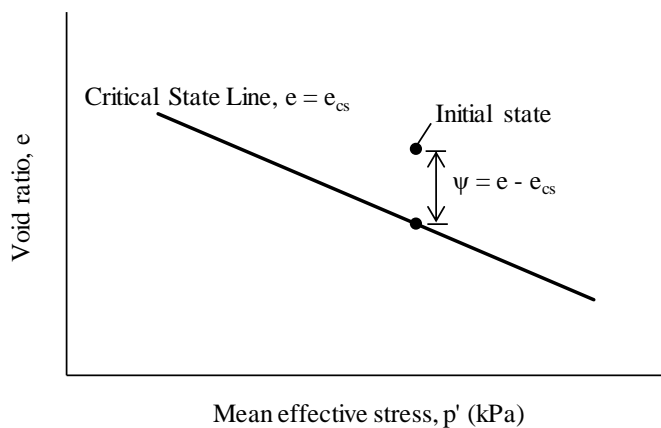
Figure 2.8 – State Parameter definition

The state parameter constitutes a powerful normalisation tool, as it translates many soil properties and behaviours (Jefferies and Been, 2016). Besides, it is often used in constitutive modelling of soil, as it takes into consideration both the density state and the stress state on soil behaviour. However, the main disadvantage of the use of the state parameter is the necessity of a very accurate determination of the critical state line, which is normally obtained from reconstituted samples in the laboratory.

2.2.2. BEHAVIOUR UNDER MONOTONIC LOADING - STATIC LIQUEFACTION

Although the focus of the present work is to study the cyclic liquefaction behaviour, understanding the behaviour of a soil subjected to monotonically increasing stresses is important to provide a context for the liquefaction interpretations.

To illustrate the behaviour of a soil under undrained monotonic loading, Figure 2.9 presents the stress path of three undrained monotonic triaxial compression tests, in specimens of granular soil with different densities. Three types of response can be identified, depending on the density of the initial state, i.e. depending on the position relative to the critical state line. Some authors (Castro, 1969; Been and Jefferies, 1985; Kramer, 1996) define as liquefaction what other authors (Lade and Yamamuro, 1997; Robertson and Wride, 1998; Viana da Fonseca et al., 2011) consider strain softening. Despite this, the definitions of behaviour have the same meaning: liquefaction corresponds to strain softening, limited liquefaction is limited strain softening, and dilation is the same as strain hardening.

The soil specimen that is in very loose conditions (specimen A), above the CSL, experiences a peak in undrained strength at low shear strain and then the shear strength drops rapidly to large strains. This behaviour is termed flow liquefaction or strain softening. On the other hand, if the soil is in a dense state (specimen B) below the CSL, it will contract at first but then dilate towards its ultimate state. The behaviour is termed dilation or strain hardening. However, at intermediate densities (specimen C) above but close to the CSL, the soil specimen can suffer limited liquefaction, or limited strain softening, which is characterised by a peak strength followed by a limited strain-softening that inverts to a dilative behaviour until the ultimate state. This reversal point is known as the phase transformation point (Ishihara et al., 1975).
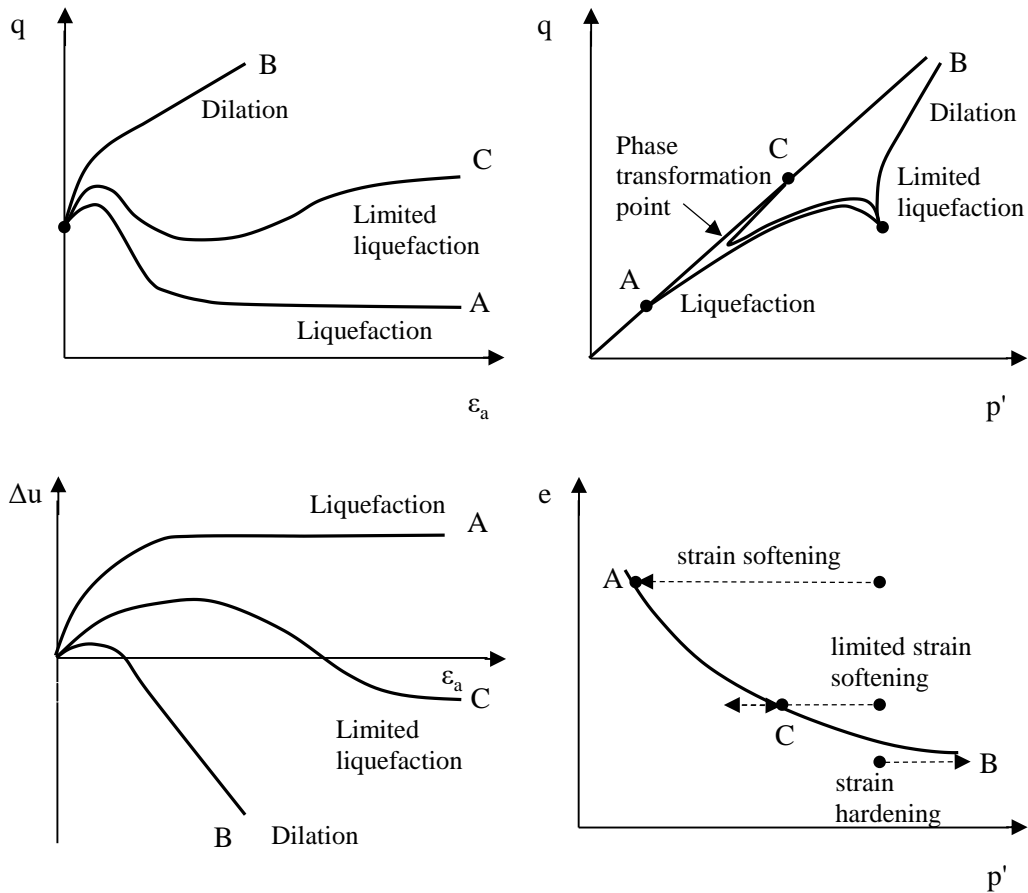
Figure 2.9 – Undrained monotonic behaviour of three specimens at different initial densities with the same initial confining pressure (adapted from Kramer, 1996)

Moreover, Kramer (1996) presented the response of a series of triaxial tests with the same initial void ratio at different effective confining pressures. Figure 2.10 illustrates the results, showing that as the specimens start at different confining pressures, they will follow different stress paths but as they start with the same initial void ratio, they will end at the same steady-state point. Specimens A and B are located below the critical state line, so the behaviour is dilative. On the other hand, specimens C, D, and E are above the CSL and contract upon shearing. The stress paths show a peak in strength, followed by a rapid strain towards the critical state. The locus of the peak points (marked with an x) is where flow liquefaction initiates, and form a straight line (Vaid and Chern, 1985), defined as flow liquefaction surface (FLS), also called the instability line (Ishihara, 1993; Lade and Yamamuro, 2011). It is important to note that Sladen et al. (1985) proposed the collapse surface, which corresponds to the line crossing the peak strength points and the steady-state (Figure 2.11).
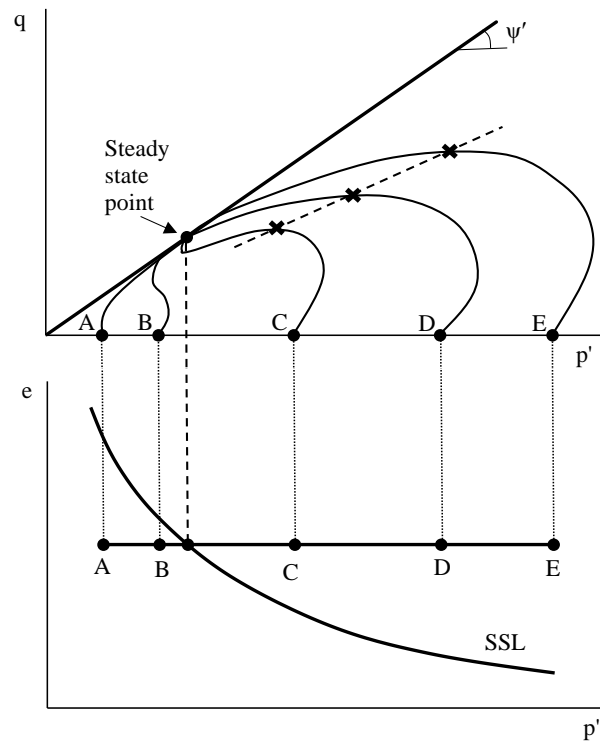
Figure 2.10 – Response of triaxial tests with the same initial void ratio at different effective confining pressures (Kramer, 1996)
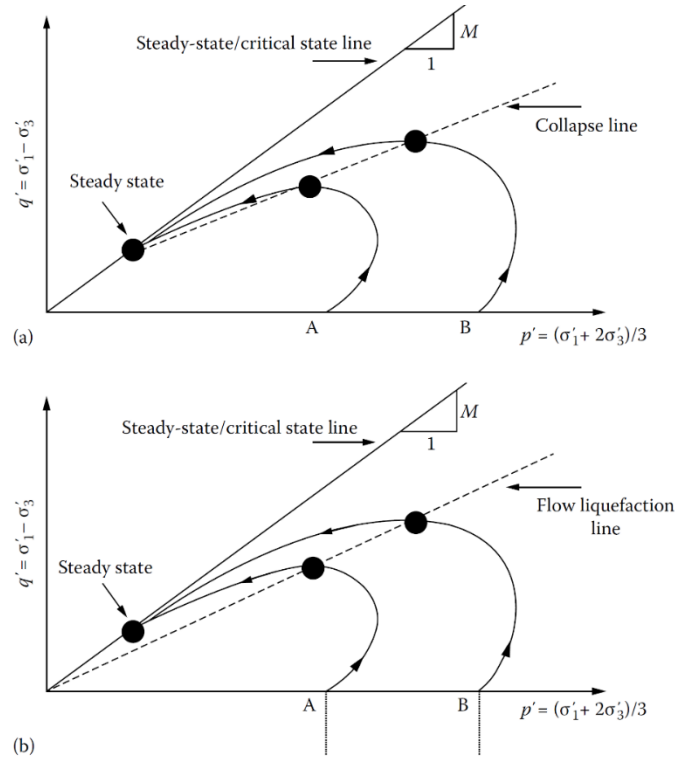
Figure 2.11 – Definition of collapse surface and flow liquefaction line (Jefferies and Been, 2016)

The flow liquefaction surface separates stable and unstable states in undrained shear. As referred above, flow liquefaction can be triggered by monotonic or cyclic loading. If the stress path of a specimen reaches the FLS, flow liquefaction is triggered, reducing the shear resistance to the steady-state. Therefore, the zone of susceptibility to flow liquefaction is marked in Figure 2.12.
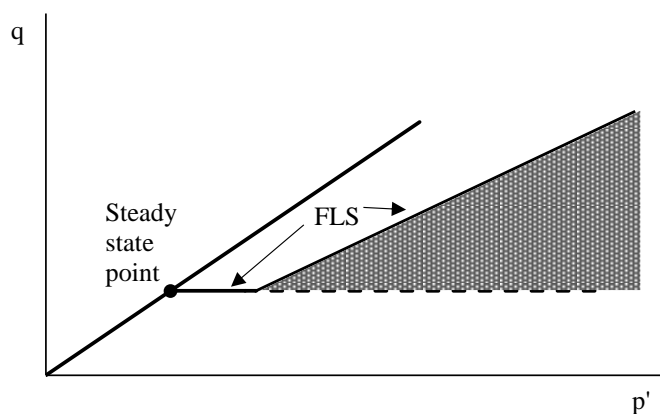
Figure 2.12 – Zone of susceptibility to flow liquefaction (adapted from Kramer, 1996)

Moreover, Carrera et al. (2011) suggested a scheme for the division of the area above the CSL for three different behaviours. The division is based on the positions of the q_{max} points in the q-p' plane in relation to the instability line. If the points are between the instability line and the CSL, the specimens will suffer strain softening but will not liquefy. In the e-$\log(p')$ plane, the horizontal asymptote for low pressures is of key importance as it bounds the instability zone. For samples with void ratios above the horizontal asymptote, total liquefaction was observed with p' dropping to zero. Samples with a void ratio between the horizontal asymptote and the linear part of the CSL showed strain softening but no liquefaction, reaching stable critical states located on the curved part of the CSL. On the other hand, for higher pressures, specimens were compressive and generally strain hardening, and reached stable critical states on the straight part of the CSL. These observations emphasise the importance of the definition of a curved CSL, especially for low confining pressures, to avoid misinterpretations of the state parameter.

Furthermore, the analyses of this Figure suggests that the state parameter might not be completely accurate to predict soil behaviour, as the soil could have the same state parameter and have different expected behaviour depending on its location above the CSL. For example, a soil with a certain state parameter that must undergo static liquefaction at low pressures when it is above the horizontal asymptote, will not undergo static liquefaction if its located at higher stresses.
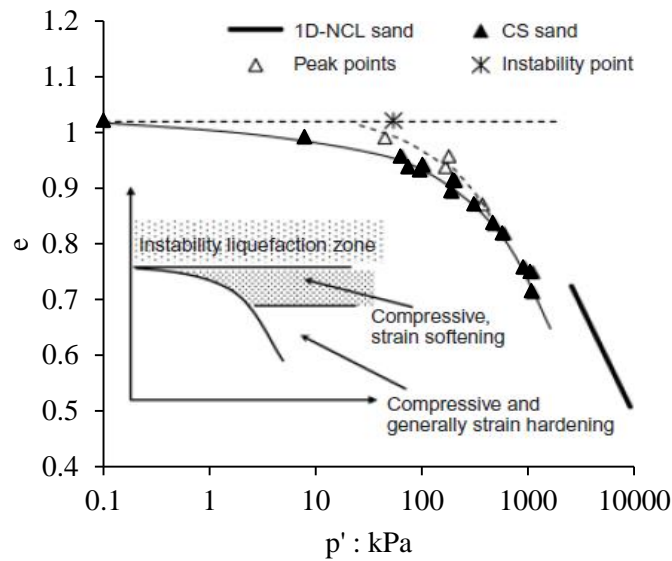
Figure 2.13 – Critical state line of Stava Tailings clean sand and suggested scheme of subdivision of the area above the CSL into three different regions connected to different behaviour (Carrera et al., 2011)

2.2.3. BEHAVIOUR UNDER CYCLIC LOADING

As referred above, when subjected to cyclic undrained loading, such as earthquake loadings, a saturated cohesionless soil tends to develop positive pore pressures. Returning to the diagram in Figure 2.3, three situations can be caused by cyclic loads: flow liquefaction, cyclic liquefaction and cyclic mobility. Flow liquefaction was discussed in the section above, and is related to the strain softening response, when static shear exceeds the steady-state strength. On the other hand, cyclic liquefaction and cyclic mobility are triggered by a progressive increase in the pore water pressure and are distinguished based on the occurrence of shear stress reversal. If there is shear stress reversal, which means that the cyclic shear stress is higher than the static shear stress, the effective stresses might reach zero, and cyclic liquefaction might occur. However, if no shear stress reversal takes place, cyclic mobility will occur, as the condition of zero effective stress does not develop and the deformations will be limited.

Figure 2.14 illustrates an example of the cyclic behaviour of a loose granular soil subjected to undrained cyclic simple shear loading. As the cyclic loading begins, the initial shear strain amplitude is small and the pore pressure ratio starts to increase, while the vertical effective stress decreases. As the cyclic loading progresses, the stress-path approaches the origin and the vertical effective stress becomes very low. At this stage, the pore pressure ratio increases more rapidly, reflecting an increase in the shear strain amplitude. When the effective stress-path reaches the origin (i.e. the pore pressure ratio equals 1), liquefaction is triggered and higher shear strain amplitudes are observed.
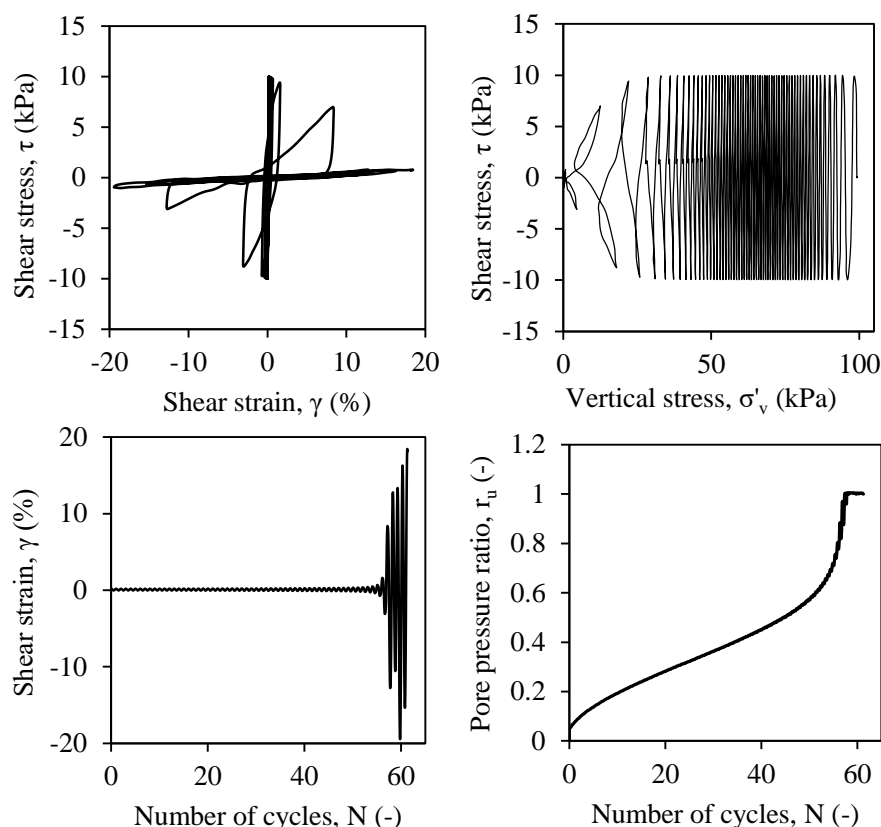
Figure 2.14 – Example of the cyclic behaviour of a loose granular soil subjected to undrained cyclic simple shear loading

Kramer (1996) considered cyclic mobility as Robertson (1994) flow chart considered cyclic softening and presented three different cyclic triaxial test scenarios that can trigger it (Figure 2.15). The first is characterised by no shear stress reversal and no exceedance of the steady-state strength. As the cyclic loading progresses, the vertical effective stress decreases significantly until it touches the failure envelope, where it stabilizes. The second scenario corresponds to no stress reversal and exceedance of steady-state strength. When the stress path reaches the FLS, some periods of instability are observed. High strains may develop but they tend to stop with the end of cyclic loading. The third scenario shows shear stress reversal with no exceedance of the steady-state strength. As the cycles progress, the specimens suffer compressions and extensions until reaching the failure envelope. During this process, a state of softening is produced with pore water pressure build-up to almost 100% and significant axial strain. When the stress-path crosses the origin, the effective stress is zero, and liquefaction is triggered. However, no complete loss of strength is verified even after liquefaction is triggered and the axial strain does not increase indefinitely (Ishihara, 1993).

Similarly to the shaded area susceptible to flow liquefaction, Kramer (1996) also presented a zone of susceptibility to cyclic mobility (Figure 2.16). The zone is characterised by stress states below the steady-state point. This behaviour can occur in both loose and dense soils, with a variety of effective confining pressures. During the current work, liquefaction is considered according to the type of loading, as the focus is to study cyclic liquefaction due to earthquake loading.
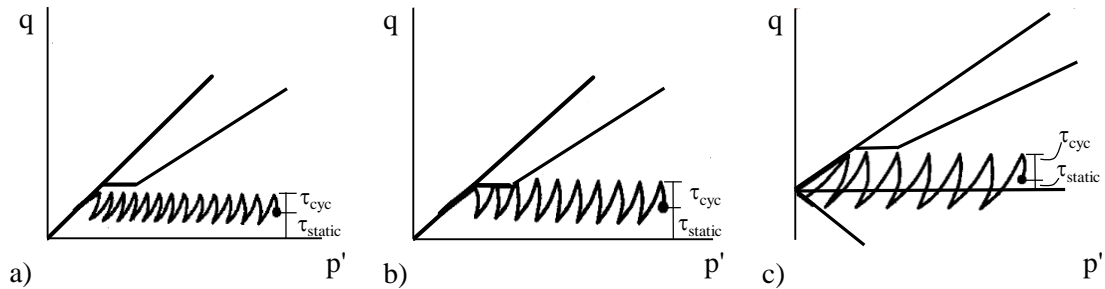
Figure 2.15 – Three cases of cyclic mobility (Kramer, 1996)
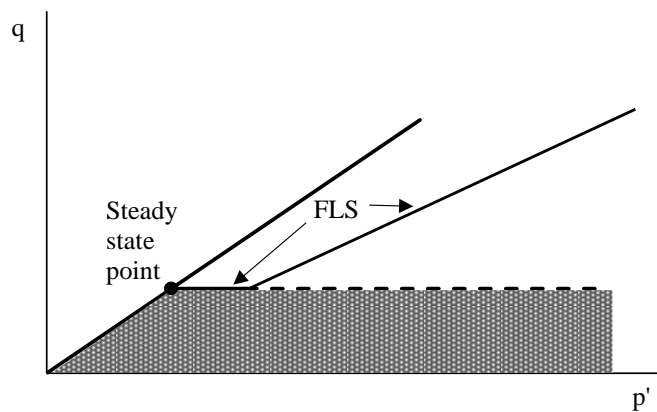
Figure 2.16 – Zone of susceptibility to cyclic mobility (adapted from Kramer, 1996)

Similarly to the analysis of liquefaction susceptibility using the state position relative to the CSL (*i.e.*, the state parameter), the liquefaction susceptibility can also be assessed through the shear wave velocity (V_S), associated to the material stiffness (G_{max}). The methods to evaluate liquefaction based on shear wave velocity are addressed in following sections. In this sense, it is important to include a section about the stiffness at very small strains, as presented below.

2.2.4. THEORETICAL BACKGROUND ON STIFFNESS AT VERY SMALL STRAINS

The vibrations produced by wave propagation in a soil specimen are responsible for very small particle movements. Therefore, the soil behaviour can be assumed to be elastic, and stress wave velocities might be used to define the shear modulus (G_0 or G_{max}) and the constrained modulus (M_0 or M_{max}). The shear

and constrained moduli are determined by multiplying the soil mass density (ρ) by shear wave (S wave) or compression wave (P wave) velocities, respectively, as follows:

$$G_{max} = \rho V_S^2 \tag{2.6}$$

$$M_{max} = \rho V_P^2 \tag{2.7}$$

The shear modulus is considered a fundamental parameter of dynamic properties of the ground, as it is in practical terms independent of the type of loading, number of cycles and strain rate and history (Viana da Fonseca et al., 2011). Moreover, G_{max} reflects the nature of interparticle contacts, as the very small strains deforms the granular skeleton at constant fabric (Cho et al., 2006).

Over the years, studies have proven that the shear modulus was dependent on a variety of parameters, such as effective stresses, void ratio, stress history, degree of saturation, shear stress, grain and mineralogical properties, excitation frequency, ageing, fabric and structure, and temperature (Hardin and Black, 1969). However, these factors have different degrees of influence in the stiffness of a soil. Hardin and Blandford (1989) gathered the most influential factors and proposed equation (2.8) to estimate G_{max}:

$$G_{0ij} = S_{ij} \times F(e) \times OCR^k \times p_a^{(1-n_i-n_j)} \times (\sigma'_i)^{n_i} \times (\sigma'_j)^{n_j} \tag{2.8}$$

where σ'_i and σ'_j are principal effective stresses in the wave propagation direction, i, and wave polarisation direction, j; k is an empirical exponent of the overconsolidation ratio OCR depending on the plasticity index, PI; F(e) is a void ratio function; S_{ij} is a non-dimensional material constant reflecting the fabric and structure of the soil; n_i and n_j are empirical stress exponents or indices, that are usually considered the same for sand; and p_a is a reference stress, considered the atmospheric pressure, 100 kPa (adapted from Ferreira, 2009).

The void ratio function accounts for the influence of the void ratio in soil stiffness, and has been defined using several expressions by various authors (Table 2.1). If no specific study is carried out to determine the characteristic void ratio function of a particular soil, one of the reference expressions can be applied directly. On the other hand, if the void ratio function considered is appropriate, the influence of the overconsolidation ratio can be neglected (Ferreira, 2009).

Table 2.1 – Reference void ratio functions

Expression	Reference
$\dfrac{(2.17 - e)^2}{1 + e}$	Hardin and Richart (1963); Iwasaki et al. (1978b)
$\dfrac{(2.973 - e)^2}{1 + e}$	Hardin and Drnevich (1972)
$\dfrac{1}{0.3 + 0.7e^2}$	Hardin (1978); Chung et al. (1984)
$e^{-1.3}$	Lo Presti (1995); Jamiolkowski et al. (1991)
$\dfrac{(1.46 - e)^2}{1 + e}$	Wichtmann and Triantafyllidis (2004)
$(1 + e)^{-3}$	Bui et al. (2010)

In the present work, the shear wave velocities were measured in the laboratory using bender elements in the vertical direction. In triaxial conditions, the influence of the principal effective stresses might be represented by considering the mean effective stress, p'. Taking into account all the considerations analysed above, the essential form of the empirical equation to estimate G_{max} can be expressed as:

$$G_{max} = A \times F(e) \times p'^n \tag{2.9}$$

where A is a material coefficient that reflects the influence of particle characteristics, anisotropy, fabric, and structure of the soil; and n varies with soil type and shear strain levels.

2.3. LIQUEFACTION SUSCEPTIBILITY CRITERIA

In this section, the emphasis is given to the simplified procedure developed by Seed and Idriss (1971), to assess liquefaction triggering, an approach based on stress measurements. Notwithstanding, there are other approaches available to study the liquefaction susceptibility of soils, such as strain-based, energy-based, laboratory-based, and computational mechanics approaches. In this work, the in situ tests were analysed with the simplified stress-based approach, while the laboratory tests were analysed from various perspectives, namely stress-based, and energy-based approaches, which are discussed in section 2.6. The simplified procedure to assess the factor of safety against liquefaction is described in detail, as

well as the adjustment factors to consider different seismic and soil conditions. Besides, the factor of safety against liquefaction is used in alternative approaches to assess liquefaction hazard in terms of qualitative risk and severity of liquefaction consequences. Some of these indexes, such as the Liquefaction Potential Index and the Liquefaction Severity Number, are explained during this section.

2.3.1. FACTOR OF SAFETY AGAINST LIQUEFACTION

After the Niigata and Alaska 1964 earthquakes, Seed and Idriss (1971) developed the "Simplified Procedure", a stress-based approach to estimate the potential for cyclic liquefaction due to earthquake loading, introducing the factor of safety against triggering of liquefaction (FS$_{liq}$). Although many modifications and improvements have been proposed over the years, the basic framework remains unchanged and this method continues to be the most commonly used stress-based approach to evaluate liquefaction triggering nowadays.

The Factor of Safety against liquefaction triggering (FS$_{liq}$) is defined as the ratio between the capacity of a soil to resist liquefaction, the Cyclic Resistance Ratio (CRR), and a measurement of the earthquake loading induced in the soil, the Cyclic Stress Ratio (CSR), as follows:

$$FS_{liq} = \frac{CRR}{CSR}$$
(2.10)

The Cyclic Stress Ratio, CSR (equation (2.11)), is a measure of the earthquake loading induced in the soil, and can be obtained by a site-specific ground response analysis. However, Seed and Idriss (1971) developed a simplified method that relates the average cyclic shear stress (τ_{av}) and the initial effective vertical stress in the ground (σ'_{v0}), where a_{max} is the horizontal component of the peak ground acceleration at the site, g is the acceleration of gravity, σ_{v0} is the initial total vertical stress in the ground and r_d is a shear stress reduction coefficient that accounts for the non-rigid response of the soil deposit subjected to a vertically propagating shear wave. The 0.65 factor was originally proposed to account for the influence of an irregular earthquake loading in the triggering of liquefaction. Since the introduction of the magnitude scaling factor (MSF), this value is no longer necessary, however, it is still the standard due to historical precedent (NASEM, 2016).

$$CSR = \frac{\tau_{av}}{\sigma'_{v0}} = 0.65 \left(\frac{a_{max}}{g}\right) \left(\frac{\sigma_{v0}}{\sigma'_{v0}}\right) r_d$$
(2.11)

The maximum ground acceleration (a_{max}) depends on the location of the site and can be calculated using formulations from Eurocode 8 – Part 1 and Part 5 and the respective National Annexes (NP EN 1998-1

and NP EN 1998-5, 2010) that address the design of structures for earthquake resistance. This calculation procedure is explained in detail further in this work, in section 3.2.1.

The shear stress reduction coefficient calculation is controversial among the geotechnical community, and different authors use distinct approaches, as it is a function of the non-rigid response of the soil deposit and the characteristics of the shear waves propagating through the soil. The initial proposal from Seed and Idriss (1971) considered r_d to be related only to the depth. Following the 1996 NCEER and 1998 NCEER/NSF workshops, Youd et al. (2001) suggested equations (2.12) and (2.13), from Liao and Whitman (1986) for estimating average values of r_d.

$$r_d = 1.0 - 0.00765z \ \ for \ z < 9.15m \tag{2.12}$$

$$r_d = 1.174 - 0.0267z \ for \ 9.15m < z < 23m \tag{2.13}$$

However, more recent procedures also consider the seismic action characteristics, including the moment magnitude and the peak ground acceleration in the calculation of r_d (Moss et al., 2006; Boulanger and Idriss, 2014). Using additional site response analyses, Idriss (1999) proposed a new procedure, in which the parameter r_d was also related to the earthquake moment magnitude (equation (2.14)). The arguments inside the sin are in radians and z is the layer depth in meters.

$$r_d = \exp[\alpha(z) + \beta(z).M] \tag{2.14}$$

$$\alpha(z) = -1.012 - 1.126\sin\left(\frac{z}{11.73} + 5.133\right) \tag{2.15}$$

$$\beta(z) = 0.106 + 0.118\sin\left(\frac{z}{11.28} + 5.142\right) \tag{2.16}$$

On the other hand, Moss et al. (2006) reassessed the equations proposed by Cetin (2000), and suggested that r_d is calculated according to equation (2.17) for depths under 20 m, where d is the depth in meters at the midpoint of the critical layer, M_w is the moment magnitude and a_{max} is the peak ground acceleration.

$$r_d = \frac{\left[1 + \dfrac{-9.147 - 4.173 \cdot a_{max} + 0.652 \cdot M_w}{10.567 + 0.089 \cdot e^{0.089 \cdot (-d \cdot 3.28 - 7.760 \cdot a_{max} + 78.576)}}\right]}{\left[1 + \dfrac{-9.147 - 4.173 \cdot a_{max} + 0.652 \cdot M_w}{10.567 + 0.089 \cdot e^{0.089 \cdot (-7.760 \cdot a_{max} + 78.576)}}\right]} \tag{2.17}$$

27

The means for calculating r_d are not strictly defined so its value depends on the method selected for liquefaction assessment. Robertson and Cabal (2015) used the r_d formulation suggested by Youd et al. (2001) while Idriss and Boulanger (2008) and Boulanger and Idriss (2014) used the relationship developed by Idriss (1999).

The capacity of a soil to resist liquefaction corresponds to the CSR required to trigger liquefaction and is represented by the Cyclic Resistance Ratio (CRR). Several field tests, such as the Standard Penetration Tests (SPT), the Cone Penetration Tests (CPT), the flat dilatometer test (DMT), or measurements of shear wave velocity (V_S), have been used to assess CRR, based on the in situ resistance parameters. The CRR corresponds to the demarcation that separates the regions of liquefaction and non-liquefaction, in the plot of CSR with in situ test parameters, for earthquakes with the reference magnitude of 7.5.

The simplified procedure was developed for standard conditions, which comprise a reference magnitude of 7.5, vertical effective stress of 1 atm, and level or gently sloping ground. Therefore, adjustment factors are included in the CRR calculation, to account for conditions different than the standard. To account for the effects of the earthquake magnitude, related to the duration of the cyclic motion, a Magnitude Scaling Factor (MSF) is used. This factor computes the equivalent CRR for a reference magnitude of 7.5. Furthermore, to consider the influence of the initial overburden pressure and static shear stress conditions, K_σ and K_α are introduced, respectively. According to Seed (1983), CRR is adjusted as follows:

$$CRR = CRR_{7.5} \times MSF \times K_\sigma \times K_\alpha$$

(2.18)

These adjustment factors are explored in detail in section 2.3.2.. Later in this Chapter, other factors that also influence the cyclic liquefaction of soils, including the initial confining stress, relative density, soil anisotropy, and fines content are discussed.

2.3.1.1. Brief reference to soil liquefaction evaluation according to the Eurocode

The Eurocode 8: Design of structures for earthquake resistance, Part 5: Foundations, retaining structures and geotechnical aspects includes a section with recommendations on the assessment of potentially liquefiable soils. Liquefaction is described as "*a decrease in the shear strength and/or stiffness caused by the increase in pore water pressures in saturated cohesionless materials during earthquake ground motion, such as to give rise to significant permanent deformations or even to a condition of near-zero effective stress in the soil*". The liquefaction susceptibility evaluation should be performed for the free-

field site conditions, based on the presence of extended layers or thick lenses of loose sand below the groundwater table, and when the groundwater table is close to the ground surface.

The minimum required investigation includes Standard Penetration Tests (SPT) or Cone Penetration Tests (CPT), and the performance of grain size analysis in the laboratory. The SPT measurements should be normalised according to the overburden stress, the energy ratio of the testing equipment used, and for depths less than 3 m, the N_{SPT} value should be multiplied by 0.75.

Furthermore, Eurocode 8 suggests a set of conditions that, if satisfied, allow the omission of a liquefaction susceptibility study, mainly:

- If the building foundations are shallow, the evaluation of liquefaction susceptibility is only required for the first 15 m from ground surface;
- "*When α·S< 0.15 and at least one of the following conditions is fulfilled:*
    - *The sands have a clay content greater than 20 % with plasticity index PI > 10;*
    - *The sands have a silt content greater than 35 % and, at the same time, the SPT blowcount value normalised for overburden effects and for the energy ratio $N_{1(60)} > 20$;*
    - *The sands are clean, with the SPT blowcount value normalised for overburden effects and for the energy ratio $N_{1(60)} > 30$.*"

The liquefaction susceptibility is assessed based on empirical liquefaction charts, based on in situ test parameters, namely SPT, CPT, and shear wave velocity measurements. Figure 2.17 shows the chart for clean sands and silty sands. The seismic shear stress, τ_c, is calculated with equation (2.19), based on the Simplified Method, where α is the ratio of the design ground acceleration on type A ground to the acceleration of gravity, S is a soil factor, and σ_{v0} is the total overburden pressure. When using this field correlation approach, soils should be considered susceptible to liquefaction whenever the earthquake-induced shear stress exceeds λ of the critical stress. In Portugal, λ is 0.8, which corresponds to a factor of safety of 1.25.
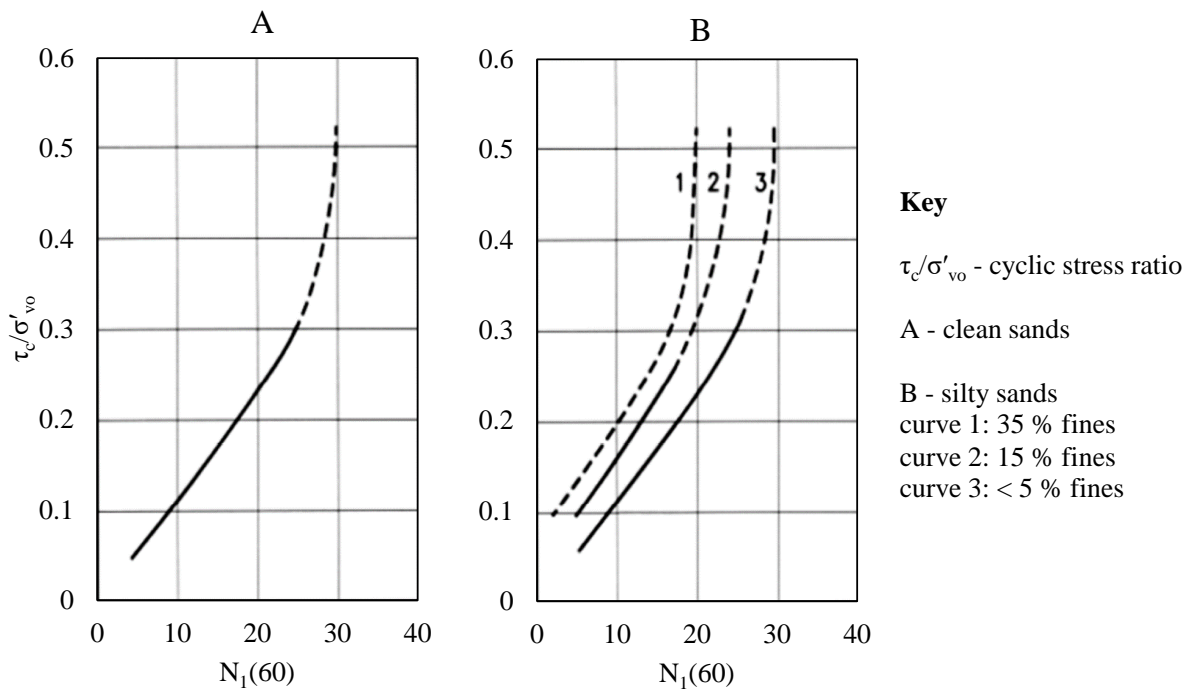
Figure 2.17 – Relationship between stress ratios causing liquefaction and $N_1(60)$ values for cleans and silty sands for $M_w = 7.5$ earthquakes

$$\tau_c = 0.65\alpha \cdot S \cdot \sigma_{v0}$$

(2.19)

Moreover, Eurocode 8 proposes the factor CM, equivalent to the MSF presented in section 2.3.2.1., to assess liquefaction susceptibility for earthquake magnitudes rather than 7.5. The ordinates of the liquefaction curves should be multiplied by CM, which values are given in Table B.1 of Eurocode 8 – Part 5. Despite not presenting the figures for liquefaction susceptibility charts based on the results of CPT, EC8 recommends the direct use of CPTu-based charts, avoiding the use of indirect correlations between SPT blowcounts and CPT cone resistance. On the other hand, as the correlations based on shear wave velocity are still under development, they are not advised without the assistance of a specialist. In terms of ground improvement to prevent liquefaction, the methodologies proposed in the Eurocode 8 include compaction to increase the penetration resistance of the soil, and drainage to reduce the excess pore water pressure generated during the earthquake.

2.3.2. ADJUSTMENT FACTORS APPLIED TO CRR

2.3.2.1. Adjustment for earthquake magnitude

As expressed above, the Magnitude Scaling Factor (MSF) is an adjustment factor used to normalise the cyclic resistance ratio or the cyclic stress ratio. Seed and Idriss (1982) introduced this factor, estimated from the average number of loading cycles for several earthquake magnitudes and laboratory test results, to account for earthquakes with magnitudes other than 7.5 (equivalent to 15 loading cycles). This way, an irregular time history of an earthquake loading is substituted by an equivalent stress history with constant amplitude. Seed and Idriss (1982) defined the equivalent stress amplitude as 65% of the maximum shear stress in the irregular history, the same factor that affects CSR, as expressed above. Youd et al. (2001) recommended the use of a range of MSF, with an upper bound proposed by Andrus and Stokoe (2000) and a lower bound proposed by Idriss (in 1995 Seed Memorial Lecture, personal communication to T. L. Youd, 1997) for magnitudes lower than 7.5. Some relationships between the earthquake magnitude and the MSF are presented in Figure 2.18.
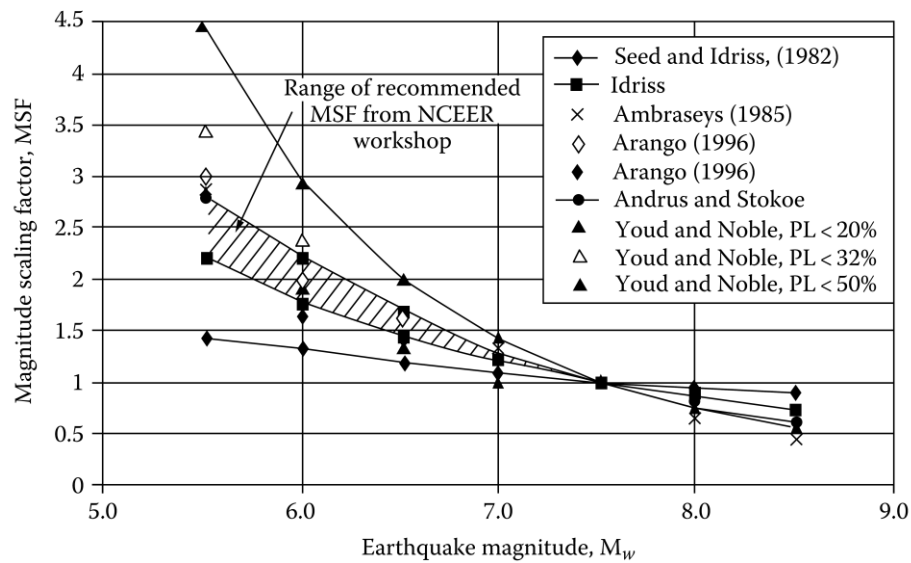
Figure 2.18 – MSF proposed by different authors (Youd et al., 2001)

A few years later, Idriss and Boulanger (2008) proposed different MSF−M_w curves according to the type of soil. For sands, an upper limit (cap) of MSF was established at 1.8, to take into consideration the time series of stress induced by a small magnitude earthquake to be dominated by a single pulse of stress (Boulanger and Idriss, 2014). Figure 2.19 presents the proposed curves for sands and clays.
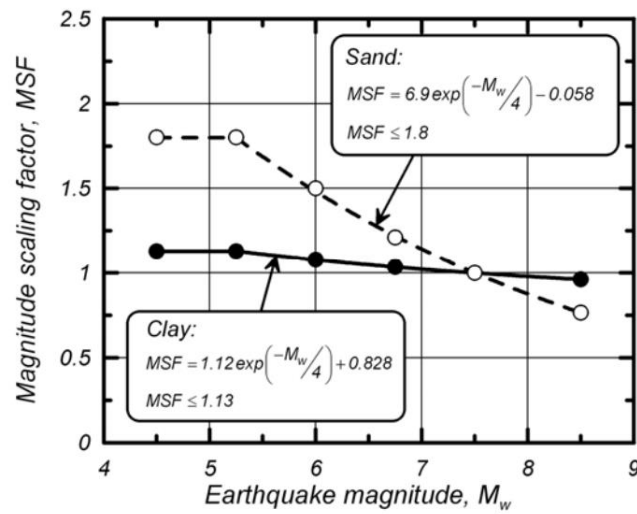
Figure 2.19 – MSF for sands and clays (Boulanger and Idriss, 2014)

More recently, Boulanger and Idriss (2014) recommended an approach based on Idriss and Boulanger (2008) that relates the MSF with the results from SPT and CPT tests (see Table 2.2). Contrary to other approaches that consider the same MSF curve for all cohesionless soils, the revised MSF attempts to include the influence of soil characteristics, through field test results.

2.3.2.2. Adjustment for effective stress, K_σ

The correction factor K_σ, introduced by Seed (1983), accounts for the dependency of the cyclic strength of sands on confining stress, and for the non-linearity of the relationship for overburden pressures greater than 100 kPa. It is defined by the ratio of the CRR at a certain effective vertical stress to the CRR at an effective vertical stress of 100 kPa. Later, Hynes and Olsen (1999) compiled a summary of K_σ curves extrapolated from laboratory tests (Figure 2.20), where K_σ is obtained by equation (2.20). The exponent function f includes the effects of the in situ conditions, mainly relative density, past stresses, ageing, and overconsolidation ratio. Youd et al. (2001) recommend $f = 0.7-0.8$ for relative densities between 40% and 60% and $f = 0.6-0.7$ for relative densities between 60% and 80%.

$$K_\sigma = (\sigma'_{v0}/p_a)^{f-1}$$

(2.20)
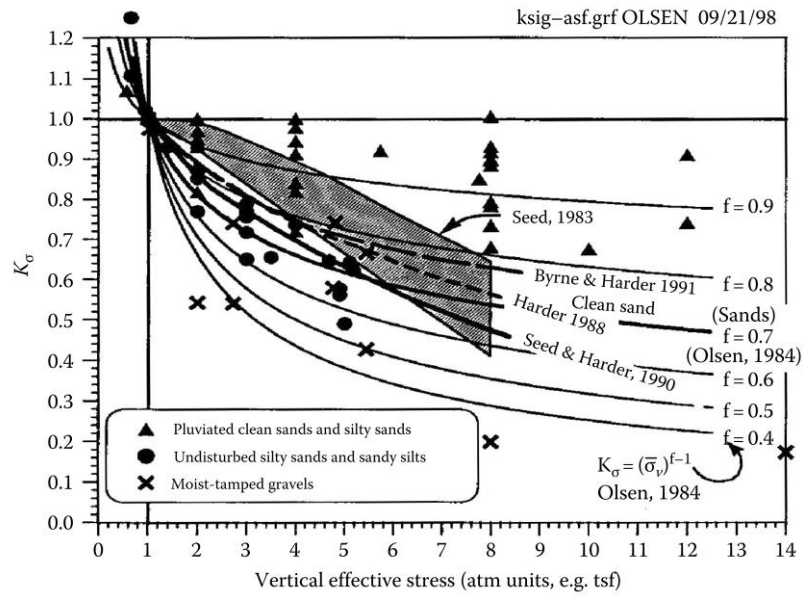
Figure 2.20 – K_σ curves extrapolated from laboratory tests (from Hynes and Olsen, 1999)

Boulanger (2003a) developed K_σ relationships, based on the critical state framework, by considering semi-empirical correlations between field CRR, penetration resistances, and the relative state parameter index, ξ_R. The relative state parameter was used only in the derivation process, so it is not computed (Idriss and Boulanger, 2008). Figure 2.21 shows the relationships for a range of $(N_1)_{60}$ and q_{c1N}.
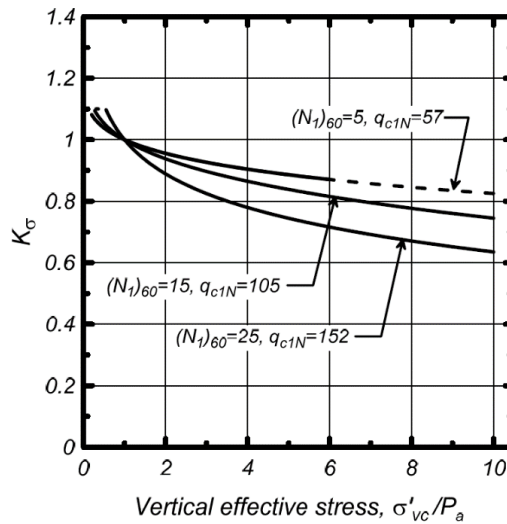
Figure 2.21 – Overburden correction factor relationship for a range of $(N_1)_{60}$ and q_{c1N} (Idriss and Boulanger, 2008)

For effective stresses ranging 0.5 to 1.2 atm, the range well represented in the liquefaction case history database, K_σ values agree among researchers. However, there is a debate about whether to restrain the value of K_σ to a maximum value when the effective stresses are small. Moreover, for effective stresses significantly larger than 1 atm, the K_σ values recommended by different researchers differ, as they are extrapolations from liquefaction case history databases. Due to the uncertainties associated with these extrapolations, it is important to use experimental data and soil mechanics principles to constrain K_σ outside the range of the known databases (NASEM, 2016).

2.3.2.3.   Adjustment for initial static shear stress, K_α

Seed (1983) introduced a shear stress adjustment factor, K_α, to account for the influence of the initial static shear stress on the horizontal plane before earthquake shaking. K_α represents the ratio between CRR at a certain value of α and the CRR at $\alpha = 0$. The parameter α is introduced as the ratio between the initial static shear stress to the normal effective stress on the horizontal plane and can be obtained from simple shear or triaxial shear tests (equations (2.22) and (2.23), respectively)

$$K_\alpha = \frac{CRR_\alpha}{CRR_{\alpha=0}}$$
(2.21)

$$\alpha = \frac{\tau_{st}}{\sigma'_{vc}}$$
(2.22)

$$\alpha = \frac{\sigma'_{1c} - \sigma'_{3c}}{\sigma'_{1c} + \sigma'_{3c}}$$
(2.23)

K_α depends on relative density and confining pressure and can decrease or increase depending on these conditions. Besides, the failure criteria to obtain CRR and the laboratory testing device also influence this parameter. Seed and Harder (1990) collected a wide variety of laboratory tests and developed a range of K_α depending on α and relative density. Later, Harder and Boulanger (1997) re-examined those values and recommended the relationships between K_α and α of Figure 2.22. However, Youd et al. (2001) did not recommend the use of this factor, as there is a lack of convergence and consistency in the existing data and more research is needed.
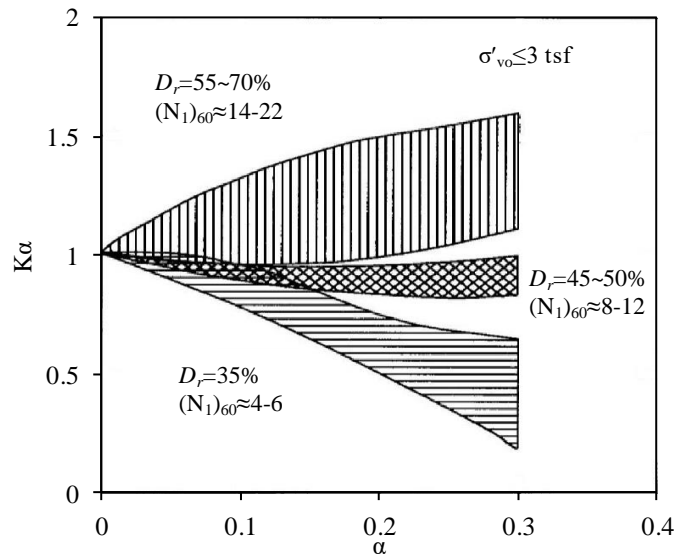
Figure 2.22 – Recommended relationships between K_α and α (Harder and Boulanger, 1997)

Since then, Boulanger (2003b) applied the critical state soil mechanics framework and explained the effects of relative density and effective stress on K_α, using a relative state parameter, ξ_R (Figure 2.23). Although there is no consensus on recommended K_α values, the proposal from Boulanger (2003b) is the most commonly used in geotechnical practice (NASEM, 2016).
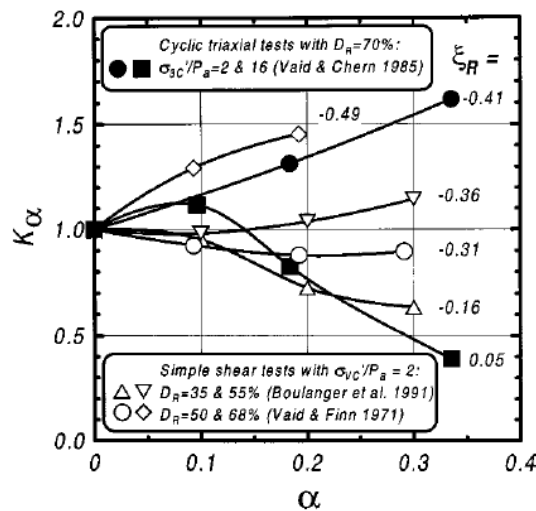
Figure 2.23 – Effect of ξ_R on K_α (Boulanger, 2003b)

2.3.2.4. Consistency of adjustment factors

The adjustment factors explored above are used in the normalisation of the cyclic resistance ratio and/or cyclic stress ratio, to account for the earthquake magnitude, overburden stress, and initial static shear stress. In the majority of methods available, these factors, as well as the shear stress reduction coefficient, r_d, were empirically determined from CSR case histories and the correspondent in situ test parameters. Therefore, the CRR curves obtained from different methods are directly dependent on the adjustment factors calculation, as they were developed based on the liquefaction triggering method considered.

For this reason, to correctly use a CRR relationship in geotechnical practice, care must be taken in the selection of the adjustment factors. According to the methodology selected to perform the liquefaction analysis, the corresponding adjustment factors should be employed and the formulas should not be mixed, to guarantee the coherence and consistency of the analysis.

Table 2.2 presents the adjustment factors used in the methods from Robertson (2009), an update from Robertson and Wride (1998), Moss et al. (2006), and Boulanger and Idriss (2014), as these were the frameworks explored in this work. The formulation used to calculate r_d are also included in the Table. On all these methods, K_α is considered 1, as its value is usually small for nearly level ground conditions and the case history databases are mainly composed of level or nearly level ground sites.

Table 2.2 – Adjustment factors for each method

Robertson (2009)	$r_d = 1.0 - 0.00765z \; for \; z < 9.15m$
	$r_d = 1.174 - 0.0267z \; for \; 9.15m < z < 23m$
	$MSF = \dfrac{10^{2.24}}{M_w{}^{2.56}}$
	$K_\sigma = 1$

Moss et al. (2006)	$r_d = \dfrac{\left[1 + \dfrac{-9.147 \; - \; 4.173 \; \cdot \; a_{max} \; + \; 0.652 \; \cdot \; M_w}{10.567 \; + \; 0.089 \; \cdot \; e^{0.089 \cdot (-d \cdot 3.28 - 7.760 \cdot a_{max} + 78.576)}}\right]}{\left[1 + \dfrac{-9.147 \; - \; 4.173 \; \cdot \; a_{max} \; + \; 0.652 \; \cdot \; M_w}{10.567 \; + \; 0.089 \; \cdot \; e^{0.089 \cdot (-7.760 \cdot a_{max} + 78.576)}}\right]}$
	$DWF_M = 17.84 \cdot M_w{}^{-1.43}$
	$K_\sigma = 1$

Boulanger and Idriss (2014)	$r_d = \exp[\alpha(z) + \beta(z).M]$
	$\alpha(z) = -1.012 - 1.126 \sin\left(\dfrac{z}{11.73} + 5.133\right)$
	$\beta(z) = 0.106 + 0.118\sin\left(\dfrac{z}{11.28} + 5.142\right)$
	$MSF = 1 + (MSF_{max} - 1)\left(8.64 \exp\left(\dfrac{-M}{4}\right) - 1.325\right)$
	$MSF_{max} = 1.09 + \left(\dfrac{q_{c1Ncs}}{180}\right)^3 \leq 2.2 \; or \; MSF_{max} = 1.09 + \left(\dfrac{(N_1)_{60cs}}{31.5}\right)^2 \leq 2.2$
	$K_\sigma = 1 - C_\sigma \ln\left(\dfrac{\sigma'_v}{p_a}\right) \leq 1.1$
	$C_\sigma = \dfrac{1}{37.3 - 8.27(q_{c1Ncs})^{0.264}} \leq 0.3 \quad or \quad C_\sigma = \dfrac{1}{18.9 - 2.55\sqrt{(N_1)_{60cs}}} \leq 0.3$

2.3.3. LIQUEFACTION POTENTIAL INDEX

The Liquefaction Potential Index (LPI) was originally proposed by Iwasaki et al. (1978a, 1982) to characterise the liquefaction potential damage. Its calculation is based on the factor of safety against liquefaction and, hence, varies depending on the method used to calculate FS$_{liq}$. It considers the first 20 m below ground surface and can be obtained using equation (2.24) where F = 1 - FS$_{liq}$ for FS$_{liq} \leq 1$, F = 0 for FS$_{liq} > 1$ and w(z) = 10 - 0.5z for $z \leq$ 20m.

$$LPI = \int_0^{20\,m} F \times w(z)\, dz \qquad (2.24)$$

The LPI admits that the severity of the liquefaction manifestation is proportional to the thickness of the liquefied layers, the proximity of the liquefied layers to the surface and depends on the safety factor against liquefaction in soils with $FS_{liq} < 1$. This factor varies between 0, for a local without liquefaction potential ($FS_{liq} > 1$ in all layers until 20 m depth), and 100 when FS_{liq} is 0 for all layers in the uppermost 20 m.

Iwasaki et al. (1978a, 1982) defined that liquefaction potential is very high at sites where LPI > 15 and is low where LPI < 5. Several researchers have proposed different intervals based on different testing sites (Toprak and Holzer, 2003; Lee et al., 2003, Papathanassiou, 2008; Sonmez, 2003). Maurer et al. (2014) analysed cone penetration test soundings and field observations following the Darfield and Christchurch earthquakes in New Zealand and concluded that the Iwasaki criterion is more applicable to assess the damage potential than the occurrence of liquefaction, is less effective for predicting marginal manifestations of liquefaction and is not appropriate for evaluation of lateral spreading potential.

2.3.4. LIQUEFACTION SEVERITY NUMBER

The Liquefaction Severity Number (LSN) was developed by Tonkin and Taylor (2013) and represents the effects of shallow liquefaction damage on residential land and foundations. This parameter considers the volumetric densification strain within soil layers to determine the severity of liquefaction land damage likely at the ground surface. The hyperbolic function (1/z) gives more weight to liquefaction at shallow depths. It considers all layers with $FS_{liq} < 2$ and the formulation is presented in the following equation, where ε_v is the calculated post-earthquake volumetric strain and z is the depth of the layer of interest.

Table 2.3 presents the expected liquefaction expression and effects on the ground surface according to the LSN value.

$$LSN = 1000 \int \frac{\varepsilon_v}{z}\, dz \qquad (2.25)$$

Table 2.3 – Observed land effect according to LSN (Tonkin and Taylor, 2013)

LSN range	Typical performance
0 – 10	Little to no expression of liquefaction, minor effects
10 – 20	Minor expression of liquefaction, some sand boils
20 – 30	Moderate expression of liquefaction, with sand boils and some structural damage
30 – 40	Moderate to severe expression of liquefaction, settlement can cause structural damage
40 – 50	Major expression of liquefaction, undulations and damage to the ground surface, severe total and differential settlement of structures
> 50	Severe damage, extensive evidence of liquefaction at the surface, severe total and differential settlements affecting structures, damage to services

2.3.4.1. Determination of volumetric strain following liquefaction

Based on experimental data from Nagase and Ishihara (1988), Ishihara and Yoshimine (1992) proposed a methodology for predicting post liquefaction volume change of clean sands, depending on the factor of safety against liquefaction, the maximum single amplitude of shear strain and the volumetric strain due to consolidation following liquefaction. Years later, Yoshimine et al. (2006) plotted the experiment from Nagase and Ishihara (1988) on the graphs from Ishihara and Yoshimine (1992) presented in Figure 2.24.
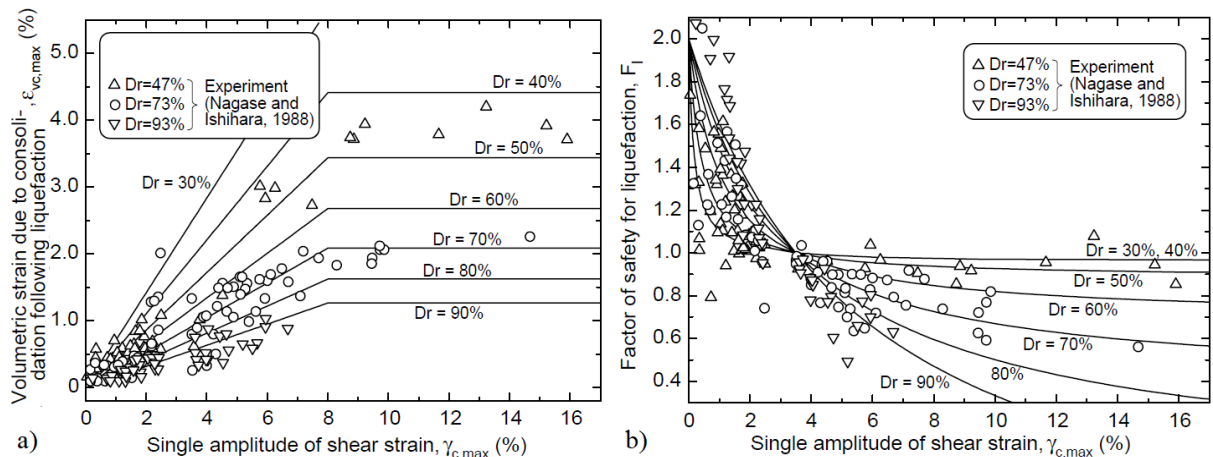
Figure 2.24 – a) Relation between reconsolidation volumetric strain and maximum shear strain; b) Relation between the factor of safety and maximum shear strain (Yoshimine et al., 2006)

The authors proposed mathematical functions to approximate the relations between the volumetric strain due to consolidation following liquefaction and single amplitude of shear strain ($\varepsilon_v - \gamma_{max}$) and between the factor of safety against liquefaction and maximum shear strain (FS$_{liq} - \gamma_{max}$). These functions are presented in equations (2.26) to (2.28).

$$\varepsilon_v = 1.5 \exp(-2.5D_R) \min(0.08, \gamma_{max}) \tag{2.26}$$

$$\gamma_{max} = 0 \ \text{if} \ FS_{liq} \geq 2$$

$$\gamma_{max} = \min\left(\gamma_{lim}, 0.035(2 - FS_{liq})\left(\frac{1 - FS_\alpha}{FS_{liq} - FS_\alpha}\right)\right) \ \text{if} \ 2 > FS_{liq} > F_\alpha \tag{2.27}$$

$$\gamma_{max} = \gamma_{lim} \ \text{if} \ FS_{liq} \leq F_\alpha$$

$$F_\alpha = 0.032 + 4.7D_R - 6.0(D_R)^2 \tag{2.28}$$

The limiting shear strain (γ_{lim}) can be expressed as a function of D_R, and approximated by:

$$\gamma_{lim} = 1.859(1.1 - D_R)^3 \geq 0 \tag{2.29}$$

The calculation procedure above allows the determination of the volumetric strain following liquefaction for each layer considered in the calculation of LSN. Moreover, the combination of the equations provides the relationship between the factor of safety against liquefaction and the volumetric strains following liquefaction (Figure 2.25), which is currently used for estimating liquefaction induced ground settlements (Zhang et al., 2002).
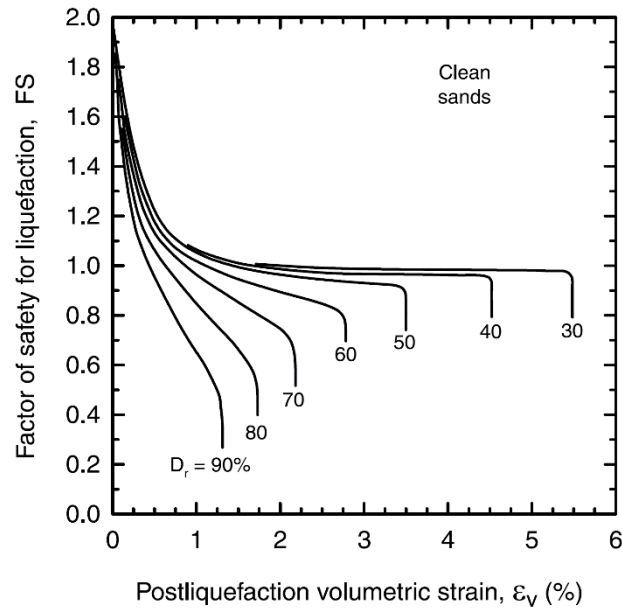
Figure 2.25 – Estimation of post-liquefaction volumetric strain of clean sands (Zhang et al., 2002)

2.4. Evaluation of Liquefaction from Empirical Criteria

Before performing more costly and time-consuming tests, such as field and/or laboratory tests, it is interesting to evaluate the liquefaction susceptibility of a site based on empirical criteria. It is clear that purely empirical criteria are not enough to define liquefaction susceptibility, however, they can provide a preliminary assessment based on the location and site conditions. In this section, emphasis to the historical, geologic, and compositional criteria is given.

The historical criteria are based on past experience and collected databases. Post-earthquake field investigations can produce very important information about the liquefaction susceptibility of some locations. The study of case histories helps to identify sites where liquefaction occurred and, if the ground conditions remain unchanged, where it can happen again.

The geologic criteria are based on the depositional and hydrological environments, and age of the soil deposit. Among the geologic factors affecting liquefaction susceptibility are the grain size distribution, the drainage conditions and the groundwater depth. Saturated soil deposits in a loose state (fluvial, colluvial and aeolian) show high liquefaction susceptibility (Kramer, 1996). On the other hand, more recent soils from the Holocene age are more prone to liquefaction than older soils from Pleistocene age. As liquefaction occurs in saturated soils, the position of the groundwater level influences liquefaction susceptibility, in a way that liquefaction is more prone to occur in sites where the groundwater is closer to the ground surface.

Another factor that influences liquefaction susceptibility is the soil composition, which refers to particle size, shape and gradation of the soil. The composition of soil has an impact on its volume change behaviour and consequently on the development of excess pore pressure required for liquefaction.

Tsuchida (1970) collected grain size distribution curves of both liquefiable and non-liquefiable soils of various case history earthquakes and proposed the grain size boundaries for most liquefiable and potentially liquefiable soils presented in Figure 2.26. It is noticeable that soils with high fines content, such as clays or fine silts, are less susceptible to liquefy, due to the difficulty of particle rearrangement prevented by the high plasticity of these soils. Coarse sands and gravels are also less susceptible as the space between the particles allows the dissipation of pore water pressure. However, more recent earthquakes such as the 1999 Kocaeli earthquake in Turkey and the 2011 Tohoku earthquake in Japan induced liquefaction in sands with considerable non/low plastic fines and the 1983 Borah Peak earthquake in the USA and the 1995 Kobe earthquake in Japan incurred liquefaction in well-graded gravelly soils (Kokusho, 2017). These examples highlight the importance of considering other parameters, as grain size alone is not enough to assess liquefaction susceptibility.
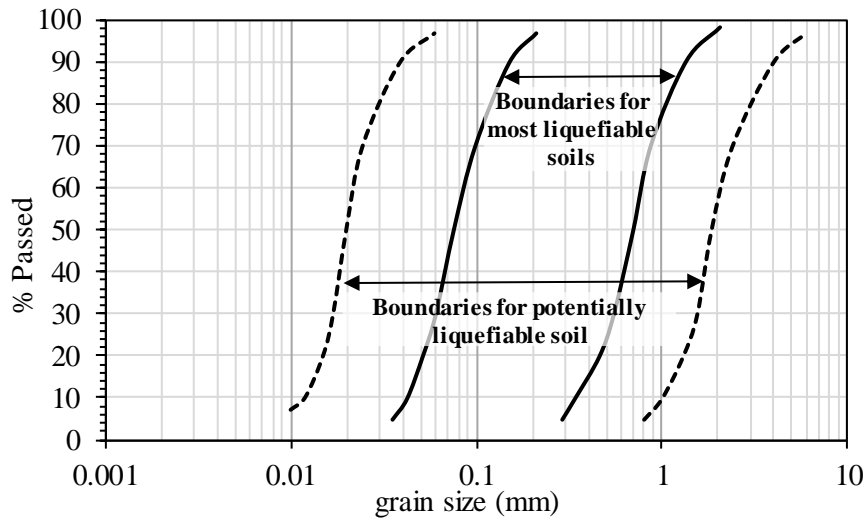
Figure 2.26 – Boundaries for liquefaction susceptibility according to the grain size distribution (adapted from Tsuchida, 1970)

A few years later, Wang (1979) suggested that fine-grained soils can be susceptible to liquefaction if they satisfy certain criteria, known as the Chinese Criteria. Later, Seed and Idriss (1982) adapted these criteria and created the "Modified Chinese Criteria" that defines a soil as susceptible to liquefy if its composition meets the following requirements:

Fraction finer than 0.005 mm ≤ 15 %;

Liquid Limit, LL ≤ 35 %;

Natural water content ≥ 0.9LL.

More recently, Seed et al. (2003) introduced a substitute for these criteria, considering the liquid limit, plasticity index and water content (Figure 2.27). Those criteria are applicable for soils with fines content higher or equal to 20% and plasticity index higher than 12%, or for FC higher or equal to 35% and PI lower than 12%. The chart is divided into three zones that represent the cyclic liquefaction susceptibility: a soil in Zone A is potentially liquefiable if the water content (*w*) is higher than 0.8LL, a soil in Zone B may be susceptible to liquefaction if *w* is higher than 0.85LL, and a soil in Zone C is not susceptible to cyclic liquefaction.
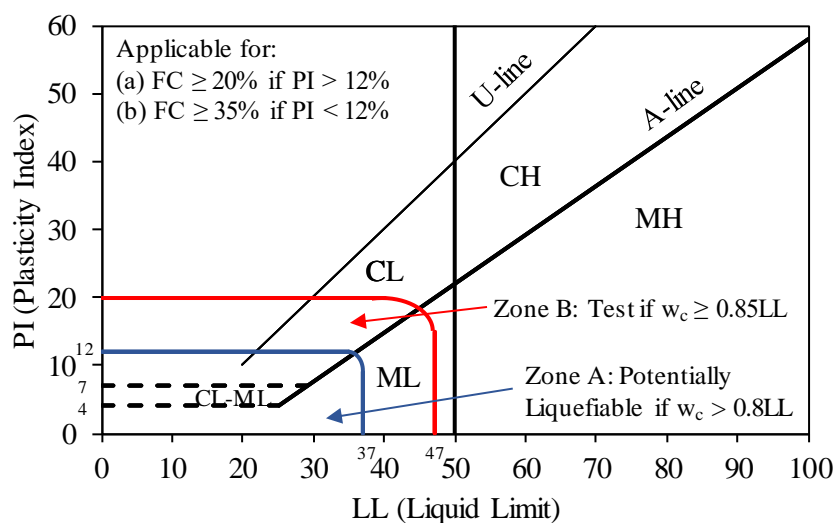
Figure 2.27 – Recommendation Regarding Assessment of "Liquefiable" Soil Types (Seed et al., 2003)

In addition, Bray and Sancio (2006) realised that some fine-grained soils that liquefied during recent earthquakes did not meet the Chinese Criteria. The authors declared that the plasticity index (PI) is a better indicator of liquefaction susceptibility. Young, non-plastic silts and clayey silts (PI < 12) with high water content to liquid limit ratios (w/LL > 0.85) are susceptible to liquefy, and clayey silts and silty clays with 12 < PI < 18 and (w/LL > 0.80) can also undergo liquefaction. The authors concluded that other factors affect liquefaction susceptibility, such as mineralogy, void ratio, overconsolidation or age.

On the other hand, Boulanger and Idriss (2006) proposed a criterion based on the plasticity index. These criteria separate soils according to a sand-like or clay-like behaviour and recommend PI = 7 as the boundary between the two behaviours. They consider that soils that exhibit sand-like behaviour (PI < 7) are susceptible to liquefaction, while soils that exhibit clay-like behaviour (PI ≥ 7), although being susceptible to some strength loss, will not experience cyclic liquefaction with total stiffness and strength loss.

2.5. EVALUATION OF LIQUEFACTION FROM IN SITU TESTS

The liquefaction susceptibility of a soil can be determined by field or laboratory-based methods. As laboratory tests involve either the collection of high-quality samples, which requires expensive and very complex procedures, or the preparation of reconstituted specimens, which can be less representative of the natural soil conditions, in situ tests are commonly preferred by geotechnical engineers. In situ testing

is a simpler, effective and more economical procedure, and is supported by the accumulated past case history experiences.

The liquefaction hazard assessment based on field tests began with the "Simplified Procedure" developed by Seed and Idriss (1971), which correlated the cyclic stress ratio with the blow counts from the standard penetration test (SPT), and is still the most accepted and widely used framework.

Over the years, the original "Simplified Procedure" was refined and adapted to include other in situ test results, such as piezocone penetration test (CPTu), flat dilatometer test (DMT) or Becker penetration test (BPT). More recently, the use of shear wave velocities to assess liquefaction resistance has gained relevance, as V_S is a basic mechanical property of soils related to small-strain shear modulus (G_{max}), and the in situ V_S measurements can be directly compared with laboratory measurements for sample quality evaluation (Andrus and Stokoe, 2000).

The development of field-based liquefaction triggering procedures has been the object of study of many researchers and different methodologies have been proposed to estimate the cyclic resistance of soil. Therefore, the liquefaction assessment procedures available are based on different quantity and quality case histories and are constantly being improved with the implementation of new data. Each methodology requires a set of parameters obtained by empirical correlations that vary according to the selected method. This section presents a summarised state of the art of the methods used in the present research work, for estimating the cyclic resistance and consequently the factor of safety against liquefaction, based on the results of standard penetration (SPT), piezocone penetration (CPTu), and flat dilatometer (DMT) tests, as well as shear wave velocity measurements (V_S).

2.5.1. METHODS BASED ON SPT

As stated above, the "Simplified Procedure" to assess liquefaction susceptibility was first developed based on SPT blow counts (Seed and Idriss, 1971). Since then, several authors have proposed correlations to predict CRR from SPT blow count (Youd et al., 2001; Cetin et al., 2004; Idriss and Boulanger, 2008). These proposals come from the evaluation of different case histories and the use of different adjustment factors. Thus, the direct comparison of the CRR values for a certain blow count can be misleading, as it depends on the methodologies used and the adjustment factors considered in the evaluation of each case. One thing the SPT-based CRR correlations have in common is the use of $(N_1)_{60}$, the SPT blow count normalised to an overburden pressure of 100 kPa and hammer energy of 60 %.

The normalisation is performed with parameters that account for: the energy transmitted to the rod train (C_E), the rod train length (C_R), the borehole diameter (C_D), the use of split spoons with room for liners

but with the liners absent (C_S), and the level of effective overburden stress depending on the depth of the test (C_N). The value of the normalised result is given by equation (2.30).

$$(N_1)_{60} = C_E C_R C_D C_S C_N N \qquad (2.30)$$

In the present work, the correction factors applied were based on Idriss and Boulanger (2010). The value of C_N was obtained through an iterative process using equations in (2.31), where σ'_{v0} is the effective overburden pressure and the exponent m is related to $(N_1)_{60cs}$.

$$C_N = \left(\frac{p_a}{\sigma'_{v0}}\right)^m \le 1.7$$

$$m = 0.784 - 0.0768\sqrt{(N_1)_{60cs}} \qquad (2.31)$$

Over the years, the initial CRR−$(N_1)_{60}$ relation proposed by Seed and Idriss (1982) for sand suffered minor adjustments. However, in the report from the 1996 NCEER and 1998 NCEER/NSF workshops (Youd et al., 2001), a personal communication from Rauch (1998) recommended equation (2.32) as the approximate base curve to predict CRR for clean sands. For $(N_1)_{60} \ge 30$, clean granular soils are considered too dense and categorised as non-liquefiable.

$$CRR_{7.5} = \frac{1}{34 - (N_1)_{60}} + \frac{(N_1)_{60}}{135} + \frac{50}{[10 \cdot (N_1)_{60} + 45]^2} - \frac{1}{200} \qquad (2.32)$$

More recently, incorporating an updated case history database compiled by Cetin et al. (2000), Idriss and Boulanger (2004, 2008) developed a correlation between the cyclic resistance ratio and the equivalent clean sand $(N_1)_{60cs}$ value for cohesionless soils (equation (2.33)). As shown in Figure 2.28, the recommended curve agrees well with the proposal from the NCEER/NSF workshop.

$$CRR_{7.5} = \exp\left[\frac{(N_1)_{60cs}}{14.1} + \left(\frac{(N_1)_{60cs}}{126}\right)^2 - \left(\frac{(N_1)_{60cs}}{23.6}\right)^3 + \left(\frac{(N_1)_{60cs}}{25.4}\right)^4 - 2.8\right] \qquad (2.33)$$
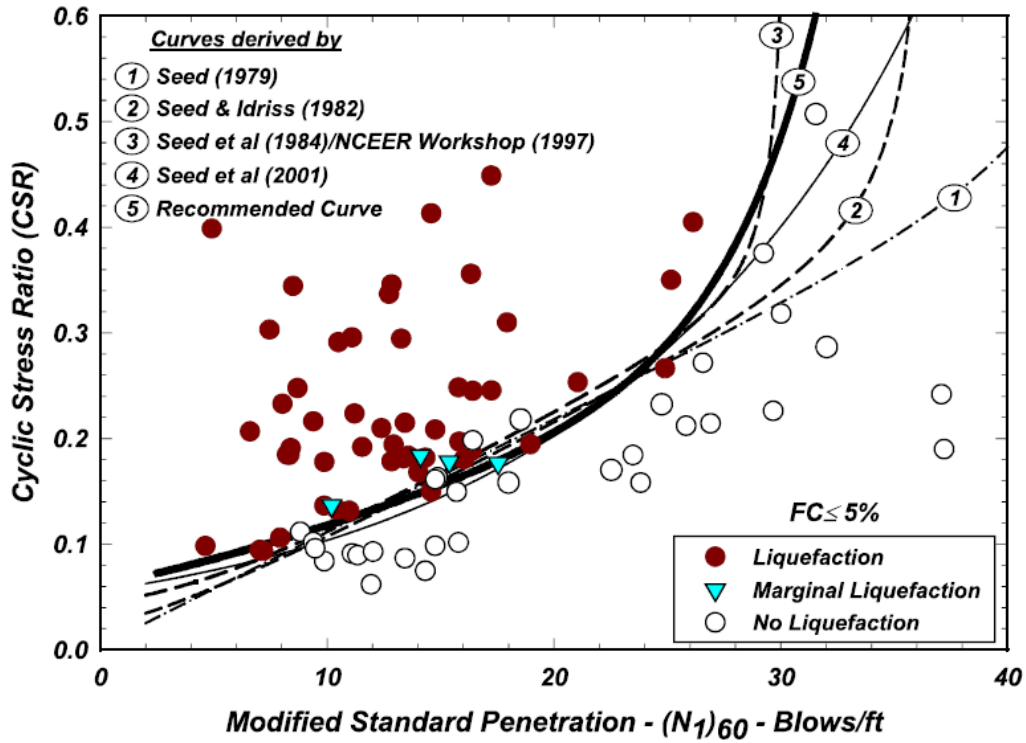
Figure 2.28 – Curves relating CRR to $(N_1)_{60}$ for clean sands with M = 7.5 and σ'_v = 1 atm and recommended curve by Idriss and Boulanger (2004)

The proposal presented above was developed for clean sands, soils with fines content lower than 5%. Therefore, an adjustment factor was proposed to account for the influence of fines content in the boundary curves (Idriss and Boulanger, 2008). The SPT penetration resistance is adjusted to equivalent clean sand resistance according to the following expressions:

$$(N_1)_{60cs} = (N_1)_{60} + \Delta(N_1)_{60} \tag{2.34}$$

$$\Delta(N_1)_{60} = \exp(1.63 + \frac{9.7}{FC + 0.01} - \left(\frac{15.7}{FC + 0.01}\right)^2) \tag{2.35}$$

The use of these expressions requires knowledge about the accurate fines content of each soil layer. Due to the difficulty in obtaining the exact fines content of each layer, habitually it is estimated based on the type of soil found, as will be explained later. Additionally, the plasticity of the fines is also a key parameter affecting the cyclic behaviour of soils. Boulanger and Idriss (2008) stated that the above SPT-based procedures are only applicable to soils with fines with plasticity index under 7, which means non-plastic to very low plasticity fines.

It is also important to state that the quality of the site characterisation is decisive for the accurate assessment of liquefaction susceptibility. The fact that SPT tests are performed every 1 m (in the present work) can produce misleading $(N_1)_{60}$ values and might miss critical thin layers.

2.5.2. METHODS BASED ON CPTu

The CPT has become more popular and common to predict CRR because it is a continuous, reliable test and the databases are increasing in number and quality of the information. Over the years, several authors have proposed correlations between CRR and CPT results, using databases from a variety of case histories with CPT measurements (Ishihara, 1993; Robertson and Wride, 1998; Moss et al., 2006; Idriss and Boulanger, 2008). In this section, the general frameworks of three methods, namely Robertson (2009), Moss et al. (2006) and Boulanger and Idriss (2014), are summarised and discussed, as these are the methodologies used in the present work.

One of the first "steps" in the liquefaction assessment procedure based on CPT is to obtain the soil behaviour type index for each layer (Robertson, 1990). The Robertson (1990) charts (Figure 2.29) were the base of soil classification by CPTu results, stating that soils are divided into 9 types: 1 – sensitive, fine grained; 2 – organic soils: peats; 3 – clays: clay to silt clay; 4 – silt mixtures: clayey silt to silt clay; 5 – sand mixtures: silty sand to sand silty; 6 – sands: clean sands to silty sands; 7 – gravelly sand to sand; 8 – very stiff sand to clayey sand; 9 – very stiff, fine grained. These charts have been adapted to various characterising parameters, allowing an in depth mechanical and geotechnical characterisation of soil profiles. Jefferies and Davies (1993) proposed that the soil behaviour type boundaries can be defined as concentric circles, with a radius identified as the soil behaviour type index, I_c (represented in Figure 2.29). Thereby, soil behaviour type is given in terms of I_c: $I_c < 1.31$ corresponds to gravel; $1.31 \leq I_c < 2.05$ is for sand; $2.05 \leq I_c < 2.60$ corresponds to silty sand to sandy silt; $2.60 \leq I_c < 2.95$ is for silty clay to clayey silt and $I_c \geq 2.95$ refers to clay (Robertson and Wride, 1998).
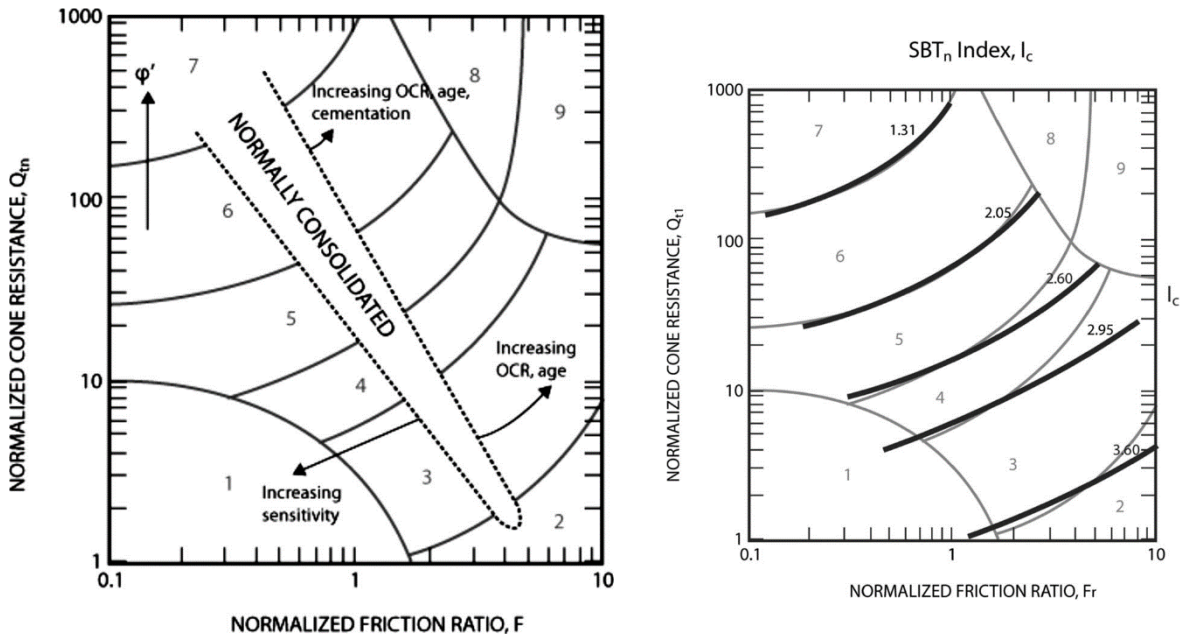
Figure 2.29 – Normalised CPT Soil Behaviour Type charts (Robertson, 1990, 2009)

The soil behaviour type index, I_c, is obtained through an iterative process that relates the cone resistance, sleeve friction and vertical stress normalisation. The normalised cone resistance and normalised friction ratio are calculated using equations (2.36) and (2.37) respectively, where q_c is the cone resistance, σ'_{v0} is the initial effective vertical stress, σ_{v0} is the initial total vertical stress and f_s is the sleeve friction stress.

$$Q_{tn} = \left(\frac{q_c - \sigma_{v0}}{p_a}\right) \times \left(\frac{p_a}{\sigma'_{v0}}\right)^n \qquad (2.36)$$

$$F_r = \left(\frac{f_s}{q_c - \sigma_{v0}}\right) \times 100\% \qquad (2.37)$$

Over the years, the stress exponent has been discussed and the most recent proposals (Robertson, 2009; Robertson, 2016), based on the critical state soil mechanics framework, suggested that *n* varies with I_c and the effective overburden stress using equation (2.38). The soil behaviour type index is defined by equation (2.39).

$$n = 0.381 \times I_c + 0.05 \times \left(\frac{\sigma'_{v0}}{p_a}\right) - 0.15 \qquad (2.38)$$

$$I_c = [(3.47 - \log Q_{tn})^2 + (\log F_r + 1.22)^2]^{0.5} \qquad (2.39)$$

Similarly to the SPT, CPT−based curves that separate liquefiable from non-liquefiable regions are defined by a CRR expression, related to the normalised cone resistance. As mentioned before, the CRR can be obtained using different methodologies.

Robertson and Wride (1998) suggested a relationship between the normalised cone resistance for clean sands with the cyclic resistance ratio for an earthquake with 7.5 moment magnitude, depending on the resistance value, later updated by Robertson (2009) to consider the stress exponent in equation (2.38), and recommended by the CPT Guide for Geotechnical Engineering from Robertson and Cabal (2015). The correlations between CPT parameter $Q_{tn,cs}$ and CRR are expressed in equation (2.40) and Figure 2.30 shows the curve plotted with results of liquefiable and non-liquefiable soils.

$$
\begin{aligned}
if\ 50 \leq Q_{tn,cs} \leq 160 \quad & CRR_{7.5} = 93\left[\frac{Q_{tn,cs}}{1000}\right]^3 + 0.08 \\
if\ Q_{tn,cs} < 50 \quad & CRR_{7.5} = 0.833\left[\frac{Q_{tn,cs}}{1000}\right] + 0.05
\end{aligned}
\tag{2.40}
$$
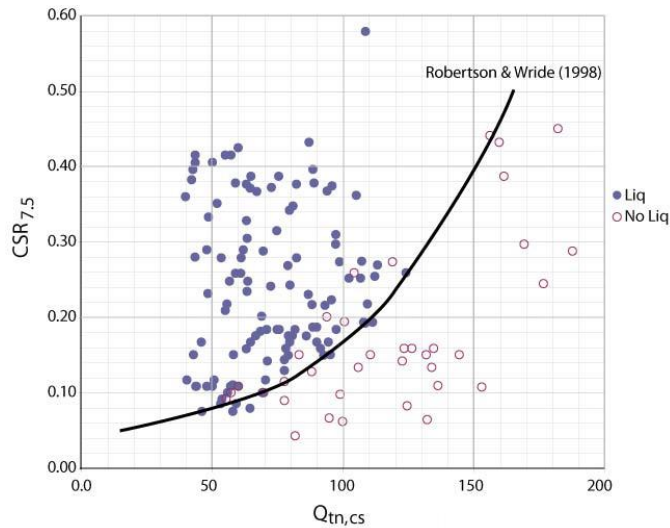
Figure 2.30 – Cyclic resistance ratio (CRR$_{7.5}$) from CPT normalised clean sand equivalent cone resistance (Q$_{tn,cs}$) (updated by Robertson, 2009)

The cyclic resistance curves are determined based on the equivalent clean sand penetration resistance that is influenced by soil type. Robertson and Wride (1998) suggested the use of a normalisation parameter, K_c, function of the soil behaviour type, for estimating $Q_{tn,cs}$, expressed as follows:

$$
Q_{tn,cs} = K_c \times Q_{tn}
\tag{2.41}
$$

$$
\begin{aligned}
&if\ I_c \leq 1.64 \qquad\qquad\qquad K_c = 1.0 \\
&if\ I_c > 1.64 \quad K_c = -0.403I_c{}^4 + 5.581I_c{}^3 - 21.63I_c{}^2 + 33.75I_c - 17.88
\end{aligned}
\tag{2.42}
$$

Moreover, Robertson and Wride (1998) suggested a method to calculate the apparent fines content directly from CPT results, shown in equations (2.43), as I_c increases with increasing apparent fines content and soil plasticity. This correlation is approximate, as many other factors affect the response of the CPT, such as soil plasticity, mineralogy, sensitivity, and stress history.

$$
FC\ (\%) = 0\ if\ I_c < 1.26
$$

$$
FC\ (\%) = 1.75I_c{}^{3.25} - 3.7\ if\ 1.26 \leq I_c \leq 3.5
\tag{2.43}
$$

$$
FC\ (\%) = 100\ if\ I_c > 3.5
$$

On the other hand, Moss et al. (2006) presented a correlation that employs a larger database of high-quality field case histories, using a Bayesian framework to account for all the uncertainties associated with seismic demand and liquefaction resistance. This method is strongly based on the proposals from Cetin (2000) and Cetin et al. (2004), and was developed directly from measured CPT data. Equation (2.44) presents the expression used to calculate CRR, where $q_{c,1,mod}$ is the normalised cone tip resistance (in MPa), R_f is the friction ratio (f_s/q_c, in percent), c is a normalisation exponent, M_w is the moment magnitude, σ'_v is the effective vertical stress and $\Phi^{-1}(P_L)$ is the inverse cumulative normal distribution function. The proposed relationship is probabilistic, however, they suggested the consideration of P_L=15% for deterministic purposes and comparison with other methods.

$$
CRR = \exp\left\{\frac{X}{7.177}\right\}
$$

$$
X = q_{c,1}{}^{1.045} + q_{c,1}(0.110R_f) + (0.001R_f) + c(1 + 0.850R_f) - 0.848\ln M_w - 0.002\ln\sigma'_v - 20.923 \\
+ 1.632\Phi^{-1}(P_L)
\tag{2.44}
$$

Once again, the cone tip resistance is normalised for a given level of overburden stress, using equation (2.45), and following an iterative procedure. The normalisation exponent c depends on the friction ratio and the tip resistance to account for the variability in the response of different soil types and is obtained by equation (2.46).

$$
q_{c,1} = C_q q_c
$$

$$
C_q = \left(\frac{p_a}{\sigma'_v}\right)^c \leq 1.7
\tag{2.45}
$$

$$c = f_1 \left(\frac{R_f}{f_3}\right)^{f_2}$$

$$f_1 = 0.78 q_c^{-0.33}$$

$$f_2 = -(-0.32 q_c^{-0.35} + 0.49)$$ (2.46)

$$f_3 = \text{abs}[\log(10 + q_c]^{1.21}$$

Moss et al. (2006) considered a modification of the normalised cone tip resistance to account for the frictional effects of apparent "fines". According to the authors, the fines adjustment was regressed from the liquefaction database and represents the change in liquefiability correlated to the change in friction ratio, as a function of CSR.

$$q_{c,1,mod} = q_{c,1} + \Delta q_c$$

$$\Delta q_c = (0.38 R_f - 0.19) \ln CSR + (1.46 R_f - 0.73)$$ (2.47)

Figure 2.31 presents the probability curves proposed by Moss et al. (2006) compared with other proposals, including the one from Robertson and Wride (1998) presented above. It is relevant to note that the curve by Robertson and Wride (1998) for clean sand with $K_c = 1.0$ is compatible with a probability of 15% curve, selected for the representation of the deterministic boundary.
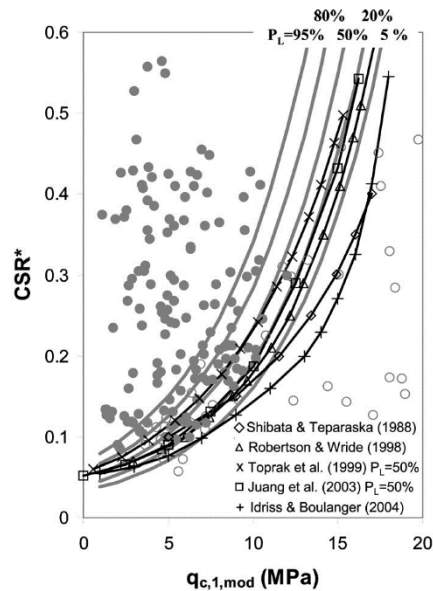
Figure 2.31 – Combination of probability curves by Moss et al. (2006) with other proposals

Alternatively, when realizing that the correlations of liquefaction potential move to the left with the increase in fines content, Idriss and Boulanger (2008) proposed a different approach taking into account the fines content. More recently, Boulanger and Idriss (2014) updated those correlations, in agreement with new adjustment factors and an updated case history database. Figure 2.32 presents the comparison between the two proposals, along with the updated case history database of liquefaction in cohesionless soils. The proposed correlation between $CRR_{7.5}$ and the normalised cone resistance for equivalent clean sand, q_{c1Ncs}, is presented in equation (2.48).
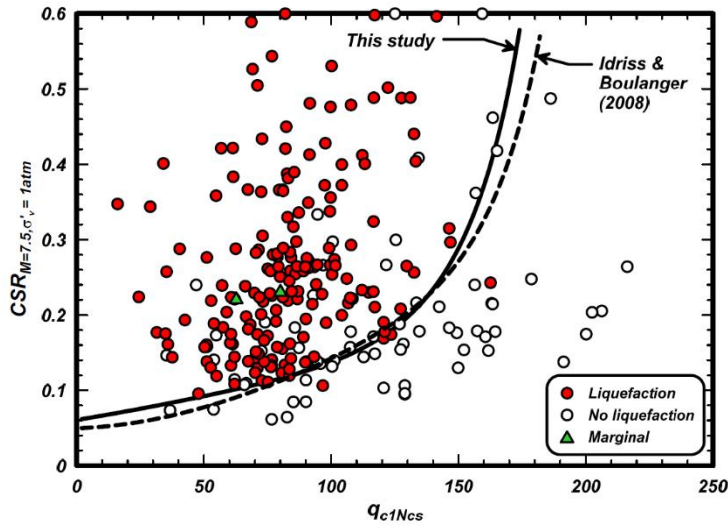
Figure 2.32 – CPT case history database used by Boulanger and Idriss (2014)

$$CRR_{7.5} = \exp\left(\frac{q_{c1Ncs}}{113} + \left(\frac{q_{c1Ncs}}{1000}\right)^2 - \left(\frac{q_{c1Ncs}}{140}\right)^3 + \left(\frac{q_{c1Ncs}}{137}\right)^4 - 2.8\right) \qquad (2.48)$$

To account for the effect of fines (fines content and plasticity) on the CPT-based liquefaction triggering correlations, an equivalent clean sand cone resistance is obtained using the adjustment Δq_{c1N} (equation (2.49)). According to the updated case history database, the new MSF, and an improvement in consistency with empirical q_c/N_{60} ratios, Boulanger and Idriss (2014) changed the adjustment proposed by Idriss and Boulanger (2008) and suggested equation (2.50) for obtaining Δq_{c1N}.

$$q_{c1Ncs} = q_{c1N} + \Delta q_{c1N} \qquad (2.49)$$

$$\Delta q_{c1N} = \left(11.9 + \frac{q_{c1N}}{14.6}\right) \exp\left(1.63 - \frac{9.7}{FC + 2} - \left(\frac{15.7}{FC + 2}\right)^2\right) \qquad (2.50)$$

On the other hand, the cone tip resistance is normalised to account for overburden stress effects. The value of q_{c1N} is obtained from equation (2.51), where the C_N is a factor to account for the overburden stress, p_a is the atmospheric pressure, and q_t is the corrected cone tip resistance. The value of C_N is obtained through equation (2.52), where σ'_{v0} is the effective overburden pressure and the exponent m is related to q_{c1Ncs}.

$$q_{c1N} = C_N \frac{q_t}{p_a} \tag{2.51}$$

$$C_N = \left(\frac{p_a}{\sigma'_{v0}}\right)^m \leq 1.7 \tag{2.52}$$

$$m = 1.338 - 0.249(q_{c1Ncs})^{0.264}$$

Furthermore, Boulanger and Idriss (2014) also developed a probabilistic study for liquefaction potential assessment, based on CPT results. The probability curves for P_L equal to 15%, 50% and 85% are plotted in Figure 2.33 for all the sands studied. The deterministic relation presented above corresponds to a probability of liquefaction of approximately 16%, considering just the model uncertainty, which is compatible with the probability of 15% in the Moss et al. (2006) proposal.
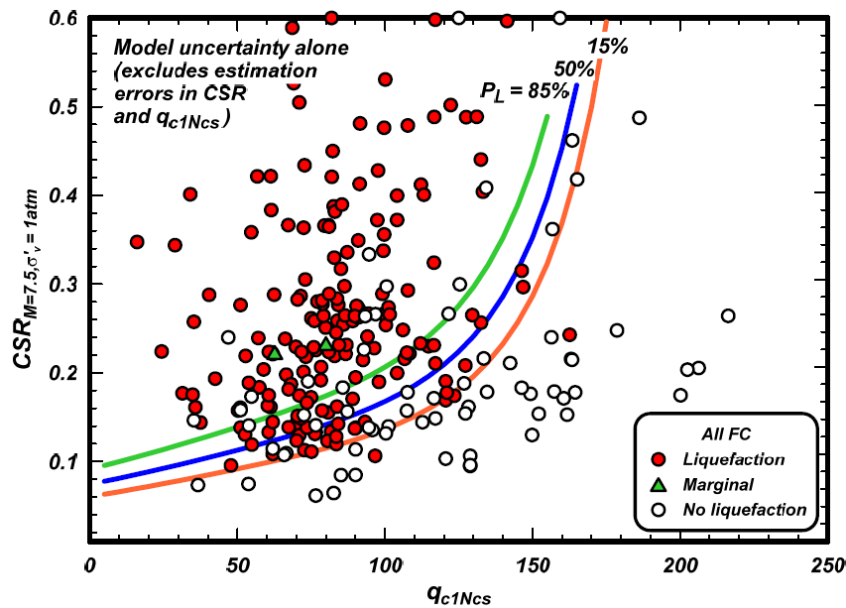
Figure 2.33 – Curves of CRR$_{M=7.5,\sigma'v=1atm}$ versus q$_{c1Ncs}$ for probabilities of liquefaction of 15 %, 50 %, and 85 % for all sands studied (Boulanger and Idriss, 2014)

The three methods presented above allow the determination of the cyclic resistance ratio based on CPT test results. However, the proposals differ, especially in terms of the estimation of the equivalent clean

sand cone resistance and the consideration of different normalisation factors for overburden stress and soil type. Another clear difference between the three methods are the approaches used to estimate the effect of fines (fines content and plasticity). While Robertson and Wride (1998) and Moss et al. (2006) consider a correlation based on the tip resistance and sleeve friction ratio measurements, Boulanger and Idriss (2014) focus on the independent specification of fines characteristics, through the use of measurements of FC from soil samples.

It is very important to maintain the coherence within the method, which means that it is crucial to use the normalisation factors corresponding to the method chosen, and thus avoid mixing different expressions, both on the calculation of CRR and CSR.

2.5.3. METHODS BASED ON DMT

The flat dilatometer test (DMT) allows the measurement of in situ strength and deformation properties of a wide variety of soil types. One of the outputs of this test is the parameter, K_D, which can be used to evaluate liquefaction resistance of soils as it is highly sensitive to stress history, pre-straining, cementation and structure (Marchetti et al., 2008). In the last decades, correlations of K_D with CRR have been developed, such as the ones presented in Figure 2.34.
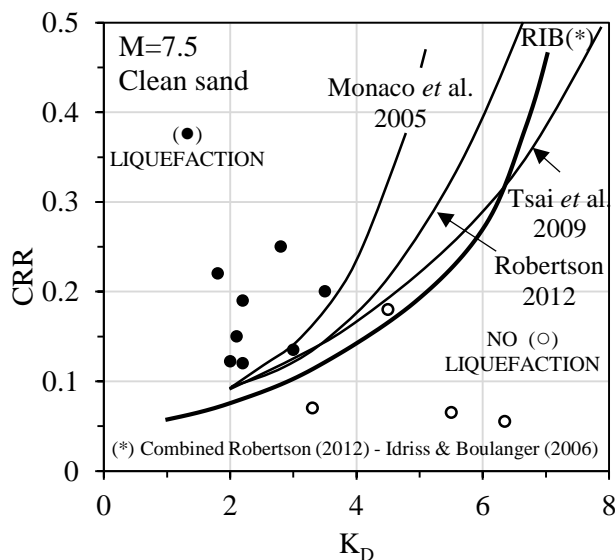
Figure 2.34 – Correlations for estimating CRR from K_D (adapted from Marchetti and Marchetti, 2016)

Marchetti (2016) summarised the most recent advances in the DMT interpretation of the estimation of liquefaction resistance in clean sand. The recommended correlation between CRR and K_D is presented in equation (2.53), which combines the correlation from Idriss and Boulanger (2006) to estimate CRR from Q_{cn} and the interrelationship between Q_{cn} and K_D from Robertson (2012).

$$CRR = \exp\left[\left(\frac{Q_{cn}}{540}\right) + \left(\frac{Q_{cn}}{67}\right)^2 - \left(\frac{Q_{cn}}{80}\right)^3 + \left(\frac{Q_{cn}}{114}\right)^4 - 3\right]$$

(2.53)

$$Q_{cn} = 25K_D$$

Marchetti (2016) presented a method for incorporating the stress history parameter into the liquefaction correlations, by combining CRR-Q_{cn} and CRR-K_D correlations. The proposal is on equation (2.54) and is the geometric average between the CRR estimated by Q_{cn} and CRR obtained with equation (2.53). Figure 2.35 shows the chart for estimating CRR in clean sand based on this method.

$$Average\ CRR = [(CRR\ from\ Q_{cn}) \times (CRR\ from\ K_D)]^{0.5}$$

(2.54)
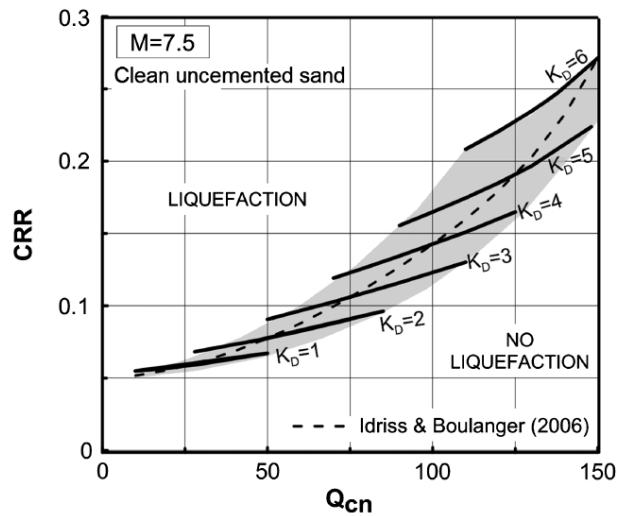
Figure 2.35 – Chart estimating CRR based on Q_{cn} and K_D (Marchetti, 2016)

2.5.4. METHODS BASED ON SEISMIC WAVES VELOCITY MEASUREMENT

Methods based on conventional in situ tests like SPT and CPTu are overall preferred over seismic methods, due to the large and strong database accumulated over the years that supported these methods with confidence. Besides, the resistance parameters (($N_1)_{60}$, q_{c1N}) are plastic strength parameters, which can be correlated to CRR, also a plastic strength parameter, to assess liquefaction potential.

The alternative use of shear wave velocity measurements to assess liquefaction potential is sustained by the fact that V_S and liquefaction resistance are influenced by many of the same factors (Andrus and Stokoe, 2000). However, some concerns have been identified when using V_S for liquefaction resistance evaluation, considering that wave propagation through soil is associated with very small strains of around 10^{-6} to 10^{-5} and the deformations exhibited are purely elastic, while liquefaction is a medium to high strain phenomena associated with failure (Ishihara, 1996). Moreover, the seismic tests do not allow the collection of samples for soil classification, and, depending on the measurement interval, they might not detect thin, low V_S strata (Andrus and Stokoe, 2000). Nonetheless, the use of V_S measurements is favourable in certain situations, such as the penetration of hard to sample soils where SPT and CPT may be unsuitable. Besides, V_S is a basic mechanical soil property that is directly related to the small-strain shear modulus, G_{max}, which is considered a fundamental parameter of dynamic properties of the ground commonly used in numerical analyses.

Nowadays, with the improvement of in situ seismic wave velocity measurement methods, the shear wave velocity (V_S) has been an increasingly used parameter to evaluate the liquefaction resistance of soils. To allow more accurate comparisons of results, it is usual to normalise V_S according to the vertical effective stress, using equation (2.55) (Robertson et al., 1992).

$$V_{S1} = V_S \times \left(\frac{p_a}{\sigma'_{v0}}\right)^{0.25} m/s \tag{2.55}$$

Andrus and Stokoe (2000) proposed a relationship between CRR and V_{S1}, based on 225 case histories of Holocene soils with less than 5% fines, where V_{S1}^* is the maximum limit of V_{S1} for the occurrence of liquefaction and a and b are curve fitting parameters (0.022 and 2.8, respectively). This relationship was updated by Andrus et al. (2004), as given in equation (2.56), which includes two extra factors to account for the effect of ageing on V_{S1} and CRR, K_{a1} and K_{a2}, respectively. These factors take the value of 1.0 for uncemented soils of the Holocene. The value of V_{S1}^* varies between 200 and 215 m/s for soils with fines content between 5% and 35%, according to (2.57).

$$CRR = \left[a\left(\frac{K_{a1}V_{S1}}{100}\right)^2 + b\left(\frac{1}{V_{S1}^* - K_{a1}V_{S1}} - \frac{1}{V_{S1}^*}\right)\right]K_{a2} \tag{2.56}$$

$$V_{S1}^* = 215 \text{ m/s for } FC \leq 5\% \tag{2.57}$$

$$V_{S1}^* = 215 - 0.5(FC - 5) \text{ m/s for } 5\% < FC \leq 35\%$$

$$V_{S1}^* = 200 \text{ m/s for } FC \geq 35\%$$

More recently, Kayen et al. (2013) also presented a relationship of shear wave velocity (V_S) with the occurrence of liquefaction, based on 422 historical cases. Similar to Zhou and Chen (2007), they do not limit the maximum boundary of V_{S1} to 215 m/s, but performed a probabilistic study to determine CRR based on the probability of liquefaction occurrence (P_L). Equations (2.58) and (2.59) present the formulations to calculate P_L and CRR based on V_{S1}.

$$P_L = \Phi \left\{ -\frac{[(0.0073V_{S1})^{2.8011} - 1.946 \ln CSR - 2.6168 \ln M_w - 0.0099 \ln \sigma'_{v0} + 0.0028FC]}{0.4809} \right\} \quad (2.58)$$

$$CRR = \exp \left\{ -\frac{[(0.0073V_{S1})^{2.8011} - 2.6168 \ln M_w - 0.0099 \ln \sigma'_{v0} + 0.0028FC - 0.4809\Phi^{-1}(P_L)]}{1.946} \right\} \quad (2.59)$$

In Figure 2.36, graphs with the relation of CSR and V_{S1} proposed by Andrus and Stokoe (2000), Zhou and Chen (2007), and the new proposal of Kayen et al. (2013) for previous data and data collected by Kayen et al. (2013) are illustrated. Dark circles are cases of liquefaction and open circles are instances where liquefaction did not occur. It is observed that some points where liquefaction occurred are on the right side of the line of Andrus and Stokoe (2000), especially for higher CSR values.
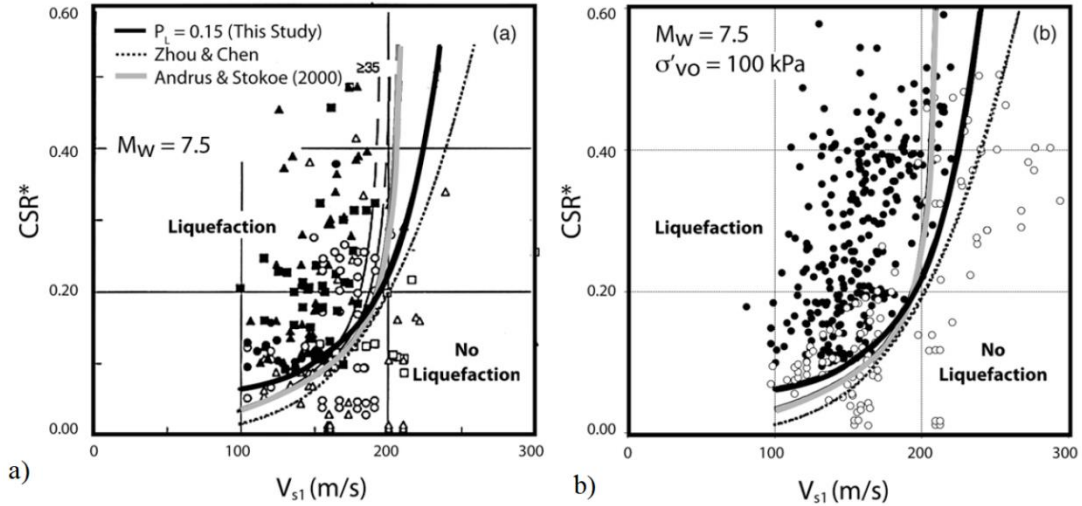
Figure 2.36 – CSR and V_{S1} correlation curves: a) Andrus and Stokoe (2000) data; b) Kayen et al. (2013) data

Kayen et al. (2013) have shown that measurements of V_S have difficulty detecting small differences in the percentage of fines. The occurrence of liquefaction based on V_{S1} is relatively insensitive to the fines content since the test only measures the frictional and modulus components (consistent with previous studies, e.g. Andrus and Stokoe, 2000). Figure 2.37 shows the difference in the adjustment curve for

fines content (FC) of 0 and 35%. The maximum difference between them is about 5 m/s, which is a very small adjustment when it comes to liquefaction evaluation.
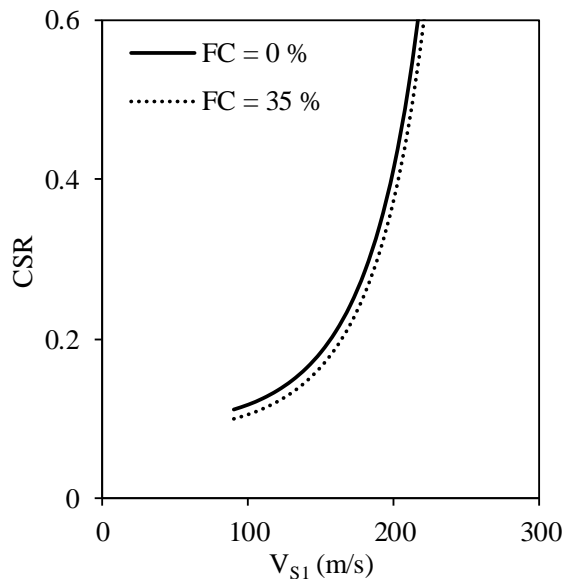
Figure 2.37 – Adjustment curves for FC = 0% and 35%, for P_L = 50%, M_w = 7.5, σ'_{v0} = 1 atm (Kayen et al., 2013)

2.6. EVALUATION OF LIQUEFACTION FROM LABORATORY TESTS

The study of liquefaction in the laboratory was initiated by Seed and Lee (1966) and Lee and Fitton (1969) with tests on saturated sands in undrained triaxial conditions, and by Peacock and Seed (1968) testing saturated sands in undrained cyclic simple shear tests. At in situ conditions, the liquefaction assessment is based on the comparison of the CSR (characterising the seismic action) and the resistance of the soil obtained through laboratory testing.

According to NASEM (2016), there have been few developments in laboratory testing for liquefaction assessment since the 1985 report (NRC, 1985) probably due to the difficulty in collecting high-quality samples (with relatively undisturbed structure) for testing. Nevertheless, laboratory tests are a valuable means to study the influence of numerous parameters, such as fines content or effective overburden pressure in the triggering of liquefaction, to evaluate if a soil is suitable to in situ sampling, and to calibrate numerical models.

Over the years, different laboratory tests were used to study the cyclic behaviour of soils, to better understand how the soils respond to cyclic loading and which factors influence these behaviours and how. The triaxial test is one of the most used tests due to the availability of these apparatuses in most laboratories and the gathered knowledge associated with the procedures and interpretation of the results.

However, the cyclic triaxial test does not allow principal stress rotation, but rather principal stress inversion which is not ideal to study the influence of cyclic loading on soil behaviour.

Alternatively, the cyclic simple shear test imposes shear in the horizontal direction, enabling a more accurate reproduction of the earthquake stress conditions. The specimen is restrained against lateral expansion and the cyclic horizontal stresses are applied to the top or bottom, trying to simulate the shear wave vertical propagation (Kramer, 1996). More recently, the independent control of horizontal and vertical stresses has been developed, improving the quality of this type of tests.

Apart from cyclic triaxial and cyclic simple shear tests, there are other laboratory equipment that allow the investigation of soil behaviour to cyclic loading, namely the hollow cylinder, torsional shear apparatus, and shake tables. The Hollow Cylinder allows the control of the three principal stresses and the definition of multiple stress-paths. However, it requires a difficult specimen preparation procedure, is very complex and not available for most research groups.

Jefferies and Been (2016) distinguished three different cyclic loadings, presented in Figure 2.38, where the major principal direction, σ_1, is considered the initial vertical stress and the angle α measures the orientation of σ_1. The first case (a) corresponds to a cyclic variation of the deviatoric stress, without crossing the $q=0$ axis, where the direction of the principal stress σ_1 never changes (α is always 0°). In the second case (b), the orientation of the principal stresses is fixed, although principal stress flips (jumps) are observed, which means that the vertical and horizontal stresses alternate in being the major principal stress. The deviatoric stress changes between positive and negative and the principal stress direction, α, jumps from 0° to 90°. This corresponds to a cyclic triaxial test with consecutive changes between compression and extension. The third case (c) also includes a shear stress, along with horizontal and vertical stresses. The shear stress varies with time, so σ_1 is not aligned with the vertical direction. The principal stresses directions also vary with time, which means that the principal stresses rotate (α varies cyclically). This is the case of the cyclic simple shear test, and is the closer simulation of the vertical propagation of shear waves from seismic loading.

	(a)	(b)	(c)
At maximum load			
At minimum load			
Stress path			
Principal stress direction			
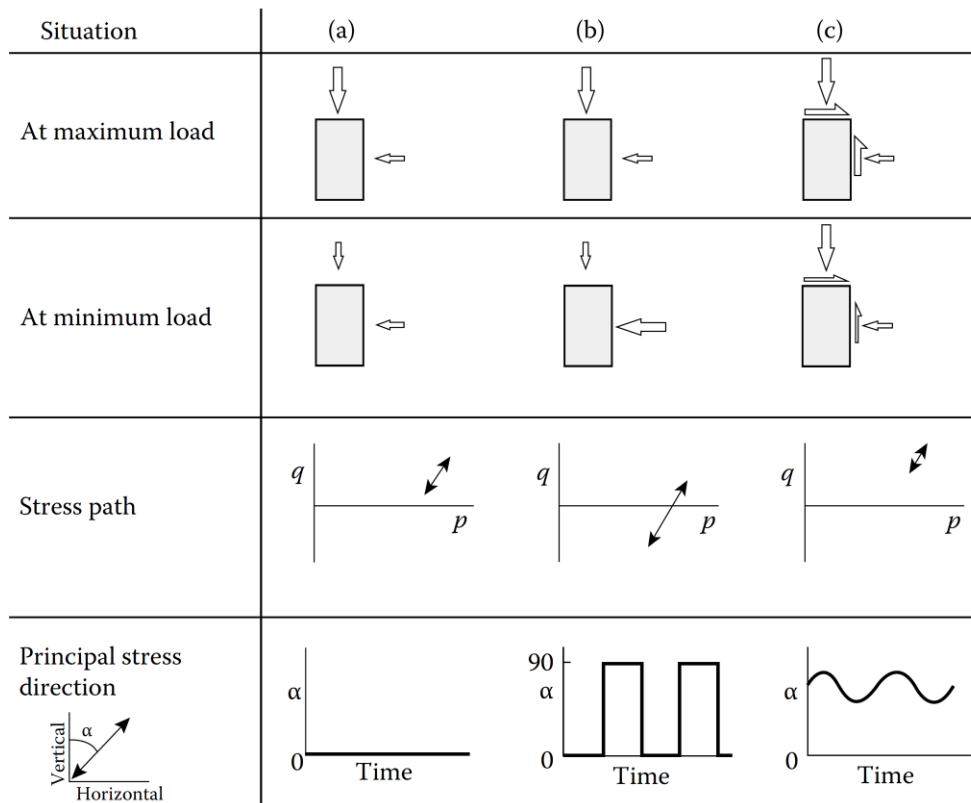
Figure 2.38 – Different forms of cyclic loading (Jefferies and Been, 2016)

2.6.1. LABORATORY SIMULATION OF EARTHQUAKE LOADING ON SOILS

The accurate simulation of field conditions, both in situ state and seismic loading, is essential for the representativeness of the results and its application in design practice and numerical modelling. A representation of a shear stress wave propagating in a single vertical plane is shown in Figure 2.39 (Jefferies et al., 2015). The upward shear stress wave imposes on the element of soil a horizontal shear stress, the vertical total stress remains constant, and the principal stresses rotate. As discussed above, this behaviour is closely simulated by the cyclic simple shear test, which enables a more accurate reproduction of the earthquake stress conditions.
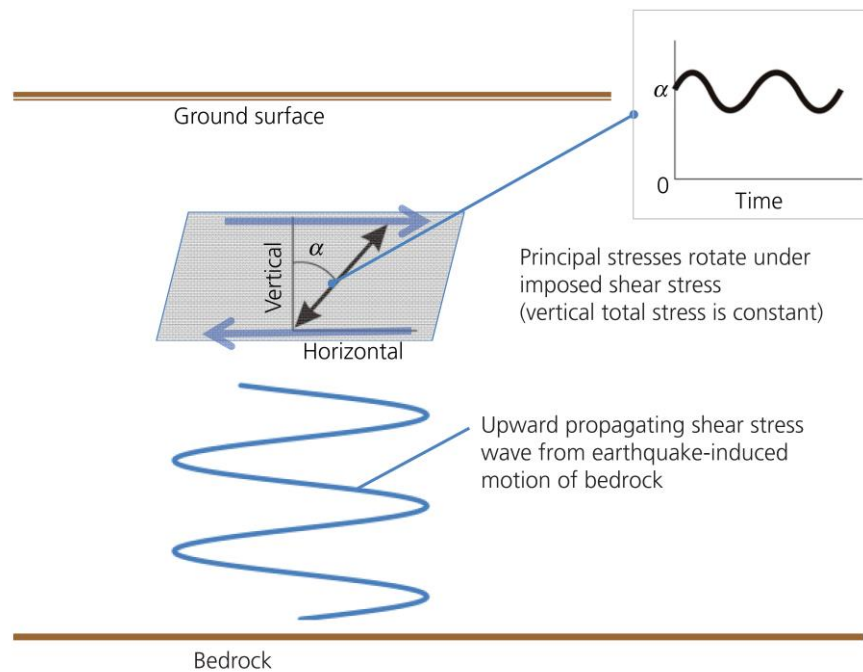
Figure 2.39 – Imposed loading on the soil due to earthquake-induced motion (Jefferies et al., 2015)

However, it is not always possible to simulate the exact field conditions in the laboratory. The triaxial test is the most commonly used for being available in the majority of laboratories. In triaxial conditions, the cyclic loading is imposed by a variation of deviatoric stress, and there is no principal stress rotation. The major principal stress direction varies between 0º and 90º. Therefore, care should be taken when comparing the results from different types of tests, namely triaxial and simple shear tests, with field results. Later in section 2.7.3.3, some considerations about the comparison between field, triaxial, and simple shear conditions are discussed.

Another concern is the selection of the confining pressure to simulate the field conditions in the laboratory, especially in the triaxial test. The cyclic triaxial tests may be performed under anisotropic loading, however the stress rotations induced are not comparable to those that occur in situ. Therefore, isotropic consolidation is the most commonly used confining configuration (Taylor, 2015). Moreover, Cubrinovski (1993) showed that in cyclic torsional tests with initial anisotropic stress conditions, sands tend to approximate an isotropic stress state during cyclic loading. The decision of the appropriate confining pressure for undisturbed specimens is not straightforward. Some authors applied the estimated σ'_v from in situ as the isotropic confining pressure (Yoshimi et al., 1989; Huang et al., 2008), Ishihara et al. (1978) and Taylor (2015) applied confining stresses higher than σ'_v, while Pillai and Stewart (1994) applied p'_0 to triaxial specimens and σ'_v to simple shear tests.

On the other hand, the interpretation of the laboratory test results depends on the identification of liquefaction initiation, which is usually performed based on either pore pressure, shear strength, shear strain/deformation, or energy-based criteria. However, the choice of the criteria is not consensual in the liquefaction study groups. Wu et al. (2004) discussed some of these criteria and emphasised the details of each one. Pore water pressure criterion is widely used and states that soil liquefaction occurs when the excess pore water pressure ratio ($r_u = \Delta u/\sigma'_{3c}$ in triaxial condition and $r_u = \Delta u/\sigma'_{v0}$ in simple shear conditions) equals 1.0, i.e., the pore pressure builds up to equal the initial confining pressure. However, the generation of pore pressure is associated with the type of soil and compaction conditions, so not all soils that liquefy reach a r_u of 1.0. Ishihara (1993) suggested that for silty sands or sandy silts, the value of r_u should be reduced to 0.90 or 0.95 (corresponding to about 5% of double amplitude axial strain in triaxial conditions). Another relevant aspect is the compaction of the specimen. It is understood that in loose sands the generation of high pore pressures results in large shear strains. On the contrary, in denser sands, high pore pressures can be observed but with limited shear strain potential due to their dilatant tendency. Therefore, this criterion should be used together with deformation development information.

The strain/deformation-based criteria are interrelated with the pore pressure generation (Dobry et al., 1982). After analysing many laboratory cyclic triaxial tests, Ishihara (1993) proposed the use of 5% double amplitude axial strain as a criterion to define the occurrence of liquefaction and cyclic softening for clean sands and sands with fines. However, the measurement of shear strain depends on the deformation mode (e.g. triaxial or simple shear) and the strain levels are not consensual, varying between 2 and 10% for different authors (Wu et al., 2004), which has a great influence on the liquefaction definition. In cyclic simple shear, liquefaction is usually defined at 3.75% single amplitude shear strain, which corresponds to the 2.5% single amplitude of axial strain in cyclic triaxial tests (Vaid and Sivathayalan, 1996). The relationship between double amplitude axial strain and double amplitude shear strain is made through the Poisson's ratio as $\varepsilon_{DA} = \gamma_{DA}/(1+\upsilon)$. In undrained conditions, the Poisson's ratio is 0.5 so $\gamma_{DA} = 1.5\varepsilon_{DA}$ (Kokusho, 2017).

2.6.2. CYCLIC RESISTANCE CURVES

Normally, a soils resistance to liquefaction is represented by the cyclic resistance curve/cyclic strength curve, which relates the Cyclic Stress Ratio (CSR) with the number of cycles required for liquefaction to occur (N_{liq}). Depending on the type of test, the CSR is defined according to the cyclic stresses induced in the specimen. For cyclic simple shear tests, CSR is the ratio between the cyclic shear stress and the initial vertical effective stress ($CSR_{ss} = \tau_{cyc}/\sigma'_{v0}$). On the other hand, for cyclic triaxial tests, it is the ratio between the maximum cyclic shear stress and the initial effective confining pressure ($CSR_{tx} = q/2\sigma'_c$)

(Kramer, 1996). The number of cycles required for liquefaction to occur is determined at initial liquefaction that, as mentioned above, can be considered based on stress or strain. The initial liquefaction is considered when pore pressure ratio reaches 1, or when double amplitude shear strain of 5% and 7.5%, in triaxial and simple shear tests, respectively, is achieved (Ishihara, 1993; Vaid and Sivathayalan, 1996).

The CSR-N_{liq} curve is determined based on at least 3 laboratory tests, performed under the same initial state conditions (same relative density and confining pressure), at different CSR. The number of cycles required for liquefaction triggering increases with the decrease of shear stress amplitude, as observed in Figure 2.40.
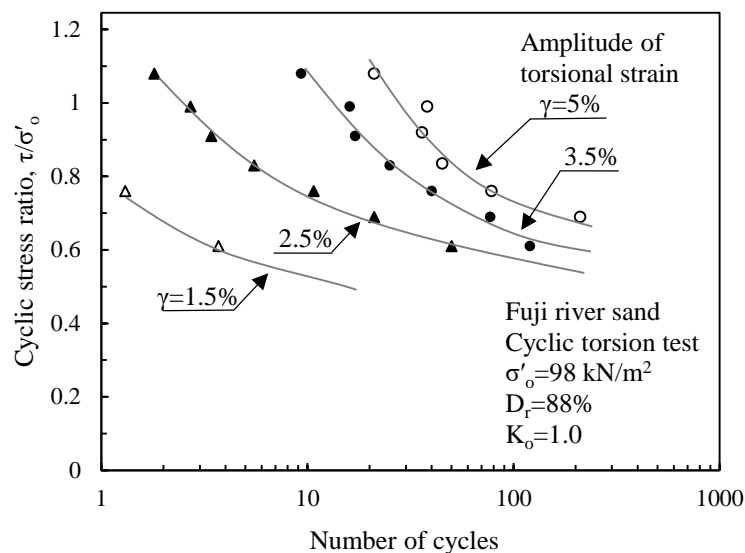
Figure 2.40 – Example of cyclic resistance curves (adapted from Ishihara, 1985)

2.6.3. METHOD BASED ON STATE PARAMETER

The critical state soil mechanics has been increasingly used as a framework for liquefaction analysis, both for static (Carrera et al, 2011; Bedin et al., 2012) and cyclic loading (Qadimi and Coop, 2007; Huang and Chuang, 2011). The most commonly used framework was proposed by Jefferies and Been (2006), based on the state parameter, ψ. Similarly to the liquefaction assessment charts developed for SPT, CPT, DMT and V_S data presented in section 2.5, charts using the state parameter were also developed over the years. Robertson and Wride (1998) used data from Stark and Olson (1995) and Suzuki et al. (1995) to plot CRR-q_{c1N} liquefaction resistance curves, to separate sites where liquefaction occurred from those where it did not occur. Using the same data, Jefferies and Been (2006) plotted the cyclic resistance curve, by determining the state parameter from CPT results, following the screening

method of Plewes et al. (1994). Later, in the second edition of their book, Jefferies and Been (2016) used data from Moss (2003) to determine the liquefaction susceptibility chart using the state parameter. Figure 2.41 and Figure 2.42 show the two curves, adjusted to the data available. Both curves dividing liquefied and non-liquefied sites are given by:

$$CRR = a \exp(-b\psi) \qquad (2.60)$$
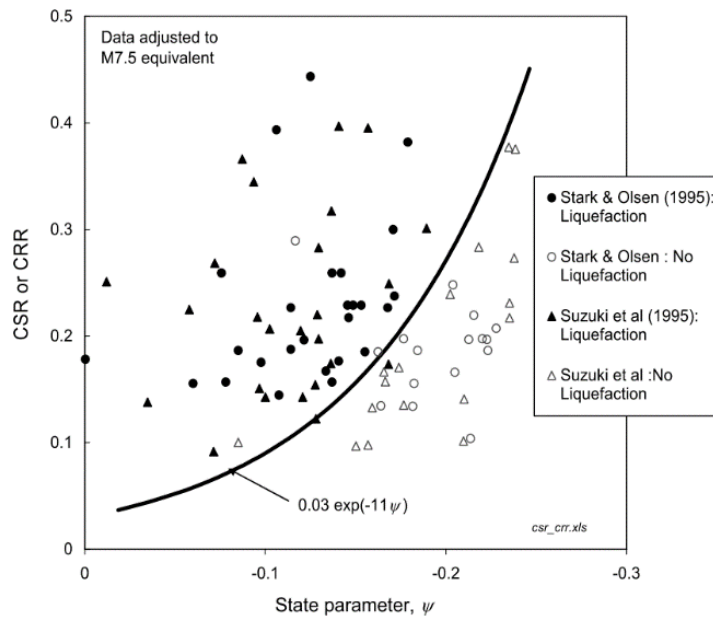
Figure 2.41 – Liquefaction assessment charts based on state parameter (data from Stark and Olson (1995) and Suzuki et al. (1995), in Jefferies and Been, 2006)
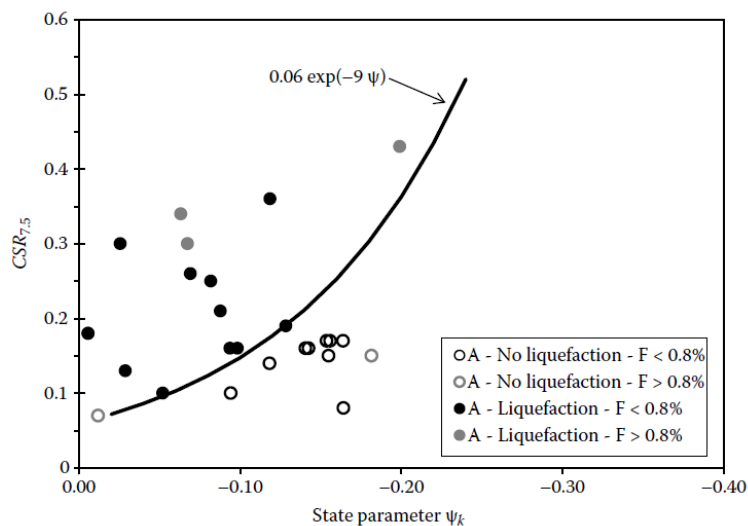
Figure 2.42 – Liquefaction assessment charts based on state parameter (data from Moss (2003), in Jefferies and Been, 2016)

Depending on the database selected, the curves change slightly and the parameters *a* and *b* are different, to better adjust the curve to the results. In the case of the curves above, *a* and *b* are 0.03 and 11, respectively, to fit the data from Stark and Olson (1995) and Suzuki et al. (1995), and are 0.06 and 9, respectively, to fit the data from Moss (2003).

Moreover, Jefferies and Been (2016) present a relationship between CRR for failure in 15 cycles (CRR$_{15}$) and state parameter, from laboratory tests in a variety of sands (Figure 2.43). There seems to be a clear trend, however, there is some scatter in the results, as the state parameter is not the only parameter that affects the cyclic behaviour. Fabric effects play a relevant part on cyclic response and are not captured in the state parameter. These effects will be explored further in section 2.7.3.1, where the sample preparation methods are compared.
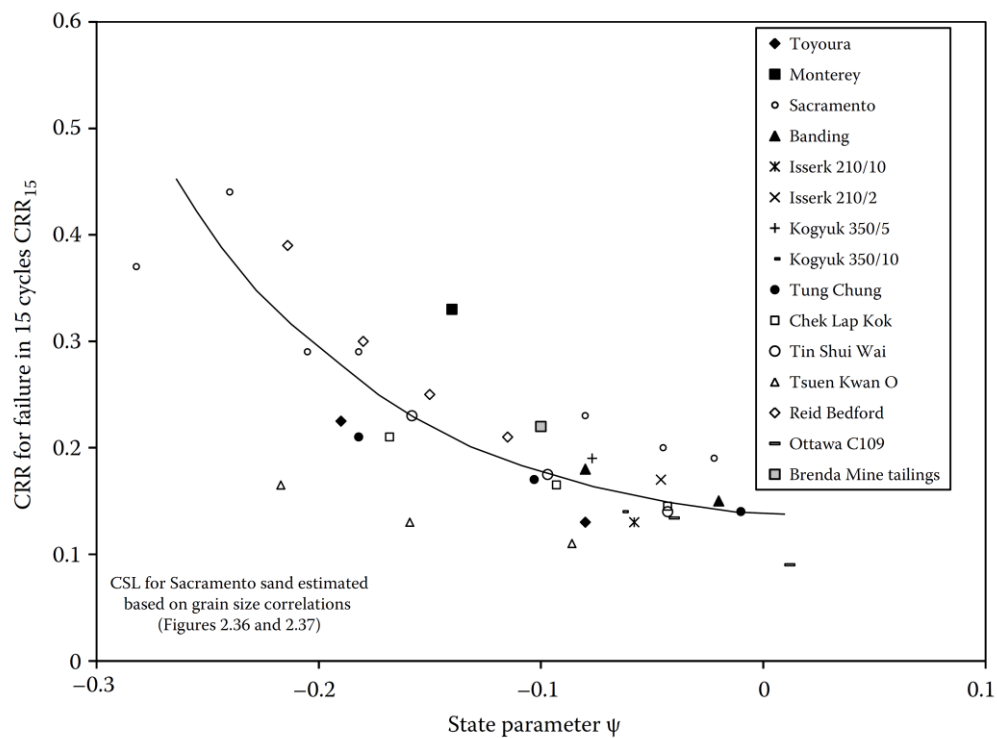
Figure 2.43 – CRR$_{15}$ as a function of state parameter (Jefferies and Been, 2016)

The use of an approach based on the state parameter has the clear advantage of not requiring a stress level correction since, for a constant void ratio, the state parameter explains the influence of stress level change. Contrary to the Simplified procedures that use field test results to assess liquefaction potential, the use of the state parameter estimated from CPT results includes the effect of stress level and soil properties. Therefore, the critical state approach is free from sometimes dubious corrections and adjustment factors (Jefferies and Been, 2016).

As stated above, one main disadvantage of using this approach is the determination of an accurate critical state line through laboratory tests. The collection of high-quality undisturbed samples is not a simple and inexpensive process, so most laboratory tests are performed in reconstituted specimens. It is known that fabric affects the cyclic behaviour of soil, hence the reconstitution technique will influence the CSL determination. Besides, the determination of in situ state parameter is not direct and requires the accurate measurement of in situ G_{max} and K_0, which, especially the last, can be challenging (Jefferies and Been, 2016).

2.6.4. METHOD BASED ON SHEAR WAVE VELOCITY MEASUREMENTS

The shear wave velocity approach was already discussed in terms of in situ tests, with the relationships between CRR and V_S proposed by Andrus and Stokoe (2000) and Kayen et al. (2013). Alongside the in situ correlations, various studies relate the laboratory-determined shear wave velocity and the CRR, in order to assess liquefaction resistance based on laboratory tests. Dobry et al. (1981, 1982) might have been the first to study the laboratory V_S-based method, which curiously provided the basis of the Andrus and Stokoe (2000) methodology. Their studies were followed by many others, such as De Alba et al. (1984), Tokimatsu and Uchida (1990), Rauch et al. (2000), and Zhou and Chen (2007).

The integration of bender elements on cyclic triaxial apparatus allowed the measurements of the shear wave velocities of specimens before cyclic shearing (Lee and Santamarina, 2005; Zhou and Chen, 2007). These piezoelectric transducers and the interpretation of the results are detailed in section 5.3.1.

Zhou and Chen (2007) summarised the semitheoretical considerations that allow to correlate the cyclic resistance ratio in undrained cyclic triaxial conditions, CRR_{tx}, with the shear wave velocity measured before cyclic shearing, V_S. As already explained, the cyclic stress ratio is defined as the cyclic shear stress (τ_d) and the initial effective vertical stress in the ground, which in cyclic triaxial conditions is replaced by the mean effective confining stress. Moreover, CRR_{tx} can be related to the CRR_{tx} at 100 kPa using K_σ (equation (2.20)), where the exponent f includes the effects of the soil conditions. From here, it is clear that the maximum shear stress is proportional to $(\sigma'_m)^f$, as:

$$\left(\tau_d = \frac{\sigma_d}{2}\right) \propto (\sigma'_m)^f \tag{2.61}$$

On the other hand, the small-strain shear modulus, G_{max}, is defined by equation (2.9), so, combining these expressions discussed above, the following relationship is obtained:

$$\left(\tau_d = \frac{\sigma_d}{2}\right)^{n/f} \propto G_{max} \tag{2.62}$$

This proportionality can be expressed by means of a constant of proportionality, introducing the factor k in the equation. Moreover, Tokimatsu and Uchida (1990) proposed the use of a void ratio function with the minimum void ratio to normalise G_{max} and eliminate the effect of soil type. Taking all the above into consideration, equation (2.62) becomes:

$$(\tau_d)^{n/f} = k\frac{G_{max}}{F(e_{min})} \tag{2.63}$$

Considering the relationship between CRR and τ_d, the equation above can be rewritten based on CRR, replacing the small strain shear modulus by the relationship with V_S (equation (2.6)), where ρ is the total mass density of the soil. It is important to note that f/n depends on soil type and relative density, therefore this expression is material-dependent.

$$CRR_{tx} = \frac{1}{\sigma'_m}\left[k\frac{\rho V_S^2}{F(e_{min})}\right]^{f/n} \tag{2.64}$$

2.6.5. METHOD BASED ON ENERGY APPROACHES

Besides the stress and strain-based approaches, there is a set of methods that use intensity measurements (commonly termed energy measurements) to assess liquefaction potential. These energy-based methods arose due to two main reasons. The first is the possibility to quantify earthquakes in terms of energy, through simple correlations with common seismological parameters such as the earthquake magnitude (Gutenberg and Richter, 1956). The second was the pioneering work of Nemat-Nasser and Shokooh (1979) that developed a relationship between dissipated energy and pore pressure generation, which was followed by several other studies later detailed in section 2.6.6. Besides, the energy per unit volume of soil is a function of both stress and strain, so energy-based methods have the possibility of encompassing the strengths of each approach (Green, 2001).

As discussed above, a dry loose soil has the tendency to densify under cyclic shear, which involves particle rearrangement that expends energy. As the soil gets denser, and approaches the minimum void ratio, the energy required to rearrange the soil particles increases. However, in a saturated loose soil under undrained conditions, the tendency to densify will result in an increase in pore pressure, and consequently a decrease in the intergranular forces, which translates in a decrease in the incremental

energy. On the other hand, the accumulated energy increases with plastic strain accumulation (Figueroa et al., 1994).

When a soil is dynamically sheared, part of the energy is dissipated throughout the soil, and the other part is dissipated into the soil. The accumulated dissipated energy might be related to the cumulative area bounded by stress-strain hysteresis loops (Green, 2001). Figure 2.44 represents a typical hysteresis shear stress-strain loop, where the shaded area corresponds to the total dissipated energy, ΔW.
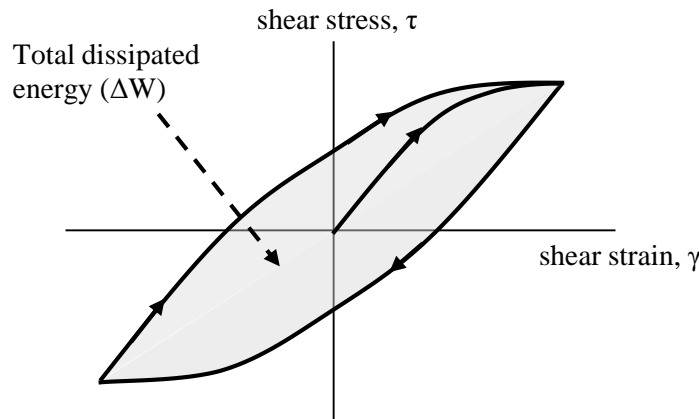
Figure 2.44 – Typical hysteresis shear stress-strain loop (based on Green, 2001)

In a cyclic laboratory test, the stress, strain, and pore pressure are recorded over time which allows the determination of the hysteresis loops. For the cyclic triaxial test, the dissipated energy is calculated with the deviatoric stress-axial strain hysteresis loops, following equation (2.65), where ΔW is the dissipated energy per unit volume of material up to the nth load increment, $\sigma_{d,i}$ is the ith increment in deviatoric stress, $\varepsilon_{a,i}$ is the ith increment in axial strain, and n is the total number of increments.

$$\Delta W = \frac{1}{2} \sum_{i=1}^{n-1} (\sigma_{d,i+1} + \sigma_{d,i})(\varepsilon_{a,i+1} - \varepsilon_{a,i}) \qquad (2.65)$$

On the other hand, for cyclic simple shear the dissipated energy is calculated with the shear-strain hysteresis loops, following equation (2.66), where τ_i is the ith increment in shear stress, γ_i is the ith increment in shear strain, and n is the total number of increments.

$$\Delta W = \frac{1}{2} \sum_{i=1}^{n-1} (\tau_{i+1} + \tau_i)(\gamma_{i+1} - \gamma_i) \qquad (2.66)$$

Similarly to the stress-based approach, the basic premise of the energy-based approaches is to compare the seismic demand and the soil capacity, i.e. the soil liquefaction resistance. Green (2001) presented a thorough summary of the most used energy-based liquefaction evaluation procedures, developed from earthquake case histories and laboratory data. One of the first energy approaches for liquefaction evaluation is based on the dissipated energy and was proposed by Davis and Berrill (1982), and modified by Berrill and Davis (1985). The seismic demand is estimated from the seismic wave energy released by the earthquake (Gutenberg and Richter, 1956), modified to account for the distance from site to centre of energy release and material damping. The correlation between the seismic demand and the normalised number of blow counts from SPT databases, proposed by Berrill and Davis (1985), is presented in Figure 2.45.
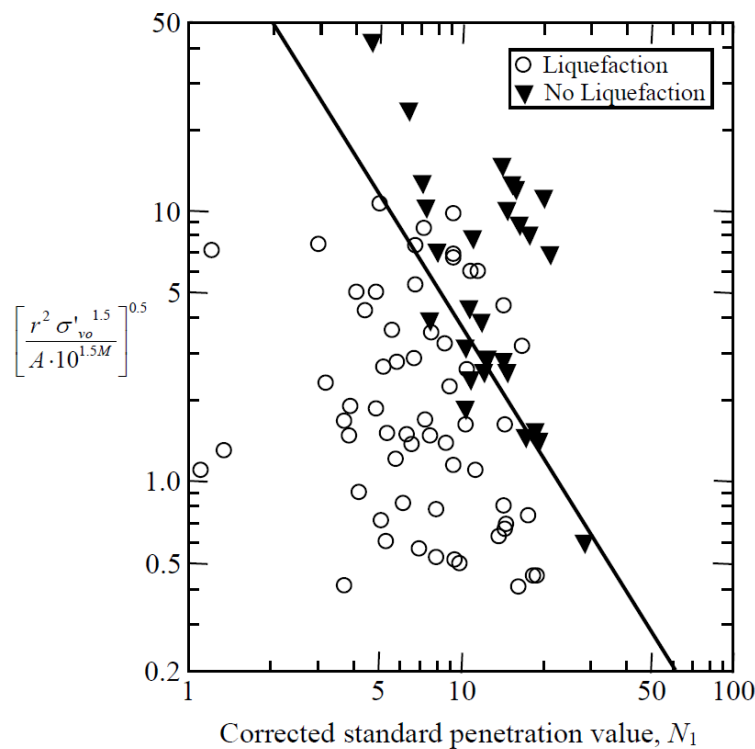
Figure 2.45 – Liquefaction chart proposed by Berrill and Davis (1985)

The liquefaction resistance of soils, hence the accumulated dissipated energy until liquefaction, is influenced by several factors, namely grain size distribution, relative density of the deposit, type of applied loading, drainage conditions, confining pressures, soil structure and cementation, intensity and duration of ground shaking, strain history and thickness of the deposit, and amount of entrapped air in the deposit (Figueroa et al., 1994). Figueroa et al. (1994) performed several torsional shear tests in a hollow cylinder device and concluded that the energy per unit volume required for liquefaction increases

with an increase in relative density and with an increase in effective confining pressure, while the amplitude of shear strain is not relevant. They proposed an expression to assess the capacity energy based on the relative density and the effective confining pressure. Likewise, Baziar et al. (2011) proposed an expression to determine the capacity energy, based on effective confining pressure, relative density, fines content, uniformity coefficient (C_U) and mean grain size (D_{50}). These expressions enable the estimation of the capacity energy that might be used to assess the liquefaction potential of a soil deposit when compared to the demand energy released by a seismic source.

The energy-based approaches have been increasingly used and developed over the years, especially because of the relationship between dissipated energy and pore pressure generation introduced by Nemat-Nasser and Shokooh (1979). Their potential advantages are recognised and make these approaches promising for future use in practice (NASEM, 2016).

2.6.6. METHODS TO ESTIMATE PORE PRESSURE EVOLUTION

As discussed above, earthquake-induced soil liquefaction is a phenomenon typically associated with the increase in pore water pressure, causing a significant loss of soil strength and stiffness. Therefore, it makes sense that researchers focusing on liquefaction study dedicate time to development of pore pressure generation models. The pore pressure models are usually computed in terms of pore pressure ratio (r_u), defined as the ratio between the excess pore water pressure to the initial effective confining pressure. This ratio varies between zero (when no excess pore pressure exists) and one (when the pore pressure equals the initial effective confining pressure, i.e. liquefaction occurs). There is a variety of pore pressure generation models, including stress-based (Seed et al., 1975; Booker et al., 1976), strain-based (Martin et al., 1975; Dobry et al., 1982), and energy-based models (Berrill and Davis, 1985; Green et al., 2000; Polito et al., 2008). In this section, the emphasis is given to the Seed et al. (1975) stress-based model and the GMP energy-based model (Green et al., 2000).

The most used stress-based pore pressure generation model was proposed by Seed et al. (1975) using empirical data from laboratory tests on clean sands, and simplified by Booker et al. (1976) as equation (2.67). This equation has two calibration parameters, N_{liq} and α, that can be calibrated with undrained cyclic tests, namely cyclic triaxial tests. The parameter N_{liq} can only be determined if the soil liquefies, which is a setback as some dense soils do not liquefy but experience significant pore pressure increases and deformations due to cyclic softening (Idriss and Boulanger, 2008). On the other hand, α is an empirical constant that depends on soil type and test conditions. The pore pressure ratio is usually plotted against the cycle ratio (i.e. the ratio of the number of cycles to the number of cycles required for liquefaction to occur). Lee and Albaisa (1974), after gathering the results of stress-controlled cyclic tests

in sands of various densities, concluded that the pore pressure ratio curves fall between an upper and lower limit, as illustrated in Figure 2.46. When α is 0.7, the curve is approximately the average between the upper and lower bound, and this is the recommended value for clean sands according to Booker et al. (1976). If the purpose is to use this expression in earthquake site response analyses, the earthquake motion needs to be converted to an equivalent number of uniform cycles (Seed et al., 1983), which constitutes a disadvantage of the use of this stress-based model.

$$r_u = \frac{2}{\pi}\arcsin\left(\frac{N}{N_{liq}}\right)^{1/2\alpha} \tag{2.67}$$
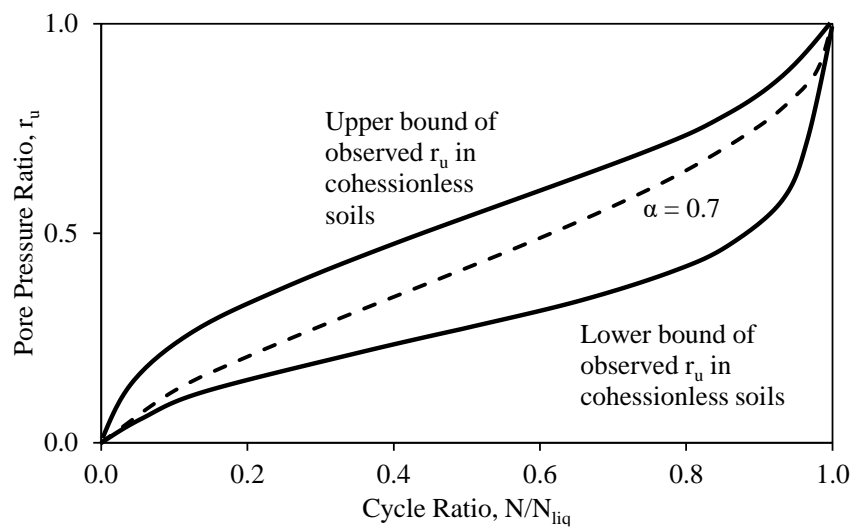
Figure 2.46 – Observed bounds of excess pore pressure generation as a function of cycle ratio and the approximate average of bounds given by equation (2.67) for $\alpha = 0.7$ (adapted from Seed et al., 1975)

Pore pressure generation models based on energy were firstly introduced by Nemat-Nasser and Shokooh (1979) that assumed that there is a unique relationship between pore water pressure generation and the cumulative dissipated energy per unit volume of soil up to the onset of liquefaction. Thereafter, many other researchers concluded the same and proposed correlations to assess pore pressure generation from cumulative dissipated energy (Berrill and Davis, 1985; Towhata and Ishihara, 1985; Green et al., 2000; Kokusho, 2013; Azeiteiro et al., 2017; Millen et al., 2020). One of the most generic formulations was proposed by Berrill and Davis (1985), as a simple empirical formulation in equation (2.68), where W_s is the normalised energy dissipated per unit volume of soil ($\Delta W/\sigma'_o$), and α and β are calibration parameters.

$$r_u = \alpha W_s{}^\beta \tag{2.68}$$

More recently, Green (2001) provided a detailed review of several energy-based pore pressure generation models. Herein, the model proposed by Green et al. (2000), referred to as GMP (Green-Mitchell-Polito) model is briefly summarised, as an alternative to the use of stress-based models. The empirical expression proposed (equation (2.69)) was obtained using data from tests with a variety of fines content, and relates the pore pressure rate with the dissipated energy per unit volume of soil. W_s is the dissipated energy (ΔW) normalised by the initial effective mean stress, as expressed in equation (2.70) for undrained cyclic triaxial tests.

$$r_u = \sqrt{\frac{W_s}{PEC}} \leq 1 \tag{2.69}$$

$$W_s = \frac{1}{\sigma'_o} \sum_{i=1}^{n-1} \frac{(\sigma_{d,i+1} - \sigma_{d,i})}{2} (\varepsilon_{a,i+1} - \varepsilon_{a,i}) \tag{2.70}$$

The calibration parameter PEC (pseudoenergy capacity) can be obtained graphically from cyclic test data, by plotting r_u versus the square root of W_s, as shown in Figure 2.47. Equation (2.71) presents the numerical simplification of the calculation of PEC, where $W_{s,r_u=0.65}$ is the value of W_s corresponding to $r_u = 0.65$.
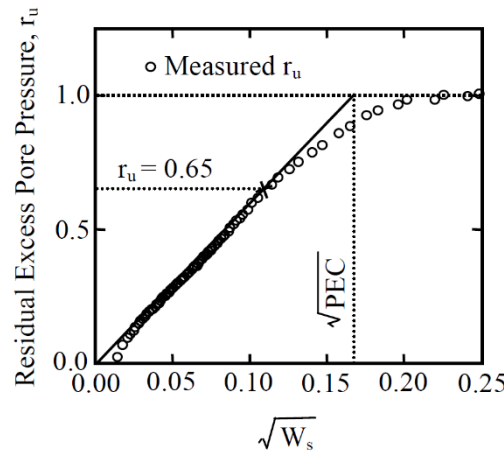
Figure 2.47 – Determination of PEC from cyclic test data (Green et al., 2000)

$$PEC = \frac{W_{s,r_u=0.65}}{0.4225} \tag{2.71}$$

In the same study referred above, Polito et al. (2008), proposed a correlation to obtain PEC from fines content and relative density. Equation (2.72) presents this correlation depending on a fines content

threshold of 35 %, where c_1, c_2, c_3, and c_4 are regression coefficients. The value of PEC increases with the increase of relative density, and decreases with an increase in fines content. These effects are more significant for soils with FC < 35%.

$$\ln(PEC) = \begin{cases} \exp(c_3 \cdot D_R) + c_4 & \text{if } FC < 35\% \\ c_1 \cdot FC^{c_2} + \exp(c_3 \cdot D_R) + c_4 & \text{if } FC \geq 35\% \end{cases}$$

$$c_1 = -0.597; \ c_2 = 0.312; \ c_3 = 0.0139; \ c_4 = -1.021$$

(2.72)

2.7. FACTORS AFFECTING CYCLIC LIQUEFACTION

The behaviour of soils under cyclic loading is affected by several factors that depend on the material characteristics or the testing procedures, such as particle size and gradation, relative density, soil structure and cementation, confining pressure, type of applied loading, loading wave form, frequency of loading, pre-straining conditions, drainage conditions, overconsolidation ratio, specimen preparation method, and specimen size. Over the years, these factors have been studied in detail, to better understand how they influence the undrained shear response of soils. Townsend (1978) and Vaid and Sivathayalan (2000) presented comprehensive reviews of many of these factors. In this section, the factors studied in this work are discussed, including the state conditions (confining stress, relative density, and state parameter), soil type (fines content and plasticity), sample preparation method, structure and fabric, and cyclic loading conditions.

2.7.1. INFLUENCE OF THE STATE CONDITIONS

The influence of confining stress and relative density on cyclic strength have been documented by many authors (Castro and Poulos, 1977; Townsend, 1978; Vaid and Sivathayalan, 1996). Based on laboratory tests performed in Fraser Delta sand in simple shear conditions, Vaid and Sivathayalan (1996) presented the relationships between the cyclic stress ratio to cause liquefaction in 10 cycles of loading, effective confining stress, and relative density (Figure 2.48). It is shown that the increase in soil density increases the cyclic resistance ratio, while an increase in confining stress decreases the cyclic resistance. The effect of confining stress is more relevant in denser specimens (due to dilatancy), and is almost negligible for loose specimens, illustrated by a less steep curve.
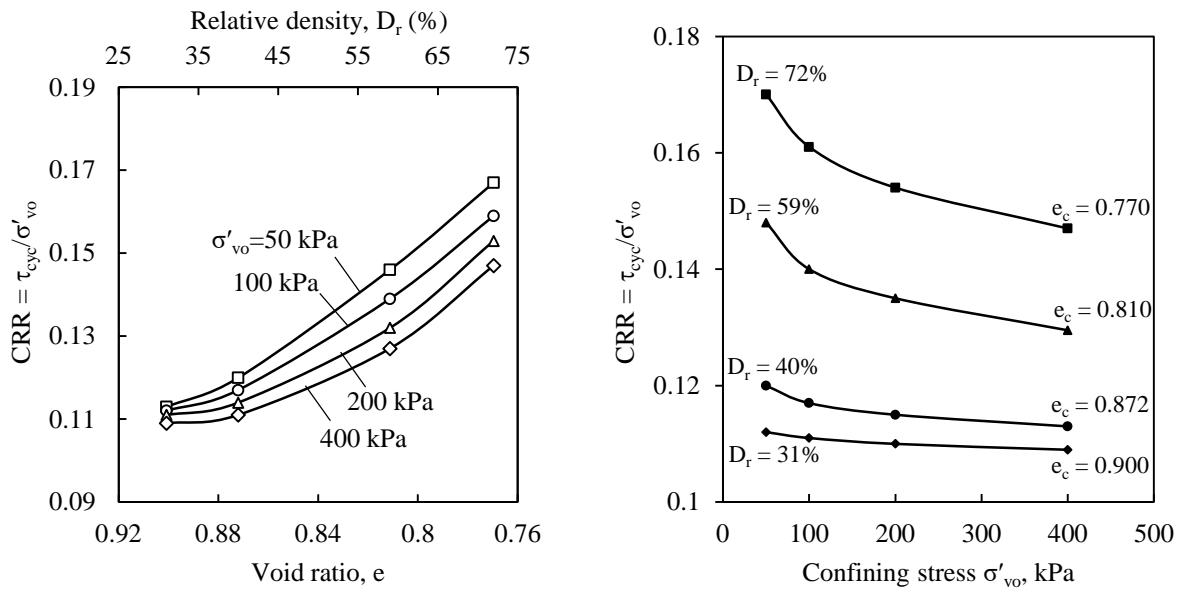
Figure 2.48 – Liquefaction resistance of Fraser Delta sand in cyclic simple shear showing the effect of confining stress and relative density on liquefaction resistance (adapted from Vaid and Sivathayalan, 1996)

As discussed before, the critical void ratio decreases with the increase of confining pressure. For low confining pressures, a dense sand has the tendency to dilate, as it is often located on the left side of the CSL. However, for higher confining pressures, this tendency for dilation decreases. Therefore, for the same void ratio and the same CRR, a dense specimen under high confining pressure is less stable than under lower confining pressures, which justifies the decrease in CRR with increase of confining pressure. This tendency was also observed by Yoshimi et al. (1984).

On the other hand, the denser a soil is, the more difficult it is for the pore pressure to build-up, as the contact forces among the soil particles are higher, and the soil has a tendency to dilate. The relative density is a parameter that reflects how dense a soil is, according to its particular particle size, grading and shape, and is defined by equation (2.73), where e_{max} and e_{min} correspond to the maximum and minimum void ratios, i.e. loosest and densest states respectively, and e is the natural void ratio.

$$D_R = \frac{e_{max} - e}{e_{max} - e_{min}}$$
(2.73)

2.7.2. FINES CONTENT AND PLASTICITY

One of the main factors that affect the behaviour of a soil is the soil type, which refers to physical characteristics as soil gradation, mineralogy, particles shape or soil plasticity. The fines content (FC) is the percentage of particles with diameter smaller than 0.075 mm (passing through the sieve #200) and

can be used to compare soils regarding their cyclic strength. However, FC does not characterise other important features, such as the soil gradation or plasticity of the fines. As discussed in section 2.4, the plasticity of fines strongly influences liquefaction potential as an increase in plasticity is associated with an increase in liquefaction resistance (Bray and Sancio, 2006). It is then important to firstly distinguish if the fines are plastic or non-plastic.

The effect of non-plastic fines on soil behaviour has been the focus of much research work. Cubrinovski & Ishihara (2002) and Lade et al. (1998) studied the effect of fines in the packing of particles (maximum and minimum voids ratio), Carrera et al. (2011) tested mine tailings and found that the location of NCL varied with fines content (FC), and Soares and Viana da Fonseca (2016) showed the same for a silt and a silty sand. Furthermore, several authors (Chang, 1990; Polito, 1999; Cubrinovski et al., 2010) have studied the influence of FC in the cyclic behaviour of soils. However, this has been a controversial theme. While some studies suggest that the addition of fines to sand increases liquefaction resistance (Chang et al., 1982; Amini and Qi, 2000), others report that liquefaction resistance decreases with increase of fines content (Chang, 1990; Polito and Martin, 2001, Thevanayagam, 2007b). Chang et al. (1982) verified a general increase of liquefaction resistance with the addition of fines, for FC > 20%, which was proceeded by a drop in resistance for FC < 10%. Amini and Qi (2000) also experienced an increase in resistance with increase of fines content, when 10% < FC < 50%. On the other hand, many other studies state that liquefaction resistance reduces with increase of fines content up to a threshold value. After this value is surpassed, the liquefaction resistance increases (Chang, 1990; Polito and Martin, 2001; Thevanayagam, 2007b; Huang and Chuang, 2011). Examples of the influence of fines content in the cyclic strength of soils are presented in Figure 2.49.
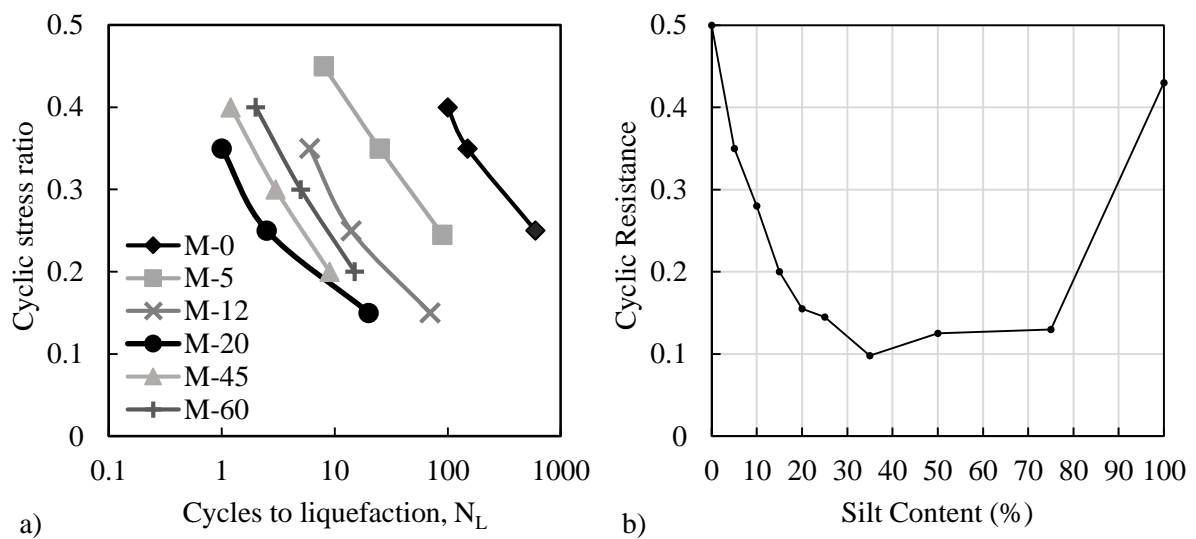
Figure 2.49 – a) Liquefaction resistance curves for different fines content values (Chang, 1990); b) Variation of cyclic resistance with fines content (Polito, 1999)

To better understand this behaviour, some authors have studied reconstituted soil samples of sand mixed with different percentages of fines and compared the results, having as reference the behaviour of the clean sand (with less than 5% fines content). Polito and Martin (2001) found that there seems to be a "limiting silt content", around 25 to 45%, which is the maximum silt content that can fill the voids created by the sand skeleton. If the silt content is below the limiting value, the cyclic resistance is controlled by the relative density of the specimen (high relative density means higher cyclic resistance). If it is above the limiting silt content, the sand grains are suspended within the silt matrix. The relative density also controls the cyclic resistance but the increase occurs at a slower rate. Moreover, Thevanayagam (2007a) presented the idea of equivalent intergranular void ratio and stated that liquefaction resistance decreases when the fines content increases until a certain value that depends on the grain characteristics, size disparity ratio and global void ratio. Past that value, the resistance increases with an increase in silt content.

The concepts of limiting silt content and intergranular void ratio are based on previous works by Ladd et al. (1998) and Cubrinovski and Ishihara (2002). The influence of fines content in cyclic strength is related to the soils skeleton, hence to the soil matrix being controlled by the sand or fines particles. Cubrinovski and Ishihara (2002) showed the relationship between limiting void ratios and fines content and found that there is a transition zone around 25-35% of FC (Figure 2.50). Below these values, the fine particles fill-in the void between the sand particles and do not influence the sand skeleton structure, hence the microstructure of the granular mix is defined by the sand matrix, and the limiting void ratios decrease with increase of FC. On the other hand, for FC above that threshold, the fines matrix controls the microstructure and the sand particles are separated by the fines particles. However, when dealing with natural sands, the grain-size distribution changes gradually from coarser to finer particles, so the absence of a gap in the soils gradation reduces (or eliminates) the effects of filling the voids with fines for FC below 25% (Cubrinovski and Ishihara, 2002).
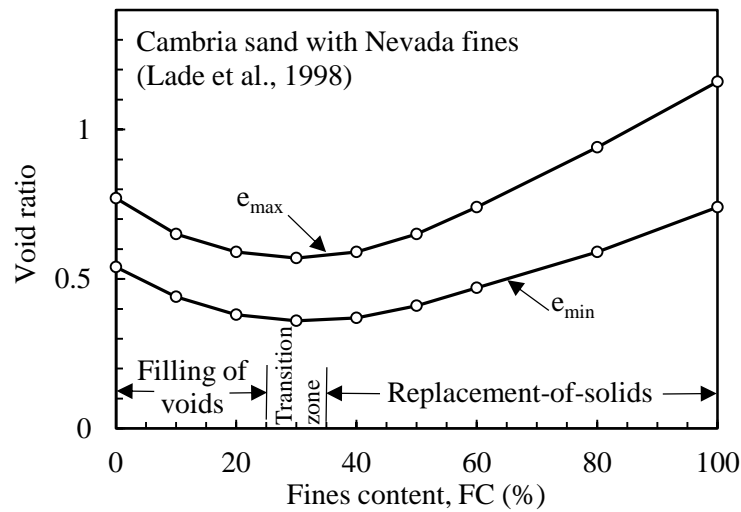
Figure 2.50 – Variation in e_{max} and e_{min} with fines content for mixtures of Cambria sand and Nevada fines (adapted from Cubrinovski and Ishihara, 2002)

Thevanayagam (1998) proposed that two different void ratios are used to characterise the mechanical behaviour of soils, according to the matrix that defines the soil microestructure. The intergranular and interfine void ratios, e_c and e_f, were proposed as equations (2.74) and (2.75), respectively. At low fines content, the sand particles form the major soil skeleton and the fines fill-in the voids between the sand particles, not having influence in the soil behaviour. The soil state depends on the intergranular void ratio, which is equivalent to the sand skeleton void ratio. On the other hand, at high fines content, the fines contacts govern the soil behaviour, and the state is defined by the interfine void ratio.

$$e_c = \frac{e + FC}{1 - FC} \tag{2.74}$$

$$e_f = \frac{e}{FC} \tag{2.75}$$

Over the years, these expressions were improved to include more than the FC, as this parameter is not sufficient to characterise the mechanical behaviour of mixtures. Thevanayagam et al. (2002) introduced the concepts of equivalent intergranular contact void ratios, $(e_c)_{eq}$ and $(e_f)_{eq}$, to characterise the behaviour of gap-graded granular mixtures. Different proposals for the equivalent intergranular void ratios are reported by various authors (Rahman et al., 2008; Gobbi, 2020).

The effect of fines is also presented in the empirical curves from case history databases. An example is presented in Figure 2.51a, and it is observed that with increasing fines content the curve moves to the left, presenting higher resistance for the same penetration resistance. This appears to be contrary to the

considerations made based on the laboratory tests. However, according to Cubrinovski and Ishihara (1999), the penetration resistance, after normalisation with confining pressure, depends on the relative density and fines content. For the same relative density, soils with fines normally exhibit lower penetration resistance than clean sand. Cubrinosvki et al. (2010) reinterpreted empirical field data in terms of relative density and concluded that liquefaction resistance of sandy soils decreases with increasing fines content (Figure 2.51b), confirming the laboratory determined tendencies.
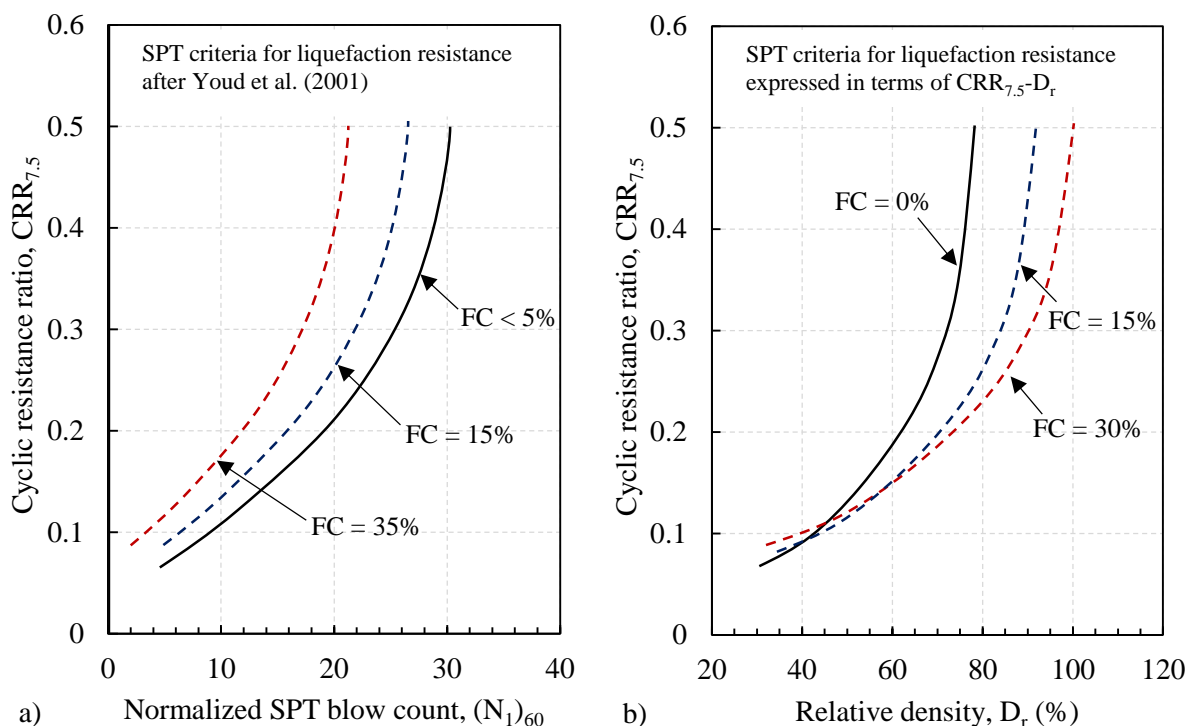
Figure 2.51 – SPT-based criteria for liquefaction resistance of Youd et al. (2001): a) relationship between normalised SPT blow count and fines content; b) relationship between relative density and fines content (Cubrinovski et al., 2010)

2.7.3. SOIL ANISOTROPY EFFECTS FOR LIQUEFACTION EVALUATION

Soil anisotropy might be of two types: inherent anisotropy, that is related to the natural fabric (orientation of particles) and structure (influence of lamination, layering or bedding) of the soil; and induced anisotropy, related to the stress induced to the soil. Moreover, inherent anisotropy is attributed to the particle arrangement during deposition, so it is influenced by particle shape, angularity and roughness, particle size distribution and mineralogy.

It is known that anisotropy affects the behaviour of soils, however its influence is not straightforward and its complexity has led to many studies over the years (Lee and Fitton, 1969; Oda, 1972; Ishihara, 1993; Høeg et al., 2000; Wang et al., 2006). On one hand, the deposition mode, particle shape and creep

influence the fabric and structure of soil (Høeg et al., 2000; Ishihara, 1993). On the other hand, the orientation of loading also has a significant influence on the soil response. Youd (1977) created a particulate model to show how packing changes during cyclic straining. The rotation of principal stresses reflects on the rotation of grains that rearrange their position which might cause excess pore pressure generation during undrained loading. Yamada et al. (2010) performed systematic cyclic triaxial tests to analyse the effects of anisotropy on reliquefaction resistance and found that anisotropy can be more influential of soil behaviour than density. During the liquefaction process, the soil goes through successive states of anisotropy. Depending on the level of anisotropy after liquefaction, the sand will exhibit a different behaviour, despite the relative density increase after each stage. In cases where the anisotropy after liquefaction is higher than before, the sand will behave as an extremely loose sand and liquefaction resistance decreases. Contrarily, if the anisotropy after liquefaction is lower than before, the sand will not exhibit a behaviour resembling an extremely loose sand and liquefaction resistance increases.

The following sections discuss the influence of both types of anisotropy on the cyclic strength of soils, focusing on specimen fabric and structure, through the consideration of various sample preparation methods and the differences between undisturbed and reconstituted specimens (inherent anisotropy), and on cyclic loading conditions (induced anisotropy).

2.7.3.1.   The influence of sample preparation on cyclic strength

As the collection of high quality samples in saturated sands from the field is an expensive and difficult procedure, the majority of laboratory tests in granular soils is performed on reconstituted specimens (Castro, 1969; Ishihara, 1993; Soares, 2014). There are several sample preparation methods that differ in terms of deposition procedure (e.g., pluviation, spooning, or flowing), soil moisture condition (e.g., dry, moist, or wet), the placement medium being air or water, and the densification technique (e.g., tamping, tapping, vibrating) (Frost and Park, 2003). Therefore, it is important to assess the influence of each method, and consequently of the fabric produced by each method, in the cyclic behaviour of soil. The selection of the most suitable reconstitution method is not easy, as many studies show different preparation methods result in different soil fabrics and stress-strain response (Ladd, 1974; Ishihara, 1993; Vaid et al., 1999; Frost and Park, 2003; Kwan and El Mohtar, 2018). Mulilis et al. (1977) performed several cyclic triaxial tests on the Monterey Sand No. 0, a clean sand, to study the effect of different preparation techniques on cyclic resistance (Figure 2.52). The cyclic liquefaction resistance increases with the energy input per unit weight of soil applied during specimen preparation. Therefore, it is observed that tamped or vibrated specimens exhibit higher resistance than pluviated specimens, and

specimens prepared by dry pluviation are less resistant than specimens prepared using moist or saturated soil for the same relative density. Likewise, Tatsuoka et al. (1986) performed cyclic triaxial tests on Toyoura sand and had similar results, with air pluviated specimens showing lower resistance. It is important to mention that there are several studies on the influence of specimen preparation technique in cyclic triaxial tests, but not many have been performed in cyclic simple shear conditions. Kwan and El Mohtar (2018) compared data from different reconstitution methods and also found that air pluviated specimens had lower resistance when compared to water sedimentation.
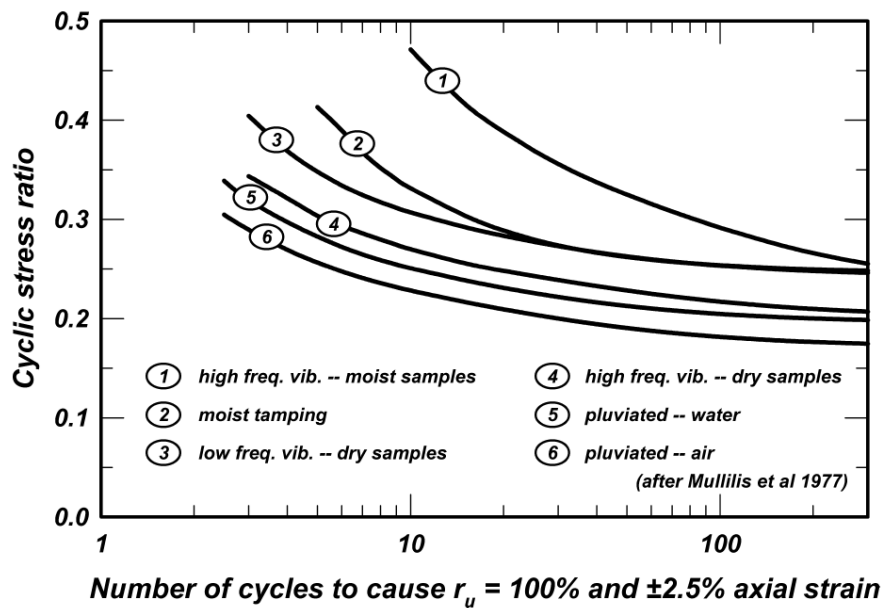
Figure 2.52 – Effect of sample preparation on cyclic strength (after Mulilis et al., 1977, from Idriss and Boulanger, 2008)

In addition to comparing different reconstitution techniques, it is relevant to compare them with undisturbed samples, to understand the effect of the fabric produced by each technique on the prediction of in situ liquefaction resistance.

Yoshimi et al. (1984) compared the cyclic resistance of dense Niigata sand samples, collected with the frozen and tube sampling techniques and reconstituted with moist-tamping and air pluviation to the same relative density (Figure 2.53). It was found that the tube samples had lower resistance than the frozen samples and air pluviation was the reconstituted technique that approximated the tube sampling resistance curve. This can be justified by a loss of some characteristics such as age, cementation, and stress and strain history during tube sampling that were not recreated in the reconstitution of specimens in the laboratory (Idriss and Boulanger, 2008).
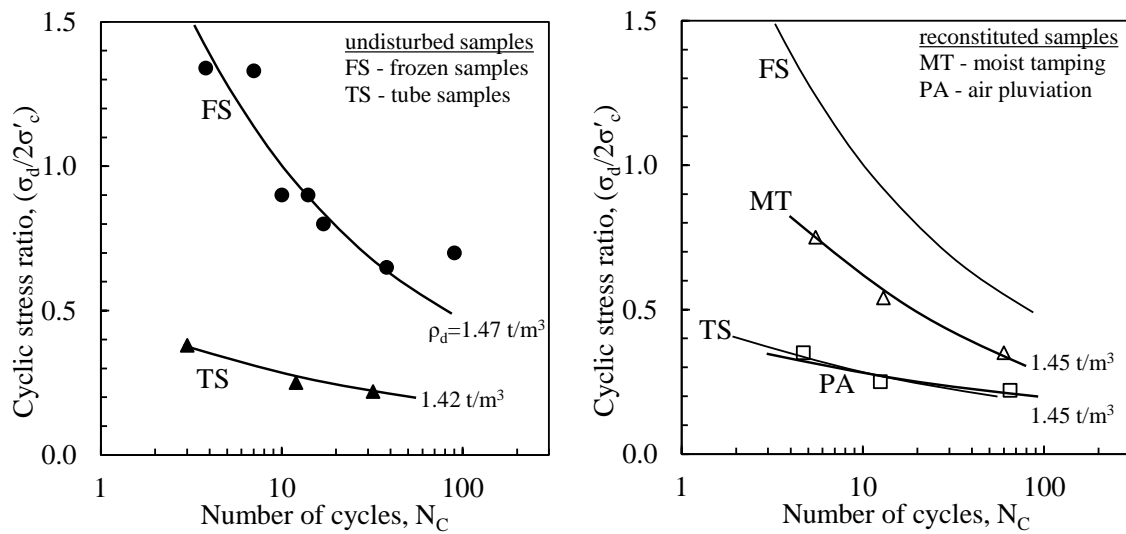
Figure 2.53 – Cyclic resistance curves of in-situ frozen samples (FS), conventional "undisturbed" tube samples (TS), samples reconstituted by moist tamping (MT), and air pluviation (PA) (after Yoshimi et al., 1984)

More recently, Ghionna and Porcino (2006) studied liquefaction resistance of undisturbed and reconstituted samples of a natural coarse sand (Figure 2.54). Once again, the air pluviation (AP) method produced lower resistance specimens. It is observed that the wet sedimentation method is the preparation procedure that provides the closest results to undisturbed specimens, which was also reported by other authors (Vaid et al., 1999; Høeg et al., 2000). However, the wet sedimentation method can cause fine separation, as larger particles sediment faster than finer particles.

A recent study from Wang et al. (2006) found that there is a good agreement between the cyclic resistance ratio of intact and reconstituted specimens of sand and silts, as long as they have the same initial shear wave velocity values and liquefaction is defined at peak-to-peak axial strain lower than 6%. The results are based on over 200 cyclic triaxial tests with intact samples extruded from tube samples and specimens reconstituted with the moist tamping technique. The limit of peak-to-peak is due to the differences in fabric from intact to reconstituted specimens. Intact specimens are stiffer than specimens reconstituted to the same V_S, so they strain less. However, reconstituted specimens were able to capture the onset of liquefaction. These results are promising, as they show that specimens reconstituted in the laboratory can predict the cyclic in situ behaviour, proved that they are prepared to the same initial shear wave velocity.
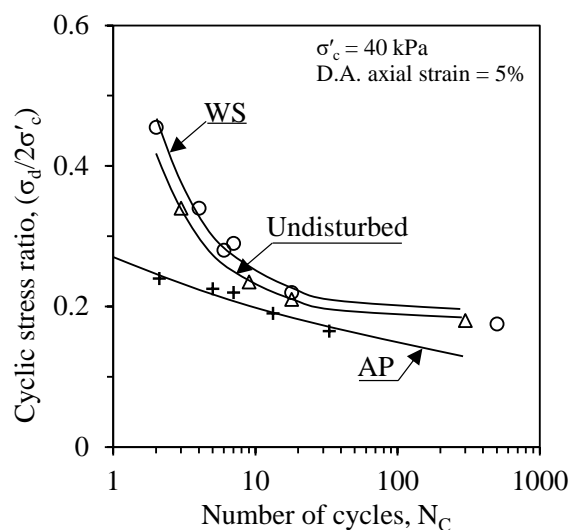
Figure 2.54 – Cyclic strength of undisturbed and reconstituted isotropically consolidated specimens (Ghionna and Porcino, 2006)

2.7.3.2. The influence of sample homogeneity on cyclic strength

Laboratory tests are usually performed with reconstituted specimens of homogeneous soil. However, soils in their natural condition might not be homogeneous, as layering of different soil types may occur during the deposition process. The layering refers to the intercalation of layers of different soil types, such as small sand layers between thicker clay layers or sand-silt-clay interlayers.

The influence of a layered structure or stratification in sand deposits has been studied recently. Amini and Qi (2000) performed tests in specimens reconstituted by moist-tamping and water pluviation (sedimentation), to reproduce homogeneous and stratified soil conditions, respectively, and concluded that the liquefaction resistance of layered and uniform soils was not significantly different. These conclusions followed similar ones presented by Vasquez-Herrera and Dobry (1972).

On the other hand, Kokusho and Kojima (2002) tested various soil layering systems in a lucite tube and found that water films can be formed in all of them once liquefaction occurs, often beneath or within less permeable sublayers. These water fills develop due to differences in the permeability of the different layers and work as sliding surfaces, being probably involved in seismically induced land and submarine slides in liquefied loose sand deposits.

Yoshimine and Koike (2005) conducted a series of undrained triaxial tests in monotonic and cyclic loading conditions, performed in uniform and stratified specimens of the same well graded clean sand. The stratified specimens were obtained by sieving and separating four different ranges of particle size and depositing them alternately. The stratified specimens were found to be much more dilative and

stiffer than the uniform sand at the same density. Figure 2.55 presents the comparison between the stratified and uniform deposits, where the relative density of the stratified specimens was determined by a weighted average of the various layers. It is observed that stratified specimens present a higher liquefaction resistance than uniform specimens.
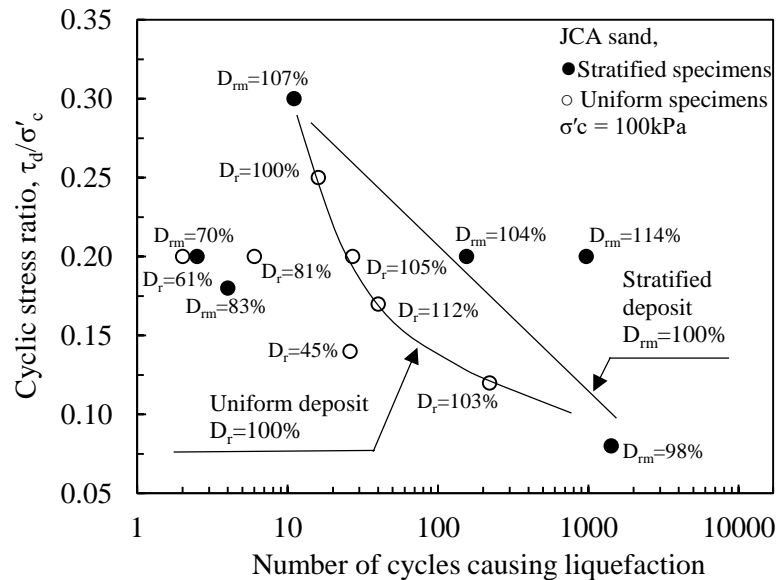
Figure 2.55 – Undrained cyclic loading tests on uniform and stratified JCA sand compared through the modified relative density (Yoshimine and Koike, 2005)

2.7.3.3. Cyclic loading conditions

As was discussed above, cyclic triaxial and cyclic simple shear tests impose different stress conditions to the specimens, which are also different from the stresses experienced by the soil in the free field during an earthquake event. Although the cyclic simple shear simulates better the field conditions, the cyclic triaxial test is one of the most commonly used tests in the laboratory, as referred before. The triaxial test has the added advantages of offering principal stress control and a large database of cyclic resistance results for a variety of soil types and state conditions. Therefore, over the years, researchers have tried to understand the relationship between the cyclic resistance of triaxial and simple shear tests.

The relationship between the cyclic resistance of simple shear and triaxial tests is often represented by the factor c_r, i.e., the ratio between CRR of simple shear tests (CRR_{ss}) and CRR of triaxial tests (CRR_{tx}). Seed et al. (1975) proposed that the relation between the CRR required to trigger liquefaction in the field was about 10% less than the required in laboratory testing, to account for the multidirectional shaking effect of earthquakes on the site that is not reproduced in the laboratory in unidirectional cyclic simple shear tests. These relationships are expressed as follows:

$$CRR_{field} = 0.9 CRR_{ss} = 0.9 c_r CRR_{tx} \qquad (2.76)$$

Silver et al. (1980) compared cyclic triaxial and simple shear test results in specimens reconstituted by moist tamping and air pluviation (Figure 2.56). They found that the sample preparation method did not affect the resistance of simple shear tests. However, triaxial tested specimens prepared with moist tamping showed higher resistance than air pluviated, and the specimens prepared with air pluviation sheared under triaxial conditions showed similar resistance to the simple shear specimens.
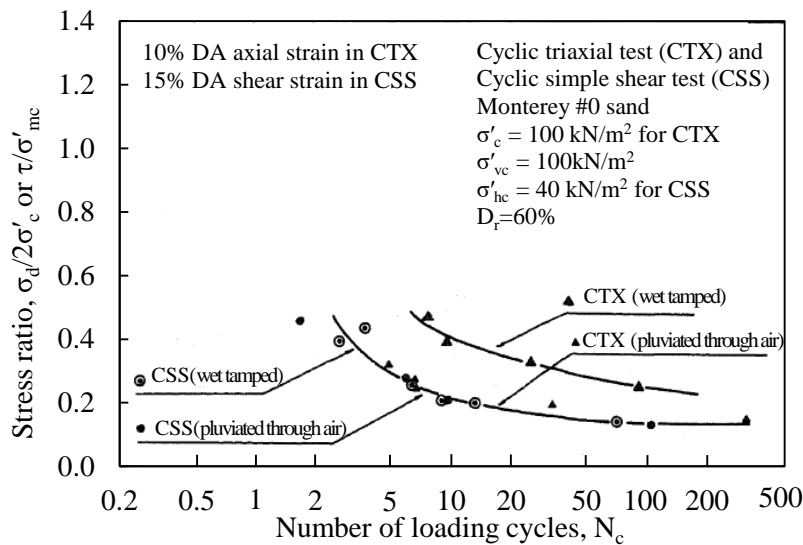
Figure 2.56 – Stress ratio versus number of loading cycles to 15% double amplitude strain for wet tamped and air-pluviated Monterey No. 0 sand at D_r=60% (Silver et al., 1980)

In the triaxial test, specimens can be consolidated either isotropically or anisotropically. However, in simple shear tests, specimens are usually anisotropically consolidated, as the vertical stress is imposed and the specimen is confined laterally by a set of rings, which do not allow lateral strain. The specimens are subjected to an initial effective stress system of σ'_{v0} vertically and $K_0 \times \sigma'_{v0}$ horizontally. Taking this into consideration, Finn et al. (1971) proposed a correlation where the initial effective stress ratio is $R=\Delta\sigma_d/2(\sigma'_c)_0$ for the triaxial test and $r=2\Delta\tau_{xy}/(\sigma'_y+K_0\sigma'_y)_0$ for the simple shear test. The relationship between simple shear and triaxial liquefaction resistance is given by $(1+K_0)/2$.

On the other hand, Ishihara et al. (1985) performed cyclic torsional shear tests with different K_0 values, and suggested that the cyclic resistance of anisotropically consolidated specimens could be related to the cyclic resistance of isotropically consolidated specimens, hence, the CRR from the simple shear test could be related to the CRR from the undrained isotropically consolidated triaxial test as:

$$CRR_{ss} = \left(\frac{1 + 2(K_0)_{ss}}{3}\right) CRR_{tx} \tag{2.77}$$

However, Tatsuoka et al. (1986) and Vaid and Sivathayalan (1996) concluded that the use of reduction factors only based on K_0 was conservative, as the relationship between cyclic resistance of triaxial and simple shear tests was dependent on several other parameters, such as sample preparation, soil type and fabric, relative density, and confining pressure. Vaid and Sivathayalan (1996) presented Figure 2.57 that shows how c_r varies with relative density and confining pressure. It is observed that, for lower relative density, c_r varies less and decreases with the increase of confining stress. On the contrary, for higher densities, c_r increases with increase of confining stress at a higher variation rate. Moreover, the values of c_r are higher for lower relative densities than for higher densities, emphasising that the difference between CRR_{ss} and CRR_{tx} increases with the increase of relative density.
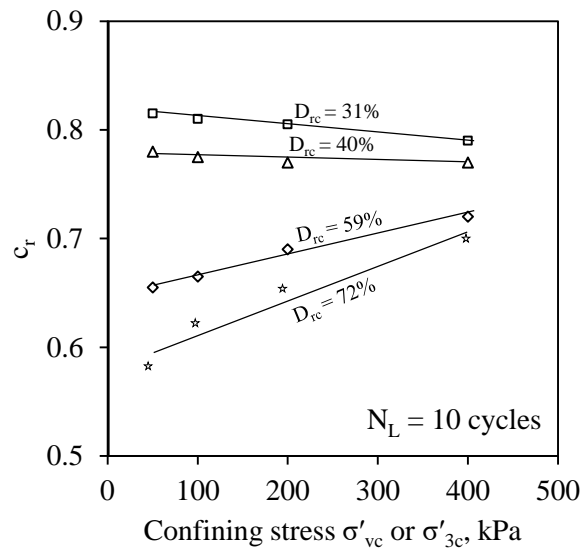
Figure 2.57 – The ratio c_r of cyclic resistance of Fraser Delta sand under simple shear and triaxial stress conditions (Vaid and Sivathayalan, 1996)

Table 2.4 summarizes the recommended relationships between the cyclic resistance from triaxial and simple shear tests, proposed over the years. The most commonly used proposal is the one from Ishihara et al. (1985). However, other studies have reported that c_r depends on factors other than K_0, such as relative density, confining pressure, fabric, soil type and the number of cycles required for liquefaction to occur.

Table 2.4 – Values of CSR correction factor c_r, relating cyclic simple shear and triaxial testing (after Jefferies and Been (2006) and Taylor (2015))

Reference	Equation	Factor c_r	
		$K_0 = 0.4$	$K_0 = 1.0$
Castro (1969)	$c_r = 2(1+K_0)/3\sqrt{3}$	0.69	1.15
Finn et al. (1971)	$c_r = (1+K_0)/2$	0.7	1
Seed and Peacock (1971)	Varies	0.55-0.72	1
De Alba et al. (1976)	Varies with N_c	0.6-0.65	
Ishihara et al. (1985)	$c_r = (1+2K_0)/3$	0.6	1
Tatsuoka et al. (1986)*	Varies with D_R, fabric and soil type	0.35-1.5	1
Vaid and Sivathayalan (1996)	Varies with D_R and σ'_{3c} or σ'_{vc}	0.58-0.82	

*results comparing triaxial and torsional shear strengths

As was discussed above, one of the main differences between triaxial and simple shear equipment is the cyclic shear system. While in the triaxial test, there is a principal stress reversal, with the principal stresses angle changing between 0º and 90º, in the simple shear test the principal stresses rotate. The principal stress rotation has been studied as one of the main aspects to assess cyclic liquefaction potential of soils.

Arthur et al. (1980) were the first to study the importance of principal stress rotation on soil behaviour, as they stated that if the sands are anisotropic, a change in loading direction would mean a change in soil response. Later, Wong and Arthur (1986) concluded that "*cyclic rotation of principal stress directions in sand which causes strain radically alters the behaviour of the material from that seen in shear under constant directions of principal stress*". Besides, Ishihara and Towhata (1983) also supported the idea that a pure cyclic rotation of principal stresses caused irrecoverable volumetric strain.

Following the work of Arthur et al. (1980), Jefferies and Been (2016) stated that the principal stress rotation causes changes in the yield surface (Figure 2.58). As "*the yield surface reflects the mobilisation of particle contacts at a micromechanical level*", the soil fabric evolves during cyclic loading. Therefore, the cyclic undrained behaviour is dominated by the shrinkage and dilation of the yield surface. On the other hand, DeGennaro et al. (2004) performed undrained cyclic triaxial tests on Hostun sand and found that the elastic parameters did not change during the test, so changes in fabric during cycles were not significant. This difference in fabric evolution during cyclic shear might be the cause for the differences between cyclic resistance of specimens tested under triaxial and simple shear conditions, as the principal stress rotation in the simple shear causes soil yielding, and consequently lower undrained cyclic shear strength.
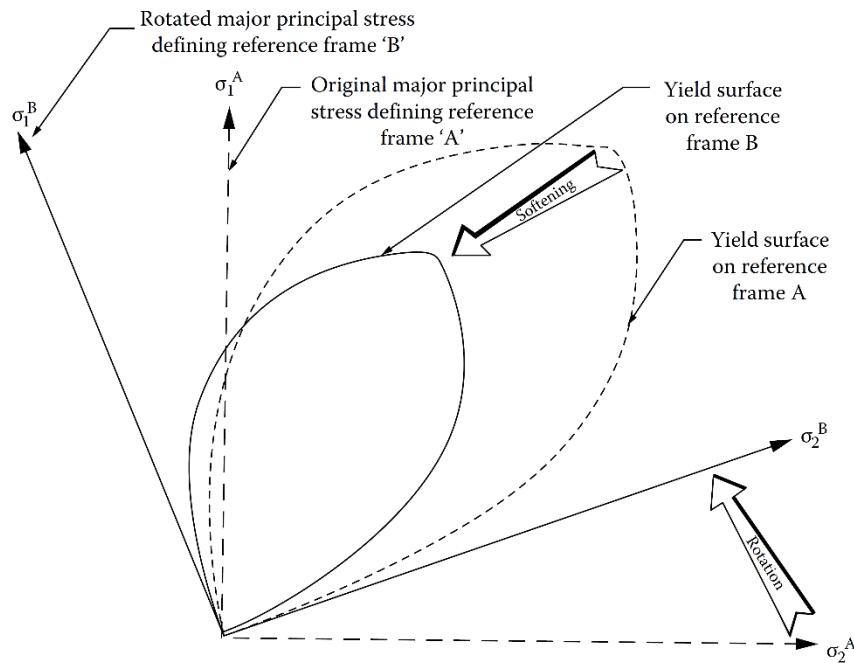
Figure 2.58 – Schematic of yield surface softening induced by principal stress rotation (from Jefferies and Been, 2016)

2.7.3.4.   Undisturbed sampling

Although the use of reconstituted samples is more practical and less expensive, as they can be reproduced indefinitely, the test results might not reflect the real behaviour of soils in the field. Reconstituted specimens fail to replicate the in situ fabric and structure from natural sands, as the natural stratification and layering of natural soils is hard to reproduce in the laboratory. Moreover, the cementation and stress-strain history, that are effects of the ageing of the deposits, are not reproduced in reconstituted laboratory specimens. Therefore, if the objective is to accurately evaluate the behaviour of soil deposits during earthquake loading, tests on high-quality undisturbed samples should be performed (Ishihara, 1993; Idriss and Boulanger, 2008). The collection of high-quality undisturbed samples of sandy soils is challenging, as samples can undergo significant changes during sampling and preparation procedures. These issues will be addressed later in this work.

PART II - FIELD-BASED EVALUATION OF LTV SOILS

3. CHARACTERISATION OF THE EXPERIMENTAL SITE AND FIELD TESTS PERFORMED

3.1. INTRODUCTION

The first part of this research involved the performance of field tests to characterise the liquefaction susceptibility of an area located in the south-west of Portugal. This Chapter explains the process behind the selection of the experimental site where the field tests were performed and soil samples were collected. To begin with, the seismicity of Portugal is detailed, describing the main faults and activity, as well as the considerations of the National Standards to assess seismic risk. The criteria and specifications of Eurocodes 7 and 8 (NP EN 1997-1:2010, NP EN 1998-1:2010) to assess the design peak ground acceleration and moment magnitude of the area are detailed. A context of historical liquefaction in Portugal is presented, with the description of some liquefaction cases that occurred over the years.

The experimental site campaign was located in the municipalities of Vila Franca de Xira and Benavente, in the lower Tagus river valley, near Lisbon, and involved the performance of several field tests and the collection of high quality samples. The soil profiles were composed of young Holocene alluvial soils, deposited over the years. To better understand the soils composition and behaviour, it is fundamental to comprehend how the geological formations evolved over the years and what is their origin. Therefore, a summary of the geologic, geomorphologic and hydrogeological characteristics of the experimental site area is also presented.

The last part of the Chapter describes the field tests performed at each experimental site, and documents the sampling programme, including a description of the three samplers used and the procedures of soil sample retrieval, transportation, extrusion, and storage in the laboratory. The main objective is to summarize the characteristics of the site location and provide a framework for the interpretation of the field and laboratory tests.

3.2. SEISMICITY OF PORTUGAL

Portugal is located on the western and southern margins of the Iberian Peninsula. The seismicity is characterised by different regions and increases from north to south, with prevalence in the south and adjacent Atlantic margins. The seismicity near the coast is related to the proximity to the boundary between the African and Eurasian plates (Ferrão et al., 2016). In terms of magnitude, Portugal is characterised by low-magnitude (M_w<5.0) events on the mainland and Atlantic margin and stronger ones (5.0<M_w<7.8) offshore. The seismic risk of south-west coast of Portugal derives mainly from moderate earthquakes with local sources, as the 1531 and 1909 earthquakes, and large events from offshore sources, responsible for the 1755 earthquake (Carvalho et al., 2008). The main faults are located in the south-west coast and south of Portugal, near the Lisbon region, the Lower Tagus Valley, Évora and the Algarve region, especially in Cape of São Vicente and the Gorringe Bank (Ferrão et al., 2016)

A maximum observed intensities (MOI) map of Portugal was produced by Ferrão et al. (2016), reflecting the seismic activity that occurred between the years of 1300 to 2014, based on the Modified Mercalli Intensity (MMI) scale (Figure 3.1a). The zones of Benavente, Lisbon and Algarve present the highest intensities.

Silva et al. (2014) presented a complete study about seismic hazard and risk for mainland Portugal, including a map (Figure 3.1b) with the peak ground accelerations for rock for a return period of 475 years (for a probability of exceedance of 10% in 50 years). The higher values of PGA are in agreement with the exposed above, identifying the Lower Tagus Valley and the southwest of Portugal as the highest risk-prone regions. The work of Silva et al. (2016), along with Carvalho et al. (2008) and Sousa and Campos Costa (2009), were the basis of the Eurocode 8 formulations about seismicity and seismic hazard in Portugal.
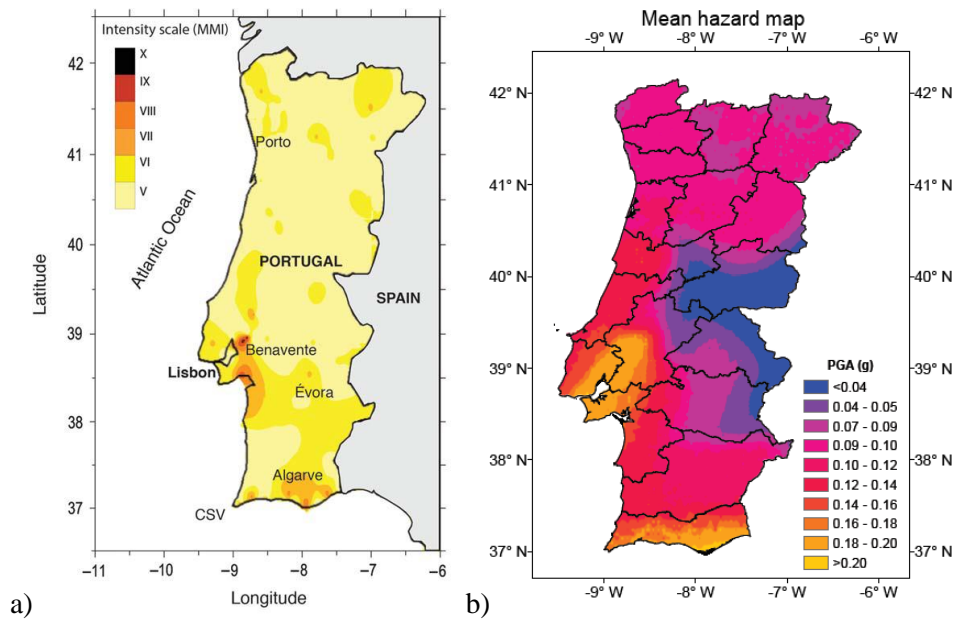
Figure 3.1 – a) MOI map (Ferrão et al., 2016); b) Mean seismic hazard map (Silva et al., 2014)

3.2.1. SEISMIC DESIGN: APPLICATION OF EC8 IN PORTUGAL

The EN Eurocodes are a series of European Standards that define the technical rules for the design of civil engineering works and contribute for a more consistent and harmonised practice of engineering in Europe. Eurocode 7 focuses on the geotechnical design while Eurocode 8 specifically sets the normalisation for the design of structures for earthquake resistance. Although this work does not comprise design of structures, together, these two Eurocodes prescribe some useful information about the determination of the seismic action and the moment magnitude for each municipality in Portugal. The correct determination of these parameters is essential for every seismic and liquefaction analysis and is described here for the municipalities of Vila Franca de Xira and Benavente, where the experimental campaign was set up.

The National Annex of Eurocode 8 – Part 1 (NP EN 1998-1:2010) presents a map of the seismic zonation of Continental Portugal (Figure 3.2). The zones are represented for two types of seismic action, Type 1, that corresponds to a "far" scenario, earthquakes with epicentre in the Atlantic region, and Type 2, that corresponds to a "close" scenario, earthquakes with epicentre in the Continental territory. An example of Type 1 earthquake is the 1755 Lisbon earthquake and of Type 2 are the 1909 Benavente and the 1531 earthquakes, described in section 3.3 of this Chapter.
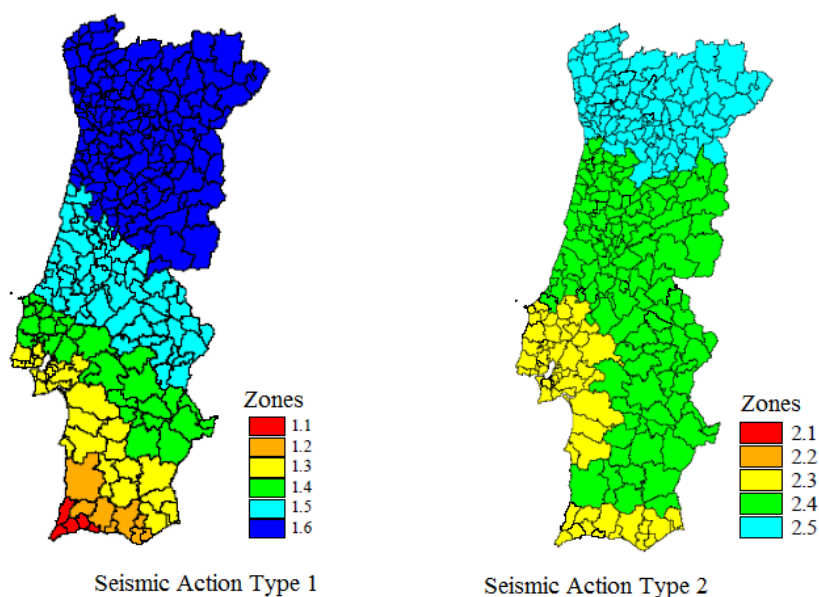
Figure 3.2 – Seismic zonation of Portugal mainland

The National Annex of NP EN 1998-1:2010 prescribes the values of reference peak ground acceleration on type A ground (a_{gR}) for each zone and type of seismic action. This value defines the zone hazard and has to be normalised according to the stratigraphic soil profile type, the building importance class and the elastic response spectrum parameters.

To each building importance class, an importance factor (γ_I) is attributed, that comprises the consequences of collapse for human life, the importance for public safety and civil protection in the immediate post-earthquake period and the social and economic consequences of collapse. The importance class is also related to the return period of the earthquake. The ground type takes into account the influence of local ground conditions on the seismic action and is used in the definition of the elastic response spectrum, characterised by the parameter *S*.

The calculation procedure to obtain the design peak ground acceleration is the following:

a) a_{gR} is defined according to the seismic zone for each seismic action type (Table NA.I of NP EN 1998-1:2010)

b) The building importance class is assessed, and the corresponding importance factor is determined (Table NA.II of NP EN 1998-1:2010)

c) The design ground acceleration on type A ground is $a_g = a_{gR} \times \gamma_I$

d) According to the stratigraphic profile, the ground type is determined (Table 3.1 of NP EN 1998-1:2010)

e) S_{max} depends on the ground type (Tables NA-3.2 and NA-3.3 of NP EN 1998-1:2010)

f) The elastic response spectrum parameter *S* is calculated according to S_{max} and a_g:

$$S = S_{max} \text{ for } a_g \leq 1 \ m/s^2$$

$$S = S_{max} - \frac{S_{max}-1}{3}(a_g - 1) \text{ for } 1 \ m/s^2 < a_g < 4 \ m/s^2$$

$$S = 1.0 \text{ for } a_g \geq 4 \ m/s^2$$

g) The design ground acceleration is defined by $a_{max} = a_g \times S$

The values of moment magnitude for each municipality are catalogued on Eurocode 8 – Part 5 (NP EN 1998-5:2010) and depend on the seismic action type and return period/importance class. The return period considered in this work was 475 years for a building importance class II.

Table 3.1 presents the results of these calculations for the municipalities of Vila Franca de Xira and Benavente. These municipalities are located very close to each other, so the seismic zone and moment magnitudes are the same for each type of seismic action.

Table 3.1 – Seismic action parameters for Vila Franca de Xira and Benavente

	Seismic action Type 1	Seismic action Type 2
Seismic zone	1.4	2.3
M_w	7.5	5.2
a_{gR} (m/s^2)	1	1.7
γ_I	1	1
a_g (m/s^2)	1	1.7
Ground type	D	D
S_{max}	2	2
S	2	1.77
a_{max} (m/s^2)	2	3
a_{max} (g)	0.20	0.31

3.3. HISTORICAL LIQUEFACTION IN PORTUGAL

The knowledge about historical liquefaction is a fundamental step to understand future occurrences, as liquefaction related earthquakes are normally a periodic phenomenon. Historical records of liquefaction in Portugal began after the 1531 earthquake, with epicentre in the Lower Tagus Valley, near Lisbon. However, these records were mainly based on the stories and reports of the affected population, such as the following descriptions:

"as terras baychas e húmidas abrirão gretas e bocas vomitando agoa e area com grande violência..." *("Low and humid lands with open cracks and holes, spewing water and sand with great violence")*

"observei uma das melhores ruas afundar-se na terra e todas as pessoas nelas…" *("I watched one of the best streets sink into the earth and all the people on them")*

After the 1755 Lisbon earthquake, complete information on seismic activity started to be available in Portugal. Jorge (1993) collected and catalogued information on the historical liquefaction occurrences in Portugal and proposed a liquefaction zonation map for the Portuguese territory (Figure 3.3). As the majority of information was qualitative and based on population reports, the liquefaction was categorised according to the quality of the information available. The classification includes three categories concerning liquefaction related descriptions (certain liquefaction, doubtful liquefaction, and very doubtful liquefaction) and one category concerning not direct descriptions of liquefaction but reports that could be related to the phenomenon (possible liquefaction). The coast of Portugal is the area where most earthquakes have occurred and more liquefaction phenomena were observed.
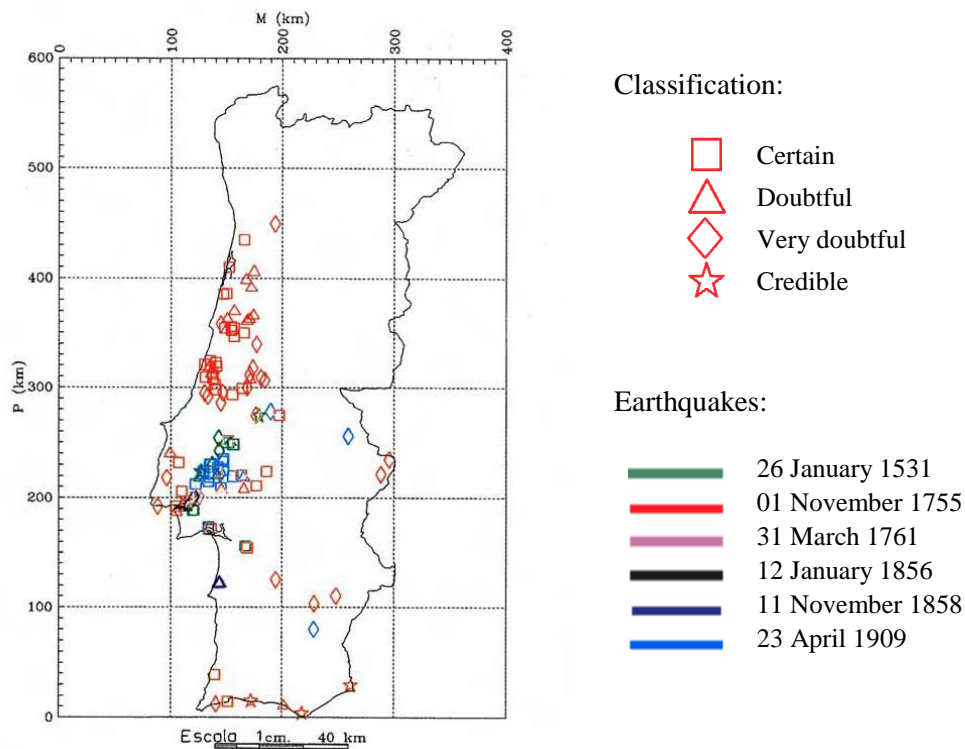
Figure 3.3 – Location of liquefaction events associated with historical earthquakes (adapted from Jorge, 1993)

Additionally, Jorge (1993) presented a liquefaction opportunity map, with the zonation according to the return period of liquefaction related earthquakes (Figure 3.4). The lower return periods are located in

the central and south west of Portugal, mainly in the Lower Tagus Valley and in Algarve. Combining the liquefaction opportunity and susceptibility maps, Jorge and Vieira (1997) presented a detailed representation of liquefaction potential zonation in Lisbon and Setubal regions (Figure 3.5). The Lower Tagus Valley presents high to very high liquefaction susceptibility.
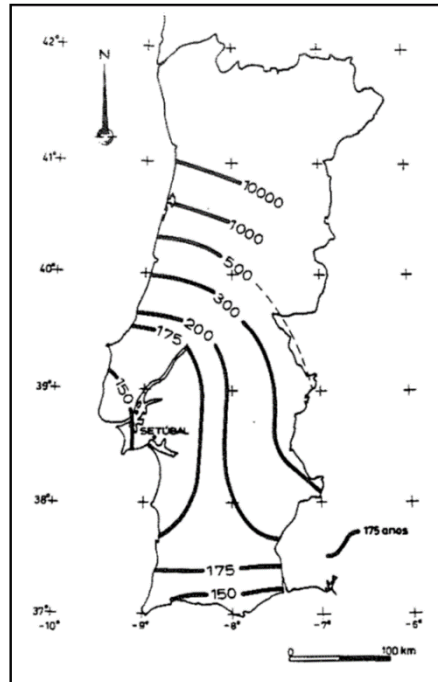
Figure 3.4 – Map of return period of the liquefaction opportunity (Jorge, 1993)
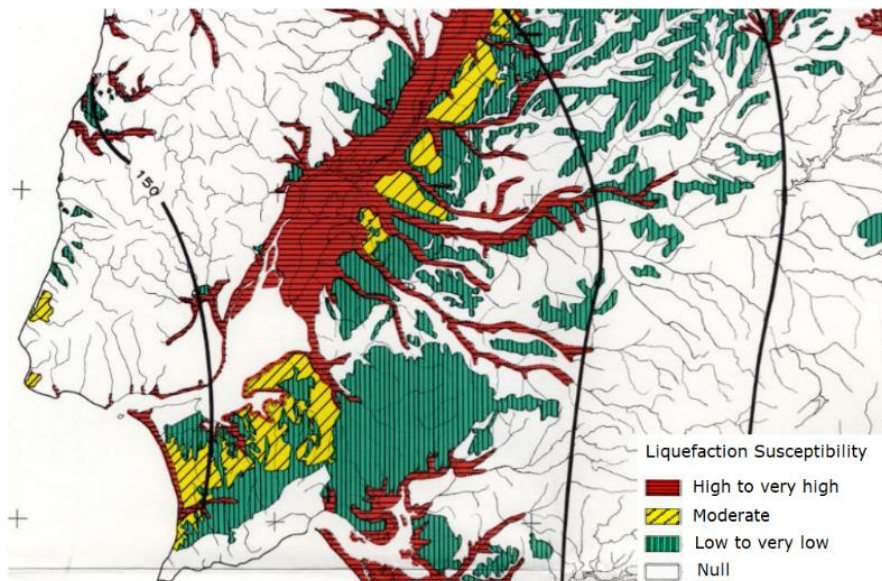
Figure 3.5 – Liquefaction zonation map of LTV region (Jorge, 1993, Jorge and Vieira, 1997)

More recently, Mazzocchi (2016) developed a structured catalogue of soil liquefaction based on Jorge and Vieira (1997) catalogue and the correlation of historical events to geology and to peak ground acceleration on stiff ground. Mazzocchi (2016) overlapped the map of Portugal geology with historical events and the peak ground acceleration on stiff ground (Figure 3.6). The majority of events occurred in limestones, sands and sandstones (light blue, yellow and light brown areas), and in areas with PGA higher than 0.075g. The events seem to be concentrated on the coast of Portugal, mainly in the Lower Tagus Valley (LTV), a zone with high liquefaction risk.
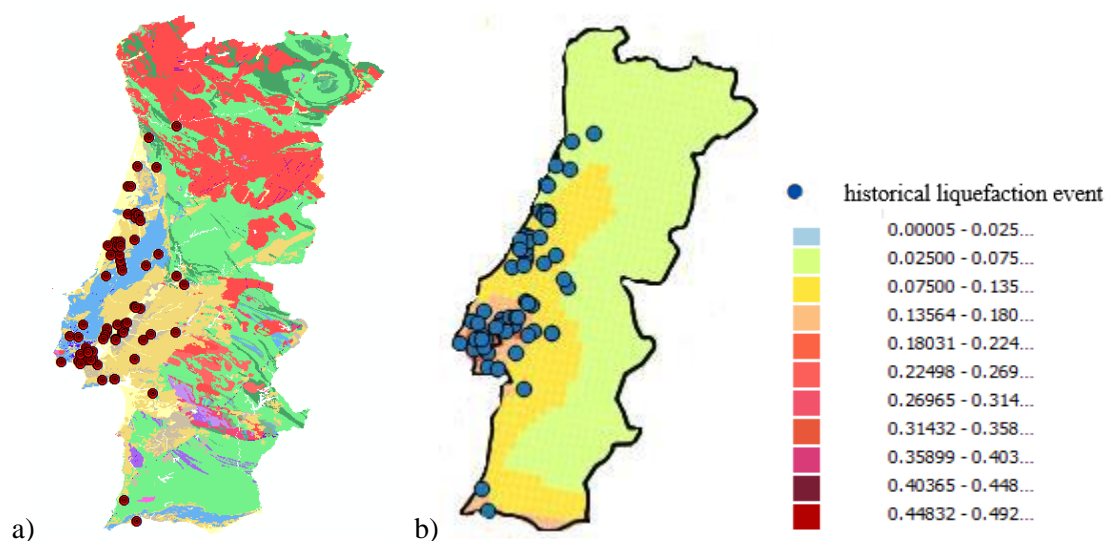
Figure 3.6 - Historical liquefaction events: a) Geology map; b) PGA map (Mazzocchi, 2016)

3.3.1. LISBON AND BENAVENTE EARTHQUAKES

Two of the most destructive earthquakes that took place in Portugal were the 1755 Lisbon earthquake and the 1909 Benavente earthquake.

The 1755 Lisbon earthquake occurred on November 1st, reaching a magnitude of 9 on the moment magnitude scale. It was responsible for many deaths and injured, as well as the destruction of almost the entire city of Lisbon. The earthquake, which epicentre was located in the Atlantic Ocean, about 200 km SW Cape St. Vincent, lasted 6 to 10 minutes and affected an area of 800 000 km^2, being considered one of the greatest seismic disasters to have struck western Europe (Chester, 2001).

Lisbon geology is complex and heterogeneous, with the western part constituted by basalt, limestone and marble of Cretaceous age and the south and west covered by Miocene formations. The centre is dominated by low-lying valleys filled with water-saturated alluvial sediments, highly susceptible to liquefaction hazard, which is the reason why this was the most affected area. Damage to structures and buildings was caused by liquefaction, landslides and slope failure (Chester, 2001). However, Lisbon

was not the only city affected by this earthquake. There are records of damage throughout Iberia and northwest Africa, and especially in the southern Portugal. Cities in Algarve such as Lagos, Portimão or Albufeira were almost entirely devastated. Figure 3.7a presents an isoseismal (MSK, Medvedev-Sponheuer-Karnik scale) map of the earthquake, showing the higher seismic intensities concentrated on the centre and south of Portugal.

The 1909 Benavente earthquake occurred on April 23rd, with epicentre near Benavente (Portugal). With a moment magnitude of 6.0, it is considered one of the largest crustal earthquakes in the Iberian Peninsula during the 20th century and caused several fatalities and the destruction of several towns near the Tagus river valley (Teves-Costa and Batlló, 2010). Figure 3.7b shows the isoseismal map and the intensity data points for this earthquake.
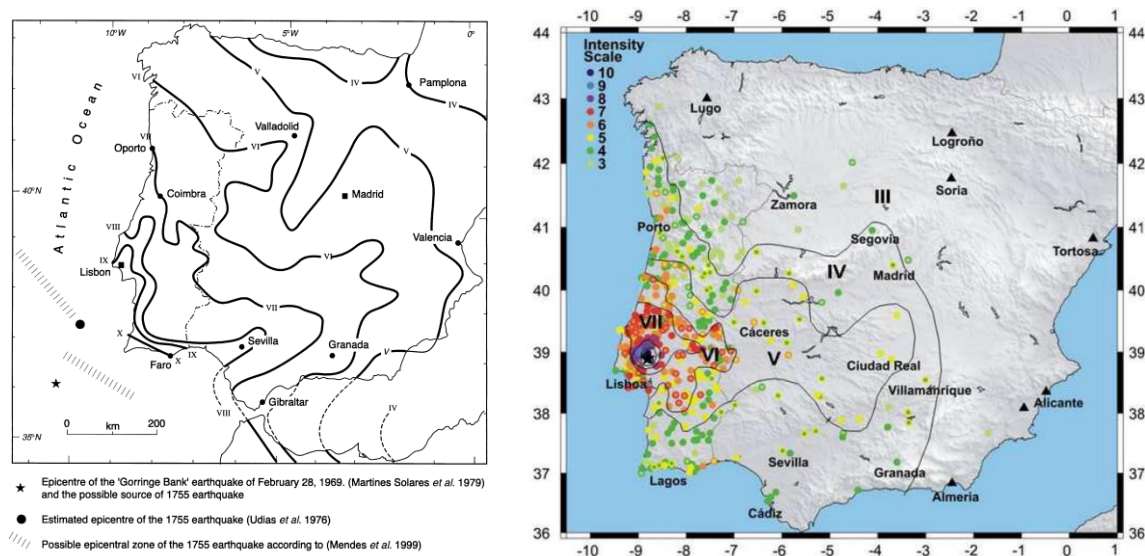
Figure 3.7 – a) Isoseismal (MSK) map of the 1755 Lisbon earthquake (Chester, 2001); b) Intensity data points and tentative isoseismal map of the 1909 Benavente earthquake (Teves-Costa and Batlló, 2010)

In the Tagus and Sorraia rivers alluvial plain, liquefaction related damages were observed, including sand boils, soil cracks and ejected sand (Teves-Costa and Batlló, 2010). The phenomenon is probably related to the combination of regional geology and local site effects. As described above, this is a zone highly susceptible to liquefaction. Cabral et al. (2013) focused their research in finding the source of the 1909 Benavente earthquake. However the location of the earthquake was difficult due to poor instrumental data, occurrence of site effects (as liquefaction) as a result of unconsolidated alluvia and fluvial terraces, and the possible interference of rupture directivity. The possible sources are an ENE reverse fault, an ENE hidden structure linking the Vila Franca de Xira fault and the Azambuja faults, or the hidden southern sector of the Azambuja fault (Cabral et al., 2013). Nevertheless, within their

research, some traces of liquefaction evidence were found (Figure 3.8), proving the occurrence of liquefaction related damages during the 1909 Benavente earthquake.
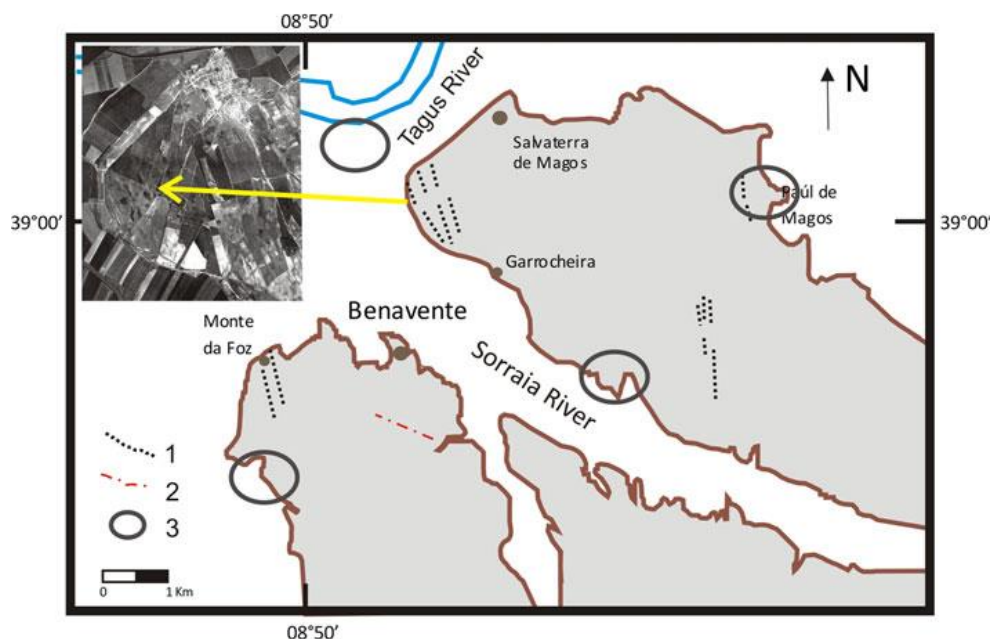
Figure 3.8 - Location of probable liquefaction features recognised in aerial photos (1:18,000 scale) of the Benavente region (crop of photo showing example). Grey area, Upper Pleistocene fluvial terrace; white area, alluvial plain of the Tagus and Sorraia rivers; 1, linear features interpreted as remnants of the surface trace of cracks injected with liquefied sands generated during the 1909 earthquake; 2, lineament corresponding to small scarp; 3, area with circular features interpreted as remnants of sand blows generated by the 1909 earthquake (Cabral et al., 2013)

3.4. SELECTION OF THE EXPERIMENTAL SITE AREA

As one of the main objectives of this research was to study liquefaction susceptibility, the selection of the adequate experimental site for the performance of field tests and collection of samples was very important. The liquefaction susceptibility analysis based on Eurocodes 7 and 8 requires the existence of loose granular soils, where the water level is close to the ground surface, and a certain level of seismic action. The study of historical liquefaction cases and the evaluation of the seismic risk in Portugal, presented above, showed that the Lower Tagus Valley was an area of interest. A more deep analysis on the geologic, geomorphologic and hydrologic settings, as well as the study of existing data in the area (in situ tests and boreholes), sustained the choice.

The experimental site is defined by two main areas located in a piece of land near the municipalities of Vila Franca de Xira and Benavente, where on April 23rd of 1909 the Benavente earthquake occurred. The area chosen belongs to the Lower Tagus River Valley (LTV) and is located on Lezíria Grande de Vila Franca de Xira, a property that is managed by the Associação dos Beneficiários da Lezíria Grande

de Vila Franca de Xira. The Lezíria Grande de Vila Franca de Xira is an area of 13420 ha and is divided by the National Road 10. Many construction works associated with the construction of the A10 motorway, a 12 km bridge and viaduct crossing the Tagus River, and the agricultural plains demanded an extensive experimental campaign with tests for geological and geotechnical characterisation. As described before, the land use is mainly agricultural and the area is surrounded by the Tagus and Sorraia rivers. Four experimental points were selected, where an extensive field test campaign was implemented (Figure 3.9). Saldanha (2017) analysed a series of geological and geotechnical reports collected from companies that developed works in the site over the years. These reports corroborate the information that the area presents soils with liquefaction susceptibility, making it the ideal experimental site.
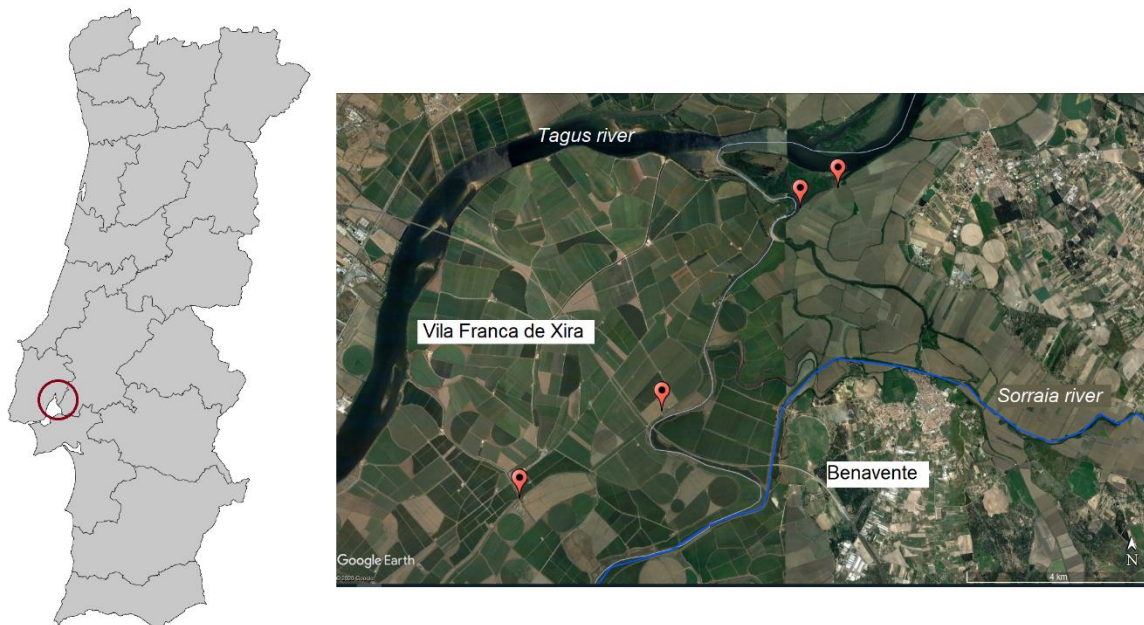
Figure 3.9 – Location of the experimental site

3.4.1. GEOLOGICAL, GEOMORPHOLOGICAL, AND HYDROGEOLOGICAL SETTINGS

The LTV is sited in the Lower Tagus Cenozoic Basin defined as "*a NE–SW elongated tectonic depression which evolved since the Eocene as a transpressive foredeep related to the tectonic inversion of the Mesozoic Lusitanian Basin (LB), located at the W*" by Cabral et al. (2013). It is composed of about 2000 m of Tertiary (Paleogene to Pliocene) sediments, Pleistocene fluvial terraces and about 70 m of Upper Pleistocene to Holocene alluvial soils. The depositional history and paleogeographic changes since ~ 20 000 cal BP, *i.e.*, calibrated years before present, considered before the origin of practical radiocarbon dating in 1950, were described by Vis et al. (2008), illustrating that the main contributing factors were the relative sea level rise and fluvial sediments supply. In the beginning (around 20 000 cal BP), Tagus was a deeply incised braided river. However, due to warmer climate during the deglaciation

period the river changed to a single-channel. The relative sea level rise caused a transgression in the Lower Tagus Valley, establishing extensive tidal environment. The fluvial wedge gradually filled the valley. After ~ 1000 cal BP, human land-use increased sediments input.

1 - Palaeozoic basement
2 - Jurassic sediments of LB
3 - Cretaceous sediments of LB
4 - Sintra Late-Cretaceous massif
5 - Paleogene sediments of the LTCB
6 - Miocene sediments of the LTCB
7 - Pliocene sediments of the LTCB
8 – Pleistocene fluvial sediments of Tagus river
9 - Holocene fluvial sediments of the Tagus river
10 - mapped fault
11 - mapped reverse fault
12 - isoseismals for the 1909 event (Teves Costa and Batlló, 2011)
13 - site of paleoseismic studies
AB - Algarve Basin
LB - Lusitanian Basin
LTCB - Lower Tagus Cenozoic Basin

Figure 3.10 – Geological Map of the Lower Tagus Valley region, adapted from Carta Geológica de Portugal, 1: 500,000 scale (Cabral et al., 2013)

The quantification of sediment volumes of the Lower Tagus Valley was presented by Vis et al. (2008, 2016), in the form of a representation of cross sections across the LTV (Figure 3.11). These cross sections illustrate the distribution of the deposited sediments throughout the years. The maximum flooding surface (MFS) defines the transition from a transgression (sea level rises relative to the land) to a regression (exposure above land of submerged seafloor) and is represented in Figure 3.11 between the blue and yellow sediments.
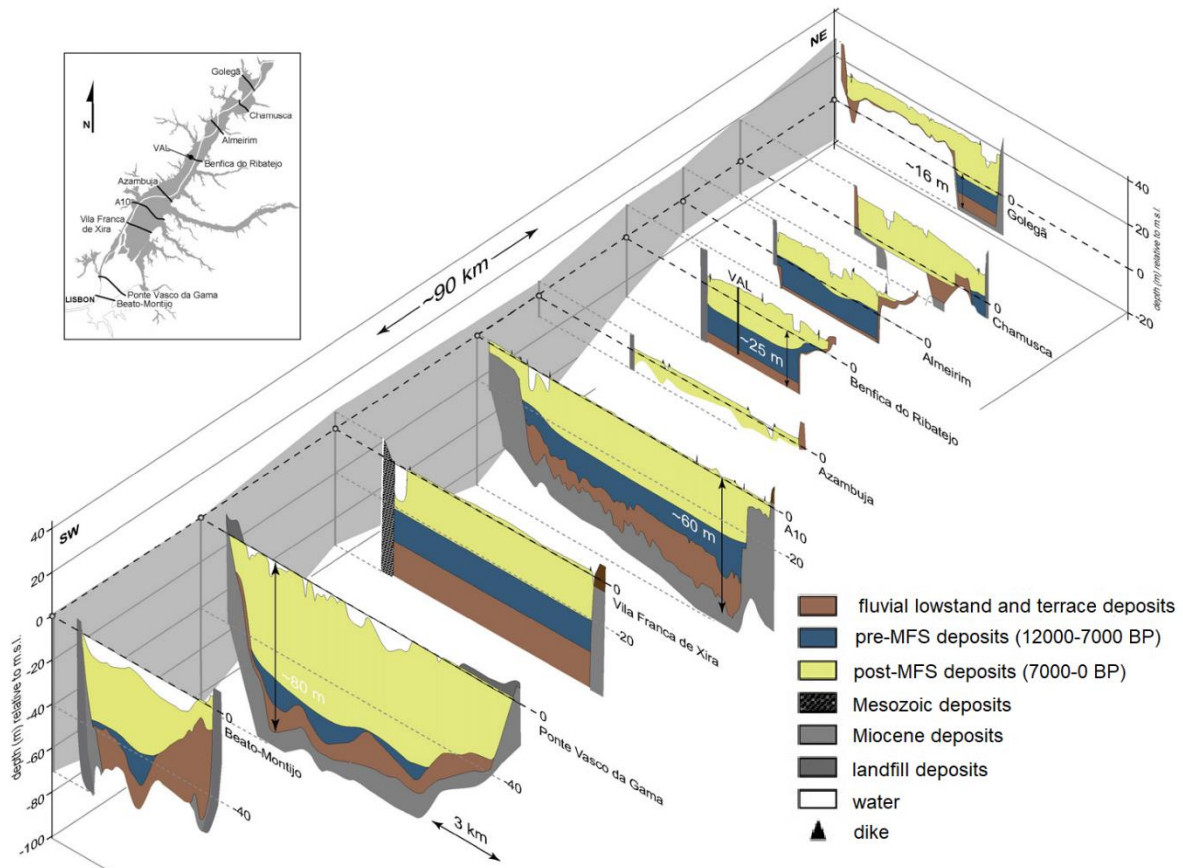
Figure 3.11 – Simplified 3D representation of cross sections across the Lower Tagus Valley (Vis et al., 2016)

The experimental sites selected for this work are located between the cross sections of Vila Franca de Xira and Azambuja, including the A10 profile. They are characterised by an upper layer of around 60 m of fluvial lowstand and terrace deposits, pre-MFS and post-MFS deposits, corresponding to the upper Pleistocene and Holocene alluvial cover. The depositional system of young Holocene alluvial soils is responsible for the coarse-fine interlayers detected on the CPTu profiles and for the laminations found in the natural soil samples.

Simões (1998) detailed the study of the subterranean water-level in the LTV. The underground flux has a global tendency for the Tagus River bed, where the discharge occurs following the orientation transversal to the river flow. The model admits the possibility of mixtures in the alluvium waters, some with origin in the Miocene in the right margin and others with origin in the Pliocene in the left margin. Therefore, the alluvium waters must have an intermedium physical and chemical composition. The Lower Tagus Cenozoic hydrogeological unit can be subdivided in three aquifer subunits: Miocene, Pliocene and Plisto-Holocene, considering the lithological heterogeneity of the sedimentary basin. These

subunits are composed of sandy deposits, sometimes permeable calcarenites, intercepted with clay layers.

3.5. EXPERIMENTAL SITE – LOCATION OF THE TESTS

In the experimental site of Lezíria Grande de Vila Franca de Xira, mechanical and geophysical in situ tests were performed, as well as the collection of high-quality soil samples for subsequent laboratory testing. An extensive experimental campaign, including standard penetration (SPT), piezocone penetration (CPTu), flat dilatometer (DMT), and geophysical SCPTu and SDMT tests, was carried out in four locations. The best location for the tests was initially chosen with the help of Dr. Sara Amoroso and Dr. Geologist Luca Minarelli, who defined the paleo-channels of the zone and guided the planning of the test locations. The owners of each piece of land were contacted and gave authorisation for field testing in each area.

Figure 3.12 presents the experimental site area, in the south-west of Portugal, near Lisbon, with the identification of each site and the distances between them. A total of four sites were selected, S1, S2, NB1, and NB2. S1 and S2 were the first sites where field tests were performed and are in Lezíria Grande de Vila Franca de Xira, while NB1 and NB2 are in the north of Benavente municipality and were investigated several months later. In NB1 and NB2, the main objective was the collection of soil samples with high-quality samplers Gel-Push and Dames and Moore, hence less penetration tests were performed. At each experimental site, different tests were carried out, as described in Table 3.2.

Figure 3.12 – Location of the four experimental sites

Table 3.2 – Field tests performed

Location	Ground water table depth (m)	Test performed	Depth (m)		Coordinates	
					Latitude	Longitude
S1	0.94	SPT	32.5		38.977081°	-8.875356°
		CPTu	27.6		38.977099°	-8.875400°
		SDMT	4		38.977178°	-8.875417°
		Sampling with Mazier	*		38.977128°	-8.875363°
S2	1.60	SPT	63.5		38.960431°	-8.911013°
		CPTu	22.8		38.959983°	-8.911465°
		SDMT	30		38.960335°	-8.910821°
		Sampling with Mazier	*		38.960475°	-8.911042°
NB1	2.50	CPTu	30		39.020935°	-8.830965°
		SDMT	20		39.020827°	-8.830960°
		Sampling with Gel-Push	*	F1	39.021163°	-8.830972°
				F2	39.021146°	-8.830975°
				F4	39.020957°	-8.830962°
				F5	39.020962°	-8.830940°
		Sampling with Dames and Moore	*	F3	39.021130°	-8.830976°
NB2	2.44	SCPTu	30		39.016881°	-8.840525°
		Sampling with Gel-Push	*	F1	39.016937°	-8.840471°
				F2	39.016929°	-8.840491°
		Sampling with Dames and Moore	*	F3	39.016916°	-8.840485°

* NOTE: the collection depth of high-quality samples is discussed in section 3.6.4.

The in situ tests were performed within the scope of two investigation projects in CONSTRUCT-GEO centre of FEUP, the National project "Liquefaction Assessment Protocols to Protect Critical Infrastructures against Earthquake Damage: LIQ2PROEARTH", funded by the Portuguese Foundation for Science and Technology (FCT) and the European project LIQUEFACT (Assessment and mitigation of liquefaction potential across Europe: a holistic approach to protect structures/infrastructures for improved resilience to earthquake-induced liquefaction disasters), funded by the European Union's Horizon 2020 research and innovation programme.

The collaboration of external companies was essential for the performance of field tests with the quality required for this research, and the help of many people and collaborators allowed obtaining high quality test results and samples for laboratory testing. The boreholes for the SPT tests and Mazier sampling

were executed by the company Teixeira Duarte – Engenharia e Construções, S.A., under directions of geologists Dr. Costa Vilar and Pedro Nunes. The CPTu and SDMT tests were performed by Instituto Politécnico da Guarda, under the supervision of Professor Carlos Rodrigues. The Gel-Push and Dames and Moore sampling campaigns were performed by Teixeira Duarte – Engenharia e Construções, S.A. in collaboration with the Italian company TECNOIN.

3.5.1. EXPERIMENTAL SITE S1

The experimental site S1 was the first to be explored. Two boreholes were drilled, one for SPT testing and another, of larger diameter, where samples were retrieved using the Mazier sampler. The boreholes were 5 m away from each other. At around 4.5 m from the sample collection borehole, a CPTu test was performed and at 7 m north, a SDMT was carried out. However, the SDMT was not successful and only recorded the first 4 m depth. The ground water table was measured with a level probe inserted inside the CPTu hole and was located at 0.94 m from the ground surface. Figure 3.13 shows the relative location of every test performed at S1.
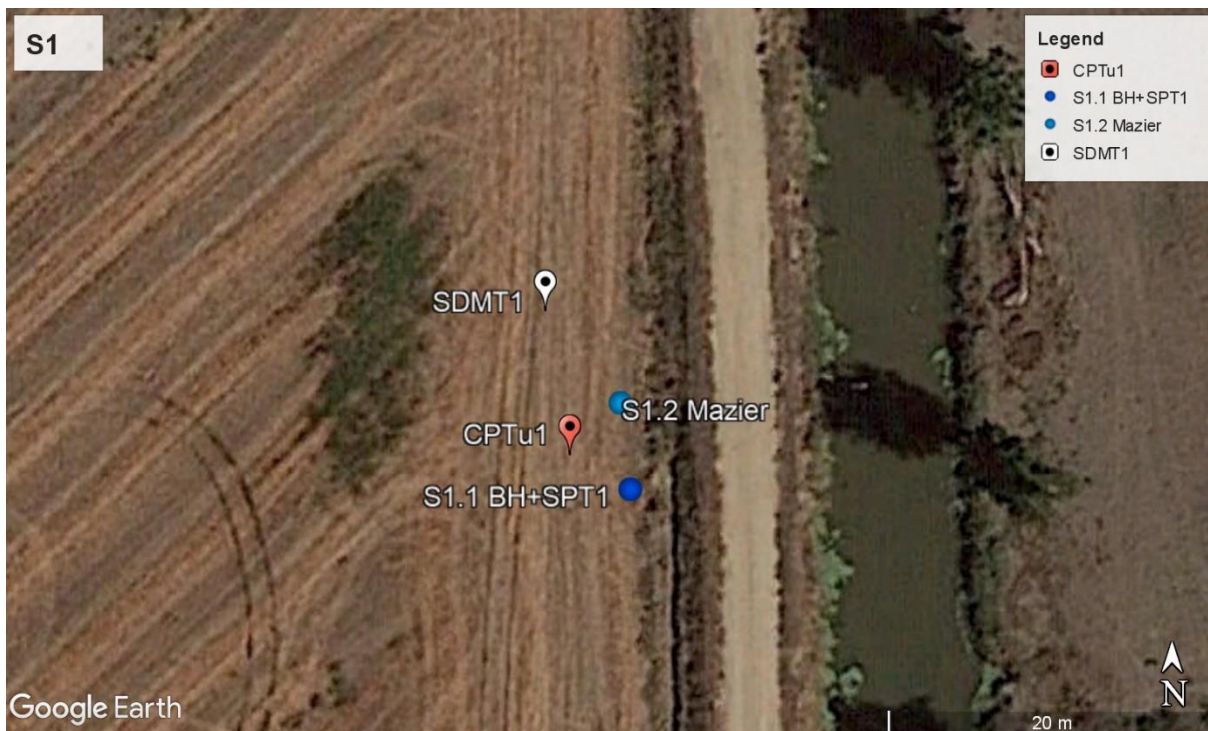
Figure 3.13 – Location of field tests in S1

3.5.2. EXPERIMENTAL SITE S2

The experimental site S2 was located south of S1, near a water path that is used to irrigate the adjacent agricultural fields (Figure 3.14). There, two boreholes 5 m apart were carried out, one for SPT testing and another for collection of samples using the Mazier sampler. A SDMT test, which includes direct measurement of seismic waves in depth, was performed at about 25 m from the sampling site. For equipment mobility and placement reasons, the CPTu test was performed on the other margin of the water path, at 67 m from the sampling borehole. However, the existence of this water path does not affect the measurements in depths, or the correlations between strata found with each test. The ground water table was found at 1.60 m depth.
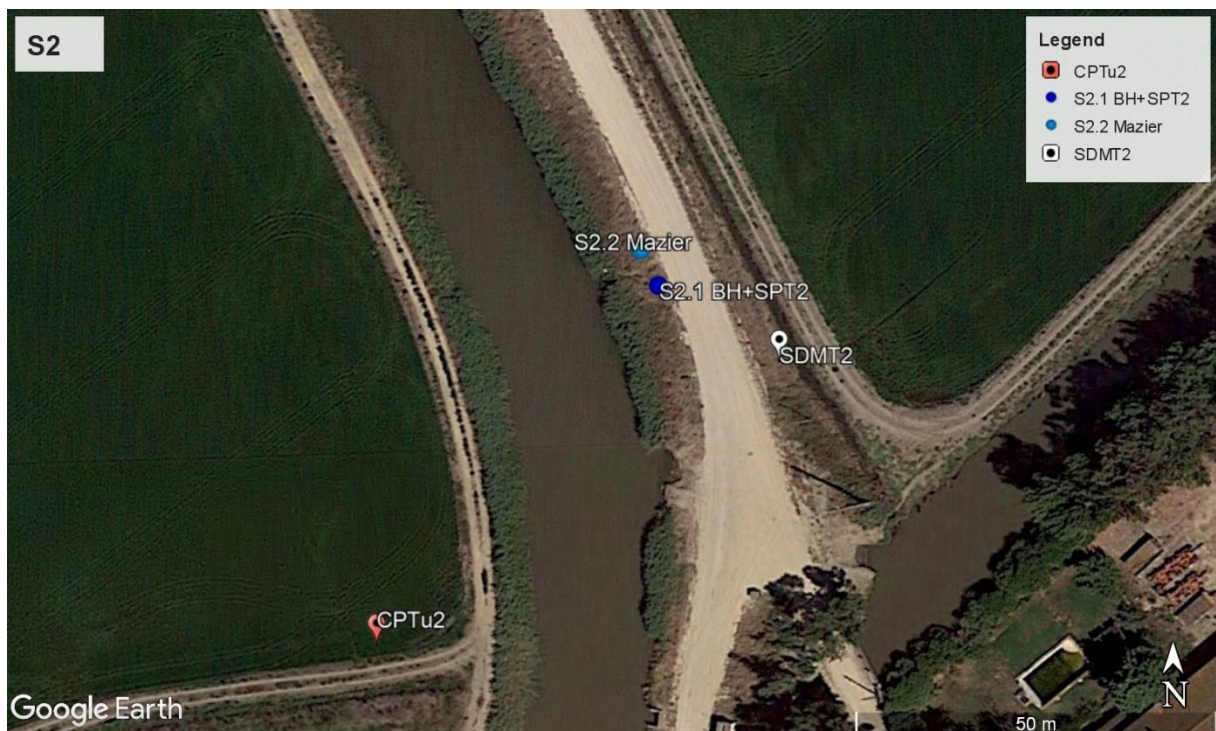
Figure 3.14 – Location of field tests in S2

3.5.3. EXPERIMENTAL SITE NB1

The NB1 site was set in an area in the north of Benavente. The geotechnical tests included one CPTu and one SDMT, 12 m apart (Figure 3.15). The ground water table, measured in the CPTu hole, was located at 2.50 m depth. One SDMT was performed 12 m south of the CPTu hole, with direct measurement of seismic waves. In this experimental site, the objective was to collect undisturbed samples of sands and silty sands, typically liquefiable materials. The CPTu soil behaviour type index profile showed a 4 m sand layer between 3 and 7 m depth. This was the selected layer for collection of soil samples, so five boreholes were performed, four using the Gel-Push sampler (NB1_F1, NB1_F2,

NB1_F4, and NB1_F5) and one using the Dames and Moore sampler (NB1_F3). For the first time in Portugal, the innovative sampling technique Gel-Push was performed to collect high-quality sand specimens, hence the necessity of performing many boreholes until the technique was controlled and the procedures optimised.
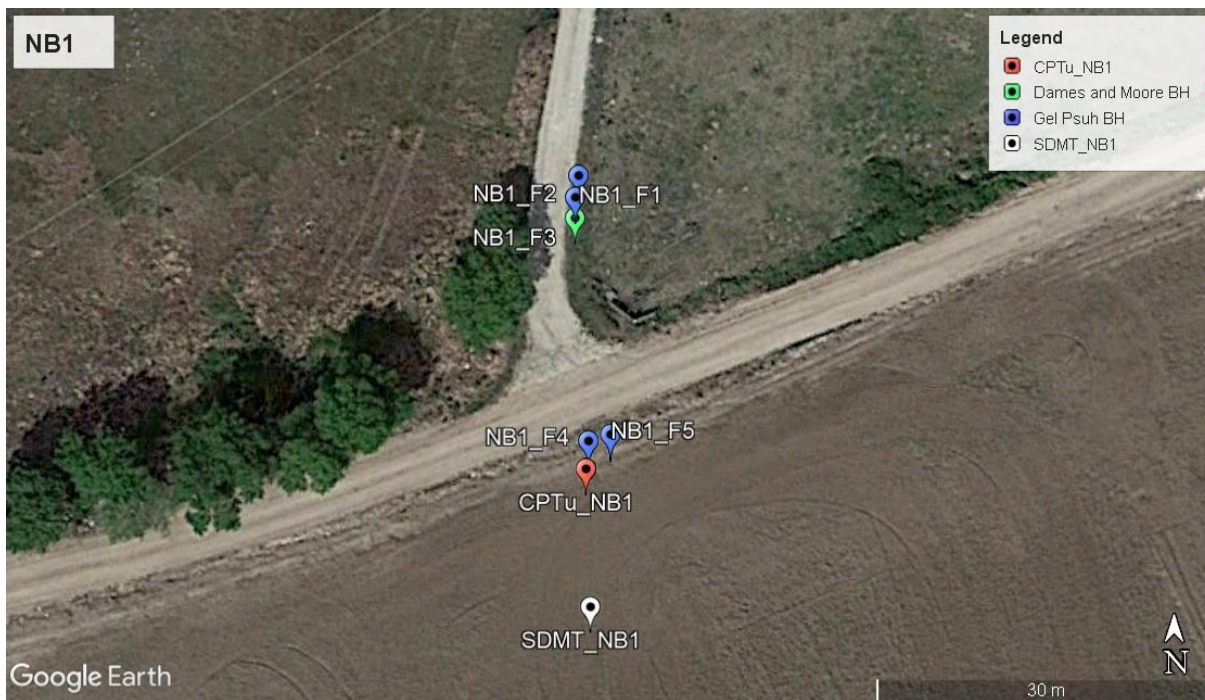
Figure 3.15 – Location of field tests in NB1

Moreover, a considerable quantity of soil (about 200 kg) was collected at around 4.5 m depth using a Cat Backhoe Loader. The soil was identified as "NB1" and was considered a case study soil for the region. In the laboratory, the soil was dried, homogenised and separated into small bags of 1.5 kg to be used in the performance of reconstituted tests, for the assessment of physical characterisation and mechanical behaviour under monotonic and cyclic tests (Figure 3.16).
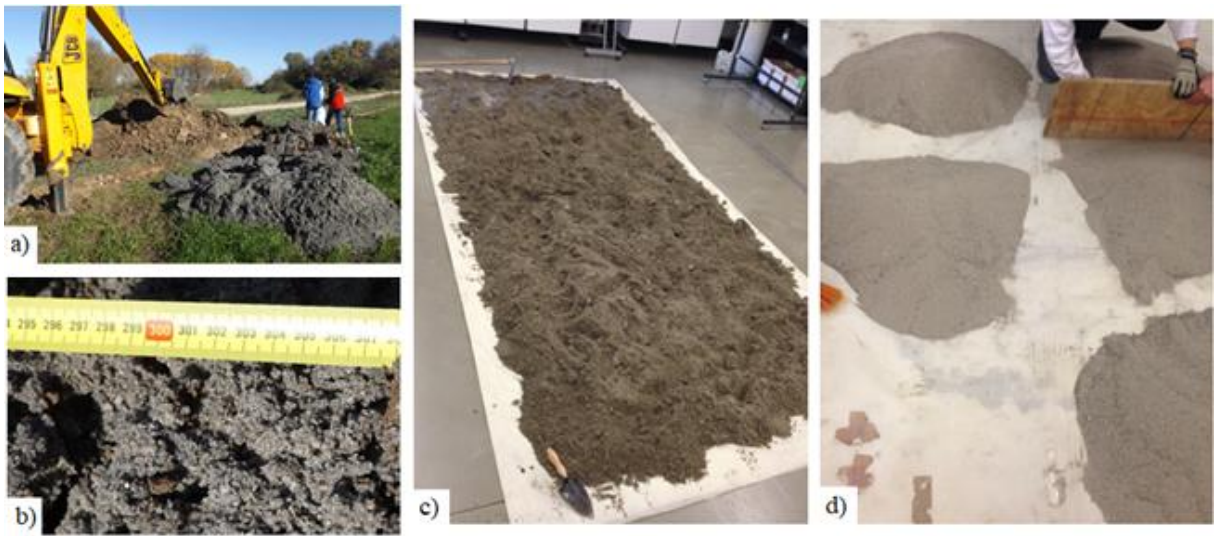
Figure 3.16 – a) Collection of the NB1 soil; b) soil in the field; c) drying process; d) homogenisation in the laboratory

3.5.4. EXPERIMENTAL SITE NB2

The experimental site NB2 was located south-east of NB1. One SCPTu was performed, with measurement of seismic waves, and three boreholes were carried out for sample collection, two using the Gel-Push sampler and one using Dames and Moore (Figure 3.17). The SCPTu is 7 m apart from the boreholes location, which are 2 m away from each other. The ground water table is at a depth of 2.44 m from the ground surface.

Figure 3.17 – Location of field tests in NB2

3.6. SAMPLING PROGRAMME

The sampling programme consisted of the extraction of high-quality soil samples from the four experimental sites. Three sampling techniques were implemented: Mazier sampler, Gel-Push sampler and Dames and Moore sampler. The use of Mazier sampler in Portugal is common and the sample collection was performed by Teixeira Duarte - Engenharia e Construções, S.A.. However, the use of Gel-Push and Dames and Moore is not widespread in Portugal. For the performance of the Gel-Push sampling, the Italian company TECNOIN collaborated with Teixeira Duarte and conducted the sampling procedures. The Dames and Moore sampling was performed by Teixeira Duarte: the company has adapted the drilling equipment for the acquired Dames and Moore sampler used in this work. The work performed allowed for the introduction in the Portuguese market of an innovative sampling technique, allowing the collection of higher quality samples. In this section, the three samplers and sampling procedures are described and recommendations for sample transportation, extrusion and storage in the laboratory are proposed.

3.6.1. MAZIER SAMPLER

The Mazier sampler is manufactured by the French company Seditech and is used for obtaining undisturbed samples of different types of soil. This sampler is composed of a rotary triple tube with outer and inner barrels, containing a PVC liner inside the tube. Its capacity for static boring and its flexibility in driving in harder soils make it an interesting sampler for research and industry purposes. Long samples of 1000 mm can be retrieved and the internal diameter of the PVC liner can vary between 61 and 108.5 mm. The sampler consists of three main parts: the sampling tube, the sampling head and the coring tube. A schematic diagram and a photo of the Mazier sampler are shown in Figure 3.18.
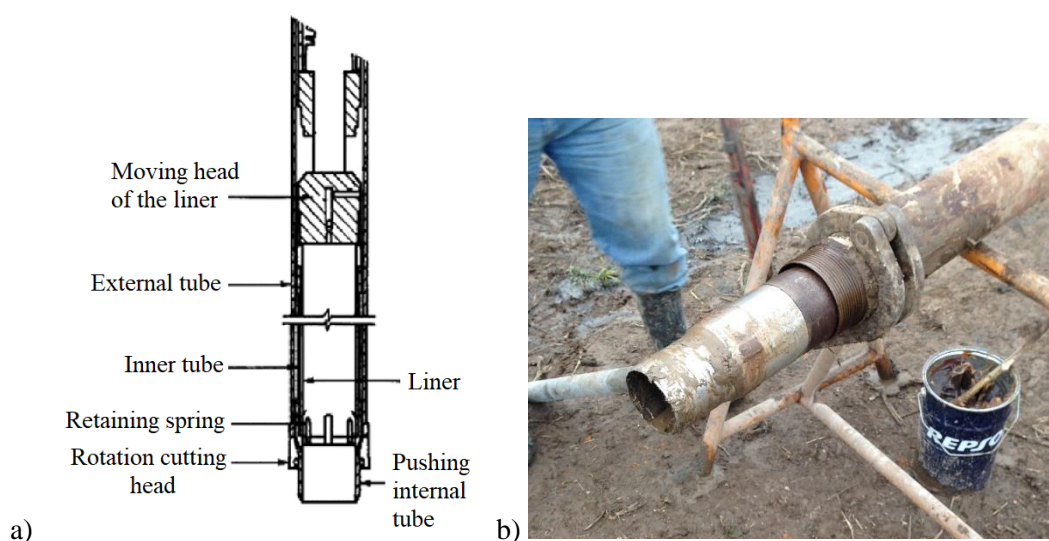
Figure 3.18 – Mazier sampler: a) diagram; b) photo of the equipment

The collection of samples is processed as follows. First, the sampler is lowered to the inside of the borehole until the required sampling depth. The drilling rods rotate, and a downward thrust is applied using the rig's hydraulic system. The drill cuts the soil, while the outer tube rotates. The inner tube stays static and the soil sample is collected within the PVC tube. When the required penetration length is achieved, the sampler is pulled out the borehole. The PVC tube is extracted from the sampler and the extremities are sealed with wax to avoid loss of water and drying. The principles of operation are schematised in Figure 3.19, for soft and hard soils, illustrating that the main difference is the advancement of the cutting shoe.

a) Coring Soft Material
(Inner tube extended)

b) Coring Harder Material
(Inner tube retracted)
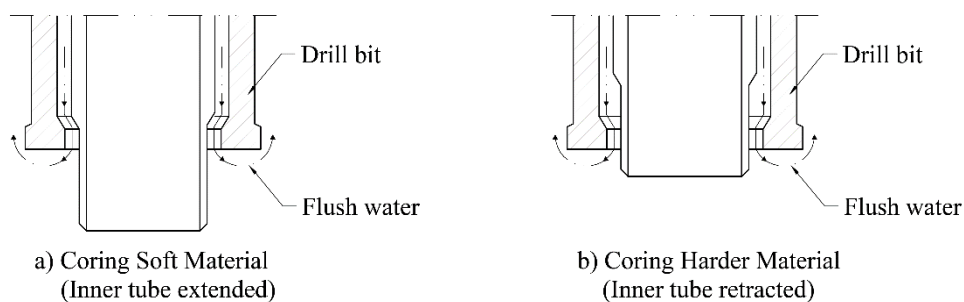
Figure 3.19 – Schematic operation of Mazier cutting shoe

3.6.2. GEL-PUSH SAMPLER

The Gel-Push technique was introduced by Kiso-Jiban Consultants, a Japanese geotechnical consulting company, and proved to collect high quality undisturbed samples from sites where recent earthquakes have occurred (Lee et al., 2012; Taylor et al., 2012; Ishihara et al., 2016; Viana da Fonseca et al., 2019a). This sampler is composed of a triple core barrel and its name derives from the use of a viscous polymer gel as the drilling fluid. The innovative use of a polymer gel (lubricant) reduces friction during sampling and during extrusion, preventing the sample tube friction to increase the stress on the sample. The gel also supports the samples standing and prevents slaking during laboratory extrusion.

There are four sampler line-up models of Gel-Push (from now on referred as GP), GP-Drilling, GP-Rotary, GP-Triple and GP-Static, which differ in terms of the penetration method, the sample diameters available and the material intended to be collected. The GP-Static (GP-S) was used in this work and is described in detail herein. Further information on the other models can be found in Mori and Sakai (2016) and in Stringer et al. (2015). Contrary to the other GP samplers, the GP-S is a static penetration sampler that follows the concepts of fixed-piston sampling (Mori and Sakai, 2016). It has a triple core barrel that includes three pistons: a fixed stationary piston, the sampling tube-advancing piston and the

core-catcher activating piston (Figure 3.20). The GP-S collects samples with 73.5 to 75.5 mm of diameter and is recommended to obtain high-quality samples of silt, sandy silt and loose sand.
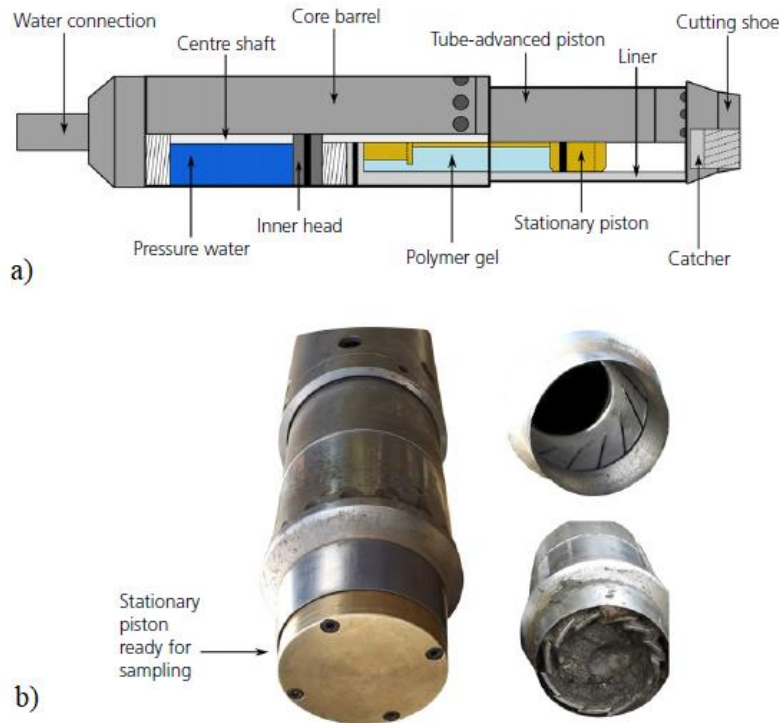
Figure 3.20 – GP sampler: a) schematic view; b) field operation (Molina-Gómez et al., 2020a)

The sampling procedure is represented in Figure 3.21. The sampler is assembled, and the gel is prepared at a concentration ratio of 1% v/v of the viscous polymer in clean water and inserted into the device. The polymer solution flows between the sample tube and the inner tube of the sampler and is injected to coat around the soil sample concurrently with penetration of the sampler. The sampler is placed carefully on the surface of the soil at the base of the borehole and the sampling tube advancing piston is activated by hydraulic pressure and pushes the shoe, the sampling tube and the liner tube downwards into the ground simultaneously. At the same time, the polymer solution is dispensed to coat the sample and the exterior wall of the sampling tube, lubricating it and reducing the penetration resistance. After reaching the maximum length (1 m), the core catcher activating piston is triggered. The piston forces the liner tube to move down, causing the core catcher to lower. The catcher fins extend out and compress the cored sample, preventing the sample from falling out of the sampling tube while it is retracted from the ground.
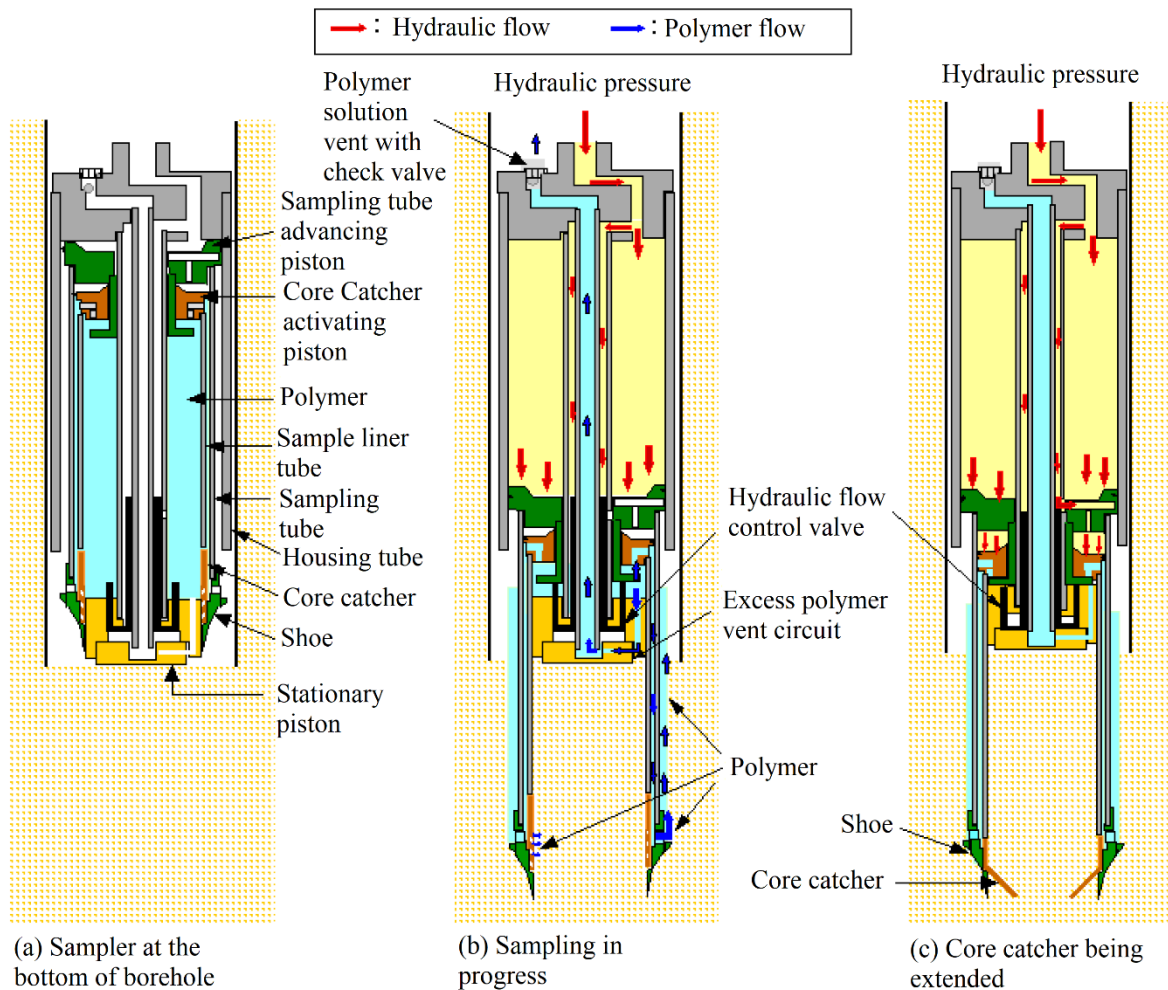
Figure 3.21 – GP-S operation scheme (adapted from Mori and Sakai, 2016)

3.6.3. DAMES AND MOORE SAMPLER

The Dames and Moore (D&M) sampler is a device that operates with the same principles as the Osterberg-type hydraulic activated fixed piston sampler, and has been used for the collection of high-quality soil samples mainly in fine sands and silty soils (Bray and Sancio, 2006; Markham et al., 2016). The equipment has some improved characteristics that allow the collection of undisturbed soil samples. The fact that the liner is made of smooth brass and is only 50 cm long, minimizes friction between the tube walls and reduces disturbances in the soil during penetration. Moreover, the existence of a neoprene skirt seal in the transition of the pressure cylinder with the lines, prevents the entrance of disturbed soil from the bottom of the borehole in the liner. The seal is also responsible for keeping the sample from falling into the borehole, by ensuring vacuum during the retrieval of the sampler.
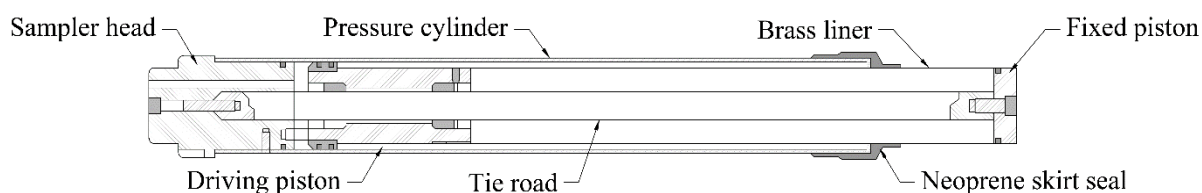
Figure 3.22 – D&M sampler

The D&M sampler has the same operation principle of the Osterberg (1973). The sampler is introduced in a pre-drilled borehole until the collection depth. A hydraulic pressure is applied, and a thin-walled tube or liner is carved in the soil, at constant rate. When it reaches the maximum length (50 cm), the tube stops and remains stationary for at least one minute. The sampler is then removed from the interior of the borehole and the liner is detached from the sampler and sealed. The operation phases of a fixed hydraulic piston sampler, such as the D&M, is presented in ASTM D6519-15 (2015) and detailed by Markham et al. (2016).

3.6.4. COLLECTION OF SOIL SAMPLES

The collection of high-quality samples was performed at the four experimental sites. At S1 and S2, the Mazier sampler was used, while at NB1 and NB2, samples were collected from different boreholes with Gel-Push and Dames and Moore. The focus of the sampling campaign was the collection of sands and silty sands, more susceptible to liquefaction. Hence, the results of soil behaviour type index of the CPTu performed at each site were used as a reference to select the depths of collection.

As was mentioned above, the Mazier sampling technique was implemented at S1 and S2, collecting samples with 1 m length and 85 mm diameter. According to the location of the most critical layers, 12 samples were collected at each site, illustrated in Figure 3.23 and Figure 3.24, for S1 and S2, respectively. Table 3.3 presents the percent recovery of each sample, i.e. the percentage of the PVC tube actually filled with soil. The overall percent recovery is high, meaning that this sampler was suitable for collecting soil of silty to sandy soils. No specific trend was found to relate the percentage of recovery and the type of soil, as the heterogeneous interlayered soil profiles make it difficult to identify a unique soil type for each sample. However, at S1 the lower recovery percentages correspond to silty sand to sandy silt (7 – 10.50 m and 25.50 – 26.50 m) and at S2 corresponds to clean sand and silty sand to sandy silt (6 – 8 m).
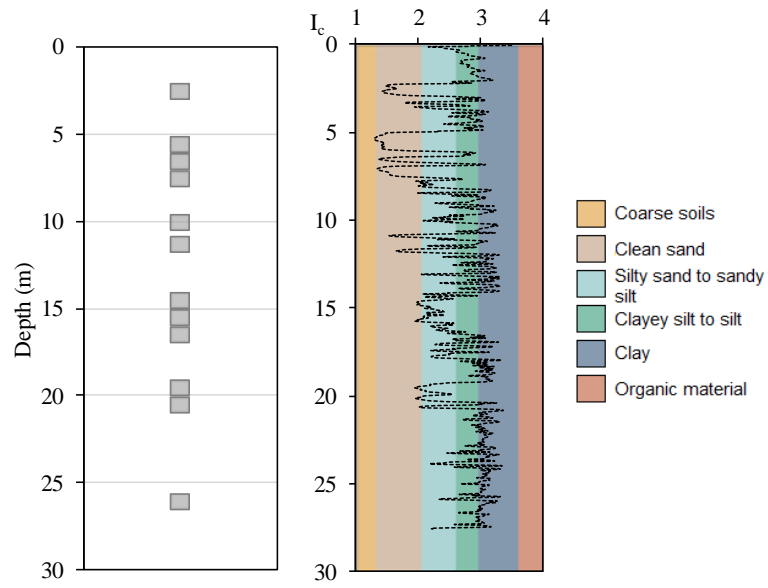
Figure 3.23 – Samples retrieved at S1 with Mazier sampler
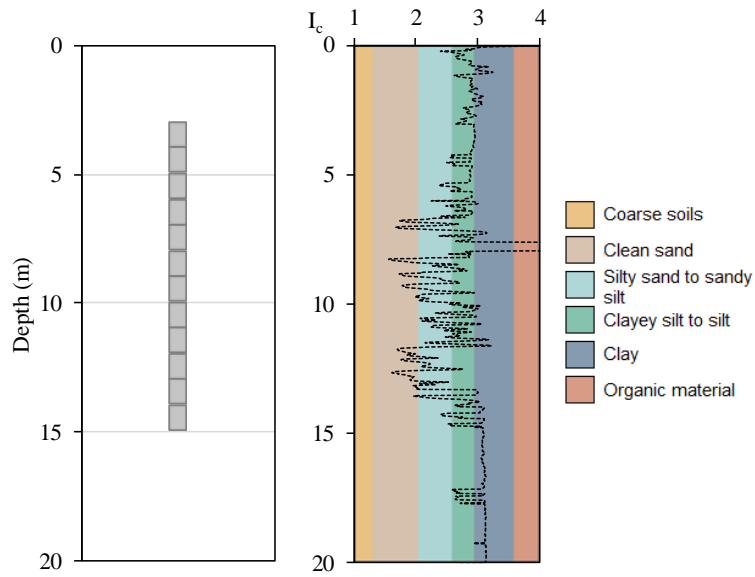
Figure 3.24 – Samples collected at S2 with Mazier sampler

Table 3.3 – Recovery percentage of each collected sample at S1 and S2

S1	Recovery (%)	S2	Recovery (%)
2 - 3 m	83	3 - 4 m	100
5 - 6 m	92	4 - 5 m	89
6 - 7 m	73	5 - 6 m	100
7 - 8 m	62	6 - 7 m	50
9.50 - 10.50 m	65	7 - 8 m	55
10.80 - 11.80 m	100	8 - 9 m	95
14 - 15 m	100	9 - 10 m	100
15 - 16 m	100	10 - 11 m	100
16 - 17 m	100	11 - 12 m	100
19 - 20 m	100	12 - 13 m	95
20 - 21 m	85	13 - 14 m	100
25.50 - 26.50 m	50	14 - 15 m	90

At NB1 and NB2, both Gel-Push (GP) and Dames and Moore (D&M) samplers were used. As the objective was to collect samples representative of the sand layers, at each site more than one GP borehole was performed, in order to retrieve a large number of good samples for laboratory tests. At NB1, a total of 12 samples were collected with GP and 16 with D&M (Figure 3.25). At NB2, 18 samples were collected with GP and 12 with D&M (Figure 3.26). The recovery percentages varied between 43% and 88% for the Gel-Push and between 80% and 94% for D&M. The higher recovery percentage of D&M can be related to the sampler size, as the D&M sampler is half the length of the Gel-Push. Moreover, the existence of the neoprene skirt, that secures the sample through vacuum, prevents it to fall during extraction from the borehole, increasing the recovery efficiency.
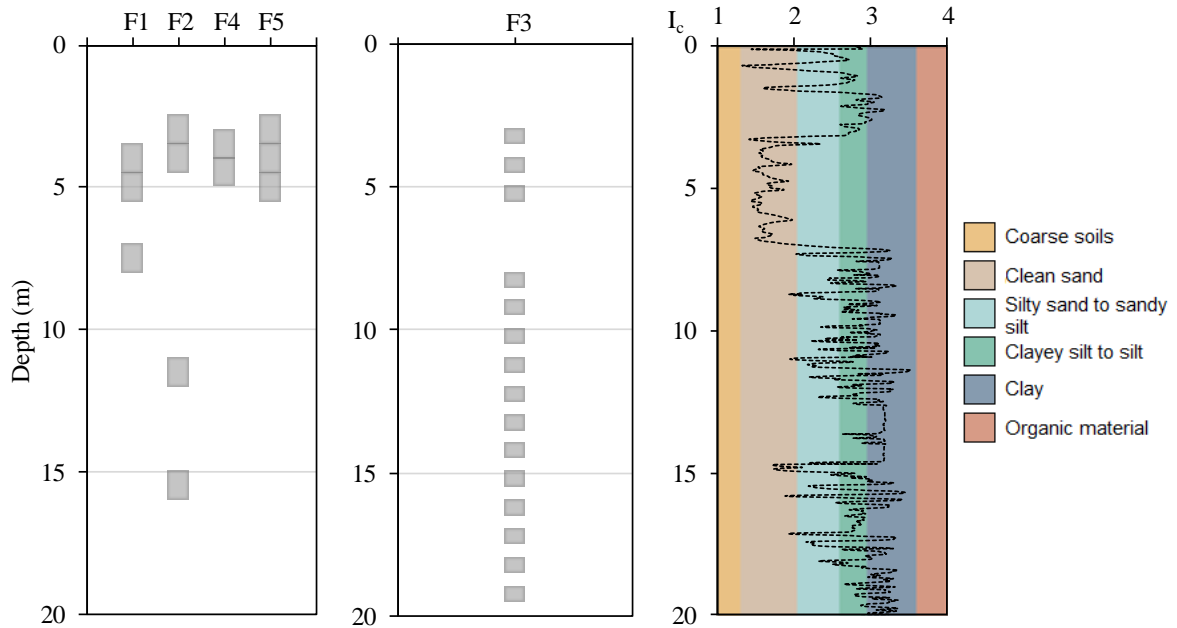
Figure 3.25 – Samples collected at NB1 with GP and D&M
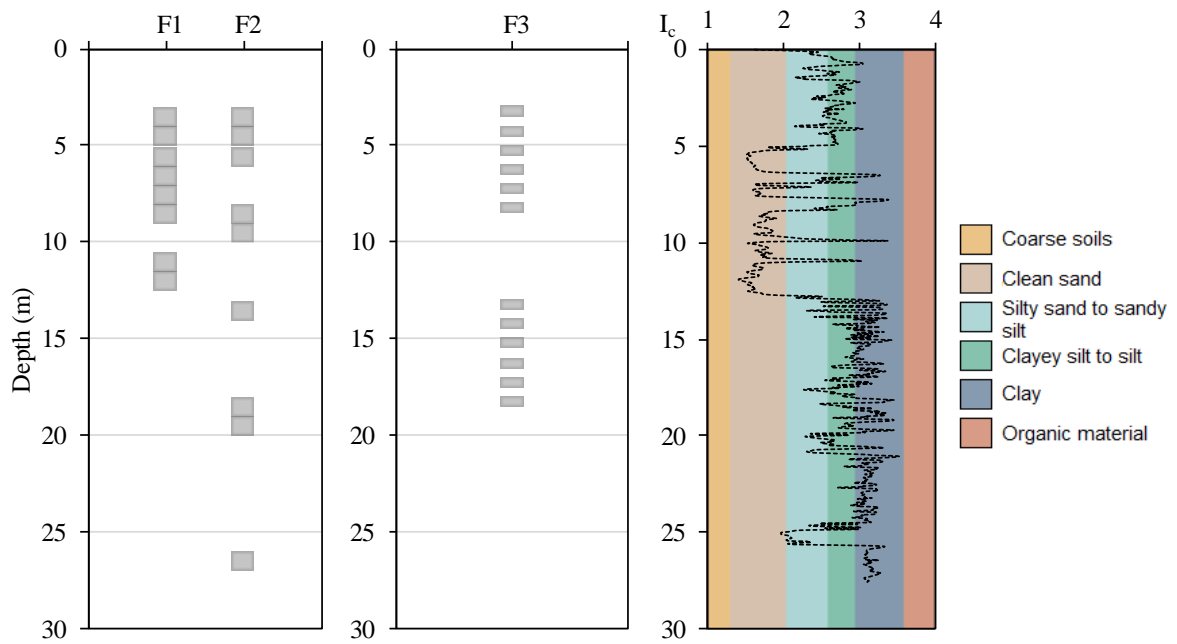
Figure 3.26 – Samples collected at NB2 with GP and D&M

Similarly to what other authors had verified (e.g. Mori and Sakai, 2016; Markham et al., 2016), the two samplers were successful in the retrieving of medium dense sands, fine sands, silts and clays. However, they were not able to collect coarse-grained soils, as the sampling tubes and liners were damaged during penetration in the soil. Contrary to the Mazier sampler, that penetrates the soil with a rotation movement,

the GP and D&M are static driven so, when reaching coarser soil layers, the metallic liners bended or were smashed (Figure 3.27). A compilation of the performance of both samplers according to the soil type is presented in Figure 3.28, where some examples of samples collected with both samplers are shown. It is evident that both samplers were suitable for the collection of most soil types. However, at 6 m to 7 m in NB1 and at around 10 m in NB2, the GP and D&M were incapable of collecting any samples, as the sampling tubes came out empty. This might be explained by two different reasons. On the one hand, the damaged cutting shoes might have prevented the soil to enter the liners. On the other hand, the very loose soil conditions or the fact that the core catcher of the GP-S could not close, might have caused the fall of the soil sample during extraction from the borehole.

Figure 3.27 – Gel-Push core catcher and D&M liner damage
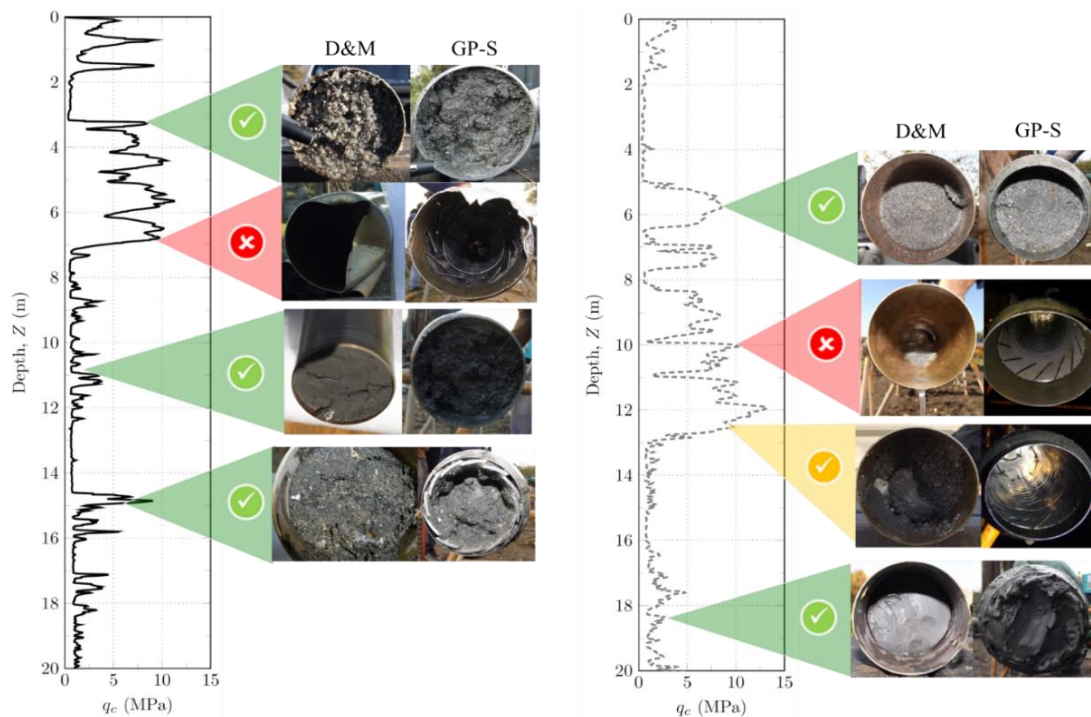
Figure 3.28 – Performance of GP and D&M: a) NB1; b) NB2 (Molina-Gómez et al., 2020b)

3.6.5. TRANSPORTATION, EXTRUSION AND STORAGE

To ensure the quality of the samples collected, certain care needs to be accounted for after sampling. Once extracted from the inside of the borehole, the sampler was carefully laid down horizontally to allow the liner to be removed from the equipment with the least vibration possible. If the liner was not filled with soil, the top or bottom parts of the tubes were filled with bags of soil, to prevent soil movement during handling of the liners. The sampling tubes were hermetically sealed using paraffin wax (in the PVC tubes from the Mazier sampler) or with plastic caps fixed with tape (in the case of the metallic tubes from GP and D&M samplers). This allowed the maintenance of the in situ water content of the samples. The liners were transported vertically, in the retrieval direction. The laboratory at FEUP is located at around 300 km from the experimental site, so specially designed wooden boxes were constructed, to transport the liners in the vertical position. The boxes were also adapted with a built-in vibration isolation system, consisting of foam on the bottom, top and around the liners, to reduce vibrations during transportation (Figure 3.29).

Figure 3.29 – Transportation box with liner confinement foam

The process of sample extrusion in the laboratory depends on the type of sampler used. These procedures will be explained in detail in section 6.5.1.1. At this point, it is important to note that the samples were extruded from the inside of the sampling tubes using a vertical hydraulic piston and smaller individual samples were prepared. To facilitate handling during test setup, the size of the specimens corresponded to the dimensions required for the triaxial chamber. The individual samples were confined inside PVC tubes, sealed with cling film and tape, and labelled. The name of each sample defines the site, the

sampler used, the borehole where it was collected, the collection depth and the order inside the sampling tube (see Figure 6.14 for details). They were individually measured (diameter and length) and weighted to estimate the unit weight. The samples were stored in boxes inside a room with controlled temperature and humidity conditions until testing, so the expected alterations in water content are minimum.

3.7. CHAPTER SUMMARY

This Chapter presented the results of a careful and detailed study of the experimental site where the field tests and collection of samples were carried out. The experimental site is located in the municipalities of Vila Franca de Xira and Benavente, places known to have been affected by major seismic activity in the past. Among the earthquakes that affected the area are the 1531 earthquake, the 1755 Lisbon earthquake and the 1909 Benavente earthquake, responsible for liquefaction related damages, described in historical records. The historical information collected, combined with the study of the seismic risk of Portugal allowed the selection of the pilot site, in an area known to have suffered liquefaction in the past. The geological, geomorphological, and hydrogeological settings of the zone, composed of Holocene alluvial soils, highlight the importance of further studies in this area, as it is very susceptible to liquefaction in case of another seismic event.

Following the characterisation of the experimental site area, the extensive experimental campaign carried out in the four locations selected was documented, including the type and location of all field tests performed. Moreover, the sampling programme was described in detail, focusing on the three samplers used (Mazier, Gel-Push, and Dames and Moore), on the samples collected and initial assessment of the performance of each sampler, and on the transportation, extrusion and storage procedures. The samplers proved to be competent for the majority of soil types collected, however the GP and D&M were incapable of collecting coarser soils due to a combination of factors: the damaged cutting shoes during the sampling process and the very loose soil conditions that might have caused the fall of the soil sample during extraction from the borehole. The investigation of the liquefaction susceptibility of the four locations and a more detailed sampling quality evaluation are presented in the following chapters.

4. FIELD TESTS RESULTS AND ANALYSIS

4.1. INTRODUCTION

The main objectives of the performance of field tests was to investigate the liquefaction susceptibility of the studied zone and identify the best strata for the collection of high-quality samples.

The following Chapter describes the field tests performed at the experimental sites, namely the standard penetration test (SPT), the cone penetration test (CPTu), the flat dilatometer (DMT), and the methods to determine the shear wave velocity profiling of the four experimental sites. A preliminary liquefaction assessment is performed based on each individual test.

The second part of this Chapter deals with the liquefaction susceptibility assessment of each experimental site, focusing on the influence of the consideration of fines content determined in the laboratory, the comparison between different methods of CPTu-based liquefaction analysis, and the elimination of transitional layers. There are different methodologies available to assess liquefaction potential according to the field test performed. When analysing the CPTu results, three different methodologies were compared. However, when comparing the different tests, the Boulanger and Idriss (2014) method was selected, so there is coherence in the comparisons. The shear wave velocities were assessed using direct methods based on the measurements of SDMT and SCPTu. However, some correlations with other field test parameters exist and were investigated and compared with the direct measurements, to assess their reliability.

The end of the Chapter presents a summary of the main findings and some recommendations for the study of liquefaction based on field tests. As this is a research work, it was possible to perform detailed field-testing using a variety of equipment, each with advantages and disadvantages. However, this type of detailed analyses is rare when dealing with the design of low to moderate risk projects, as they involve high costs and are time consuming. Therefore, this Chapter aims to compare the results obtained by different tests and suggest adequate procedures and methods to study liquefaction based on in situ tests. Moreover, it addresses questions such as the worth of performing index testing (as grain size analyses or Atterberg limits) for each layer and the influence of this information on liquefaction susceptibility

assessment, or the changes between different methods on the identification of critical layers, liquefaction potential risk and severity of the possible damage.

4.2. PRELIMINARY RESULTS OF IN SITU TESTS PERFORMED

As described in Table 3.2, a variety of field tests were performed in each experimental site. This section addresses the equipment and procedures to perform each test, as well as a preliminary assessment of the soil profiles and liquefaction susceptibility for each experimental site obtained with SPT, CPTu, DMT, and V_S measurements. The preliminary assessment was performed using Boulanger and Idriss (2014) method, and considering the fines content determined from empirical correlations. In section 4.3, the consideration of fines content determined in the laboratory and the use of different CPTu-based liquefaction assessment methodologies are discussed in more detail.

4.2.1. SPT TESTING

The Standard Penetration Test (SPT) consists of the driving at the bottom of a borehole of a hollow thick-walled tube by blows from a slide hammer with a mass of 63.5 kg falling from 0.76 m height. The penetration on the soil is facilitated by a bipartite steel sampler with a cutting ring at the end. The test result is the number of blows necessary for the sampler to advance 30 cm into the ground. The procedures are detailed in EN ISO 22476-3 (2005). Figure 4.1 shows a photo of the equipment.
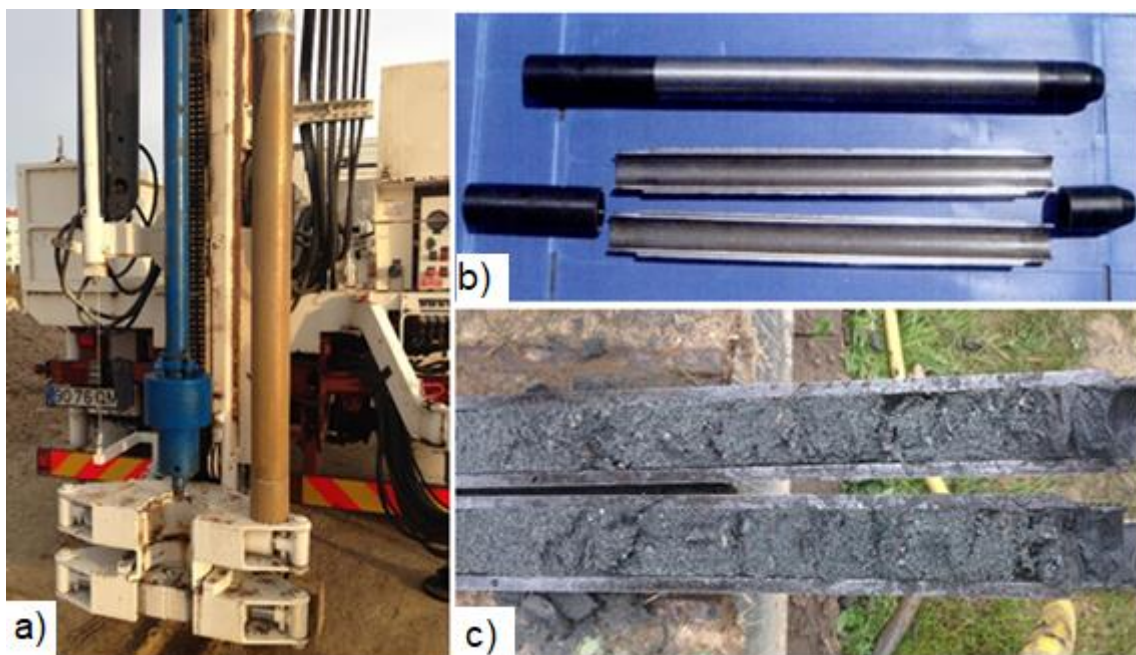
Figure 4.1 – SPT equipment: a) slide hammer; b) steel sampler; c) sample collected

The SPT has the advantages of being simple, low-cost, and suitable for various types of soil, from clays to fine gravels, at any depth. Another good feature is that it allows the collection of soil samples, as the soil remains inside the sampling tube, useful for the performance of physical identification tests in the laboratory. It is an interesting test for having an estimate of the soil types and existing geological-geotechnical profile of the site, based on soil samples collected.

However, the limitations of this test come from the empirical correlations for geotechnical parametrisation. From a single value, N_{SPT}, numerous resistance and stiffness parameters are obtained, through empirical correlations. It is questionable how this is possible. Additionally, it is obviously not suitable for identifying small changes in soil layers, as one parameter characterises a layer of around 50 cm, considered homogeneous. As Mayne et al. (2009) said "*(The SPT gives) a false sense of reality in the geotechnical engineer's ability to assess each and every soil parameter from the single N-value.*".

Despite efforts to improve the degree of standardisation of the SPT, many correlations were obtained based on tests performed with different kinds of hammers and sampling tubes, different energy systems and different degrees of efficiency, raising awareness for the consistency of N_{SPT} values used in the development of correlations to determine soil resistance to liquefaction.

In the present research, two SPT were performed at two different locations, S1 and S2 (see Figure 3.12). The SPT were performed with intervals of 1.00 m to fully characterise all crossed soil layers. The depth of the boreholes was 32.50 m and 63.50 m, in S1 and S2, respectively.

As mentioned before, the SPT allows the collection of a small soil sample. The grain size curve and Atterberg limits of samples from all depths were analysed in the laboratory. The SPT results in terms of normalised blow-count number, $(N_1)_{60cs}$, are presented in Figure 4.2, for both sites, and together with the grain size profile defined based on laboratory tests. A preliminary analysis of the liquefaction susceptibility, considering Type 1 and Type 2 of seismic action, defined in subsection 3.2.1, is also shown. The factors of safety against liquefaction are plotted only for the sandy layers (fines content lower than 35%). A colour code for FS_{liq} is represented, defining in red the FS_{liq} lower than 1, as this is the conventional minimum limit for liquefaction safety, in yellow the FS_{liq} between 1 and 1.25, a more conservative boundary prescribed in the Eurocode 8, and in green FS_{liq} higher than 1.25. Observing Figure 4.2, some layers have high to very high liquefaction susceptibility. The two profiles are different but converge on the fact that they both have sandy layers with low factor of safety against liquefaction. Profile S1 is composed of a 1.5 m thick crust of clay, followed by sand layers at 2.5–7.5 m, 10.5–16.5 m, 19.5–21.5 m and at 28.5 m. The FS_{liq} profile shows that a medium dense sand layer at 5–8 m is not susceptible to liquefaction, confirmed by high values of $(N_1)_{60cs}$. On the other hand, the other sandy layers have FS_{liq} below 1, being at risk of liquefaction for both types of seismic action. As for S2, it

presents a 10 m thick sand layer, between 5.5 m and 15.5 m, with high liquefaction risk, confined by low resistance clay layers. The consideration of the two different types of seismic action seem to not influence the selection of critical layers in terms of liquefaction susceptibility, as they coincide in most cases.
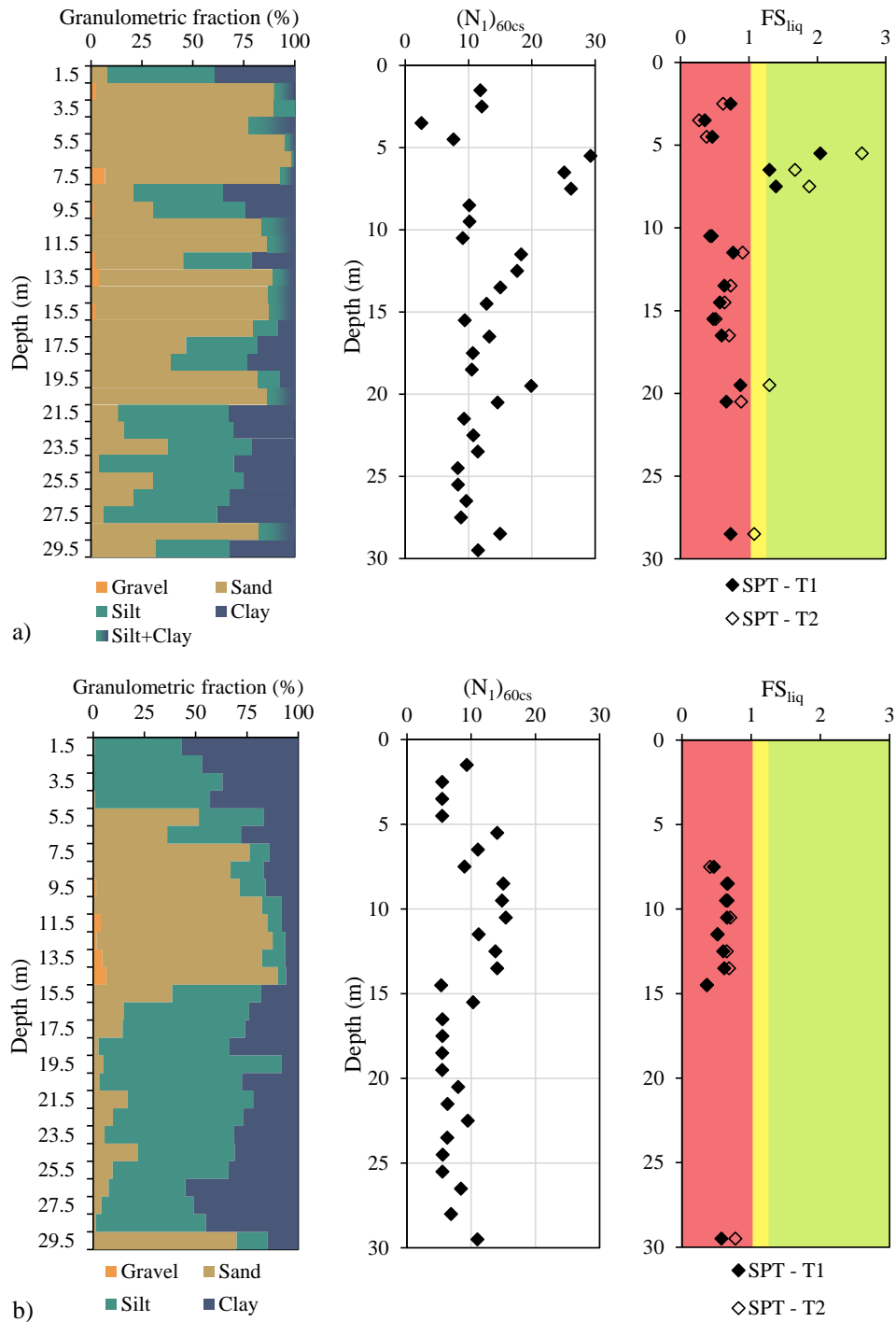
Figure 4.2 – SPT-based liquefaction susceptibility analysis: a) S1; b) S2

4.2.2. CPTu TESTING

The Cone Penetration Test (CPT) is currently one of the most used in situ tests, as it is fully automated and allows continuous in-depth results. The procedures are expressed in EN ISO 22476-1 (2012).

The CPT is a high complexity test, which requires a skilled operator to run and demands a high investment. However, it is recommended as it can be performed in soils from clay to coarse sand and provides a fast and continuous profiling, allowing the detection of thin layers interspersed with thicker layers. Thanks to a continually increasing and reliable database, the estimation of several parameters is done with strong theoretical basis in interpretation. It has the disadvantage of not allowing the collection of soil samples, hence the soil type is assessed indirectly according to the measured parameters or through the execution of boreholes in the vicinity.

The equipment is composed of a steel tip with a conical end (with cone base area of 10 cm^2 and apex angle of 60º) and a sleeve (134 mm extension and 150 cm^2 area), as shown in Figure 4.3. The CPTu consists of a piezocone which contains an annular filter located at the end of the sleeve, behind the cone tip, and transducer that measures the pore water pressure during the piezocone penetration into the soil.
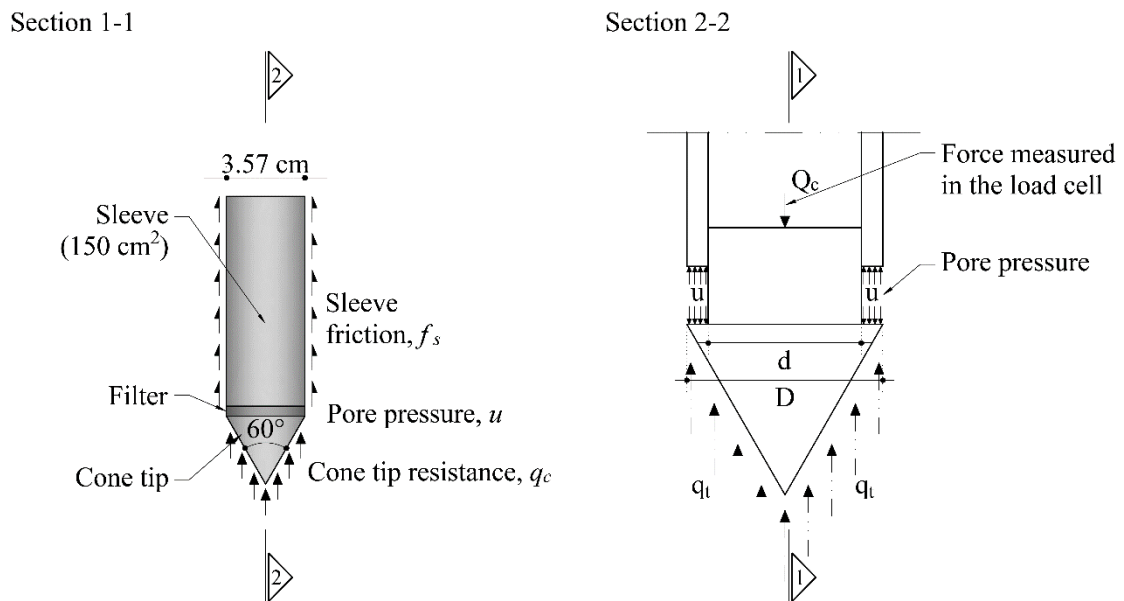
Figure 4.3 – CPTu piezocone scheme

The tip is continuously driven into the ground by means of a hydraulic system at a rate of 2 cm/s. A set of rods is added as the depth increases and an electric wire passes through the rods and transmits the signals from the transducers. The test allows the measurement of three parameters every 2 cm depth: the cone tip resistance, q_c, the lateral friction resistance, f_s, and the pore water pressure, u. The interpretation of CPTu tests allowed the development of classification maps and identification of the type of soils

crossed. The classification is based on the soil behaviour, which means that the resistance and pore pressure developed during cone penetration predict the type of soil present.

As the CPTu is considered the most complete test and the equipment was available for several days at the experimental site, it was performed at every site. In addition, at NB2 a seismic cone penetration test (SCPTu) was performed, by including shear wave measurements every 1 m.

The results were interpreted with Cliq ® software, developed by Geologismiki, sponsored by Gregg Drilling and Testing Inc. and with technical support and comments of Professor Peter Robertson, Professor Robb Eric S. Moss and Professor Ross W. Boulanger. The software allows the selection of different methodologies and the input of variables to adjust parameters, allowing more accurate analyses. The seismic conditions considered were $a_{max} = 0.20$ g and $M_w = 7.5$ and $a_{max} = 0.31$ g and $M_w = 5.2$ for seismic action type 1 and type 2, respectively (see Table 3.1). Moreover, to avoid calculation errors, a symbolic value of 0.01 kPa, that has no implication in the results, was introduced when q_c or f_s were zero.

The methodology used in the preliminary liquefaction susceptibility analysis was proposed by Boulanger and Idriss (2014) (from now on abbreviated to B&I2014). This approach was chosen as it is correlated with the SPT and DMT approaches selected and is useful for the comparison of different field test procedures performed below. However, there are other methodologies available that are also going to be considered further ahead in this work. For this preliminary analysis, the fines content was calculated with the formula suggested by B&I2014 method.

The cone resistance measurements, as well as the pore pressure developed during cone penetration, are presented in Figure 4.4 for the four testing sites. Besides, the soil behaviour type index and the factor of safety against liquefaction are also represented, with reference to the limits considered. In the FS_{liq} profiles, only soils with $I_c > 2.6$ are represented, as $I_c = 2.6$ is the commonly used limit value for the occurrence of liquefaction, since it separates the sand and clay behaviour types. Furthermore, it corresponds to FC of approximately 35% in the Robertson (2009) method, which was also defined in this research as the liquefaction susceptibility threshold.

The I_c plots show the soil type profile, based on the proposal of Robertson and Wride (1998). Simplified I_c profiles are also represented, defined by the approximation of the original I_c by constant values, as proposed by Cubrinovski et al. (2017). These simplified profiles consider: gravel and coarse sand ($I_c \leq 1.3$); clean sand ($1.3 \leq I_c \leq 1.8$); sands with low fines content ($1.8 \leq I_c \leq 2.1$); silty sand, sandy silt and non-plastic silt ($2.1 \leq I_c \leq 2.6$); and non-liquefiable silt or clay ($I_c \geq 2.6$). This soil classification is slightly different from the proposal from Robertson (1990), as it is focused on soil response to liquefaction. Thereby, silts, clays and organic soils are grouped in the non-liquefiable category, and the sandy soils

are sub-divided according to the fines content, as it is known that small variations in FC strongly influence liquefaction behaviour.
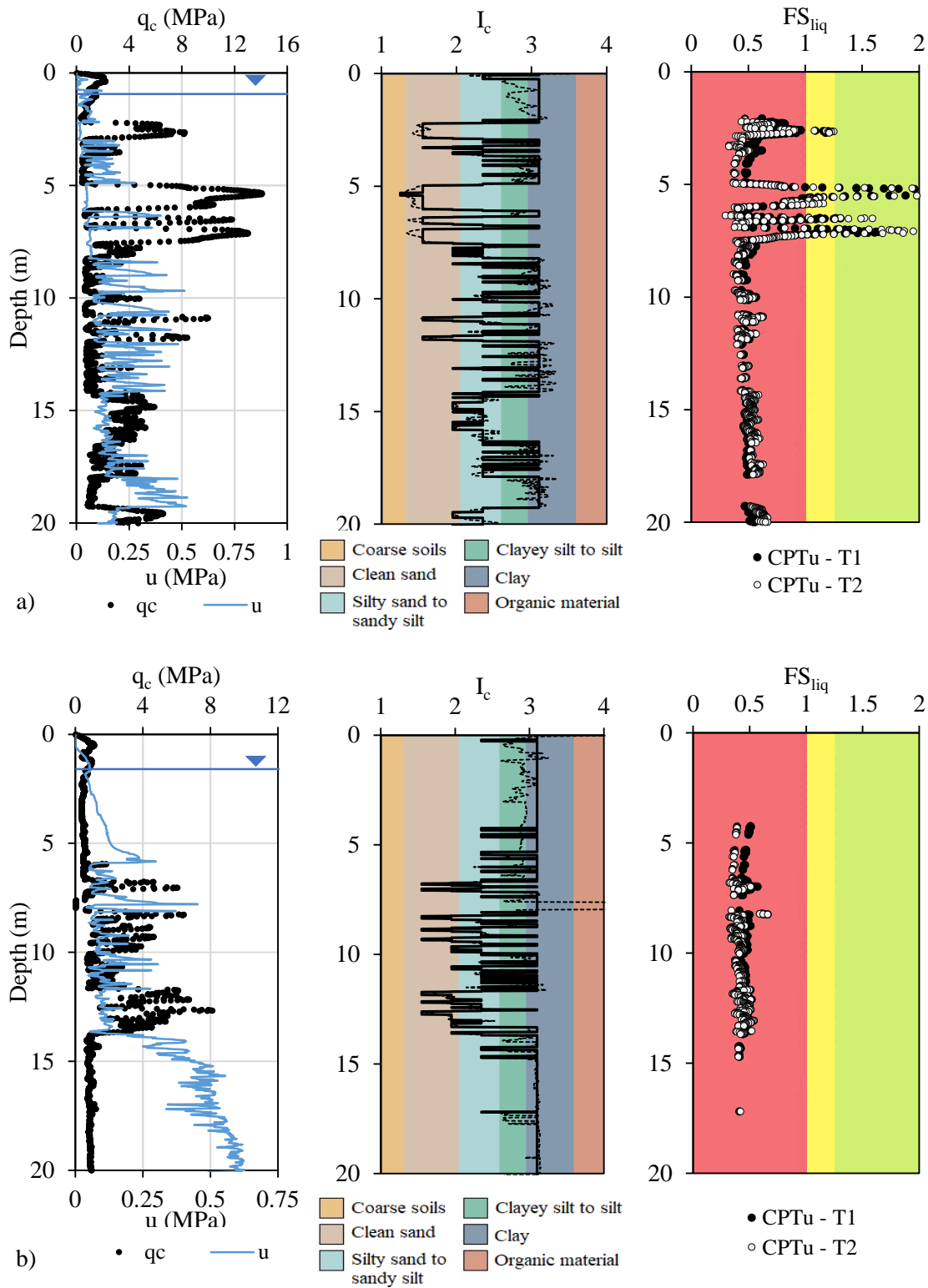
Figure 4.4 – CPTu-based liquefaction susceptibility analysis: a) S1; b) S2; c) NB1; d) NB2
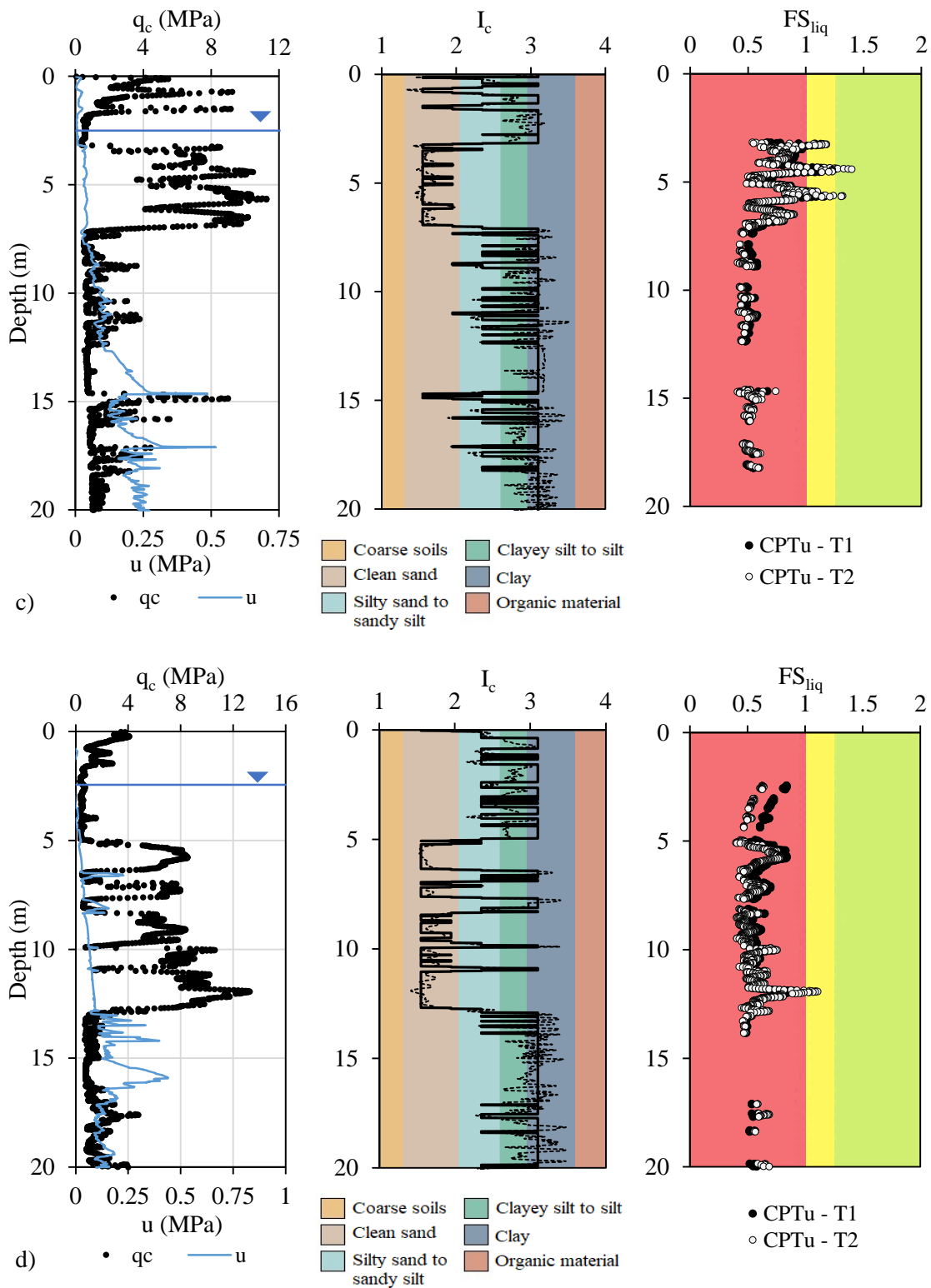
Figure 4.4 (continued) – CPTu-based liquefaction susceptibility analysis: a) S1; b) S2; c) NB1; d) NB2

Despite the variability among the different tests, all soil profiles show critical layers with liquefaction susceptibility.

Analysing profile S1, it is evident that it is a very heterogeneous profile, including many small layers of sand and clay. However, some clear layers are detected, with higher values of q_c and no excess pore pressure, corresponding to coarser-soil behaviour. Most of the profile is composed of sand-silt-clay layers, which makes it difficult to determine the liquefaction risk, as the behaviour of interlayer soils is complex. However, two liquefiable layers at 2 m to 3 m and at 5 m to 7 m are distinguished, although in some points the sand is more resistant and presents FS_{liq} greater than 1.

S2 profile follows the same trends, a very heterogeneous layer between 6 m and 14 m presents low factor of safety against liquefaction. The profile is composed of low resistant clay except for this middle layer of interbedded sand-silt-clay soils.

On the other hand, NB1 and NB2 present less interbedded layers, and show clear liquefiable sand layers. In NB1, the liquefiable layer is located at 3.5 m to 7 m, with no excess pore pressure and higher cone resistance. The critical layer presents most factor of safety against liquefaction lower than 1. Likewise, in NB2, a liquefiable sand layer is found at 5 m to 13 m. In both profiles, some silty layers are also classified as susceptible to liquefaction, being this more evident in NB1 profile. These coarse-fine interlayers were expected as they are characteristic of young Holocene alluvial soils, deposited over time due to river flow.

4.2.3. DMT TESTING

The Flat Dilatometer Test (DMT) was conceived by Marchetti (1980) and is commonly used to obtain the soil stratigraphy and estimate at rest lateral stresses, elastic modulus, and shear strength of soils. The equipment consists of a stainless steel cell with a bevelled end that is grounded at a rate of 20 mm/s. On one side of the blade, a flexible circular steel membrane with 60 mm diameter is attached to a displacement transducer in the inner face. The blade is shown in Figure 4.5, as well as the control unit equipment. The test procedures are detailed in EN ISO 22476-11 (2017). The result parameters obtained are the material index (I_D), the Horizontal Stress Index (K_D) and the Dilatometer Modulus (E_D). The soil type can be identified according to the I_D as: $0.1 < I_D < 0.6$ for clay; $0.6 < I_D < 1.8$ for silt; and $1.8 < I_D < (10)$ for sand (Marchetti, 1980).
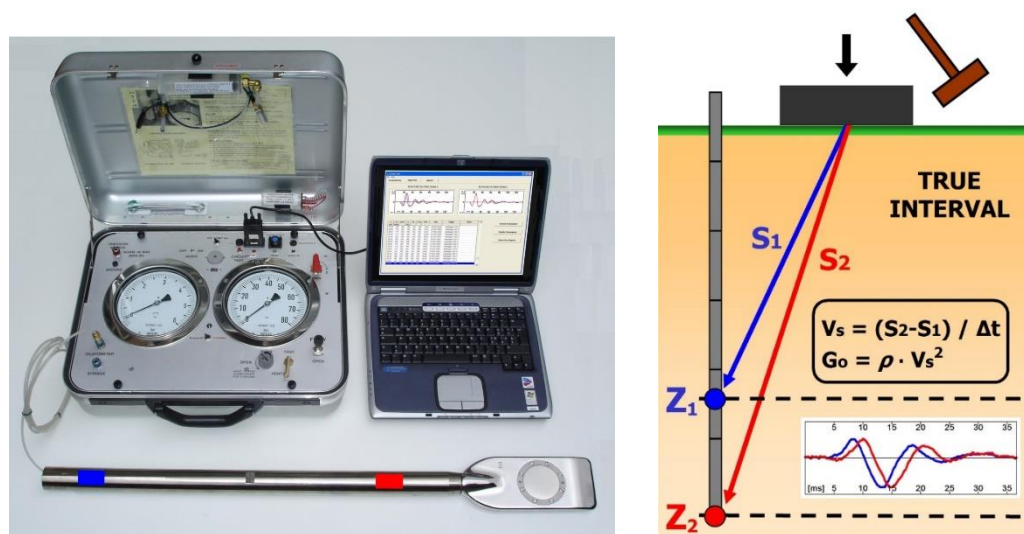
Figure 4.5 – Seismic dilatometer equipment and seismic scheme (Amoroso, 2014)

The DMT has the advantages of being low complexity and average cost, suitable for clays and sands. It has a good results reproducibility, there are several correlations to evaluate the resistance parameters and deformability, and the stress history information can improve liquefaction resistance estimates (Marchetti, 2016). It can also be coupled with a seismic module, placed above the blade, becoming a seismic dilatometer (SDMT). The rod is equipped with two geophones spaced 0.5 m, which allow the measurement of the shear wave velocity (V_S) when a hammer blow is produced on the ground surface. The scheme of the seismic procedure is also presented in Figure 4.5.

In the present research, two SDMT were performed, at S2 and NB1 sites. Both tests were conducted with the traditional execution of the DMT, with measurements every 20 cm, while the measurements of V_S were performed every 50 cm. Figure 4.6 presents the results of the material index and horizontal stress index, as well as a preliminary assessment of liquefaction susceptibility, based on the simplified procedure, for the two sites.

S2 profile shows a silty sand layer from 5.5 to 14 m, where the factor of safety against liquefaction is lower than 1. This is in accordance with the results obtain with SPT and CPTu tests that also identified this as the most critical layer in S2. At a depth of 30 m, a sandy layer is also identified. However, the K_D is around 1, being outside the limits considered in the liquefaction susceptibility method used (Robertson, 2012). Moreover, due to the high depth where this layer is, the liquefaction potential would probably be low.

On the other hand, the interpretation of NB1 is not so clear. A silty sand layer is found at 3 to 9 m; however, those points are not considered in the liquefaction susceptibility interpretation as the approach

is only valid for $I_D > 1.2$ and $2 < K_D < 6$ (Robertson, 2012). Therefore, based on DMT results, the critical layers are at 5 – 6 m, 11 – 12 m and 14 – 15.5 m.
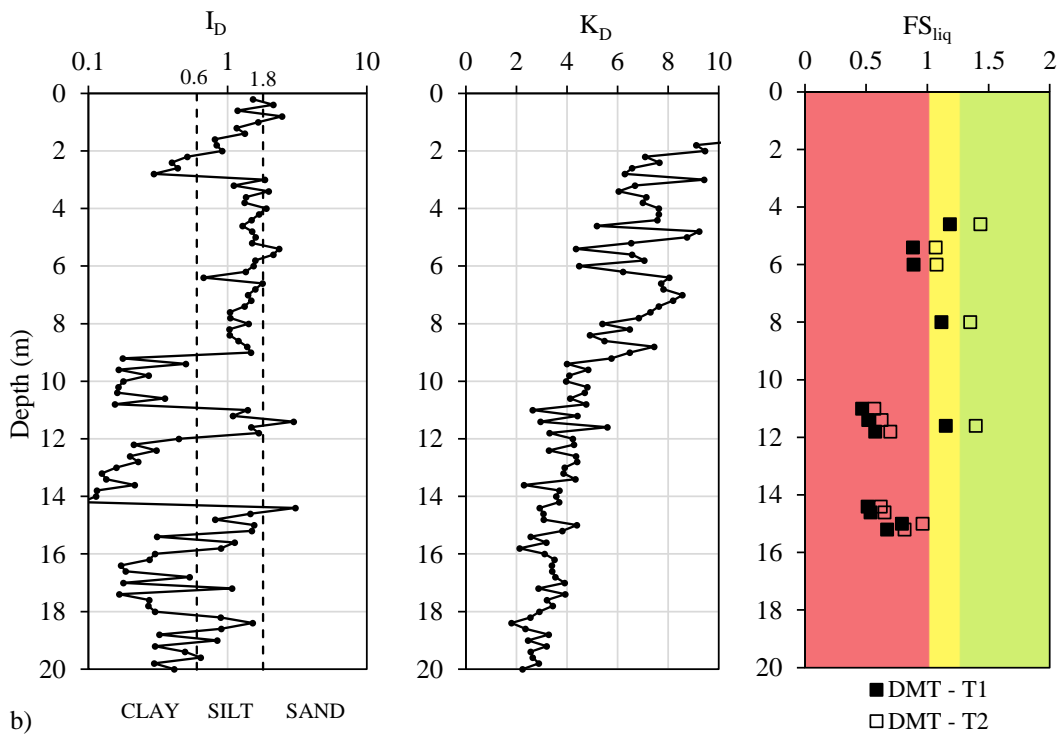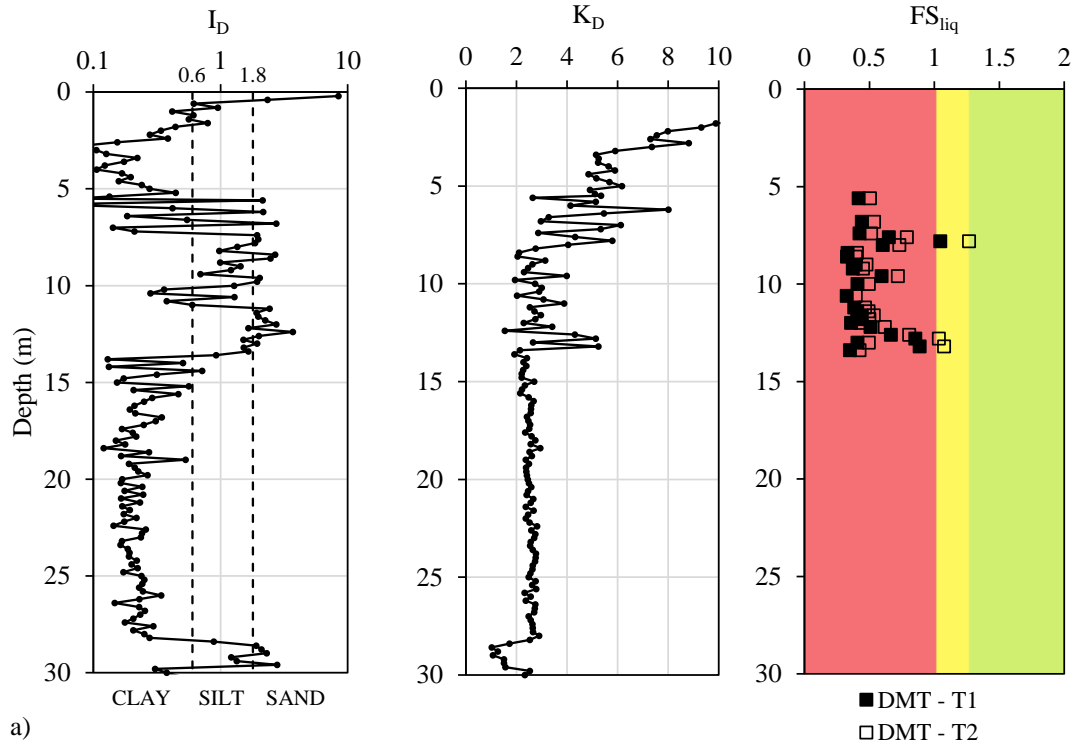
Figure 4.6 – DMT-based liquefaction susceptibility analysis: a) S2; b) NB1

4.2.4. SHEAR WAVE VELOCITY PROFILING

One of the objectives of this research was to evaluate the quality of samples collected at each experimental site, using high-quality samplers (discussed in detail in Chapter 5). The most common methodology to study sampling quality involves the comparison of direct seismic wave measurements from in situ tests with laboratory measurements. Therefore, the shear wave velocities were measured at each site, using seismic devices attached to either the DMT or the CPTu. The readings were performed every 0.5 m in the SDMT tests and every 1 m in the SCPTu test. As explained above, the SDMT performed at S1 was unsuccessful, so there is no record of direct seismic wave velocities at this site.

Notwithstanding, there are indirect correlations with penetration tests to predict shear wave velocity profiles. In this section, the CPT-V_S, SPT-V_S and DMT-V_S correlations are studied and compared with the direct measurements, when available.

For the estimate from SPT test results, the recommendations from Wair et al. (2012) were adopted. The authors suggest V_S estimates for Quaternary soils based on the number of SPT blows and the effective vertical stress. According to soil type, V_S is estimated through equations (4.1) and (4.2) for clays and silts, and sands, respectively. As the soils tested are from the Holocene, age scaling factors were applied to each equation.

$$V_S = 0.88 \times 26 N_{60}^{0.17} \sigma'_v{}^{0.32} \quad \text{for clays and silts} \tag{4.1}$$

$$V_S = 0.90 \times 30 N_{60}^{0.23} \sigma'_v{}^{0.25} \text{ for sands} \tag{4.2}$$

For the CPT-V_S correlations, the prediction proposed by Robertson (2009) was found to be the most appropriate for these soils, as detailed in Ferreira et al. (2018). For all soils, the proposal for V_S estimation is based on the soil behaviour type index, I_c, the cone resistance, q_t, and the effective vertical stress, σ'_{v0}, as follows:

$$V_S = \left[10^{(0.55 I_c + 1.68)}(q_t - \sigma'_{v0})/p_a\right]^{0.5} \tag{4.3}$$

As for the estimate of V_S from DMT results, Marchetti et al. (2008) created a diagram based on the seismic dilatometer results obtained at 34 research sites, comprising a variety of soil types (Figure 4.7). From the diagram, estimates of the small-strain shear modulus, G_0 (hence V_S) are obtained from DMT parameters I_D, K_D and M_{DMT}, as expressed in Table 4.1. The shear wave velocity is then obtained with $V_S = (G_0/\rho)^{0.5}$, where ρ is the soil density.
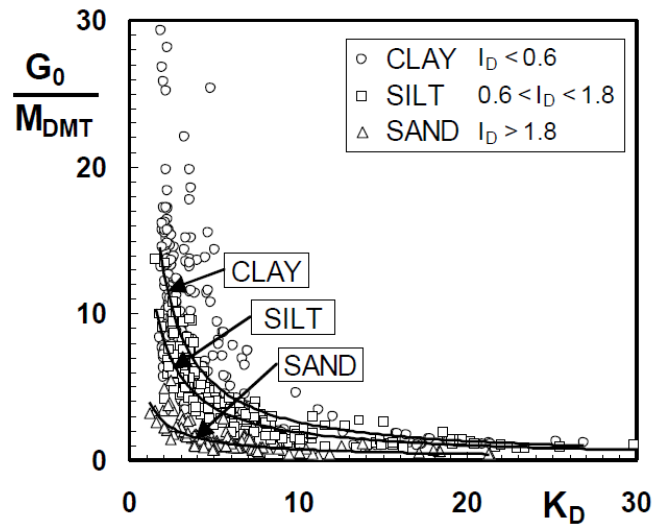
Figure 4.7 – Ratio G_0/M_{DMT} vs. K_D for various soil types (Marchetti et al., 2008)

Table 4.1 – Proposals for G_0 from DMT results (Marchetti et al., 2008)

Material Index	Interpolated correlation
$I_D < 0.6$	$G_0/M_{DMT} = 26.177 K_D^{-1.0066}$
$0.6 < I_D < 1.8$	$G_0/M_{DMT} = 15.686 K_D^{-0.921}$
$I_D > 1.8$	$G_0/M_{DMT} = 4.56137 K_D^{-0.7967}$

Figure 4.8 to Figure 4.11 present the shear wave velocities obtained from the direct measurements (SDMT or SCPTu), and from the correlations with SPT, CPTu and DMT results, for each experimental site. The computed factors of safety against liquefaction are also included, liquefaction susceptibility was assessed with Andrus and Stokoe (2000) and Kayen et al. (2013) methodologies (abbreviated to A&S2000 and Kea2013, respectively), for the two types of seismic action (T1 and T2). In accordance to previous considerations, the factors of safety against liquefaction are only represented for soils with FC < 35%. However, the direct V_S measurements and associated FS$_{liq}$ are represented for the entire soil profile, to clarify the interpretation of results. The FS$_{liq}$ boundaries defined at 1 and 1.25 are also represented.
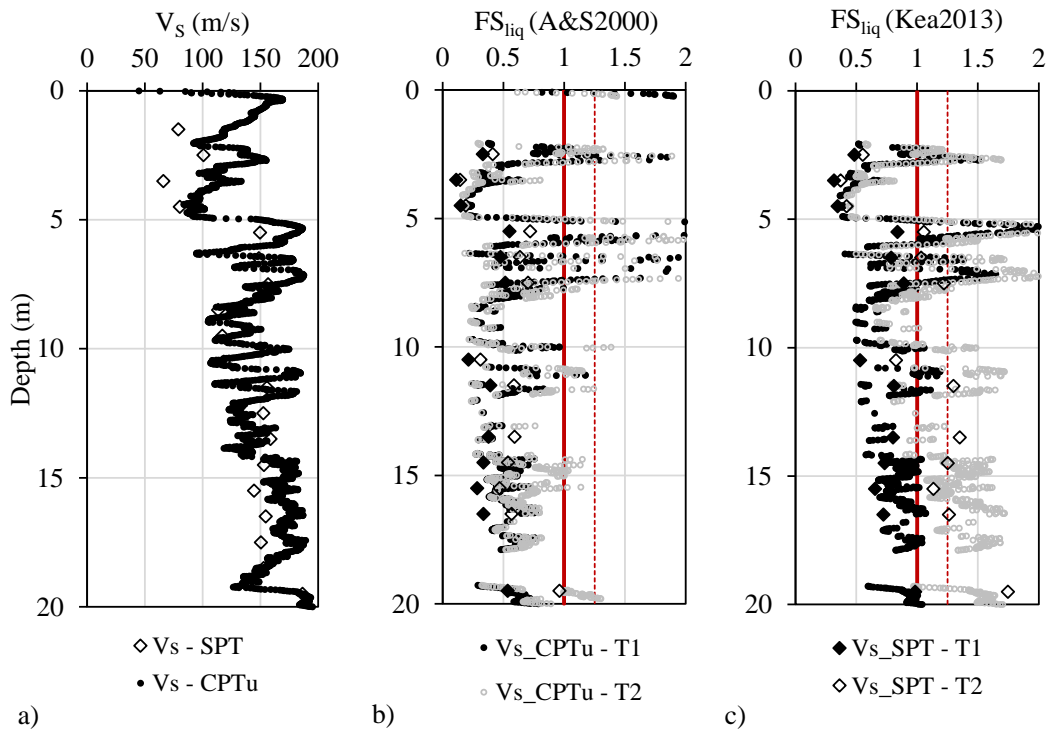
Figure 4.8 – V_S-based liquefaction susceptibility in S1: a) V_S profile; b) FS_{liq} from A&S2000; c) FS_{liq} from Kea2013
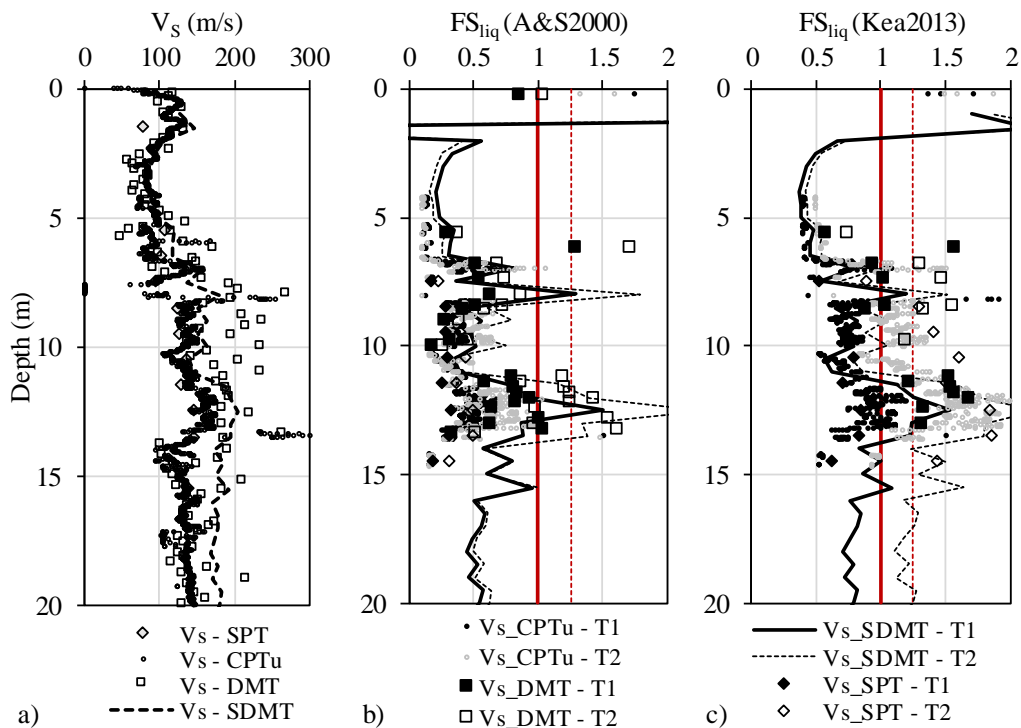
Figure 4.9 – V_S-based liquefaction susceptibility in S2: a) V_S profile; b) FS_{liq} from A&S2000; c) FS_{liq} from Kea2013
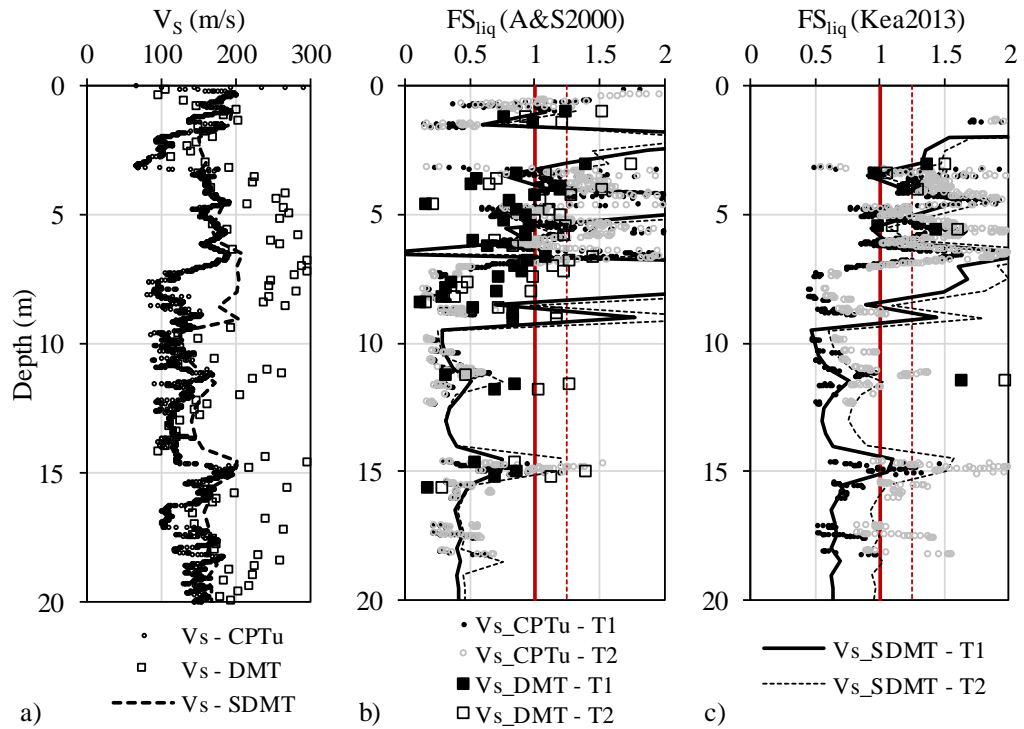
Figure 4.10 – V_S-based liquefaction susceptibility in NB1: a) V_S profile; b) FS_{liq} from A&S2000; c) FS_{liq} from Kea2013
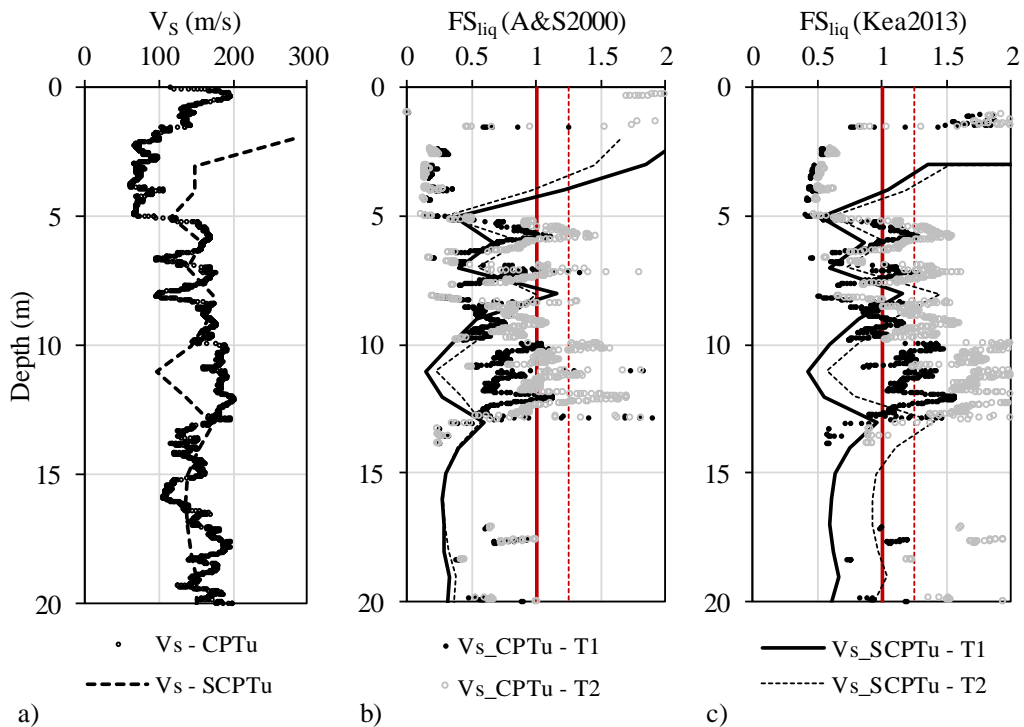
Figure 4.11 – V_S-based liquefaction susceptibility in NB2: a) V_S profile; b) FS_{liq} from A&S2000; c) FS_{liq} from Kea2013

In general, a good agreement between the predictions and the direct measurements was found. In some soil layers, DMT-based V_S values are higher than those obtained with other tests. Despite that, the liquefaction susceptibility based on different predictions is quite similar, enabling the identification of critical liquefiable layers in all the sites. In general, A&S2000 methodology is more conservative than Kea2013, providing lower values of factor of safety against liquefaction. The reason why Kea2013 is less conservative, especially for seismic action type 2, is probably the low moment magnitude value (M_w = 5.2) that has a significant impact on the factor of safety in this methodology. This suggests that the magnitude scaling factor DWF might need further adjustments.

At S1 site, since the SDMT test was unsuccessful, there is no direct measurement of V_S. The comparisons are performed between the predictions with SPT and CPTu results. The SPT-based predictions are more conservative, identifying the entire soil profile as susceptible to liquefaction, in the A&S2000 approach. On the other hand, the CPTu-based results identify two layers with FS_{liq} higher than 1, at 3 m and between 5 m and 7.5 m. As illustrated before, this is a very heterogeneous soil profile, with sand-silt-clay interlayers, reflected in the V_S and FS_{liq} profiles.

As for S2, the shear wave velocities predicted with penetration test results show good agreement with the direct measurement, which is also reflected on the FS_{liq} profiles. The DMT-based predictions are closer to the SDMT measurements, demonstrating a good performance of Marchetti et al. (2008) methodology, as also evidenced by Amoroso (2014). This is clear at 11 m to 13 m, where the direct and DMT-based FS_{liq} is higher than the SPT or CPTu-based results. A thick liquefiable layer is found between 6 m and 14 m, where the majority of FS_{liq} values are below 1. Once again, the Kea2013 method for type 2 of seismic action is less conservative.

At NB1, the results are not so clear. There is a general good agreement between the direct measurements and the predictions, even though DMT-based V_S are higher. In the liquefaction susceptibility analysis, some critical layers are identified at 1-2 m, 4-7 m, 10-12 m and 15 m, despite some discrepancies in the results. There is no clear correlation between the results of the different tests. However, the CPTu results show a better agreement with the direct measurement than the DMT.

At NB2, the direct measurements were obtained using a SCPTu, coupled to the CPTu cone so the reading were performed in the exact same borehole. The seismic wave measurements are similar to the CPTu-based predictions, except in the beginning of the profile and at 10 m to 13 m. Despite that, a clear thick liquefiable layer is found at 5 m to 13 m.

The direct measurement of seismic waves is certainly the best way to obtain the shear wave velocities profile in depth. However, this is not always possible, as was the case of S1. Therefore, in the subsequent analyses the shear wave velocities used will be the direct measurements, except at S1, where the CPTu-

based predictions will be adopted. This approach was considered better than the SPT-based predictions, in the sense that it is more accurate and allows the identification of smaller layers, particularly relevant in S1 profile. Besides that, the CPTu-based correlation showed good agreement with the direct measurements in the other soil profiles, validating its further use in S1.

4.3. LIQUEFACTION SUSCEPTIBILITY ASSESSMENT

The liquefaction susceptibility is investigated in terms of the factor of safety against liquefaction (FS_{liq}), the Liquefaction Potential Index (LPI), and the Liquefaction Severity Number (LSN). Based on the procedures recommended in Eurocode 8, two seismic actions were considered: SA type 1 and SA type 2, defined by $a_{max} = 0.20$ and $M_w = 7.5$, and by $a_{max} = 0.31$ and $M_w = 5.2$, respectively.

This section presents an extensive study of some factors that influence the assessment of liquefaction susceptibility based on different field tests. Firstly, a study comparing the use of fines content estimated or directly obtained through particle size analyses of SPT samples in the laboratory is conducted. The influence of different fines content in the results of SPT and CPTu is analysed, focusing on the critical layers identification. Due to the lack of consensus about the best criteria for evaluating liquefaction resistance, a comparative study between three CPTu-based methods is performed, to evaluate the differences between them and the influence on liquefaction assessment. The normalisation procedures adopted by each method are detailed in Chapter 2, as well as the calculation formulas. Moreover, the transitional layer influence is also discussed, reflecting on the necessity of excluding these layers in the analysis of strongly interlayered profiles. Finally, the overview of the liquefaction susceptibility of the four experimental sites is presented, with a comparison between liquefaction susceptibility based on different field tests. The performance of each in situ test in the assessment of liquefaction is evaluated.

4.3.1. REFLECTION ON FINES CONTENT

Over the years, the importance and influence of fines content in the liquefaction susceptibility of soils has been the focus of many research studies. It is now well accepted within the geotechnical community, that the fines content and its plasticity play a very important role in the liquefaction susceptibility of soils, both in field tests (Robertson and Wride, 1998; Boulanger and Idriss, 2016) and in laboratory tests (Polito et al., 2001; Cubrinovski and Rees, 2008).

It is recognised that soils with high percentage of fines and, more importantly, high plasticity are less susceptible to liquefaction (Kramer, 1996). Nowadays, several methods used to normalise field test results include, in one way or another, the effect of fines content, making its correct determination of

great importance. As stated in Chapter 2, Boulanger and Idriss (2014) proposed the normalisation of SPT-blow count and CPTu cone resistance using fines content, by introducing equivalent clean sand adjustments, $\Delta(N_1)_{60}$ and Δq_{c1N}, for SPT and CPTu, respectively.

Within the current research work, for sites S1 and S2, fines content and plasticity index from each SPT depth were analysed in the laboratory. The grain size and plasticity index of all samples tested in the cyclic triaxial apparatus were also determined. This detailed grain size information allowed the performance of an in depth study concerning the influence of fines content in liquefaction assessment based on field penetration tests, presented in Ramos et al. (2020). In this section, a description of the different methodologies to determine FC and a reflection on its influence in liquefaction susceptibility assessment are presented and discussed.

4.3.1.1. Fines content on SPT

For the liquefaction assessment based on Boulanger and Idriss (2014) methodology, the N_{SPT} value is normalised using fines content, introducing the equivalent clean sand adjustment, $\Delta(N_1)_{60}$. Therefore, the knowledge of the most accurate value of fines content for each soil layer is crucial. However, a correlation between FC and N_{SPT} is non-existent, leading to the necessity of estimating fines content. In the current research, two different methodologies were considered: i) the estimation of FC based on the lithological description of the SPT borehole log, provided by the field operator or by the geotechnical company, and ii) the determination of grain size and plasticity index from the soil samples collected in the SPT sampler tube, at each depth. Table 4.2 presents the values of fines content according to the type of soil described on the SPT log. These values were empirically determined, using a conservative approximation and considering the evolution chart of $\Delta(N_1)_{60}$ with the percentage of fines by Boulanger and Idriss (2014).

Table 4.2 – Fines content values depending on soil type

Type of soil	Fines content (%)
Fine non-liquefiable soil	100
Silty sand	30
Sand with fines	10
Clean sand	5

In two of the experimental sites, S1 and S2, SPT tests were performed. The fines content profiles for both sites are illustrated in Figure 4.12, using the estimated and laboratory approaches described previously. The plasticity indexes obtained in the laboratory are also represented as the values next to the FC point at each depth. It is important to keep in mind that the SPT estimate is a gross approximation

as one value represents a 1 m thick layer, homogenised, not considering the discretisation of the different interlayers. As can be seen in the Figure, the two approaches give similar values of FC, with some exceptions, particularly at S1. This can be related to the strong heterogeneity of the profile that can induce errors in the assessment of the soil layer characteristics described in the SPT log.
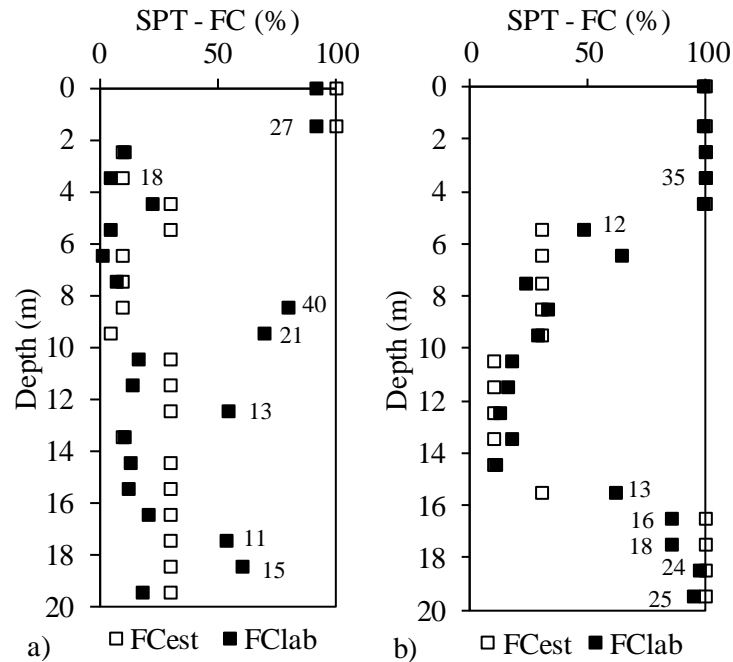
Figure 4.12 – Profiles in depth of the FC from SPT: a) S1; b) S2

4.3.1.2. Fines content on CPTu

In a similar way as for the SPT-based liquefaction assessment from B&I2014 method, the cone resistance from CPTu must be normalised according to the fines content. In this case, Boulanger and Idriss (2014) proposed a formulation to estimate fines content depending on the soil behaviour type index, I_c (equation (4.4)). The parameter C_{FC} is a fitting parameter based on site-specific data, taken equal to 0 in this work, as no site-specific data was available.

$$FC = 80(I_c + C_{FC}) - 137 \tag{4.4}$$

The results of fines content for S1 and S2 profiles are given in Figure 4.13, comparing the results from B&I2014 formulation and the values obtained in laboratory grain size tests. Contrary to the SPT results presented in 4.3.1.1, the estimated CPTu values show a very intricate profile, with constant changes from soils with 100% to 0% fines content. This is not reflected on the SPT profile, and consequently it is not represented in the laboratory measurements, as they provide constant values for each SPT sample.

To represent the FC obtained in the grain size analyses in the laboratory, the value for each 1 m thick layer is constant, which for densely layered profiles may not be fully representative of the real soil layer configuration. On the other hand, the B&I2014 formulation computes one value of FC for each 2 cm layer, being more detailed. However, the correlation was empirically obtained, based on a set of case studies and can produce inaccuracies. Nonetheless these differences, the results show good agreement between the B&I2014 interpretation and the laboratory results.

The fines content of high-quality specimens collected using a Mazier sampler are also illustrated in Figure 4.13. It is observed that the results from the Mazier sampler are not always in good agreement with the SPT collected soils, as observed at 2 m, 9 m, 11 m in S1 profile, and at 6 m and 7 m at S2 profile. However, at most depths, the results are similar, which was expected as the two boreholes are only 5 m apart.
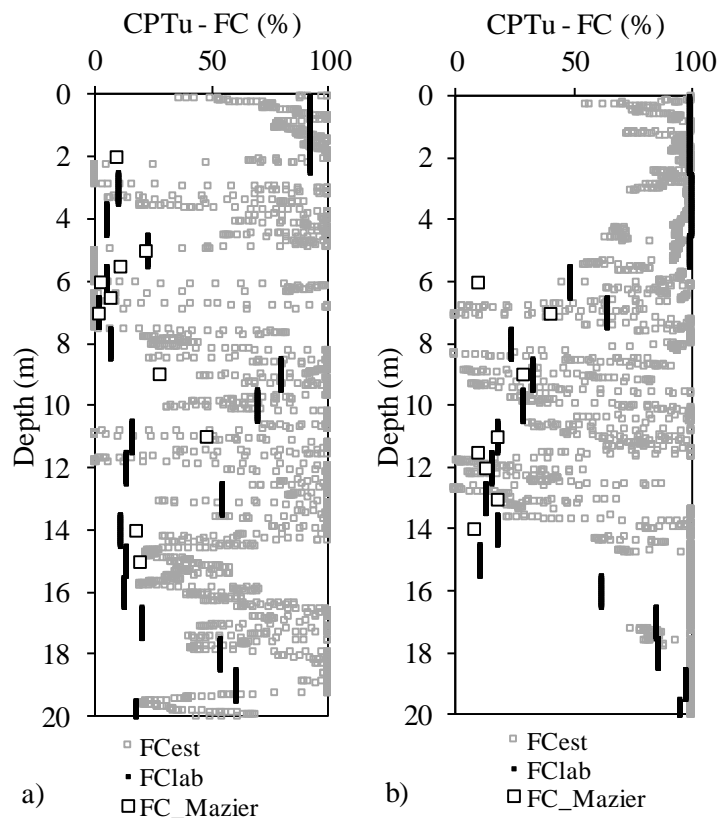
Figure 4.13 – Profiles in depth of the FC from CPTu: a) S1; b) S2

4.3.1.3. Influence of FC on liquefaction susceptibility

To discuss the influence of the consideration of different methods for FC estimation, a comparative analysis of the effect of each FC profile on liquefaction assessment was performed, based on the factor of safety against liquefaction, the LPI and the LSN.

Figure 4.14 and Figure 4.15 present the liquefaction susceptibility assessment for S1 and S2, respectively, in terms of factor of safety against liquefaction. The representation is firstly performed for the SPT results (a), then for the CPTu (b) and lastly for both tests, considering only the layers with FC < 35% and seismic action type 1 (c). It appears that the consideration of estimated or laboratory measured values, in both SPT and CPTu, does not influence the identification of liquefiable layers. Even though some FS_{liq} values are slightly different, especially in the CPTu results where the estimated values are higher than laboratory measurements, there is a consistency regarding the values lower than 1. For that reason, the same layers are considered susceptible to liquefaction (FS_{liq} < 1.0). Moreover, different seismic action type considerations do not interfere with the results, neither in the SPT nor in the CPTu. Observing Figure 4.14c and Figure 4.15c, it is recognizes that the consideration of FC_{lab} in the SPT analysis refines the results and approximates the results to the more detailed CPTu results. This conclusion is more significant when analysing the S2 profile, as it presents more homogeneous layers. The SPT analysis suggests that all the 20 m profile is susceptible to liquefaction, almost considering the entire profile as one layer. However, when analysing the CPTu results, the separation between layers is evident. When the layers with more than 35% FC are hidden, a single critical layer is detected, and the representation is clearer. Once again, the SPT results with FC_{est} show some values out of the critical layer, meaning that the consideration of FC_{lab} improves the results and approximates them to the CPTu results.
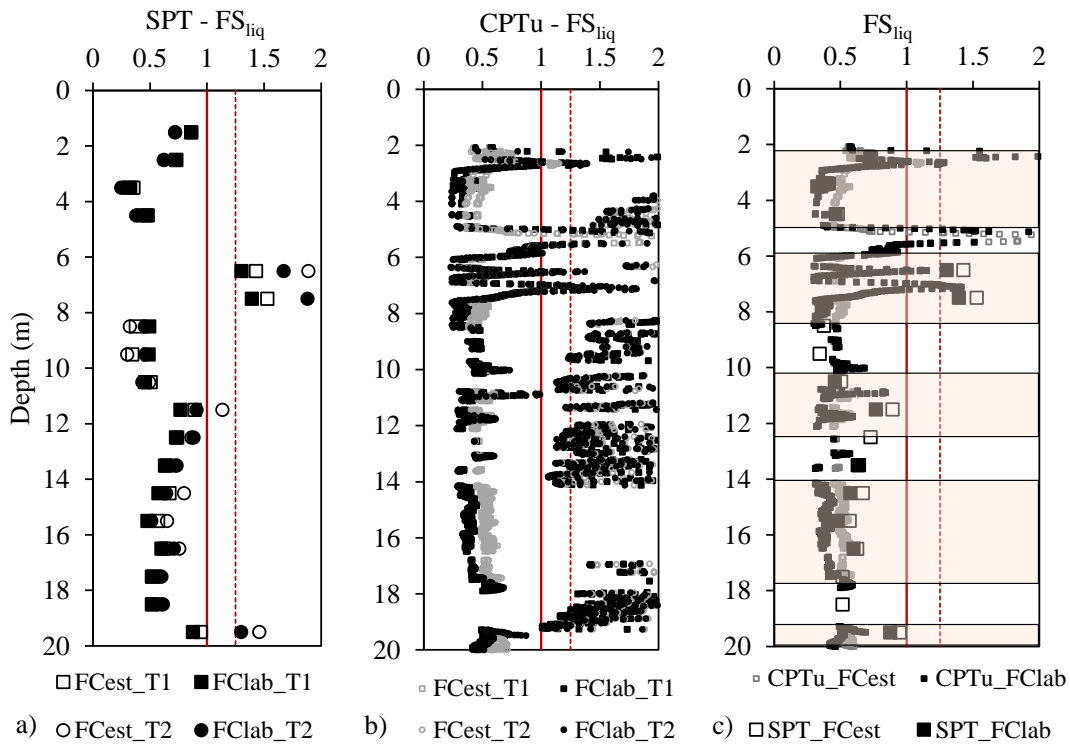
Figure 4.14 – Factor of safety against liquefaction for S1: a) SPT; b) CPTu; c) definition of critical layers
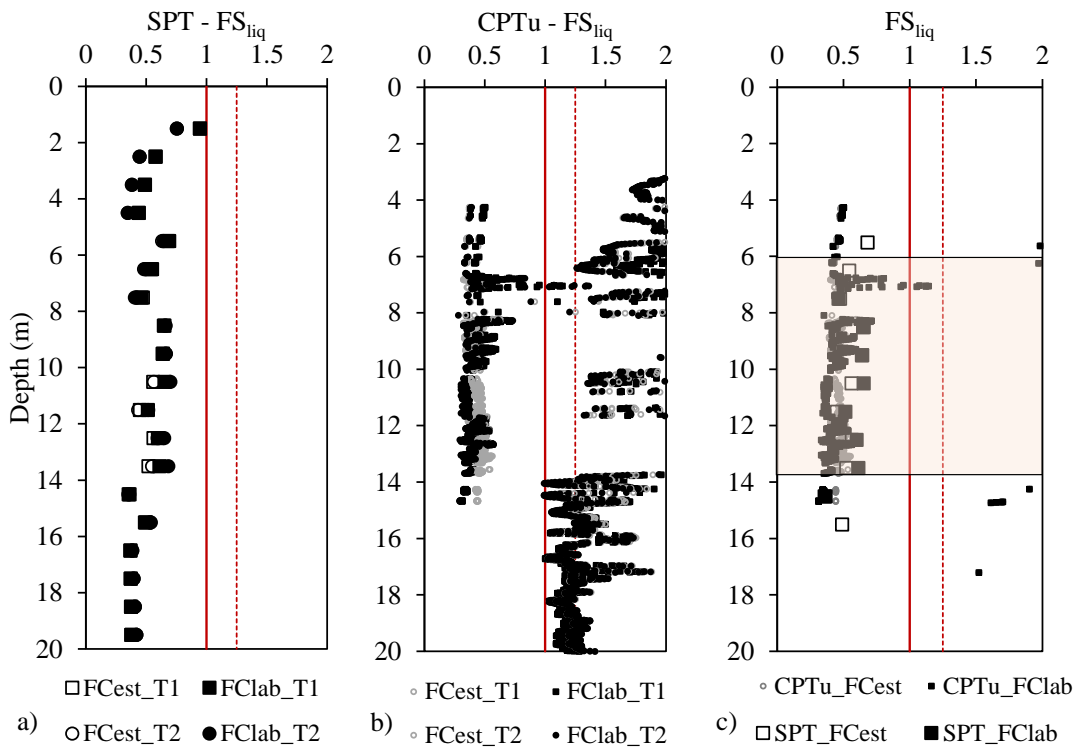
Figure 4.15 – Factor of safety against liquefaction for S2: a) SPT; b) CPTu; c) definition of critical layers

To fully understand the influence of different considerations and to provide information about the damages induced by soil liquefaction, the values of LPI and LSN were computed for the SPT and CPTu results of the two soil profiles, using both types of seismic action and both the estimated fines content (FC_{est}) and the laboratory-measured values (FC_{lab}). The results are illustrated in Figure 4.16 and Figure 4.17, including a coloured background shading based on the classification of Iwasaki et al. (1978a) and Tonkin and Taylor (2013), respectively.
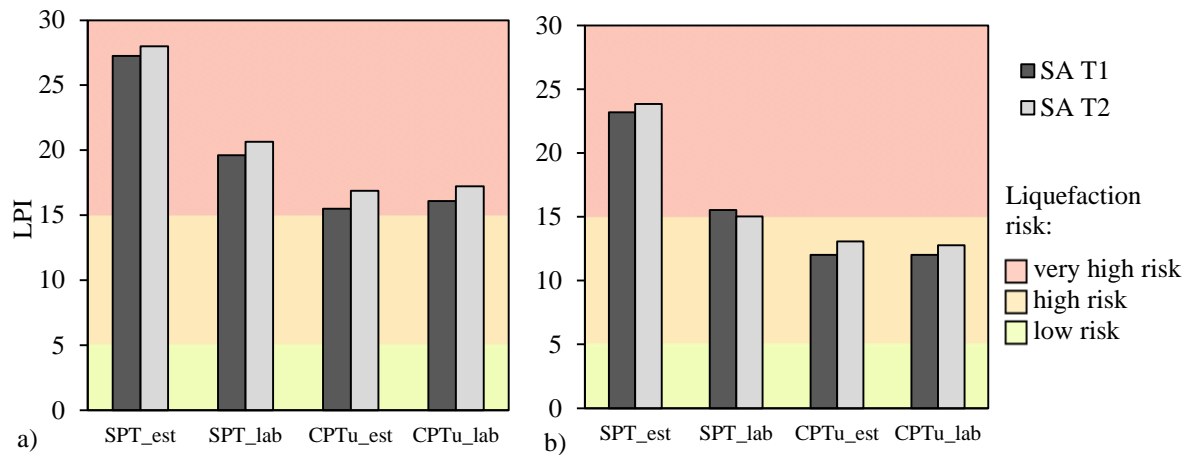
Figure 4.16 – LPI results: a) S1; b) S2
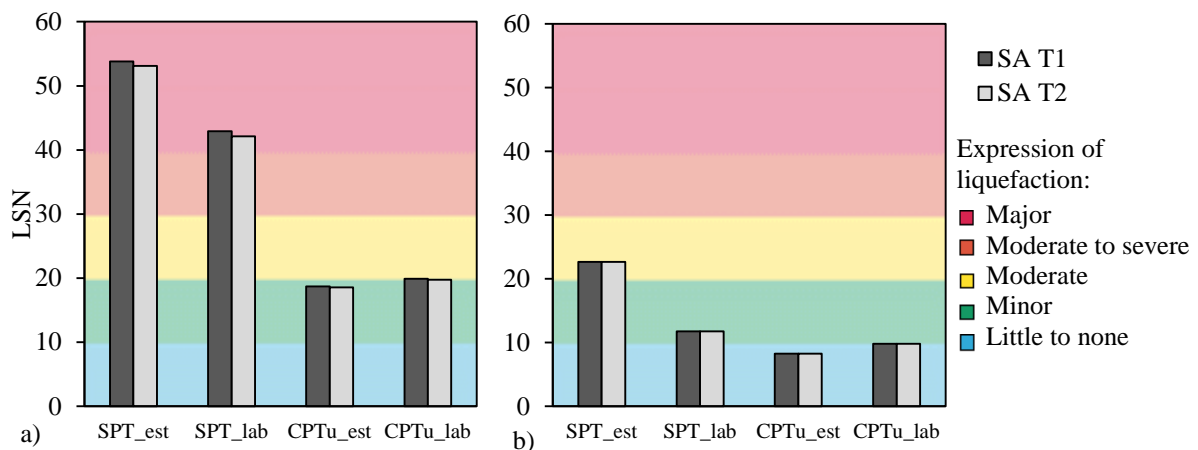
Figure 4.17 – LSN results: a) S1; b) S2

It is noticeable that, similarly to what occurred in FS_{liq}, the seismic action type does not significantly change the values of LPI and LSN. Moreover, in the CPTu case, the use of estimated or laboratory measured FC provides almost the same results. This confirms that the formulation used for the estimation of FC (proposed by Boulanger and Idriss (2014)) appropriately estimates the fines content and validates the use of estimated FC in the analyses. On the other hand, this is not verified in the SPT

result. There are no significant changes in the LPI and LSN values for different seismic action type, but there is a considerable difference between the results using FC_{est} and FC_{lab}. The results of LPI and LSN when using FC_{lab} are closer to the CPTu results, reinforcing the importance of the use of the laboratory FC in the SPT analyses.

4.3.2. COMPARISON BETWEEN DIFFERENT METHODOLOGIES

As mentioned before, the piezocone penetration test (CPTu) is a widely used field test, as it provides an almost continuous soil profile analysis, based on the soil resistance and the pore pressure developed during penetration. Over the years, methods to evaluate liquefaction susceptibility based on different in situ tests have been extensively studied. However, there is not much consensus with regard to the best criteria for evaluating liquefaction resistance based on CPT results. According to each methodology, the correlations and normalisation factors are obtained differently, since the expressions were derived from different earthquake databases that have been updated over the years. In this section, three methodologies were selected and discussed in detail, namely Robertson (2009), Moss et al. (2006), and Boulanger and Idriss (2014) (referred to as R2009, MEA2006, and B&I2014 from here on). The main differences in the normalisation parameters for each test were introduced in Chapter 2 and justify some comparisons presented here.

The four CPTu performed at the experimental sites were analysed using the three methods, in terms of factor of safety against liquefaction, LPI and LSN. The seismic action applied is the same as before for types 1 and 2 of seismic action.

4.3.2.1. Factor of safety against liquefaction

Figure 4.18 presents the factor of safety against liquefaction for the four profiles, comparing the results of each method, for seismic action type 1 and 2, respectively. Only FS_{liq} for layers with $I_c < 2.60$ are represented, as $I_c = 2.60$ corresponds to FC of approximately 35% in the Robertson (2009) method.

Seismic action type 1 is characterised by a lower a_{max} and higher M_w. In this case, the magnitude corresponds to the reference value of 7.5, so MSF is 1 and does not affect the results. In the more interlayered profiles, S1 and S2, the R2009 and MEA2006 seem to deliver more conservative results, with lower FS_{liq} values. However, in the more homogeneous layers (for example between 4 m and 7 m in NB1 or between 5 m to 14 m in NB2), the B&I2014 is more conservative, generally resulting in lower values of FS_{liq}.

When treating the results for seismic action type 2, with higher a_{max} and lower M_w, the results seem to invert. R2009 and MEA2006 are less conservative, presenting higher values of FS_{liq}. Despite these differences, it is perceptible that all methods identify the same critical layers, being B&I2014 the most conservative in general, as it delivers lower values of FS_{liq}.
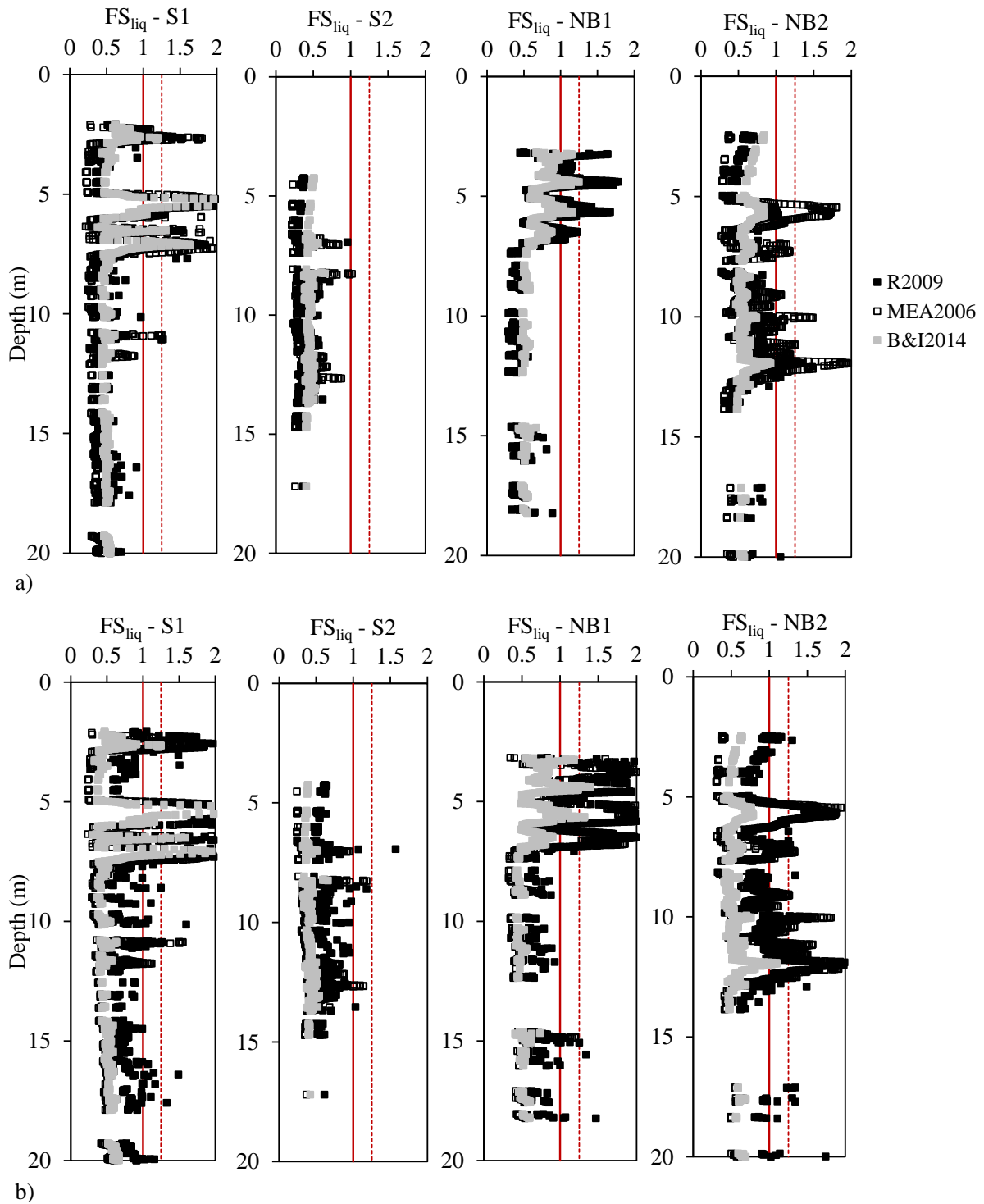
Figure 4.18 – Factor of safety against liquefaction: a) SA type 1; b) SA type 2

To better understand the differences between methods, Figure 4.19 shows the relationships between calculated FS_{liq} for paired combinations of methods, for layers with $I_c < 2.60$. Figure 4.19 (a, b, c) presents the comparison between R2009 vs MEA2006, R2009 vs B&I2014, and MEA2006 vs B&I2014, respectively, for seismic action type 1, while the same comparisons for seismic action type 2 are in Figure 4.19 (d, e, f).

When comparing R2009 and MEA2006, there are some points of S1 that fall in the 1:1 line, meaning that both methods deliver approximately the same results. However, for the majority of points, R2009 is more conservative, and MEA2006 recurrently produces FS_{liq} higher than 1.0, corresponding to no liquefaction susceptibility. When comparing R2009 and MEA2006 with B&I2014, a steeper trend is identified, especially in MEA2006. B&I20014 computes almost all values below 1.0, being the most conservative method. For seismic action type 2, the values of FS_{liq} for R2009 are higher, as the trends rise in the graphs. This is justified by the lower value of M_w, which produces a higher MSF and thus decreases the CSR, lowering the seismic action and delivering higher FS_{liq} values. This is particularly relevant for the R2009 method as it computes a very high MSF value. This tendency also occurs for MEA2006, although less pronounced. For this action, B&I2014 also yields more conservative results, confirming what was previously evidenced in the FS_{liq} profiles in depth (Figure 4.18). It is also relevant to note that in all graphs there is a concentration of points around $FS_{liq} = 0.5$, which means that for lower FS_{liq}, the methods identify more or less the same critical layers, also highlighted in the FS_{liq} profiles in depth. Moreover, there seems to be no clear distinction between the results of the different sites, suggesting that FS_{liq} is mainly affected by the design seismic action, at least for soils with $I_c < 2.60$.
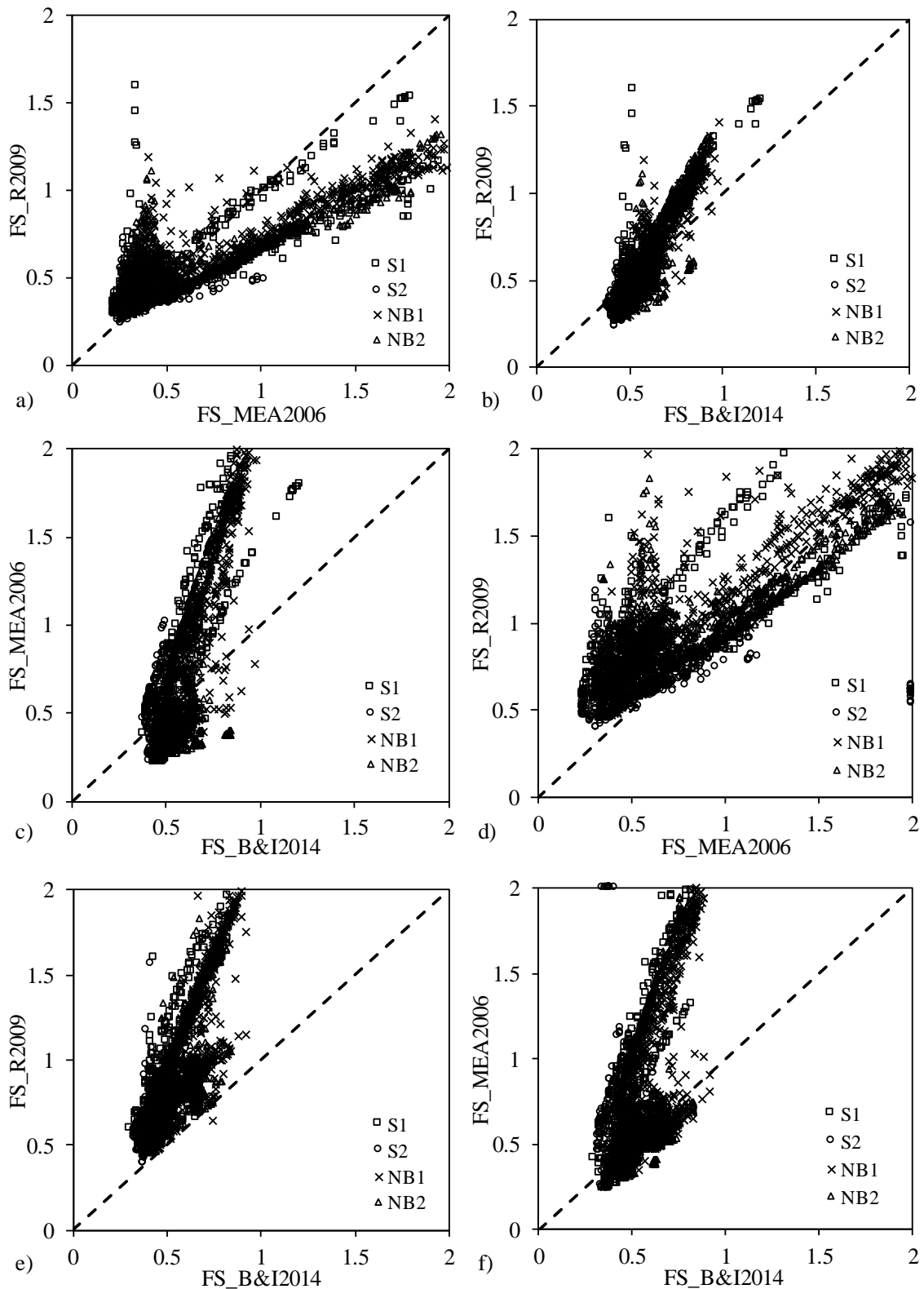
Figure 4.19 – Comparison of FS results between methods for seismic action type 1: a) R2009 vs MEA2006, b) R2009 vs B&I2014, c) MEA2006 vs B&I2014; and for seismic action type 2: d) R2009 vs MEA2006, e) R2009 vs B&I2014, f) MEA2006 vs B&I2014

4.3.2.2.   LPI and LSN

As mentioned above, the factor of safety against liquefaction is insufficient to provide indications about the severity of the manifestation or the cumulative effect throughout the soil profile. To better understand the influence of different methods and assess the damages induced in the soil in case of liquefaction, the liquefaction potential index, LPI (Figure 4.20) and the liquefaction severity number, LSN (Figure 4.21) were analysed for the four profiles using the three methods.

As evidenced in the comparison of Figure 4.20, for the LPI, the seismic action type plays an important role. The values from R2009 decrease significantly for SA type 2 (higher a_{max} and lower M_w) while B&I2014 values increase. The values of MEA2006 are nearly unaffected with the seismic action type, despite a minor decrease for type 2. As expected, for this parameter, the soil profile highly influences the results. All soil profiles are identified as high to very high risk of liquefaction, except for NB1 and NB2 for R2009 method with seismic action type 2. These results can be justified by the significant influence of MSF on the factor of safety and hence on the LPI. Once again, R2009 demonstrates higher dependency with MSF, as for the lower value of M_w ($M_w = 5.2$), the computed MSF value is very high, thus strongly decreasing CSR and delivering higher FS_{liq} values, hence lowering LPI.

As for LSN, the differences are not so significant. Once again, the selection of the method influences the trends and the differences between the two seismic action types. The R2009 method is the most affected by the seismic action parameters, as MSF strongly varies according to the moment magnitude, producing higher values of FS_{liq} for seismic action type 2. In turn, MEA2006 and B&I2014 are less influenced by the seismic action type. This is due to the influence of FS_{liq} in the ε_v calculation. Zhang et al. (2002) suggestion for determining ε_v presents a lower limit value for FS_{liq}, $FS_{liq} = 0.5$. Since the majority of low FS_{liq} values for MEA2006 and B&I2014 are close to or lower than 0.5, the changes due to seismic action type are not visible. This also justifies the nearly identical results for S2, even from R2009 method. The more interlayered profiles, S1 and S2, reveal minor to moderate expression of liquefaction. NB1 presents minor to moderate expression of liquefaction, except for R2009 type 2 that has little to none liquefaction expression. NB2 is the most critical profile, presenting moderate to severe liquefaction expression. This is a consequence of the type of soils above 10m, composed mainly by sands and silty sands with low FS_{liq}.
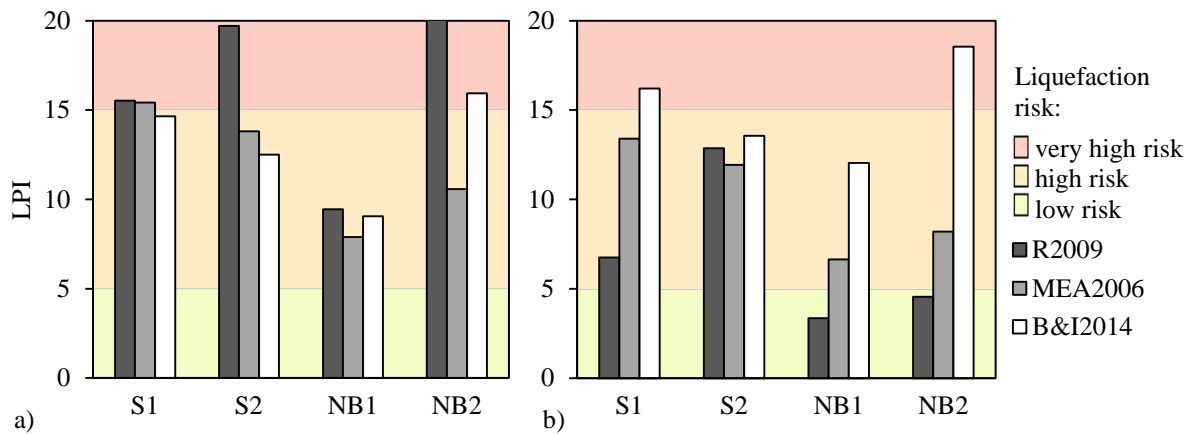
Figure 4.20 – LPI results: a) SA type 1; b) SA type 2
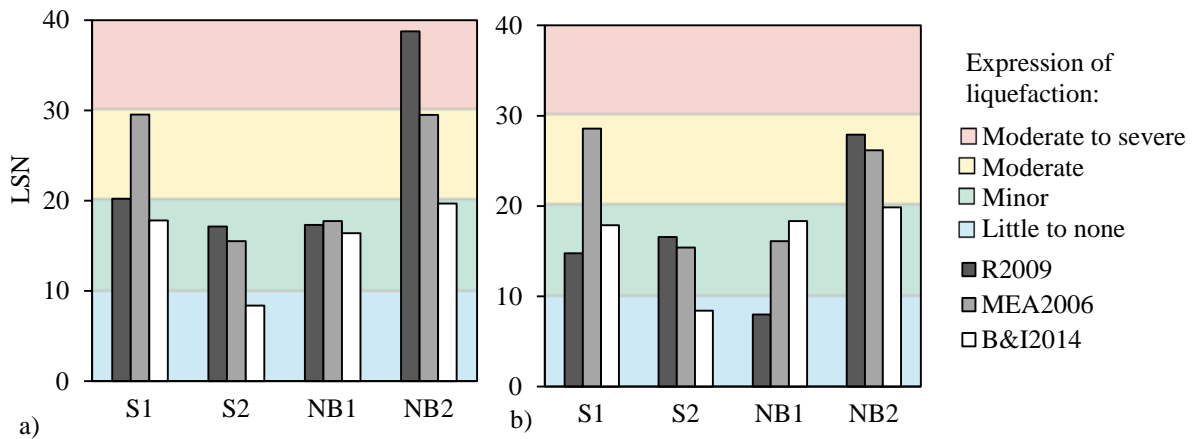
Figure 4.21 – LSN results: a) SA type 1; b) SA type 2

4.3.3. REFLECTION ON TRANSITIONAL LAYERS

As stated by Robertson and Wride (1998), the cone resistance is influenced by the soils ahead and behind the cone tip. Near the interface of two distinct soil layers, the changes in CPTu measurements are difficult to interpret and may be misleading. When the cone is moving from one soil type to another, especially if there is significant difference in soil stiffness or strength (e.g. soft clay to sand), the CPT data within the transition zone is usually excessively conservative. This is particularly relevant when dealing with thinly interbedded soils. The analysed soil profiles are very heterogeneous, with sand-clay interlayers that affect the sensitivity of the CPTu measurements. Therefore, a complementary analysis was performed excluding the transitional layers from the calculations, to highlight and detect the differences between the consideration (or not) of those layers in the liquefaction assessment frameworks.

The method is based on the identification and elimination from the liquefaction calculation of the points that belong to transitional layers, i.e. when the cone is in transition from clay to sand or from sand to

clay. This procedure is already implemented in Cliq®, the software used to perform the CPTu calculations. The range of I_c where the transitional layers can be found was set to $1.80 < I_c < 3.00$ as these were the values considered to include silts and sandy silts. The transitional points are found when the I_c changes rapidly, defined as a rate of $\Delta I_c = 0.01$. The analysis presented below refers only to seismic action type 1, as the comparison between the two seismic actions would be identical to previous discussion. Figure 4.22 shows the profiles of the factor of safety against liquefaction for each site and for the three methods studied in section 4.3.2. It is clear that the transitional layer correction eliminates some points. However, approximately the same critical layers are identified.
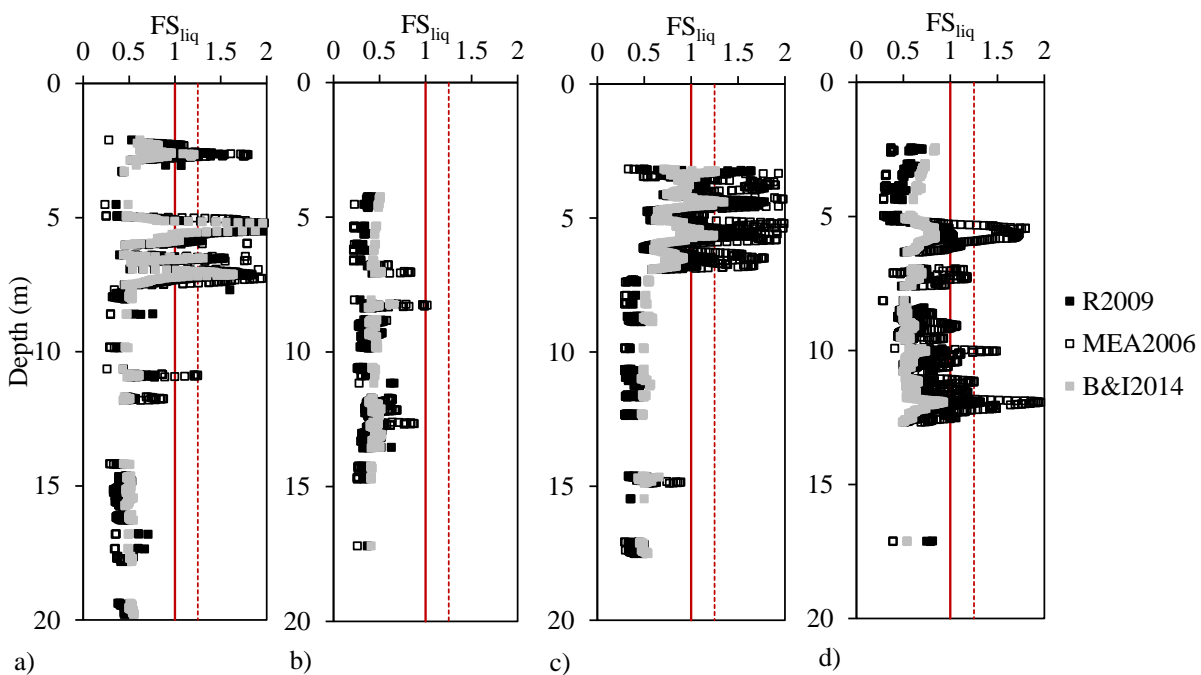
Figure 4.22 – Factor of safety against liquefaction with transitional layer correction: a) S1; b) S2; c) NB1; d) NB2

Figure 4.23 presents the LPI and LSN values obtained with the correction of transitional layers, overlapping the results considering all layers. The values considering the correction of transitional layers are clearly lower, and consequently, the liquefaction hazard is lower than when considering all layers. This is due to the elimination of some layers from the calculations. It can be concluded that the initial analysis is very conservative and the elimination of transitional layers increase the accuracy of the results. The comparison between different methods show similar trends. For the LPI, R2009 and B&I2014 are more conservative than MEA2006 and all methods are highly dependent on the soil type profile. For the LSN, the transition layer correction affects especially S1 and S2, which was expected, since these are the most interlayered profiles.
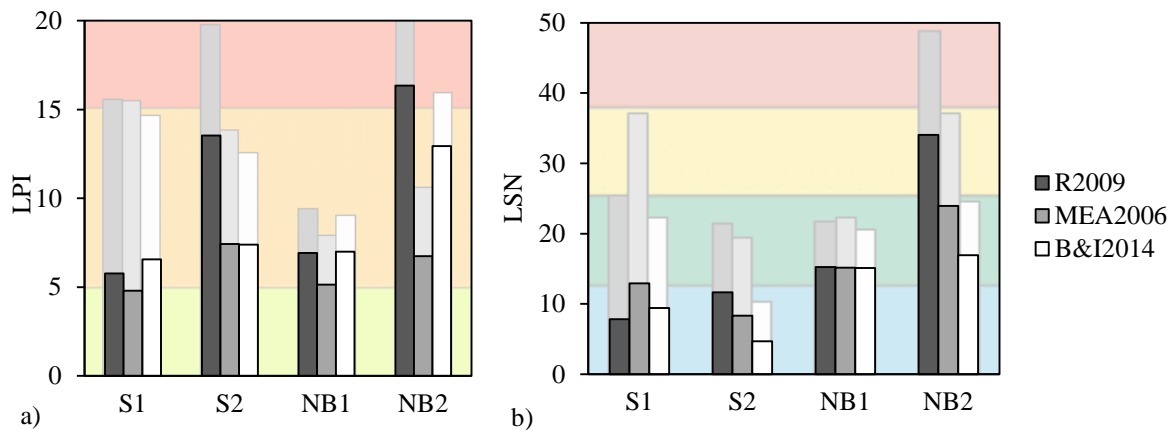
Figure 4.23 – Impact of the consideration of transitional layers correction in the reduction of liquefaction hazard:
a) LPI, b) LSN

4.3.4. OVERVIEW OF LIQUEFACTION SUSCEPTIBILITY OF THE PILOT SITE

After studying the influence of different factors, such as fines content, CPTu-based liquefaction assessment methods, and transitional layer correction on the liquefaction susceptibility of the experimental sites, an overview of the liquefaction susceptibility is presented. The liquefaction susceptibility assessment of the pilot site was based on the comparison of results of the field tests performed in each experimental location. At S1 and S2, where SPT were performed and a thorough study of the grain size and Atterberg limits in the laboratory allowed the identification of the fines content and plasticity index for each depth, the accurate measure of FC is used in conjunction with CPTu soil behaviour type index (I_c) to produce a simplified soil type profile and identify the layers most susceptible to liquefaction. At NB1 and NB2, as SPT tests were not performed, the soil profile was obtained through the I_c results from CPTu. To enable a precise comparison between the different test results, the B&I2014 method was used for the interpretation of SPT and CPTu data. The grain size distribution obtained on SPT samples was integrated in the SPT-based liquefaction assessment. Although advised, the transitional layers correction was not used in the CPTu results as the purpose was to compare the tests performance and there is no methodology to detect and exclude transitional layers in the SPT or DMT-based liquefaction assessment methods.

Figure 4.24 presents the simplified profile for S1, obtained taking into consideration the fines content from SPT samples and the I_c from CPTu. The plasticity index is also represented in Figure 4.24a, as the number next to each square (where PI is not specified means non-plastic (NP) soil). In the I_c profile, a I_c_liq profile is also defined based on the simplified I_c approach proposed by Cubrinovski et al. (2017), and including only the values of I_c lower than 2.6 (considering soil with $I_c > 2.6$ as non-liquefiable). It is clear that the soil profile is complex, with the presence of sand layers interbedded with silts and clays.

As discussed before, the SPT was performed each 1 m, which inhibited the detection of small interbedded layers. On the other hand, the CPTu was performed each 1 cm, allowing an almost continuous measurement, hence the definition of more detailed soil profiles. For this reason, the SPT alone is not enough to accurately define the soil profile, as it fails to identify the existence of small thickness silt and clay interlayers. Notwithstanding, the measurement of fines content in the laboratory is very important as it refines the simplified profile defined based on lithology from SPT analyses, as was discussed in section 4.3.1. The fines content obtained from SPT samples allowed a more accurate identification of the types of soil in the field, which the estimated FC from the SPT lithology clearly missed. The SPT laboratory-measured FC plays a very important role, especially in the subsequent liquefaction susceptibility analyses, as it provides a more accurate characterisation of the fines content in each soil layer.
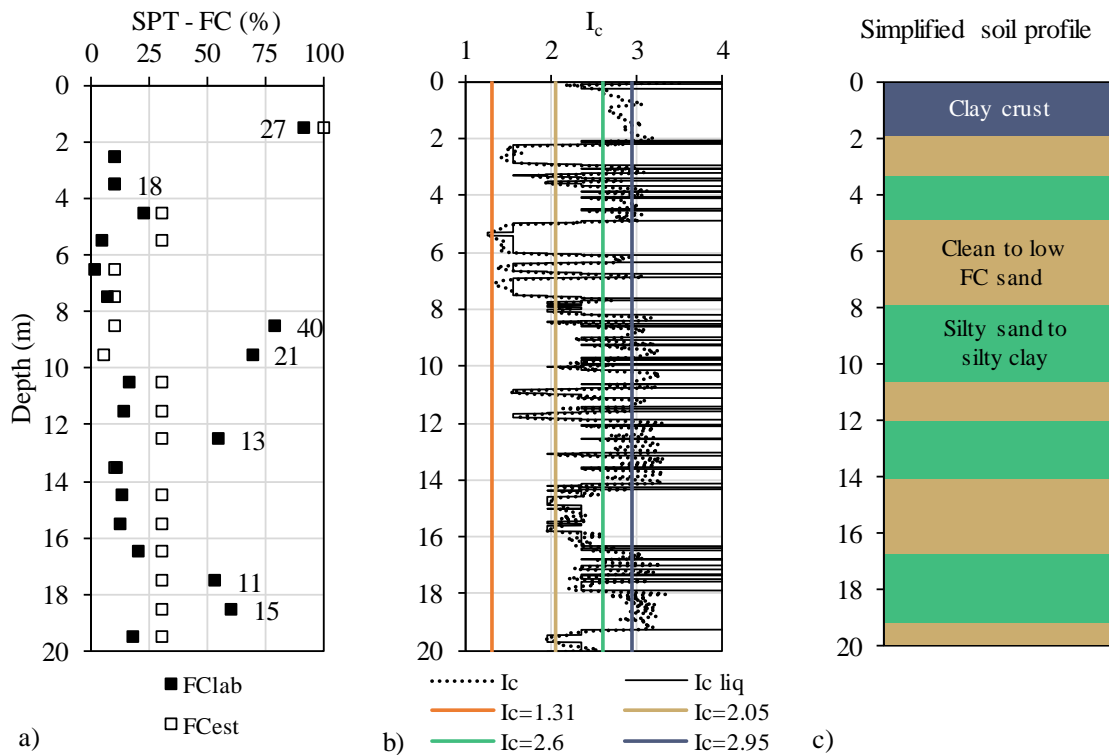
Figure 4.24 – S1 results: a) SPT laboratory-measured fines content and plasticity index; b) simplified I_c for liquefaction; c) simplified soil profile

Taking into consideration the simplified soil type profile, and considering that soil with $I_c > 2.6$ are non-liquefiable, the analyses of liquefaction susceptibility were revised and are illustrated in Figure 4.25. Three highly liquefiable layers were identified as critical, between 2 m and 4 m, at 10 – 12 m, and at 14 – 17 m. Moreover, a thin liquefiable layer was identified at 19 m, but due to the distance to ground surface, the effects on the surface might be negligible. Apart from those, a moderate to low liquefaction

susceptibility layer was detected at 5 to 8 m, composed by higher resistance sands. It is interesting to note that despite the scatter of V_S–FS_{liq} values (approach from Andrus and Stokoe, 2000), they identify approximately the same critical layers.
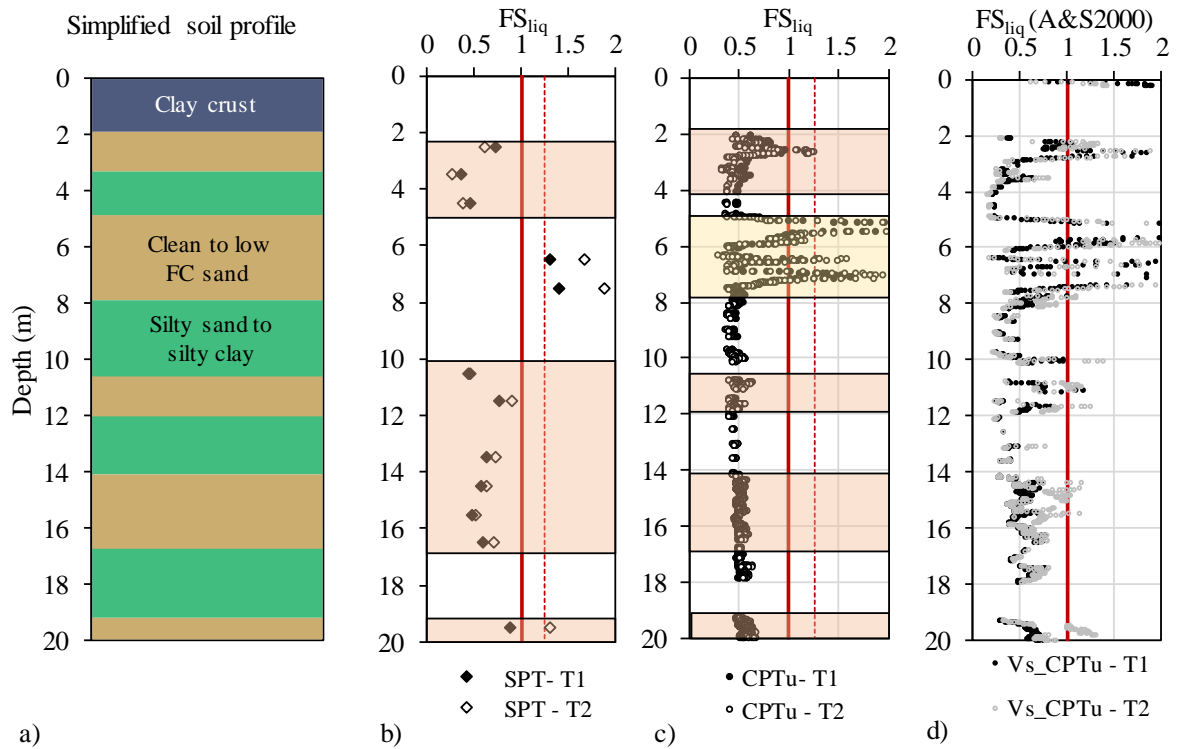
Figure 4.25 – Identification of critical layers in S1: a) soil profile; b) SPT FS_{liq}; c) CPTu FS_{liq}; d) V_S FS_{liq}

The same analysis was performed for S2, as illustrated in Figure 4.26, with the consideration of laboratory-measured fines content from SPT samples and the I_c profile excluding layers with $I_c > 2.6$. In this case, the simplified profile is defined as a 10 m thick fine to medium sand layers with silt-clay interlayers, from 4 to 14 m, confined by layers of non-liquefiable clay. The estimated fines content from SPT lithology are different from the laboratory-measured values, especially in the transition between soil layers, as verified for S1 profile. In the liquefaction susceptibility analyses (Figure 4.27), the critical layers differ slightly: the SPT defined a critical layer with 7 m thickness from 7 – 14 m; the CPTu defined a critical layer from 5 to 14 m, with a few interbedded layers of fine soil better identified in Figure 4.26b, which was also detected on the DMT results. Considering all the field tests, it is reasonable to consider that the critical layer is located between 5 and 14 m. The V_S–FS_{liq} results show good agreement with the other tests plots. The inclusion of the soil type information in the V_S–FS_{liq} profile, allows for a more clear identification of the critical layers, making the V_S-based liquefaction susceptibility assessment more reliable.
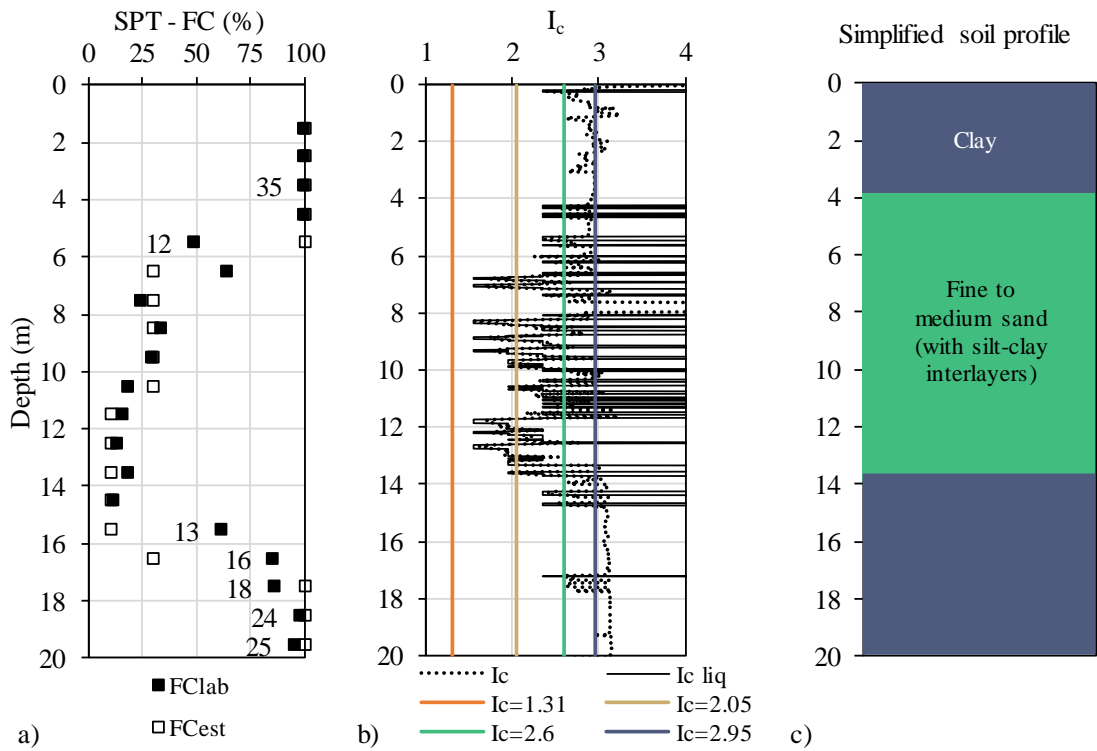
Figure 4.26 – S2 results: a) SPT laboratory-measured fines content; b) simplified I_c for liquefaction; c) simplified soil profile
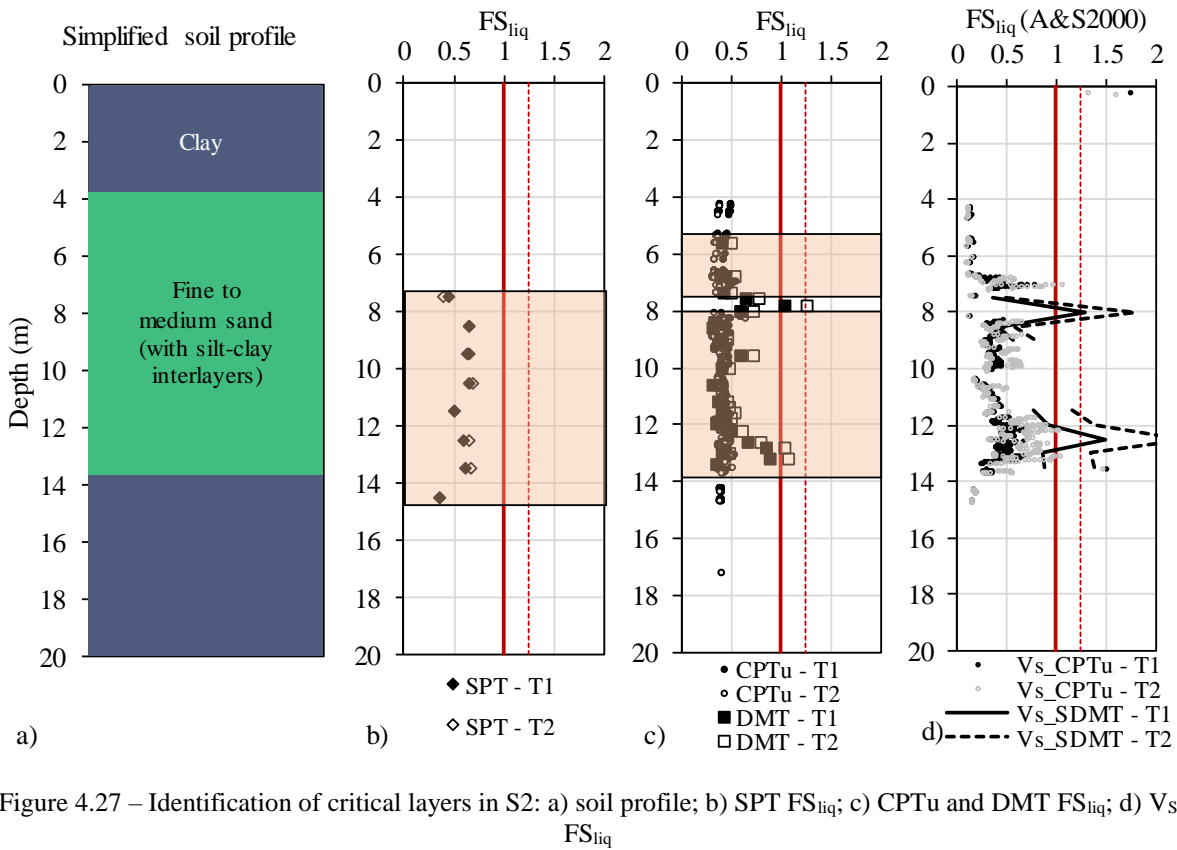
Figure 4.27 – Identification of critical layers in S2: a) soil profile; b) SPT FS_{liq}; c) CPTu and DMT FS_{liq}; d) V_S FS_{liq}

A similar analysis was performed for NB1 and NB2. However, contrary to the previously studied sites, SPT tests were not performed, nor were the grain size and plasticity index for each depth assessed. Despite that, simplified profiles of soil type were defined based on the I_c from CPTu, considering the I_c cut-off value of 2.6 to define non-liquefiable layers.

The NB1 profile is heterogeneous, with interlayers of silty sand and clay. However, a clean sand layer was identified at 3 to 7 m. The silty sand layers are interbedded with silty clay and clay (Figure 4.28). The liquefaction susceptibility analysis is presented in Figure 4.29, where five critical layers were identified. The clean sand layers present some FS_{liq} values higher than 1 in the CPTu-based analyses, probably layers with slightly higher resistance, but it is in general susceptible to liquefaction. Despite the less refined profile, the DMT presents results in good agreement with the CPTu analysis. Five liquefaction susceptible layers were identified at 3 – 7 m, from 8 – 9 m, at 10 – 12 m, from 14 – 16 m, and at 18 – 19 m. However, the effects on the surface caused by the liquefaction of the deeper layers are probably negligible. For the studied developed in this research, the most interesting layer is at 3 to 7 m, as is a liquefiable sand layer, and is where the subsequent sample collection with Gel-Push sampler is focused. Regarding V_S–FS_{liq}, the critical layers identified are coincident with the other tests.
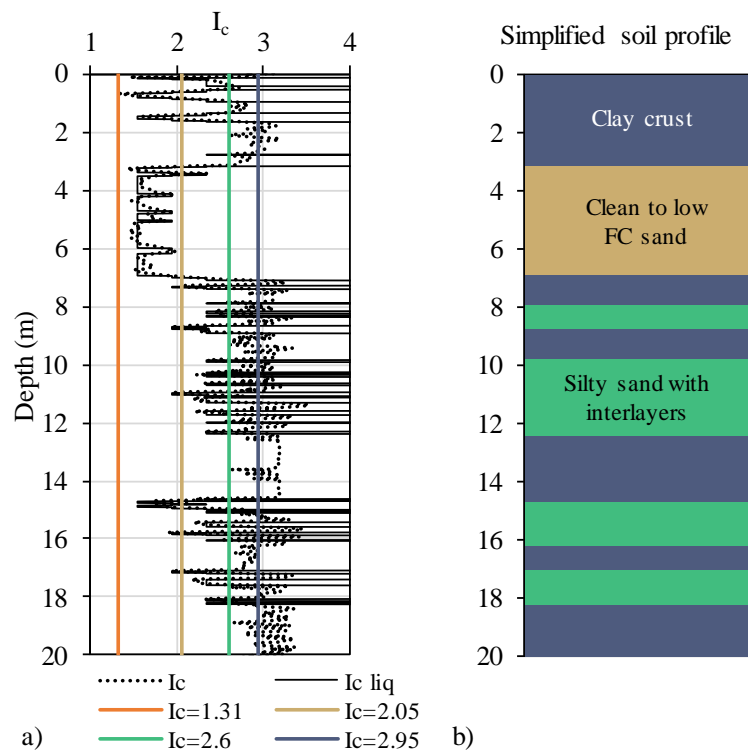
Figure 4.28 – NB1 results: a) simplified I_c for liquefaction; b) simplified soil profile
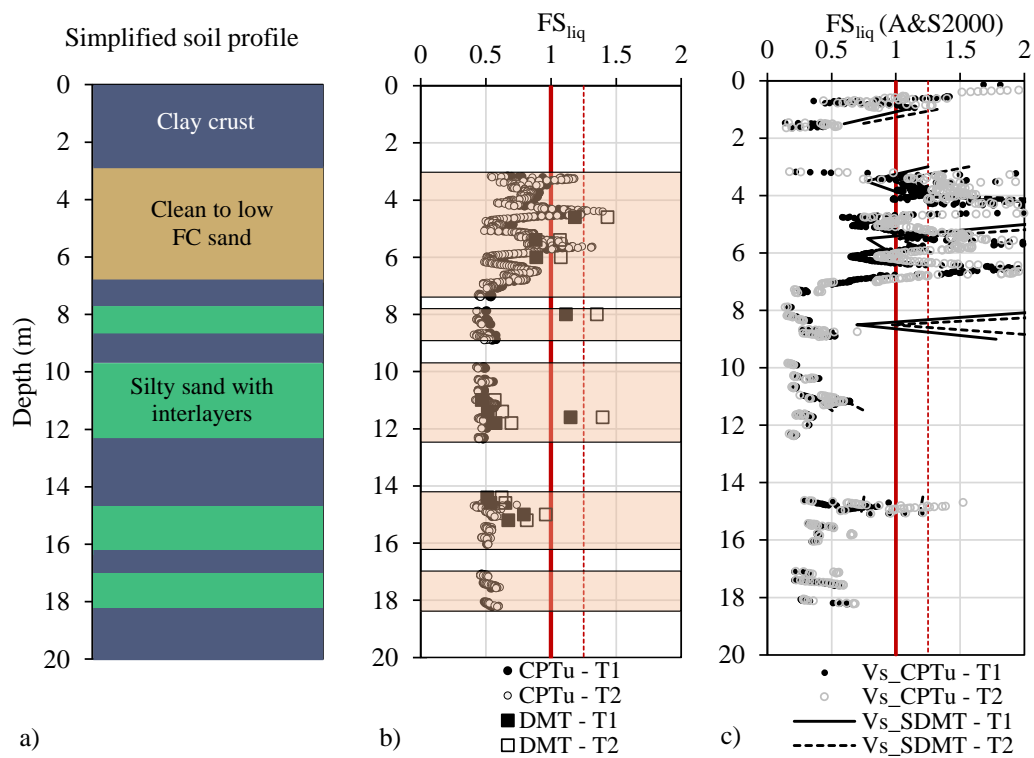
Figure 4.29 – Identification of critical layers in NB1: a) soil profile; b) CPTu and DMT FS$_{liq}$; c) V$_S$ FS$_{liq}$

As for NB2, the simplified soil profile (Figure 4.30) identified a thick clean to low fines sand layer at 5 to 13 m, confined by non-liquefiable layers of clay and silty clay. Some thin silt and clay interlayers were also identified. At NB2, the only test performed was the SCPTu, so no comparison with other tests is possible. Figure 4.30 illustrates the liquefaction susceptibility analysis, where a critical layer is identified at 5 to 14 m, corroborated by the V_S–FS$_{liq}$ results.
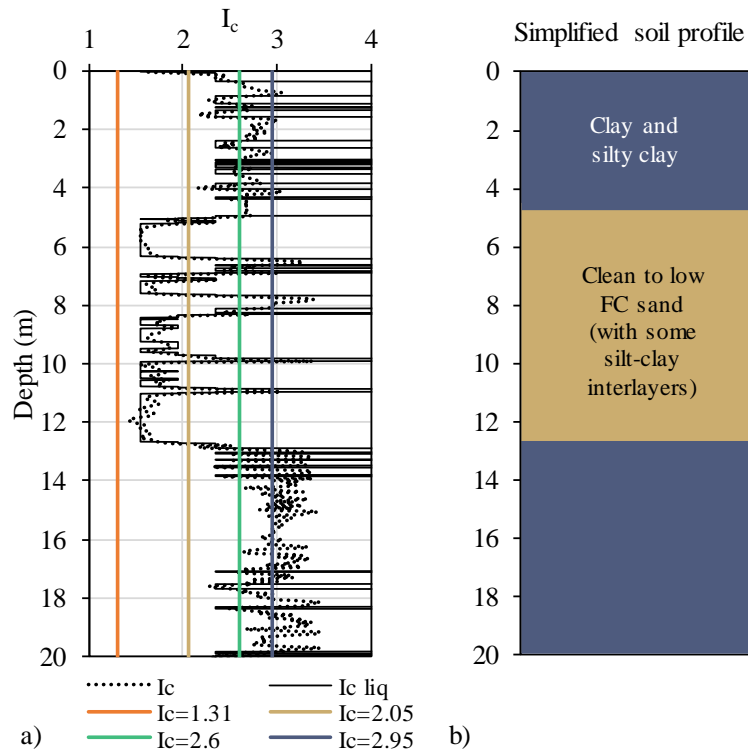
Figure 4.30 – NB2 results: a) simplified I_c for liquefaction; b) simplified soil profile
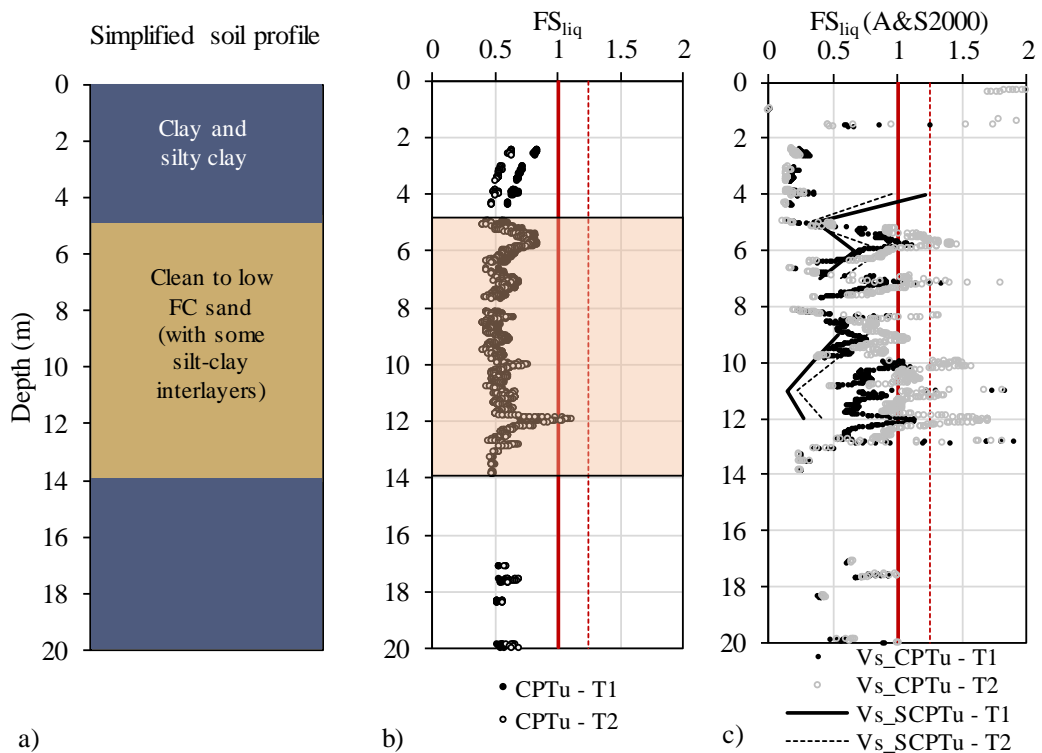
Figure 4.31 – Identification of critical layers in NB2 a) soil profile; b) CPTu FS_{liq}; c) V_S FS_{liq}

As discussed previously, the LPI and LSN are indices that provide information about the risk and consequent severity of damages induced by soil liquefaction. To further compare the performance of different field tests, the computed values of LPI and LSN from the results of SPT, CPTu, DMT, as well as V_S direct measurements are presented in Table 4.3, for both types of seismic action. The results suggest that, except for the LSN in S1, the SPT and CPTu values are similar. It is important to remember that the SPT values presented herein were calculated with the fines content from SPT samples obtained in the laboratory. As was verified in section 4.3.1.3, the use of more accurate FC in the SPT analysis have a positive impact, and should be done whenever possible.

The values from DMT are less conservative, systematically smaller than the SPT and CPTu, and apparently are very dependent on the soil profile. However, the few sites tested with DMT prevent a clear evaluation of the performance of DMT-based liquefaction indices. As was discussed in section 4.2.3, the DMT approach is only valid for $I_D > 1.2$ and $2 < K_D < 6$ (Robertson, 2012), hence few layers are considered liquefiable in NB1 profile, and consequently very low values of LPI and LSN are computed.

Table 4.3 – Comparison of LPI and LSN from different field tests

Seismic action	Type of test	LPI				LSN			
		S1	S2	NB1	NB2	S1	S2	NB1	NB2
Type 1	SPT	19.6	15.5	–	–	42.9	11.7	–	–
	CPTu	14.6	12.5	9.0	15.9	17.8	8.4	16.4	19.7
	DMT	–	11.9	2.4	–	–	7.6	0.9	–
	Vs_A&S2000	–	7.1	8.0	23.4	–	–	–	–
	Vs_Kea2013	–	3.5	2.5	14.4	–	–	–	–
Type 2	SPT	20.6	15.0	–	–	42.1	11.7	–	–
	CPTu	16.2	13.6	12.0	18.5	17.9	8.4	18.3	19.9
	DMT	–	9.8	1.5	–	–	7.4	0.6	–
	Vs_A&S2000	–	4.0	3.1	18.9	–	–	–	–
	Vs_Kea2013	–	1.6	0.5	8.4	–	–	–	–

The LPI from V_S results presented in Table 4.3 reveal that the Andrus and Stokoe (2000) method computes higher results than Kayen et al. (2013), which had already been established before. The most probable factors of the discrepancies between the results are the fact that the V_S measurements occur only every 1 m, making no discretisation of the interbedded layers, and that V_S is not adequate to distinguish sandy from clayey soils, decreasing the accuracy of the methods. In addition, the Kea2013 method is more sensible to lower moment magnitudes, which have a significant impact on the factor of safety, justifying the low values for seismic action type 2 ($M_w = 5.2$). At NB2 site, the V_S approach presents higher values, in agreement with CPTu. In this case, the shear wave velocities were measured with SCPTu and more detailed information about soil types and fines content was available, improving

the performance of FS_{liq} formulations, and consequently of LPI. The use of V_S to assess these indices is only recommended when specific soil type information (grain size from laboratory tests or I_c from CPTu) are available. The LSN was not calculated from the V_S results, as it requires the estimation of relative density, which is not empirically correlated to V_S.

Considering the values of CPTu for comparison between the different experimental sites, Figure 4.32 shows the LPI and LSN values for both types of seismic action, over a colour scale background according to the risk and surficial expression of liquefaction. From a qualitative perspective, the results suggest that S1 and NB2 present very high risk of liquefaction (with LPI higher than 15), while S2 and NB1 present high liquefaction risk (with LPI between 5 and 15). On the other hand, the LSN values predict moderate expression of liquefaction in S1, NB1 and NB2, with some structural damage, and minor expression of liquefaction in S2. Although in LPI the SA type 2 values are slightly higher, the type of seismic action does not alter the classification in terms of risk and severity of damages associated with liquefaction.
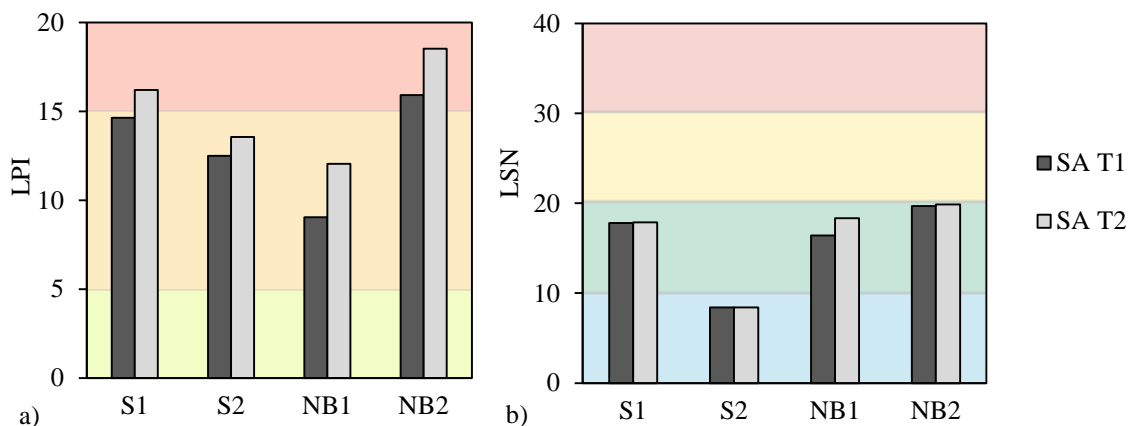
Figure 4.32 – Severity damage from CPTu at the experimental sites: a) LPI; b) LSN

Since LPI and LSN are both indices that provide information about liquefaction risk and severity of damages, some authors have proposed correlations between them, to qualitatively categorize the different sites (Wotherspoon et al, 2015, Giannakogiorgos et al., 2015). It is important to note that LPI is calculated with the layers where FS_{liq} is less than 1.0 and up to a depth of 20 m. On the other hand, the LSN is calculated on the layers where FS_{liq} is less than 2.0 and until 10 m depth. These assumptions produces differences in the calculated indices, making them not directly comparable. In order to compare the results of LPI and LSN, LSN was also calculated considering the first 20 m of depth (LSN_{20}). This approach led to a convergence of the qualitative results of LPI and LSN_{20}, as a greater similarity between the results was observed. Figure 4.33 presents the relationships between LPI and LSN, calculated for

the first 10 m and 20 m. It is clear that a convergence of the results is obtained for LSN_{20}, and the expected severity and damage are more compatible.

As a result, a suggestion of severity and damage assessment using both values of LPI and LSN_{20} is proposed on Figure 4.33b. The proposed boundaries define three severity damage categories: low to minor for LPI lower than 5 and LSN_{20} lower than 5; moderate for LPI between 5 and 15 and LSN_{20} between 5 and 25; and major to severe for LPI higher than 15 and LSN_{20} higher than 25. Note that this is a conceptual approach, as the classification is based on the LPI and LSN from field test results, not considering observed liquefaction damages. On the other hand, some other works have suggested LPI–LSN classification chart based on observed liquefaction manifestations after the Emilia-Romana 2012 earthquake and the 2010 – 2011 Canterbury earthquake sequence (Papathanassiou et al., 2015, Giannakogiorgos et al., 2015). However, in this case no data were available for that type of analysis.
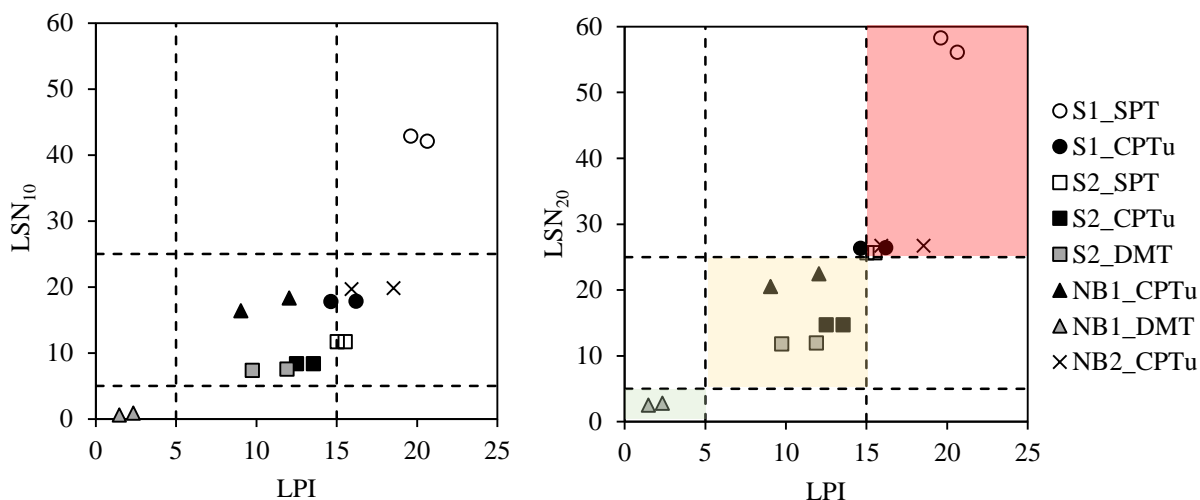
Figure 4.33 – Severity and damage assessment using LPI and LSN results: a) LSN_{10}; b) LSN_{20}

Moreover, 33 additional CPTu tests performed at the same pilot site (Ramos et al., 2021) were integrated in the new chart proposed. The location of the CPTu tests is presented in Figure 4.34. The results were obtained using B&I2014 method for SA type 1. Figure 4.35 presents the results, showing the compatibility of the expected liquefaction severity and damage, and the adequacy of the new LPI and LSN_{20} boundaries suggested.
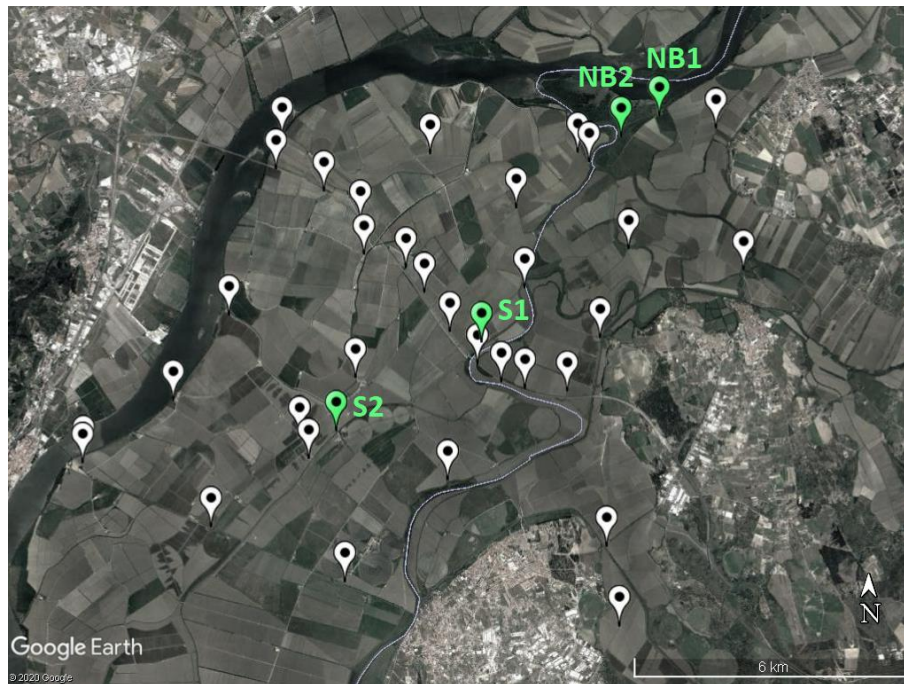
Figure 4.34 – Location of the CPTu testing sites in the LIQUEFACT pilot site area
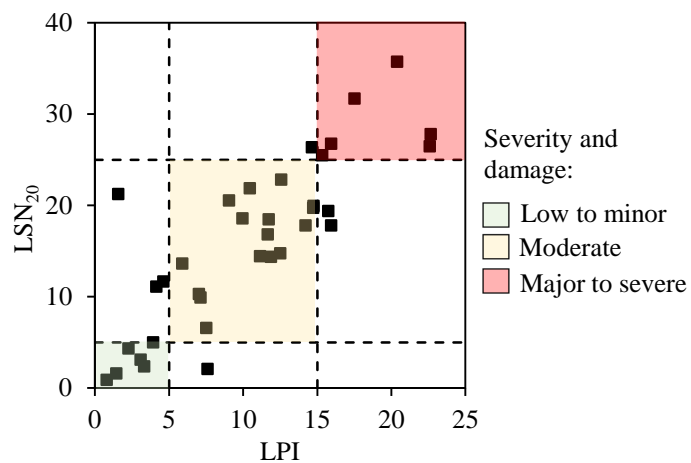
Figure 4.35 – Severity and damage assessment using LPI and LSN_{20} results for 33 CPTu profiles from the studied pilot site

4.4. RECOMMENDATIONS AND MAIN FINDINGS

Following the analysis of the different in situ tests performed at four experimental sites, focusing on the influence of fines contents, CPTu-based methodology adopted, and transitional layers consideration, on liquefaction susceptibility, a summary of the main findings and some recommendations are proposed:

- The consideration of the estimated values or the laboratory-measured values of fines content (FC), in both SPT and CPTu, does not provide different results in terms of factor of safety against liquefaction profiles, as apparently the same layers are susceptible to liquefaction. However, the exclusion of the layers with more than 35% FC and considerable plasticity facilitates the detection of the critical layers, especially in S2 profile, as the layer definition in S1 is more complex due to the heterogeneity of the profile with sand-silt-clay interlayers. It is also evident that the SPT test alone is not enough to clearly define the critical layers, as it considers a macro approach and does not detect small interlayers.

- In terms of LSN and LPI results, the consideration of FC_{lab} in the SPT analysis converges the results with the CPTu, reinforcing the importance of the use of the laboratory FC in the SPT analysis. In the CPTu case, the use of estimated or laboratory FC gives similar results, since the correlations for fines content assessment with CPTu results are already very refined. In fact, the CPTu results do not benefit from the inclusion of FC_{lab}, as liquefaction is better analysed based on the soil behaviour index and not only on fines content. It is also important to note that the SA type variation, in this case, does not provide different results.

- The use of laboratory-measured fines content, FC_{lab}, and associated plasticity is beneficial in the analysis of SPT results, as it provides additional information and allows a more accurate characterisation of soil behaviour. The necessity of complementing the SPT blow count results with a thorough FC evaluation in the laboratory was clear, as SPT results were found to be rather unreliable if based solely on the lithological description of the SPT log.

- The importance of consistency when using a CPTu-based liquefaction assessment method has been highlighted. Therefore, the implementation of the logic tree approach (Lai et al., 2020), which attributes a weight to each method and computes a weighted average of the results to obtain a representative value, should be careful as it may contradict the coherence of the analyses discussed above.

- Although there are no ideal methods, it is proposed the use of Boulanger and Idriss (2014) method, also recommended by Cubrinovski et al. (2016). This method considers the effect of fines content, by directly introducing the fines content values in the calculations, which facilitates the use of laboratory grading data. Furthermore, the methodology was also developed for standard penetration tests (SPT) allowing to contrast and compare results from both tests.

- The elimination of transitional layers is recommended, especially when dealing with interbedded soil profiles.

- The investigated experimental sites were constituted by very heterogeneous soil profiles, with interbedded sand-silt-clay layers. However, in some locations, more homogeneous layers of sand were found and critical layers were identified, at different depths. Despite the heterogeneity

162

of the soil profiles, thick potentially liquefiable layers were found, thus concluding that the experimental site area is prone to liquefaction.

- The use of different methodologies for the assessment of liquefaction susceptibility was beneficial, especially when complemented with laboratory analyses of grain size distribution and Atterberg limits. Nevertheless, some discrepancies were found in the SPT and V_S measurements, particularly in the identification of soil interlayers. The SPT was performed every 1 m, which inhibited the detection of small interbedded layers, while the CPTu was performed each 1 cm, allowing an almost continuous measurement, hence the definition of more detailed soil profiles. The CPTu is the most accurate test to identify small interlayers, and the available complete and strong databases encourage its use. The DMT results presented good agreement with the CPTu analysis. However, the available databases are not as complete as CPTu. In general, the V_S-FS_{liq} profiles identified approximately the same critical layers as the other field tests, but the values of LPI were not in agreement with the other field tests. These discrepancies might be related with the interval of V_S measurements (every 1 m), that does not allow the discretisation of the interbedded layers. However, the measurements of the field V_S are crucial for a comprehensive sample quality assessment.

- From a qualitative perspective, the results suggested that S1 and NB2 present very high risk of liquefaction, while S2 and NB1 present high liquefaction risk. On the other hand, the LSN values predict moderate expression of liquefaction in S1, NB1 and NB2, with some structural damage, and minor expression of liquefaction in S2.

- A new chart relating LPI and LSN_{20} values was proposed and might be used to assess liquefaction severity and damage. The suggested boundaries define three severity damage categories: low to minor for LPI lower than 5 and LSN_{20} lower than 5; moderate for LPI between 5 and 15 and LSN_{20} between 5 and 25; and major to severe for LPI higher than 15 and LSN_{20} higher than 25.

5. SAMPLE QUALITY ASSESSMENT

5.1. INTRODUCTION

The recovery of high-quality undisturbed samples is a challenge, especially when it comes to loose sandy soils, as samples can undergo significant changes during sampling, transport and extrusion in the laboratory. The term "undisturbed" is not literal, and is attributed to samples where the induced disturbance has been minimised and the sample closely represents the in situ soil behaviour. Independently of the sampling procedures, a soil sample will suffer disturbances. According to Taylor (2015), the quality of a sample is dependent on many factors including the type and nature of the soil being sampled, the sampling equipment design, and operational factors such as the drilling techniques adopted, transportation, sample storage and laboratory practices. Moreover, Baligh et al. (1987) listed some of the causes for soil disturbance during tube sampling: changes in soil conditions ahead of the advancing borehole during drilling operations; penetration of the sampling tube and sample retrieval to ground surface; water content redistribution in the tube; extrusion of the sample from the tube; drying and/or changes in water pressures; and, trimming and other processes required to prepare specimens for laboratory testing. Another cause of sample disturbance is the stress relief the sample suffers when removed from the ground. The zero stress condition in the laboratory may be responsible for changes in strength, stiffness, and pore pressure or volume change responses (Ferreira et al., 2011).

The collection of high-quality samples is essential for the rigorous soil characterisation and for subsequent performance of advanced laboratory tests, since the reliability of the laboratory results depends on the quality of the samples retrieved. This means that the accurate characterisation of the soil behaviour based on laboratory tests is conditioned by the representativeness and quality of the collected samples. In this sense, the assessment of the degree of sample disturbance is important before further interpretation of soil behaviour based on laboratory tests.

This Chapter addresses the assessment of the quality of samples collected with the three samplers described in section 3.6, by means of a variety of methods, such as: visual inspection, the comparison of in situ and laboratory measured seismic wave velocities, the measurement of volumetric strains during reconsolidation, and the comparison between in situ correlations and laboratory measured soil density.

The sample quality assessment allows the identification of the most suitable samples to be subjected to extensive laboratory tests and the determination of what type of sampler is more adequate for a specific site. Moreover, recommendations and main findings are summarised at the end of the Chapter.

5.2. VISUAL INSPECTION

The visual inspection is an empirical, hence subjective, quality assessment method, as it is based on the observation of the peripheral surface of the samples, when they are removed from the inside of the sampling tube.

Regarding the samples collected with Mazier (section 3.6.1), the specimens were selected based on the soil behaviour type profile from CPTu results and removed from the sampling tube before the performance of the triaxial test. According to the type of soil actually found and the external conditions of the sample, it was discarded or prepared for triaxial testing. Figure 5.1 shows some examples of samples collected with Mazier. Some radial damage is observed in samples with higher fines content, probably caused by friction between the sample and the PVC tube during extrusion. Samples with lower fines content revealed lower disturbances and were adequate to be tested subsequently.

On the other hand, the samples collected with GP and D&M samplers (sections 3.6.2 and 3.6.3) were extruded from the sampling tubes immediately after they arrived to the laboratory. The samples were divided into individual samples with the dimensions required for the triaxial tests. As the sample was extracted from the sampling tube, moved by the hydraulic piston, the visual inspection was carried out. The GP and D&M samples were identified and a description of the top and bottom soil type was recorded, for future reference and selection of the samples for further laboratory testing. Figure 5.2 shows some samples after the extraction from the liners. In the majority of samples, no radial damage was identified. The peripheral surface of the samples is smooth and does not show any damage such as holes, cracks or distortion of shape. The incorporation of the viscous polymer in the GP-S and the smooth brass sampler surface in the D&M reduced the friction between the soil and the liner wall, protecting the sample surface.

Figure 5.1 – Samples collected with Mazier sampler: a) and b) samples with damaged surface; c) and d) homogeneous samples adequate for triaxial testing

In summary, this method consists on the observation of the sample surface, the visual characterisation of the soil type that constituted the samples and the identification of visible damage on the surface, such as holes, cracks or distortions of the shape. It is not adequate to determine the sampling effects on the soil behaviour, but rather allows for the preliminary selection of samples for extensive laboratory testing.

Figure 5.2 – Samples extracted from GP sampling tubes: a) clay sample; b) and c) silty sand samples; d) and e) sand samples

5.3. COMPARISON BETWEEN FIELD AND LABORATORY DETERMINED SHEAR WAVE VELOCITIES

One of the most common non-destructive techniques to assess sample quality is based on the estimation of shear wave velocities (or small-strain shear modulus). Shear waves, contrary to compression waves, can only propagate through the soil skeleton, so they provide useful information about changes in soil fabric caused by sampling (Viana da Fonseca and Pineda, 2017).

The laboratory and field-based measurements of V_S are compared in this section to assess sample quality. The evaluation of sample quality is performed by directly comparing the two measurements and analysing the ratio $V_{Slab}/V_{Sinsitu}$, where the measurements are normalised according to mean effective stress and void ratio. Before discussing V_S comparisons, it seems appropriate to outline the methodology for measuring the V_S of soil specimens in the laboratory, using bender elements, which is done in the following section.

5.3.1. BENDER ELEMENT TESTING

The measurement of seismic waves in the laboratory plays a significant role in the present research. The shear (S) wave velocities provide information about soil stiffness and are used for the assessment of sample quality and the characterisation and comparison of the small strain behaviour of soils. On the other hand, the measurement of compression (P) wave velocities is important to assess the saturation degree (S_r) of a specimen, i.e. to ensure that the specimen is fully saturated before continuing with the test procedures.

One of the most common non-destructive techniques to assess seismic wave velocities in the laboratory is the use of piezoelectric transducers, particularly bender elements (Figure 5.3). Bender elements (BE) are composed of two piezoceramic thin plates connected to a metallic central foil and outer faces electrodes. When one plate expands and the other contracts, a bending motion is generated. The excitation frequency controls the bender element motion. Low frequencies (<10 kHz) induce a bending movement, transmitting an S wave. However, if the frequency is high enough (>10 kHz), the bending motion transforms into a compression-extending deformation, transmitting a P wave (Ferreira, 2009).
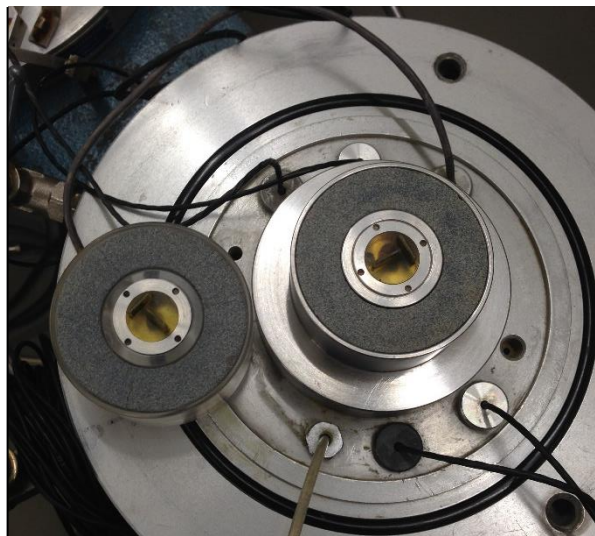
Figure 5.3 – Bender elements

Besides the piezoelectric transducers, to define the seismic wave characteristics and study the propagation velocities, a system composed of three devices is required: a function generator, a signal amplifier and an oscilloscope (Figure 5.4).
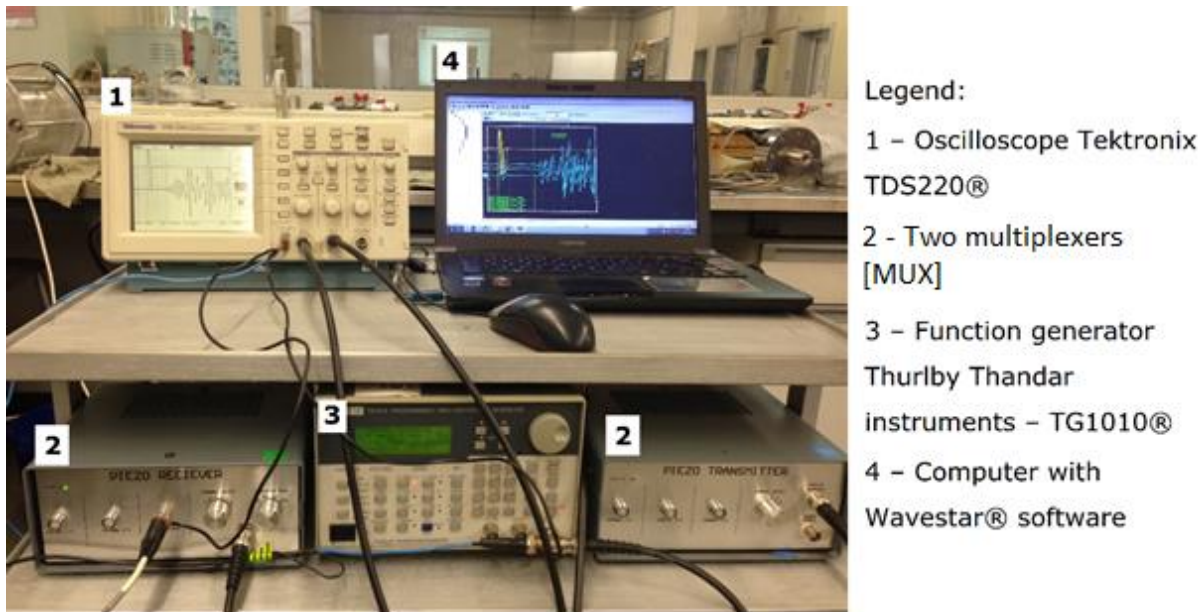
Figure 5.4 – Equipment required for seismic wave measurement

The function generator (TTi – Thurlby Thandar instruments – TG1010®) allows the creation of a variety of electric signals (sinusoidal, square, ramp, arbitrary), continuous or repeated pulses at a given frequency. The two multiplexers allow the amplification of the response wave signal and management of the channel of each transducer pair. The oscilloscope (Tektronix TDS220® model) is able to record the signals and identify the time interval between the transmitted and received waves. It is connected to a personal computer with the WaveStar® software for data acquisition and interpretation.

Most of the triaxial cells at the laboratory at FEUP have bender elements installed, to measure seismic wave velocities in the soil specimens during the different test stages. Moreover, a pair of bender elements not coupled to a triaxial chamber was used to measure the seismic waves in the specimens from GP and D&M after extrusion from the sampling tube, for a preliminary assessment of the quality of the samples.

5.3.1.1. Test procedure

In testing undisturbed specimens, the bender elements are introduced on the top and bottom ends of the specimens and are aligned in the same plane so the wave is transmitted with the maximum energy and the signal is clear. One of the benders functions as the transmitter, bending according to the produced signal with the characteristics of shape and frequency defined in the function generator, while the other receives the wave signal. Both signals are processed and displayed in the oscilloscope monitor. The

received signals were amplified with a gain of 200 and the oscilloscope was earthed to reduce noise. Figure 5.5 illustrates a typical configuration and operation of bender elements.
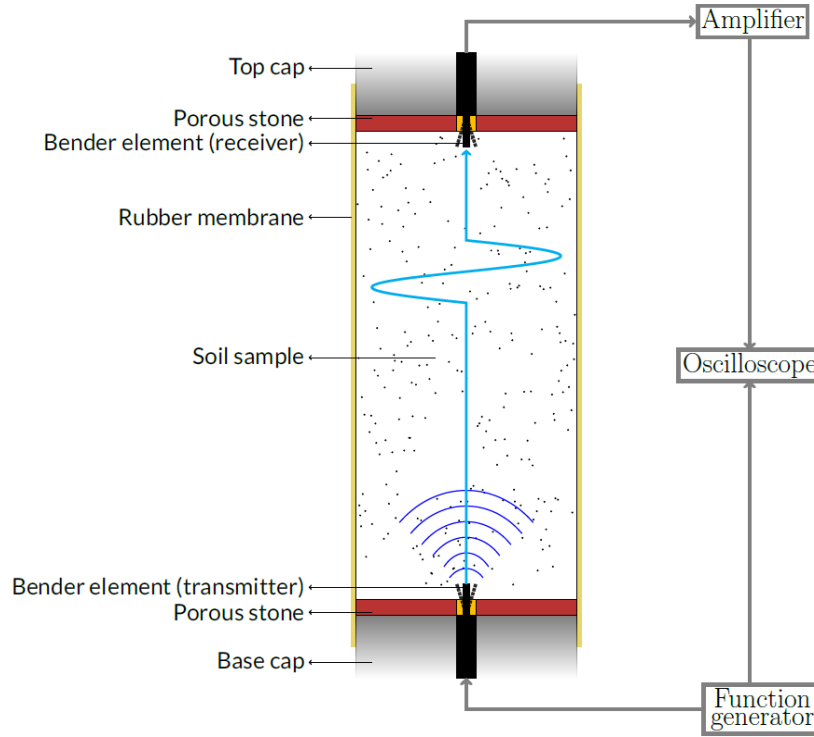
Figure 5.5 – Configuration and operation of BE test (Molina-Gómez et al., 2018)

5.3.1.2.   Interpretation of wave measurement results

The seismic wave velocity is determined by the ratio between the travel length (L_t), and the arrival time, defined by the time between the moment the wave starts to propagate and its arrival at the receiver BE (t_t), as expressed in equation (5.1).

$$V_{S\ or\ P} = \frac{L_t}{t_t} \tag{5.1}$$

However, there are conflicting guidelines for the selection of the travel length and travel time for shear wave determinations with bender elements (Lee and Santamarina, 2005). As for the travel length, the definition adopted consists on the tip-to-tip distance, i.e. the distance between the tips of the top and bottom bender elements, supported by the results of Lee and Santamarina (2005) and Ferreira (2009).

On the other hand, the travel time determination is more challenging. Figure 5.6 presents a typical signal of an S-wave. There are multiple places were the first arrival can be defined (A, B, C or D). The discussion about the different first arrival time considerations is not the focus of this work. Following

the proposals from Lee and Santamarina (2005) and Ferreira (2009), herein, the first arrival time is considered to be on point C, as points A and B indicate a polarity change that is related with near-field effects, and point D corresponds to a time when the receiver signal already started.
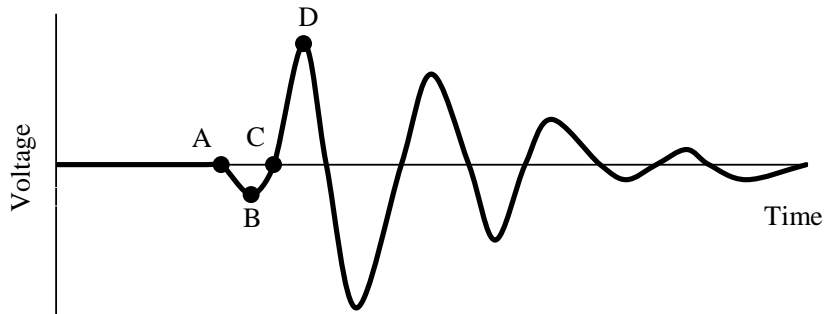
Figure 5.6 – Typical S-wave signal: A – first deflection, B – first bump maximum, C – zero after first bump, and D – major first peak

To avoid signal misinterpretations, related with near-field effects, cross-talk and reflection of P-wave in the S-wave output signal, it was necessary to perform the test measurements with a minimum of three different frequencies (Viana da Fonseca et al., 2009). Figure 5.7a and b present two examples of the plots of transmitted and received waves, for shear and compression wave, respectively. The shear waves were assessed for a range of frequencies of 2-8 kHz while the P waves were obtained for a range of frequencies of 50-100 kHz.
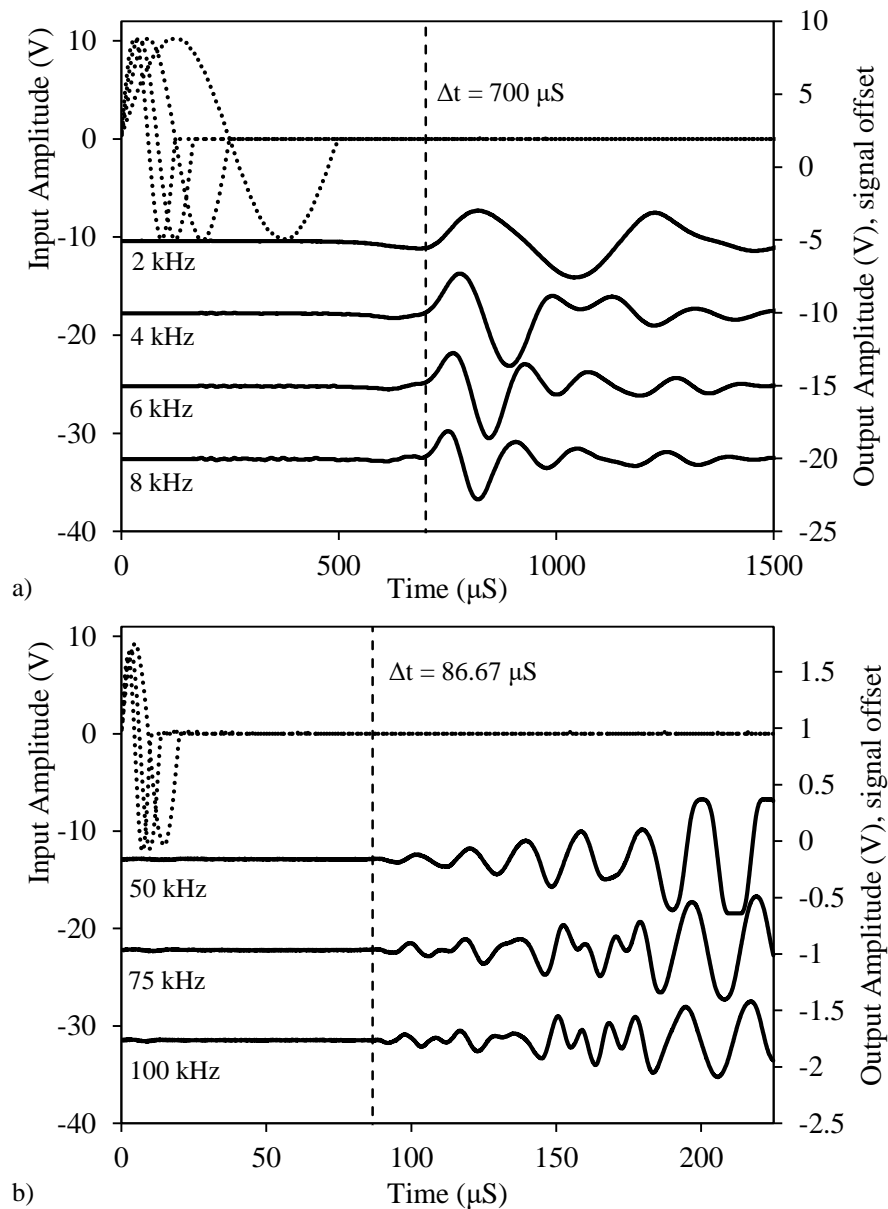
Figure 5.7 – Bender element test results: definition of the arrival time: a) S-waves; b) P-waves

5.3.2. DETERMINATION OF V_S IN THE LABORATORY

As described before, the samples collected with Gel-Push and Dames and Moore samplers were extruded from the sampling tube into individual specimens upon arrival to the laboratory. The individual samples were tested using a pair of bender elements outside a triaxial chamber, and the shear wave velocities were measured on a bench, as shown in Figure 5.8. Due to the test configuration, these tests are referred to as "bench tests".
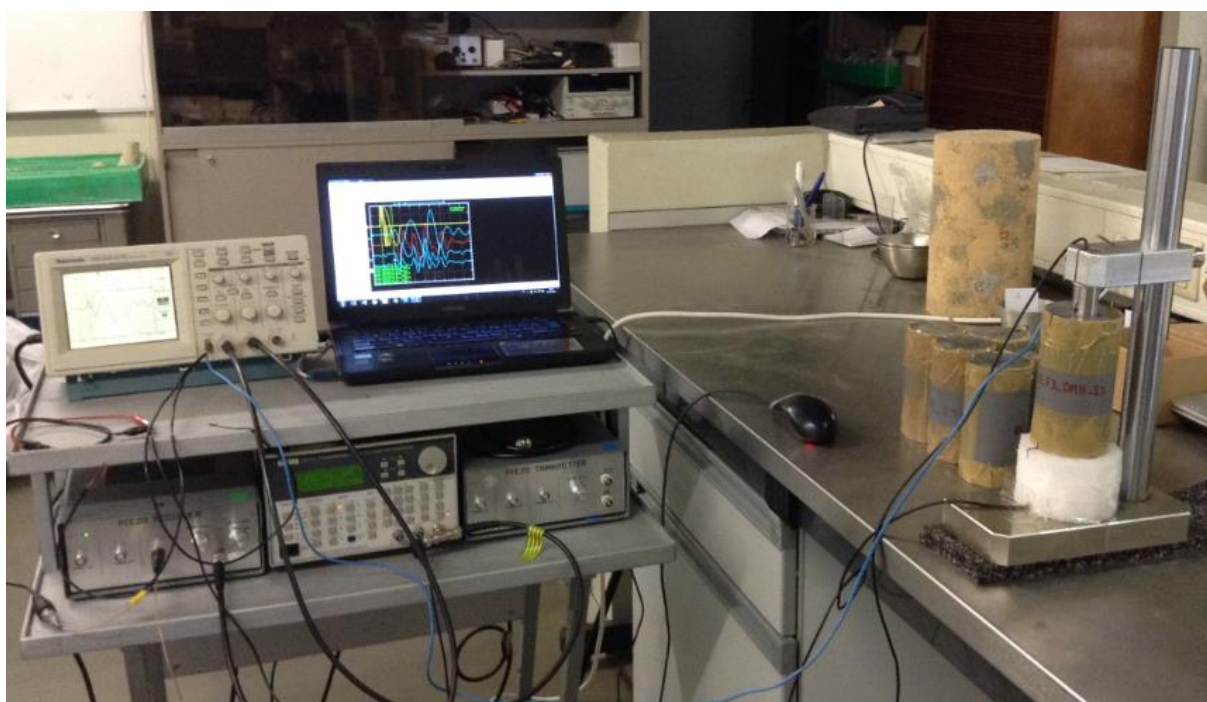
Figure 5.8 – BE bench tests configuration

On the other hand, a more selected group of specimens, including the Mazier collected and some GP, was tested in the triaxial apparatus, where bender elements are installed. The shear wave velocities were measured at different test stages including after reconsolidation to the in situ stresses. As the specimens were consolidated to the in situ mean effective stress and the determination of void ratio and unit weight is more precise than the estimated for the bench samples, these results are considered to be more accurate. It should be noted that the triaxial specimens were isotropically consolidated, which does not represent the in situ K_0 condition and might influence the results obtained.

For a more consistent comparison between laboratory and field-measured shear wave velocities, a normalisation procedure to the respective void ratio was performed. Moreover, as the bench tested specimens are unconfined, a normalisation to the in situ stresses was introduced.

a) Void ratio normalisation

The void ratio values were not directly measured in situ and, therefore, some simplifications were adopted to obtain these values. The specific gravity was considered 2.65 and the soil was considered to be fully saturated, as all samples were collected below the ground water level. The unit weight at each depth was estimated from the CPTu correlation from Robertson and Cabal (2010). As there is some uncertainty about the exact location of the samples collected, a mean value of the unit weight estimation for the first and last 25 cm from the collection depth was considered. The void ratio of the bench

specimens was estimated based on the weight and water content of each individual specimen. As the GP and D&M specimens were confined inside similar PVC tubes, a constant diameter and height was considered (72 mm diameter and 148 mm height for the GP samples and 61 mm diameter and 120 mm height for the D&M samples). The void ratio of the triaxial tested specimens was determined at the end of the test, having a more accurate determination of the water content, dimensions, weights and volumetric changes.

The influence of void ratio is accounted for by the consideration of a void ratio function, to normalise the results. Various approaches have been suggested for the definition of the void ratio function, as discussed in section 2.2.4. When no specific study is carried out to determine the void ratio function of the soil, one of the reference expression can be applied directly. Herein, the void ratio function proposed by Lo Presti et al. (1995) was used (equation (5.2)). Therefore, the measured shear wave velocities, V_S, were normalised as V_S^* (equation (5.3)).

$$F(e) = e^{-1.3} \tag{5.2}$$

$$V_S^* = \frac{V_S}{\sqrt{F(e)}} \tag{5.3}$$

b) Mean effective stress normalisation

Since the bench tested samples were only confined by the PVC tube to where they were extruded after sampling, a direct comparison of laboratory and field measured V_S is not advisable. Soil stiffness is strongly affected by effective stress, especially in sands. To overcome this issue, a normalisation to in situ stresses was implemented, where V_S^* is the shear wave velocity normalised with the void ratio function, p'_0 is the effective stress measured in situ (considering $K_0=0.5$), and p' is the estimated mean effective stress for bench conditions.

$$V_S^{**} = V_S^* \left(\frac{p'_0}{p'}\right)^{0.25} \tag{5.4}$$

The value of p' considered as the mean effective stress in bench specimens was 2 kPa, considering the sample height and a unit weight of 19 kN/m³ (average value for every sample collected). The correction values depended on the in situ confinement pressure and ranged from 1.93 and 2.82 for p'_0 of 27.5 kPa to 127 kPa, respectively (the ranges of in situ confinement of the samples tested with bench BE).

The specimens tested on the triaxial chamber were reconsolidated for the corresponding in situ stresses. Although the reconsolidation target was the in situ value, in some cases the mean effective stress in the

triaxial test was slightly different from the field value. Therefore, the mean effective stress normalisation was also implemented on the V_S values from triaxial tested specimens, to avoid misinterpretations.

The normalised shear wave velocities obtained with bench tests were compared with the respective normalised shear wave velocities obtained in the triaxial chamber, where the specimen was confined to the in situ pressure. The average difference between bench tests and triaxial tests results was 5%, which validates the choice of 2 kPa as the bench samples confinement.

5.3.3. PROFILE COMPARISONS

Figure 5.9 presents comparisons between the shear wave velocities measured in the field with SDMT and SCPTu, at each experimental site, and the CPTu-V_S correlation from Robertson (2009). Overlaying the field V_S profiles are the V_S values measured in the specimens tested in the triaxial apparatus. The profiles presented are not normalised for void ratio or mean effective stress. The laboratory results exhibit some agreement with the field values. The CPTu-based prediction is very close to the direct down-hole measurements, which validates the consideration of CPTu-V_S profile at S1, since there was no direct measurement at this site. However, these comparisons are only shown to illustrate more clearly the tests performed in depth, as the direct comparisons presented below for each specific sample allow a more accurate evaluation of each individual sample quality. Notwithstanding, the representation of Figure 5.9 shows a proximity between field and laboratory measurements even before normalisation, anticipating that the confinement induced in the laboratory simulates well the in situ conditions.
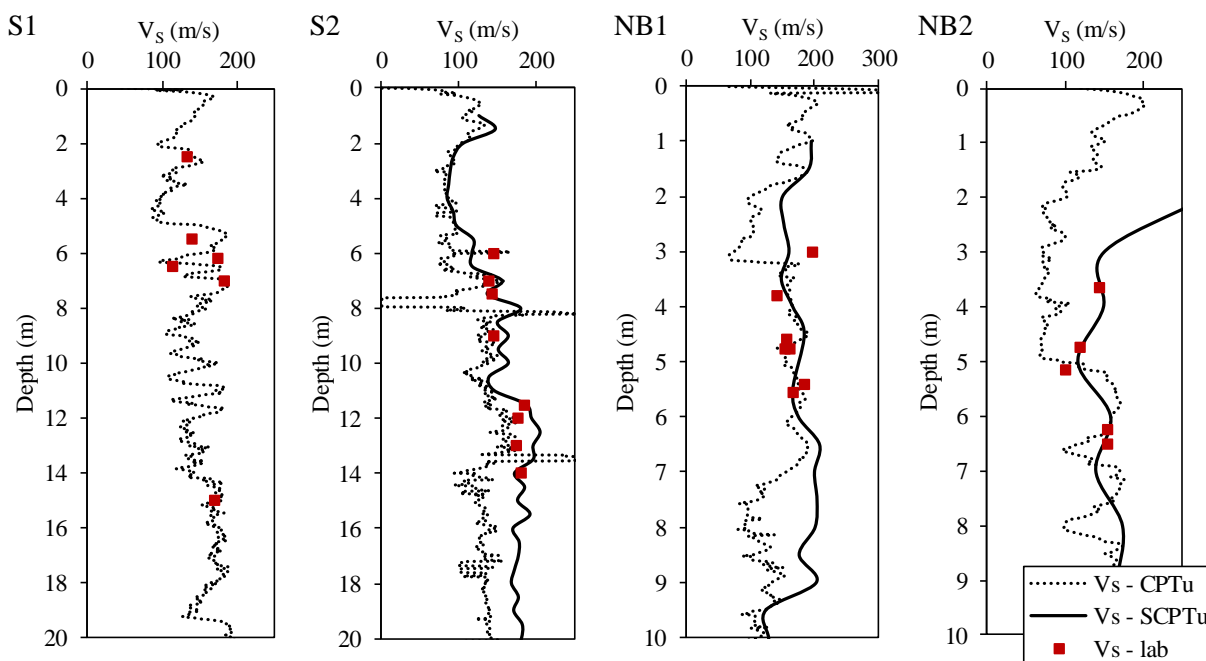
Figure 5.9 – V_S comparison profiles

5.3.4. DIRECT COMPARISONS

The comparison of laboratory and field-measured shear wave velocities of specific samples is presented first for the GP and D&M samples tested on the bench (BE-bench), and then for the Mazier and GP specimens tested under triaxial conditions (BE-CTx). The sample quality classification used was proposed by Ferreira et al. (2011) and divides samples into five categories according to their quality and condition, based on the $V_{S}^{*}{}_{lab}/V_{S}^{*}{}_{insitu}$ ratio, as expressed in Table 5.1.

Table 5.1 – Sample quality classification based on V_S normalised ratio (Ferreira et al., 2011)

Quality zone	$V_{S}^{*}{}_{lab}/V_{S}^{*}{}_{insitu}$	Sample quality	Sample condition
A	≥ 0.85	Excellent	Perfect
B	0.85 - 0.70	Very good	Undisturbed
C	0.70 - 0.60	Good	Fairly undisturbed
D	0.60 - 0.50	Fair	Fairly disturbed
E	< 0.50	Poor	Disturbed

Figure 5.10 presents the results of the samples tested with BE-bench, collected at NB1 and NB2 with GP and D&M samplers. The charts present the reference lines for the five sample quality categories from Table 5.1. The results show that only 26% of the samples collected with GP have less than 60% ratio, being fairly undisturbed to disturbed. On the other hand, within the D&M samples, only 2 samples are categorised as fairly disturbed, reflecting the better performance of D&M in this case.

Around 6% of GP and 33% of D&M samples present quality ratios above 1:1, which was not expected. In theory, the stiffness of a specimen in the laboratory are usually lower than in situ, as sampling and extrusion processes induce changes in soil conditions caused by water redistribution, and mainly by stress relief. These changes normally induce a decrease in stiffness, hence the laboratory-measured V_S are usually than the field-measured V_S. However, the transportation or water content loss (increase in suction) might influence the state of the specimens, and increase the laboratory V_S values. In the present research, additional factors may also be attributed to these results, particularly errors related with the determination of V_S of bench tests and V_S in the field.

The fact that the direct field measurements of V_S were performed at each 50 cm in SDMT and each 100 cm in SCPTu, and a mean value is considered, can produce uncertainties, since in reality the profile layers are not homogeneous. Moreover, the void ratio normalisation requires the knowledge of the void ratio at each depth. For that reason, an estimated unit weight is obtained from the CPTu results, using Robertson and Cabal (2010) proposal. Since the soil profiles are very heterogeneous, the unit weight determined might not represent accurately the real value. Therefore, the determination of in situ void ratio can induce errors on the results.

The possible causes of inaccuracies in the interpretation of bench tests derive mainly from errors associated with void ratio determination and lack of confinement of the sample during V_S measurements. Analysing the samples with ratios higher than 1:1 in more detail, it was concluded that they were mainly clays and very fine soils. The void ratio is determined based on estimation of specific gravity, dimensions and water content. As the water content is estimated from the ends of the entire sampling tube, it can induce significant errors in the void ratio assessment. On the other hand, the lack of confining pressure in the bench samples affects the coupling between the BE and the soil, leading to weaker signal and poorer resolution, obscuring signal interpretation.
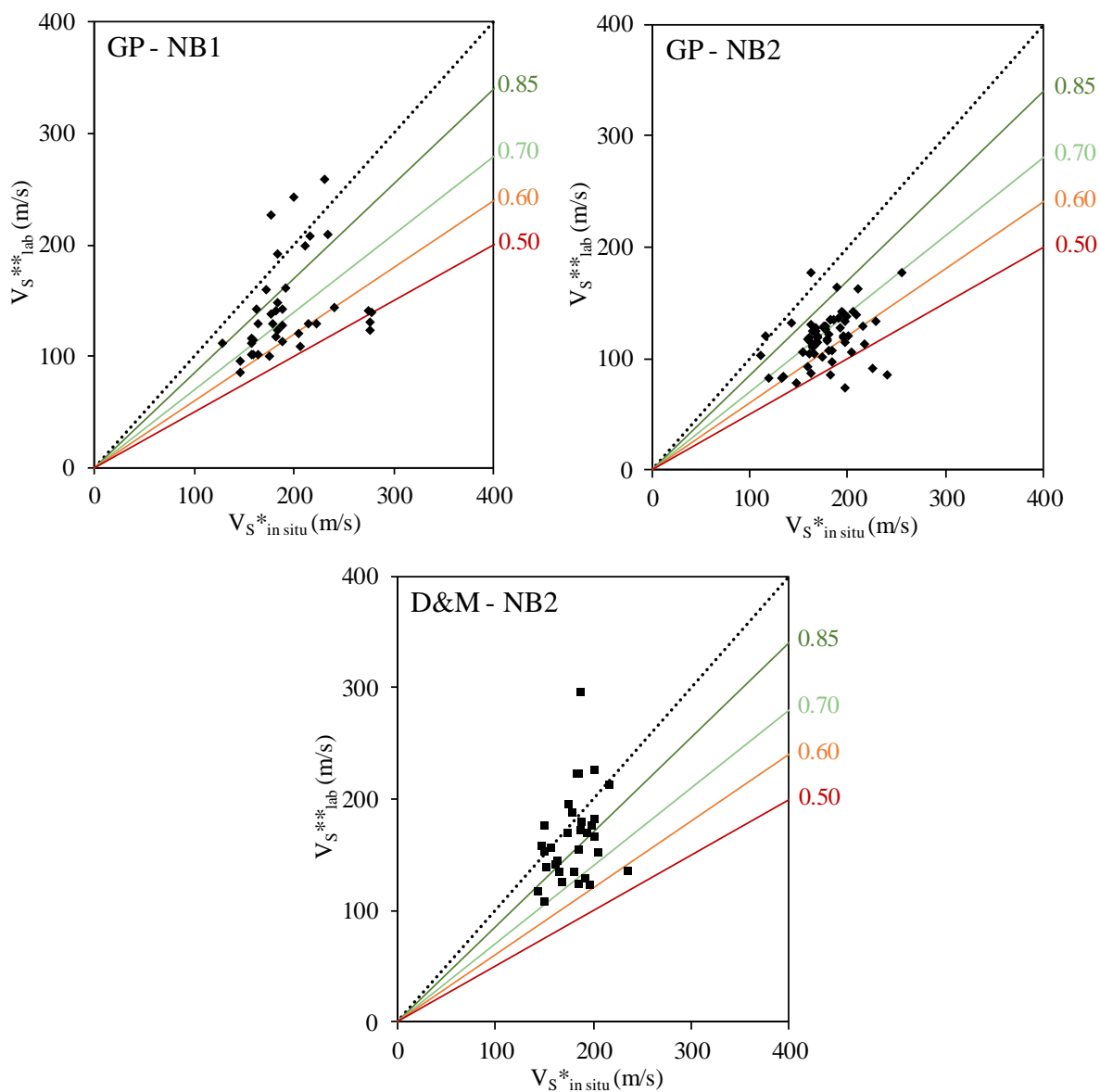
Figure 5.10 – Results of sample quality assessment from BE-bench tests

Some of these issues can be minimised by analysing the results from specimens tested under triaxial conditions. The specimens were reconsolidated to the in situ stresses and are fully saturated, simulating more accurately the field state conditions. The dimensions, void ratio and water content are also more accurately measured so fewer errors are accounted for. As the results are more precise, the assessment of sample quality is improved. However, the bench test analysis is very important for a preliminary quality assessment and to choose the least disturbed specimens to test further.

Figure 5.11 presents the results of the samples collected with Mazier and Gel-Push samplers, tested with BE-CTx. With the exception of some Mazier collected samples and one GP sample that have ratios below 0.60, the majority of samples have good to excellent quality (ratios higher than 0.60). Besides, no sample was found to be poor quality/disturbed (ratio lower than 0.5), demonstrating the adequate performance of both samplers for collecting soil samples of a variety of soil types.

The samples collected with the GP present higher quality than the ones collected with the Mazier. This was expected as the mechanism of sample retrieval with Mazier involves a rotatory movement with water injection, which disturbs the adjacent soil and can wash away particle bonds damaging the natural structure of the soil. For this reason, the samples collected with the Mazier are more disturbed. On the other hand, the GP sampling process consists on the static penetration on the soil of the sampling tube and the presence of the viscous gel lubricates the liner and decreases friction while the soil enters the liner. This is probably one of the reasons why the GP samples present higher quality.

Also illustrated in Figure 5.11b are the comparison between V_S determined from BE-bench and BE-CTx, for the selected GP samples. The inaccuracy in the estimation of void ratio and water content of samples after extrusion prevents the rigorous estimation of V_S in bench tests, reinforcing the importance of testing samples with more advanced procedures. Moreover, the ratios $V_{S\ lab}^{**}/V_{S\ insitu}^{*}$ were plotted against $V_{S\ insitu}^{*}$ and fines content (Figure 5.11c and d). A subtle correlation between FC and $V_{S\ lab}^{**}/V_{S\ insitu}^{*}$ suggests that the quality decreases with the FC increase. However, more samples with higher fines content are needed to support this assumption.

Notwithstanding, it can be concluded that both samplers are able to collect good to high-quality samples. The consideration of BE-CTx allows a more accurate determination of sample quality than BE-bench, although these provide a good preliminary assessment, allowing the selection of the best samples to invest in more advanced testing procedures.
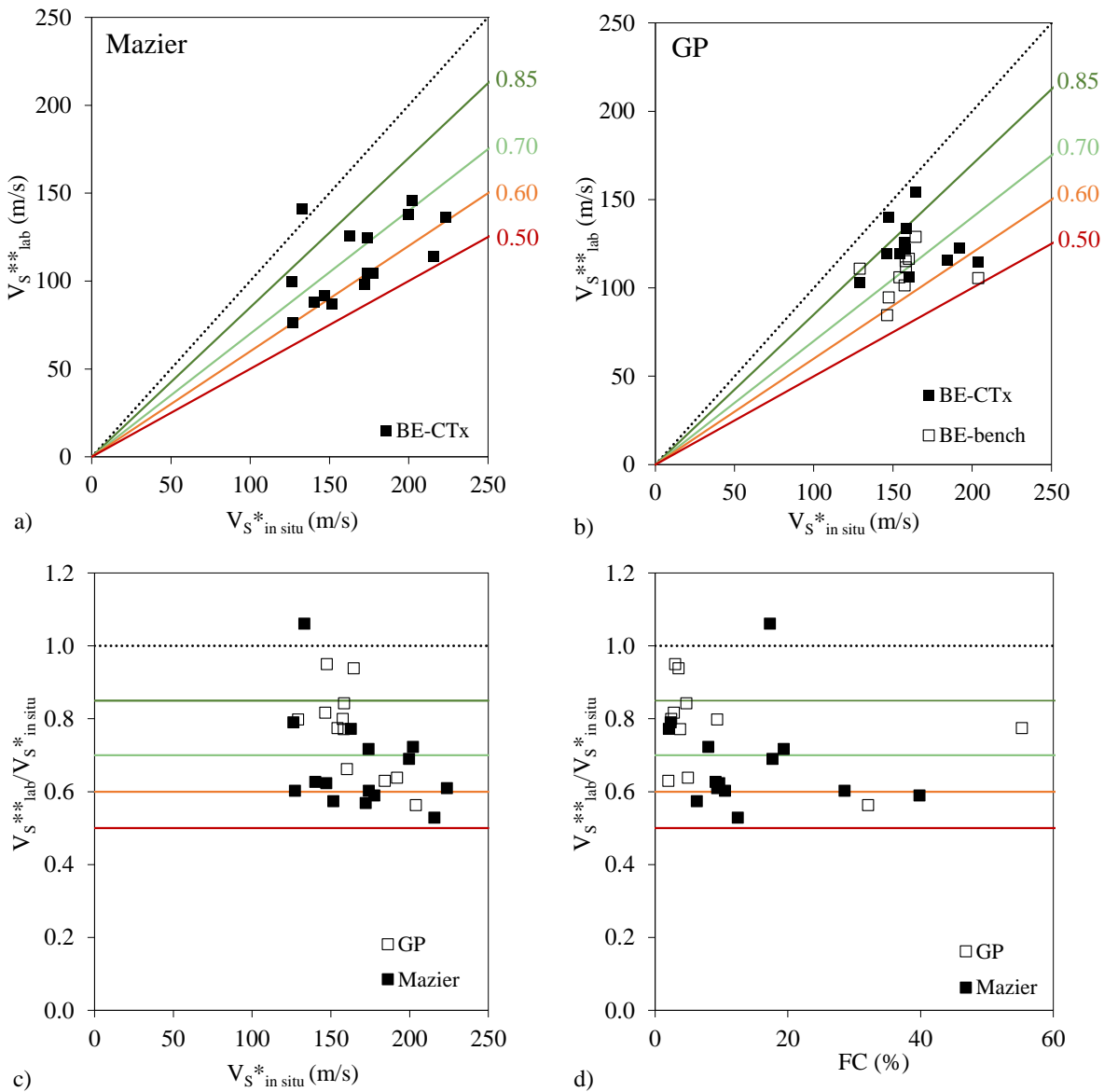
Figure 5.11 – Results of sample quality assessment from BE-CTx tests: a) Mazier samples; b) GP samples; c) correlation between $V_S^*{}_{insitu}$ and $V_S^{**}{}_{lab}/V_S^*{}_{insitu}$; d) correlation between FC and $V_S^{**}{}_{lab}/V_S^*{}_{insitu}$

5.4. EVALUATION OF VOLUME CHANGE DURING RECONSOLIDATION

The volumetric strains experienced by a specimen when reconsolidated to the in situ stresses are associated with the level of sample disturbance, as they reflect the effective stresses reduction caused by sampling procedures. Andresen and Kolstad (1979) suggested that the volumetric strains during reconsolidation are related to the sample quality. This concept was also adopted by Terzaghi et al. (1996), who suggested the Specimen Quality Designation (SQD), based on ε_v. According to this scale, the best quality samples are designated A and have $\varepsilon_v < 1\%$ while the worst quality ones are designated

by E with $\varepsilon_v > 12\%$. Specimens of intermediate quality are between these values. This characterisation of sample quality is mainly applicable to cohesive soils, especially soft clays and silts, and may not be suitable for all types of soils.

In a similar way, Lunne et al. (1997) proposed an approach based on the void ratio change, which also reflects the volumetric strains. The classification is determined by the ratio of $\Delta e/e_0$, where Δe is the difference between the initial void ratio (e_0) and the void ratio at the end of reconsolidation, and was developed with test results from marine clays with a variety of plastic indexes, water contents and overconsolidation ratios. The sample quality is categorised according to the criteria presented in Table 5.2.

Table 5.2 – Sampling quality assessment from volumetric strains (from Lunne et al., 1997)

| | OCR | | Quality [*] |
	1 - 2	2 - 4	
	< 0.04	< 0.03	Very good to excellent
$\Delta e/e_0$	0.04 - 0.07	0.03 - 0.05	Good to fair
	0.07 - 0.14	0.05 - 0.10	Poor
	> 0.14	> 0.10	Very Poor

[*] use of the soil for the characterisation of mechanical properties

The classification from Lunne et al. (1997) was applied to the intact samples collected with Mazier and Gel-Push at the four locations. Figure 5.12 presents the results, compared with the fines content of each sample. The $\Delta e/e_0$ ratio was calculated with the void ratio variations measured during the reconsolidation to in situ stresses in the triaxial chamber. There seems to be a correlation between the fines content and the sample quality, especially when analysing the Mazier collected samples, showing that samples with higher fines content have lower quality. Although the samples were collected from different depths and locations, and are composed of different soil types (reflected on the fines content), most specimens are classified as very good to excellent. As was expected, the three specimens with poor quality present high fines content and were collected with the Mazier sampler. However, with the exception of these three samples, all the other samples were categorised as good to medium or very good to excellent. Besides, all samples collected with the GP sampler were classified as very good to excellent.
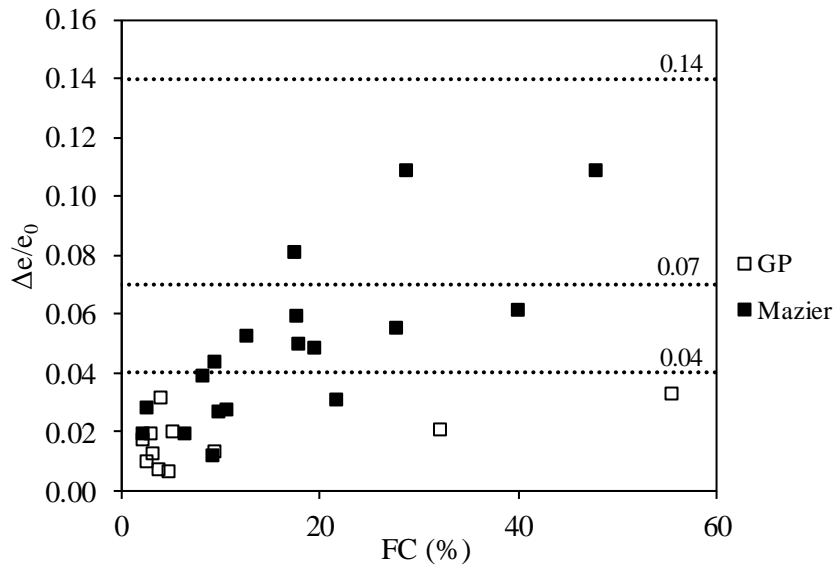
Figure 5.12 – Sample quality evaluation using $\Delta e/e_0$ ratio plotted against FC

A combined chart with the V_S ratios determined in section 5.3.4 is presented in Figure 5.13. The combined analysis is interesting as it allows to compare the performance of both methods in assessing sample quality. The chart illustrates that the majority of samples have $\Delta e/e_0$ ratios below 0.04, regardless of having a variety of V_S ratios, which reflect on different quality classifications.
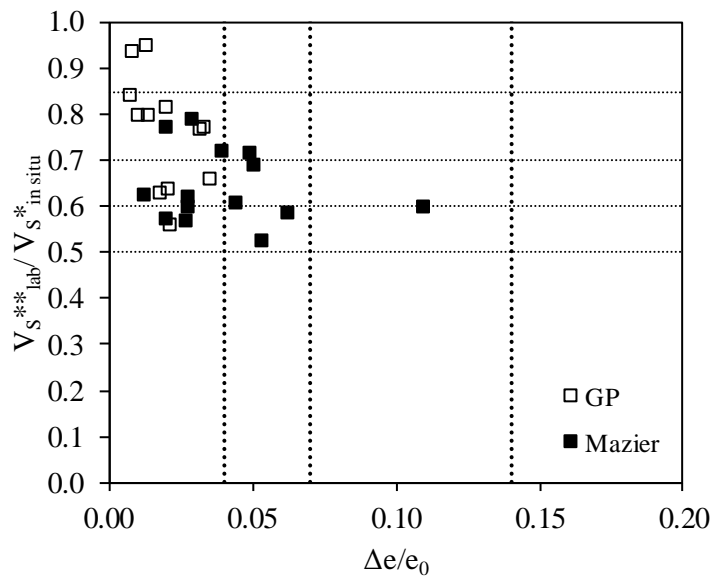
Figure 5.13 – Sample quality assessment combining V_S and $\Delta e/e_0$ ratios

It is important to note that this method was mainly developed for clays, as the differences in void ratio due to compression are more significant and the compression lines of clays are steeper. On the other

hand, the compression lines of sands are less steep, and for low compression values the variations of void ratio are very low. Therefore, the use of $\Delta e/e_0$ values might not reflect the disturbances in the sample, as the lack of precision and the small ranges of values do not guarantee the integrity of the analyses. This might be the reason why this method did not differentiate the quality of most samples. Therefore, in this case, it is considered that the shear wave velocities comparison is a good alternative to assess sample quality, as it reflects the differences in particle arrangement and fabric that occurred during the sampling process. However, the $\Delta e/e_0$ method is an interesting approach for a preliminary distinction between some samples.

5.5. SAMPLE DENSITY

As referred in other sections, the sampling process induces disturbances on the collected samples. These disturbances are oftentimes related to volumetric changes that occur during the sampling process or the extrusion of the samples from the sampling tubes in the laboratory. One of the methodologies to assess sampling quality involves the comparison between the relative density (D_R) estimated in the field and in the laboratory, which will be analysed straightaway.

Ideally, the in situ density is measured with geophysical downhole methods, such as gamma density loggings. However, those were not available in the current research so correlations with CPTu test results were consider to assess the relative density in depth of the four profiles studied. Numerous correlations were developed using large calibration chambers. However, the correlations available were developed mainly for reference clean sands, such as Toyoura or Ticino sands, with little to no fines content. As reported by Cubrinovski and Ishihara (1999), the relation between penetration resistance and relative density is highly dependent on soil gradation, and correlates to the maximum and minimum void ratio. It is important to note that the soil profiles analysed in this work are very heterogeneous, with interlayers of sand-silt-clay. For this reason, the D_R-CPT correlations, mostly developed for clean sands, are not ideal to estimate the in situ density of the soil and they must be analysed with care, as they can induce interpretation errors. The analysis was performed nonetheless, as it is interesting to assess the differences between the in situ values and the laboratory measures of D_R. It is worth mentioning that the author is aware of the fact that this is clearly not the best method to assess the quality of samples, which will be discussed later in this Chapter.

Among the different CPT-D_R correlations that exist, the ones from Baldi et al. (1986) (B-CPT), Salgado et al. (1997) (S-CPT), Jamiolkowski et al. (2001) (J-CPT), and Green et al. (2014) (G-CPT) were used herein, and a comparative performance of each method is discussed. Table 5.3 summarizes the expressions used for each method and the parameters chosen.

Table 5.3 – CPT-D_R correlations

CPT-D_R correlation	Formulation	Considerations/parameters
B-CPT	$D_R = \dfrac{1}{C_2}\ln\left(\dfrac{Q_{cn}}{C_0}\right)$	$C_0 = 15.70$ $C_2 = 2.41$
S-CPT	$D_R = 0.478(q_{c1N})^{0.264} - 1.063$	-
J-CPT	$D_R = \dfrac{1}{C_2}\ln\left[\dfrac{q_c/p_a}{C_0(\sigma'/p_a)^{C_1}}\right]$	for $\sigma' = \sigma'_{v0}$, $\;\;C_0 = 17.68$ $C_1 = 0.50$ $C_2 = 3.10$
G-CPT	$D_R = \dfrac{1}{c}\left[\dfrac{q_c/p_a}{(\sigma'_{v0}/p_a)^{0.5}}\right]$	$c = 300$ for $I_c < 1.32$ $c = 300 - (1.32 - I_c)\dfrac{300 - 400}{1.32 - 2.07}$ for $1.32 \le I_c \le 2.07$ $c = 400$ for $I_c > 2.07$

Note: q_c – cone penetration resistance; σ'_{v0} – effective vertical stress; p_a – atmospheric pressure; q_{c1N}, Q_{cn} – normalised CPT resistances, corrected for overburden pressure, $Q_{cn}=(q_c/p_a)/(\sigma'_{v0}/p_a)^{0.5}$

The determination of D_R in the laboratory was based on e_{max} and e_{min} obtained for each soil sample with the JGS method. The method was developed for soils with low fines content, so the normalisation proposed by Ishihara et al. (2016) was applied to approximate the values to the standard. In the absence of a more accurate determination of D_R in the field and in the laboratory, the comparisons are analysed with a critical eye, as some inaccuracies can come from the above considerations.

5.5.1. PROFILE COMPARISONS

Figure 5.14 presents the estimated in situ D_R profiles, where the J-CPT, S-CPT, G-CPT, and B-CPT correlations were used. The B-CPT correlation was calculated using both Q_{tncs} after Robertson and Wride (1998) and q_{c1Ncs} after Idriss and Boulanger (2008) to account for different soil type considerations. In addition, the results of relative density calculated in the laboratory for the samples collected with Mazier and Gel-Push samplers are also represented.

As previously discussed, the soil profiles are very heterogeneous and present several interlayers of sandy and clayey soils. The interlayered profile of cone resistance in depth reflects on a significant oscillation of relative densities in depth. The heterogeneity verified in Figure 5.14 hinders the interpretation of the

results. Therefore, an average value consisting on the $+-25$ cm around a certain depth was considered (e.g., for the depth 2.5 m, the value considered is the average of all computed values between 2.25 m and 2.75 m). Figure 5.15 presents the average profiles, enabling a better comparison between different D_R correlations.

In general, G-CPT returns lower values of relative density, which means that even with the association with soil behaviour type index, the correlation is not the most appropriate. On the other hand, the results from J-CPT and S-CPT correlations are very similar. The B-CPT correlation using either Q_{tncs} or q_{c1Ncs} provides the higher values of D_R, and the closest to the laboratory measurements. This is probably related to the inclusion of site-specific I_c-FC relationship in q_{c1Ncs} calculation and to Q_{tncs} being empirically based on I_c, approximating the correlations to the laboratory measured values. An example of these differences between D_R-CPT correlations is presented at 3 m to 7 m in NB1 profile (Figure 5.15c). There is a homogeneous sand layer and the calculated D_R values vary from around 30% for G-CPT, 55% for J-CPT and S-CPT, and 75% for B-CPT. This trend is verified in other layers in the four soil profiles.

Since the correlations are calculated using logarithmic functions, if the cone resistance value, Q_{cn}, is very small the calculated relative density is negative. This occurs especially for normally consolidated young finer soils, which have typically small cone resistances, reflecting on small or negative values of D_R. A simple study of the correlations of D_R-Q_{cn} (Figure 5.16) shows that, for Q_{cn} lower than 16-18 kPa, the relative density is negative (due to the logarithmic function used). The G-CPT is not represented because it also depends directly on I_c. As negative values of D_R are an impossibility and considered an error due to the formulas used, these values are not represented further.

In order to analyse the sample quality of each individual sample and the effect of the type of sampler used, a direct comparison between laboratory and field measurements is presented in the following section. The direct comparisons where performed based on the average in situ values, as explained below.
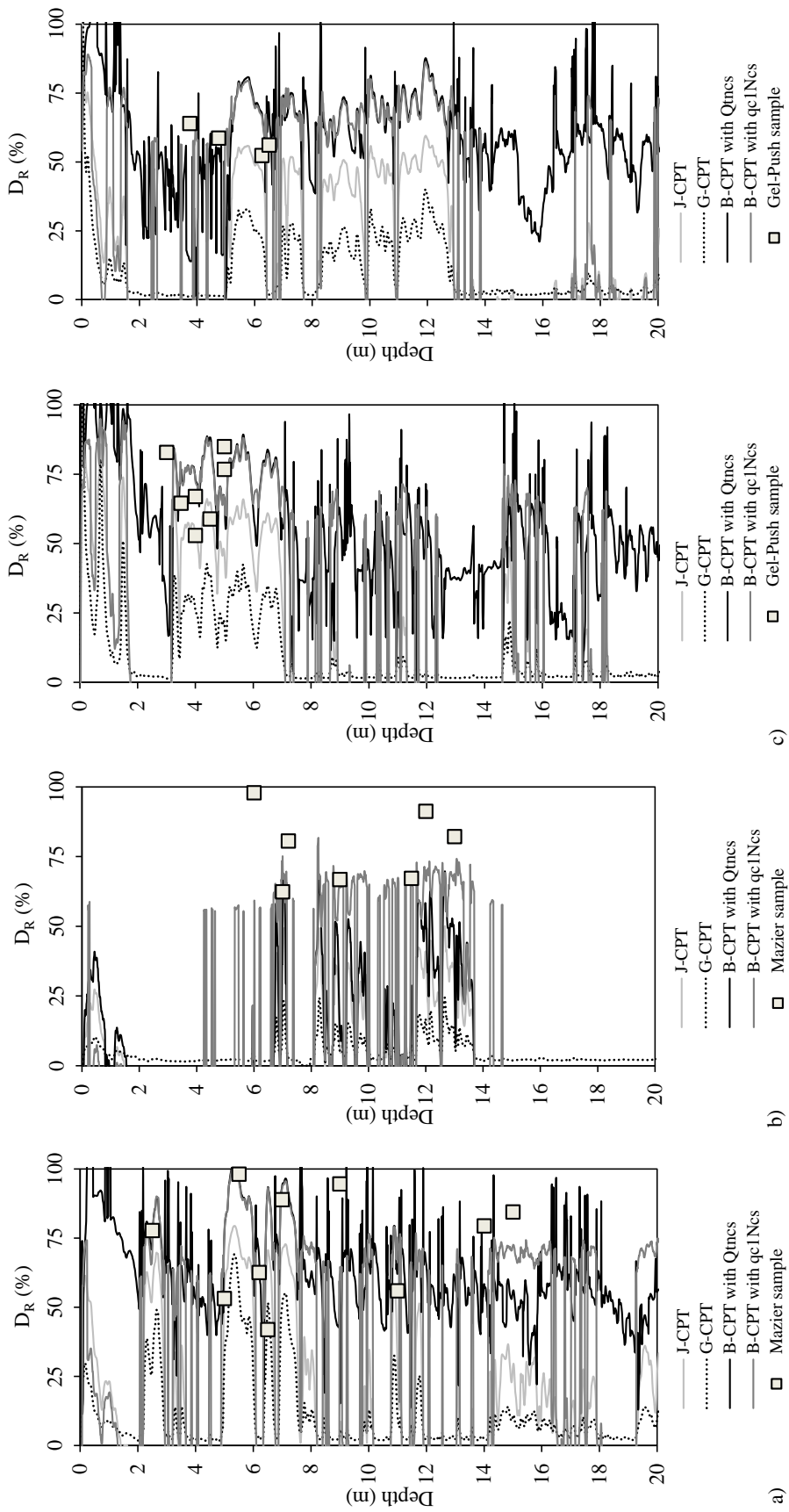
Figure 5.14 – D_R profiles: a) S1; b) S2; c) NB1; d) NB2
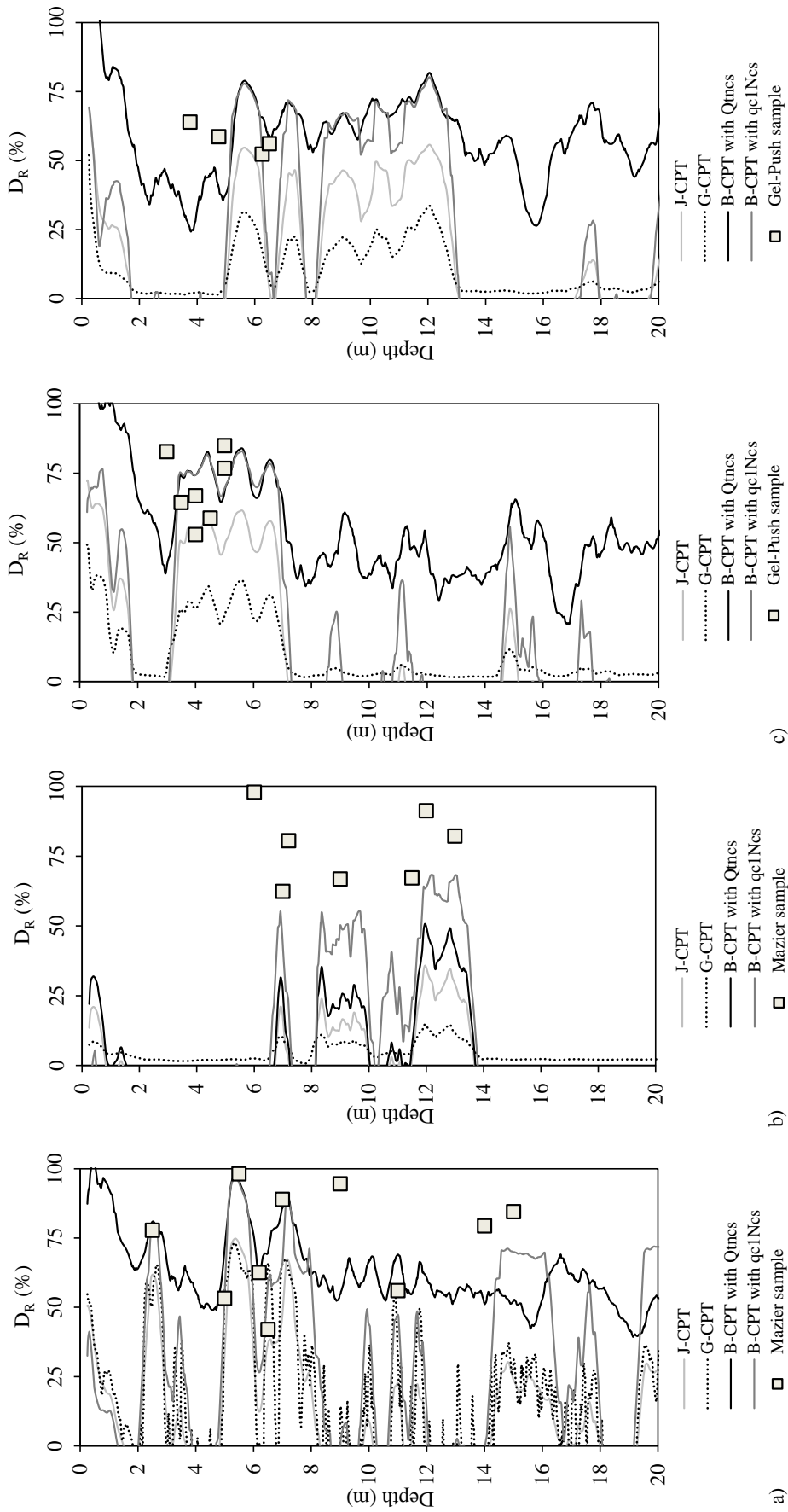
Figure 5.15 – Average D_R profiles: a) S1; b) S2; c) NB1; d) NB2
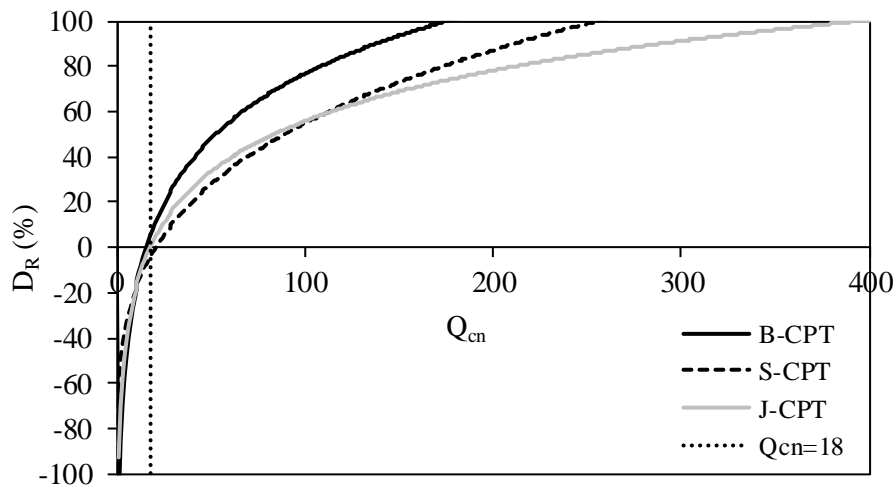
Figure 5.16 – Relationship between D_R and Q_{cn} for B-CPT, S-CPT and J-CPT correlations

5.5.2. DIRECT COMPARISONS

Direct comparisons between D_R-CPT correlations and the laboratory measured values are presented in Figure 5.17 for samples collected with Mazier and Gel-Push samplers. As verified before, the samples tested in the laboratory have high densities, which can be due to densification during sampling or extraction in the laboratory. During the extrusion using the vertical hydraulic piston, some samples seem to have densified and that is reflected on the high values of D_R measured. Following the trends verified in the profile comparisons, the correlation from G-CPT computes values of D_R lower than the other correlations and does not agree well with the laboratory measurements. Once again, it is verified that J-CPT and S-CPT provide very similar results. On the other hand, B-CPT correlations seem to be the best estimate for laboratory measurements, as the point values are located around 1:1. It is recognised that more samples collected with the Gel-Push sampler are located closer to the 1:1 line than Mazier collected samples, suggesting that the GP has a better performance, as was verified in section 5.3 for the comparison of field and laboratory-measured shear wave velocities. However, this tendency might be also related to the type of samples collected with GP (majority sands). The influence of fines content in the relative density determination will be analysed ahead.
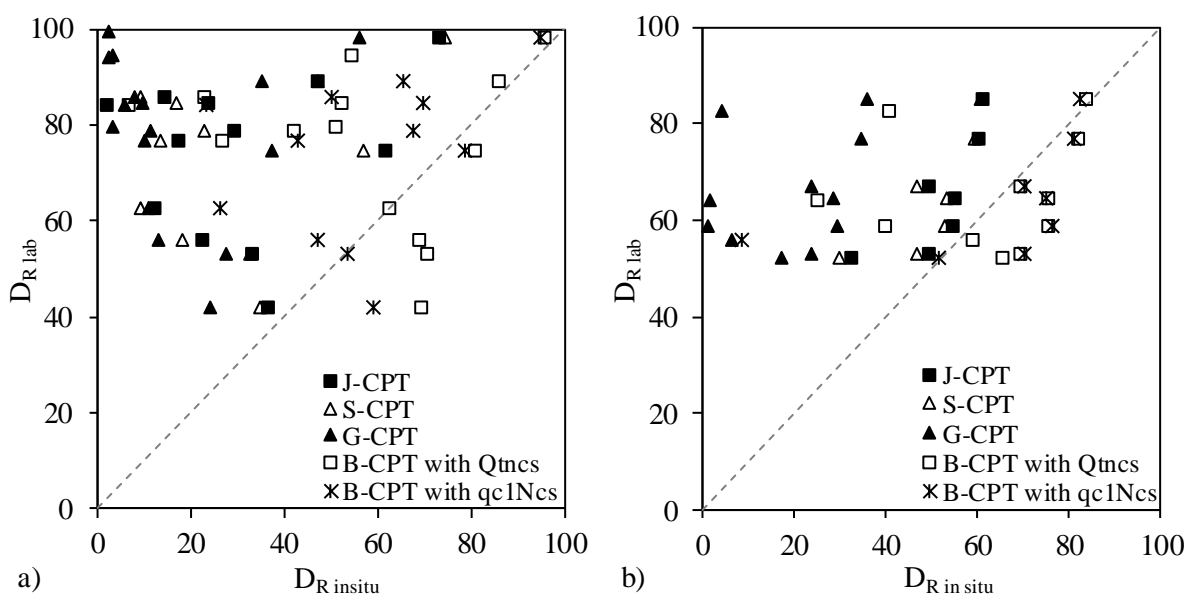
Figure 5.17 – Comparison of in situ D_R-CPT correlations to laboratory measured values in samples collected with: a) Mazier sampler; b) Gel-Push sampler

Figure 5.18 presents the same results but considering the ratio between laboratory-measured D_R and in situ correlations. It is clear that as the relative density in situ increases, the ratio is closer to one. This was expected as the D_R measured in the laboratory were higher. Once again, it is perceptible that the G-CPT correlation returns the higher ratios, reflecting the considerable difference between laboratory and in situ results. The correlation from Baldi et al. (1986) using either Q_{tncs} or q_{c1Ncs} shows ratios close to 1, reflecting good agreement between B-CPT correlation and laboratory measurements.

Additionally, Figure 5.19 presents the comparison between $D_{R\,lab}/D_{R\,insitu}$ and the fines content (FC) of the respective sample. The G-CPT correlation is not represented as it was shown to not perform well in these soils. Both Figure 5.18 and Figure 5.19 show values of $D_{R\,lab}/D_{R\,insitu}$ ratio below 1, meaning that the samples are looser after sampling. These ratios correspond to samples with low fines content, and to D_R in situ calculated with B-CPT correlations. This is a reflection of the dilation process that probably occurred during sampling and extraction processes in sandy samples. The samples with lower fines content dilated during the extraction processes, probably due to release of confining stress and low reconsolidation strains verified. On the other hand, samples with higher fines content show densification, as they probably compressed during sampling and extrusion processes. The difference in behaviour of low to high fines content samples is only reflected when using the B-CPT correlation, especially when using B-CPT with q_{c1Ncs}, as it includes a site-specific I_c-FC relationship. However, there is no clear trend between FC and laboratory-measured D_R, as some samples with low FC also compressed and have higher laboratory measured D_R than in situ estimates.

The J-CPT and S-CPT correlations were not able to predict these differences in soil behaviour, as the in situ estimate is always lower than the laboratory measure. This reveals that these two correlations may not be the most appropriate for the determination of D_R in situ for these materials, as they underestimate the compressibility of the samples by using mean compressibility coefficients.

a) b)
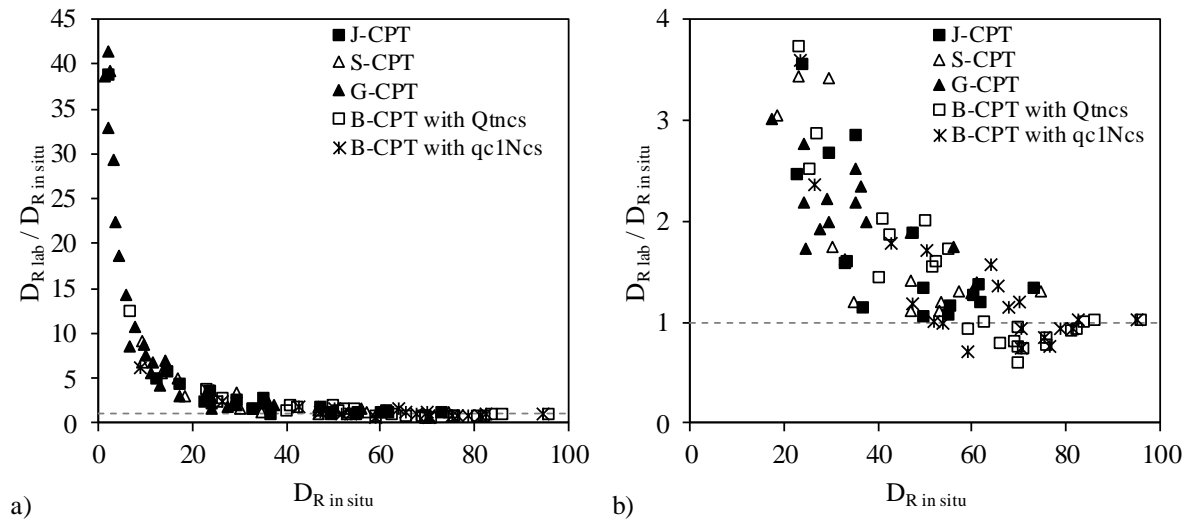
Figure 5.18 – Comparison of in situ D_R-CPT correlations to laboratory measured values using $D_{R\ lab}/D_{R\ in\ situ}$ ratio

a) b)
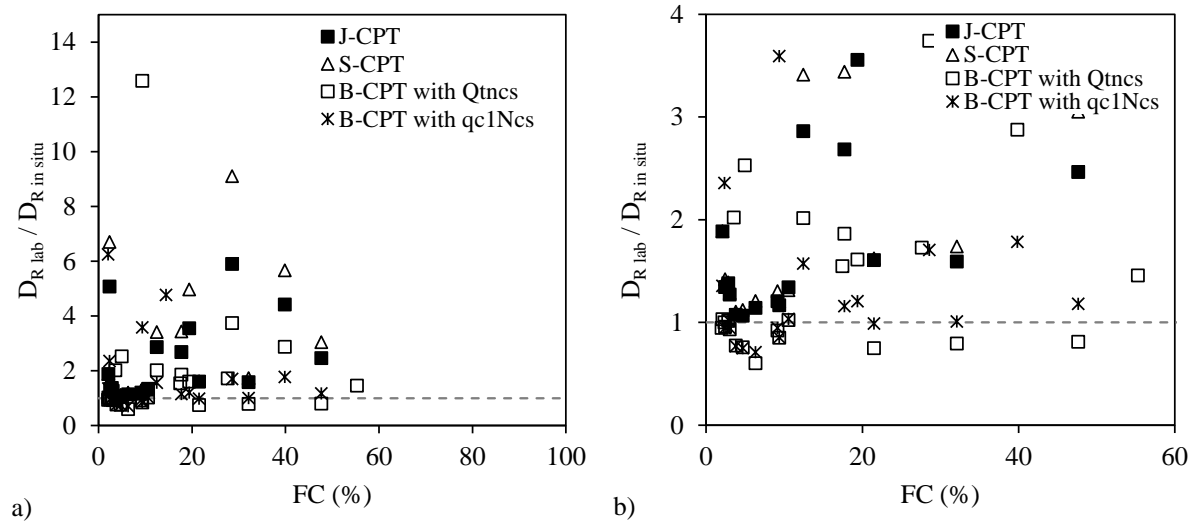
Figure 5.19 – Comparison of $D_{R\ lab}/D_{R\ in\ situ}$ ratio with fines content (FC)

As was discussed above, the uncertainties associated with the determination of D_R in the field and in the laboratory make this sample quality assessment inconclusive. However, the results presented suggest that the use of B-CPT in combination with q_{c1Ncs} is the correlation that better approximates the laboratory-measured values, for samples collected with both Mazier and GP samplers.

5.6. QUALITY EVALUATION DISCUSSION

As shown throughout this Chapter, there are different methods available for sampling quality assessment. However, no method alone is enough to perfectly assess the degree of disturbance of a soil sample, as they were developed for different soil types and strongly depend on empirical correlations based on a specific type of soil. In the present work, four different methodologies were applied: visual inspection, shear wave velocities comparison, evaluation of volumetric strains during reconsolidation and relative density comparison.

In terms of visual inspection, all samples tested in the advanced laboratory tests were of good quality, not presenting any external damage such as holes, cracks or distortion of shape. Some Mazier collected samples presented serious damages on the surface, probably due to the operation of the Mazier sampling that involves rotation with water injection. The water flow can generate disturbances on the samples, due to wash out of the finer particles. However, those samples (Figure 5.1a and Figure 5.1b) were not tested in triaxial conditions. The Gel-Push samples showed no visual signs of disturbance, as the surface was smooth and without visible cracks or holes.

The method based on the evaluation of volumetric strains during reconsolidation was considered imprecise for the soils tested, as it was developed mainly for clays and the results did not differentiate the quality of the samples (almost all specimens were of good to excellent quality). The D_R comparisons using CPT correlations were generally inconclusive as many uncertainties are associated with the in situ D_R determination, particularly due to the presence of fines and interlayers. The B-CPT correlation in combination with q_{c1Ncs} proved to be the most adequate to predict relative density in the field, especially for samples with low fines content. On the other hand, the method based on the comparison of shear wave velocities was appropriate for the samples tested. The shear wave velocities obtained directly using SDMT or SCPTu and with the correlation CPT-V_S from Robertson (2009) are in good agreement with the results from BE-CTx.

Taking all the above considerations into account, no methodology alone is satisfactory to assess correctly the sample quality. Taylor (2015) introduced a Specimen Quality Index (SQI), where a SQI is defined based on a weighted sum of selected quality assessments, the maximum being 10 points. Similarly, an SQI analysis is presented here, based on the three methods studied and taking into consideration the reliability of results. All samples tested in advanced laboratory tests were visually good so the visual inspection criterion was not included in this particular study. As the V_S comparison method is the most accurate of the three methods, a higher percentage was attributed to it (+8 points). According to the $V_S{}^{**}{}_{lab}/V_S{}^*{}_{insitu}$ ratio values, points were attributed as: +8 if V_S ratio is above 0.85: +7 if V_S ratio is between 0.70 and 0.85; +6 if V_S ratio is between 0.60 and 0.70; +4 if V_S ratio is between 0.50 and 0.6; and +0 if V_S ratio is below 0.5. The method that considers the volume change during

reconsolidation counts as +1 point, if $\Delta e/e_0$ is lower than 0.04. Due to large uncertainties in the field correlations to determine D_R, the relative density method counts as +1 point if the ratio of laboratory to in situ estimate of D_R is within ±0.15. Table 5.4 presents the SQI evaluation for each specimen, according to the three methodologies considered. Only the specimens where shear wave velocities were measured are considered. In this case, as the $\Delta e/e_0$ and D_R methods were not very reliable, the $V_S^{**}{}_{lab}/V_S^*{}_{insitu}$ ratio values rule the sample quality assessment.

Table 5.4 – Combined Specimen Quality Index assessment

Sample	Sampler	FC (%)	$V_S^{**}{}_{lab}/V_S^*{}_{in\,situ}$	$\Delta e/e_0$	$D_{R\,lab}/D_{R\,in\,situ}$	SQI	Classification
			+8	+1	+1		
S1_M2_I3	Mazier	9.15	0.63	0.012	0.96	8	Very good
S1_M5_I2	Mazier	21.50	-	0.031	0.99	-	-
S1_M5_I4	Mazier	10.56	0.60	0.028	1.03	8	Very good
S1_M6_I2	Mazier	2.35	0.79	0.029	2.36	8	Very good
S1_M6_I3	Mazier	6.31	0.57	0.020	0.71	5	Fair
S1_M7_I1	Mazier	2.10	0.77	0.020	1.36	8	Very good
S1_M9_I1	Mazier	27.61	-	0.056	-71.43	-	-
S1_M11_I1	Mazier	47.67	-	0.109	1.18	-	-
S1_M14_I1	Mazier	17.44	-	0.060	-35.60	-	-
S1_M15_I1	Mazier	19.38	0.72	0.049	1.21	7	Good
S1_M25_I1	Mazier	17.30	1.06	0.081	-4.23	8	Very Good
S2_M6_I1	Mazier	9.68	0.62	0.027	-8.71	7	Good
S2_M7_I1	Mazier	39.85	0.59	0.062	1.79	4	Poor
S2_M7_I2	Mazier	14.45	0.57	0.027	4.77	5	Fair
S2_M9_I1	Mazier	28.58	0.60	0.109	1.71	6	Good
S2_M11_I2	Mazier	9.37	0.61	0.044	3.59	6	Good
S2_M12_I1	Mazier	12.46	0.53	0.053	1.57	4	Poor
S2_M13_I1	Mazier	17.71	0.69	0.050	1.16	6	Good
S2_M14_I1	Mazier	8.03	0.72	0.039	-3.71	8	Very good
NB1_F2_GP2.5_I3	GP	3.56	0.94	0.008	-4.87	9	Excellent
NB1_F2_GP3.5_I1	GP	9.37	0.80	0.013	0.85	9	Excellent
NB1_F4_GP4_I2	GP	2.44	0.80	0.010	0.95	9	Excellent
NB1_F5_GP4_I2	GP	4.71	0.84	0.007	0.75	8	Very good
NB1_F1_GP4.5_I1	GP	3.79	0.77	0.032	0.77	8	Very good
NB1_F5_GP5_I1	GP	3.03	0.95	0.013	0.94	10	Excellent
NB1_F5_GP5_I2	GP	2.83	0.82	0.020	1.03	9	Excellent
NB2_F1_GP5_I1	GP	-	0.66	0.035	-	7	Good
NB2_F1_GP6_I2	GP	4.96	0.64	0.020	1.01	8	Very good
NB2_F2_GP4_I4	GP	55.30	0.77	0.033	-1.75	8	Very good
NB2_F1_GP3_I4	GP	32.10	0.56	0.021	-3.97	5	Fair
NB2_F1_GP6_I3	GP	2.00	0.63	0.018	6.26	7	Good

5.7. RECOMMENDATIONS AND MAIN FINDINGS

Following the evaluation of the quality of samples collected with Mazier and Gel-Push samplers, some recommendations and suggestions are proposed for future investigations:

- The three samplers used in the retrieval of samples proved to be competent for the majority of soil types collected. However, the GP and D&M samplers collected samples of higher quality than the Mazier sampler. The Mazier sampling procedure involves rotation with water injection, which can generate disturbances on the samples, due to wash out of the finer particles. Moreover, the fact that the liners from Mazier were made of PVC required a more carefully extrusion, in order to not damage the sample a consequence of the flexibility of the tube. Additionally, the internal PVC tube surface was not perfectly smooth, causing some surface damages when extruding samples of fine soil, as the soil was dragged through the surface while the PVC tube was removed. On the other hand, the gel polymer used in the GP sampler allows for a smoother extrusion of the soil samples from the metallic liner, reducing the friction during the extraction process.

- The visual inspection of samples is crucial to determine the preliminary state of the soil samples and to select the most adequate samples for extensive laboratory testing. This is ideally done by X-ray or tomography processes, which were not accessible at the time of this work. It is advised to record and photograph the specimens as they are extruded from the sampling tube, as well as labelling them for future reference.

- For sampling quality evaluation, high-quality in situ testing should be carried out. The in situ measurements of shear wave velocities are the reference for sampling quality assessment as they are the base of most comparisons. Therefore, the in situ tests need to be performed with precision and care. To assess the shear wave velocities in situ, direct measurements from downhole logging (e.g. SDMT or SCPTu) are recommended, as they are better reproduced with the bender element configuration in the laboratory. However, downhole logging measures V_S each 0.50 m or 1 m which is a rough estimate and can be misleading when analysing a smaller specimen from a particular depth. For detailed sample quality comparisons, it is suggested that a continuous profile is determined using, for example, CPTu test close to the sampling borehole. In the present work, the CPT-V_S correlation from Robertson (2009) computed results that agree well with the direct measurements. Moreover, the CPTu allows for the estimation of unit weight and relative density.

- For the determination of shear wave velocity in the laboratory, bender elements provide a non-destructive shear wave measurement procedure. The results from the specimens tested in the triaxial cell proved to be more accurate than the "bench" test results, as the specimen was submitted to the same confining stresses as in the field and was fully saturated, providing a

cleaner wave signal and facilitating the interpretation of results. The normalisation of both field and laboratory V_S with void ratio function and mean effective stress improves the comparisons and is highly recommended for a more accurate comparison of results.

- The method that considers the volume changes during reconsolidation was not successful in the present work and was not appropriate for the granular materials tested as it did not differentiate samples with different quality. The D_R-CPT correlations have large uncertainties associated with the in situ D_R determination, particularly due to the presence of fines and interlayers in the soil profiles analysed. Therefore, these two methods were considered not appropriate for the soils studied, and their results are negligible when compared to the shear wave velocities evaluation. Methods that take into account the effect of fines content, particularly in the determination of D_R from CPT tests should be further developed, as most methods available are only suited for reference clean sands.

- As each method had uncertainties mainly associated with the determination of parameters from in situ test correlations, the analyses of a variety of methods for assessing sample quality should be considered. A ponderation of various methods, such as a Specimen Quality Index (Taylor, 2015), with weights reflecting the precision and amount of confidence in each method, can be useful for assessing the global quality of samples.

PART III - LABORATORY EVALUATION OF LTV SOILS

6. LABORATORY EQUIPMENT, TESTING PROCEDURES, AND EXPERIMENTAL PROGRAMME

6.1. INTRODUCTION

This Chapter outlines the laboratory work performed, as well as the equipment and procedures used for the performance of the tests involved in this investigation. Most laboratory tests were performed at the Laboratory of Geotechnics (LabGEO) of FEUP. The particle shape analyses were conducted at University College London and a set of cyclic simple shear tests was performed at University of Ljubljana.

The Chapter begins with a brief explanation of the tests performed for physical characterisation, namely grain size, specific gravity and Atterberg limits. As the procedures to obtain the shape parameters and the maximum and minimum dry densities were new to LabGEO's research group, they are described in more detail. Aiming to understand the behaviour of soils under cyclic load, this study was focused on triaxial and simple shear tests, performed with different apparatus. The triaxial and simple shear equipment used are described, followed by the sample preparation techniques, test procedures adopted and test analyses considerations. The Chapter is concluded with a summary table of all tests performed within this research.

6.2. PHYSICAL CHARACTERISATION

6.2.1. GRAIN SIZE ANALYSIS, ATTERBERG LIMITS, AND SPECIFIC GRAVITY

As most soil samples were obtained from undisturbed samples, the physical characterisation of the materials was conducted after the performance of cyclic triaxial tests. Each specimen was homogenised, riffled, and quartered to obtain a representative soil sample. The grain size analyses involved the sieving and sedimentation methods, which procedures are presented in Figure 6.1. The Atterberg limits and specific gravity were assessed following the ISO 17892-12:2018 and ISO 17892-3:2015 standards.
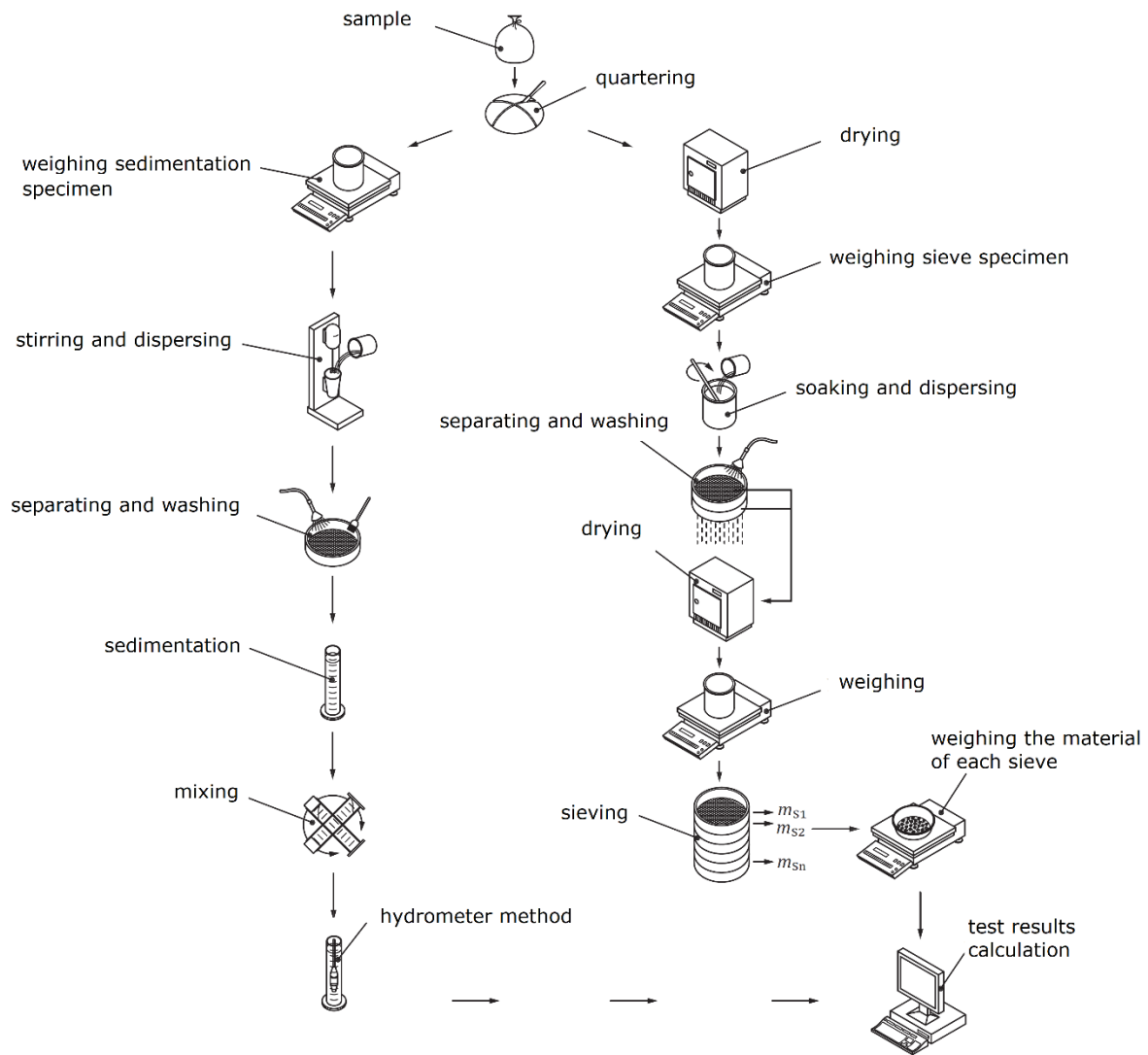
Figure 6.1 – Sieving procedure (adapted from ISO 17892-4:2016)

6.2.2. DETERMINATION OF SHAPE PARAMETERS – MORPHOLOGI G3

The shape parameters were obtained using a Malvern Morphologi G3 at the University College London, in the Department of Civil, Environmental and Geomatic Engineering. The Morphologi G3 is an automated particle characterisation system designed to measure the size and shape of particles by image analysis. It is composed of a sample dispersion unit (SDU), 5 megapixel digital camera, a motorised objective revolver for automatic magnification changeover and two light sources for reflected (episcopic) and transmitted (diascopic) illumination. Figure 6.2 shows the Morphologi G3 apparatus.

Figure 6.2 – Malvern Morphology G3 apparatus

The test procedure involves four parts: sample preparation, image capture, image processing, and results generation. The sample is placed dry on the inside of the SDU with a small spoon, which size depends on the material being tested. In this case, the spoon selected was 19 mm^3, the larger available, as the specimens are well graded and the objective was to select a representative sample. When testing finer soils, the spoon used was 5 mm^3. The dispersion unit is placed in the Morphologi G3 arm and the air supply pipe is attached.
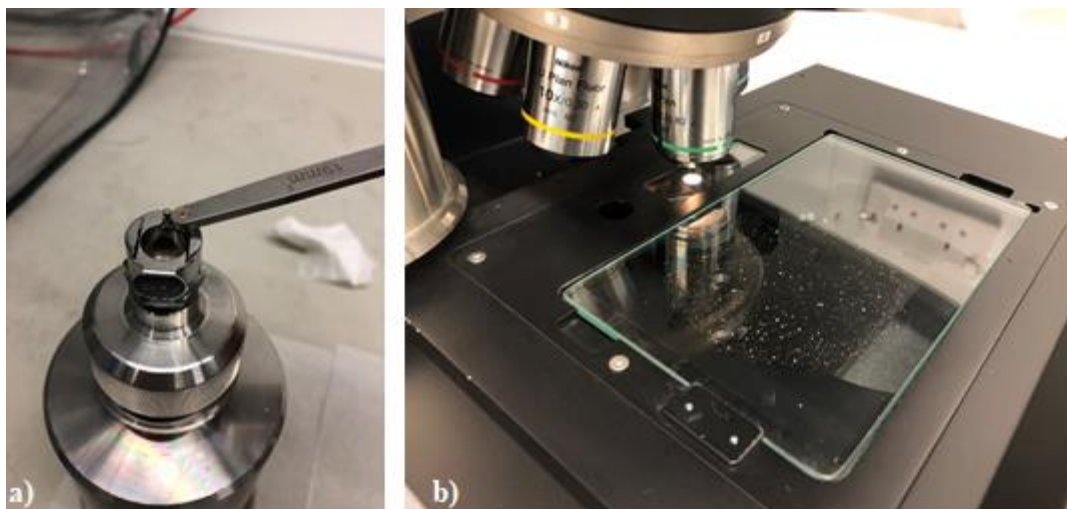
Figure 6.3 – a) Inserting the sample in the SDU; b) sample dispersed onto glass plate

In the software, the user programs a SOF (standard operation procedure) that defines the name of the sample, the objective, the scan area, the number of pixels, among other important configurations. The

objective is selected according to the particle size of the sample. In this work, the objective used was 2.5x, which measures particles from 0.013 mm to 1 mm size. The number of pixels in which each particle is divided is manually selected by the user and the recommended minimum value is 100 pixels per particle. A low energy is selected for the dispersion unit so there is no particle breakage due to high dispersion energy and the scan area is chosen, as being the circle where the sample is dispersed. The focus of the objective is also manually set. A glass plate holder receives the sample and the scanning begins. Depending on the objective and area selected, each test can last from 1 hour to 24 hours.

Each particle is recorded and analysed individually by the software. The user can visualize images of each particle in the sample and assess its properties. Some particles are displayed as two particles or are fabric fibres that land on the glass plate, as represented in Figure 6.4. Those particles can be excluded by hand or using filters for the different parameters (for example, excluding all particles with convexity higher than a certain value). When all the useless particles are excluded, the user can create and save the optimised results.
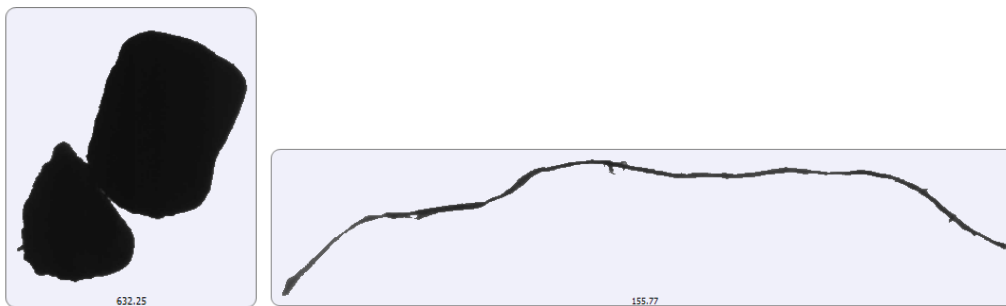
Figure 6.4 – Examples of particles excluded

The results can be downloaded in the form of a table, images of each particle or statistical graphs. For the current work, the results were exported to an excel sheet and then organised in diagrams. The parameters were plotted in terms of cumulative volume, considering the entirety of the sample. The most relevant shape parameters were obtained, based on the assessment of each individual particle tested. Table 6.1 summarizes the most relevant parameters and the respective definition.

Table 6.1 – Definition of shape parameter obtained with Morphologi G3

Parameter	Definition
CE diameter	Diameter of a circle with the same area as the particle
Length	Maximum distance between two lines which touch the particle on opposite sides
Width	Minimum distance between two lines which touch the particle on opposite sides
Perimeter	Actual perimeter of particle
Circularity	Ratio of CE perimeter to actual particle perimeter.
Convexity	Ratio of convex hull perimeter to the actual perimeter
Solidity	Ratio of the actual particle area to the convex hull area
Aspect ratio	Ratio of width to length of the particle
Elongation	1 – Aspect ratio

6.2.3. DETERMINATION OF MAXIMUM AND MINIMUM DRY DENSITIES – JGS METHOD

As mentioned in Chapter 2, the relative density is a key parameter governing the soil behaviour and liquefaction resistance. In this sense, the determination of the maximum and minimum densities of soils, and respective minimum and maximum void ratios, is crucial for the accurate determination of the relative density of each specimen.

As the majority of materials studied were retrieved using the Mazier or Gel-Push samplers, the quantity of each soil sample was limited, and not enough to determine the maximum and minimum densities following ASTM procedures D 4253-00 and D 4254-00, as the specifications require high masses of soil. Therefore, the Japanese Geotechnical Society (JGS) method, detailed in JGS 0161-2009 standard, was used, as it requires a minimum wet mass of the sample of 500 g. Figure 6.5 shows the test mould, funnel, stainless steel strait knife and hammer used in the process.

Figure 6.5 – Equipment used for the determination of maximum and minimum soil densities

The determination of the minimum dry density, ρ_{dmin}, (and corresponding maximum void ratio, e_{max}) is performed by pouring the sample into a funnel placed in the centre of the bottom of the mould and lifting it at a constant rate until overfill the mould above its top edge. Then, the sand level is trimmed with the top of the mould and the mass of the specimen is determined.

As for the maximum dry density, ρ_{dmax}, (and corresponding minimum void ratio, e_{min}), the procedure involves the separation of the sample in ten equal parts and the pouring of the sample in ten layers. To each layer, 100 impacts are applied to the side of the mould, with a wooden hammer with 30 mm diameter, rotating the mould every 5 impacts. After compaction, the sand level is trimmed and the mass of the specimen is determined.

Depending on the test procedure used, the maximum and minimum void ratio values tend to vary. For this reason, it is important to be consistent and use the same method when comparing results. According to Ishihara et al. (2016), the value for e_{max} yields approximately the same results independently of the method used, while the JGS method is known to yield larger values of e_{min} than the ASTM method, especially for sands containing silts. As the JGS method is applicable to sand with less than 5% fines content (i.e., particles with an aperture width of 75μm), the value of e_{min} determined with the JGS method must be adjusted according to the fines content (FC). Ishihara et al. (2016) proposed a correlation, based on collected data, that relates e_{min}, obtained by the JGS method, and e^*_{min}, obtained by standard compaction test by employing energy 10 to 15 times as much as that used in the standard Proctor. The e^*_{min} values obtained by the 10-15 times energy standard proctor test are approximately equivalent to the values obtained by ASTM test. Ishihara et al. (2016) plotted some data that relates e^*_{min}/e_{min} with FC and came up with a three line graph, expressed by the following equation:

$$\frac{e^*_{min}}{e_{min}} = \begin{cases} 1.0 & for\ 0 \leq FC \leq 5 \\ -0.012FC + 1.06 & for\ 5 < FC \leq 30 \\ 0.7 & for\ FC > 30 \end{cases} \tag{6.1}$$

In the present work, the value of e^*_{min} is used to calculate all relative densities, as the JGS method is applicable only to sands with less than 5% FC and some soils analysed have higher percentages of fines.

6.3. TRIAXIAL APPARATUS

6.3.1. CONVENTIONAL TRIAXIAL CELL

The triaxial test is one of the most widely used apparatus to investigate soil behaviour, due to the simplicity associated with specimen preparation, procedures and interpretation of the results and the availability of these apparatus in many laboratories. Despite not allowing the rotation of principal

stresses and only controlling the horizontal and vertical stresses, the triaxial test is perhaps the least expensive among other advanced devices, such as the Hollow Cylinder or the Simple Shear.

A total of five triaxial chambers were used for the work presented herein. For the monotonic drained tests, two chambers adapted for specimens with 70 mm diameter and 140 mm height were used, one with bender elements and other with lubricated bases. Both were equipped with a load cell of 10 kN, to account for the higher loads reached during the shear stage. For the cyclic tests, three chambers were used, equipped with a load cell of 1 kN, as the loads required for cyclic shear were small. The chambers differ in the sizes of the specimens, with the ratios between diameter and height of 85/156, 70/140, and 60/120. Figure 6.6 shows a scheme of the conventional triaxial chamber.
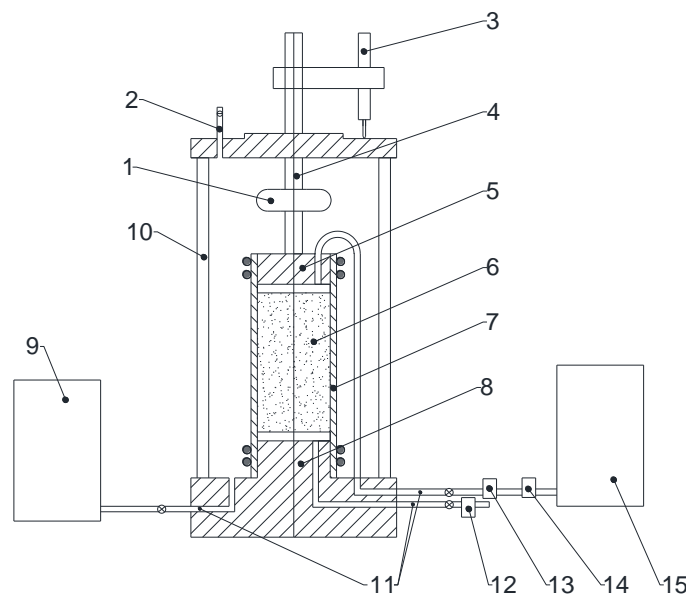
Legend
1 - load measuring device
2 - air bleed
3 - LVDT
4 - piston
5 - top cap
6 - soil specimen
7 - membrane
8 - pedestal
9 - device for measurement and control of cell pressure
10 - triaxial cell
11 - drainage tubes
12 - pore pressure sensor (bottom)
13 - pore pressure sensor (top)
14 - volume change sensor
15 - device for measurement and control of back pressure

Figure 6.6 – Scheme of a conventional triaxial cell

The triaxial chamber is made of corrosion resistant metal with a cylindrical body of transparent acrylic plastic. The cell is reinforced with fibre glass and withstands pressures up to 1700 kN/m^2. The base has three outlet ports, for pressure and drainage connections (external cell pressure, connection to base pedestal for drainage and back-pressure appliance, and connection to top cap for measuring the pore-pressure). On top of the cell there are an air relief valve and a support for an external displacement transducer (LVDT). The system also includes a data acquisition box for the installation of several channels. The software used for test control and data acquisition was LabVIEW® for monotonic tests and DynaTester V2.0 for cyclic tests. The monotonic tests were performed in a mechanical press by Wykeham Farrance® that provides the axial deformation at a prescribed rate, compressing the specimen.

6.3.2. CYCLIC TRIAXIAL APPARATUS

All cyclic triaxial tests were performed at LabGEO, at FEUP. The apparatus used is a conventional triaxial chamber where the load is applied by a hydraulic press that works with oil (Figure 6.7). The hardware consists of a motor and a hydraulic bomb, with maximum pressure of 250 bar allowing a maximum cyclic load of 10 kN, a hydraulic unit and a servo-actuator that has a hydraulic cylinder with displacement and load transducers. The servo-actuator allows the input of cyclic loads with frequencies varying between 0.001 and 2 Hz.
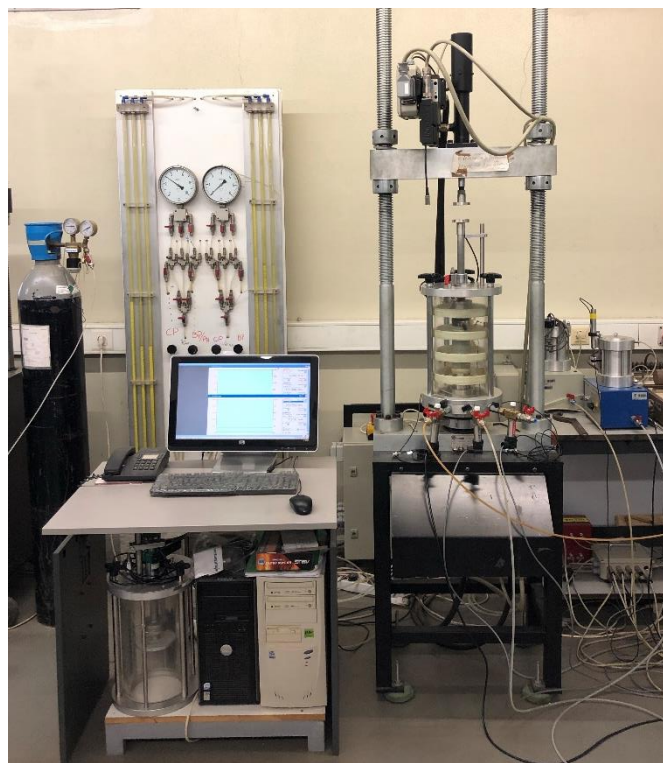
Figure 6.7 - Cyclic triaxial apparatus in LabGeo, FEUP

In order to perform isotropically consolidated cyclic tests, a rubber V-ring (Figure 6.8) is attached to the top cap, which creates vacuum when in contact with the piston plate. The plate is connected to the top of the chamber through a tube to expel the water between the two pieces and ensure full contact during compression/extension load cycles.
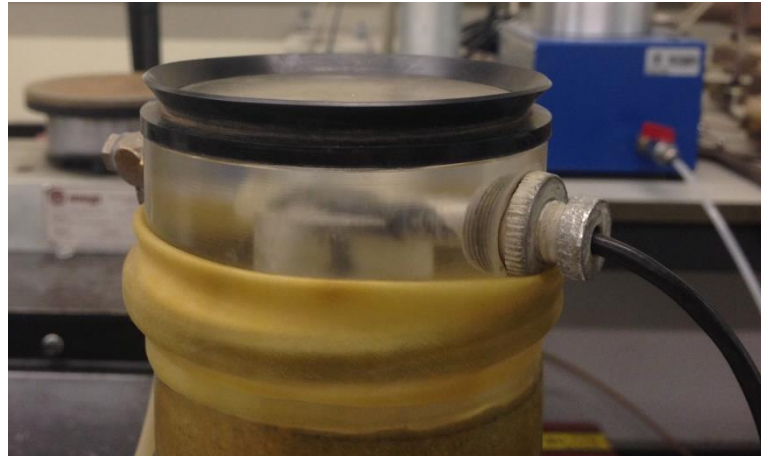
Figure 6.8 – Rubber ring on the top cap

The pressure regulation is usually performed by a motorised air compressor system that has an upper limit of 750 kPa. However, a GDS® Advanced Pressure/Volume Controller (ADVDPC) is often used for pressure/volume control, mainly when the pressures are higher than the compressor allows. Its operation is based on the movement of a piston controlled by a step-by-step motor that introduces pressures in a fluid (typically water). A photograph of two devices is shown in Figure 6.9.

Figure 6.9 – GDS® Advanced Pressure/Volume Controller

6.3.3. INSTRUMENTATION

All the triaxial chambers are supplied with instrumentation to measure stress and strain. As mentioned before, during triaxial tests the measuring devices used for stress-control are: an inner load cell that measures the vertical load, a cell pressure (CP) transducer, a back pressure (BP) transducer and a pore pressure (PN) transducer to measure pressures inside the cell, on the bottom and top of the specimen respectively. The pressure transducers have a capacity of 10 bar. As there are back and pore pressure transducers, the pore pressures are measured at the base and top of the sample.

The axial strain of the specimens was measured using external axial displacement devices. A Linear Variable Differential Transformer (LVDT) is attached to the load piston, joining its movement during shear (Figure 6.10). The LVDT used has a maximum range of 50 mm, which is enough to reach the required deformations. In addition, the servo-actuator has a hydraulic cylinder with displacement transducers. Some comparisons were made between the measurements from the external LVDT and the servo-actuator displacement transducer and the results were similar.

In this work, no internal instrumentation was used, during cyclic shear load to liquefaction the specimen experiments extreme deformation and the internal transducers could damage the membrane and the specimen.

Figure 6.10 – LVDT

The volume changes during consolidation and shearing were measured using an automatic volume gauge by VJ Tech® (Figure 6.11) with capacity of $100\ cm^3$. The device is composed of a small hydraulic cylinder whose piston is coupled to a LVDT (Soares, 2014). The volume change is measured by water flow, thus the specimen needs to be fully saturated.
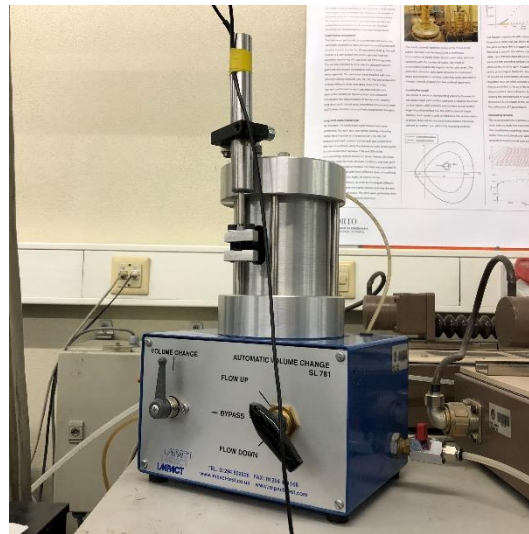
Figure 6.11 – Automatic volume change gauge by VJ Tech ®

The initial diameter and height are taken during assembly in the triaxial chamber, using a calliper. During the consolidation and shear stages, the volume gauge measures the accurate volume changes, as the specimens are saturated. After the end of the test, the accurate void ratio is determined based on the final dry weight and the water content determined at the end of the test, as will be explained later in this chapter.

6.4. CYCLIC SIMPLE SHEAR APPARATUS

6.4.1. CYCLIC SIMPLE SHEAR APPARATUS

Recently, LabGeo acquired a Cyclic Simple Shear device (also named Back-pressure dynamic simple shear device) that allows the performance of static and dynamic shear tests (Figure 6.12). The equipment allows the control of saturation conditions, with a back-pressure transducer connected to the inside of the specimen, to record pore pressure developments. The confining pressure is applied through air and the back pressure is linked to a volume change gauge that measures volume changes. Despite the possibility of performing tests with flexible membrane and cell pressure confinement, with measurement of back and pore pressures, during this research all tests were performed with the stack of rings configuration. This option was preferred since many issues arose when trying to perform tests with flexible membrane, as detailed in Appendix A. Therefore, the specimens were confined by a rubber membrane and a series of stacked copper rings (as in the SGI–type device), which restrained lateral deformations but allowed the distortion of the specimen. The apparatus includes a multi axis load cell, with capacity for maximum vertical force of 5 kN (static and dynamic) and maximum horizontal force of 4 kN (static and dynamic). The software used to control and acquire data is the GEOsys®, where the

test procedure is set and controlled. Appendix A presents a thorough description of the parts that constitute the cyclic simple shear device used.

Figure 6.12 – Cyclic simple shear equipment at FEUP

Moreover, some cyclic simple shear tests were performed at the geotechnical laboratory of University of Ljubljana (LabGeoUL). The equipment from LabGeoUL is an EP Servo Control Type, Model No. DTA-136, developed by Seiken Inc., with a pneumatic servo controller EO-260 that allows the definition of the cyclic shear conditions (Figure 6.13). The confining pressure medium is water and the specimen is not confined with rings. A rubber membrane and control of cell pressure assure an isotropic consolidation. The equipment includes cell, back and pore pressure transducers, one vertical and two horizontal displacement transducers with capacity for 20 mm, ± 25 mm and ± 1 mm, respectively, and a double tube volume gauge with 25 mL capacity. Both horizontal and vertical load cells have a capacity of 2 kN.
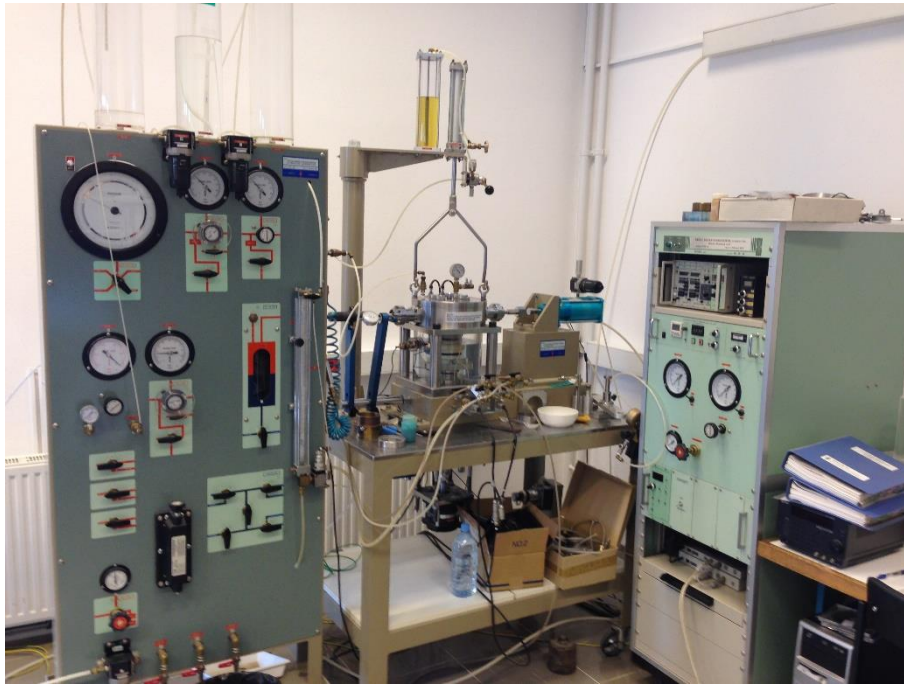
Figure 6.13 – Cyclic simple shear equipment at LabGeoUL

6.4.2. INSTRUMENTATION

As mentioned above, in the simple shear apparatus from FEUP, the horizontal and vertical loads were measured by a load cell transducer, placed on the bottom of the specimen with capacity for 4 kN horizontal force and 5 kN vertical force. Due to size constrictions, it was not possible to fit LVDT instrumentation on the simple shear chamber. Therefore, both vertical and horizontal strains are measured with the actuator. As the specimen is confined by rigid copper rings, there are no radial deformations.

In the tests performed at LabGeoUL, there are two horizontal and one vertical LVDT, The horizontal transducers are set at a fixed position, connected to the top cap. The smaller displacement transducer ($\pm$ 1 mm) is used for measuring small displacements at the beginning of the dynamic test, while the larger ($\pm$ 25 mm) measures deformation when liquefaction begins. The vertical displacement transducer is located at the bottom of the equipment, near the vertical loading pneumatic cylinder, and has a capacity for 20 mm. The volume changes were measured by water flow, as the specimen is fully saturated. The volume gauge is a double tube type volume meter with capacity for 25 mL.

6.5. SAMPLE PREPARATION AND TEST PROCEDURES

In the scope of this research, a large set of triaxial tests was performed on undisturbed and reconstituted specimens. The procedures required to prepare the samples for testing are diverse, and depend on the

type of test performed, the condition of the specimen and the preparation technique selected. The following sub-sections describe the methodologies used to prepare undisturbed specimens and reconstituted specimens for triaxial and simple shear tests and the test procedures followed. One of the objectives was to study the influence of the preparation method in the monotonic and cyclic behaviour of this soils, hence the reconstitution of specimens using both moist-tamping and dry air pluviation techniques.

The samples were identified by a nomenclature that describes the origin of the soil (Figure 6.14). The first letter and number correspond to the location of the borehole. The second letter is the sampler used (M for Mazier, GP for Gel-Push, and DM for Dames and Moore) and the second number is the initial depth of the sampling tube. The third letter is the nature of the sample (I for intact and R for reconstituted) and the third number is the position of the sample in the respective sampling tube (1 is for the first sample collected in that specific tube and so on). The last part describes the test performed and the test number. In case of the reconstituted samples, these are sometimes identified by the preparation method (MT for moist-tamping and PL for air pluviation). Moreover, in the case of the samples collected with Gel-Push, the borehole location also includes the borehole number, referenced by the letter F.
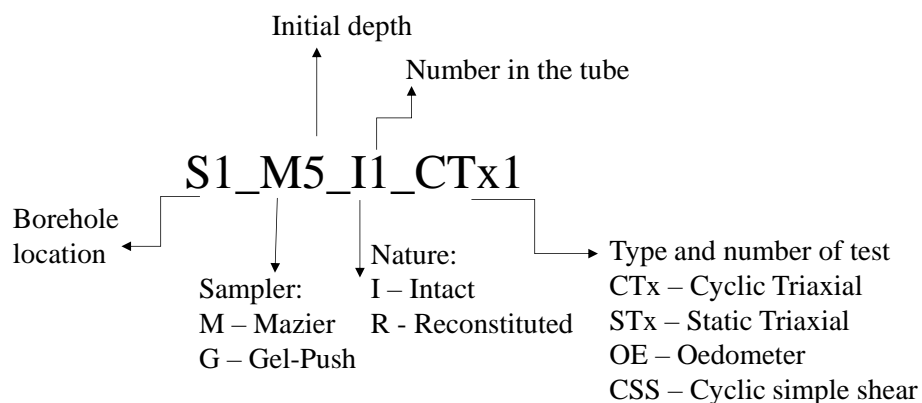
Figure 6.14 – Sample name definition

6.5.1. TRIAXIAL TESTS

6.5.1.1. Sample preparation procedures

a) Reconstituted samples

In the present work, moist tamping (MT) and dry air pluviation (PL) techniques were used to prepare reconstituted triaxial specimens, as these are the two methods most commonly used in LabGeo at FEUP.

The moist tamping technique was first proposed by Ladd (1978) and consists on the tamping of six layers of moist soil inside a split mould. The dry soil is mixed with a certain quantity of water, which

depends on the type of soil, to facilitate the compaction. The method involves a pre-determined quantity of soil to be compacted in each layer, according to the undercompaction method described by Ladd (1978). This method allows to obtain specimens with a wide range of void ratios and minimizes particle segregation. Besides, to produce specimens as homogeneous as possible, the undercompaction technique can be used, in which the lower layers are compacted looser, as the compaction of each succeeding layer can further densify the sand below it (Ladd, 1978).

On the other hand, in the dry air pluviation technique, the soil is placed with a funnel initially placed at the bottom of the mould. Slowly, the funnel is raised, maintaining a constant small drop height until the mould is totally filled. This procedure allows the creation of specimens with different void ratios by varying the drop height (Vaid and Negussey, 1984; Tatsuoka et al., 1986). In this work, very loose specimens were obtained with this method, with an initial void ratio close to the maximum void ratio.

The assembly of the reconstituted specimens involves different steps. First the membrane is placed around the base pedestal of the triaxial chamber secured with two o-rings. A metallic bipartite mould is placed around the membrane and a vacuum pressure of around 50 kPa stretches the membrane, guaranteeing the adjustment of the membrane to the mould. The specimen is prepared using either moist-tamping or pluviation. Paper filters are placed on the base and top cap, between the porous stone and the soil specimen, to prevent clogging during percolation. Once the specimen is prepared, the top cap is placed on top and the membrane is wrapped on with two o-rings. A small vacuum of 10 kPa is applied to the inside of the specimen, to prevent collapse while taking off the mould. The specimen is measured (diameter and height) and the triaxial cell is closed and filled with water. A confining pressure of 10 kPa is applied at the same time as the interior vacuum pressure is released. Figure 6.15 shows the procedures used to prepare specimens with moist-tamping and dry air pluviation.
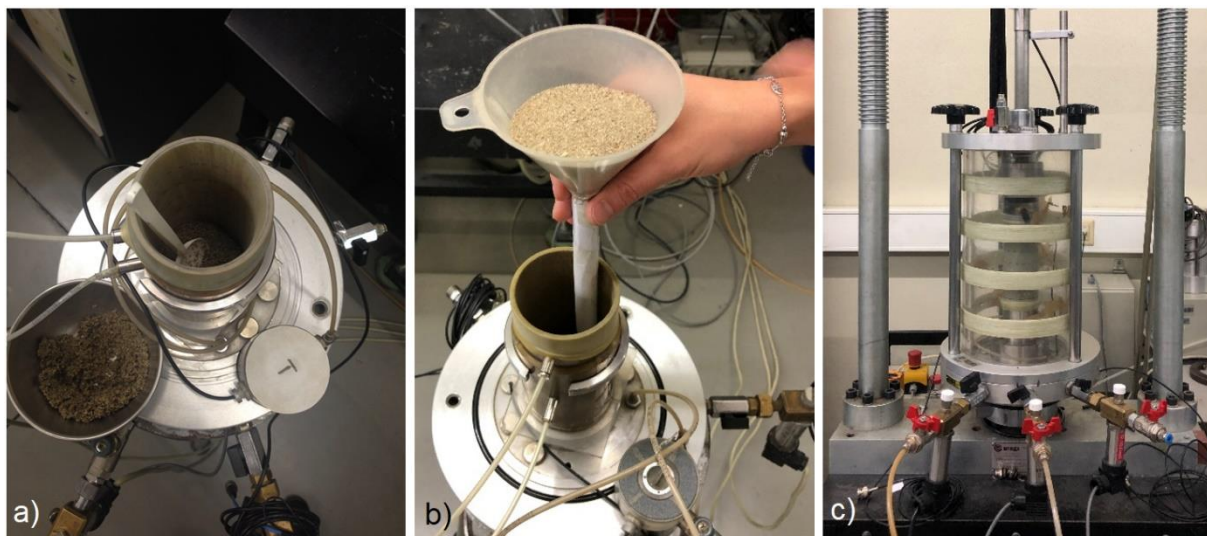
Figure 6.15 – Specimen preparation procedures for triaxial test: a) Moist-tamping; b) Air pluviation; c) Sample inside triaxial cell

b)   Undisturbed samples

The undisturbed samples were collected using two different samplers, Mazier and Gel-Push. As the samples came in different sampling tubes, the preparation of specimens for triaxial tests was slightly different. For each sampler, the diameter of the sampling tubes was the same as the diameter of the pedestal of the triaxial cells used so no trimming of the sides was necessary. The trimming of the top and bottom was performed with a steel knife, until the required height of the specimen to fit the triaxial chamber.

The Mazier collected samples were about 1 m length and confined by a PVC tube. After selecting which sample to test, a smaller specimen was cut using an electric saw, carefully, maintaining the tube in the vertical position. The specimen was then extruded from the PVC tube, cutting a vertical line in the tube to free the confinement forces and then sliding the tube. After that, the specimen was wrapped with a rubber membrane and placed in the triaxial chamber, where the top and bottom were secured with two o-rings. The diameters and height of the specimen were measured, the triaxial cell was closed and filled with water.
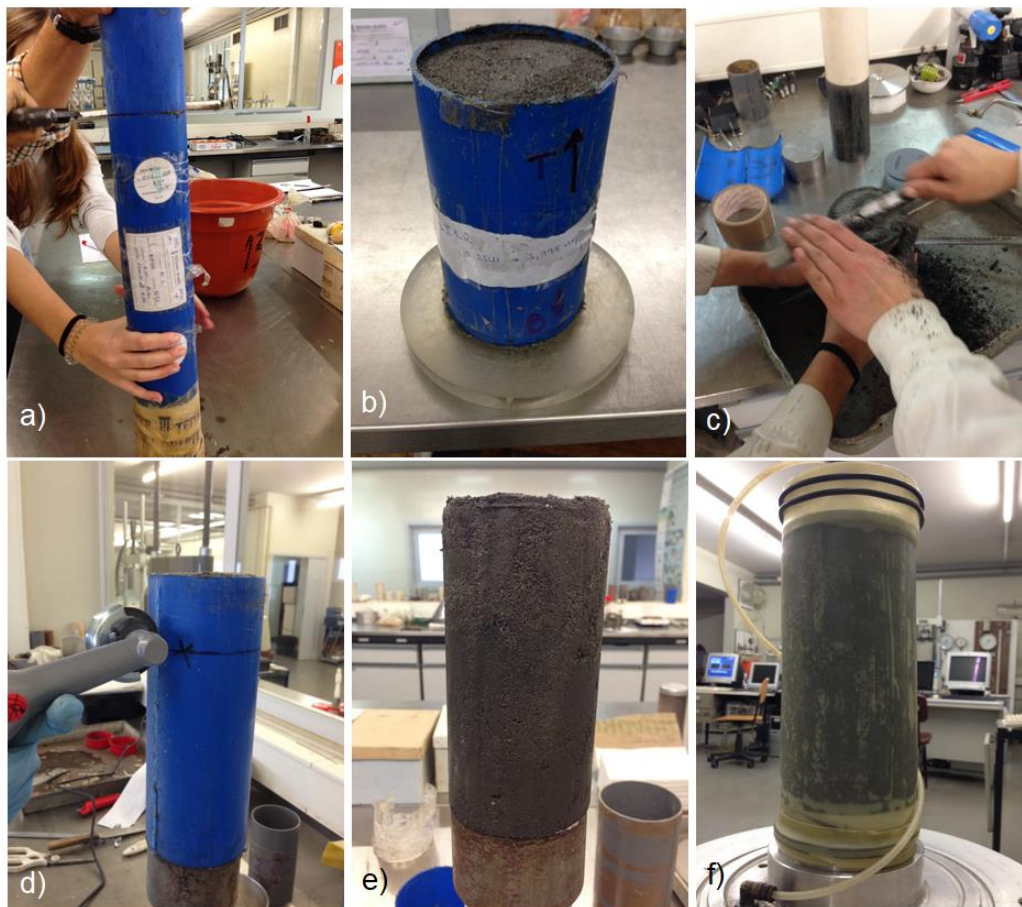
Figure 6.16 – Mazier sample preparation procedure: a) specimen horizontal cut; b) smaller specimen; c) trimming to the correct height; d) vertical cut for pressure relief; e) specimen without PVC tube; f) specimen ready for triaxial test

The Gel-Push sampling tubes were metallic, so it was not possible to cut them with a saw. Therefore, each sample was divided into smaller specimens that were extruded using a vertical hydraulic piston, cut and transferred to PVC tubes, with the appropriate dimensions for the triaxial cell. All specimens were extruded a few days after the in situ sampling and were stored inside PVC tubes, sealed with plastic wrap and tape, to avoid water content losses. After selecting which Gel-Push specimen to test, the specimen was taken out of the PVC tube and wrapped in a rubber membrane. It was then transferred to the triaxial chamber, the diameters and height of the specimen were measured, and the triaxial cell wa closed and filled with water.

Figure 6.17 – Gel-Push sample preparation procedure: a) hydraulic extractor; b) extraction of specimen; c) preparation of smaller specimen for storage; d) assemblage on the triaxial cell; e) specimen ready for triaxial test

6.5.1.2. Test procedures

Independently of the specimen preparation method, the triaxial test procedures are similar, with small alterations, explained when necessary. The triaxial test procedure involves four main stages: percolation, saturation, consolidation and shearing. These stages are summarised in the next paragraphs.

After the specimen assembling, the triaxial chamber is closed and filled with water. The specimen is maintained integral by applying 10 kPa vacuum pressure after de-moulding. A cell pressure of 10 kPa is applied, while turning off the vacuum pressure, maintaining an initial confinement of 10 kPa.

Percolation consists on the flow upwards of de-aired water through the specimen, to reduce the air present in the voids, filling them with water until close to saturation. This is performed with a confining pressure of 20 kPa and a back-pressure of 10 kPa. The recommended quantity of water to percolate corresponds to twice the voids volume (Soares and Viana da Fonseca, 2016). When the specimen was remoulded, previous to the percolation with water, it was performed a percolation with CO_2 that helps the expulsion of air during percolation with water and speeds up the saturation phase. CO_2 percolation was not performed on undisturbed specimens to avoid adulteration of the undisturbed structure.

During saturation, the confining and back pressures were increased until a BP of 300 kPa, maintaining an effective isotropic pressure of 10 kPa. The Skempton's B parameter represents the degree of saturation, i.e. the percentage of water filling the voids (Skempton, 1954). If the sample is 100% saturated, the variation of the internal pressure (Δu) is equal to the external pressure variation ($\Delta \sigma_3$), hence B=1. In this research, although the CEN ISO/TS 17892-9:2004(E) only recommends a value of at least 0.95, the saturation was assured when B Skempton parameter was higher than 0.98 (Soares and Viana da Fonseca, 2016) and, when measured, the compression wave velocity (V_P) was higher than 1500 m/s.

The isotropic consolidation was attained by increasing the confining pressure to the required effective pressure, while maintaining the back pressure constant. The objective of this phase is to stabilize the specimen for the applied effective confining stress state until it reaches equilibrium in a drained state. The specimen is considered consolidated when the volume is constant (volume change is negligible).

The last stage is shearing, that leads the specimen to failure or to critical state. The monotonic drained tests were performed under constant strain rate, until an axial strain of at least 20% or constant volume (critical state) was reached. The strain rate should be slow enough to prevent pore pressure changes during compression. The rate used in this research for the monotonic compression tests was 0.02 mm/min, which is within the prescribed values in ISO 17892-9 (2018). The cyclic tests were performed undrained under stress control, until zero effective pressure or 5% double axial amplitude was reached. The load amplitude was selected according to the desired CSR and the cycle frequency varied between 0.1 Hz and 1 Hz.

The triaxial test apparatus used allows the measurement and acquisition of confining and back pressures, axial and volumetric deformations. Besides a complete control of the total and effective stress states, pore pressure and deformation state makes this equipment a useful and reliable tool to perform quality tests.

6.5.2. CYCLIC SIMPLE SHEAR TESTS

6.5.2.1. Sample preparation procedures

a) Reconstituted samples

As described in the sample preparation procedures for triaxial tests, the cyclic simple shear specimens were also prepared using either moist-tamping or dry pluviation techniques. The specimens were about 63 mm diameter and 22.5 mm height. When using the moist-tamping technique, the specimen was compacted in two layers.

The specimen was prepared in the base pedestal outside the cell chamber. First, the membrane, mould and copper rings were placed on the base pedestal. Transparent tape was used to seal the mould, so the vacuum could be applied to the membrane. The height of the mould was measured (the average of three measurements), a paper filter was placed on the bottom pedestal, and the specimen was prepared, using the desired preparation method (dry air pluviation or moist-tamping), as shown in Figure 6.18.
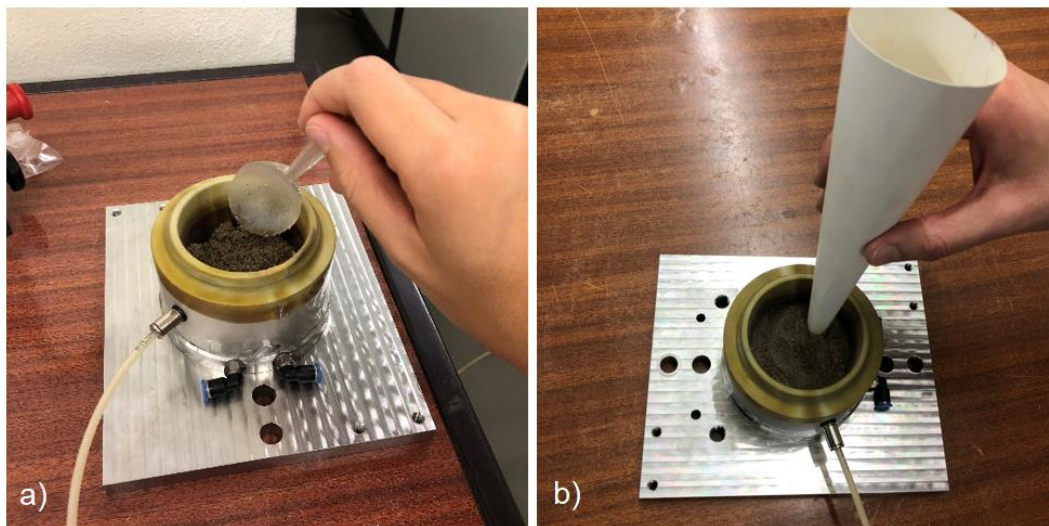
Figure 6.18 – Sample preparation for simple shear tests: a) moist-tamping; b) dry pluviation

Once the specimen is prepared, the height was measured (again the average of three measurements), to subtract to the initially measured height and assess the specimen actual height. A supporting part is attached to the base and the top cap is fixed to it. Subsequently, the top is lowered until it touches the top of the specimen, and the membrane and o-ring are secured. The mould is taken off, a bottom piece is inserted to secure the rings in place, and the bottom plate is placed on the inside of the bathtub, in the cell chamber. The bottom plate is then pushed inside the chamber and the horizontal piston is fixed and set to the zero position (using the manual controls on the software). The vertical piston is lowered (also using the software) until it touches the top cap and is attached using three screws. When the top is attached to the vertical piston, the supporting part can be removed. The chamber is closed and the test

procedures are controlled using the GEOsys software. Appendix A presents a comprehensive description of the steps involved in the preparation of a specimen.

A set of cyclic simple shear tests on reconstituted specimens of S1_M7 and S1_M2 soils (named with the reference L in Table 8.5) was performed at University of Ljubljana, all prepared by moist tamping into a mould with 70 mm diameter and 30 mm height. The sample preparation procedures comprises the placement of a rubber membrane around the base pedestal, stretching of the membrane inside the mould with vacuum, tamping of the soil in three layers and closing the chamber. The confinement is guaranteed with the rubber membrane and water pressure on the cell. Figure 6.19 shows the main parts of the procedure.
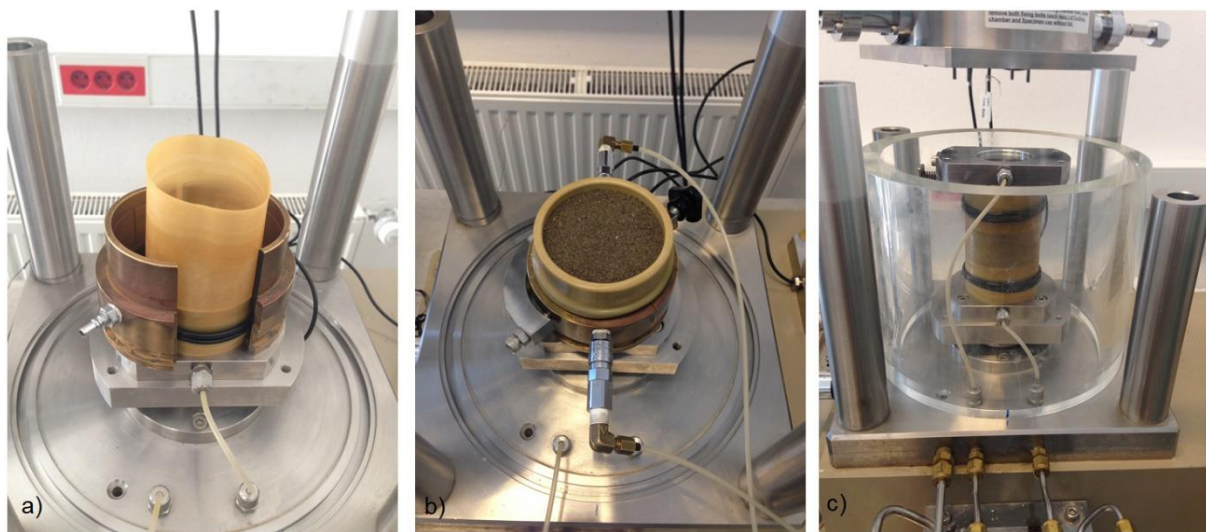
Figure 6.19 – Sample preparation in LabGeoUL apparatus: a) placement of membrane and mould; b) moist-tamped specimen; c) closing the chamber

b) Undisturbed samples

The undisturbed samples used for the performance of cyclic simple shear tests were obtained from Mazier collected samples. The performance of simple shear tests on undisturbed samples was not an objective of the work defined initially. However, the opportunity came from the fact that some Mazier collected samples, identified in the CPTu profile as having sand-silt-clay interlayers, were opened in half in order to document the presence of layers of different types of soils. Consequently, after opening and documenting the soil samples, some specimens were collected for the simple shear tests. Figure 6.20 shows the collection of a sample and the placement inside the simple shear rings. The specimens were collected using a metallic ring with the dimensions of the simple shear specimen (63 mm diameter and 24.8 mm height) and transferred to the inside of the copper rings in the base pedestal with the aid of a wooden piece.

Figure 6.20 – Sample preparation of an undisturbed specimen for simple shear tests

6.5.2.2. Test procedures

In this section, a short description of the test procedures is presented as a more detailed guide for the use of the simple shear equipment at LabGeo and test procedures is included in Appendix A.

For most tests performed with the simple shear equipment at FEUP, the specimens were not saturated and the simple shear tests were performed in specimens with different water contents depending on the preparation method. The procedure comprised two stages: consolidation to the required total vertical stress and cyclic shear. As the specimens were confined by the copper rings, the area is maintained constant and the volumetric changes are controlled by the changes in vertical displacement, i.e. changes in height. During consolidation, the vertical stress increases at a constant rate of about 2 kPa/min until reaching the required confinement and constant vertical displacement is recorded.

The shear stage was performed under stress control, until a constant low total vertical pressure (0 to 5 kPa) or 7.5% double shear strain amplitude was reached. All tests were performed with a cycle frequency of 0.1 Hz. The maximum and minimum horizontal stress depend on the selected CSR and correspond to the tangential stress. Due to the configuration of the equipment, the cyclic load was applied to the bottom of the specimen.

The simple shear tests performed at LabGeoUL followed a different test procedure. The specimens were confined with a flexible rubber membrane and the apparatus allowed the control of the lateral pressure applied to the specimen and the measurement of back and pore pressure. Therefore, the procedures were similar to the procedures of triaxial tests and involved four stages: percolation with CO_2 and water, saturation until a B parameter of more than 0.98, isotropic consolidation until constant volume changes, and cyclic shear. The cyclic load was applied through sinusoidal cycles of 0.1 Hz until zero effective pressure or a shear strain single amplitude of 3.75%. The undrained test was assured by closing the back pressure valve, and maintaining a constant sample height and total vertical stress during the loading stage.

6.6. TEST ANALYSIS

6.6.1. TRIAXIAL TESTS

Regardless the type of test performed, an accurate void ratio determination is essential for the proper interpretation of results. As no internal instrumentation was used, the void ratio is determined at the end of the test, considering full saturation of the specimen. After testing, the specimen is carefully placed in a previously weighed recipient and immediately weighed, guaranteeing the correct determination of water content and dry weight. As the majority of tests were performed in chambers with bender elements, it was not possible to use the freezing technique (Sladen and Handford, 1987) to determine the precise final void ratio. However, some tests were performed in a triaxial cell with lubricated bases, allowing the specimen to be frozen. The void ratio values determined with both techniques were found to be coincident (Figure 6.21), confirming that the determination of void ratio right after testing, without freezing, also showed precise results.
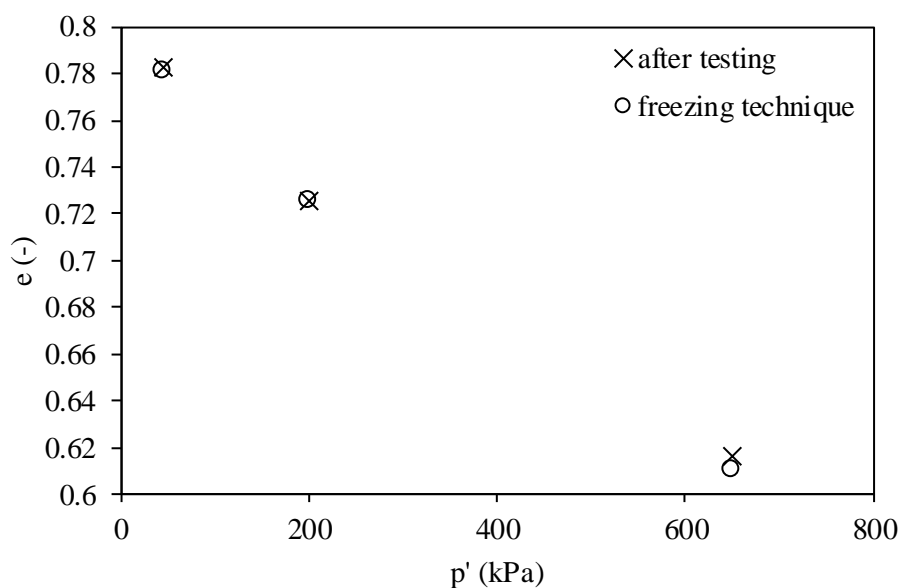
Figure 6.21 – Comparison between final void ratios determined after testing and using the freezing technique

6.6.1.1. Monotonic and cyclic shear

The monotonic tests were performed to evaluate the critical state lines of some soils and understand the behaviour of those soils when sheared drained in compression, while the cyclic tests were liquefaction assessment tests. As referred above, the precise void ratio is determined at the end of the test, considering the specimens fully saturated and using the expression $G_s \times w_f = S_r \times e$, where G_s is the soil specific weight, w_f is the final water content, S_r is the degree of saturation (considered 100%) and e is the void ratio. The sample dimensions are determined with an inverse calculation procedure, from end to beginning of the test. Table 6.2 presents the equations used to calculate height, volume and area of the specimen in each stage of the test. The subscribed 0, 1, and 2 refer to specimen measurements after preparation, consolidation and shear, respectively, while *i* and *f* refer to the initial and final values of each stage, respectively.

Table 6.2 – Calculation procedure for the evaluation of triaxial tests

Stage	ε_a	ε_v	ε_r	H	V	A
End of test	-	-	-		$V_{2f} = \dfrac{W_d\,(e_f + 1)}{G}$	
Drained monotonic shear	$\dfrac{\Delta H}{H_{2i}}$	$\dfrac{\Delta V}{V_{2i}}$	$\dfrac{\varepsilon_v - \varepsilon_a}{2}$	$H_2 = H_0 - \Delta H_2$ $\Delta H_2 = \Delta H + \dfrac{V_0 - V_{2i}}{V_0} \times \dfrac{H_0}{3}$	$V_{2i} = V_{2f} + \Delta V_2$	$\dfrac{V_2}{H_2}$
Undrained cyclic shear	$\dfrac{\Delta H}{H_{2i}}$	0	$-\dfrac{\varepsilon_a}{2}$	$H_2 = H_0 - \Delta H_2$ $\Delta H_2 = \Delta H + \dfrac{V_0 - V_{2i}}{V_0} \times \dfrac{H_0}{3}$	$V_{2i} = V_{2f}$	$\dfrac{V_2}{H_2}$
Consolidation	$\dfrac{\Delta H}{H_{1i}}$	$\dfrac{\Delta V}{V_{1i}}$	$\dfrac{\varepsilon_v - \varepsilon_a}{2}$	$H_1 = H_{2i} - \Delta H_1$ $\Delta H_1 = \dfrac{V_1 - V_{1i}}{V_0} \times \dfrac{H_0}{3}$	$V_{1i} = V_{2i} + \Delta V_1$	$\dfrac{V_1}{H_1}$

In the isotropic triaxial configuration, the axial and radial confinement pressure are the same, hence

$$\varepsilon_r = \varepsilon_a \tag{6.2}$$

$$\varepsilon_v = 2\varepsilon_r + \varepsilon_a = 3\varepsilon_a \tag{6.3}$$

The stress invariants are determined during shear stage as:

$$q = \sigma'_v - \sigma'_h = \frac{F}{A_2} \tag{6.4}$$

$$p' = \frac{\sigma'_v + 2\sigma'_h}{3} \tag{6.5}$$

In the undrained cyclic tests, the volume change during shear is null and pore pressure is generated. The excess pore pressure is determined as:

$$\Delta u = BP - BP_i \tag{6.6}$$

where, BP_i is the back pressure at the beginning of shearing and BP is the vertical stress at a certain instant of the shearing.

6.6.1.2. Membrane correction

The measurement of soil behaviour response can be influenced by the triaxial test system, mainly by membrane related causes as membrane penetration and membrane force (Taylor, 2015).

For fine soils, the potential errors due to membrane penetration are considered insignificant (Sladen and Handford, 1987). Moreover, Nicholson et al. (1993) studied factors affecting membrane compliance and stated that membrane penetration effect is only relevant if D_{20} is higher than twice the membrane thickness. As 0.4 mm thickness membranes were used and none of the soils tested had $D_{20} > 0.8$ mm, this correction was not considered in the analyses.

Membrane force corrections were applied to monotonic test results, as their effect is more pronounced when barrelling occurs and for low confining pressures. The total vertical and horizontal stresses were corrected, according to Standard ISO 17892-9 (2018), as follows:

Correction to total vertical stress

$$(\Delta\sigma_v)_m = \frac{4 \times t_m \times E_m}{D_m} \times \left[(\varepsilon_v)_m + \frac{(\varepsilon_{vol})_m}{3} \right] \tag{6.7}$$

Correction to total horizontal stress

$$(\Delta\sigma_h)_m = \frac{4 \times t_m \times E_m}{D_m} \times \frac{(\varepsilon_{vol})_m}{3} \tag{6.8}$$

where t_m is the initial thickness of the membrane, considered 0.4 mm, E_m is the elastic modulus of the membrane, considered 1300 kPa, D_m is the initial diameter of the membrane, $(\varepsilon_v)_m$ is the vertical strain of the membrane (expressed as ratio), and $(\varepsilon_{vol})_m$ is the volumetric strain of the volume enclosed by the membrane (expressed as ratio).

Besides, Fukushima and Tatsuoka (1984) described three membrane correction methods: Method I corresponds to the standard recommendation; Method II assumed that axial deformation is independent of radial deformations; and Method III assumed that the axial deformation of the membrane is negligible, so $(\Delta\sigma_v)_m = 0$. In this work, as only drained tests were performed, the results did not vary when using the Standard or Method III for membrane correction, as also verified by Fukushima and Tatsuoka (1984). However, care should be taken when analysing undrained triaxial tests, especially for lower confining pressures.

6.6.2. CYCLIC SIMPLE SHEAR TESTS

Due to equipment restrictions, the cyclic simple shear tests at FEUP were performed without water percolation and saturation of the specimen. In this type of test, the vertical stress is controlled and a horizontal cyclic force is applied to the specimen. As discussed by Reyno et al. (2005), for devices where saturation is not possible, the undrained conditions can be reproduced performing drained tests at constant volume. The cross section remains constant during the test, as it corresponds to the inside area of the copper ring, thus a constant volume condition is achieved by locking the vertical rod and guaranteeing a fixed sample height. In these constant volume tests, the change in total vertical stress corresponds to the pore pressure changes. As the soils used for this thesis were sands, the shaking produces a compaction of the specimen and a consequent reduction of vertical stress, equivalent to the increase of pore pressure in a similar undrained test (Finn et al., 1978, Dyvik et al., 1987).

The initial height is measured at the beginning of test, after specimen preparation. The area is constant throughout the test, as it corresponds to the interior area of the copper stacked rings confining the specimen. As the area is kept constant, the axial deformation is the same as the volumetric deformation, calculated based on the axial deformation of the specimen during consolidation. The axial strain, height and area are determined as:

$$\varepsilon_a = \varepsilon_v = \frac{\Delta H}{H_0} \tag{6.9}$$

$$H = H_0 - \Delta H \tag{6.10}$$

$$A = A_0 \tag{6.11}$$

In the shearing stage, the height is fixed and maintained constant, so, as the area is also kept constant, there are no volume changes. As there is no control or measurement of the back pressure, the test results are represented as total stresses. The total vertical stress (σ_v) is determined by the ratio between the

vertical load and the area, while the tangential stress (τ) is the ratio between the horizontal load and the area.

$$\sigma_v = \frac{F_v}{A} \tag{6.12}$$

$$\tau = \frac{F_h}{A} \tag{6.13}$$

The shear strain is the ratio between the horizontal displacement and the specimen height.

$$\gamma = \frac{\Delta h}{H} \tag{6.14}$$

As the specimens are not saturated and the tests are constant volume tests, the pore pressure generation corresponds to the drop in vertical stress, i.e. the difference between vertical stress at the beginning of shearing (σ_{v0}) and the vertical stress at a certain instant of the shearing (σ_{vi}):

$$\Delta u = \sigma_{v0} - \sigma_{vi} \tag{6.15}$$

$$r_u = \frac{\Delta u}{\sigma_{v0}} \tag{6.16}$$

On the other hand, as the equipment used in University of Ljubljana allowed the saturation of the specimen and the measurement of the cell and back pressures, the pore pressure generation is measured directly in a similar way as in the triaxial test procedure. Thus, the excess pore pressure and pore pressure ratio are determined as:

$$\Delta u = BP_i - BP_0 \tag{6.17}$$

$$r_u = \frac{\Delta u}{\sigma'_{v0}} \tag{6.18}$$

where, BP_0 is the back pressure at the beginning of shearing, BP_i is the vertical stress at a certain instant of the shearing, and σ'_{v0} is the effective vertical stress at the beginning of shearing.

6.7. INTRODUCTION TO THE EXPERIMENTAL WORK DEVELOPED

The experimental laboratory work developed involved the performance of tests in different equipment and with soils of variable characteristics in variable initial conditions. The work was composed of three

main parts: material properties characterisation; monotonic and cyclic triaxial and simple shear tests in reconstituted samples to define the critical state lines of the case study soils and study the influence of distinct parameters on the liquefaction behaviour of soils; and cyclic triaxial tests and simple shear tests in undisturbed and respective reconstituted specimens. The material properties characterisation included grain size analyses and the determination of specific weight, Atterberg limits, maximum and minimum void ratio, and shape parameters of all undisturbed samples tested and of the NB1 soil.

To investigate the influence of distinct parameters on cyclic liquefaction resistance of sands, a large set of cyclic triaxial and cyclic simple shear tests was performed. The effect of initial confining pressure, relative density, sample preparation method, and type of loading (depending on the equipment used) on the soils liquefaction resistance was considered. Besides, a set of monotonic triaxial tests in NB1, S1_M2, S1_M7, and S1_M6 soils and a set of monotonic direct simple shear tests in NB1 soil were performed to determine their critical state lines and to evaluate differences in behaviour of soils prepared with different methods and sheared at different rates, respectively.

Finally, to study the cyclic liquefaction resistance of the experimental sites, cyclic triaxial tests were performed with undisturbed specimens collected with Mazier and Gel-Push samplers. Moreover, the respective reconstituted specimens were prepared with the same soil and initial conditions, to assess the effect of fabric change. A set of cyclic direct simple shear tests were also performed in undisturbed samples collected with the Mazier sampler, followed by tests on the respective reconstituted specimens in the same initial conditions, for a direct comparison between the results.

In summary, the experimental laboratory work involved the performance of:

- Undrained cyclic triaxial tests on undisturbed specimens collected using Mazier and Gel-Push samplers and respective reconstituted specimens with the same soils and initial state conditions;
- Undrained cyclic triaxial tests on NB1, S1_M2 and S1_M7 soils;
- Drained monotonic triaxial tests on NB1, S1_M2, S1_M6, and S1_M7;
- Constant volume cyclic direct simple shear tests on NB1, S1_M2 and S1_M7 soils;
- Constant volume cyclic direct simple shear tests on undisturbed samples collected with the Mazier sampler and respective reconstituted specimens with the same soils and initial state conditions;
- Monotonic direct simple shear tests on NB1;
- Oedometric tests on NB1, S1_M2, S1_M6, and S1_M7.

A total of 219 tests, including 5 oedometer tests, 127 triaxial tests and 87 simple shear tests, were performed and are presented in this work, as summarised in Table 6.3. Moreover, around 82 grain size distribution curves, 68 specific gravity, 25 Atterberg limits, 28 void ratio limits determination and 22 morphology tests were performed, with the help of the LabGEO technicians.

Table 6.3 – Summary of laboratory tests performed

Apparatus	Type of loading	Soil ID	Sample Preparation method	Number of tests performed
Triaxial	Monotonic	S1_M2	MT	3
		S1_M6	MT	3
		S1_M7	MT	3
		NB1	MT	8
			PL	6
	Cyclic	Mazier and Gel-Push samples	Undisturbed	31
			Reconstituted - MT	28
		S1_M2	MT	9
		S1_M7	MT	15
		NB1	MT	18
			PL	3
Simple shear	Monotonic	NB1	MT	5
			PL	3
	Cyclic	S1_M2	MT	8
		S1_M7	MT	9
		NB1	MT	30
			PL	8
		Mazier	Undisturbed	8
			Reconstituted - MT	16
Oedometer		S1_M2	MT	1
		S1_M6	MT	1
		S1_M7	MT	1
		NB1	MT	1
			PL	1
			Total	219

7. PHYSICAL AND GEOMECHANICAL CHARACTERISATION OF CASE STUDY SOILS

7.1. INTRODUCTION

One of the objectives of this work, integrated on the FCT project LIQ2PROEARTH, was to investigate the effect of different factors on the cyclic behaviour of soils. For this purpose, four soils were selected from the collected samples and considered as case study soils. These soils were selected as there was enough soil to perform a variety of reconstituted specimens, which was not possible with the other soils collected as undisturbed samples with Mazier and Gel-Push samplers.

This Chapter presents the physical and geomechanical properties of the four selected soils, S1_M2, S1_M6, S1_M7, and NB1. First, a description of the physical properties is presented, including the grain size distribution curves, specific weight, mineralogy, shape parameters, and void ratio limits. Secondly, oedometric tests, triaxial compression tests, and shear wave velocity measurements results are discussed, in order to fully characterise the mechanical properties of the four soils, determine their critical state lines and analyse their small strain behaviour. Additionally, a set of direct simple shear tests in monotonic conditions was performed to evaluate the influence of confining pressure, sample preparation method, and shear rate in the behaviour of the NB1 sand.

7.2. MATERIAL PROPERTIES

In this section the four materials tested are presented in terms of main physical properties. Soils S1_M2, S1_M6, and S1_M7 were obtained from Mazier undisturbed samples. After performing the triaxial tests with the undisturbed samples, the soil was collected, homogenised, and prepared for the following laboratory tests. On the other hand, the NB1 soil was collected and prepared for the performance of reconstituted tests. Seven parcels of this soil were collected and the respective grain size curves were determined. As observed in Figure 7.1a, all parcels present similar grain size curves, so an average curve was used as the reference curve of particle size distribution. Figure 7.1b presents the grain size distribution curves of the four soils studied. The four soils are characterised as sands with low fines content, D_{50} ranging from 0.33 to 0.70, and coefficient of uniformity (C_U) and shape (C_C) ranging from

1.81−3.76 and 0.89−1.01, respectively. According to the ASTM D-2487-17 classification, all soils are classified as poorly graded sands (SP), with low values of C_U and C_C, which are indicative of uniform particle size. The main physical properties of the tested soils are presented in Table 7.1. The values of maximum and minimum void ratios were obtained using the Japanese Geotechnical Society (JGS) method.
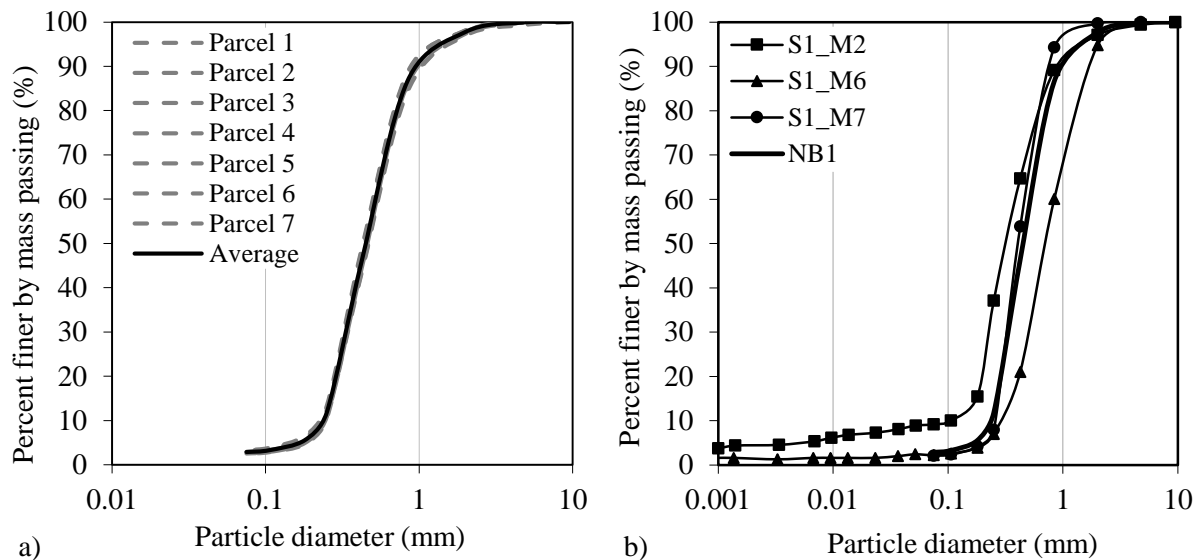
Figure 7.1 – Grain size distribution of studied soils: a) NB1 soil; b) S1 and NB1 soils

Table 7.1 – Main physical properties of tested soils

Name	Packing		FC (%)	G_s	Gradation		
	e_{max}	e_{min}			D_{50} (mm)	C_C	C_U
S1_M2	0.940	0.571	9.2	2.651	0.33	1.01	3.76
S1_M6	0.713	0.494	2.4	2.629	0.70	0.99	2.80
S1_M7	0.902	0.613	2.1	2.643	0.40	0.89	1.81
NB1	0.846	0.590	2.9	2.640	0.45	0.90	2.16

The mineralogy of some case study sands was obtained with the X-ray diffraction technique. As discussed above, these soils have an alluvial origin, and are mainly composed of quartz with traces of orthoclase, albite, and muscovite. Table 7.2 presents the results of the mineralogy tests.

Table 7.2 – Mineralogy of three studied soils

Mineral	S1_M7	NB1	NB1_F2_GP2.5
Quartz	66	65	59
Orthoclase	11	6	13
Albite	6	9	19
Muscovite	13	20	9
Kaolinite	4	-	-

To investigate the particle shape of the materials, the soils were tested in the Morphologi G3 apparatus, at University College London. Altuhafi et al. (2013) proposed a graph correlating sphericity and convexity in QicPic (which correspond to circularity and solidity in Morphologi G3, respectively) and defined angularity zones. The solidity and circularity results are plotted in Figure 7.2, showing that the four soils have similar values of circularity and solidity and are very close to the boundary between subangular and subrounded particles.
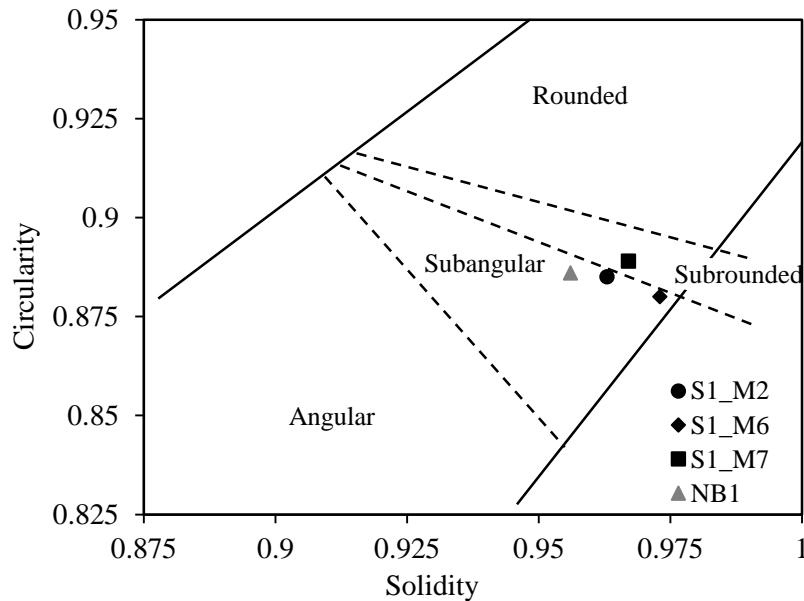
Figure 7.2 – Shape results plotted on the angularity zones plane proposed by Altuhafi et al. (2013)

7.3. OEDOMETRIC TESTS

With the objective of better characterising the soils studied, a set of oedometric tests was performed with reconstituted specimens of S1_M2, S1_M6, S1_M7, and NB1 soils. The tests were performed according to the ISO 17892-5:2017 standard. The specimens had a diameter of 50 mm and a height of 19 mm, and were moulded with the moist-tamping technique with a high void ratio (to simulate very loose conditions). Additionally, one specimen of NB1 soil was prepared with air pluviation, to assess the influence of sample preparation technique. Figure 7.3 presents the oedometric tests results, with the loading and unloading phases. To assist on the comparisons, the grain size distribution curves for each soil are also presented in Figure 7.3.
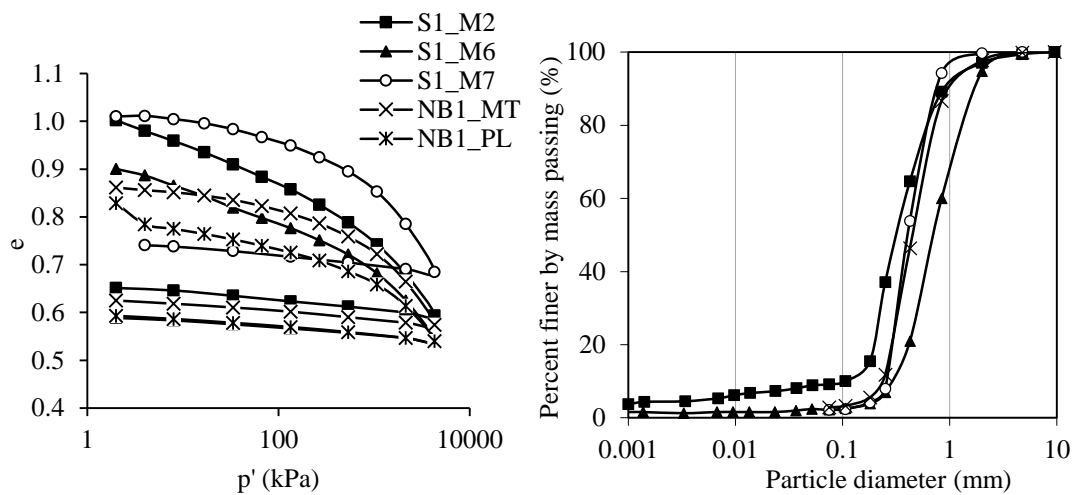
Figure 7.3 – Results of oedometric tests and grain size distribution curves for the respective soils

It seems that S1_M7 is less compressible, as the final void ratio is higher than the other soils, for the same maximum confinement of 6400 kPa. However, the tests did not start at the same void ratio, so the compressibility was assessed by the difference between the initial void ratio and the void ratio after a confinement of 6400 kPa. These results are on Table 7.3, and the S1_M2 soil was found to be the most compressible (higher e_0-e_L). This may be justified by the higher fines content of this soil, as expressed by the comparison of grain size distribution curves also illustrated on Figure 7.3. On the other hand, the unloading stage is very similar for all soils in terms of void ratio differences.

A difference in the compressibility of specimens of NB1 prepared with MT and PL is also identified. The specimen prepared with PL showed an initially higher settlement, probably due to the rearrangement of particles during the saturation of the specimen. However, when considering the entire confinement process, the difference between the initial and final void ratios is the same. This might have an impact on the cyclic behaviour of specimens prepared with the two methods, as the specimen prepared with air pluviation shows an initially higher compressibility that might influence the soil response in the first few loadings cycles.

Table 7.3 – Summary of the oedometric tests performed

Material	Depth (m)	e_0	e_L	e_U	e_0-e_L	C_C
S1_M2	2	1	0.59	0.65	0.41	0.247
S1_M6	6	0.9	0.54	0.59	0.36	0.236
S1_M7	7	1.01	0.68	0.74	0.33	0.280
NB1_MT	4-5	0.86	0.57	0.63	0.29	0.247
NB1_PL	4-6	0.83	0.54	0.59	0.29	0.196

7.4. CRITICAL STATE LINES

The critical state soil mechanics (CSSM) framework globally describes the mechanical behaviour of soils considering the volume changes during shear and has been used to characterise the monotonic and cyclic behaviour of sands (Been and Jefferies, 1985; Coop, 2005; Jefferies and Been, 2016). The state parameter, ψ, defines the position of a soil specimen in relation to the critical state line, as outlined in Chapter 2. The clear identification of the critical state line of a soil is very important to fully understand its behaviour under both monotonic and cyclic loading.

In this section, the critical state lines (CSL) of the four case study soils presented above were determined and compared. Besides, the critical state parameters were related to other materials properties, namely the maximum and minimum void ratios, mean grain size, coefficient of uniformity, fines content and shape parameters, and compared with benchmark sands from literature.

7.4.1. CSL FOR SOILS COLLECTED AT S1

Three soils collected with the Mazier sampler in site S1, at depths 2 m, 6 m and 7 m, herein labelled as S1_M2, S1_M6, and S1_M7, respectively, were characterised in terms of their behaviour under triaxial compression. Sets of three to four drained triaxial compression tests were performed with each soil, as presented in Table 7.4. All specimens were prepared using the moist tamping technique, targeting a loose initial void ratio, and isotropically consolidated to different confining pressures. The tabulated results are detailed in Appendix C, presenting an index code of the test, the void ratio after assembling (e_0), the void ratio at the end of saturation (e_{i-1}), the volumetric strain during consolidation and during shear (ε_v), the void ratio after consolidation (e_i), the applied mean effective stress (p'_i), the shear wave velocity after consolidation (V_S), the void ratio at the end of shear (e_f), the mean effective stress (p'_f), and deviatoric stress (q_f) at the end of shear.

Table 7.4 – List of monotonic triaxial tests performed with reconstituted specimens of S1 soils

Test ID	Method of sample preparation	e_i	p'_i (kPa)	Drainage conditions
S1_M2_R3_STxD1	MT	0.82	50	Drained
S1_M2_R3_STxD2	MT	0.75	200	Drained
S1_M2_R3_STxD3	MT	0.72	400	Drained
S1_M7_STxD1	MT	0.86	200	Drained
S1_M7_STxD2	MT	0.86	401	Drained
S1_M7_STxD3	MT	0.89	70	Drained
S1_M7_STxD4	MT	0.95	20	Drained
S1_M6_STxD1	MT	0.72	70	Drained
S1_M6_STxD1	MT	0.68	398	Drained
S1_M6_STxD1	MT	0.71	200	Drained

Figure 7.4 to Figure 7.6 present the results for S1_M2, S1_M6, and S1_M7, respectively, and include the stress–path, q–p', with the identification of the critical shear stress ratio, M_{cs}; the stress-strain path, q–ε_a; the evolution of volumetric strain with axial strain, ε_v–ε_a; and the e-log(p') plot with the identification of the CSL. As expected, all specimens showed a contractive behaviour with $\varepsilon_v > 0\%$ and no peak strength associated to dilation was found, as the specimens were prepared in very loose conditions, with high void ratios. These trends were expected, as they follow the CSSM theory, in which loose specimens located on the wet side of the CSL tend to contract towards the CSL. As a result, the critical state was defined by the end of the test conditions in the e-log(p') diagram. Table 7.5 summarises the critical state parameters for the S1 soils, according to the definitions of the linear and curved CSL (equations (2.1) and (2.2)). The three soils have similar critical friction angle, ϕ'_{cs}, around 33°, corresponding to critical friction ratios, M_{cs}, of around 1.35. S1_M2 curve is steeper, with a higher values of slope, λ, and void ratio intercept, Γ. The comparison between the critical state lines is addressed in section 7.4.3.

Table 7.5 – Critical state parameters for S1 soils

Material	Linear CSL parameters		Curved CSL parameters			M_{cs}	ϕ'_{cs} (°)
	Γ	λ_{10}	$e_{cs,0}$	λ	ξ_a		
S1_M2	1.031	0.146	0.815	0.075	0.5	1.37	33.92
S1_M6	0.835	0.081	0.712	0.040	0.5	1.35	33.38
S1_M7	0.957	0.065	0.881	0.043	0.5	1.33	32.98
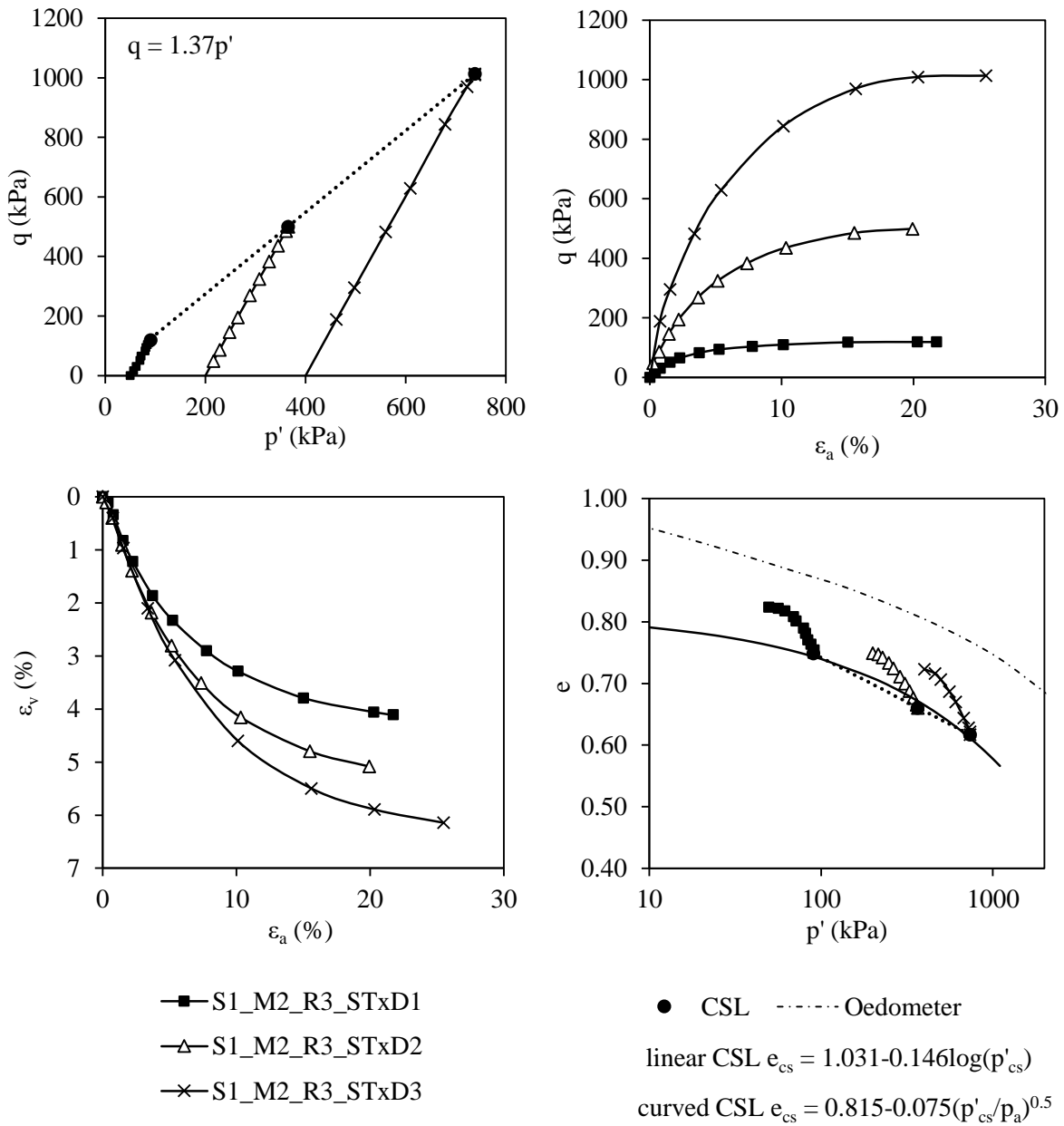
Figure 7.4 – Results of drained triaxial compression tests on S1_M2: definition of CSL
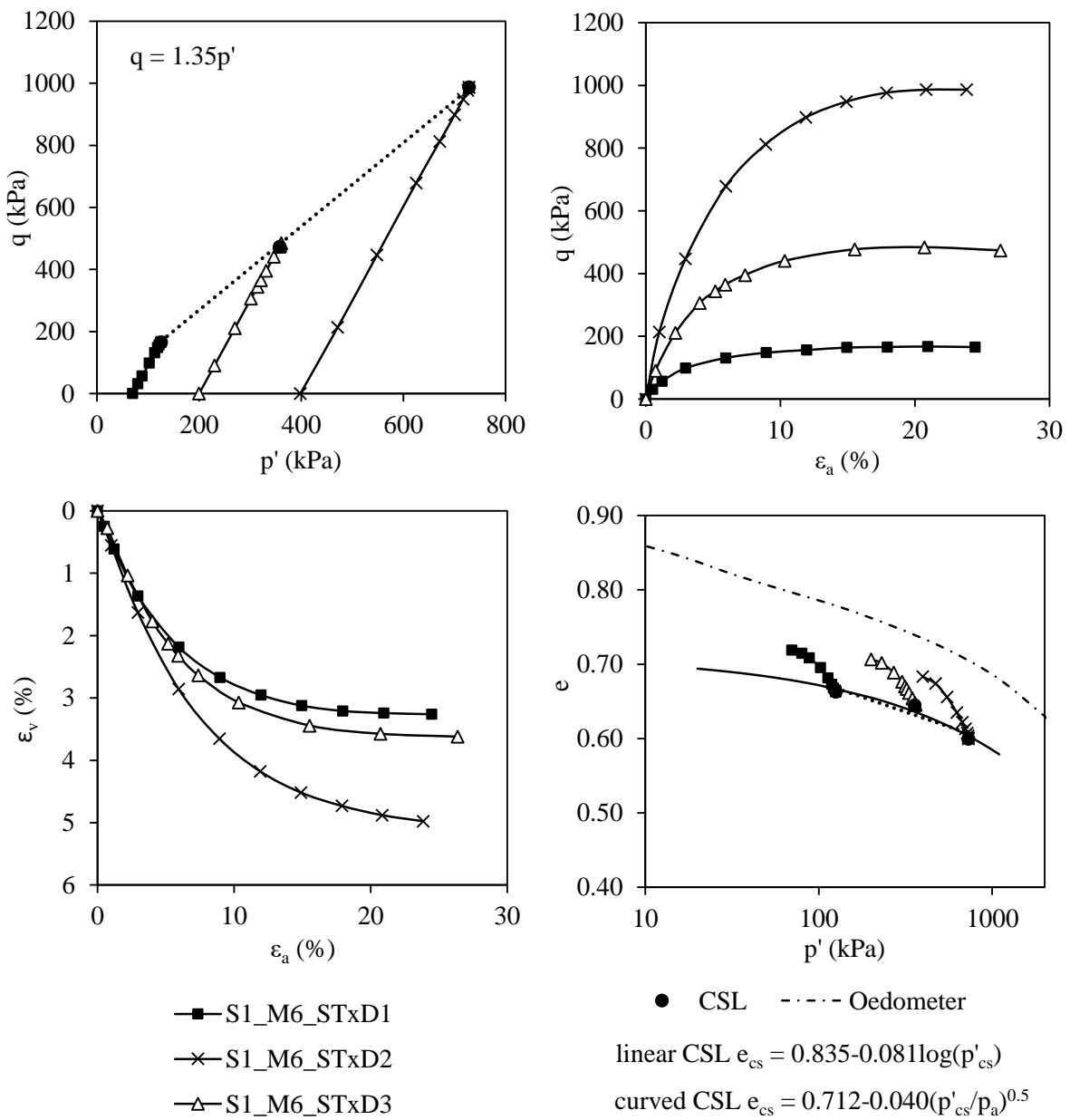
Figure 7.5 – Results of drained triaxial compression tests on S1_M6: definition of CSL
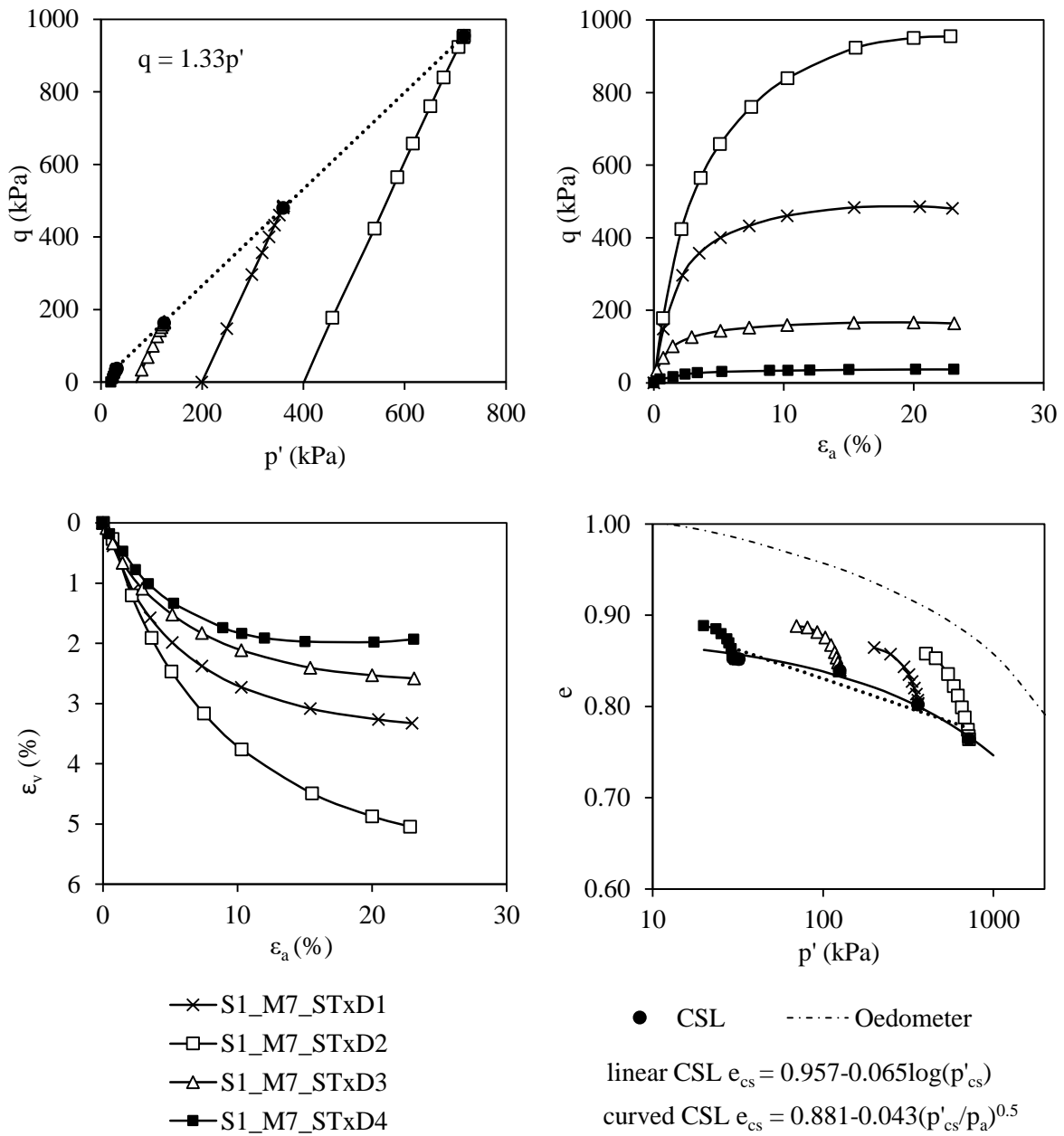
Figure 7.6 – Results of drained triaxial compression tests on S1_M7: definition of CSL

7.4.2. CSL FOR NB1 SOIL

A set of triaxial compression tests was performed under drained conditions with NB1 soil, covering a wide range of confining pressures, as reported in Table 7.6. To evaluate the fabric influence on soil behaviour to monotonic loading, a total of 14 tests were performed, 8 in specimens prepared with the moist-tamping (MT) technique and 6 in specimens prepared with dry air pluviation (PL), following the procedures described in section 6.5. As referred above for S1 soils, the tabulated results are presented in Appendix C, including an index code of the test, the void ratio after assembling (e_0), the void ratio at the end of saturation (e_{i-1}), the void ratio after consolidation (e_i), the volumetric strain during consolidation and during shear (ε_v), the applied mean effective stress (p'_i), the shear wave velocity after consolidation (V_S), the void ratio at the end of shear (e_f), the mean effective stress (p'_f), and deviatoric stress (q_f) at the end of shear.

The representation of all tests on the same plot would be confusing, so the tests results are organised according to the initial confining pressure. Figure 7.7 presents the results of the triaxial compression tests performed in NB1, grouped by initial confining pressures of 20 kPa, 45 kPa, 200 kPa, 400 kPa, and 650 kPa, respectively.

Table 7.6 – List of monotonic triaxial tests performed with reconstituted specimens of NB1 soil

Test ID	Method of sample preparation	e_i	p'_i (kPa)	Drainage conditions
NB1_MT_STx1	MT	0.71	649	Drained
NB1_MT_STx2	MT	0.78	46	Drained
NB1_MT_STx3	MT	0.77	19	Drained
NB1_MT_STx4	MT	0.78	44	Drained
NB1_MT_STx5	MT	0.79	19	Drained
NB1_MT_STx6	MT	0.75	650	Drained
NB1_MT_STx7	MT	0.76	198	Drained
NB1_MT_STx8	MT	0.76	45	Drained
NB1_PL_STx1	PL	0.78	46	Drained
NB1_PL_STx2	PL	0.73	200	Drained
NB1_PL_STx3	PL	0.73	395	Drained
NB1_PL_STx4	PL	0.80	43	Drained
NB1_PL_STx5	PL	0.80	20	Drained
NB1_PL_STx6	PL	0.71	667	Drained
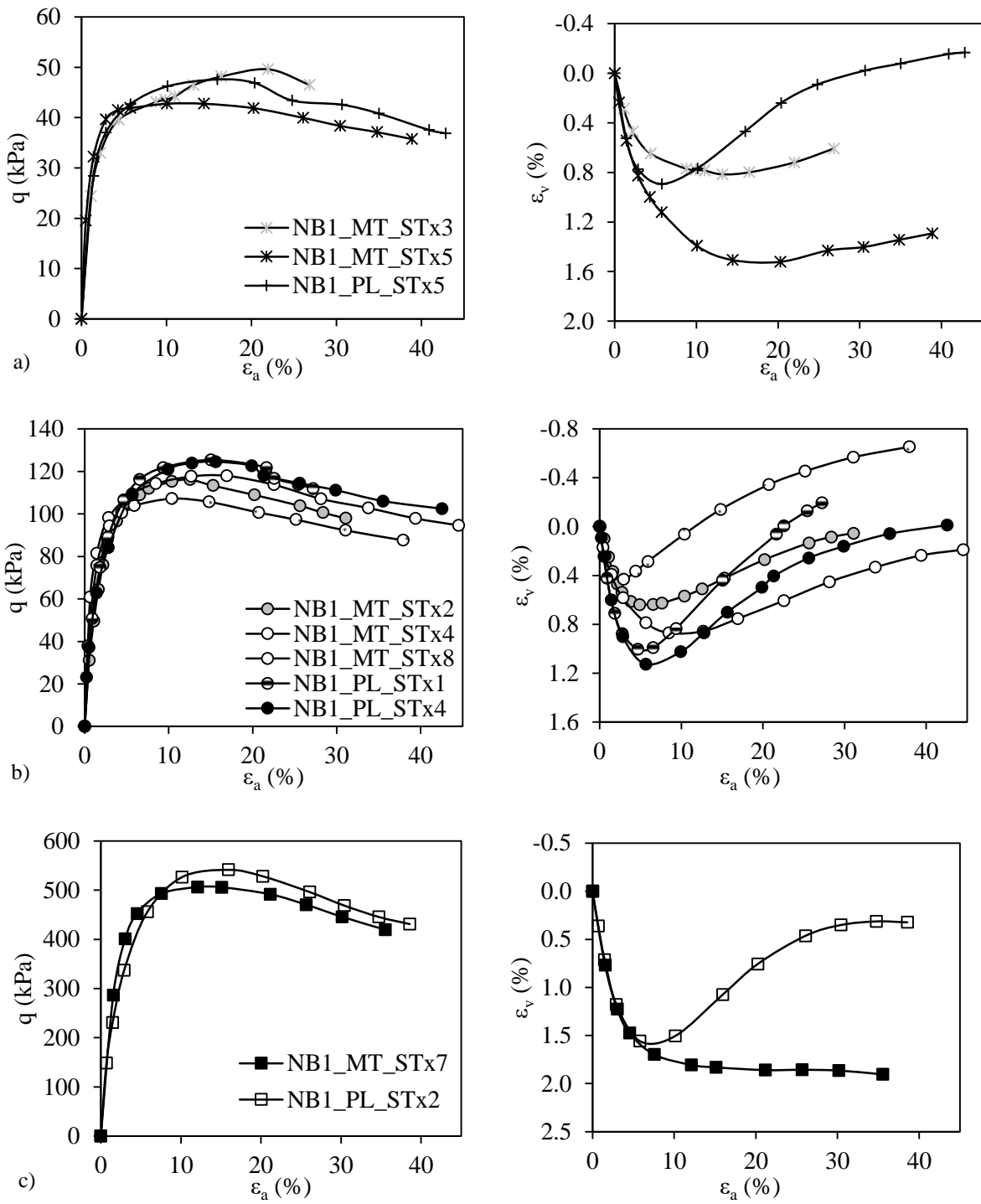
Figure 7.7 – Stress-strain and volumetric-strain behaviour of drained tests in NB1 for different initial confining stresses: a) 20 kPa; b) 45 kPa; c) 200 kPa; d) 400 kPa; e) 650 kPa
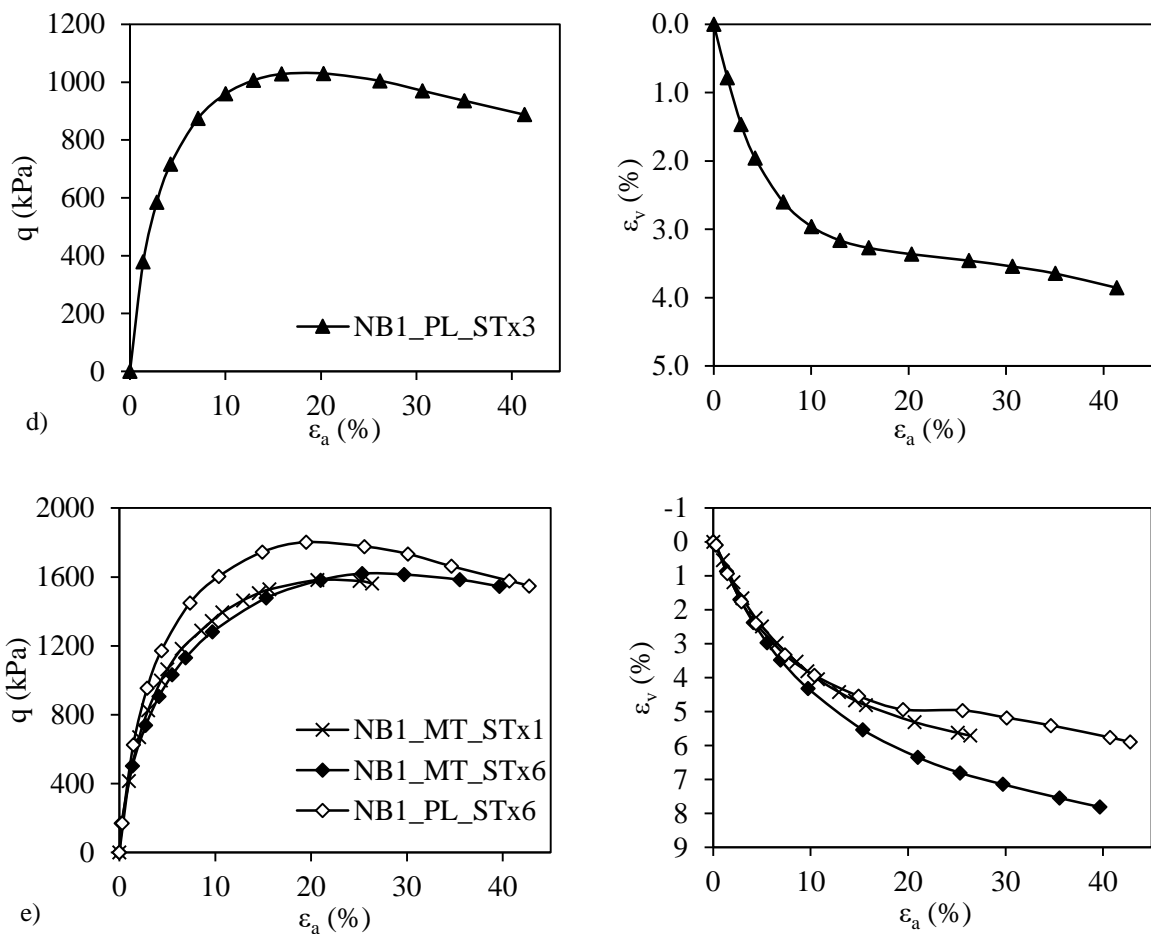
Figure 7.7 (continued) – Stress-strain and volumetric-strain behaviour of drained tests in NB1 for different initial confining stresses: a) 20 kPa; b) 45 kPa; c) 200 kPa; d) 400 kPa; e) 650 kPa

From the three specimens confined with initial confining pressure of 20 kPa (Figure 7.7a), two were prepared with MT and one with PL. NB1_MT_STx5 and NB1_PL_STx5 were prepared with the two distinct methods and, despite having similar initial void ratio of 0.795, they behave differently. While the test prepared with MT showed a more contractive behaviour, the test prepared by PL first experienced some contraction but then dilated, to a final void ratio similar to the beginning. However, this difference in behaviour is mainly because the initial void ratio is very close to the critical void ratio. For low stresses, the identification of the CSL is not always straightforward (Cubrinovski and Ishihara, 2000; Coop, 2005). Despite the same confinement, the three tests ended at different stages. The two specimens prepared with moist tamping show no evidence of a stable volumetric strain, hence no stabilisation of the critical void ratio. The dilatancy plots were studied to try to extrapolate the data to estimate the critical state conditions, according to the proposal of Carrera et al. (2011). As all tests were drained, the void ratio is plotted against the dilatancy. Figure 7.8 presents the results for all tests with initial confining pressure of 20 kPa. NB1_MT_STx3 and NB1_MT_STx5 did not reach the condition

of zero dilatancy, and it is not possible to assess the trajectory of dilatancy with precision as the final void ratio is far from the one of NB1_PL_STx5. Therefore, these two tests were excluded from the definition of the CSL.
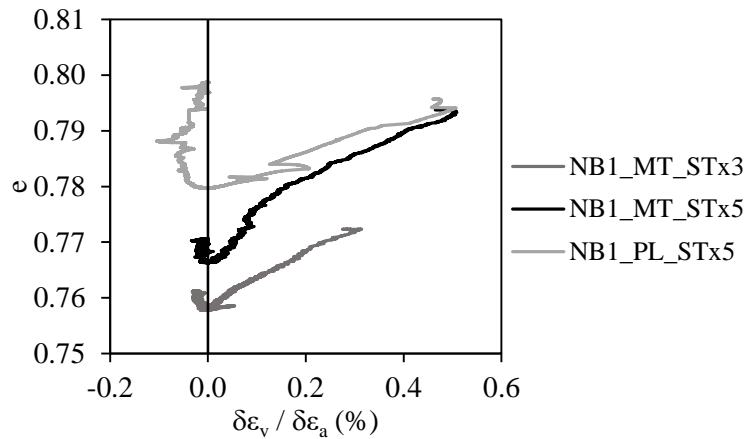
Figure 7.8 – Evolution of dilation with void ratio to extrapolate critical state

As for the tests with initial confining pressure of 45 kPa (Figure 7.7b), they all contracted at first and then dilated, despite having started at different void ratios. Four tests tend to the same final void ratio, considered the critical void ratio, while test NB1_PL_STx4 is considered an outlier as it does not follow the trend and was not considered in the CSL definition. The two tests with 200 kPa of confinement present different behaviours but end at the same critical void ratio (Figure 7.7c). There is a stabilisation of the volume and, consequently, of void ratio, so the CSL was reached and the critical void ratio determined. The test prepared with MT contracted while the test prepared by air pluviation first contracted and then dilated because the initial void ratio was lower. This might not be related to the preparation method but rather to the different initial void ratio (above or below the CSL) that conditioned the specimen behaviour. On the other hand, the test confined at 400 kPa shows contractive behaviour (Figure 7.7d). As for the three tests with initial confining stress of 650 kPa (Figure 7.7e), they all show contractive behaviour, despite there is no stabilisation of the volume. However, the void ratio shows a tendency for the same final value in each test, $e = 0.61$, considered the critical void ratio.

The critical state line was defined for NB1 soil, with specimens prepared with both moist-tamping (MT) and air pluviation (PL), as presented in Figure 7.9. Both specimens prepared with MT and PL reach the same CSL. From these results, there is no apparent difference between the critical state results for MT and PL specimens, emphasising the fact that initial fabric (produced by different preparation techniques) has no effect at large strains, as reported by other authors (Castro, 1969; Poulos, 1981; Been and Jefferies, 1985; Carrera et al., 2011; Jefferies and Been, 2016).

For high confining pressures, the line seems to change slope, probably due to the grain crushing of the soil particles, which leads to an evolution of the CSL position. As reported by Been and Jefferies (1985), an increase on FC causes an increase in the CSL slope. The CSL considered is composed of two portions, one for lower and other for higher confining stresses. Moreover, the normal consolidation line (NCL) determined by one oedometer test is also represented, confirming the change in the slope of the CSL for higher confining pressures. The two parts of the CSL equations are presented in Figure 7.9. The CSL is defined by the reference void ratio, Γ, and the slope, λ, having the values of 0.919 and 0.076, respectively. The critical friction angle, ϕ'_{cs}, was found to be 32.6°, corresponding to a critical friction ratio, M_{cs}, of 1.31.
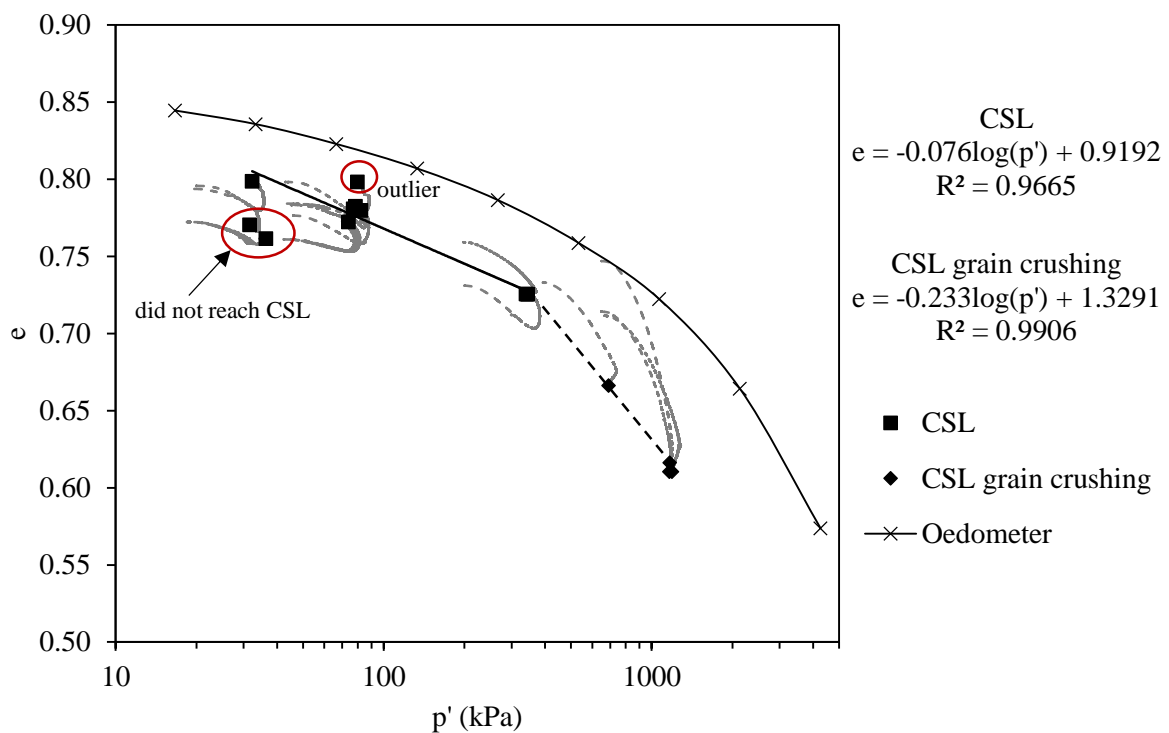
Figure 7.9 – Critical state line definition for NB1 soil

The CSL is represented in Figure 7.10, excluding the outliers and specimens that did not reach the CSL. The isotropic compression and shearing paths are also illustrated. The isotropic compression data follows the same trend as the oedometer 1D_NCL line. The curved CSL is represented, together with the correspondent equation. Although it is recognised that the curved CSL is more accurate, especially for low pressures due to the horizontal asymptote consideration, the CSL defined as linear for pressures between 30 kPa and 300 kPa was used to compute the state parameters of NB1 soil. This was considered as the specimens tested in cyclic conditions in this work were consolidated to 40 kPa and 100 kPa and the critical void ratio does not differ significantly depending on the equation used (0.85% and 0.88% for 40 kPa and 100 kPa, respectively). Moreover, this consideration allows for comparisons of λ and Γ

with benchmark soils and estimations of CSL of the undisturbed soils, as is discussed later. However, it is important to note that care should be taken when using the bilinear equation to estimate the state parameter for low pressures, because of the increasing difference between the curved and bilinear CSL for pressures lower than 20 kPa (Cubrinovski and Ishihara, 2000; Coop, 2005).
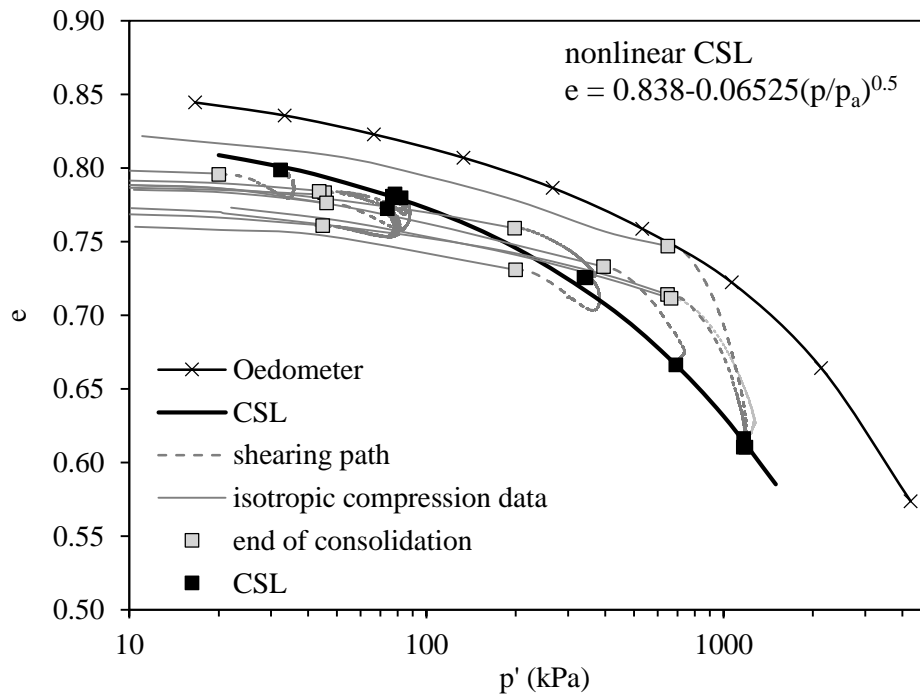
Figure 7.10 – Nonlinear CSL definition for NB1 soil

7.4.3. CSL COMPARISON

As stated above, the critical state line is a unique feature of each soil and is essential for the understanding of a soil behaviour, as its initial state position relative to the CSL will indicate a more contractive or dilative behaviour when sheared. The position and slope of the CSL is strongly influenced by grain size and particle shape, hence when comparing curves from different soils, correlations can be obtained to explain the soil behaviour disparities.

In this subsection, the four CSL determined are compared between them. The correlations between grain size and particle shape parameters with critical state parameters might explain some differences between the soils behaviours and are useful for the estimation of critical state parameters in soils when it is not possible to perform consistent reconstituted specimens for CSL determination based on triaxial tests.

Figure 7.11 presents the CSL of the soils studied in this work, which CS parameters are presented in Table 7.7. The slopes of the curves are similar, except for the S1_M2 which is steeper. This increase in slope might be due to a fines content increase, as it is recognised that fines content plays a major part

on the CSL slope and position (Been and Jefferies, 1985). As for the other three soils, despite having similar fines content, they are distinguished by the different values of the void ratio intercept (value of the void ratio when p' equals 1 kPa), with S1_M7 being the highest and S1_M6 the lowest. These differences in position might be a reflection of the packing capacity and grain size of each soil. According to Poulos et al. (1985), the vertical position of the CSL is strongly influenced by the grain size characteristics, while the slope is affected by the grain shape. Cho et al. (2006), reported that the CS intercept increases with increase in e_{min} and e_{max}, and the CS slope increases with increase in the range between e_{max} and e_{min}, which was also verified by Cubrinovski and Ishihara (2000). S1_M6 has a low maximum void ratio and its particles are coarser, which lowers the position of the CSL. On the other hand, S1_M7 has a higher maximum void ratio, justifying the higher position of its CSL.
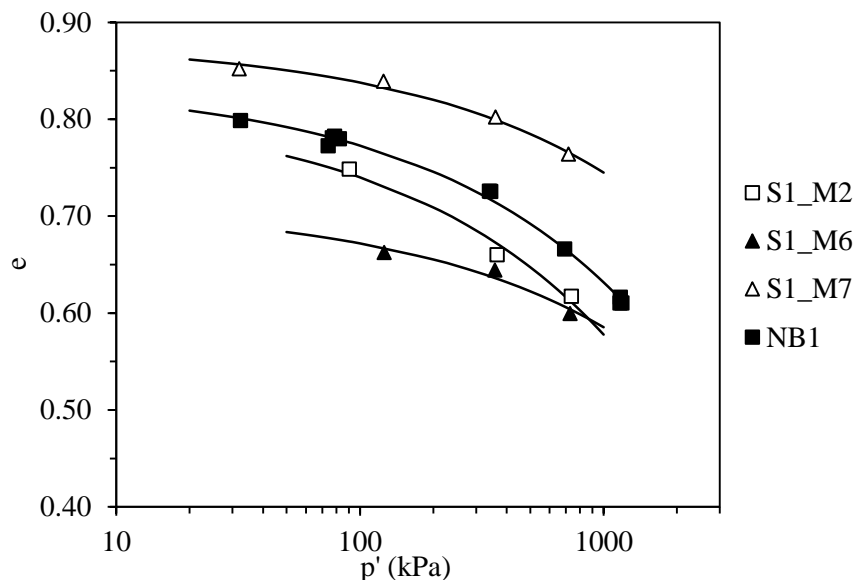
Figure 7.11 – CSL position for the soils studied

To complement this work, a selection of sands previously studied by FEUP geotechnical group CONSTRUCT-GEO (Pinto, 2014; Soares, 2014; Ramos et al., 2019) was included and used for comparison. Table 7.7 presents the material properties of those sands, that include three sands collected from experimental sites in Portugal, one sand from Algeria and the benchmark Osorio sand. All sands have a predominant quartz composition and are characterized as clean sands, with less than 8% fines content. According to the ASTM D-2487-17 classification, all are poorly graded sands (SP), with low values of C_U, which is indicative of uniform particle size. The critical state parameters were obtained from triaxial tests following the procedures described in Chapter 6.

Table 7.7 – Material properties of case study soils and soils studied in FEUP

Material	FC (%)	Gradation		Packing		CS parameters		
		D_{50} (mm)	C_U	e_{max}	e_{min}	Γ	λ_{10}	ϕ'_{cs} (^{o})
S1_M2	9.2	0.33	3.76	0.94	0.57	1.031	0.146	33.9
S1_M6	2.4	0.70	2.80	0.71	0.49	0.835	0.081	33.4
S1_M7	2.1	0.40	1.81	0.90	0.61	0.957	0.065	33.0
NB1	2.9	0.45	2.16	0.85	0.59	0.919	0.076	32.6
Terreiro do Paço (TP)	2.2	0.21	1.69	1.01	0.64	1.040	0.055	33.0
Coimbra Sand (Co)	1.8	0.36	2.13	0.81	0.48	0.850	0.062	31.4
Aveiro Sand (Av)	6.8	0.26	2.80	0.88	0.53	0.760	0.053	32.0
Algeria Sand (Al)	0.2	0.31	1.76	0.89	0.53	0.906	0.048	31.9
Osorio Sand (Oso)	4.0	0.19	1.90	0.85	0.57	0.875	0.062	32.1

The effect of a variety of parameters in the mechanical behaviour of soils have been studied over the years. Cho et al. (2006) compared the packing capacity of some benchmark sands with the critical state parameters and concluded that an increase in the range of e_{max} and e_{min} increases the slope of the CSL and the increase in e_{max} and e_{min} individually increases the intercept value. Figure 7.12 shows this study results (orange points) and the FEUP sands results (grey points) compared with the benchmark sands analysed by Cho et al. (2006). The results are consistent with the trends found for benchmark sands, which explains the variations in CS parameters displayed in Figure 7.11, especially in the CS intercept values. Furthermore, Cubrinovski and Ishihara (2000) reported the same trends, showing that an increase in the range of e_{max} and e_{min} increases the slope of the CSL.
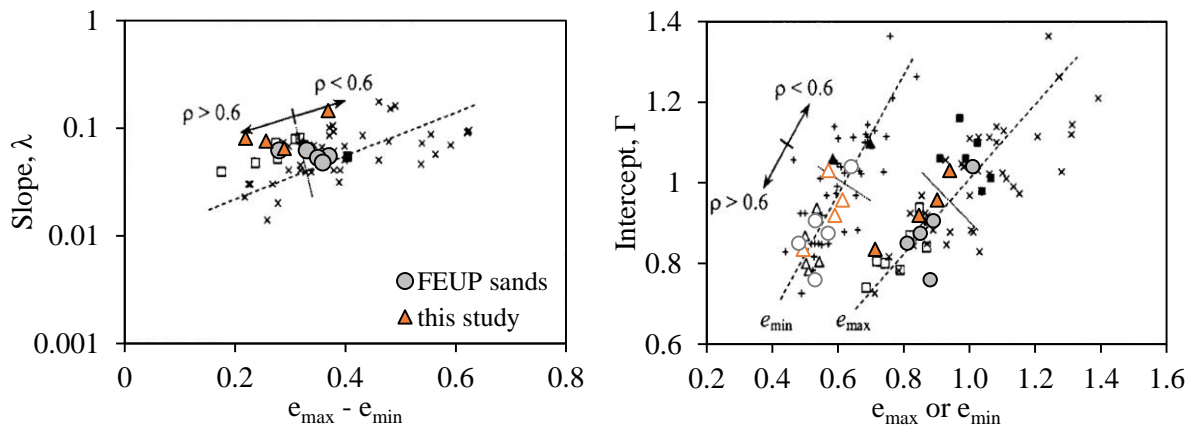
Figure 7.12 – Correlations between CS parameters and void ratio limits (data compiled by Cho et al. (2006) and completed with present data)

The CS parameters are often correlated to grain size characteristics. In this sense, the CS parameters were related to grain size parameters, namely the mean grain size (D_{50}), coefficient of uniformity (C_U), and fines content (FC), as illustrated in Figure 7.13. It is recognised that only nine sands were tested and compared, so no universal conclusions can be drawn. However, these correlations provide valuable

insight to possible trends. The D_{50} and FC results show some scatter, so no clear trends were defined. Nevertheless, it seems that the CS intercept has a tendency to decrease with increase of D_{50}, and the CS slope seems to increase with increase in FC. On the other hand, the correlations between CS parameters and C_U are clearer, showing the increase of λ and the decrease of Γ with increase in C_U.
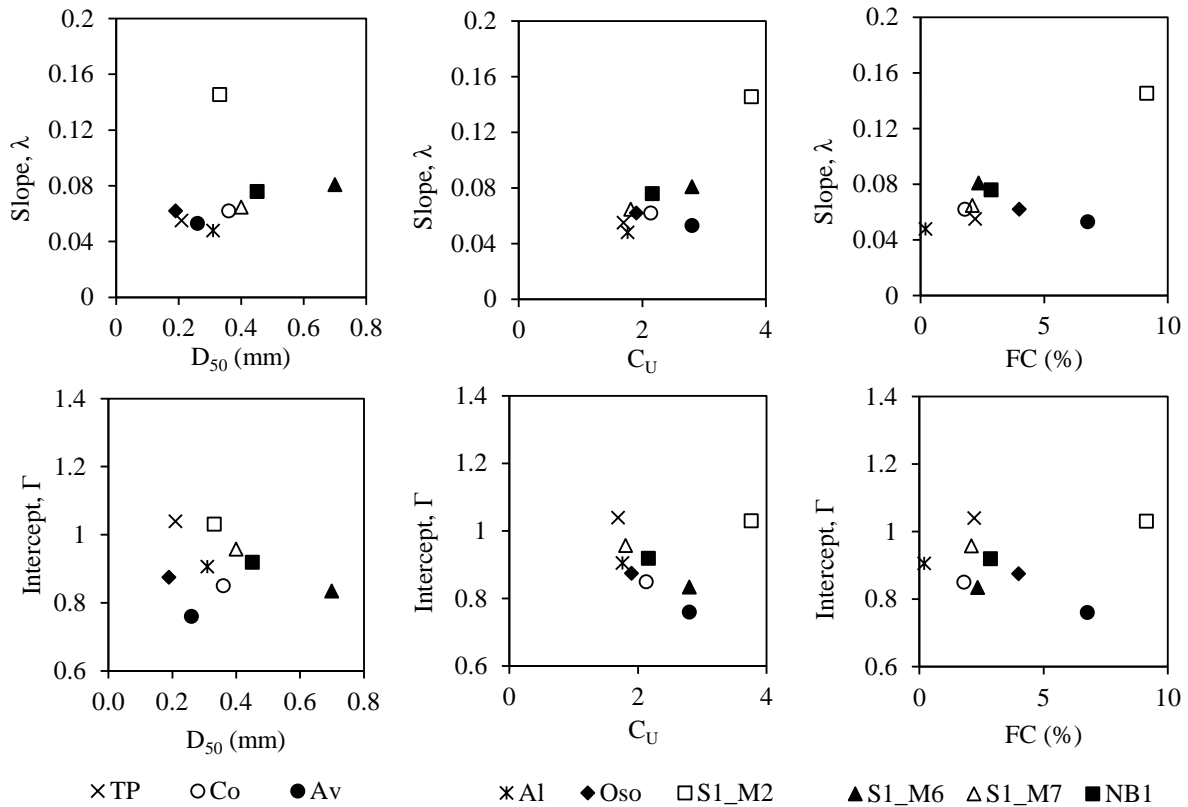
Figure 7.13 – Correlations between grain size and critical state parameters

The critical state parameters were also correlated to the shape parameters determined with the Morphologi G3 at University College London, framed within benchmark soils presented by Altuhafi et al. (2016), which values are tabulated in Table B.4 of Appendix B. Figure 7.14 presents correlations of the CSL slope with shape parameters and SAGI (shape-angularity group indicator). The scatter of the data is observed, indicating that this parameter must be influenced by other factors, such as the fines content. Nevertheless, the soils studied herein are well framed within the benchmark sands. On the other hand, the CS intercept (Figure 7.15) and critical friction angle (Figure 7.16) of the studied soils fit well with the correlations defined for the benchmark soils, especially in terms of aspect ratio and circularity. Both the CS intercept and critical friction angle decrease with increase in circularity. This two parameters are mostly affected by packing ability, as the void ratio limits decrease as the particles become more round (Youd, 1973; Cho et al., 2006; Altuhafi et al., 2016). Therefore, the effect of the

shape factors is clear on the CS intercept and critical friction angle, as rounder particles exhibit lower Γ and ϕ'_{cs}.
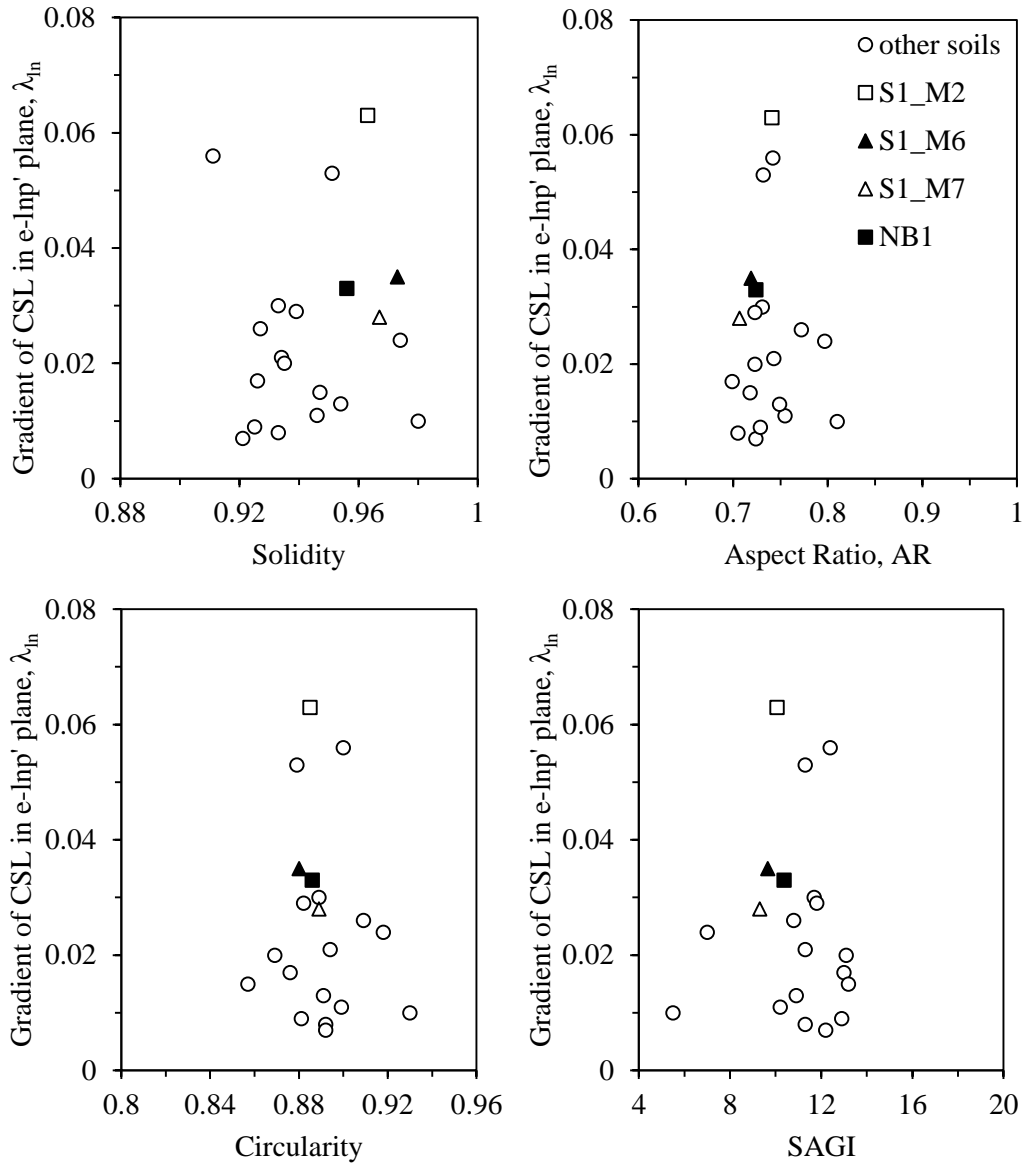
Figure 7.14 – Effect of shape parameters and SAGI on the CSL slope
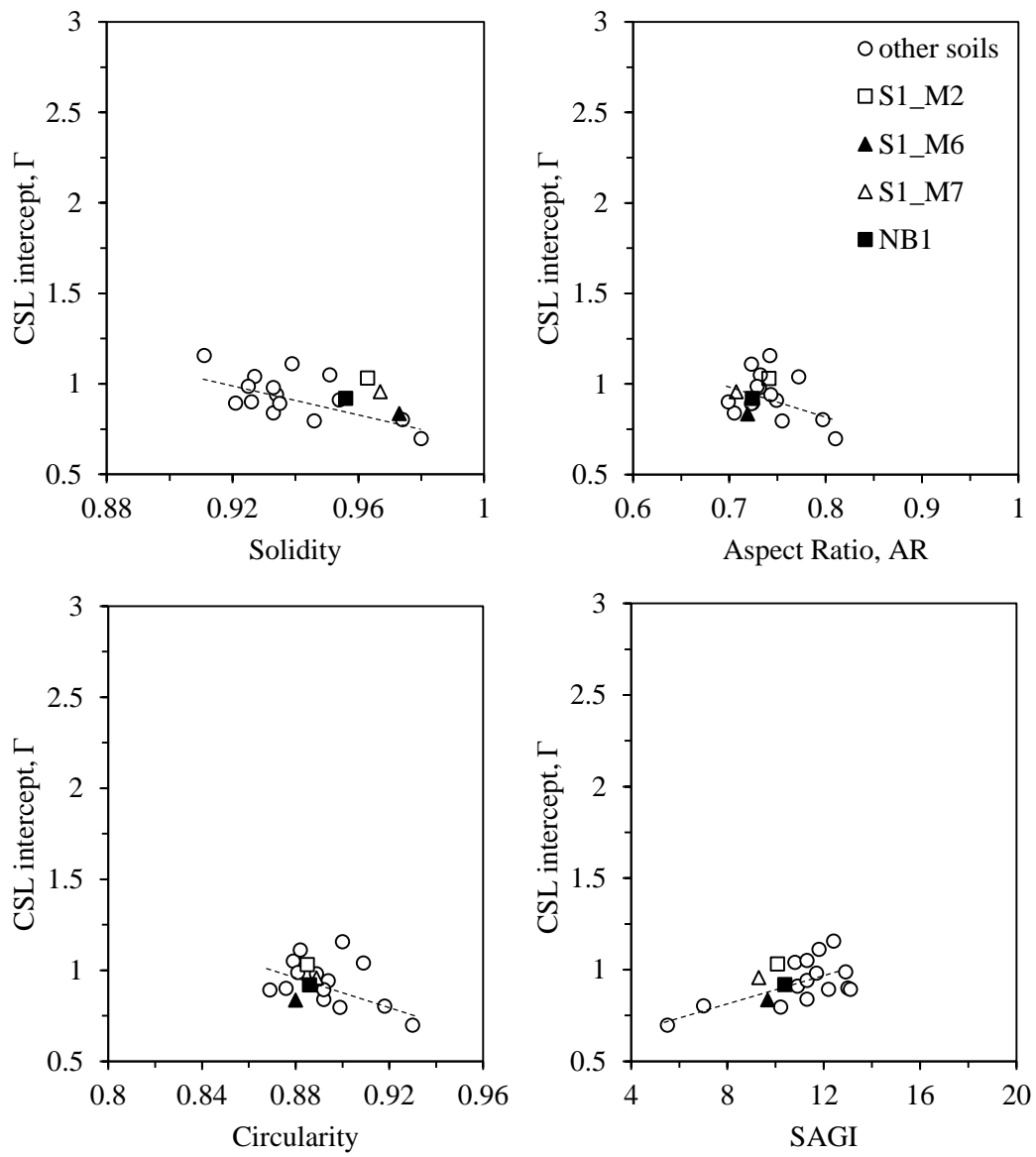
Figure 7.15 – Effect of shape parameters and SAGI on the CSL intercept
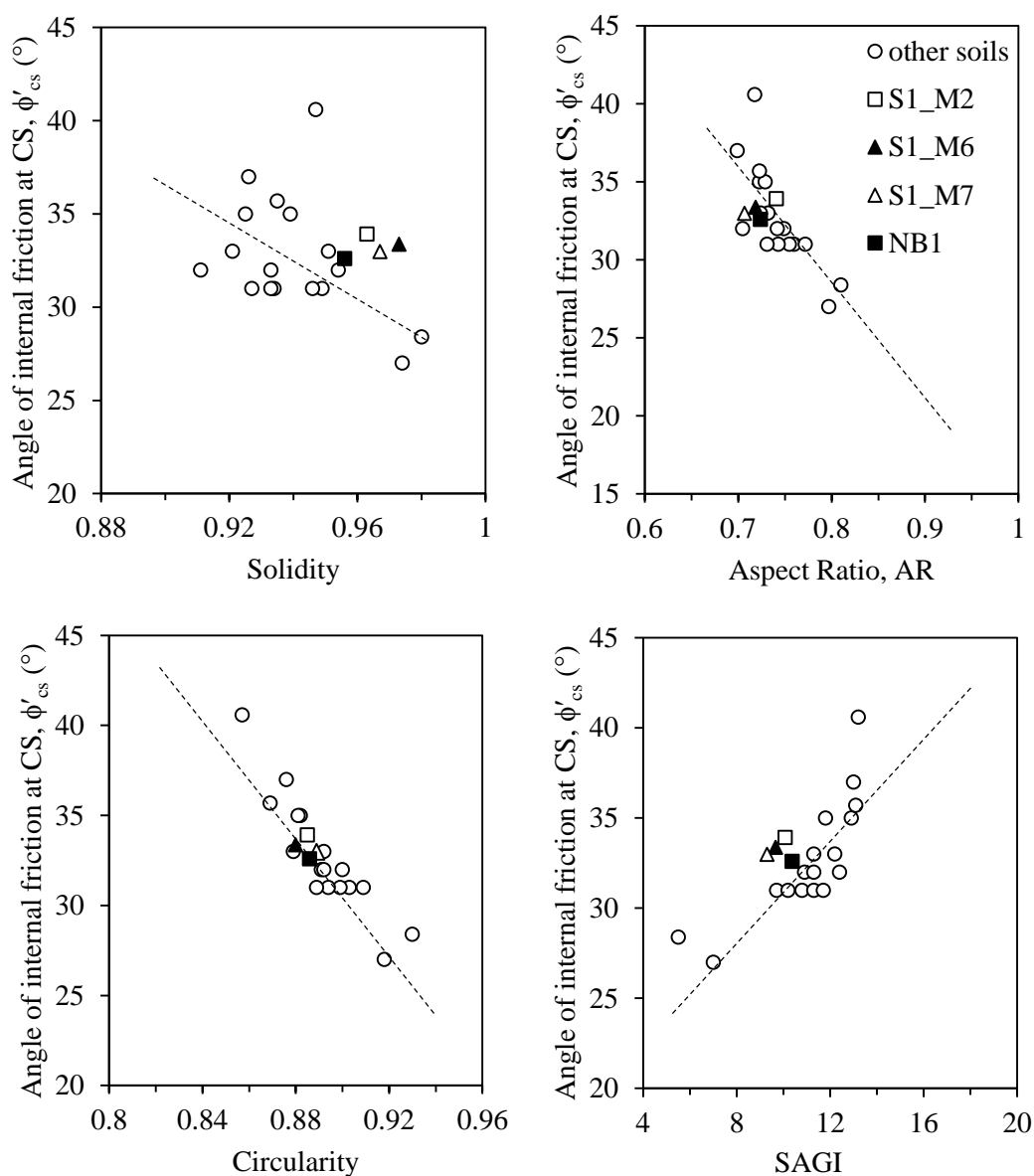
Figure 7.16 – Effect of shape parameters and SAGI on the critical friction angle

7.5. SMALL STRAIN BEHAVIOUR – STIFFNESS RESULTS AND ANALYSES

The small-strain shear modulus, G_{max}, of a soil represents the nature of interparticle contacts. It provides important soil information for a variety of purposes such as design of foundations subjected to dynamic loading, liquefaction assessment, and soil improvement control (Lee and Santamarina, 2005). Shear wave velocity measurements were obtained with bender elements implemented on the triaxial chambers. The small strain behaviour was studied based on the shear wave velocities measured at the end of the consolidation phase, for different confining stresses. Different trends were obtained for each soil, following equation (7.1), where α is the shear wave velocity when $p' = 1$ kPa and β is a parameter that accounts for the sensitivity of V_S with respect to p' (Cho et al., 2006). Figure 7.17 presents the shear

wave velocity evolution with confining stress, and includes the identification of the respective fitting equations. The curves of S1_M2 and S1_M7 soils are very close. On the other hand, NB1 curve is located slightly above the others and the S1_M6 curve is located the lowest.

$$V_S = \alpha(\sigma'_m)^\beta \tag{7.1}$$
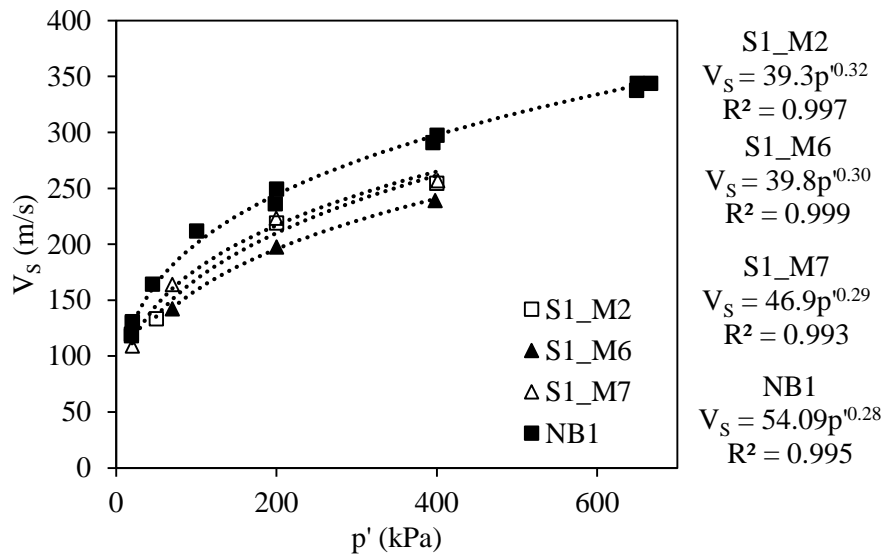
Figure 7.17 – Shear wave velocity evolution with confining stress for S1 and NB1 soils

Table 7.8 summarizes the computed α and β values for the soils studied in this work, together with the results of the FEUP sands introduced before. Based on tests performed in a wide range of soils, Santamarina et al. (2001) proposed a relationship between β and α, expressed as $\beta = 0.36-\alpha/700$, which is plotted in Figure 7.18 with the α and β values from Table 7.8. The parameters of the materials studied show good agreement with the proposed equation, emphasising that the shear wave velocities found are well framed with other benchmark soils. S1_M2 and Aveiro sand results are located slightly above the trend with a higher value of β, which was expected since these materials have higher fines content.

Table 7.8 – Shear wave velocity parameters

Material	α	β
S1_M2	39.264	0.317
S1_M6	39.831	0.300
S1_M7	46.893	0.289
NB1	54.089	0.285
Terreiro do Paço (TP)	50.869	0.290
Coimbra Sand (Co)	60.258	0.273
Aveiro Sand (Av)	45.993	0.326
Algeria Sand (Al)	54.69	0.278
Osorio Sand (Oso)	58.916	0.276
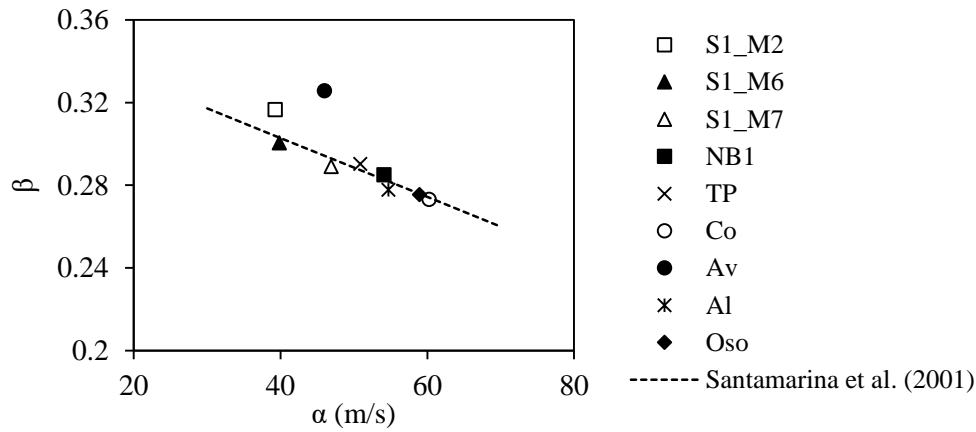
Figure 7.18 – Relationship between β and α for the different soils

Cho et al. (2006) reported that, with the increase in particle roundness and sphericity, the value of *β* decreases, while *α* increases. These trends are due to two effects. As discussed above, the void ratio limits increase with the decrease in particles circularity and solidity. Therefore, irregular particles are responsible for looser states. On the other hand, contacts between irregular particles are more deformable. For these reasons, a soil with more angular particles has lower stiffness and higher sensitivity of stiffness to the state of stress (i.e., lower *α* and higher *β*). Figure 7.19 shows the results and possible trends that relate circularity (a measure of the closeness to a perfect circle) with *α* and *β*. As predicted, as circularity increases (the particles become rounder), *α* increases and *β* decreases.
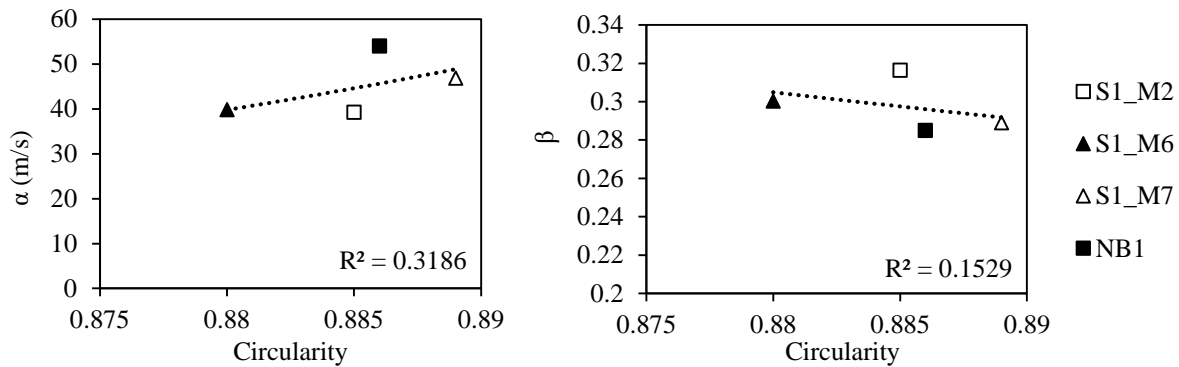
Figure 7.19 – Effect of circularity on α and β

Furthermore, the trends of V_S–p' seem to be related to the trends of the CSL determined for each material, as the materials with lower CSL showed lower shear wave velocities, hence lower stiffness. An exception was found for S1_M7, which despite presenting a CSL higher than the others, showed V_S–p' trend between NB1 and S1_M2. The relation between the CSL (large strain level) and V_S (small

247

strain level) is explained as the stiffness of sands is controlled by the confining stress, void ratio, and stress history, which also govern the soil behaviour when sheared.

In section 7.4.3, it was concluded that the shape factors (circularity, solidity, and aspect ratio) had poor correlations with the slope of the CSL, λ, but satisfactory correlations with the CS intercept, Γ, and critical friction angle, ϕ'_{cs}. Following the discussion above, as circularity increases, the value of α increases, while β decreases. Therefore, it should be expected that as CS intercept and critical friction angle increase, the values of α would decrease and β would increase. These trends are presented in Figure 7.20, confirming the predictions for the correlations with ϕ'_{cs}. However, the correlations between α and β and the CS intercept are poor, as the results are very scattered. Moreover, satisfactory correlations were found between the CS slope and α and β. As the slope of the CSL increases, β also increases, while α decreases.
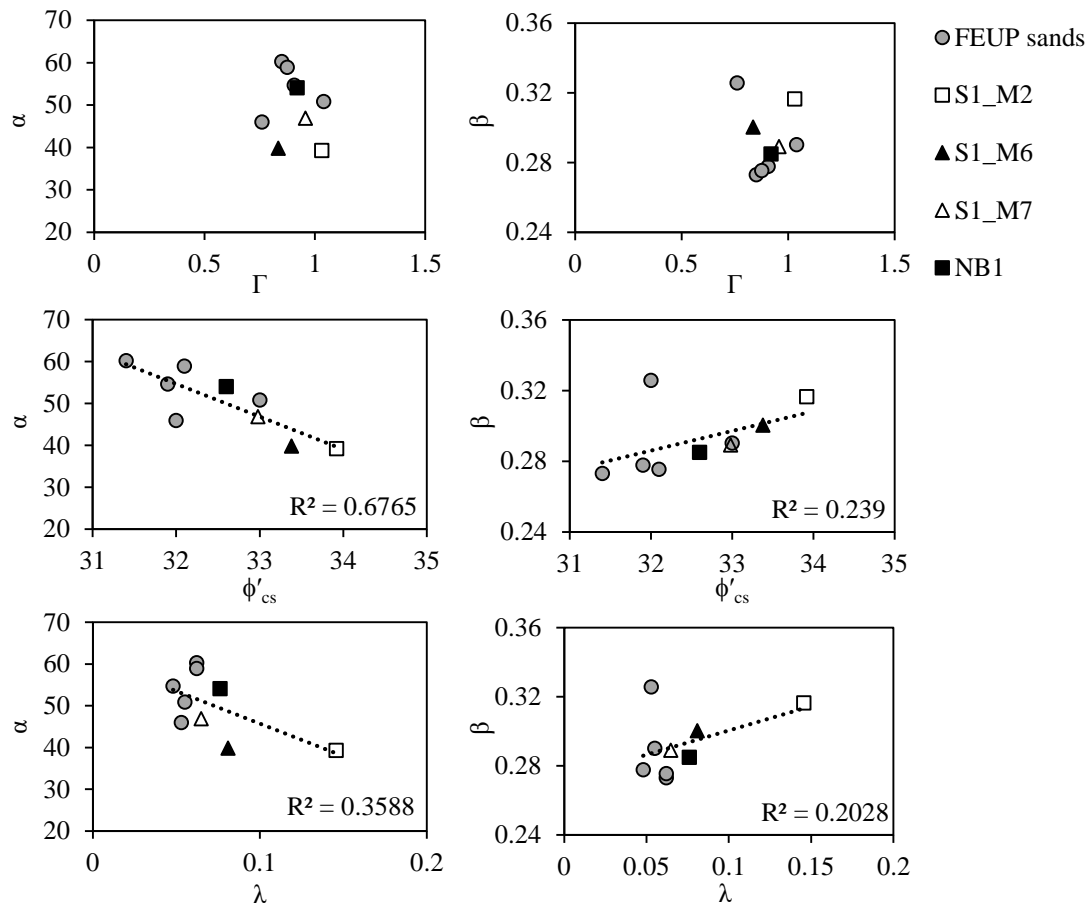
Figure 7.20 – Correlations between CS parameters and V_S-p' parameters

Following the trends found between CS parameters and V_S-p' parameters, the results of α and β were correlated with some grain size characteristics, namely the mean grain size (D_{50}), coefficient of uniformity (C_U), and fines content (FC), as illustrated in Figure 7.21. The correlations between α and β

with D_{50} are not clear, as the results show some scatter. However, it is observed that α decreases and β increases with the increase in both C_U and FC, which, as expected, is consistent with the results found previously.
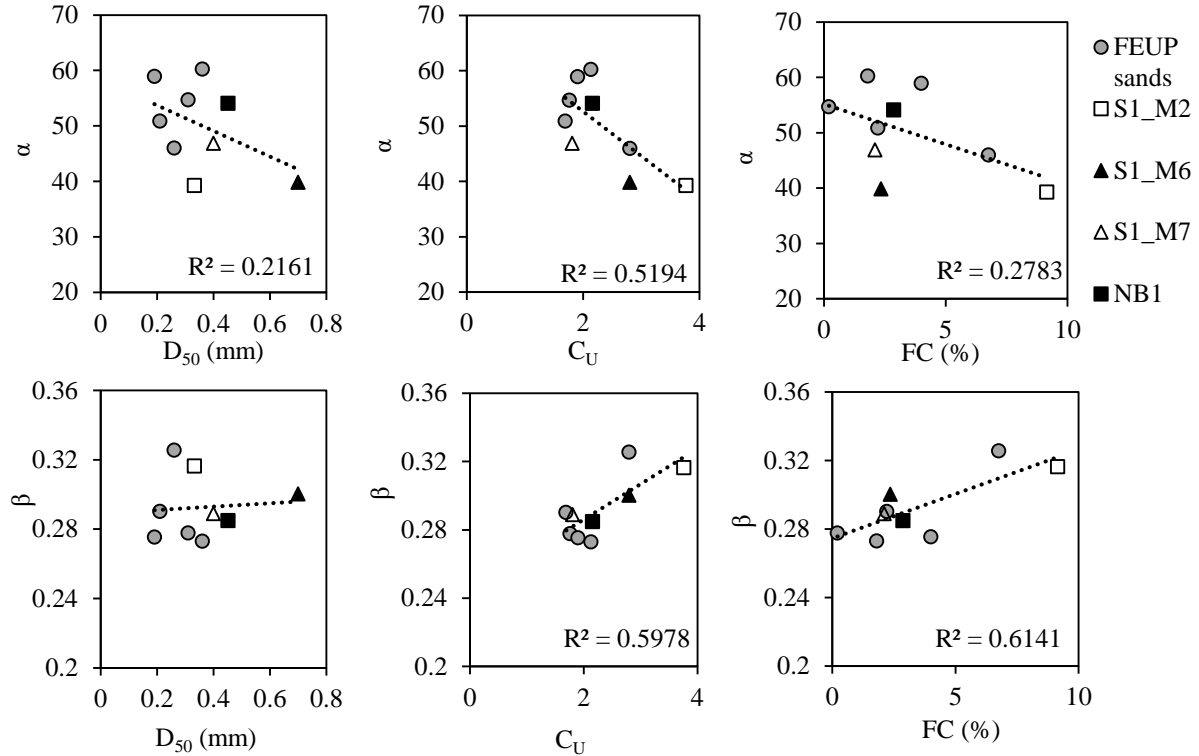
Figure 7.21 – Correlations between grain size and V_S-p′ parameters

Additionally, the values of the small-strain shear modulus, G_{max}, were computed using equation (7.2). Figure 7.22 presents the evolution of the shear moduli with the mean effective stress for the four soils studied. Following the trends defined by $V_S - p'$ results, the curves of S1_M2 and S1_M7 soils are very close, the NB1 curve is located above the others, and the S1_M6 curve is located the lowest.

$$G_{max} = \rho V_S^2 \tag{7.2}$$
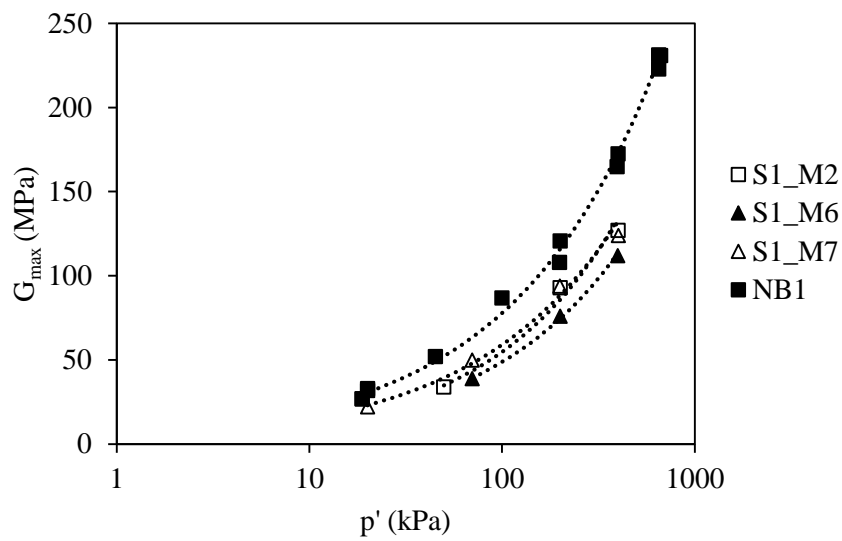
Figure 7.22 – Evolution of shear moduli with mean effective stress

To account for the influence of void ratio in the results, the shear moduli were normalised with a void ratio function. The void ratio function adopted was $F(e)=e^{-1.82}$, defined based on a specific study carried out in NB1 soil by Molina-Gómez et al. (2020a). As all the studied soils come from nearby sites, this void ratio function was adopted to normalise all the results. It is important to note that this might not be the best fit for the S1 soils, however, as no specific study was carried out to evaluate the characteristic void ratio function of these soils, the void function ratio selected is the best choice. On the other hand, the maximum correlation coefficient (R^2) values of the best fitting curves are high, around 0.99, so the choice of the void ratio function seems adequate.
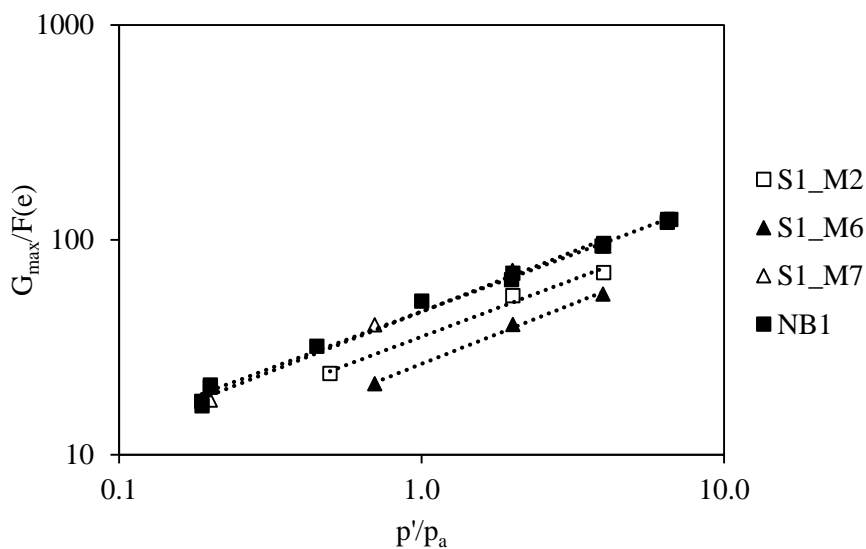
Figure 7.23 – Normalised maximum shear moduli to void ratio function for different mean effective stresses

The derived expressions of G_{max} are presented in Table 7.9 for each soil, following the formula discussed in section 2.2.4.

Table 7.9 – Derived expression of G_{max} for each soil

Material	Equation	R^2
S1_M2	$G_{max} = 35.412 \times e^{-1.82} \times \left(\dfrac{p'}{p_a}\right)^{0.53}$	0.9875
S1_M6	$G_{max} = 26.458 \times e^{-1.82} \times \left(\dfrac{p'}{p_a}\right)^{0.56}$	0.996
S1_M7	$G_{max} = 46.317 \times e^{-1.82} \times \left(\dfrac{p'}{p_a}\right)^{0.56}$	0.9913
NB1	$G_{max} = 46.426 \times e^{-1.82} \times \left(\dfrac{p'}{p_a}\right)^{0.53}$	0.9937

7.6. MONOTONIC DIRECT SIMPLE SHEAR TESTS

To evaluate the influence of confining pressure, sample preparation method, and shear rate in the behaviour of the NB1 sand, a set of monotonic direct simple shear tests was performed. The specimens were prepared following the procedures described in section 6.5, using both moist-tamping and air pluviation techniques. The specimens were confined by cooper rings and the consolidation consisted on the increase of the vertical stress until the desired confining stress. All specimens were sheared monotonically at constant rate until reaching the horizontal displacement limit of 8.0 mm imposed by the equipment, which corresponds to a shear strain of 30 to 40%. Figure 7.24 shows the shear stress-strain responses and Figure 7.25 illustrates the results the vertical displacements corresponding to volumetric strains. Tabulated test results for the monotonic simple shear tests are detailed in Table 7.10, presenting an index code of the test, the applied vertical stress (σ_v), the shear rate, the void ratio after consolidation (e_i), the void ratio at the end of the test (e_f), the specimen's water content (w) and the final shear stress (τ).

Table 7.10 – Monotonic direct simple shear test results for reconstituted specimens

Test ID	Method of sample preparation	σ_v (kPa)	shear rate (mm/min)	e_i	e_f	w (%)	τ (kPa)
NB1_Mon1	MT	50	0.02	0.70	0.73	3.27	30.42
NB1_Mon2	MT	100	0.02	0.69	0.70	3.59	54.71
NB1_Mon3	MT	20	0.07	0.74	0.75	3.28	11.25
NB1_Mon4	MT	200	0.01	0.65	0.64	3.32	105.35
NB1_Mon5	PL	50	0.07	0.68	0.68	0.3	27.88
NB1_Mon6	PL	100	0.02	0.68	0.65	0.17	54.01
NB1_Mon7	MT	20	0.02	0.74	0.75	3.57	8.92
NB1_Mon8	PL	50	0.02	0.71	0.70	0.40	24.82
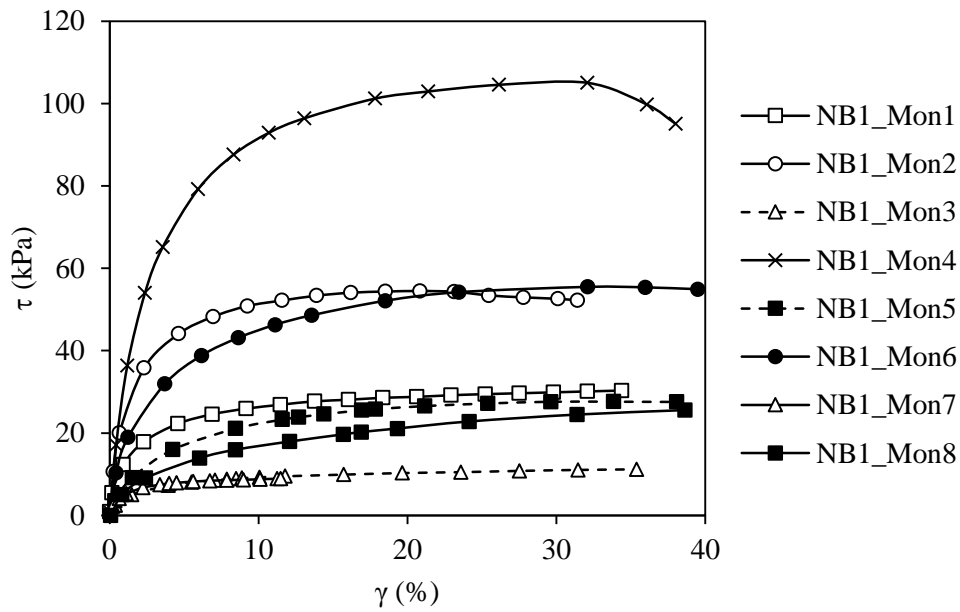
Figure 7.24 – Results of simple shear tests in the shear stress and shear strain plane
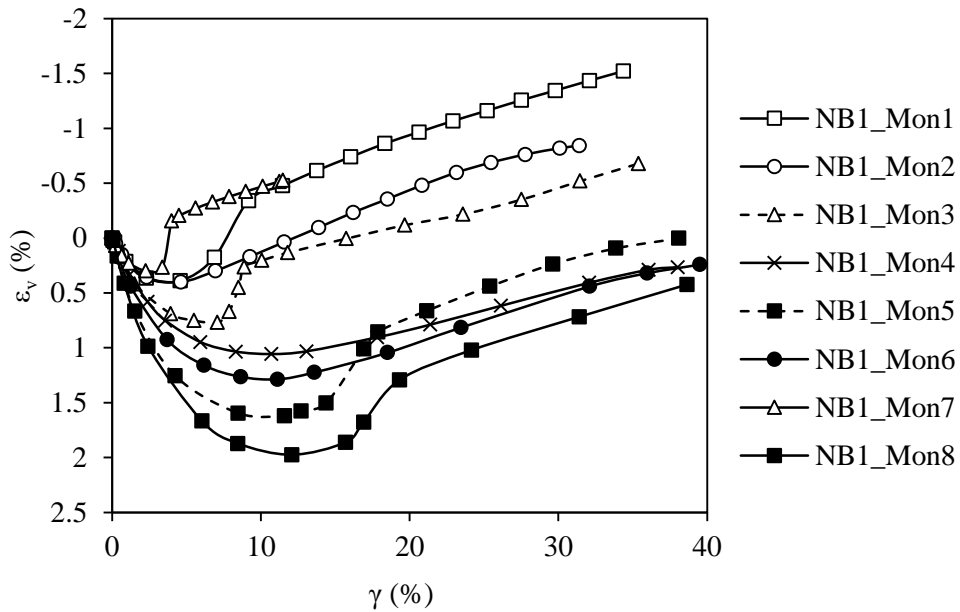
Figure 7.25 – Results of simple shear tests in the volumetric strain and shear strain plane

The results of tangential stress show typical curves, with no peak strength found as the specimens were prepared loose. On the other hand, the volumetric strain results show an initial compression, which was expected, followed by a dilation of the specimens. This dilation might be explained by the relationship between the principal stresses. At the beginning of the shear phase, the specimen is consolidated at K_0, and the major principal stress corresponds to the vertical stress. However, during the monotonic loading, the major principal stress rotates as shear strains increase. According to the results of DEM analyses

performed by Dabeet (2014), at 0% shear strain, the strong force chains, that represent the contact forces between the soil particles, are generally aligned in the vertical direction. However, at large shear strains, the strong force chains rotate and become inclined in a direction consistent with the direction of major principal stress. This rotation and inclination of the force chains might cause the dilatancy of the specimen, as observed in Figure 7.25.

The effect of sample preparation method and shear stress rate on the behaviour of NB1 specimens is assessed by comparing the behaviour of different pairs of tests. In terms of tangential shear stress, neither the preparation procedure nor the shear stress rate influenced the final strength result, which was expected as for a drained test the fabric does not affect the critical state. However, the PL specimens showed a slower rise of tangential stress for lower strains, when compared with the MT specimens.

On the other hand, the shearing rate was found to influence the soil response in both MT and PL specimens. This effect is verified when comparing two sets of tests: specimens NB1_Mon3 and NB1_Mon7 prepared with MT, consolidated for 20 kPa, and sheared at 0.07 and 0.02 mm/min, respectively, and specimens NB1_Mon5 and NB1_Mon8 prepared with PL, consolidated for 50 kPa, and sheared at 0.07 and 0.02 mm/min, respectively. In both cases the specimens sheared at a higher rate showed differences in behaviour. The initial deformation of the MT specimen confined for 20 kPa sheared at 0.07 mm/min was higher than that of the specimen sheared at 0.02 mm/min, showing that a higher rate produced a more compressive behaviour. However, the opposite was observed in the specimens prepared with PL and confined at 50 kPa, as the specimen sheared at a higher rate showed lower compressive behaviour. As there were several variants between the two sets of tests (sample preparation method, confining stress and initial void ratio), no definite conclusions could be drawn about the influence of shear rate.

To evaluate the influence of the specimen preparation technique on the monotonic simple shear behaviour of NB1 sand, two tests for two different confining stresses were performed. NB1_Mon2 and NB1_Mon6 were prepared by MT and PL, respectively, and consolidated for 100 kPa of vertical stress, while NB1_Mon1 and NB1_Mon8 were prepared by MT and PL, respectively, and consolidated for 50 kPa of vertical stress. As can be seen in Figure 7.25, the specimens prepared with air pluviation are much more compressible, showing higher values of volumetric strain for low shear strains.

The friction angle was determined in Figure 7.26, which relates the final values of tangential stress with the respective vertical stress. The friction angle, ϕ'_{ss}, was found to be 28.1°, lower than the critical friction angle found with the monotonic triaxial tests.
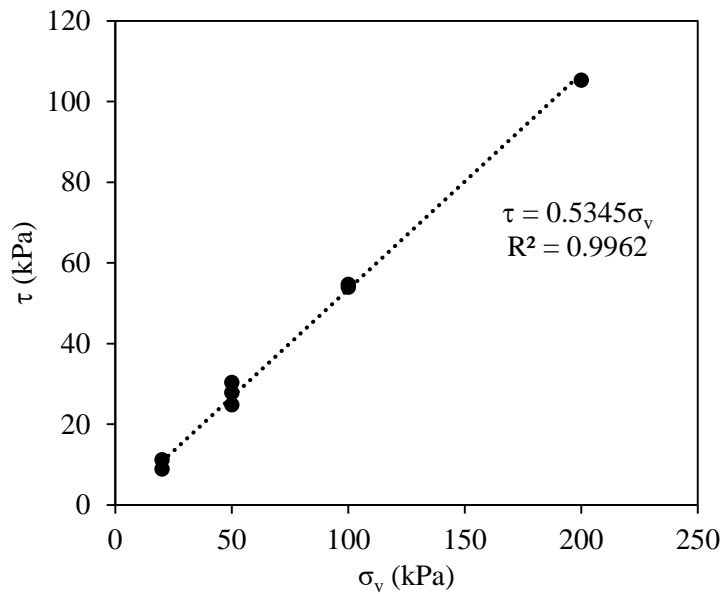
Figure 7.26 – Results of simple shear tests in the shear stress and vertical stress plane

7.7. CHAPTER SUMMARY

This Chapter presented the physical characteristics of four case study soils, S1_M2, S1_M6, S1_M7, and NB1, in terms of grain size distribution analysis, with indices such as fines content (FC), mean grain size (D_{50}), coefficient of shape (C_C), and coefficient of uniformity (C_U); specific gravity (G_s); mineralogy; void ratio limits; and particle shape.

The critical state soil properties of the four soils were established, including the slope (λ) and intercept (Γ) of the CSL in e-log(p') plane, and the critical friction angle (ϕ'_{cs}). Besides, five other sands studied at FEUP were also included in the analyses. The CS parameters were correlated with other material properties, and the observations followed the trends defined for other benchmark sands in the literature. Both the CS slope and intercept increase with increase in e_{max} and e_{min} and e_{max}-e_{min}, respectively. Moreover, the CS parameters were correlated to grain characteristics, and it was found that Γ decreased with increase of D_{50} and C_U, and λ increased with increase of C_U and FC. As for correlations with shape parameters, it was observed that Γ and ϕ'_{cs} decrease with increasing circularity, solidity, and aspect ratio. On the other hand, no correlations were found between λ and the shape parameters due to the scatter of the data, which follows the findings for other benchmark soils.

The small strain behaviour was studied based on shear wave velocity measurements obtained with bender elements implemented on the triaxial chambers. The V_S-p' trends obtained for each soil were different, and defined by the shear wave velocity when p' = 1 kPa (α) and a parameter that accounts for the sensitivity of V_S with respect to p' (β). The impact of FC was revealed by a higher value of β in S1_M2 and Aveiro sand, the soil with higher FC. Moreover, with increasing particle circularity (the

254

particles become rounder), α increases while β decreases, following the results reported by Cho et al. (2006). The V_S-p' parameters were compared with CS parameters, showing that α decreased and β increased with increasing CS intercept, critical friction angle, and CS slope. The V_S-p' parameters were also compared with grain size characteristics, showing that α decreased with increasing D_{50}, C_U and FC, while β increased with increasing C_U and FC.

Additionally, a set of direct simple shear tests was performed under monotonic conditions. These results showed that the final tangential shear stress value is not affected by preparation technique or shear stress sate, and it increases with increase of confining pressure, as expected. Besides, the preparation technique seems to affect the initial increase of tangential stress, as the PL specimens showed a slower rise of tangential stress for lower strains than MT specimens. On the other hand, the specimens prepared with air pluviation were found to be much more compressible, showing higher values of axial strain for low shear strains than MT specimens.

8. FACTORS AFFECTING CYCLIC LIQUEFACTION RESISTANCE OF CASE STUDY SOILS

8.1. INTRODUCTION

As discussed in Chapter 2, the behaviour of soils under cyclic loading is affected by several factors that depend on the material characteristics and the testing procedures. This Chapter outlines the cyclic triaxial and cyclic direct simple shear tests performed in reconstituted specimens of S1_M2, S1_M7, and NB1 soils, analysing the effect of a variety of factors on the cyclic behaviour of these materials. To allow the analysis of the influence of each factor separately, the tests were grouped according to their initial conditions (relative density, confining pressure, sample preparation technique, boundary conditions, and water content) and loading conditions.

8.2. CYCLIC TRIAXIAL TESTS (CTX)

A total of 45 cyclic triaxial tests were performed in reconstituted specimens of S1_M2, S1_M7, and NB1 soils, which results are presented in this section. The list of tests performed is presented in Table 8.1. The main objectives were to study the cyclic response of the three soils and to assess the effect of changes in state, loading, and preparation procedures in their cyclic behaviour. Therefore, the following sections are divided according to the effects of different factors on liquefaction resistance and the results are analysed in detail.

All cyclic triaxial tests were isotropically consolidated and the cyclic loading was performed with shear stress reversal, as the load altered between compression and extension. The S1_M2 and S1_M7 soils were consolidated to 70 kPa, as this was the consolidation used in the cyclic simple shear tests and the final goal was to compare the behaviour of both types of tests. The NB1 specimens were consolidated to 100 kPa, except for a set of three tests in which the confining stress was 40 kPa, to assess the effect of initial confining stress. The shear wave velocities at the end of consolidation were measured with bender elements, when they were applied to the triaxial chamber. As for the loading stage, at first, the frequency of cycles was defined to 1 Hz (1 cycle/s). However, it was found that with this frequency, when the specimen liquefied, the cell and back pressure would oscillate very quickly. For this reason, in order to more accurately record the data, a lower frequency of 0.1 Hz (i.e., 1 cycle per 10 seconds)

was selected. These changes in frequency did not affect the cyclic resistance curve position, hence this factor was considered negligible, as will be shown below.

Two different types of liquefaction failure were observed, flow liquefaction and cyclic mobility. Flow liquefaction corresponds to a complete loss of strength, as the deviatoric and mean effective stresses drop abruptly to zero and large deformations are produced, as observed in Figure 8.1. On the other hand, cyclic mobility (also referred to as cyclic liquefaction) is also characterised by a state of softening produced by a pore pressure build-up of 100% (corresponding to r_u of 1) and the consequent development of 5% double amplitude axial strain. However, the deformation is more contained and the specimen does not lose its strength entirely after the initial liquefaction. The specimen preserves some strength and the stress-path continues with increases and decreases of stresses, going up and down the failure envelope (Figure 8.2).
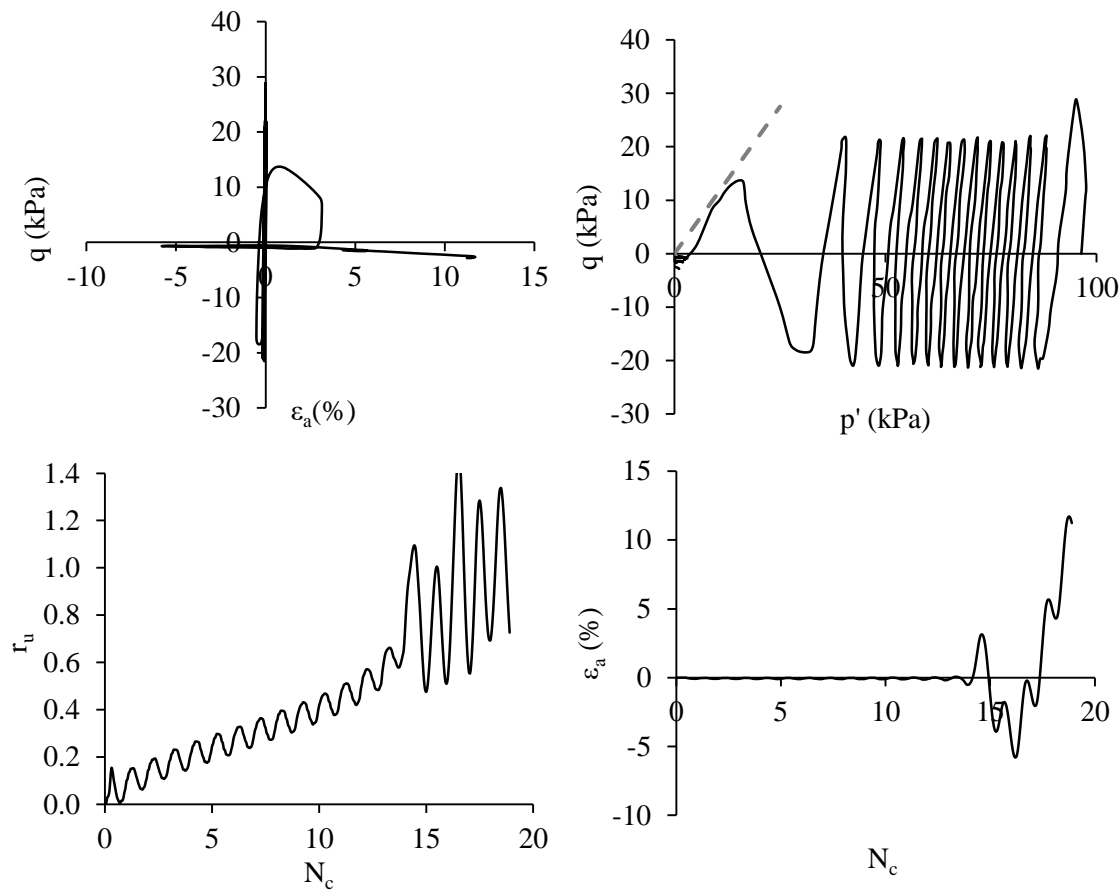
Figure 8.1 – Plot of typical cyclic triaxial test with flow liquefaction (Test ID: NB1_MT_CTx6, D_R=24%, FC=2.86%, p'_i=96 kPa, CSR=0.113)
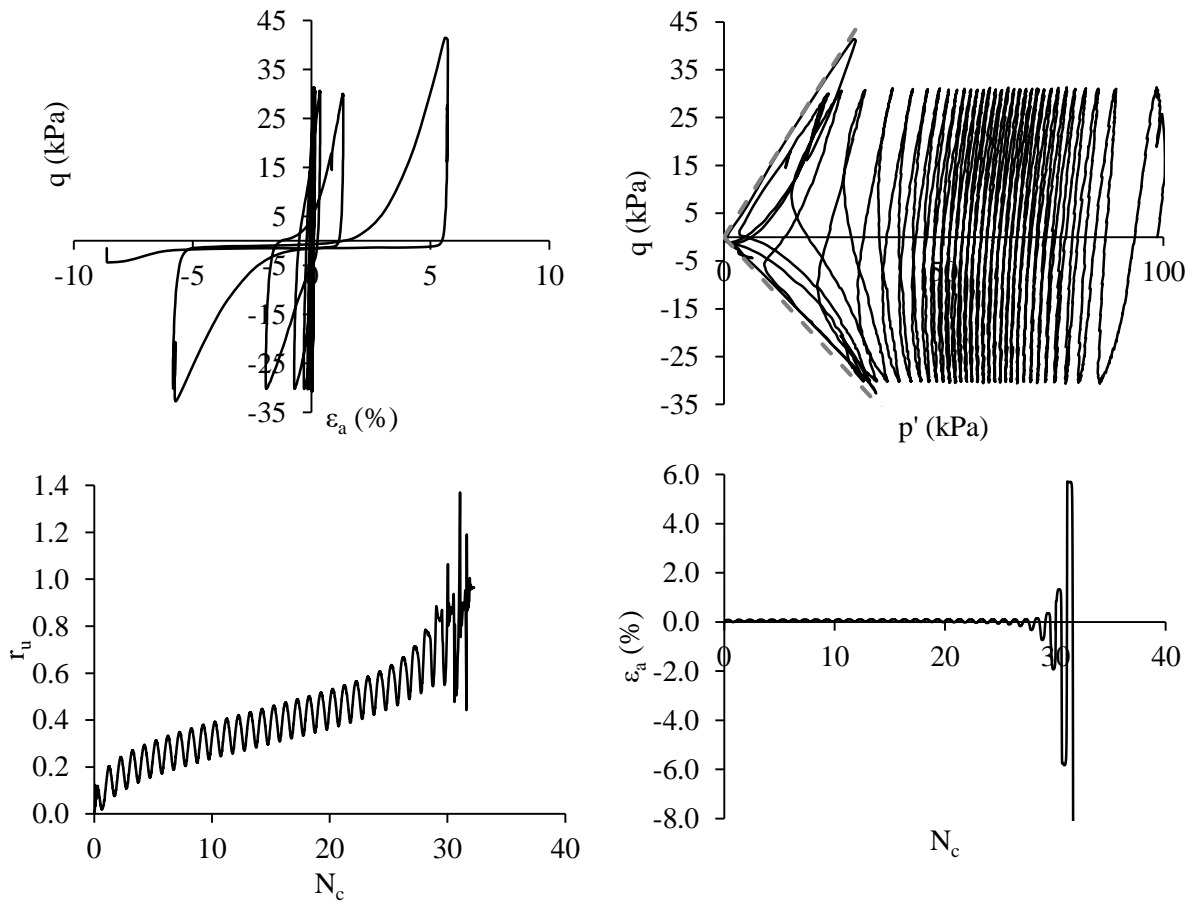
Figure 8.2 – Plot of typical cyclic triaxial test with cyclic liquefaction (Test ID: NB1_E2_3, D_R=56 %, FC=2.86%, p'_i=100 kPa, CSR=0.158)

The tabulated results for all tests can be found in Table C.2 in Appendix C, that includes the test identification (Test ID), the void ratio after specimen preparation (e_0), at the beginning of consolidation (e_{i-1}) and after consolidation (e_i), the volumetric change during consolidation (ε_v), the relative density (D_R), the confining pressure (p'_i), the shear wave velocity after consolidation (V_S), the state parameter (ψ), the frequency of cycles (Freq), the cyclic stress ratio (CSR), the number of cycles (N_{liq}) required to develop 5% axial strain in double amplitude ($\varepsilon_{a,DA}$) and required to develop 100% excess pore pressure ratio (r_u), the cumulative dissipated energy until liquefaction (ΔW_{liq}), and the type of liquefaction failure.

Table 8.1 – List of cyclic triaxial tests performed with reconstituted specimens

Test ID	Preparation Method	e_i	p'_i (kPa)	D_R (%)	Freq (Hz)	CSR ($\tau/2\sigma'_{h0}$)	N_{liq} (r_u=100%)	N_{liq} ($\varepsilon_{a,DA}$=5%)
NB1_MT_CTx1	MT	0.776	100	27	0.1	0.131	7	7
NB1_MT_CTx2	MT	0.780	100	25	1.0	0.115	32	32
NB1_MT_CTx3	MT	0.760	100	34	1.0	0.041	-	-
NB1_MT_CTx4	MT	0.767	100	31	1.0	0.127	4	4
NB1_MT_CTx5	MT	0.788	100	23	1.0	0.050	1072	1073
NB1_MT_CTx6	MT	0.784	100	24	1.0	0.113	14	14
NB1_MT_CTx7	MT	0.759	100	34	1.0	0.081	132	132
NB1_MT_CTx8	MT	0.780	100	26	0.1	0.173	1	1.2
NB1_PL_CTx1	PL	0.758	100	34	0.1	0.131	4	4
NB1_PL_CTx2	PL	0.763	100	32	0.1	0.106	18	18
NB1_PL_CTx3	PL	0.762	100	33	0.1	0.096	26	26
NB1_E2_1	MT	0.718	100	50	1.0	0.107	172	173
NB1_E2_2	MT	0.687	100	62	1.0	0.132	281	282
NB1_E2_3	MT	0.703	100	56	0.1	0.158	30	31
NB1_E2_4	MT	0.706	100	55	0.1	0.181	9	10
NB1_E2_5	MT	0.703	100	56	0.1	0.137	71	71
NB1_E2_5_REP	MT	0.694	100	59	0.1	0.139	128	130
NB1_E2_6	MT	0.693	100	60	0.1	0.208	8	9
NB1_C40_1	MT	0.702	40	56	0.1	0.161	65	66
NB1_C40_2	MT	0.702	40	56	0.1	0.209	16	17
NB1_C40_3	MT	0.691	40	60	0.1	0.144	296	298
S1_M2_CTxR1	MT	0.720	70	60	1	0.09	43	43
S1_M2_CTxR2	MT	0.720	70	60	1	0.09	107	107
S1_M2_CTxR3	MT	0.690	70	68	1	0.04	-	-
S1_M2_CTxR4	MT	0.720	70	60	1	0.09	18	17
S1_M2_CTxR5	MT	0.715	70	61	0.1	0.09	35	35
S1_M2_CTxR6	MT	0.735	70	56	1	0.08	67	67
S1_M2_CTxR7	MT	0.708	70	63	1	0.10	34	34
S1_M2_CTxR8	MT	0.712	70	62	1	0.12	10	10
S1_M2_CTxR9	MT	0.705	70	64	0.1	0.16	2.8	3
S1_M7_CTxR1	MT	0.81	70	32	1	0.09	336	337
S1_M7_CTxR2	MT	0.80	70	35	1	0.11	17	17
S1_M7_CTxR3	MT	0.78	70	42	1	0.04	-	-
S1_M7_CTxR4	MT	0.81	70	32	1	0.07	342	343
S1_M7_CTxR5	MT	0.82	70	27	0.1	0.07	286	284
S1_M7_CTxR6	MT	0.86	70	13	1	0.08	70	69
S1_M7_CTxR7	MT	0.83	70	26	1	0.10	47	47
S1_M7_CTxR8	MT	0.81	100	31	1	0.06	945	946
S1_M7_CTxR9	MT	0.80	70	37	1	0.13	44	45
S1_M7_CTxR10	MT	0.80	70	35	1	0.08	607	609
S1_M7_CTxR11	MT	0.81	70	32	1	0.11	40	40
S1_M7_CTxR12	MT	0.82	70	29	1	0.09	119	119
S1_M7_CTxR13	MT	0.81	70	30	0.1	0.13	38	39
S1_M7_CTxR14	MT	0.81	70	32	0.1	0.18	5	5
S1_M7_CTxR15	MT	0.82	70	28	0.1	0.16	6	6

8.2.1. EFFECT OF STATE PARAMETERS AND FREQUENCY OF LOADING ON LIQUEFACTION RESISTANCE

From the results of the cyclic triaxial tests performed with reconstituted specimens of S1_M2, S1_M7, and NB1, cyclic resistance curves were obtained. These curves are defined by the number of cycles required for liquefaction and the respective cyclic stress ratio. As already mentioned, liquefaction is triggered when the excess pore water pressure ratio (r_u) reaches 1, that usually corresponds to 5% of double amplitude axial strain, following the strain-based criterion. As all specimens were prepared loose or medium dense, the number of cycles obtained with the two criteria was similar, with a maximum difference of 2 cycles (see Table C.2). To assess the influence of density and stress state on cyclic resistance, the void ratio and confining stresses were considered. Moreover, the effect of state parameter was also considered, as it defines the position of a soil specimen in relation to the CSL and it encompasses the influence of both density and stress states on the soil behaviour.

The results for S1_M2 soil are illustrated in Figure 8.3, where the studied factor was the frequency of cycles, as some tests were performed with 0.1 Hz while others were sheared with 1 Hz. Moreover, since the initial target void ratio was not always reached, there is a slight variance in the void ratios, ranging from 0.69 and 0.74, which correspond to state parameters of -0.07 to -0.03. The results show that the slight differences in state parameter did not affect the cyclic strength curve. Additionally, the frequency of loading seems to not influence the position of the cyclic resistance curve, which is accordance with other works (e.g., Tatsuoka et al., 1986).
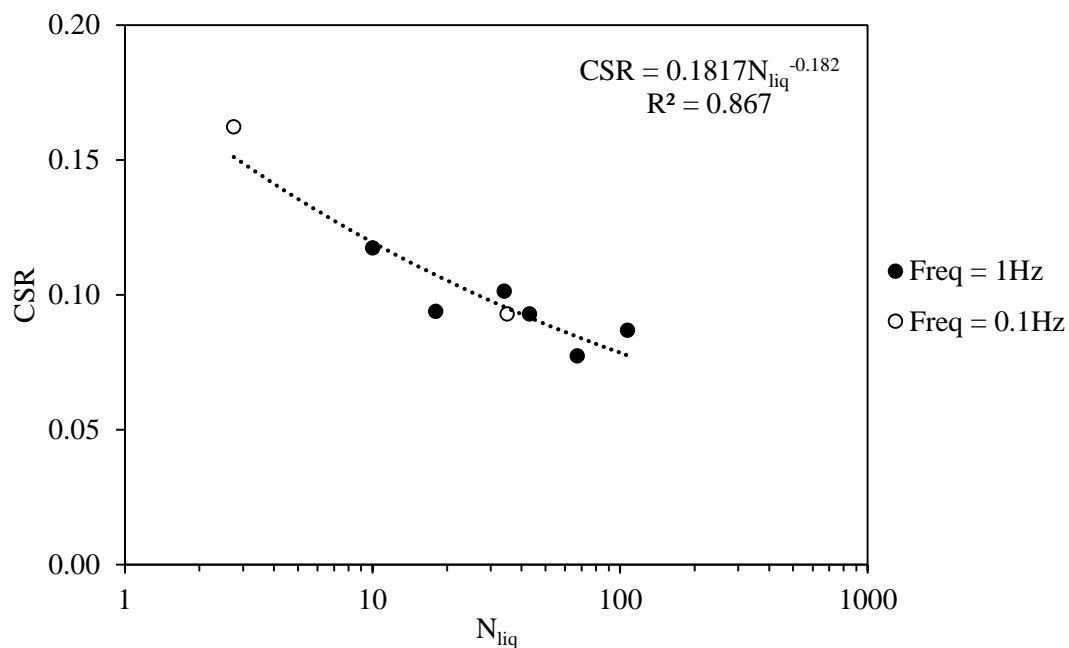
Figure 8.3 – Cyclic resistance curve for S1_M2

Figure 8.4 presents the cyclic resistance curve obtained with the tests performed with S1_M7 soil. Once again, the differences in void ratio, ranging between 0.80 and 0.86 (corresponding to state parameters of -0.04 to 0.03) seem to not influence the position of the cyclic strength curve. Moreover, the cyclic loading frequency appears to not influence the liquefaction response of the specimens as the results of tests with different frequencies fit the same liquefaction resistance curves. It is important to note that the variation of frequency was between 1 Hz and 0.1 Hz, so these conclusions are valid for these two frequencies in this soil. If the changes in frequency were higher, the curves might vary, as reported by Rascol (2009). In this case, the change of confining pressure between 70 and 100 kPa does not influence the position of the cyclic curve. However, only one test with 100 kPa of confining pressure was performed, so further investigation is needed to confirm the trend.

$$CSR = 0.2183N_{liq}^{-0.178}$$
$$R^2 = 0.8536$$

• Freq = 1Hz
○ Freq = 0.1Hz
△ p' = 100kPa
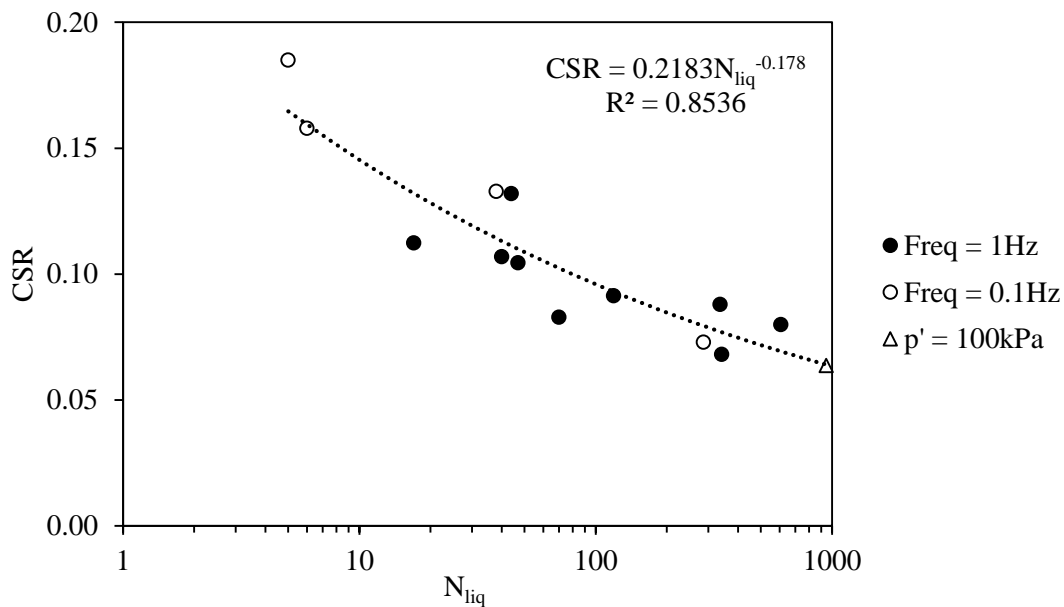
Figure 8.4 – Cyclic resistance curve for S1_M7

As for NB1 sand, tests were performed with varying sample preparation techniques, confining stresses, initial void ratio, and frequency of cyclic loading. Figure 8.5 presents the different cyclic strength curves obtained according to the test and specimen conditions. The open symbols correspond to specimens sheared with a loading frequency of 0.1 Hz, while black symbols correspond to 1 Hz of frequency of loading. On the other hand, different symbols represent different sample preparation techniques, initial void ratios and initial confining pressures.

It seems that small differences in void ratio have low impact on the resulting cyclic strength curve, so the specimens were grouped in ranges of void ratio, as it is observed by the three cyclic resistance curves obtained. However, as expected, higher changes in void ratio alter the cyclic strength curve. As expected, specimen with higher void ratios (that correspond to lower relative densities) have lower

liquefaction resistance than specimens with lower void ratios, as for the same CSR a lower number of cycles is required to trigger liquefaction in looser specimens.
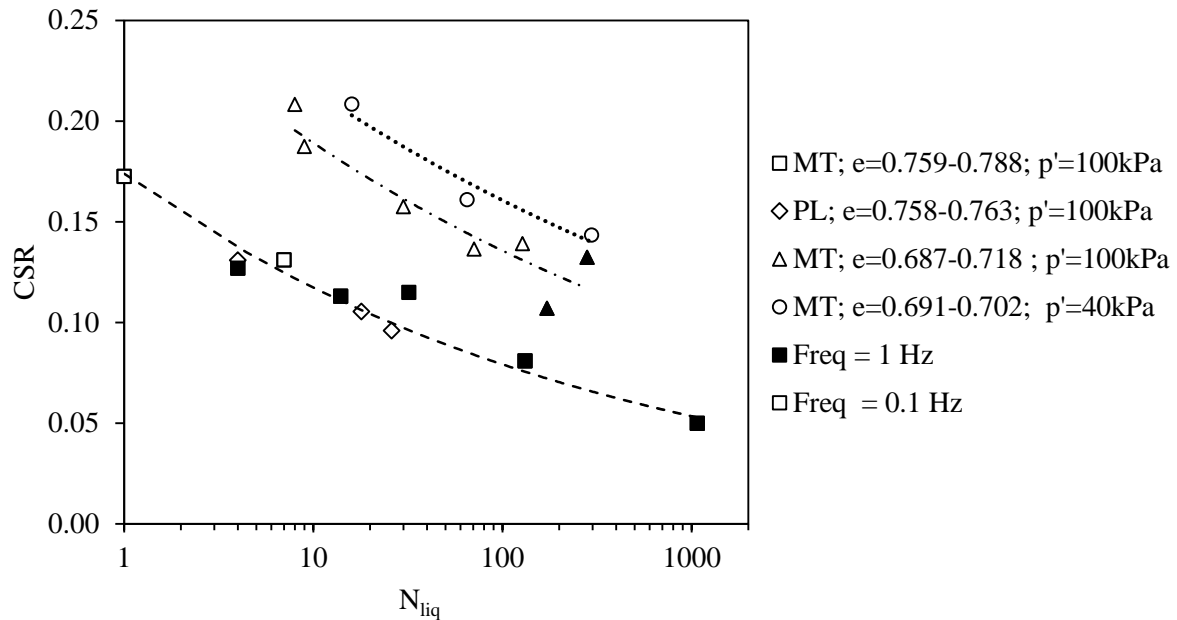
Figure 8.5 – Cyclic resistance curves for NB1 soil

To isolate the influence of the initial confining pressure, two sets of tests with specimens prepared with moist tamping with similar ranges of void ratio were compared (represented by the circles and triangles in Figure 8.6). It was found that the cyclic resistance curve for lower confining pressure was higher than the one for 100 kPa, considering approximately the same void ratio. The tests performed with 40 kPa show higher resistance, as a higher number of cycles is required to trigger liquefaction for the same CSR. This is in good agreement with results reported by other authors (Vaid and Sivathayalan, 1996).

As referred above, the state parameter takes into consideration the effect of density and stress states on the soil behaviour. Therefore, Figure 8.7 presents the cyclic resistance curves for NB1 soil, identified by the ranges of state parameters. The two lower curves were obtained from specimens tested at the same confining pressure, hence the void ratio was the changing parameter. On the other hand, the two higher curves had the same void ratio but were tested at different confining pressures. It is observed that lower state parameters, which correspond to specimens located below the CSL, exhibited higher cyclic resistance.
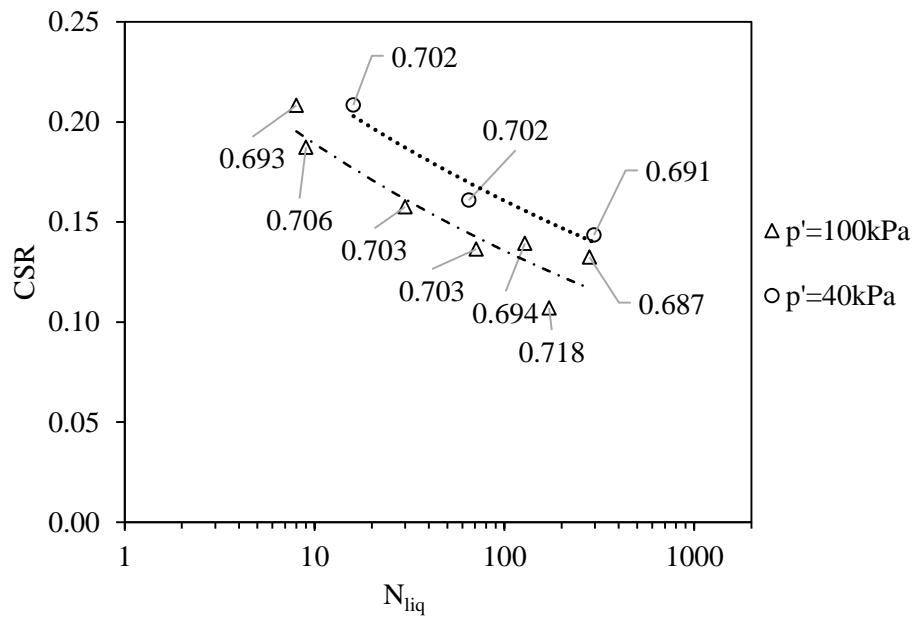
Figure 8.6 – Comparison of cyclic resistance curves for NB1 with initial confining pressures of 40 kPa and 100 kPa (the number beside the symbols are the respective void ratio)
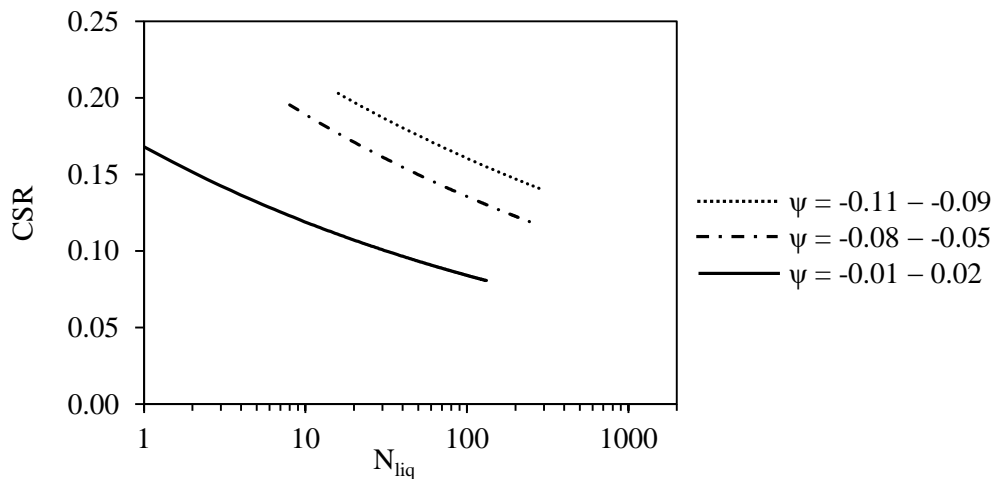
Figure 8.7 – Comparison of cyclic resistance curves for NB1 with different state parameters

8.2.2. EFFECT OF SAMPLE PREPARATION METHOD ON LIQUEFACTION RESISTANCE

The influence of two sample preparation methods (moist-tamping and air pluviation) was discussed previously in the construction of the critical state line of NB1, where it was concluded that the preparation method did not influence the position of the CSL, as it is unique for each soil. However, it might influence the volumetric changes that occur during compression. In this section, moist tamping (MT) and air pluviation (PL) were compared in terms of cyclic behaviour, to assess the influence of sample preparation method on the behaviour of NB1 sand. The specimens were prepared using the moist tamping and air pluviation techniques, following the procedures described in Chapter 6. As

discussed above, samples were prepared to high initial void ratios and were confined to 100 kPa. Analysing the tests results in Figure 8.8, it seems that the preparation method does not affect the cyclic resistance curve of NB1 specimens prepared for high void ratios. This behaviour contradicts some trends found by other authors that stated that MT specimens were more resistant than PL specimens (Mulilis et al., 1977; Tatsuoka et al., 1986). On the other hand, the moist tamping procedure at low compaction levels might result in the presence of macropores within the sand structure (Benahmed et al., 2015), which lowers liquefaction resistance. This effect might be responsible for a lower cyclic resistance curve obtained for MT specimens and the similarities between the two sample preparation technique results. It would be interesting to perform some triaxial tests with specimens prepared with air pluviation for higher densities, and compare the results with denser MT specimens, to confirm the trend found and assess if the low compaction of the MT was responsible for these results.
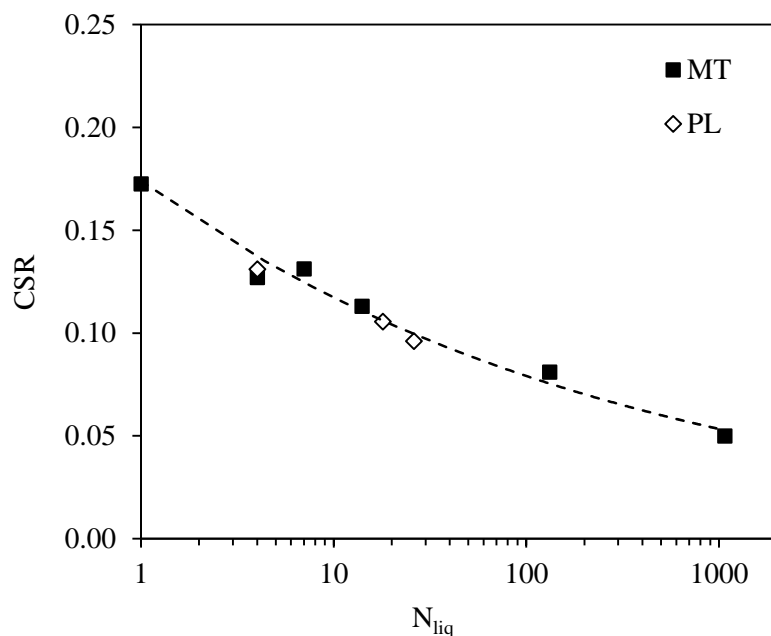
Figure 8.8 – Comparison of sample preparation methods in the assessment of NB1 cyclic resistance curve for *e* = 0.76–0.79 and *p'* = 100 kPa (ψ = -0.01–0.02)

Despite the cyclic resistance in terms of number of cycles to trigger liquefaction was found to be similar, the specimens behaviour during the shear load might be different. To better understand the behaviour of MT and PL specimens, two pairs of specimens were directly compared in terms of effective stress path, stress-strain, and evolution of pore pressure ratio and axial strains with number of cycles. Figure 8.9 presents the results for NB1_PL_CTx1 and NB1_MT_CTx4. The specimens were prepared for a void ratio of 0.76, confined to 100 kPa, sheared at CSR = 0.13, and liquefied at 4 cycles. Figure 8.10 presents the results for NB1_PL_CTx2 and NB1_MT_CTx6. The specimens were prepared for a final void ratio of 0.76 and 0.78, respectively, confined to 100 kPa, and sheared at CSR = 0.11. The MT

specimen liquefied for 14 cycles, while the PL specimens liquefied for 18 cycles. The pore pressure increase was similar for both pairs of tests. In the first one, the MT showed consistently higher values of r_u, probably due to a rapid increase in the excess pore pressure in the first cycle, which governed the r_u behaviour throughout the cyclic loading. Nevertheless, the r_u increase rate was similar for both tests. The main difference between MT and PL specimens was the strain development. The initial increase of strain is similar on both specimens, however, upon reaching r_u of 1, the PL specimen developed very large strains, while in the MT specimen the axial strains developed slower.
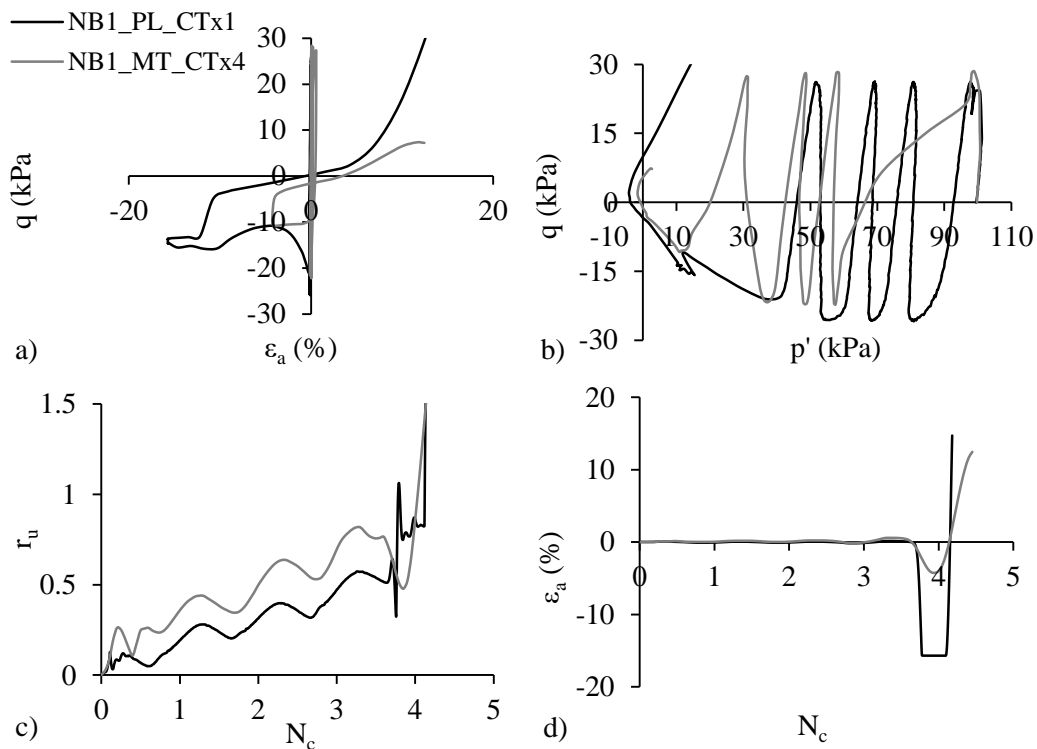
Figure 8.9 – Comparison of MT and PL specimens cyclic response: a) stress-strain curves; b) effective stress path; c) pore pressure ratio; and d) axial strain with number of cycles
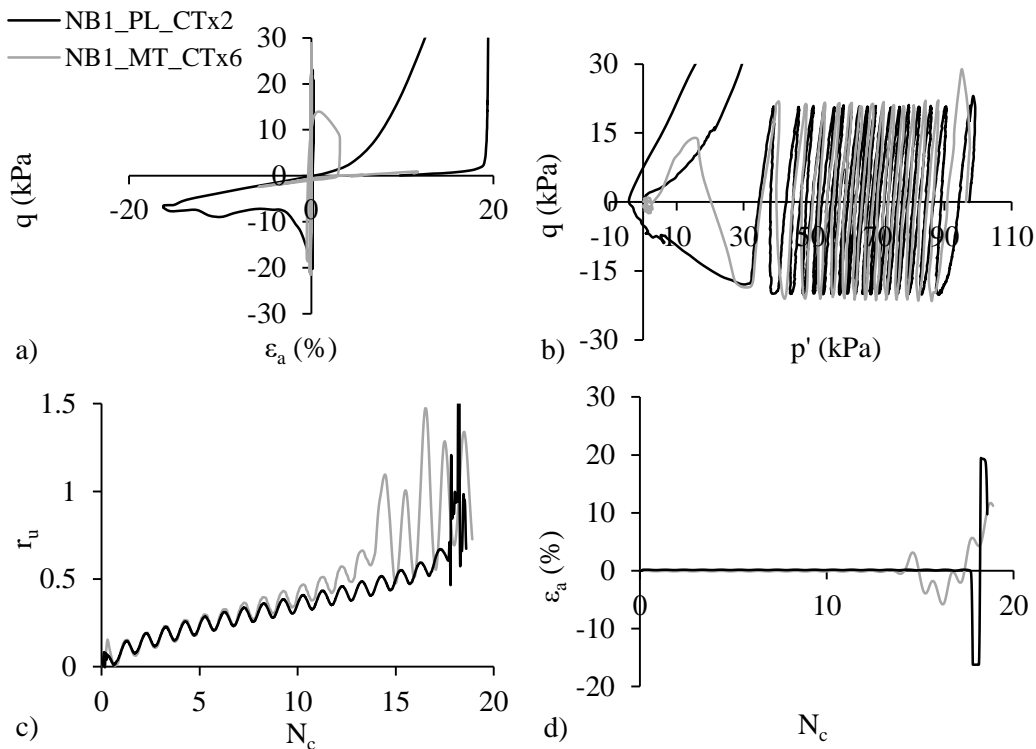
Figure 8.10 – Comparison of MT and PL specimens cyclic response: a) stress-strain curves; b) effective stress path; c) pore pressure ratio; and d) axial strain with number of cycles

8.2.3. SMALL STRAIN BEHAVIOUR – STIFFNESS RESULTS AND ANALYSIS

As discussed above, the shear wave velocities were measured at the end of the consolidation. Therefore, the shear modulus were determined for each test. The results were compared with the small-strain shear modulus curves determined with the results of monotonic triaxial tests, reported in Table 7.9. Figure 8.11 to Figure 8.13 present the results of S1_M2, S1_M7, and NB1, respectively. All S1_M2 and S1_M7 specimens were prepared with moist tamping for approximately the same initial void ratio, hence their fabric was expected to be similar. This is reflected in the results, as the values show good agreement with the previously determined curves. On the other hand, the NB1 results correspond to specimens prepared under different conditions, as some were prepared with moist tamping for different initial void ratios, while others were prepared with air pluviation. The void ratio does not reflect the fabric of the specimens, as specimens with the same void ratio but prepared with different techniques have different behaviour. Hence, the small oscillations in the G_{max}/F(e) values might be due to different fabric and particle arrangement from the preparation process. Despite this, the oscillations were not significant and the results are consistent with the previously determined stiffness curves. In this case, the values of G_{max} of MT and PL specimens were similar, which means that the intergranular contacts were not affected by the different preparation methods. After consolidation, the number of particle

contacts was the same, hence the shear wave velocities were similar. However, the void distribution might be different, which explains the differences in cyclic behaviour.

$$G_{max}/F(e) = 35.41(p'/p_a)^{0.53}$$
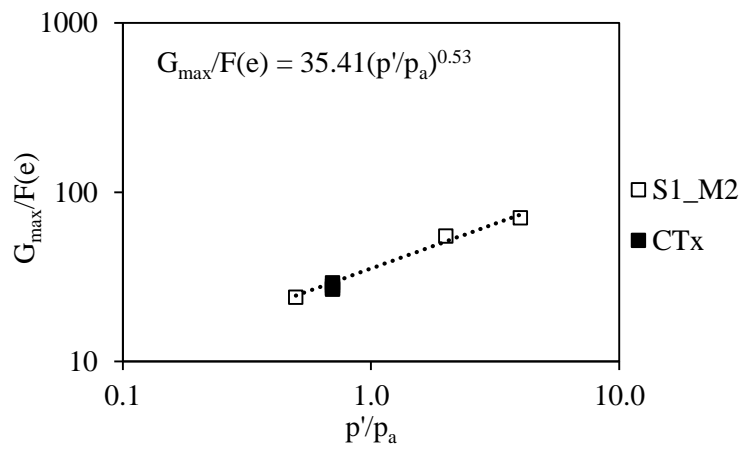
Figure 8.11 – Normalised maximum shear modulus to void ratio function for different mean effective stresses of S1_M2 soil

$$G_{max}/F(e) = 46.32(p'/p_a)^{0.56}$$
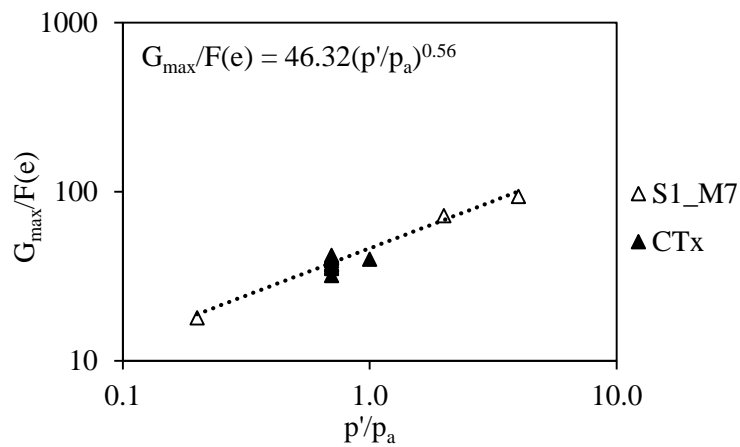
Figure 8.12 – Normalised maximum shear modulus to void ratio function for different mean effective stresses of S1_M7 soil

$$G_{max}/F(e) = 46.43(p'/p_a)^{0.53}$$
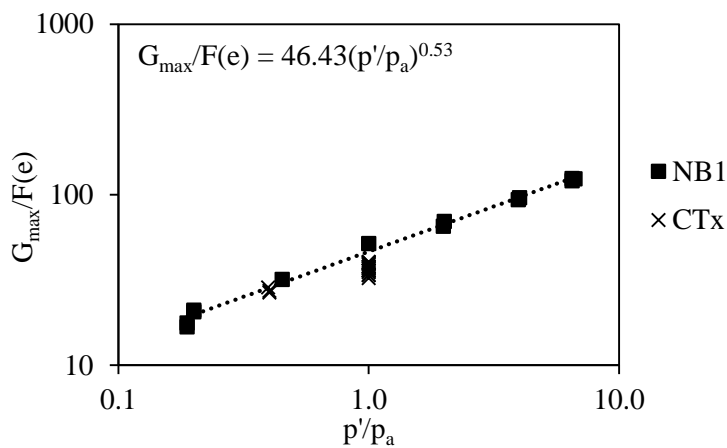
Figure 8.13 – Normalised maximum shear modulus to void ratio function for different mean effective stresses of NB1 soil

8.2.4. INTERPRETATION OF CYCLIC TRIAXIAL RESULTS THROUGH STATE PARAMETER

After collecting the cyclic triaxial results of around 13 benchmark soils, that had different cyclic resistance curves relative to variable relative densities, confining pressure, and fabric, Jefferies and Been (2016) compared the CRR normalised to the CRR for 15 cycles (CRR_{15}) with the number of cycles required to trigger liquefaction (N_{liq}) and found a correlation between CRR/CRR_{15} and N_{liq}. The triaxial tests results from this work were plotted against the Jefferies and Been (2016) results (Figure 8.14) and it was observed that the results have good agreement with the correlation obtained for other soils. This correlation is interesting as it allows to estimate approximately the CRR_{15} of soils when there is no possibility of performing more cyclic triaxial tests to obtain the entire cyclic resistance curve. The equation that best fits this study results is presented in Figure 8.14, and will be used later to estimate CRR_{15} of the cyclic resistance curves of the undisturbed specimens.
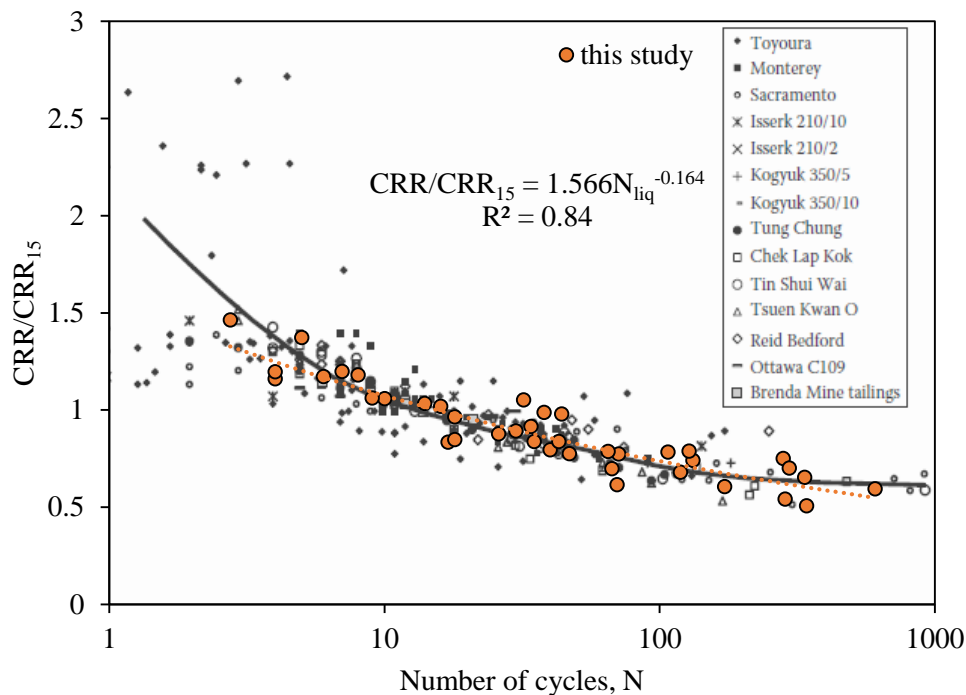
Figure 8.14 – Cyclic triaxial data normalised to CRR for 15 cycles compared with data reported by Jefferies and Been (2016)

Following the investigation discussed above that related the CRR normalised to the CRR at 15 cycles with N_{liq}, Jefferies and Been (2016) proposed a correlation between the cyclic stress ratio corresponding to a liquefaction triggered at 15 cycles and the state parameter. An analogous study was performed for the different curves presented above, for the materials and conditions studied in this research. The critical state lines of the materials tested were determined and presented in sections 7.4.1 and 7.4.2. The existence of the CSL allows the determination of the state parameter, defined above as being the parameter that identifies the state of a soil in terms of void ratio and confining pressure and that is often

used to predict soil behaviour. Table 8.2 summarizes the state parameters and CRR_{15} obtained for each curve. The state parameter was considered the mean value of all tests that defined each cyclic resistance curve, as the mean value is very close to the state parameter value for the tests that liquefied at around 15 cycles for each group of tests. The results from Jefferies and Been (2016), together with the results from this work are displayed in Figure 8.15. The studied curves parameters show good agreement with the curve plotted using other benchmark sands. However, care should be taken when considering this correlation as unique. There is some scatter in the results that might be a reflection of differences in fabric that are not captured by the state parameter. As Jefferies and Been (2016) mentioned, the principal stress direction and fabric are fundamental drivers of cyclic mobility and the grain contact arrangements play a decisive role in cyclic behaviour. Therefore, the relationship between CRR_{15} and ψ might not be unique. However, it is interesting to reflect on the results, as the CRR_{15} increases with the decrease of state parameter, and tends to a horizontal asymptote for state parameters higher than zero. This was expected as negative values of state parameter suggest a dilatant behaviour, hence these specimens require more cycles to reach liquefaction and consequently the value of CRR_{15} is higher. On the other hand, specimens with positive state parameters are looser and behave in a compressive manner, liquefying for lower number of cycles and presenting lower CRR_{15}. The horizontal asymptote is probably related to the asymptote of CRR-N_{liq}, as for the test conditions studied with principal stress inversion, it is not common that very lower values CSR induce liquefaction for several hundred cycles (Jefferies and Been, 2016).

Table 8.2 – Average values of state parameter and CRR_{15} for the cyclic resistance curves of S1_M2, S1_M7, and NB1 soils

Test ID	ψ	ψ (average)	CSR_{15}
S1_M2	-0.07 – -0.03	-0.05	0.110
S1_M7	-0.04 – 0.03	-0.02	0.135
NB1_MT	-0.01 – 0.02	0.007	0.109
NB1_E2	-0.08 – -0.05	-0.066	0.177
NB1_40	-0.11 – -0.09	-0.095	0.205
NB1_PL	-0.01 – 0.0	-0.006	0.109
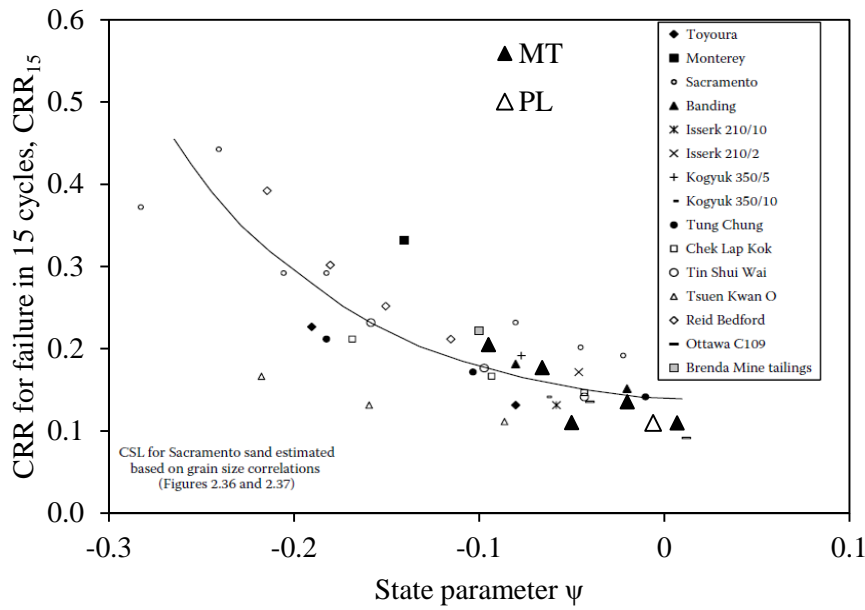
Figure 8.15 – CRR at 15 cycles as a function of state parameter

8.2.5. PORE PRESSURE BUILD-UP IN CTX

As discussed in the literature review, in saturated soils, liquefaction is associated with the increase in pore water pressure. Therefore, as liquefaction failure is related to the pore pressure evolution, an analysis of pore pressure generation has been done for the specimens tested under cyclic triaxial conditions. The results were interpreted by using equation (2.67), proposed by Booker et al. (1976), where the parameter α was calibrated to provide the best fit with the actual test results. The calibrations were performed by means of the R^2 value proposed by Polito et al. (2008), that was determined by equation (8.1), where Y_i is the r_u measured at the ith cycle ratio, $\bar{Y}$ is the average value of all r_u recorded during the test, and $\hat{Y}_i$ is the r_u predicted by equation (2.67) for the ith cycle ratio.

$$R^2 = \frac{\sum_{i=1}^{n}(Y_i - \bar{Y})^2 - \sum_{i=1}^{n}(Y_i - \hat{Y}_i)^2}{\sum_{i=1}^{n}(Y_i - \bar{Y})^2} \tag{8.1}$$

Figure 8.16 to Figure 8.21 present the pore pressure ratio evolution with N_c/N_{liq} for NB1, S1_M2, and S1_M7 soils, grouped according to the preparation technique used, void ratio, and confining pressure (refer to Table 8.1). The plot represents the maximum value of r_u for each cycle, to allow the calculation of R^2 and a better comparison between the estimated and measured results. It is observed that the pore pressure evolution curves vary depending on the type of soil, confining pressure, relative density and sample preparation technique. Focusing on each Figure individually, the pore pressure evolution of the different tests show good agreement, except for some tests which curves are far from the trends. Examples of those tests were NB1_MT_CTx2, NB1_MT_CTx4, S1_M2_CTx2, S1_M2_CTx4, and

S1_M7_CTx2. These tests were characterised by a rapid increase in excess pore pressure at the beginning of shear, which caused their pore pressure generation curve to be higher than the other curves.
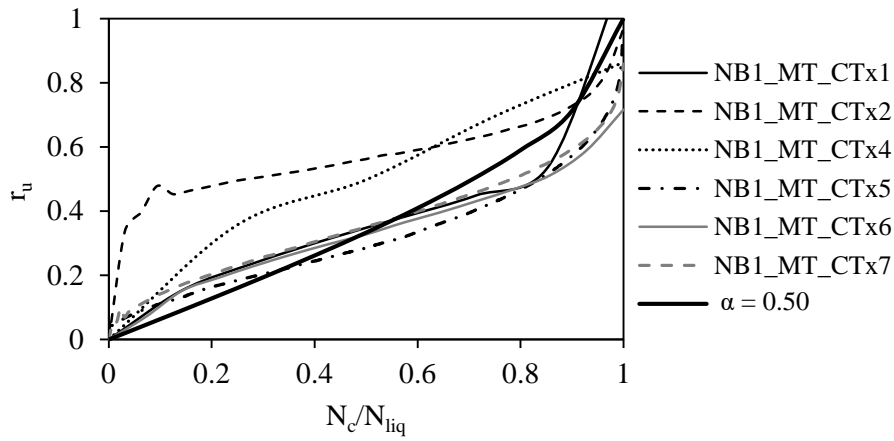
Figure 8.16 – Pore pressure ratio evolution with N_c/N_{liq} for NB1_MT tests
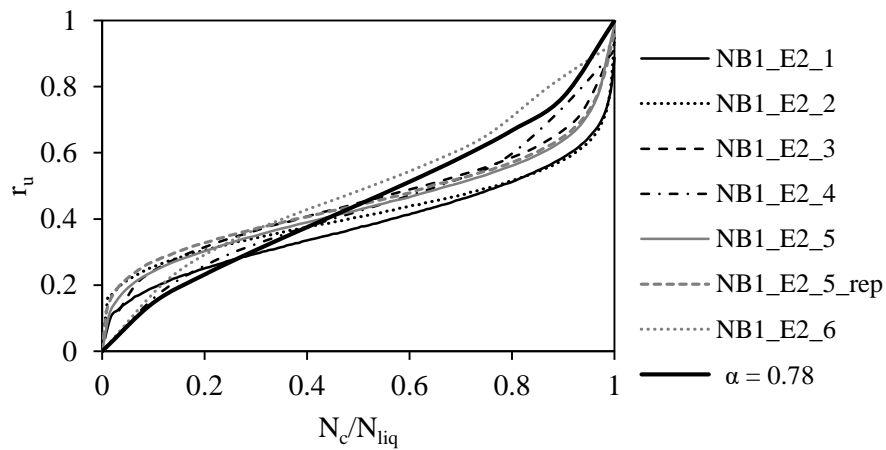
Figure 8.17 – Pore pressure ratio evolution with N_c/N_{liq} for NB1_E2 tests
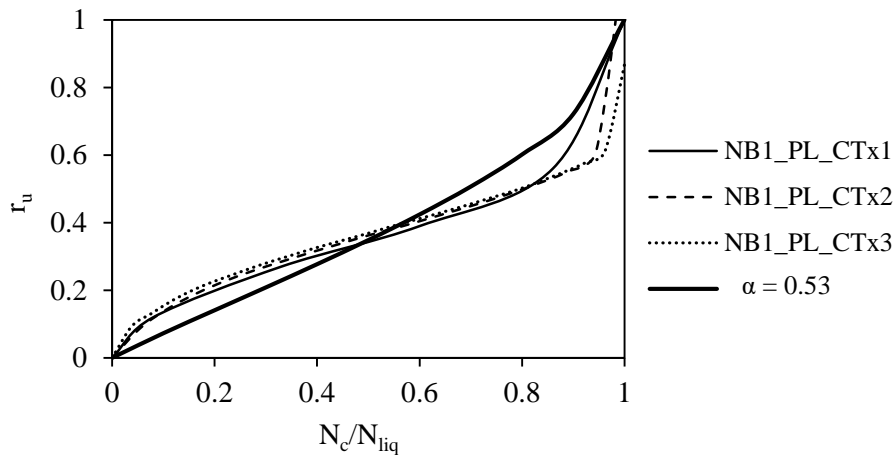
Figure 8.18 – Pore pressure ratio evolution with N_c/N_{liq} for NB1_PL tests
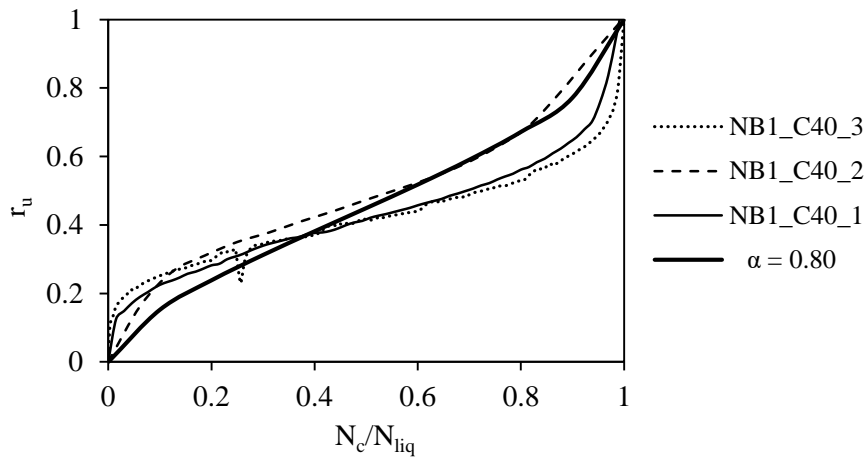
Figure 8.19 – Pore pressure ratio evolution with N_c/N_{liq} for NB1_C40 tests
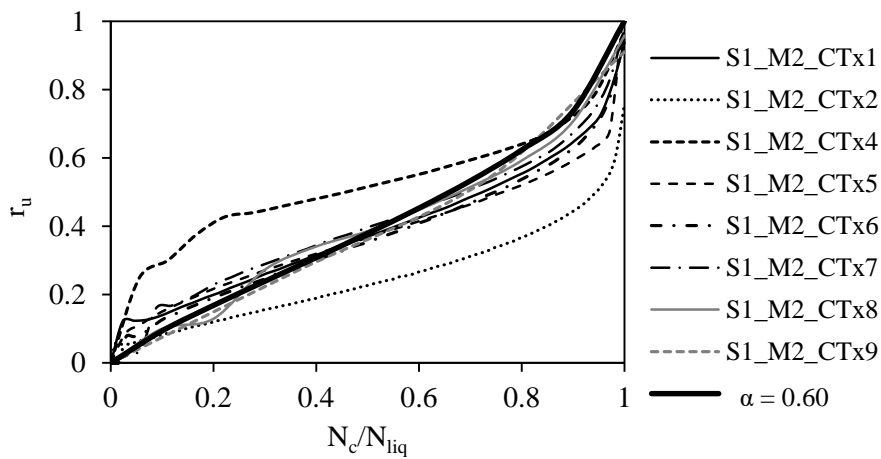
Figure 8.20 – Pore pressure ratio evolution with N_c/N_{liq} for S1_M2 tests
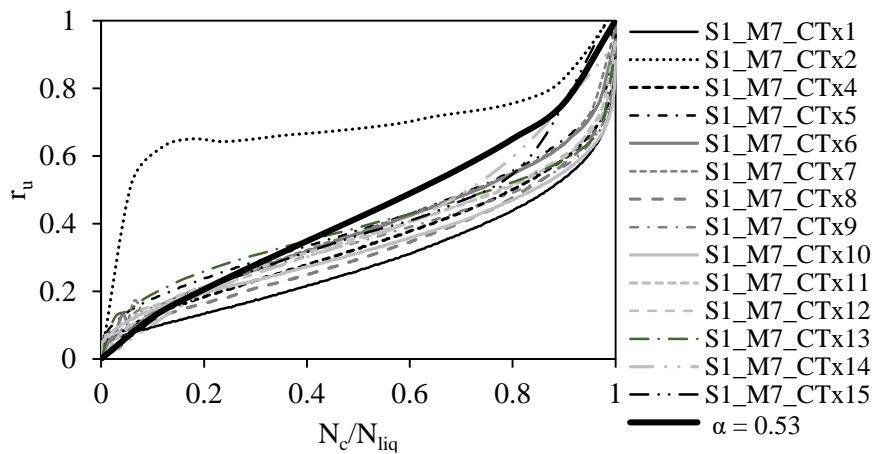
Figure 8.21 – Pore pressure ratio evolution with N_c/N_{liq} for S1_M7 tests

For each test, the value of α was determined to estimate the best fit with the measured results, by finding the highest value of R^2. Although the tests within each group were prepared for the same conditions, the results of α for each individual test varied. The results of the range of α obtained for each group of tests are presented on Table 8.3, as well as the average α and R^2. Additionally, Figure 8.22 presents the histogram of the percentage of occurrence of each range of R^2 values, considering all tests performed. Over 75% of tests showed R^2 higher than 0.80, evidencing the good performance of equation (2.67) in modelling the pore pressure generation over these range of soils. It is important to note that the tests with lower R^2 were the ones referred above as having a rapid increase in excess pore pressure at the beginning of shear, therefore their behaviour was poorly estimated by Booker et al. (1976) equation.

Table 8.3 – Calibration of α for tested sands

Test ID	range of α	α (average)	R^2 (average)
NB1_MT	0.4 – 1.16	0.77	0.84
NB1_E2	0.59 – 0.96	0.78	0.77
NB1_PL	0.50 – 0.54	0.53	0.88
NB1_40	0.72 – 0.97	0.80	0.81
S1_M2	0.25 – 1.18	0.60	0.89
S1_M7	0.34 – 0.62	0.52	0.86
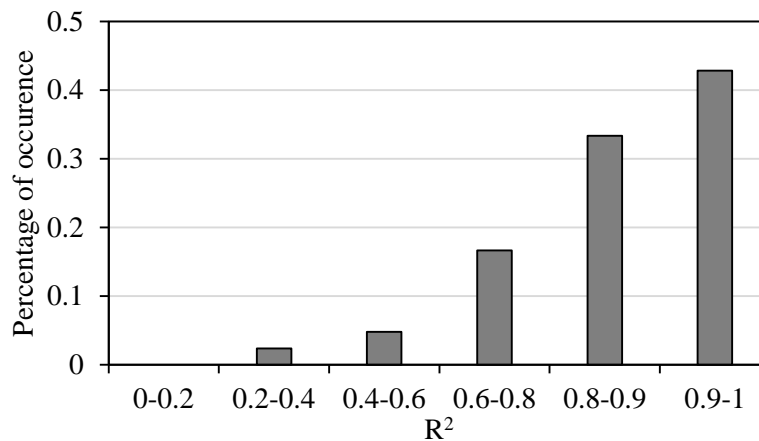
Figure 8.22 – Histogram of R^2 values for Booker et al. (1976) model fit to data from cyclic triaxial tests

8.3. CYCLIC DIRECT SIMPLE SHEAR TESTS (CDSS)

Most cyclic simple shear tests were performed at LabGEO, at FEUP, using an apparatus in which the sample is laterally confined with a rigid boundary consisting on a stack of copper rings. It is important to emphasize that the configuration with rings did not allow the measurement of pore pressure, hence the tests were not conventionally undrained, but were instead constant volume tests. As discussed before, the undrained conditions can be reproduced by performing drained tests at constant volume (Reyno et al., 2005). The constant volume is assured by maintaining the specimens' height constant during cyclic shear. The consolidation is made by applying the vertical stress. It is expected that the effective stress confinement follows an anisotropic condition ruled by K_0, with $\sigma_h = K_0 \times \sigma_v$ (total stress equals effective stress in this configuration). The S1_M2 and S1_M7 soils were consolidated to 70 kPa, to compare the behaviour of cyclic triaxial and cyclic direct simple shear tests. The NB1 specimens were consolidated to 100 kPa, except for a set of five tests in which the confining stress was 40 kPa, to assess the effect of initial confining stress. The loading waveform applied to the specimens was sinusoidal with a frequency of cycles of 0.1 Hz (i.e., 1 cycle per 10 seconds). Due to difficulties with the equipment, most tests were performed without percolation of water through the specimen. The specimens were prepared with the moist tamping technique with a low water content (around 5% which in the end was measured to come to a lower value of 3.5%). However, after observing significant differences between MT specimens with low water content and dry PL specimens, an additional set of tests in specimens prepared with higher water content was performed to assess the influence of water content in the cyclic behaviour of NB1 soil. Moreover, in the final part of this research work, it was possible to flush water through the specimen and produce specimens with high degrees of saturation (refer to Appendix A).

Additionally, a set of six cyclic simple shear tests in S1_M2 and S1_M7 soils (named with the reference L in Table 8.5) was performed at University of Ljubljana, at LabGeoUL. As described in section 6.4.1, the equipment allowed the use of a flexible membrane and no rings, as the confinement was provided by the cell water pressure. The specimens were prepared with the moist tamping technique, saturated and isotropically consolidated to 70 kPa. The loading waveform applied to the specimens was sinusoidal with a frequency of cycles of 0.1 Hz.

As already mentioned, two criteria are more frequently used to identify liquefaction triggering. In the case of cyclic direct simple shear tests, "full" liquefaction is assumed when the double amplitude shear strain reaches 7.5% (or the single amplitude reaches 3.75%) or when the σ_v drops to close to zero. However, as discussed by Ishihara (1993), for silty sands or sandy silts, the value of r_u should be reduced to 0.90 or 0.95, for compliance limits, which corresponds to a final σ_v=5 kPa for a confining pressure of 100 kPa. Analysing the tests performed in this work, with the exception of three tests performed with consolidation pressure of 40 kPa, the two criteria presented approximately the same number of cycles to trigger liquefaction, with a maximum difference of 3 cycles (refer to Table 8.4). As the strain criteria (γ_{SA}=3.75%) is more consistent, it was adopted to identify the number of cycles required to trigger liquefaction (N_{liq}). It is worth mentioning that the consistency of the analysis is of utmost importance. Therefore, as the same criterion is used for the analyses of all tests, the comparisons were assumed valid.

A total of 55 cyclic simple shear tests were performed in reconstituted specimens of S1_M2, S1_M7, and NB1 soils. The main objectives were the study of the cyclic response of the three soils and the assessment of the effect of changes in confinement (rigid or flexible boundary), state parameters (void ratio and confining pressure), and sample preparation procedures in their cyclic behaviour. Therefore, the following sub-sections are divided according to the effects of different factors on liquefaction resistance and the results are analysed in detail. The cyclic simple shear tests performed are summarised in Table 8.4 and Table 8.5. The more detailed tabulated results are reported in Table C.5 and Table C.6 in Appendix C, presenting the test identification (Test ID), the preparation method selected, the vertical stress (σ_v), the void ratio after specimen preparation (e_0) and after consolidation (e_i), the initial and final water content (w_i and w_f, respectively), the state parameter (ψ), the cyclic stress ratio (CSR), the number of cycles (N_{liq}) required to develop 3.75% axial strain in single amplitude (γ_{SA}) and to develop r_u=0.95, and the cumulative dissipated energy until liquefaction (ΔW_{liq}).

Table 8.4 – List of cyclic simple shear tests performed with NB1 reconstituted specimens

Test ID	Preparation method	w_f (%)	S_r (%)	e_i	σ_v (kPa)	CSR (τ/σ'_{v0})	N_{liq} (γ_{SA}=3.75%)
NB1_070_MT1	MT	3.2	12.0	0.66	100	0.20	13.0
NB1_070_MT2	MT	3.1	11.6	0.70	100	0.15	66.2
NB1_070_MT3	MT	3.1	11.5	0.71	100	0.21	2.0
NB1_070_MT4	MT	6.0	22.6	0.70	100	0.18	7.0
NB1_080_MT1	MT	4.0	14.4	0.73	100	0.15	5.3
NB1_080_MT2	MT	3.9	14.5	0.72	100	0.12	58.8
NB1_080_MT3	MT	3.7	13.1	0.75	100	0.13	6.8
NB1_080_MT4	MT	3.5	12.6	0.72	100	0.16	4.8
NB1_080_MT5	MT	3.4	12.1	0.74	100	0.16	1.8
NB1_MT_w10	MT	6.7	26.0	0.69	100	0.15	5.2
NB1_MT_w10_2	MT	7.1	26.0	0.72	100	0.13	14.2
NB1_MT_w10_3	MT	6.4	24.7	0.69	100	0.10	407.0
NB1_MT_sat1	MT	12.5	46.1	0.72	100	0.17	3.2
NB1_MT_sat2	MT	15.9	61.2	0.69	100	0.15	5.8
NB1_MT_sat3	MT	25.0	97.0	0.68	100	0.13	9.3
NB1_MT_sat4	MT	24.2	91.8	0.70	100	0.15	3.8
NB1_MT_sat5	MT	26.2	100.0	0.69	100	0.11	13.8
NB1_MT_sat6	MT	26.1	96.6	0.71	100	0.09	29.2
NB1_MT_sat7	MT	24.5	91.3	0.71	100	0.07	190.3
NB1_MT_sat8	MT	21.7	83.4	0.69	100	0.08	321.0
NB1_50_1	MT	3.3	12.3	0.70	50	0.15	24.0
NB1_40_1	MT	3.4	12.9	0.69	40	0.15	27.0
NB1_40_2	MT	3.4	13.6	0.67	40	0.20	17.9
NB1_40_3	MT	3.8	14.3	0.70	40	0.12	192.0
NB1_40_4	MT	3.1	11.7	0.70	40	0.17	11.5
NB1_40_5	MT	3.4	12.9	0.70	40	0.19	5.8
NB1_100_PL1	PL	0.3	1.1	0.65	100	0.15	5.2
NB1_100_PL2	PL	0.2	0.6	0.69	100	0.12	3.2
NB1_100_PL3	PL	0.2	0.6	0.66	100	0.08	254.0
NB1_100_PL4	PL	0.2	0.6	0.67	100	0.10	5.3
NB1_100_PL5	PL	0.2	0.7	0.68	100	0.12	0.8
NB1_100_PL6	PL	0.2	0.6	0.71	100	0.10	4.2
NB1_100_PL7	PL	0.2	0.6	0.70	100	0.08	7.2
NB1_100_PL8	PL	0.2	0.8	0.66	100	0.06	184.3
Test_layers1	MT	26.1	104.4	0.66	100	0.12	6.2
Test_mixture1	MT	23.3	91.4	0.68	100	0.12	6.2
Test_layers2	MT	25.4	91.9	0.73	100	0.11	15.9
Test_mixture2	MT	22.1	82.5	0.71	100	0.11	7.2

Table 8.5 – List of cyclic simple shear tests performed with S1 reconstituted specimens

Test ID	w_f (%)	S_r (%)	e_i	σ_v (kPa)	CSR (τ/σ'_{v0})	N_{liq} $(\gamma_{SA}=3.75\%)$
S1_M2_1	3.9	15.9	0.66	70	0.15	35.0
S1_M2_2	3.8	14.7	0.69	70	0.17	7.0
S1_M2_3	3.8	14.1	0.71	70	0.12	140.0
S1_M2_4	3.7	13.6	0.71	70	0.19	7.0
S1_M2_5	4.0	14.9	0.71	70	0.21	2.0
S1_M7_1	3.7	12.8	0.76	70	0.15	10.0
S1_M7_2	2.6	8.6	0.80	70	0.12	12.0
S1_M7_3	3.3	11.1	0.78	70	0.19	2.7
S1_M7_4	3.4	11.9	0.76	70	0.17	4.0
S1_M7_5	3.3	10.9	0.80	70	0.08	-
S1_M7_6	3.7	12.7	0.78	70	0.10	35.2
S1_M2_L1	27.0	100.7	0.71	70	0.16	6.1
S1_M2_L2	26.0	98.5	0.70	70	0.22	1.5
S1_M2_L3	27.1	103.9	0.69	70	0.09	36.2
S1_M7_L1	31.0	99.9	0.82	70	0.27	1.5
S1_M7_L2	30.8	100.4	0.81	70	0.16	12.5
S1_M7_L3	31.0	101.9	0.80	70	0.09	163.3

8.3.1. EFFECT OF STATE PARAMETERS ON LIQUEFACTION RESISTANCE

Analysing Table 8.4 and Table 8.5, it is possible to infer that a variety of factors were considered when planning the experimental work. In order to correctly assess the influence of the different factors, the specimens were grouped according to void ratio, confining pressure, sample preparation procedure, water content, and boundary conditions. In this section, the comparisons are made between groups of tests with the same preparation technique and water content, varying the void ratio or the vertical confining stress. The initial target void ratio within each group of specimens was the same. However, due to the processes of sample preparation and the volume variations during consolidation, the final void ratios showed slight differences in specimens from the same group of tests. Therefore, to help the analysis of results, the symbols on the figures are identified with the corresponding specimens void ratios.

The effect of confining stress was assessed by comparing two sets of tests with the same target void ratio, consolidated at 40 kPa and 100 kPa of vertical stress (Figure 8.23). Unlike the observations in the triaxial tests, the consideration of 40 kPa or 100 kPa had no influence in the definition of the cyclic resistance curve. Moreover, one test was performed with a vertical confining stress of 50 kPa, and the result corroborates these findings.

The results from Figure 8.23 also show that the NB1 soil exhibits higher cyclic resistance for lower void ratios, as evidenced by the comparison between three groups of void ratio ranges defined as 0.66-0.67, 0.69-0.71, and 0.72-0.75. The results show that, as expected, looser specimens require lower number of cycles to trigger liquefaction.
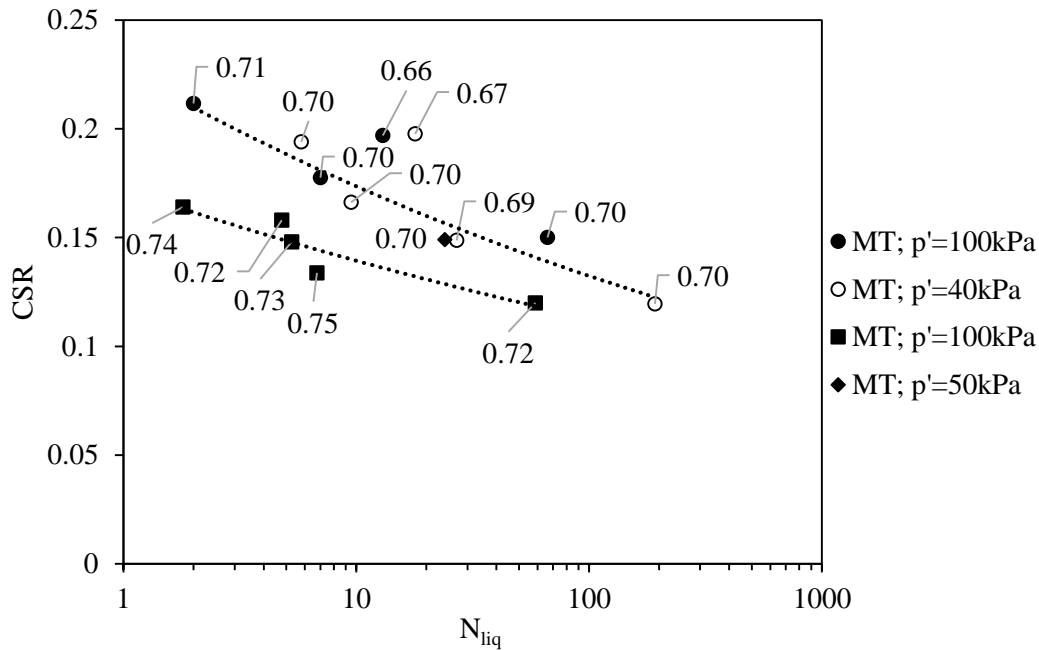
Figure 8.23 – Cyclic resistance curves for NB1 prepared with MT with 3.5% water content with identification of correspondent void ratio

The void ratio influence on cyclic strength was also assessed for the tests performed on specimens prepared with dry air pluviation (Figure 8.24). One cyclic resistance curve is defined for specimens with void ratios ranging between 0.67 and 0.71 (average value of 0.686), while the other curve was defined by two specimen with *e* around 0.65. The same tendency is observed, as specimens with lower void ratio are more resistant to liquefaction, and the corresponding cyclic resistance curve is located above the curve of higher void ratios.

The CRR_{15} was calculated for each cyclic resistance curve and correlated according to the variations in void ratio. It was found that an increase in the void ratio of around 5% (in MT specimens from 0.665 to 0.70 and in PL specimens from 0.65 to 0.686) corresponds to a decrease in resistance of around 16% in the MT specimens and around 34% in the PL specimens. The percentage of decrease in resistance (CRR_{15}) in PL specimens was more than two times the percentage of decrease in resistance in MT specimens, for the same variation in void ratio. These results suggest that the PL specimens resistance was more sensible to changes in void ratio.
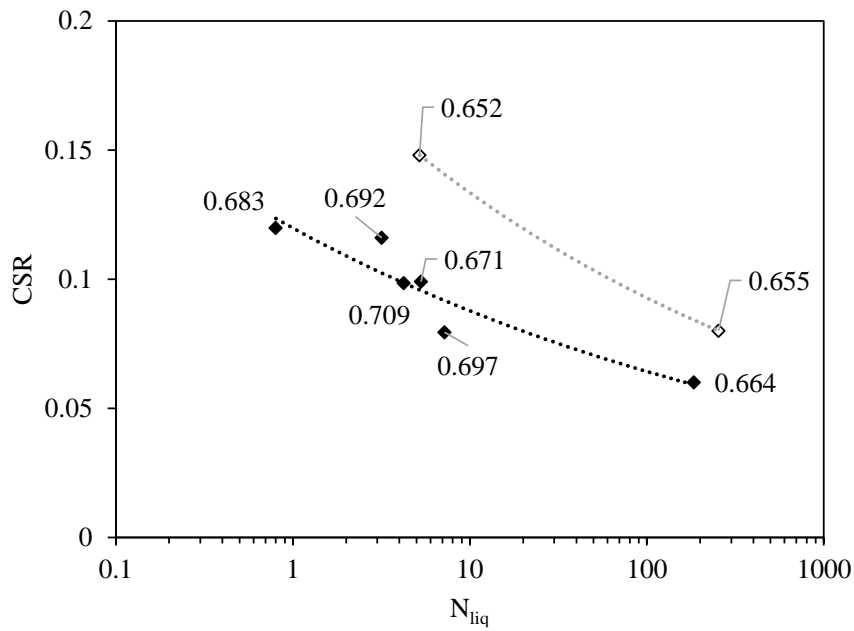
Figure 8.24 – Cyclic resistance curves for NB1 prepared with dry air pluviation

Additionally, the tests performed with S1_M2 and S1_M7 were also analysed in terms of the effect of void ratio in cyclic strength. The specimens were confined to the same vertical stress, 70 kPa, and the target initial void ratio was the same. However, due to the processes of sample preparation and the volume variations during consolidation, the final void ratios showed slight differences. Despite the small variances in *e*, the cyclic resistance curves were not affected, as evidenced in Figure 8.25 and Figure 8.26.
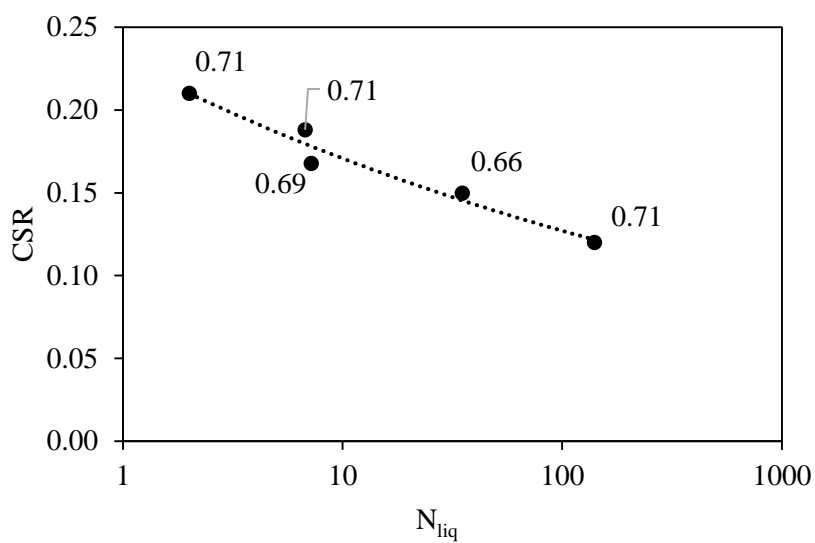
Figure 8.25 – Cyclic resistance curves for S1_M2 with identification of corresponding void ratio
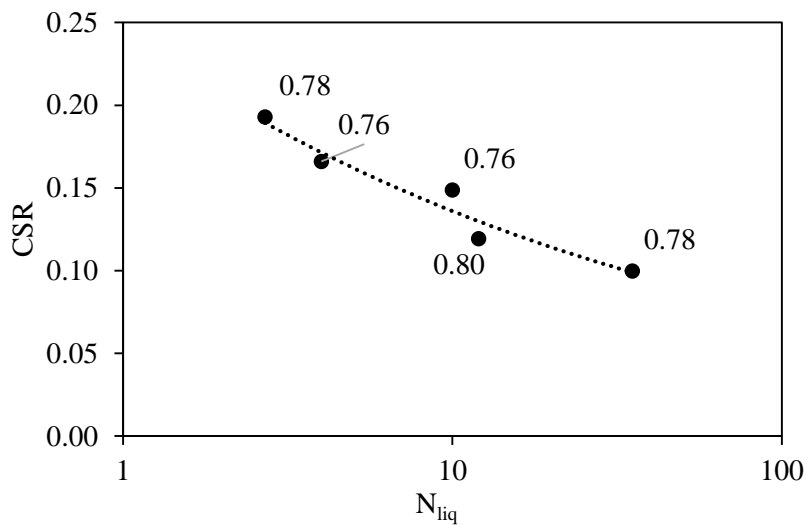
Figure 8.26 – Cyclic resistance curves for S1_M7 with identification of corresponding void ratio

8.3.2. EFFECT OF BOUNDARY CONDITIONS ON LIQUEFACTION RESISTANCE

To evaluate the effect of confinement type, cyclic simple shear tests were carried out in two distinct simple shear apparatus, one where the specimen is confined by a stack of copper rings (at LabGeo, at FEUP) and another where the specimen is isotropically consolidated by controlling the cell pressure (at LabGeoUL), both described in detail in section 6.4. The two types of specimens will be referred to as rigid boundary and flexible boundary, respectively, due to the type of boundary condition that is imposed on the specimen.

The specimens were prepared with MT, with the same initial water content and void ratio. As mentioned before, the rigid boundary apparatus is composed of a stack of copper rings that confine the specimen, and the lateral stress is unknown. The undrained condition during the loading stage is guaranteed by fixing the sample height and allowing changes in the vertical stress. As discussed before, the reduction of vertical stress is analogous to the increase of pore pressure in a similar undrained test. On the other hand, in the flexible membrane apparatus, the specimen is confined by a rubber membrane, and the lateral stress is controlled. Moreover, the back and pore pressure are also controlled and measured, allowing the saturation of the specimen.

Figure 8.27 presents the results of tests performed in S1_M2. Analysing the results, it is observed that the cyclic resistance curve of tests performed with flexible membrane is located below the cyclic resistance curve of rigid boundary specimens and has a higher slope. For low number of cycles, the cyclic resistance of tests performed with rigid and flexible boundaries are very close, and might be assumed to represent the same cyclic resistance curve. Therefore, the test result for lower CSR, and

consequently higher number of cycles required to trigger liquefaction, might not be a reliable result. To confirm this trend, more tests should be performed with flexible membrane and low values of CSR.
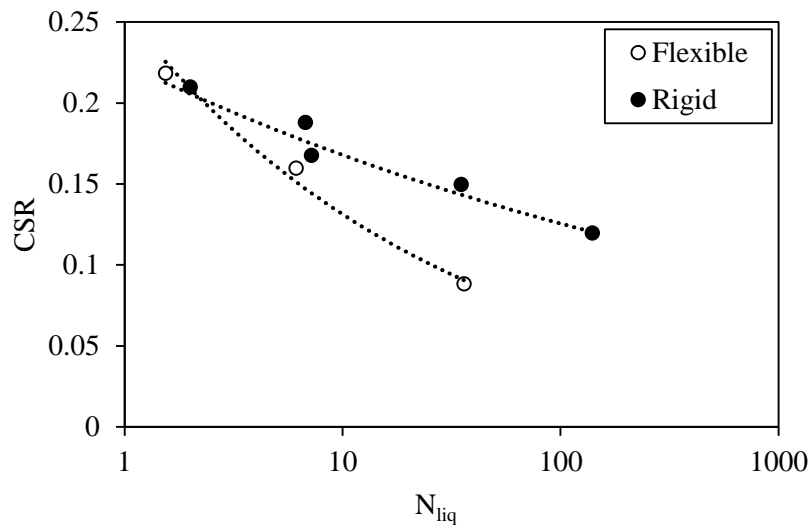
Figure 8.27 – Cyclic resistance curves comparing rigid and flexible boundaries in specimens of S1_M2

On the other hand, the results of tests performed with S1_M7 show a contradictory tendency. There is a difference between the cyclic resistance curves of specimens with rigid and flexible boundary, as specimens confined with flexible rubber membrane were more resistant, with higher number of cycles required to trigger liquefaction, than specimens confined with rigid rings. These results are in accordance with the works of Sharma et al. (2017), which showed different curves for different boundary conditions, where CSR-N_{liq} curves obtained using a rigid boundary apparatus generally lie below the curve obtained using flexible boundary apparatus. The differences in the soil response due to the two boundary conditions might be explained by different strain distribution. While the rigid boundary condition imposes a relatively uniform deformation (Sharma et al., 2017), tests with flexible boundary may be subjected to strain localisations, which increases their cyclic resistance.
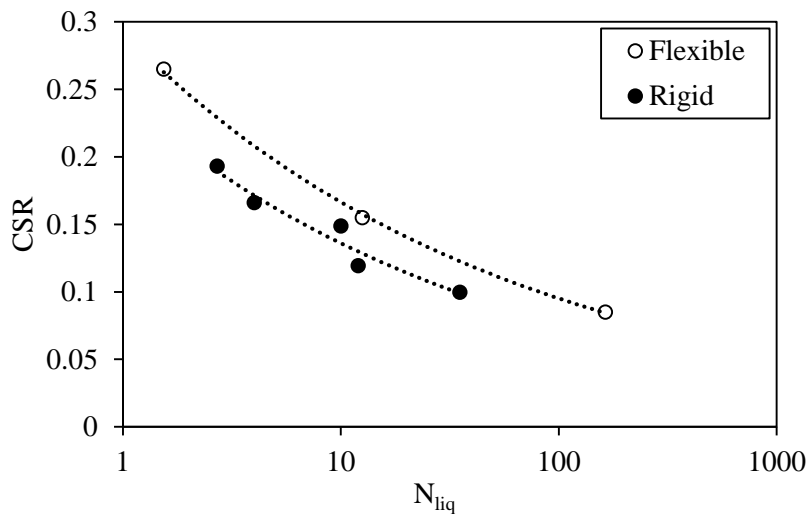
Figure 8.28 – Cyclic resistance curves comparing rigid and flexible boundaries in specimens of S1_M7

To better understand the effects of different boundary conditions, the results of some tests were compared. For S1_M2 soil, tests S1_M2_L1 and S1_M2_2 were selected as they were carried out at approximately the same CSR, 0.16 and 0.168, respectively. The results comparisons are plotted in Figure 8.29. On the other hand, for S1_M7, Figure 8.30 shows the comparison between S1_M7_L2 and S1_M7_1, which were carried out with CSR of 0.155 and 0.149, respectively. The results are presented in terms of shear-strain response, shear strain, and pore pressure ratio evolution with number of cycles.

For the two types of sand, it is observed that the shear-strain responses of tested soils differ according to the type of boundary. The secant shear modulus, G_{sec}, is clearly higher for specimens confined with flexible membrane (Figure 8.29c and Figure 8.30c), which is reflected in the lower increase in shear strain in the beginning of cyclic shear. On the other hand, the results of tests with rigid boundary show lower shear modulus, hence a higher rate of shear-strain accumulation with increasing number of cycles when compared with flexible boundary tests. However, once liquefaction occurs, the flexible membrane specimens show higher levels of deformation, as can be verified in Figure 8.29b and Figure 8.30b.

The number of cycles at which liquefaction occurs is very similar in both pairs of tests. S1_M2_L1 and S1_M2_2 required 6 and 7 cycles to trigger liquefaction, respectively, while S1_M7_L2 and S1_M7_1 required 12.5 and 10, respectively. It is important to mention that the pore pressure ratio evolution of specimens confined with rings was assessed indirectly through the decrease of vertical stress, as the ratio between ($\sigma_{v0}-\sigma_v$) and σ_{v0}, where σ_{v0} is the initial vertical stress and σ_v is the current vertical stress. Nevertheless, it is observed that the pore pressure ratio evolution is faster on the specimens confined with rigid rings (Figure 8.29d and Figure 8.30d) which is consistent with the assumption that rigid boundary specimens are less resistant than flexible boundary specimens.
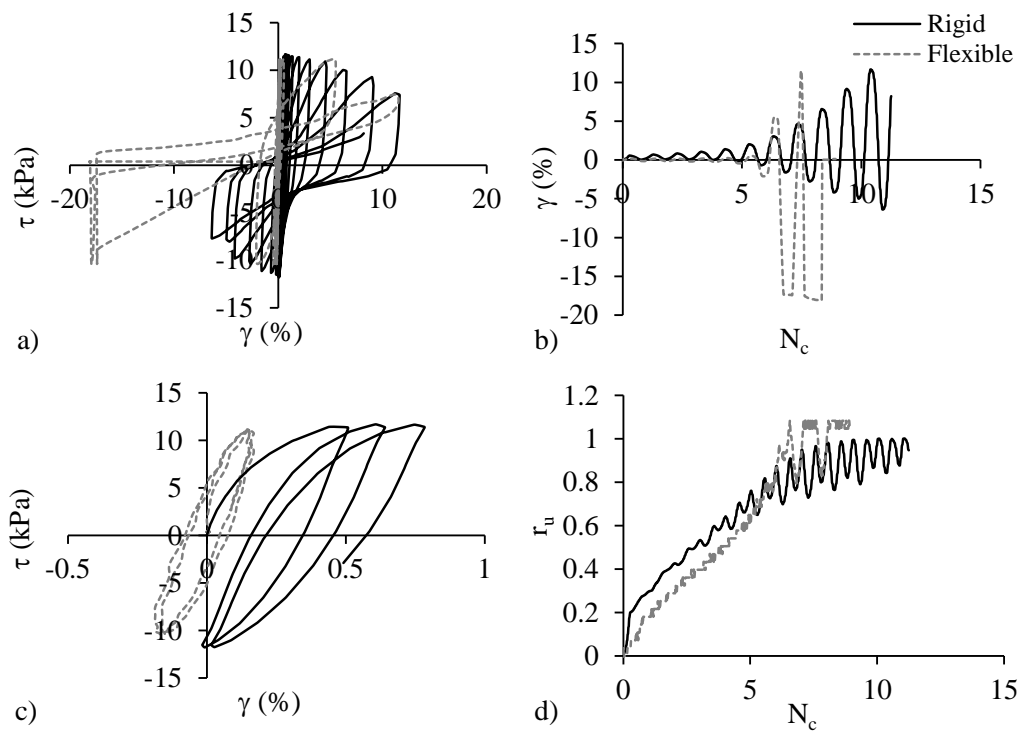
Figure 8.29 – Comparison of cyclic results of tests performed with different boundary conditions for S1_M2: a) τ−γ; b) γ−N_c; c) τ−γ for the first cycles; d) r_u−N_c
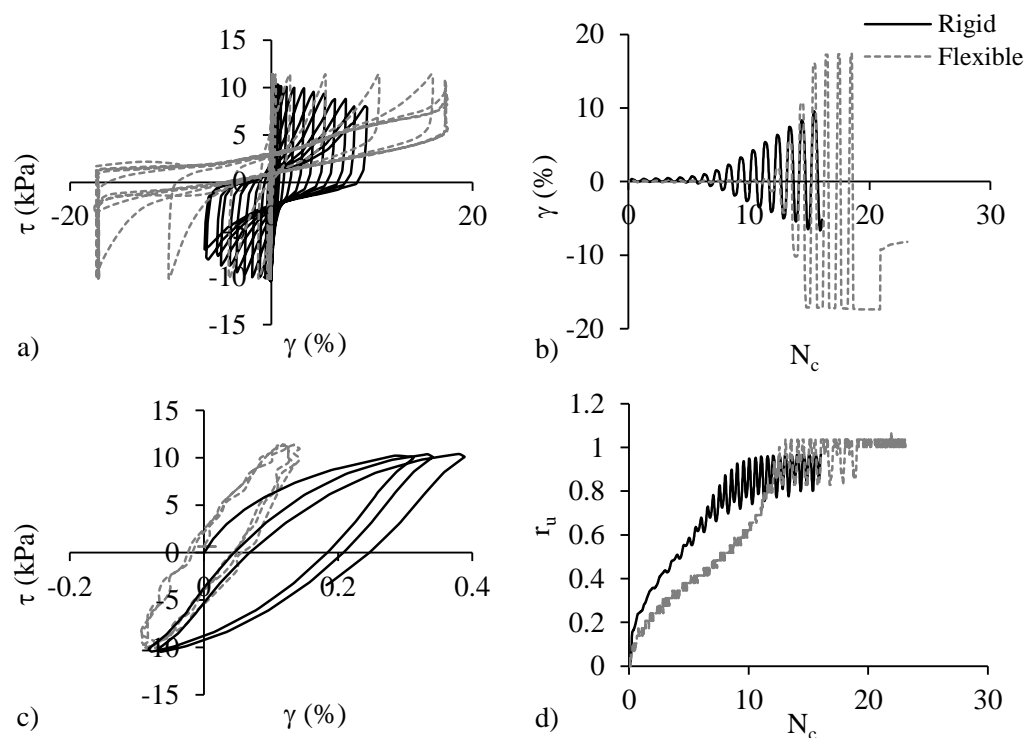
Figure 8.30 – Comparison of cyclic results of tests performed with different boundary conditions for S1_M7: a) τ−γ; b) γ−N_c; c) τ−γ for the first cycles; d) r_u−N_c

8.3.3. EFFECT OF WATER CONTENT ON LIQUEFACTION RESISTANCE

As explained above, at first, the simple shear apparatus did not allow the saturation of the specimens so the majority of MT specimens were prepared with a low water content (3.5% that correspond to a saturation degree of around 12%). However, at the final stage of this research, the author was able to saturate the specimens with CO_2 and water percolation, reaching saturation degrees very close to 100% (more details in Appendix A). Moreover, other tests were performed with intermediate water content, varying between 7% and 12−16%, that correspond to saturation degrees of 26% and 46−61%, respectively. The results are plotted together in the plane CSR−N_{liq} (Figure 8.31), showing a decrease in cyclic resistance with increase of water content. It is worth noting that the specimens with 7% and 12%−16% of water content have similar cyclic resistance. The CRR_{15} of each cyclic resistance curve is plotted in Figure 8.32 against the average water content of the specimens. The rate of CRR_{15} decrease reduces as the water content increases, which might be due to the decrease of suction with the increase of water content.
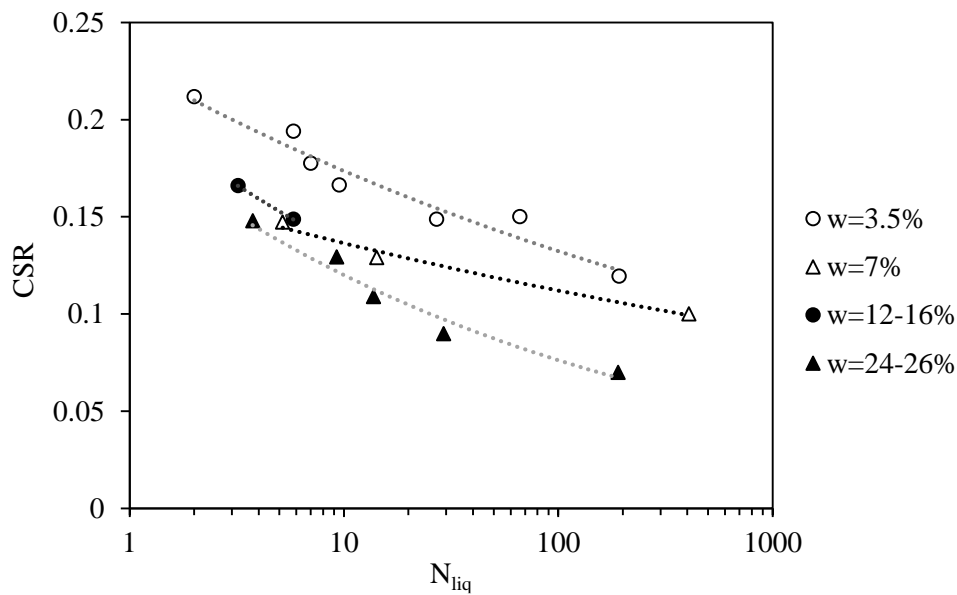
Figure 8.31 – Effect of water content on cyclic resistance curves of NB1 sand
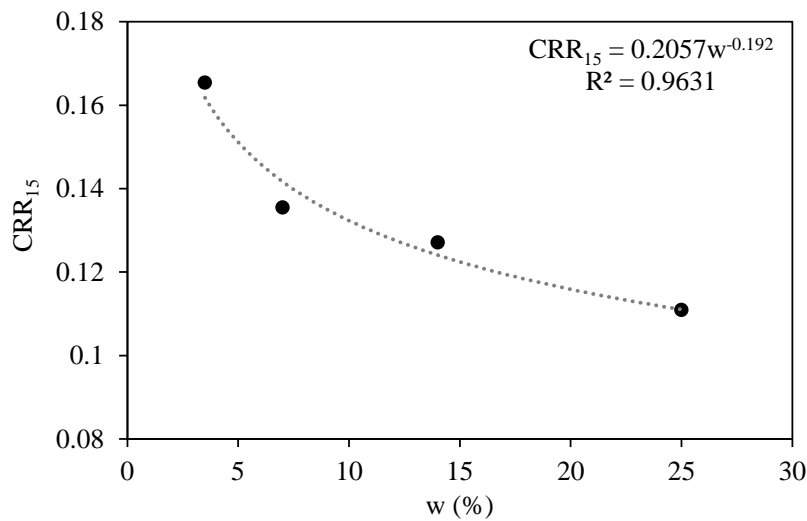
Figure 8.32 – Relationship between CRR_{15} and water content

It is known that, in moist tamped specimens, the suction effects due to partial saturation lead to the development of more stable fabrics, as discussed by Cappellaro (2019). Therefore, effects of suction might be the cause of the increase in resistance for specimens with lower water content. Filter paper tests were performed to assess the matric suction in specimens with 3.5% water content, but the results were inconclusive as the final water content of the paper filter was higher than 100%. Despite the inconclusiveness of the filter paper tests, it is clear that suction effects exist, conferring a higher resistance to specimens with lower water content. Figure 8.33a presents the water retention curve (also referred to as soil-water characteristic curve) of Ottawa sand. It is observed that for 3.5% of water content, the suction is around 15 – 30 kPa, which is a considerable value that might influence the soil resistance. Assuming that the grain size distribution curves of Ottawa and NB1 sands are similar, the water retention curve will probably be similar, hence the suction corresponding to 3.5% will also be similar, which explains the higher cyclic resistance found in the specimens with lower water content.
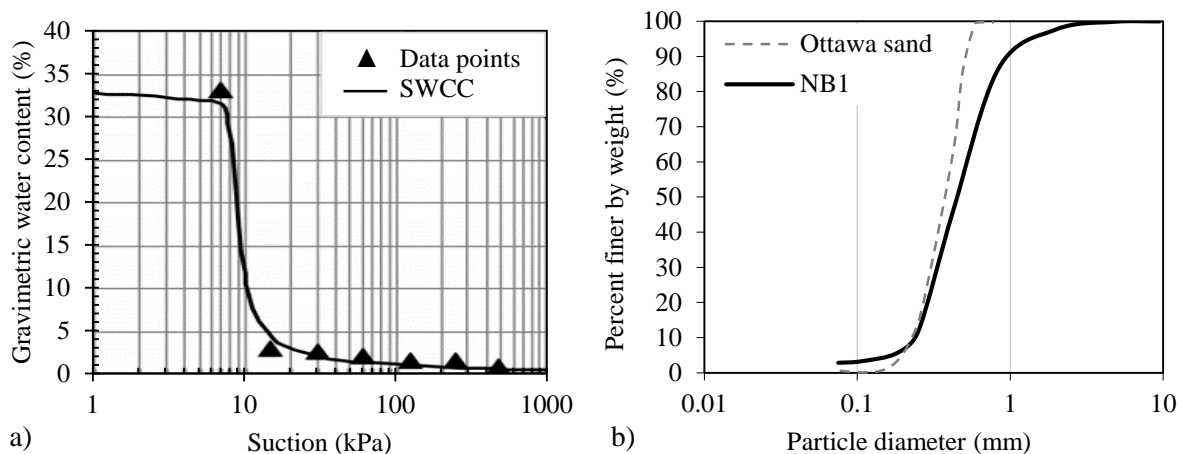
Figure 8.33 – a) Soil-water characteristic curve for Ottawa sand (adapted from Tran et al., 2016); b) GSD curves of Ottawa and NB1 sand

A detailed analysis of the influence of water content in cyclic behaviour of soil was performed by comparing the cyclic results of three specimens, NB1_070_MT2, NB1_MT_w10, and NB1_MT_sat4 with 3.5%, 6.7%, and 24.2% of water content, respectively (corresponding to saturation degrees of 11.6%, 26% and 91.8%, respectively). The three specimens were consolidated to 100 kPa and the cyclic loading was carried out for CSR of 0.15. The results are presented in Figure 8.34, reporting the evolution of shear strain with number of cycles (N_c–γ), the stress-strain path (τ–γ), the decay of vertical stress with increasing number of cycles (σ_v–N_c), and the stress path (τ–σ_v). In order to clarify the comparison between the cyclic behaviour of the three specimens, the same initial plots were reproduced for lower number of cycles, and are presented on the right (figures with index 2).

As it was previously discussed, the number of cycles required to liquefaction decreases with increase of degree of saturation (Figure 8.34a_1 and a_2). However, the number of cycles corresponding to the intermediate water content (6.7%) is closer to N_c of the saturated specimen than to the N_c of the drier specimen, despite the differences between water content being higher. This behaviour might be justified by the effects of suction. Returning to Figure 8.33, it is observed that the water retention curve is very steep for water content of 7% to 30%. Assuming that the NB1 water retention curve follows approximately the same trend, the suction will be similar for this range of water contents, approximating the results of cyclic resistance of the specimens with 6.7% and 24.2% of water content. The small differences in behaviour might be due to the compressibility of the air present in the soil (Mele et al., 2019). On the other hand, it is observed that once the strain criteria is reached, the saturated specimen has a rapid increase in shear strain, also verified by the fast decrease in vertical stress that remains low showing a complete loss of strength corresponding to flow liquefaction. On the contrary, the specimens with lower saturation degrees show cyclic mobility, as the specimens conserve some strength and the stress-path continues with increases and decreases of stresses, going up and down the failure envelope (Figure 8.34d_1 and d_2). It is worth mentioning that the secant shear modulus, G_{sec}, is lower for NB1_MT_w10 and approximately the same for NB1_070_MT2 and NB1_MT_sat4. This is reflected on a higher increase in shear strain of the specimen with intermediate S_r. However, the shear strain increase is more regular, and hence it takes more cycles to reach the shear strain criteria for failure than in the saturated specimen, which fails more rapidly.
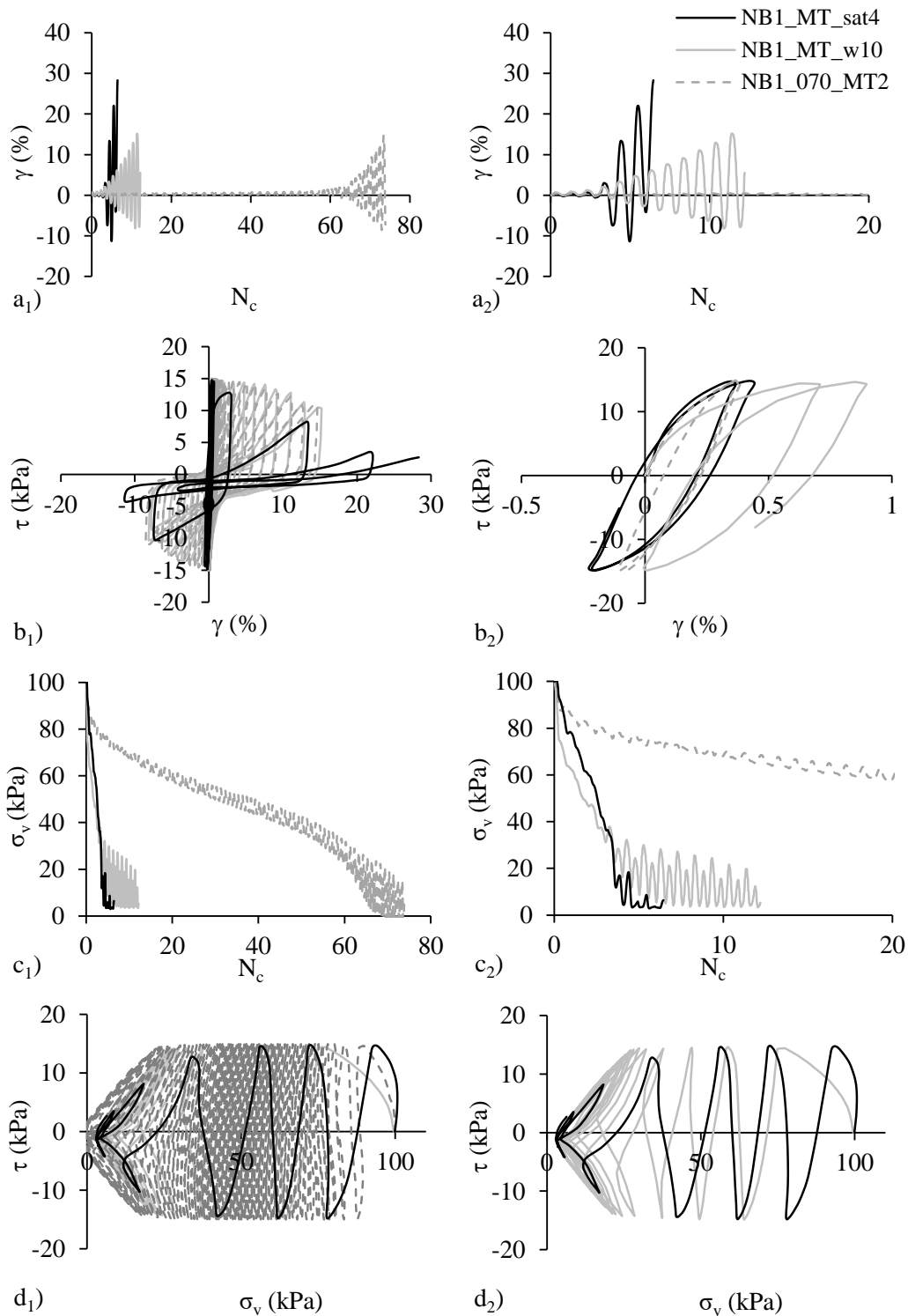
Figure 8.34 – Comparison of cyclic results of tests performed in specimens with different water content: a_1) γ−N_c; a_2) γ−N_c for lower number of cycles; b_1) τ−γ; b_2) τ−γ for the first cycles; c_1) σ_v−N_c; c_2) σ_v−N_c for lower number of cycles; d_1) τ− σ_v; d_2) τ− σ_v of NB1_MT_sat4 and NB1_MT_w10

8.3.4. EFFECT OF SAMPLE PREPARATION ON LIQUEFACTION RESISTANCE

The effect of sample preparation technique on liquefaction resistance was assessed by comparing specimens prepared with moist-tamping and air pluviation. As referred above, the water content of the specimens plays an important role in their cyclic resistance. Therefore, the comparisons were made between dry specimens prepared with air pluviation (NB1_100_PL in Table 8.4) and saturated specimens prepared with MT (specimens with a degree of saturation from 83–100%, NB1_MT_sat in Table 8.4), to eliminate the effects of suction in unsaturated specimens. All tests were performed with a vertical stress of 100 kPa and the specimens had similar void ratios. The cyclic resistance curves are plotted together in Figure 8.35, showing that PL specimens have lower liquefaction resistance than MT specimens. In terms of CRR_{15}, the MT specimens have a CRR_{15} 35% higher than the CRR_{15} of PL specimens. These results are in accordance with experimental results from other researchers (Mulilis et al., 1977; Kwan and El Mohtar, 2018).
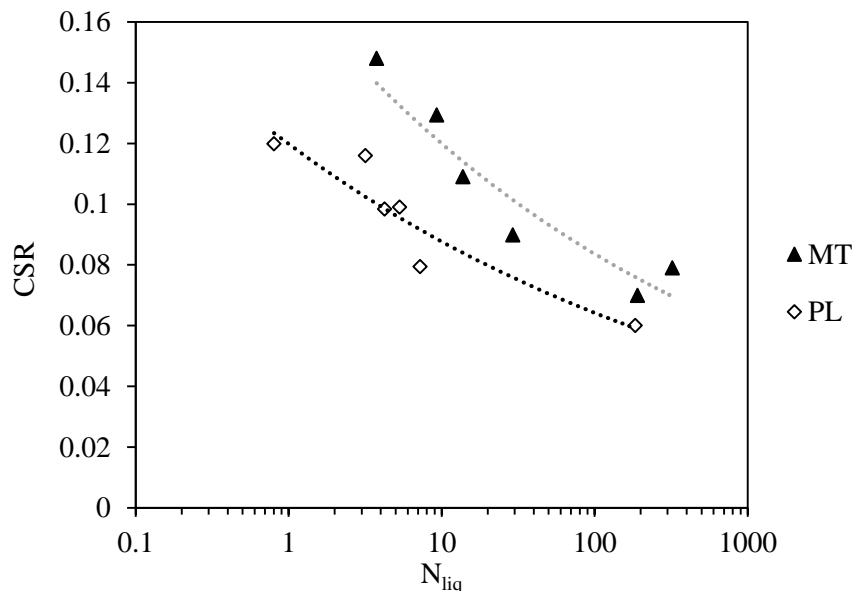
Figure 8.35 – Effect of sample preparation on cyclic resistance curves of NB1

8.3.5. EFFECT OF LAYERING ON LIQUEFACTION RESISTANCE

In order to study the effect of layering in cyclic resistance, cyclic simple shear tests were carried out on layered specimens, and mixture specimens. The layered specimens were prepared in two different layers, as illustrated in the scheme of Figure 8.36. The grain size distribution curves of the two materials is also presented in Figure 8.36, for reference. The S1_M25 soil was collected on the experimental site, at S1, and is generally finer than NB1 with a fines content of 17.3%. The material properties of the soil are presented in Table B.3. The mixture specimens were prepared by mixing the same quantity of each soil, to produce a homogeneous specimen of a combination of both materials (50% of each). The

specimens were prepared with MT and an initial water content of 5%, were percolated with CO_2 and water, and considered saturated (confirmed at the end of the test by high saturation degrees). A vertical stress of 100 kPa was applied before percolation, and the cyclic loading was carried out with CSR of 0.12 and 0.11, with a loading frequency of 0.1 Hz.
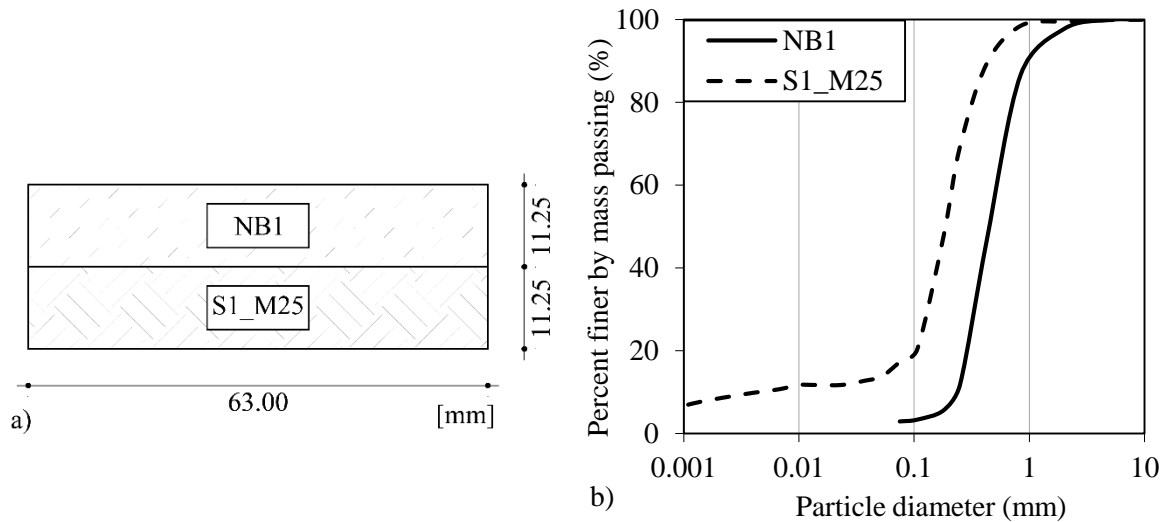
Figure 8.36 – a) Scheme of the layered specimen; b) Grain size distribution curves for the respective soils

In the first set of tests, the specimens were prepared to a target void ratio, thus the initial void ratio of the two layers was similar (the NB1 layer had a void ratio of .78 and the S1_M25 layer had a void ratio of 0.79), and to the mixture specimen (with a void ratio of 0.77). However, it was not possible to determine the final void ratio of the two separate layers as the specimen is confined by the cooper rings and the compressibility of the separate layers was probably different. Nonetheless, the final void ratios of the layered and mixture specimens were 0.66 and 0.68, respectively. Figure 8.37 presents the results, reporting the stress-strain path (τ–γ), the evolution of shear strain with number of cycles (γ–N_c), the stress path (τ–σ_v), and the decay of vertical stress with increasing number of cycles (σ_v–N_c). The results did not show significant differences between the cyclic behaviour of the two tests, as both specimens reached the liquefaction strain criteria (γ_{SA}=3.75%) in the same number of cycles. The pore pressure ratio, obtained with the decay of vertical stress, and the shear strain developments were also similar. These results are in agreement with the findings of Cappellaro (2019) that studied the effect of layering in specimens tested under cyclic direct simple shear and found that the layered structure did not result in significant differences in terms of liquefaction response.
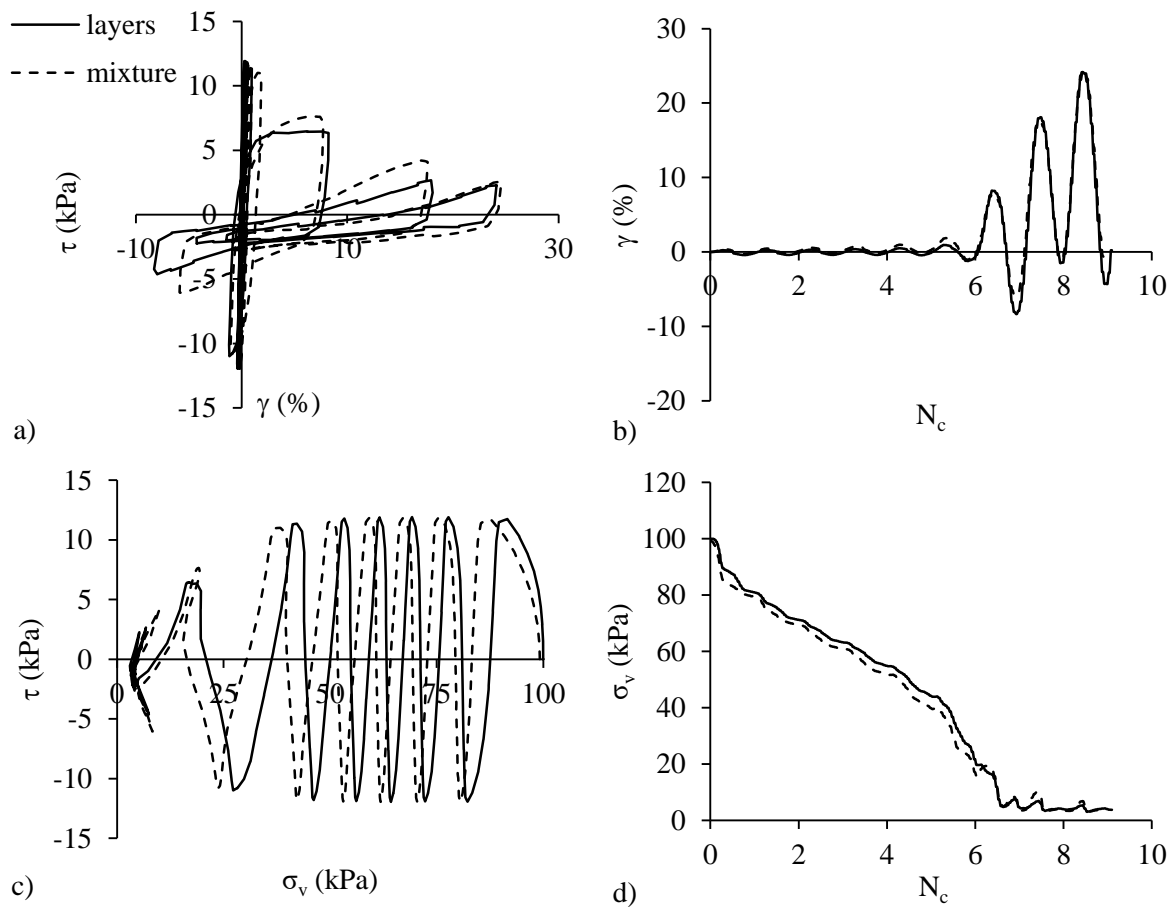
Figure 8.37 – Comparison of cyclic results of a layered and a mixture specimens, prepared to the same target void ratio: a) τ–γ; b) N_c–γ; c) τ–σ_v; d) σ_v–N_c

Additionally, another set of tests was performed, with the same layered and mixed configurations, but prepared with the same compaction, without an initial void ratio target. This meant that the same compaction effort (obtained by gently putting the soil inside the mould and tapping with a spoon to even it out) was applied to both layers. After moulding, the fines layer had a higher void ratio (1.31) than the sand layer (0.69). On the other hand, the mixture specimen had an initial void ratio of 0.98. Once again it was not possible to determine the final void ratio of each individual layer. However, the general final void ratio of the layered specimens was obtained by considering the specimens weight and final volume. The final void ratio of the layered and mixture specimens was similar (0.73 and 0.71, respectively). Figure 8.38 presents the results, reporting the stress-strain path (τ–γ), the evolution of shear strain with number of cycles (N_c–γ), the stress path (τ–σ_v), and the decay of vertical stress with increasing number of cycles (σ_v–N_c). In this case, the results of the two specimens show significant differences. The layered specimens exhibited higher resistance, and liquefaction occured after 16 cycles of loading. On the other hand, the mixture specimen liquefies at 7 cycles. The fact that the layers were compacted with the same compaction effort simulates natural sediments better, therefore, the fabric and

291

structure of the layered specimens was closer to what is found in situ. It is understood that the in situ layering, and consequently the layering found on the undisturbed specimens, is more heterogeneous than the representation in these tests. However, these findings corroborate the results of cyclic triaxial tests of undisturbed specimens, which showed that undisturbed specimens with FC > 6% are more resistant than the correspondent reconstituted specimens, as will be discussed in Chapter 10.
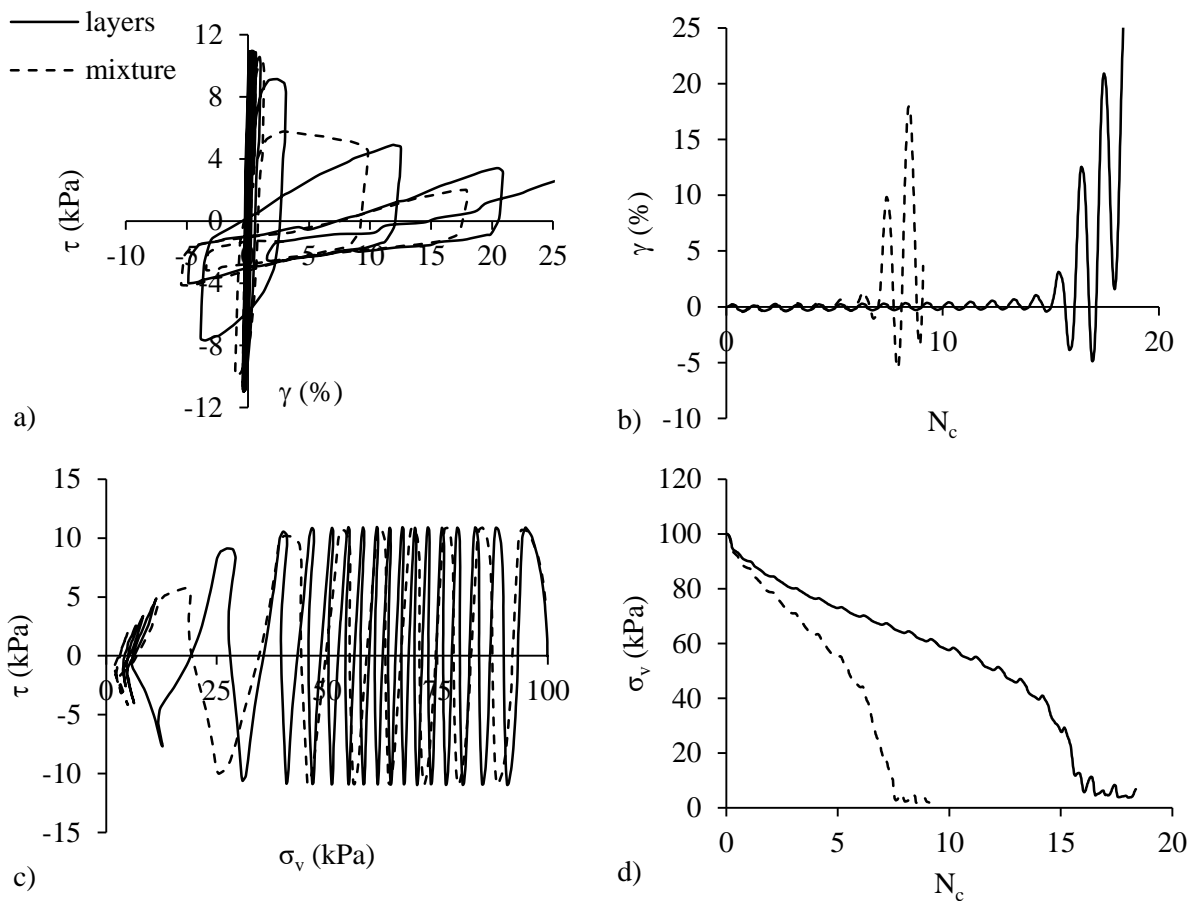
Figure 8.38 – Comparison of cyclic results of a layered and a mixture specimens, prepared with the same compaction: a) τ–γ; b) N_c–γ; c) τ–σ_v; d) σ_v–N_c

The undisturbed specimens collected with Mazier and Gel-Push samplers were composed of layered soil. However, the complex layering structures and the liquefaction of the specimens during the trixial tests prevented the determination of the void ratio of the separate layers. Despite that, due to the natural sedimentation process, it can be assumed that the layers composed of finer soils were probably less dense, with higher void ratios. The respective reconstituted specimen was prepared to simulate the global void ratio of the undisturbed specimen. Therefore, the comparison between undisturbed and reconstituted specimens is more comparable with the second pair of tests presented in this section. This discussing will be addressed later, when the undisturbed specimens results are explored. It is also important to note that the tests performed in undisturbed specimens were mainly triaxial tests, hence

the cyclic action was applied vertically and not horizontal to the layering. Future developments should focus on the performance of cyclic direct simple shear tests on undisturbed specimens, to assess the effect of layering when the specimen is subjected to horizontal cyclic loadings.

8.4. COMPARISON BETWEEN TRIAXIAL AND SIMPLE SHEAR RESULTS

In this section, the results of cyclic triaxial (CTx) and cyclic direct simple shear (CDSS) tests are compared, for the same soils in similar conditions, in terms of liquefaction resistance. The relationship between the CSR_{ss} and CSR_{tx} is defined by the factor c_r, which depends on K_0. The correlation proposed by Ishihara et al. (1985) was used (equation (2.77)) to compare the data from CTx and CSS. As discussed above, two types of simple shear tests were performed, with flexible and rigid membrane, hence the considerations are different, and the results have been presented separately.

Figure 8.39a-b presents the results for S1_M2 and S1_M7. Both the cyclic triaxial tests and the cyclic simple shear tests were performed with saturated specimens under isotropic conditions, as the CSS tests were performed with flexible membrane and $K_0=\sigma'_h/\sigma'_v=1$. The results show a good correspondence between CSR_{ss} and CSR_{tx} and are in accordance with the correlation proposed by Ishihara et al. (1985), that states that for $K_0=1$, the c_r factor is 1, hence the $CSR_{ss}=CSR_{tx}$.

293
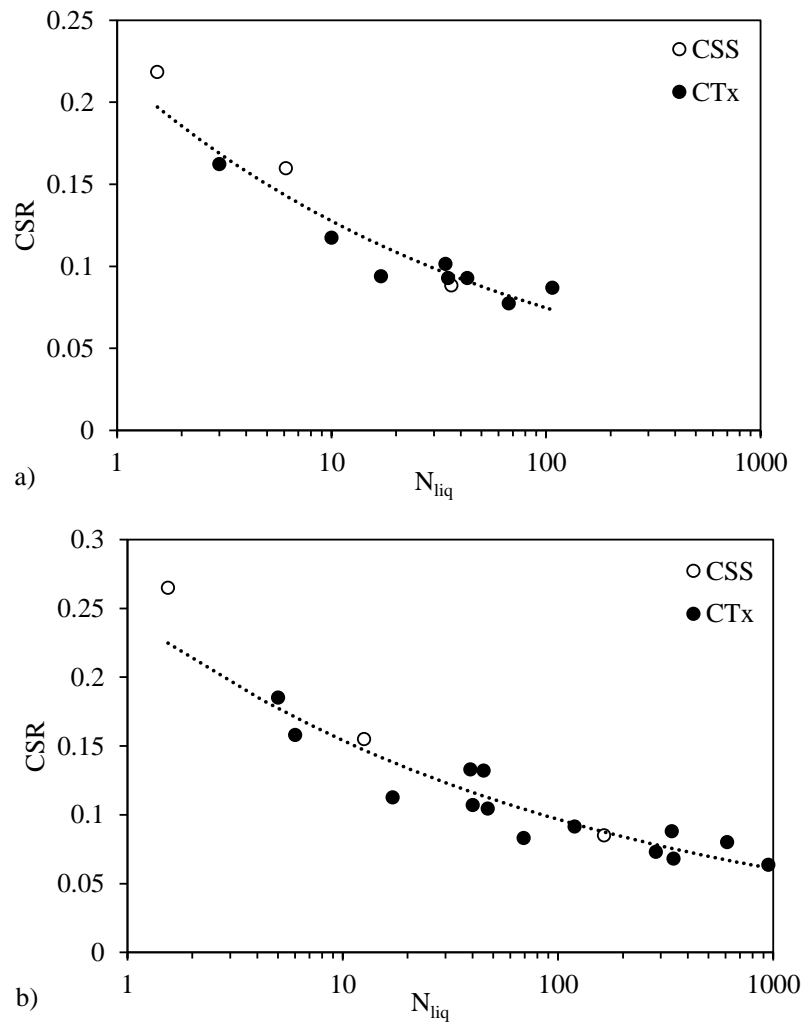
Figure 8.39 – Comparisons between CTx and CSS tests for: a) S1_M2 and b) S1_M7

The NB1 cyclic direct simple shear (CDSS) tests were performed with rigid boundary conditions. The specimens are anisotropically consolidated, as the vertical stress is imposed, and the specimen is confined laterally by a set of rings. On the other hand, the CTx tests were isotropically consolidated, hence, to make the CTx and CDSS comparable, the c_r factor must be applied. As discussed above, the c_r factor depends on K_0. However, the determination of K_0 in the laboratory is not easy, so the Jaky's formula ($K_0 = 1 - \text{sen} \phi$) was used (Jaky, 1948), where the friction angle was evaluated from the monotonic tests performed in the same conditions as the cyclic tests. Figure 8.40a presents the results of CTx and CDSS without c_r normalisation. The tests selected for comparison had similar state parameters (-0.10 to -0.05) and correspond to the tests designated by NB1_E2 and NB1_MT_sat, for CTx and CDSS, respectively. It is observed that the cyclic resistance is higher for CTx tests. Figure 8.40b presents the same results, with CSR_{tx} normalised by c_r, calculated from equation (2.77). It is verified that the results

fall on the same cyclic resistance curve, hence the c_r proposed by Ishihara et al. (1985) provides a good method to relate the results of the two types of tests.
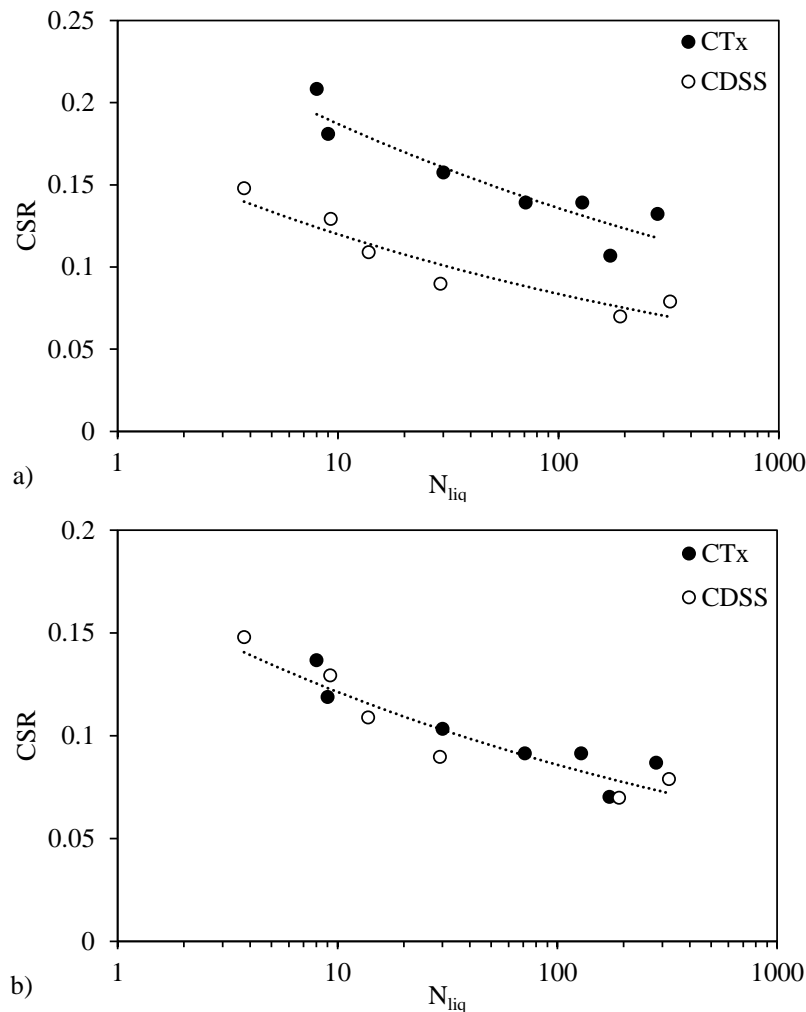
Figure 8.40 – Comparisons between CTx and CDSS tests on NB1 sand: a) without c_r normalisation; b) with c_r normalisation

Some authors presented results showing that c_r depended not only on K_0, but also on several other parameters, such as relative density, confining pressure, type of soil and fabric (Tatsuoka et al., 1986; Vaid and Sivathayalan, 1996). In the present work, there are not enough results to conclude about the influence of these parameters as the cyclic direct simple shear tests were not performed in saturated conditions (except for the results of NB1 presented in Figure 8.40) and the comparisons would not be accurate. However, the cyclic resistance curves of CSS and CTx tests corresponding to the same material were related and correlations between CSR_{ss} and CSR_{tx} based on N_{liq} were found (Table 8.6). The plot of these curves is in Figure 8.41. These results show that the c_r is not constant and varies significantly with number of cycles, as its value decreases with increase in N_{liq}. However, focusing the attention on the number of cycles that defines an earthquake motion to trigger liquefaction (15 cycles),

the values of c_r are around 1 (1.05-1.12) for S1_M2 and S1_M7, and 0.63 for NB1, which are similar to those obtained by other authors (see Table 2.4).

Table 8.6 – C_r equations depending on N_{liq} for the soils studied

Material	c_r
S1_M2	$c_r = 1.3963 N_{liq}^{-0.105}$
S1_M7	$c_r = 1.326 N_{liq}^{-0.063}$
NB1	$c_r = 0.7256 N_{liq}^{-0.052}$
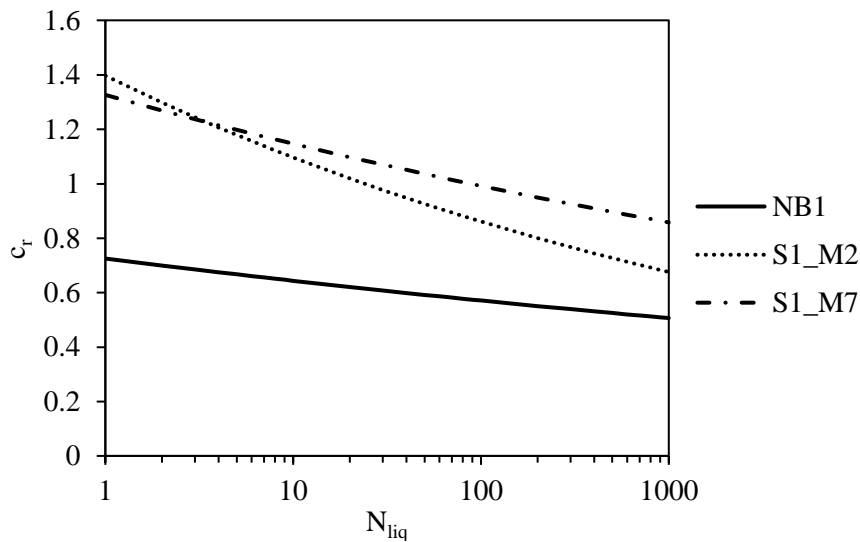
Figure 8.41 – Evolution of c_r with N_{liq}

8.5. CHAPTER SUMMARY

This Chapter presented the results of cyclic triaxial and cyclic direct simple shear tests performed on reconstituted specimens of three selected sandy soils: S1_M2, S1_M7, and NB1. The variety of parameters considered allowed the investigation of the effects of several state parameters and soil properties on the cyclic liquefaction resistance and behaviour of the three soils. Following the analysis of the results, a summary of the main findings is presented for each factor:

State parameters: The state parameters comprised the effect of void ratio and confining pressure. In the CTx tests, it was observed that slight variances in void ratio did not affect the location of the cyclic resistance curves. However, as expected, higher changes in *e* affected the cyclic resistance of soils, as loose specimens exhibited lower liquefaction resistance than denser specimens. The same trends were

observed for the CDSS tests, where small variances in e did not affect the location of the cyclic resistance curve, but for higher changes in void ratio, the NB1 soil exhibited decreasing cyclic resistance with increasing void ratio, in specimens prepared with both MT and PL. The confining pressure variation range was small, so major conclusions were difficult to make. However, it was observed that in cyclic triaxial tests performed with specimens with the same void ratio, the increase in p'_i lowered the cyclic resistance curve, hence specimens confined at lower p'_i showed higher resistance. On the other hand, in the cyclic direct simple shear tests, the consideration of confining pressure of 40 kPa, 50 kPa, or 100 kPa had no influence in the position of the cyclic resistance curve. It was concluded that specimens with lower state parameter (ψ) exhibited higher resistance, as they were located on the dense side of the CSL.

Frequency: Differences in frequency loading from 1 Hz to 0.1 Hz seemed to not influence the position of the cyclic resistance curve, as expected.

Sample preparation method: For CTx tests performed with loose specimens no difference was observed in the cyclic resistance curve, while for the CDSS tests performed with higher void ratio (denser specimens), the cyclic resistance curves from MT and PL specimens were clearly different, showing that PL specimens had lower liquefaction resistance than MT specimens. The CTx tests contradicted the expected trends found by several other authors (Mulilis et al., 1977; Tatsuoka et al., 1986). However, the specimens were prepared very loose which might have caused macropores to be present in the MT specimens, decreasing liquefaction resistance and minimizing the fabric effects that normally are reflected on the cyclic resistance of MT specimens.

Boundary conditions: The effect of boundary conditions was assessed by comparing the results of tests performed in two different simple shear devices, one where the specimens were confined by rigid copper rings and other where the specimens were confined by a flexible rubber membrane and the confinement was imposed by the cell pressure. The direct comparison between cyclic resistance curves of specimens tested with flexible membrane and rigid rings for S1_M2 was inconclusive. On the other hand, for S1_M7 specimens the flexible membrane specimens showed higher resistance than specimens tested with rigid boundary. When comparing the cyclic behaviour of flexible and rigid boundary specimens, it was observed that the secant shear modulus, G_{sec}, was higher for specimens confined with flexible membrane, which was reflected in the lower increase in shear strain in the beginning of cyclic shear. Once liquefaction occurs, the flexible membrane specimens showed higher levels of deformation. On the other hand, the pore pressure evolution was faster on the specimens confined with rigid rings, which supports the assumption that the rigid boundary specimens had lower cyclic resistance.

Water content: The effect of water content was studied for the CDSS tests, as not all specimens were saturated. The results showed a decrease in cyclic resistance with increase of water content. The higher

resistance of specimens with 3.5% water content might be related to matric suction effects due to the unsaturated state of the specimens. However, the water retention curve of the soil should be performed to confirm these effects.

Layering: The effect of layering in liquefaction behaviour was investigated for two pairs of tests. When the layered and mixed specimens were prepared to the same target void ratio (0.78), the behaviour of the two specimen was similar, and they liquefied for the same number of cycles. Similar results were found by Cappellaro (2019) that concluded that the layered structure did not result in significant differences in terms of liquefaction resistance. On the other hand, when the specimens were prepared with the same compaction effort, and consequently the initial void ratio of the fines and sand layers were different, the layered specimen exhibited higher resistance.

Laboratory device: The results of tests performed with CTx and CDSS devices were compared to evaluate the effect of the laboratory device on cyclic resistance. When the CTx and CSS tests were both performed with saturated specimens under isotropic conditions, the results showed a good correspondence between CSR_{ss} and CSR_{tx}. On the other hand, when the NB1 CDSS tests were anisotropically consolidated, they showed lower resistance than the CTx tests. However, when normalising the results of CTx with c_r, the results fell on the same cyclic resistance curve. Moreover, the value of c_r was found to decrease with the increase of N_{liq}.

Besides the effect of the factors referred above, other relevant themes were investigated, especially for the cyclic triaxial tests. The results of the small strain shear modulus found for the cyclic triaxial tests showed good agreement with the $G_{max}/F(e)–p'/p_a$ curves determined for the monotonic triaxial tests.

Additionally, the results of cyclic triaxial results were interpreted through the state parameter. The CRR_{15} for each cyclic resistance curve was determined and the results of CRR/CRR_{15}-N_{liq} showed good agreement with the correlation obtained for other soils (Jefferies and Been, 2016). Moreover, the state parameters of each curve were determined and related to the respective CRR_{15}, showing good agreement with the curve plotted using other benchmark sands. However, care should be taken when considering the relationship between CRR_{15} and ψ unique, as differences in fabric are not captured by the state parameter, and might influence the cyclic resistance of soils. Despite this, it was observed that the CRR_{15} decreases with the increase of state parameter, and tends to a horizontal asymptote for state parameters higher than zero.

The pore pressure generation was related to N_c/N_{liq} and, for each group of tests performed with similar conditions and initial parameters, the results showed good agreement, as the $r_u–N_c/N_{liq}$ curves are relatively convergent. Using the Booker et al. (1976) model, the best fit α values were computed for each specimen. The values of α that best fit the $r_u–N_c/N_{liq}$ curves measured were ranged between 0.25 and 1.18 (with averages between 0.53 and 0.78), with R^2 values higher than 0.77.

9. PHYSICAL AND GEOMECHANICAL CHARACTERISATION OF UNDISTURBED SOILS

9.1. INTRODUCTION

Part of the research programme, integrated on the FCT project LIQ2PROEARTH, was to characterise the behaviour of the soils from the Lower Tagus River Valley. Therefore, as explained before, the collection of undisturbed samples from the experimental site at different depths was an essential part of this work. The undisturbed samples collected were carefully treated in the laboratory, and prepared for the performance of advanced laboratory tests.

This Chapter aims to characterise the soils from undisturbed specimens tested under cyclic triaxial and simple shear conditions. The soils are characterised in terms of particle size distribution, particle shape parameters, and void ratio limits. Besides, some undisturbed samples were opened vertically in half and analysed for the identification of interlayers, laminations, and changes in soil type. Moreover, comparisons are made against benchmark soils tested by other authors.

As discussed in previous chapters, there was not enough undisturbed samples soil for the performance of triaxial compression tests to determine the critical state lines. Therefore, an empirical procedure was employed to assess the CS parameters based on e_{max} and e_{min}. The estimated CS parameters are compared and framed within the previous results and benchmark soils tested by other authors. The cyclic liquefaction behaviour of these materials is discussed later in Chapter 10.

9.2. MATERIAL PROPERTIES

The materials used in this work have variable properties, as they represent natural soils collected in heterogeneous profiles with interlayers. Therefore, when presenting the material properties, distinction between the four experimental sites is made. Moreover, the materials properties are compared with other published data, to frame these soils among other benchmark soils.

9.2.1. GRAIN SIZE, ATTERBERG LIMITS, AND SPECIFIC WEIGHT

Grain size analysis is crucial to assess soil type and is one of the first tests performed to characterise a material. On the other hand, the specific weight is essential to reconstitute samples to a required void ratio and for the correct determination of void ratio at the end of the saturated tests. Therefore, the grain size analysis and specific weight were determined for all soils tested in this work, according to the standards described in Chapter 6.

The first grain size analyses were performed in soil collected with the SPT tube, to have a more clear idea of which soils were at each depth and to compare with the fines content and soil type obtained empirically by the CPTu tests. This procedure was only applied to the S1 and S2 profiles, as these were the ones were SPT tests were performed. Figure 9.1 presents the grain size curves determined with the SPT soils for S1 and S2. As expected, it is observed that there is a great variety of soil types, from sands to clays. Table B.1 and Table B.2 in Appendix B present the detailed results of the grain size characteristics of these soils and the Atterberg limits of the finer soils.
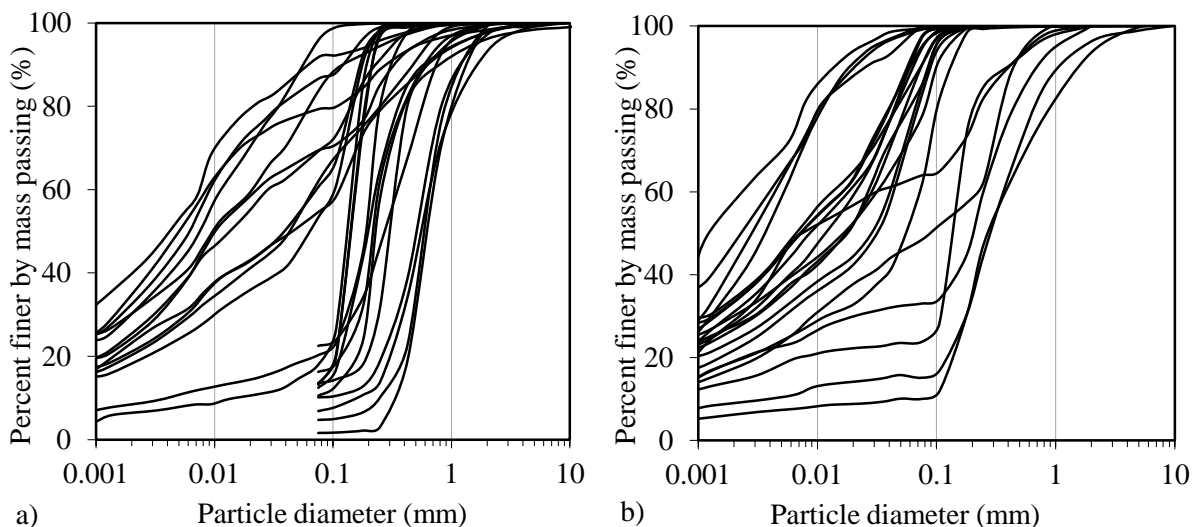
Figure 9.1 – Grain size distribution of SPT soils from: a) S1; b) S2

After performing the triaxial tests with the undisturbed samples, the soil was collected, homogenised and dried. Figure 9.2, Figure 9.3, and Figure 9.4 present the grain size distribution (GSD) curves of the soils tested under triaxial conditions, collected with both Mazier and Gel-Push samplers in S1, S2, NB1 and NB2. The GSD curves of the soils discussed in Chapter 7 are represented with a different colour (orange) to frame them among the other soils. The samples were selected based on the CPTu results, and as the objective was to assess liquefaction resistance, the aim was to select samples with sand and silts. This is the reason why the clayey soils captured by the SPT grain size analysis above are not represented, as few triaxial tests were performed on those soils.

Especially on S1 and S2 soils, there is a clear variety of grain size curves, with samples within a range of fines content between 2.1% and 39.9%. Excluding some specimens with higher fines content, the majority of specimens tested are poorly graded sands with very steep grain-size distribution curves framed mostly between 1.0 and 0.1 mm. The detailed results of the grain size characteristics of each specimen are presented in Table B.3. Table 9.1 presents the ranges of fines content (FC), percentage of clay, mean grain size (D_{50}), specific gravity (G_s), coefficient of shape (C_C), and coefficient of uniformity (C_U) for the different experimental sites. The specific gravity of soils ranges between 2.60 and 2.69, which was expected for sands mainly composed by quartz. The Atterberg limits test were not performed as the majority of the samples selected for the cyclic triaxial tests were mostly sands and the fines were non-plastic, as assessed in the samples from the same depths collected with the SPT tube.
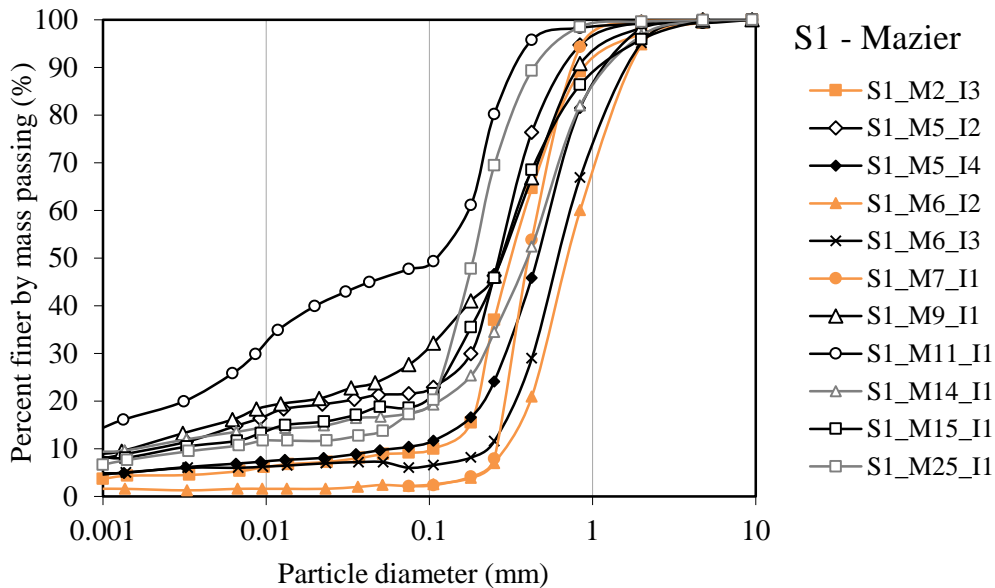
Figure 9.2 – Grain size distribution of soil samples collected from S1 with Mazier sampler tested under cyclic triaxial conditions
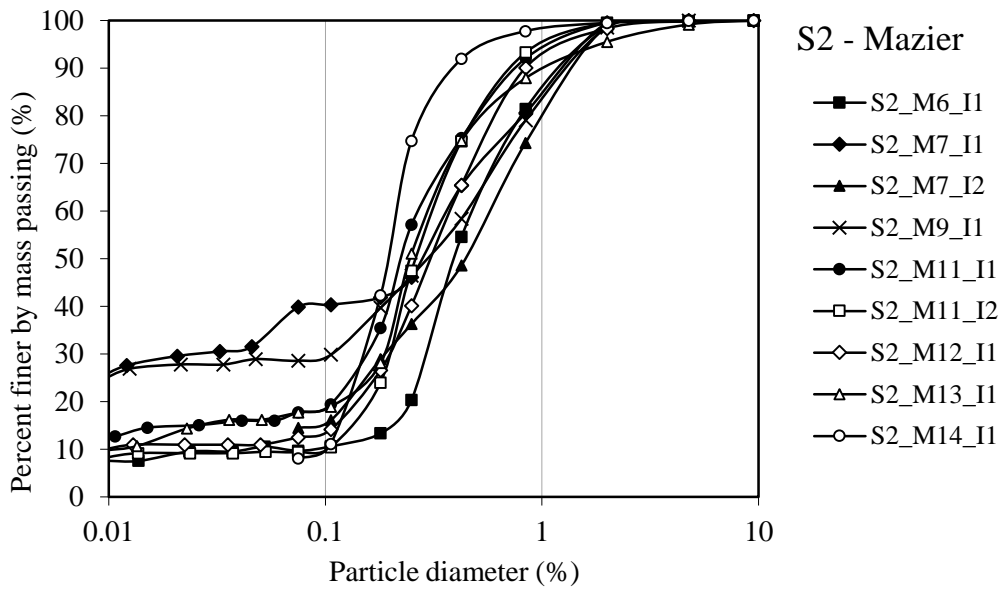
Figure 9.3 – Grain size distribution of soil samples collected from S2 with Mazier sampler tested under cyclic triaxial conditions
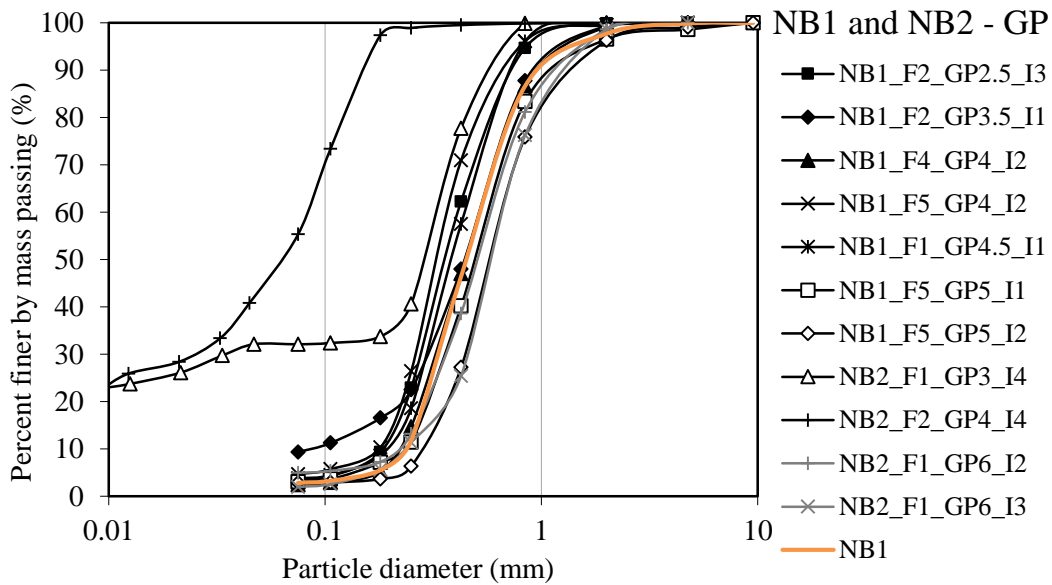
Figure 9.4 – Grain size distribution of soil samples collected from NB1 and NB2 with Gel-Push sampler tested under cyclic triaxial conditions

Table 9.1 – Ranges of parameters in each experimental site

Site	FC (%)	Clay percentage (%)	G_s	D_{50} (mm)	C_C	C_U
S1	2.1 - 27.6	1.5 - 11.4	2.615 - 2.690	0.185 - 0.7	0.89 - 56.9	1.81 - 294
S2	8.0 - 39.9	5 - 16.5	2.620 - 2.692	0.20 - 0.4	1.11 - 24.5	2.10 - 450
NB1 and NB2	2.0 - 55.3	GSC performed by sieving	2.601 - 2.689	0.065 - 0.6	0.86 - 7.6	2.06 - 330

9.2.2. PARTICLE SHAPE

The particle shape parameters were obtained using the Morphologi G3 equipment, available at the University College London. As described in section 6.2.2, the equipment scans the individual soil particles and provides information about its shape.

The Morphologi G3 provides useful information about shape parameters such as circularity, solidity and aspect ratio. These shape factors describe the particle in terms of form and angularity. The circularity is a measure of the closeness to a perfect circle (i.e. the perfect circle has a circularity of 1). The solidity describes the compactness of the particle, while the aspect ratio (AR) is a relationship between the width and length, so the more elongated the particle, the lower is its AR. The results of each soil are represented in particle shape distributions based on cumulative volume, maintaining the consistency of using sieve weights. The representative value selected was at 50% of cumulative volume, similar to the determination of the mean grain size, D_{50}. The tabulated results of these shape factors are presented on Table B.3 of Appendix B. The circularity values range from 0.86 and 0.90, the solidity ranges from 0.945 and 0.973, and the aspect ratio ranges from 0.70 and 0.79. This means that in general, all soils have particles with shape close to a circle and not very elongated.

The Morphologi G3 does not allow the determination of particle roundness, however Altuhafi et al. (2013) proposed a graph correlating sphericity and convexity in QicPic (which correspond to circularity and solidity in Morphologi G3, respectively) and defined angularity zones. The results were plotted in this graph (Figure 9.5). It is observed that clean sands (soils with FC < 5 %) particles are rounder than particles of soils with higher FC. The shape of particles might be a consequence of the mineralogy of the soil, as soils with higher FC might be composed by higher percentages of orthoclase and muscovite, minerals that are typically more elongated, while soils with lower FC might have higher percentage of quartz minerals. Nonetheless, all soils tested were classified as either subangular or subrounded, probably due to their transportation and sedimentation processes.
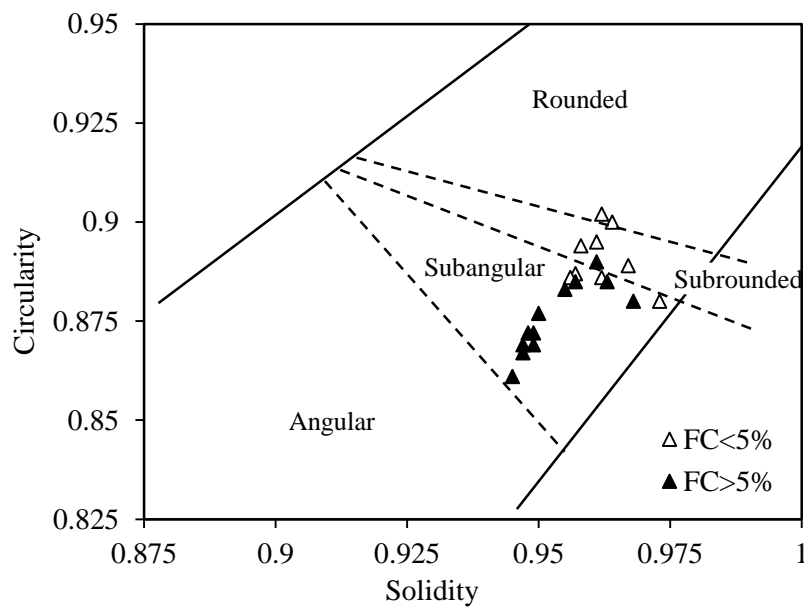
Figure 9.5 – Shape results from the selection of undisturbed specimens collected plotted on the angularity zones plane proposed by Altuhafi et al. (2013)

9.2.3. VOID RATIO LIMITS

The maximum and minimum void ratios of all soil samples were obtained using the Japanese Geotechnical Society (JGS) method. Although the JGS method is recommended for clean sands with FC < 5%, it was selected in this work for two main reasons. The first was the small quantities of each soil sample available that were not sufficient to determine the maximum and minimum densities according to the ASTM procedures. The other reason was the recommendation of Cubrinovski and Ishihara (2002) that stated that the method was applicable for soils with FC < 30%. As most soil samples tested had FC lower than 30%, the method was considered appropriate. Moreover, the correction proposed by Ishihara et al. (2016) was used to adjust the minimum void ratio according to the respective fines content (refer to section 6.2.3). Regardless of these cares, all values were determined with the same method, enabling comparisons between the results.

The tabulated results of the maximum and minimum void ratios are presented in Table B.3 in Appendix B. Figure 9.6 provides the results of e_{max} and e_{min} plotted against the fines content. A trend of increasing e_{max} with FC is observed, and e_{max} ranges from 0.713 and 1.583. On the other hand, the values of e_{min} are located within the small range of 0.47 and 0.69, and no clear trend is identified. The scatter of the results does not allow the identification of a fines transition zone (Figure 2.50). However, the limiting fines content is probably low, below 20%. The difference between e_{max} and e_{min} with fines content is presented in Figure 9.7, where the increase with FC is observed. This is due to the higher increase in e_{max} with increase in FC, which does not occur in e_{min}. The mean grain size, D_{50}, is also related to FC

(Figure 9.8), and as expected it decreases with increase of fines content, due to the high degree of uniformity of these soils.
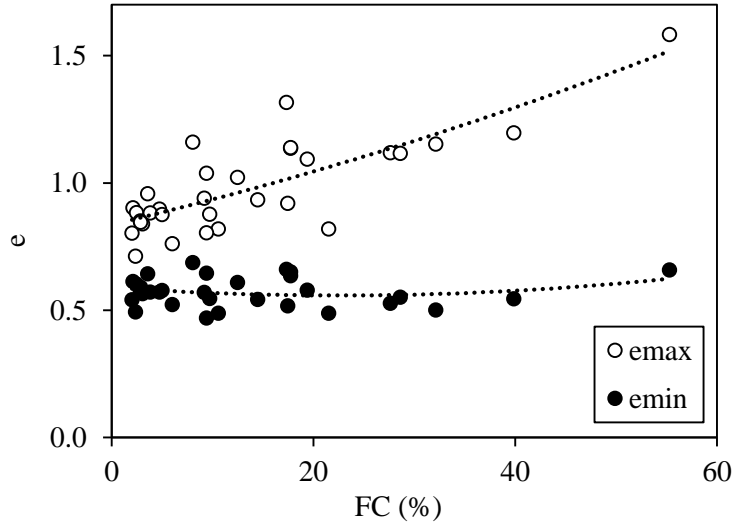
Figure 9.6 – Variation of void ratio limits with fines content
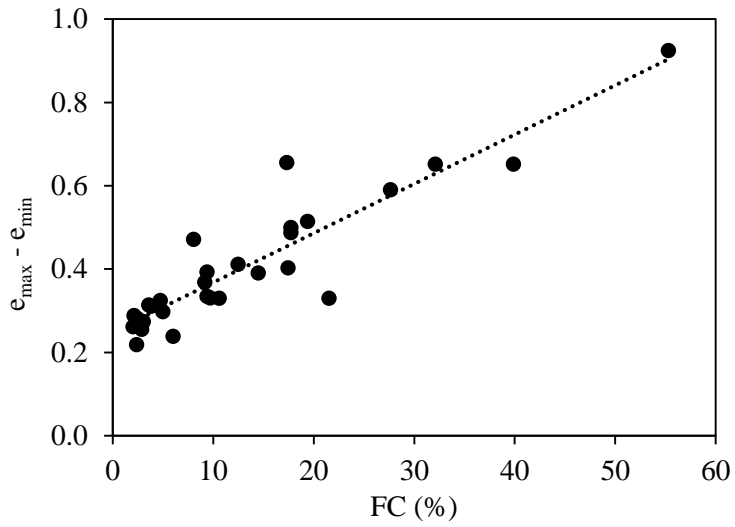
Figure 9.7 – Variation of void ratio limits with fines content
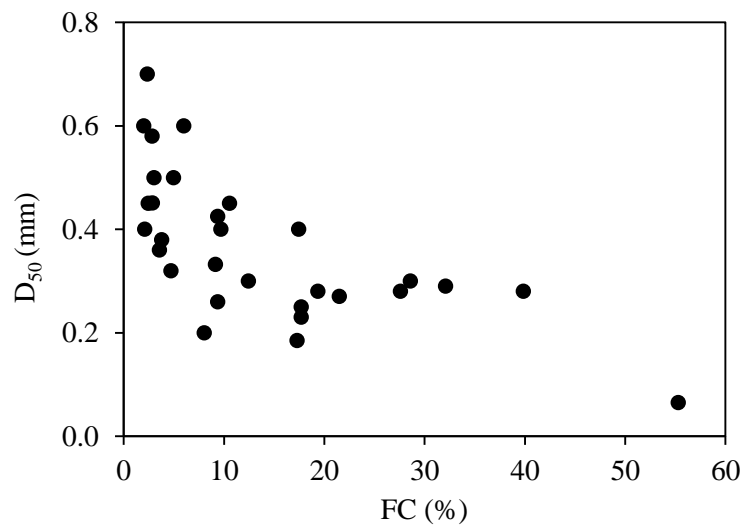
Figure 9.8 – Variation of D_{50} with fines content

9.2.4. VISUAL INSPECTION OF SELECTED UNDISTURBED SMAPLES

The cyclic triaxial tests performed on undisturbed specimens collected with the Mazier sampler showed clear impact on soil behaviour due to differences in fines content and fabric, as is discussed in Chapter 10. However, to perform the triaxial tests, the specimens were used directly from the sampling tube and the identification of the structure of each specimen, regarding interlayers and lamination, was not possible. Therefore, a selection of specimens were opened vertically, to document the internal structure of the specimens and identify interlayers, laminations, or changes in soil type. The samples selected correspond to depths where transitional layers between sands and fine soils were identified in the CPTu I_c profile. However, it is known that the cone tip resistance (q_t) and sleeve friction (f_s) measurements are influenced by the volume of soil around the cone tip. The q_t measurements might be affected by influence zones of 0.35-1.3 m thickness, hence the measurements depend on the soil sequence and properties (Mayne, 2007; Boulanger and DeJong, 2018). For that reason, the CPTu acts like a filter and smooths the interfaces of interlayers, failing to detect very small layering, as the laminations presented in the laboratory samples (with heights around 0.14 m). Therefore, opening some samples to analyse the actual interlayers and laminations is crucial for the understanding of these soils behaviour.

The photographs of the samples are presented in this section, and an attempt is made to identify changes in soil type, and the interlayers and laminations that can be recognised with the naked eye are discussed, as well as the possible causes of their existence. The examined samples were collected at the S2 site, at different depths. The samples are identified with the site and collection depth, according to the sample name definition presented in Figure 6.14.

Figure 9.9 shows a photograph of sample S2_M9. The sample is mainly constituted by clay, with fine grey sand identified on the top. The identification of clear interlayers is very difficult, however it is

observed that parts of the sample are clay and other parts are sand, mixed together. There is a clear clay centre, marked with a white shape, surrounded by a mixture of sand and clay. On the side of the PVC tube, a brown sand is observed, which was probably dragged during the Mazier rotation and does not reflect the original deposition of the soil strata.

Figure 9.9 – S2_M9 sample

Sample S2_M12_I2 is presented in Figure 9.10a. The sample is constituted mostly by brown sand with thin layers of finer soil, inclined diagonally, as marked by the white shapes. The sample has some small shells, probably due to the sedimentation process of the alluvial soils, where sea and fluvial creatures inhabited. On the other hand, in sample S2_M12_I3 (Figure 9.10b), some interlayers are visible with 1-2 mm thickness. The specimen might be divided into some larger layers, with coarser sand on top and finer sand in the middle and bottom. Moreover, a grey sand core is observed on the bottom of the sample.

Parts of the samples were collected and mixed, to determine the grain size distribution curves for each undisturbed sample (Figure 9.11). The S2_M12_I1 sample was the one tested under triaxial conditions. The fines content of S2_M12_I1 and S2_M12_I2 are similar (around 10%), while the FC of S2_M12_I3 is lower (6%). Despite having lower FC, the S2_M12_I3 has more fine particles in general, as 70% of the retained particles are located left of the other two curves.
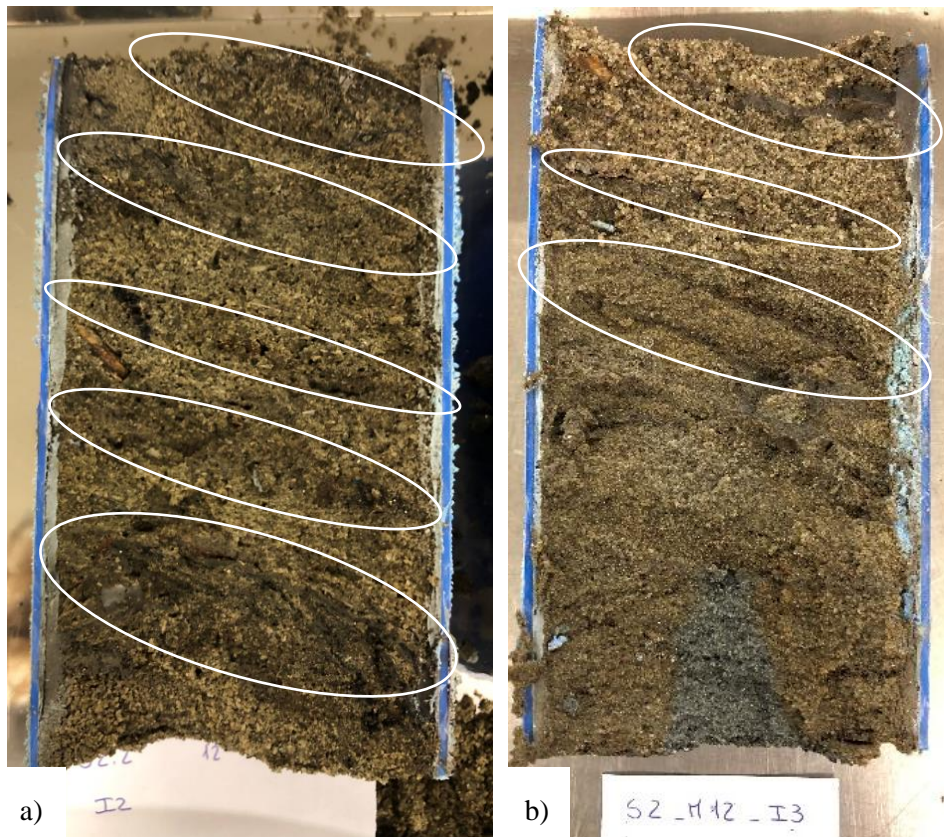
Figure 9.10 – a) S2_M12_I2 sample; b) S2_M12_I3 sample
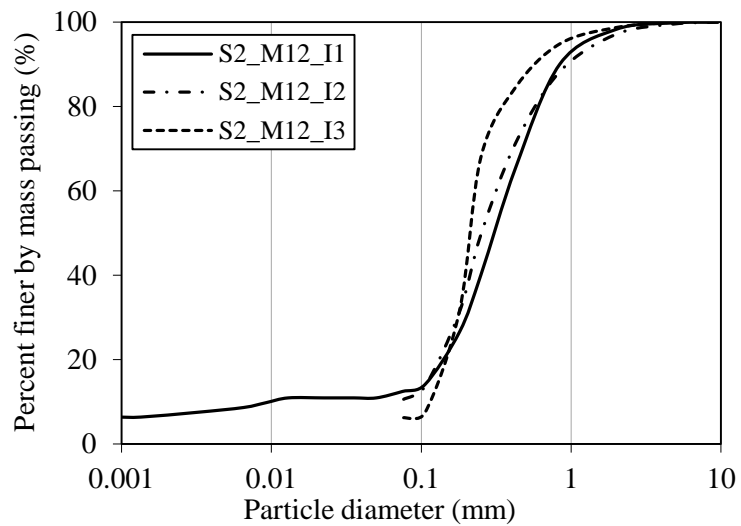
Figure 9.11 – Grain size distribution of S2_M12 soils

Figure 9.12a shows the S2_M13_I2 sample. There is no evidence of macroscopic interlayers, however, some gas bubbles are detected, maybe due to the presence of living organisms. There seems to be two types of sand, one dark grey and another brown. The sampling procedure might have dragged soil from above, identified on the sides of the sample. Some shells and small thin layers of clay (2-3 mm) are also observed. The S2_M13_I3 sample (Figure 9.12b) is mainly composed of fine sand, with two clearly different colours, brown and grey. There is brown sand on the sides of the sample, probably due to the sampling procedure, as already observed for other samples. The brown sand parts in the middle and top of the sample might be caused by the sedimentation process or the presence of organic matter (vegetation) that changed the soil colour.

Figure 9.12 – a) S2_M13_I2 sample; b) S2_M13_I3 sample

The grain size curves are illustrated in Figure 9.13. S2_M13_I2 and S2_M13_I3 are similar in terms of fines content (11.6% and 11.34%) and shape, showing high uniformity of particles size. On the other hand, the S2_M13_I1 sample (the specimen tested under triaxial conditions) has higher fines content but generally coarser particles, as its curve is located on the right.
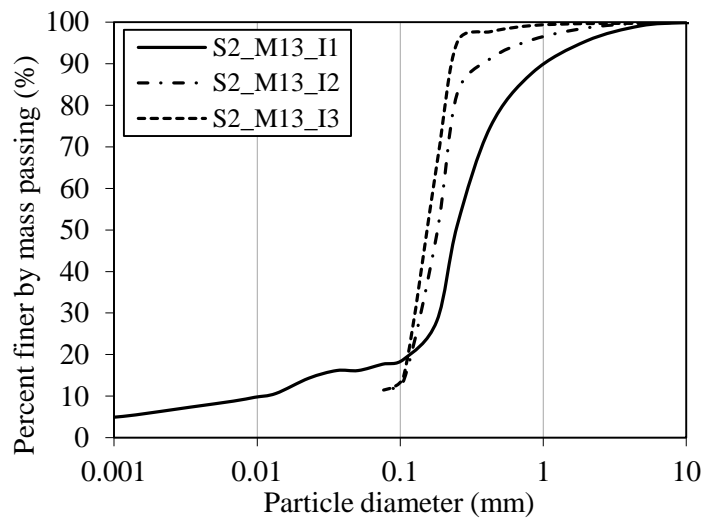
Figure 9.13 – Grain size distribution of S2_M13 soils

The S2_M14_I2 sample is shown in Figure 9.14a, where two different types of sand are observed, one brown and another grey. Some dragging of sand from the upper layers is observed, with brown sand accumulated on the edges. The S2_M14_I3 sample (Figure 9.14b) seems to be composed of finer soil, with a dark grey colour. Small horizontal and vertical microlayers are identified, with a brownish colour, but they were hard to detect with the naked eye.

The grain size curves for S2_M14 samples are presented in Figure 9.15. S2_M14_I1 and S2_M14_I2 curves are similar in terms of fines content (8.03% and 8.72%, respectively), however, the triaxial test curve presents more particles with lower diameter, as it is a finer soil in general. S2_M14_I3 soil has a higher fines content of 25%, confirming the prediction based on visual inspection.
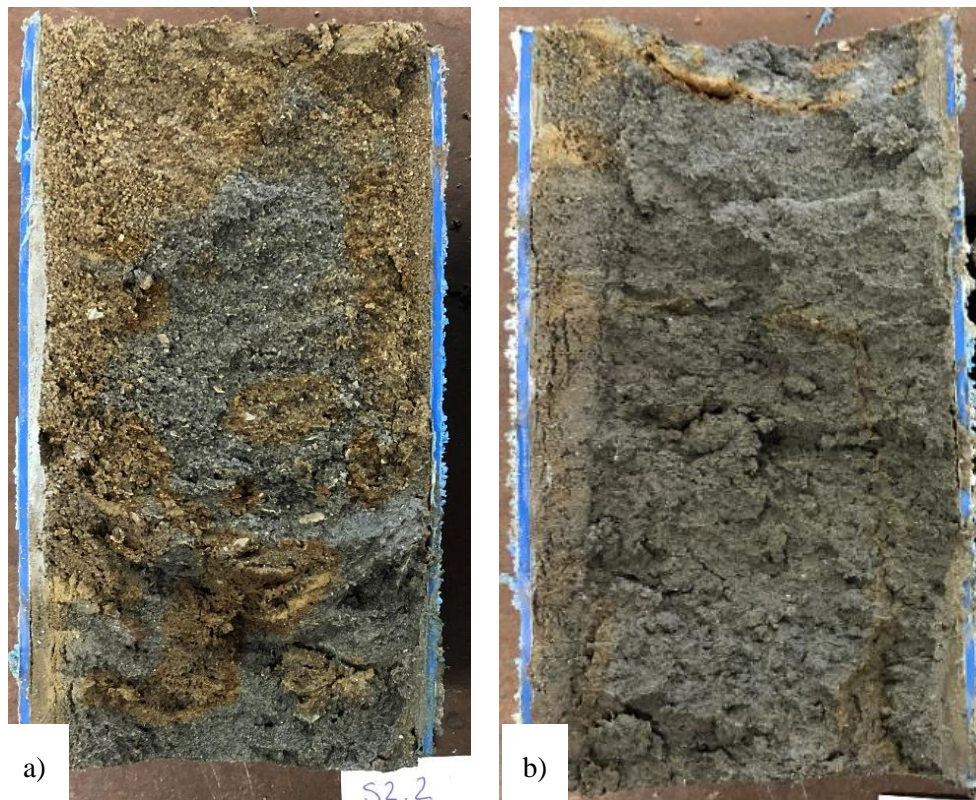
Figure 9.14 – a) S2_M14_I2 sample; b) S2_M14_I3 sample
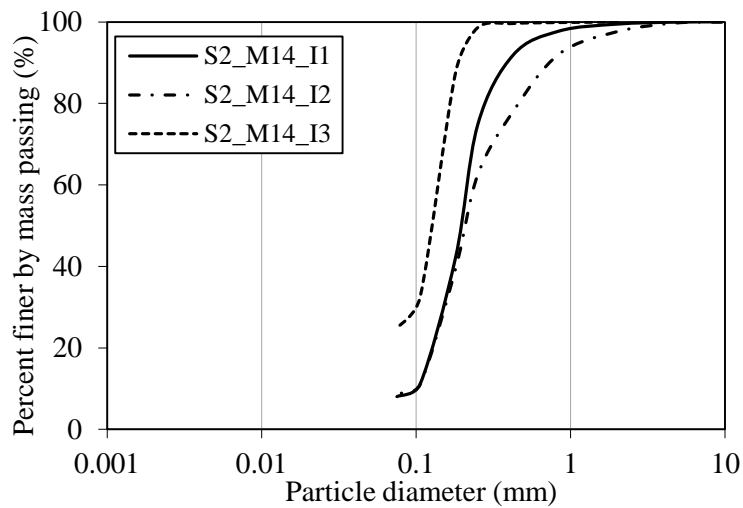
Figure 9.15 – Grain size distribution of S2_M14 soils

9.2.5. COMPARISONS WITH PUBLISHED DATA

Many researchers have focused their work on relationships between material properties, mainly how the soil gradation parameters can be related to each other and how the particle shape might affect the soils mechanical behaviour. A compilation of data from a variety of natural soils already published by other authors was used for comparison with the soils studied in this work. The main data sources were

Cubrinovski and Ishihara (2002), that studied the maximum and minimum void ratio characteristics of sands, and Cho et al. (2006), Altuhafi et al. (2013), and Altuhafi et al. (2016), that focused on the effect of particle shape on the mechanical behaviour of soils, namely on the critical state parameters. Summary tables of the benchmark soils used in the comparisons are presented in Appendix B. For the comparisons with data from Cubrinovski and Ishihara (2002), e_{min} was not adjusted with the correction from Ishihara et al. (2016) as they used results obtained with the JGS method and did not consider this correlation.

The void ratio characteristics of the soils studied in this work were compared with data from Cubrinovski and Ishihara (2002) and Cho et al. (2006) that compiled the results of a variety of sands with different fines content. Figure 9.16 shows the variation of void ratio limits (e_{max} and e_{min}) with fines content. The soils studied in this work show good agreement with the other soils, especially when comparing the minimum void ratios. The maximum void ratio values seem to be slightly lower, which is reflected on the lower void ratio range represented in Figure 9.17. However, this tendency is more significant for lower fines content, as for FC higher than around 20% the values of this study show good agreement with other sandy soils. The effect of lower void ratio range for soils with lower FC might be explained by the grain shape, as Miura et al. (1997) showed that the void ratio range increases with increasing angularity of sands. As observed in Figure 9.5, the sands with lower fines content had rounder particles, with higher values of circularity and solidity, hence they would have lower void ratio range. The data from Cubrinovski and Ishihara (2002) did not include angularity or roundness indices which hindered the comparisons between particle shapes. However, when comparing the void ratio ranges with benchmark sands from the database of Altuhafi et al. (2016) in Figure 9.18, it is observed that the sands studied in this work are well framed within other sands in terms of circularity and void ratio ranges.
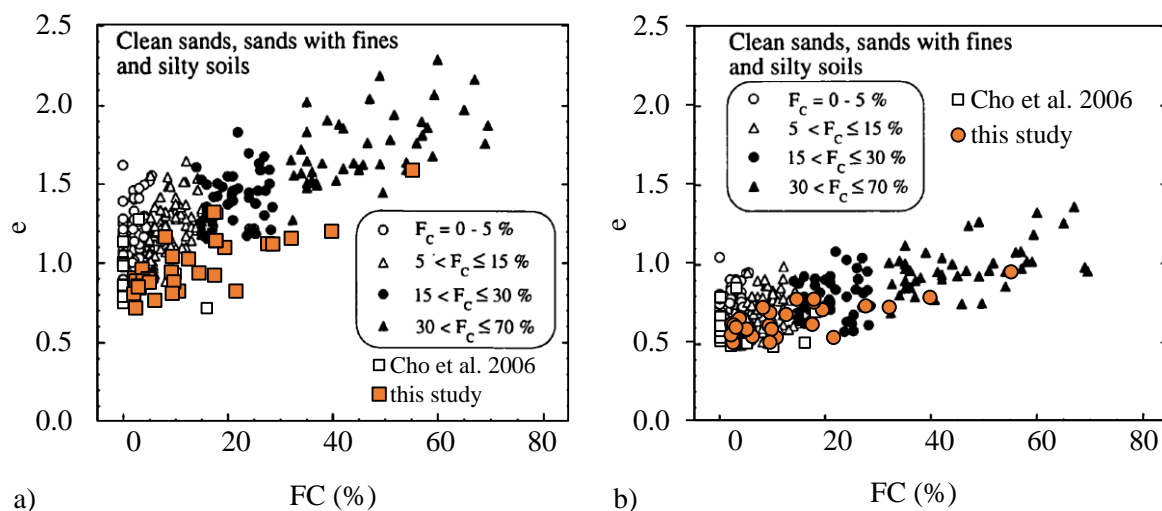
Figure 9.16 – Effect of fines content on void ratio limits: a) e_{max} and b) e_{min}
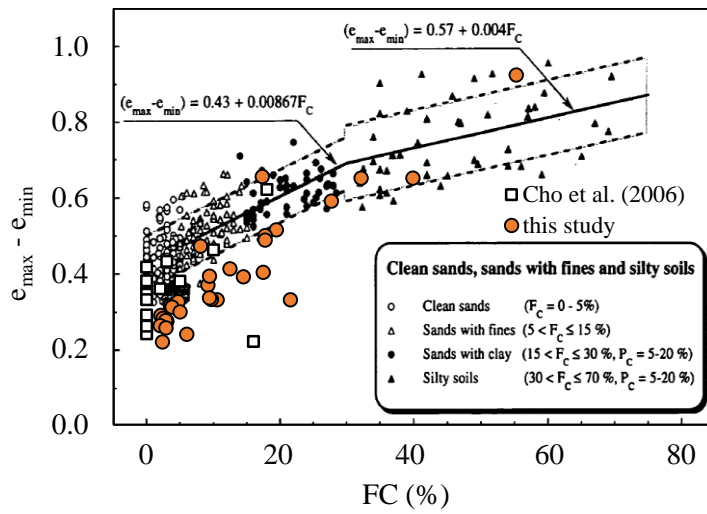
Figure 9.17 – Variation of void ratio range with fines content: comparison with benchmark sands
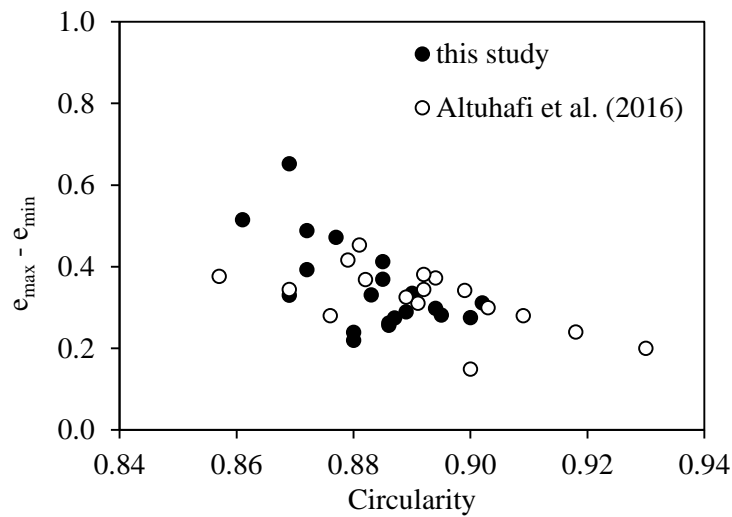
Figure 9.18 – Variation of void ratio range with circularity

The packing characteristics were also related to the grain size of the soils, by plotting $e_{max}-e_{min}$ against the D_{50}. The data from this study falls within the trend from Cubrinovski and Ishihara (2002), as illustrated in Figure 9.19.
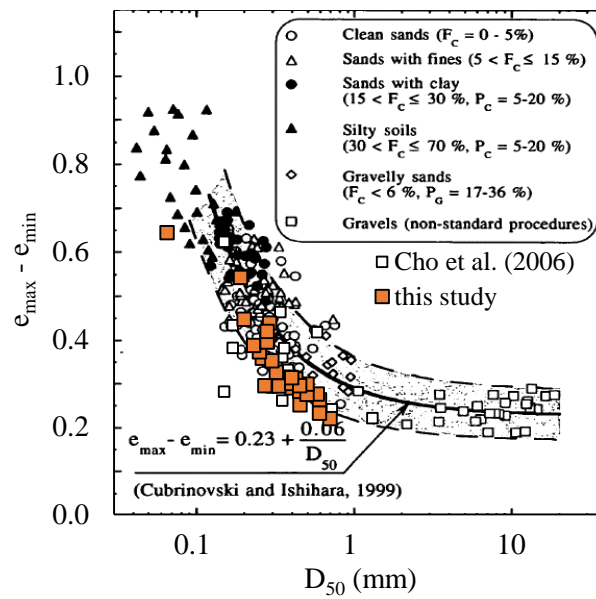
Figure 9.19 – Relationship between mean grain size D_{50} and void ratio range: comparison with other sandy soils (Cubrinovski and Ishihara, 2002)

The results of the variation of void ratio limits with different shape parameters of the soils from this study and some benchmark uniformly graded silica soils (selected from the database presented by Altuhafi et al. (2016) and summarised in Table B.4) are presented in Figure 9.20. The shape parameters studied were the circularity, solidity, and aspect ratio, as well as the parameter SAGI introduced by Altuhafi et al. (2016) to identify the angularity group based on the aspect ratio, circularity, and solidity. The SAGI value increases with the increase in soil particles angularity.

It is known that the packing ability of a soil depends on the grain size distribution and the particle shape. In this case, the values of e_{max} and e_{min} decrease with increase of solidity, circularity, and aspect ratio, which was also verified by other authors (Youd, 1973; Cho et al., 2006; Altuhafi et al., 2016). In general, it is observed that the data from this study falls within the trends defined by the benchmark soils. Despite the different fines content and consequent differences in e_{max} and e_{min}, it is observed that the shape parameters of the soils studied in this work are within a small range as they all come from the same sites and suffered similar transportation and sedimentation processes.
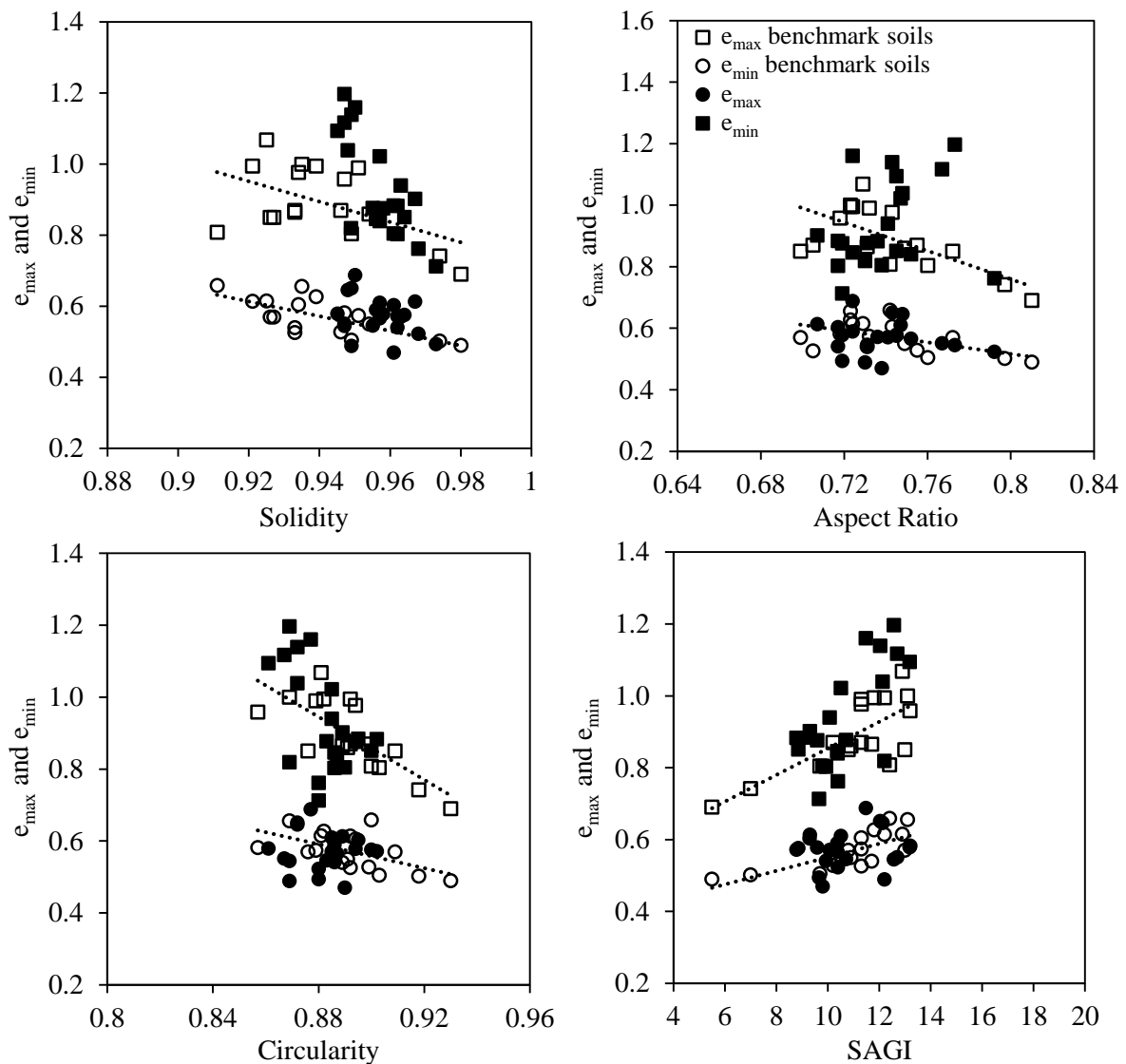
Figure 9.20 – Effect of shape parameters and SAGI on e_{max} and e_{min}

9.3. ASSESSMENT OF THE CSL OF MAZIER AND GEL-PUSH SAMPLES

Previously, in Chapter 7, the critical state lines of four soils were determined based on the results of drained compression triaxial tests. The specimens were prepared with either moist-tamping or air pluviation, but they all consisted of homogeneous profiles. However, it is known that natural soil is rarely homogeneous, and is often subjected to layering or lamination (Yoshimine and Koike, 2005), which influences the position of the CSL. In this work, no monotonic triaxial tests were performed using undisturbed specimens, so their CSL had to be determined using empirical correlations with material properties. Besides, the definition of the CSL requires at least three tests at different state conditions for the exact same soil, which is not reliable to do with undisturbed samples.

As discussed above, the critical state parameters vary widely depending on grain size, particle shape and void ratio limits (Poulos et al., 1985; Been and Jefferies, 1985) and can be correlated with different material properties. Cubrinovski and Ishihara (2000) proposed a methodology to estimate the critical state parameters from the maximum and minimum void ratios, based on a database of 52 sandy soils, with particle shapes ranging from rounded to angular. Both the slope (λ) and void ratio intercept (Γ) of the critical state lines are computed according to the void ratio range depending on the particle shape.

Figure 9.21 presents the relationships between the CSL slope and void ratio limits range of the sands studied by Cubrinovski and Ishihara (2000) separated according to the particle shape, together with benchmark sands from Cho et al. (2006), which results are in Table B.5 of Appendix B. Moreover, the results from the 4 sands tested within this study are also presented. The results from this study are closer to the angular particles trend, located higher than the rounded particles, which was expected as the soil particles were classified as sub-angular and sub-rounded according to the angularity zones plane proposed by Altuhafi et al. (2013).
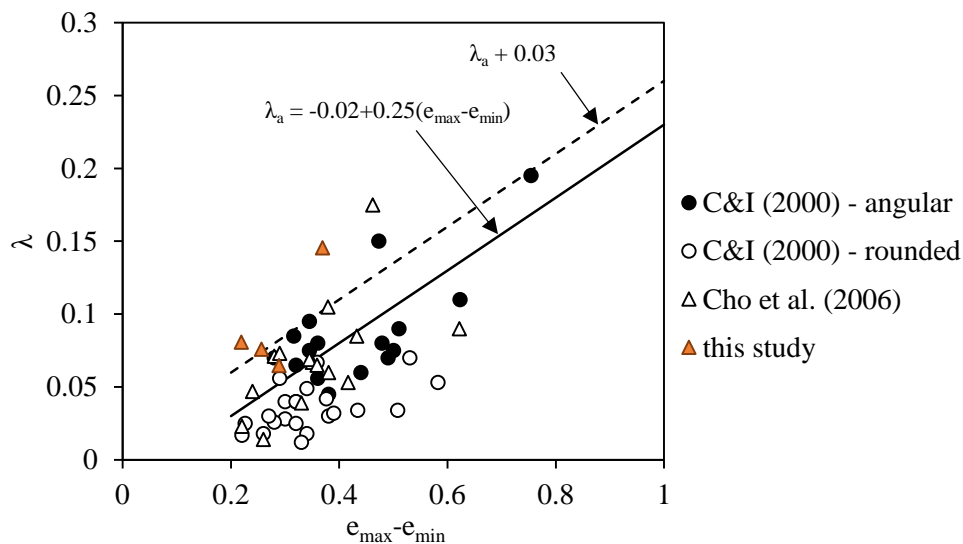
Figure 9.21 – CSL slope as function of void ratio range

Equation (9.1) was used to compute the slope of the CSL of the undisturbed specimens, as it fit the results of the S1 and NB1 soils. The equation is based on the proposal from Cubrinovski and Ishihara (2000) for angular sands, and considers the upper boundary as S1 and NB1 soils are located slightly above the other angular sands. The equation choice was based on the fact that the majority of undisturbed specimen's soils were classified as sub-angular or sub-rounded (see Figure 9.5). Besides, the CSL of natural soils with laminations and layering (reflected on the CPTu profiles and on the fines content present on the samples collected) are often located above and on the right of the CSL of

homogeneous soils (Yoshimine and Koike, 2005), hence the selection of the upper boundary to compute λ.

$$\lambda = -0.02 + 0.25(e_{max} - e_{min}) + 0.03 \tag{9.1}$$

The void ratio intercept was computed with the correlation of relative density at the steady state line, D_{ro} also proposed by Cubrinovski and Ishihara (2000). The procedure is described in equations (9.2), where D_{ro} is computed from the void ratio range, e_0 is the threshold void ratio that identifies the conditions for flow with zero residual strength, and e_1 corresponds to the void ratio intercept when p' equals 1 kPa (in this work represented by Γ).

$$\Gamma = e_1 = e_0 - 0.01 + \lambda$$

$$e_0 = e_{max} - \frac{D_{ro}(e_{max} - e_{min})}{100} \tag{9.2}$$

$$D_{ro} = -40 + 140(e_{max} - e_{min})$$

Using the method described above, the values of CS slope and reference void ratio for the undisturbed specimens soils were obtained and are presented in Table B.6 in Appendix B. The results of the critical state line parameters of all the undisturbed specimens tested were compared with benchmark sands and framed within the previous results in terms of void ratio, grain size characteristics, and shape factors. Figures with the results were included in Appendix B.

In general, the results fit well with the trends defined previously, which confirms that the decisions made were valid. In terms of void ratio limits, the estimated CS parameters follow the trends proposed by Cho et al. (2006) based on the packing ability of a variety of benchmark sands, as an increase in the range of e_{max} and e_{min} increases the slope of the CSL and the increase in e_{max} and e_{min} individually increases the CS intercept value. Moreover, the new CS parameters values strengthen the tendencies defined in Figure 7.13, in which both CS slope and intercept decrease with increase in mean grain size, D_{50}, and increase with increase in the coefficient of uniformity, C_U, and fines content, FC. However, it should be noted that the undisturbed specimens have, in general, higher fines content and grain size distributions positioned at the left of the four sands studied, hence the C_U values are higher. Some scatter is observed when comparing CS parameters with C_U, especially for lower values of C_U.

As for the shape parameters, similarly to what was verified before, there is not a good correlation between them and the slope of the CSL. On the other hand, the CS intercept values are well framed within the previously defined trends and its value decreases as the particles roundness increases (defined as increasing values of circularity, solidity, and aspect ratio and decreasing SAGI).

Zhang et al. (2020) studied the influence of particle shape and mineralogy on the particle strength, breakage and compressibility, and concluded that the mineralogy played a minor role but the particle shape influenced the compressibility behaviour of the soils. By comparing four sands, they found that the increase in aspect ratio and sphericity (similar to circularity) was reflected on an increase in strength and yielding stress, which was considered the point of maximum curvature on the e-logσ_0. Besides, the initial void ratio was lower on the rounder soil, which is in agreement with the results found in this work as the CS intercept (Γ) decreased with increase in aspect ratio and circularity. The curvature of the compressibility line might be correlated to the slope of the CSL as the two lines are assumed parallel. Zhang et al. (2020) found that the slope of the lines increased with decrease in aspect ratio and sphericity, suggesting that the slope of the CS (λ) would decrease with increase in AR and circularity. However, the results relating λ to the shape parameters were scattered and trends between shape parameters and λ were not found.

More recently, Torres-Cruz (2019) collected a database of 149 non-plastic soils with FC ranging from $0 - 100\%$, to identify trends between critical state parameters and index properties. The critical state parameters used were the CS slope (λ) and Γ_{100}, which corresponds to the void ratio of the critical state when p'=100 kPa. The results showed a strong correlation between Γ_{100} and e_{min}, but a weak $\lambda-e_{min}$ correlation. The estimated CS parameters of the soils studied in this work were compared with the results from Torres-Cruz (2019) and are presented in Figure 9.22. It is observed that the estimated CS parameters show a very good agreement with the trends defined by Torres-Cruz (2019), especially the $\Gamma_{100}-e_{min}$. These results support the selection of the Cubrinovski and Ishihara (2000) methodology to determine CS parameters from the void ratio range. Moreover, Torres-Cruz and Santamarina (2020) incorporated new results from a large database of tailings and found that non-plastic tailings fall on the same trends defined in Figure 9.22.
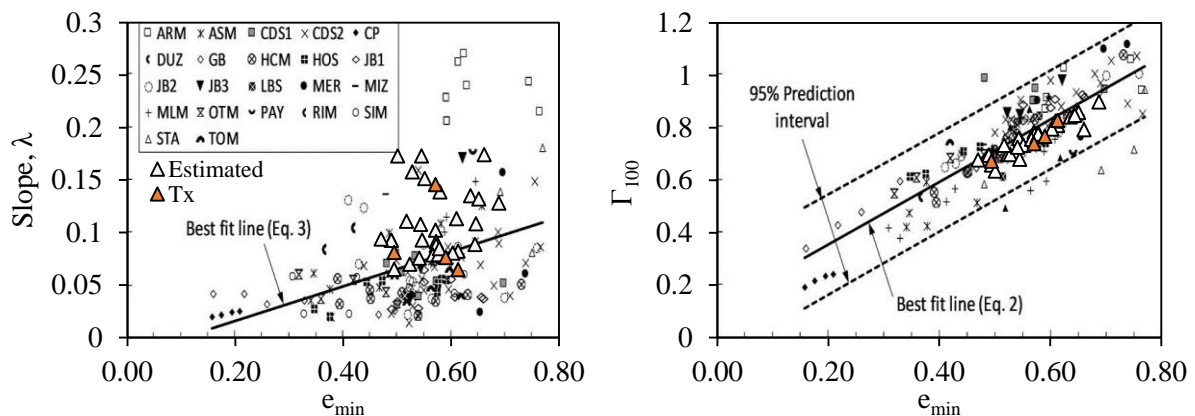
Figure 9.22 – Critical state parameters λ and Γ_{100} variation with e_{min} plotted against Torres-Cruz (2019) results

Furthermore, the CSL determined with the empirical correlations proposed by Cubrinovski and Ishihara (2000) were compared with the CSL obtained using reconstituted specimens in section 7.4. Figure 9.23 illustrates these comparisons for S1 soils. The estimated and triaxial compression tests results show good agreement. Beside, Figure 9.24 presents the comparisons of CSL of the soils from undisturbed specimens collected at NB1 and NB2 sites with the CSL of NB1 soil. The grain size characteristics of the soils are similar (Figure 9.4), however, the e_{max} and e_{min} had slight differences, which justify the range of CSL curves determined for different specimens. However, the similarities are clear, as the curves present approximately the same slope (0.076-0.094) and the CS intercepts vary between 0.866 and 0.956. These results support the use of empirical CSL to determine the state parameters of undisturbed soils like these, when it is not possible to determine the CSL with triaxial compression tests data. It can also be concluded that the determination of CSL based on representative reconstituted specimens is a viable and reliable process to obtain the CSL of the natural undisturbed material.
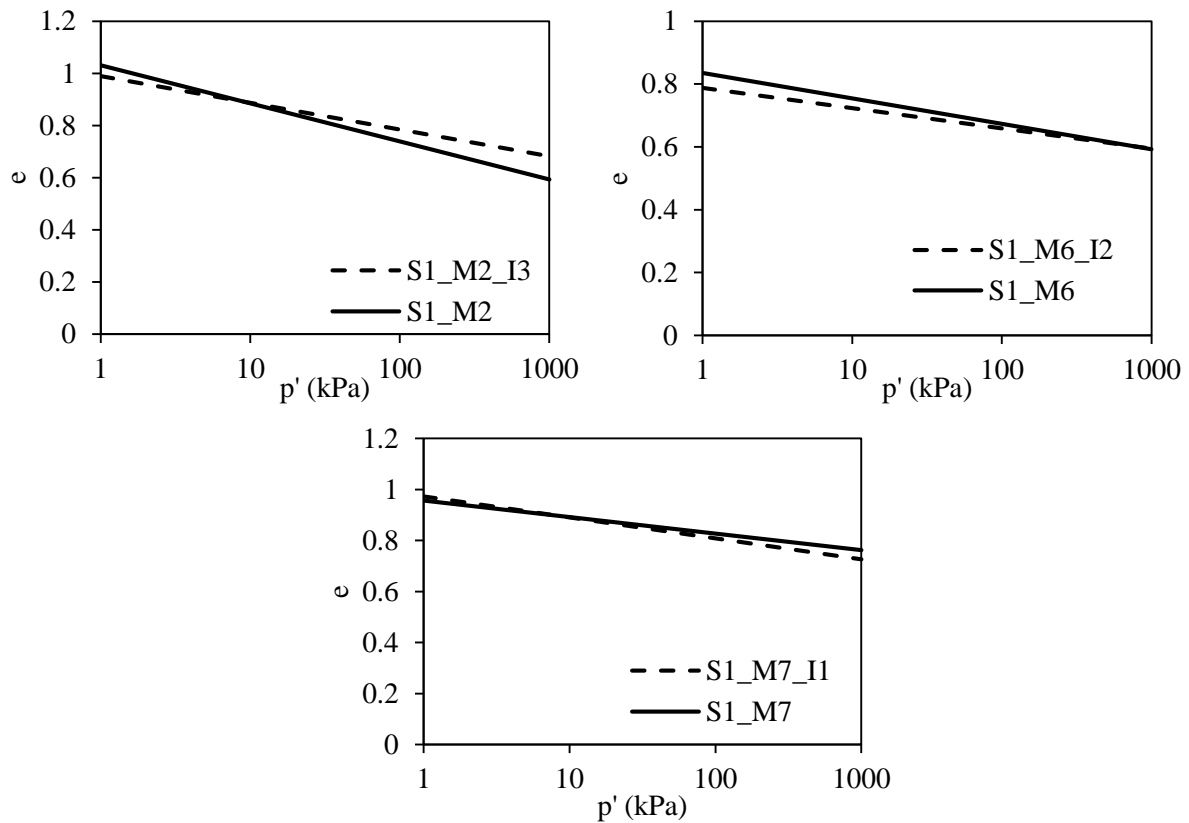
Figure 9.23 – Comparison between empirically determined CSL of undisturbed soils and the CSL of S1 reconstituted soils
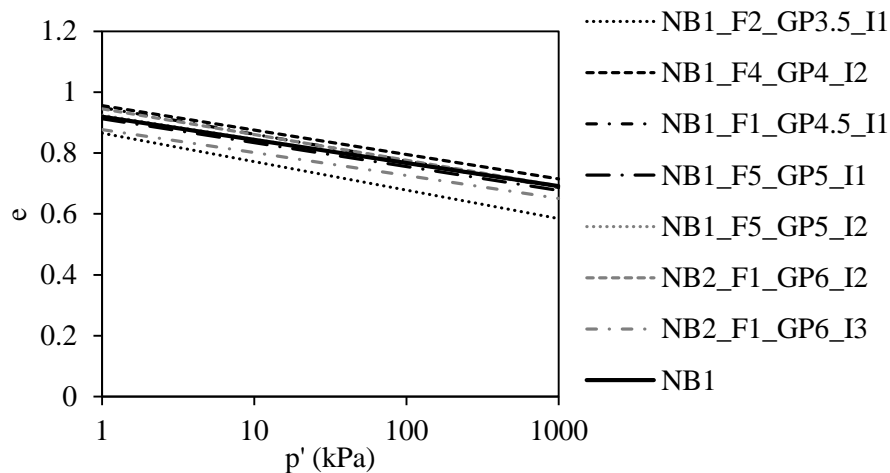
Figure 9.24 – Comparison between empirically determined CSL of undisturbed soils and the CSL of NB1 reconstituted soil

9.4. STATE PARAMETER PROFILES

The state parameter of each undisturbed specimen was computed using the critical state lines defined above, for the confining pressure and the void ratio of the specimen after consolidation. These results may be found in Table C.3 of Appendix C. Figure 9.25 illustrates the results of the estimated state parameter with depth. It is worth mentioning that at S1 and S2, specimens were collected using the Mazier sampler while at NB1 and NB2 specimens were collected using the Gel-Push sampler. The state parameters determined in the laboratory were negative, as the specimens were on the dense side of the CSL. Additionally, the state parameter was also computed using the empirical CPT-ψ relationship proposed by Robertson (2010) at the equivalent depth in the CPTu adjacent to the sampling borehole (equation (9.3)). These results were also plotted in Figure 9.25.

$$\psi = 0.56 - 0.33 \log Q_{tn,cs} \tag{9.3}$$

The results show that the formulation in equation (9.3) computed higher values of state parameter than those estimated with the empirical CSL determined using the Cubrinovski and Ishihara (2000) relationship of λ with e_{max}-e_{min} (refer to section 9.3). Moreover, it is observed that the GP specimens presented ψ values closer to the empirical CPT determined values than the Mazier specimens, suggesting a better performance of the GP in the collection of high quality samples. These results are confirmed when comparing directly the two state parameters (Figure 9.26). To obtain the state parameter value from CPTu-based correlations, an average value consisting on the $+ - 25$ cm around the sample collection depth was considered. The differences between the empirical and CPTu-based results might be explained by the densification of the samples during the sampling process, which is translated in a lower state parameter value in the laboratory as the specimens were denser than in the *in*

situ state. Moreover, there are significant uncertainties associated with both the empirical CSL relationship and the field-based relationship.

The empirical correlation proposed by Cubrinovski and Ishihara (2000) was obtained by compiling and analysing 52 sandy soils. The CSL were obtained from triaxial compression tests on reconstituted samples of clean sand and sands with non-plastic fines (FC < 20%). As discussed by Yoshimine and Koike (2005), the CSL of natural layered specimens exists above and to the right of the CSL of homogeneous specimens. Therefore, the state parameters of the undisturbed soils might be even lower than the results obtained with the empirical relationship. However, due to the lack of a more accurate definition of the undisturbed soils CSL, these values are considered in the following analyses.
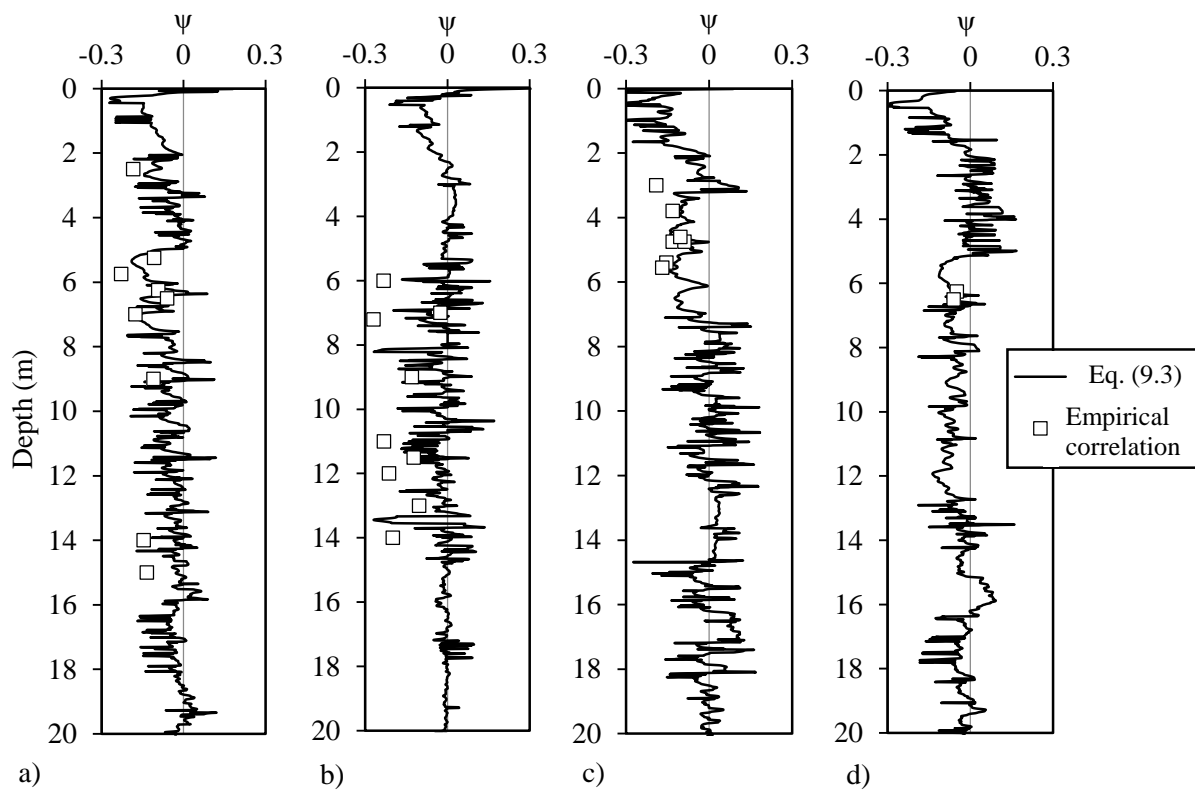
Figure 9.25 – State parameter profiles: a) S1; b) S2; c) NB1; d) NB2
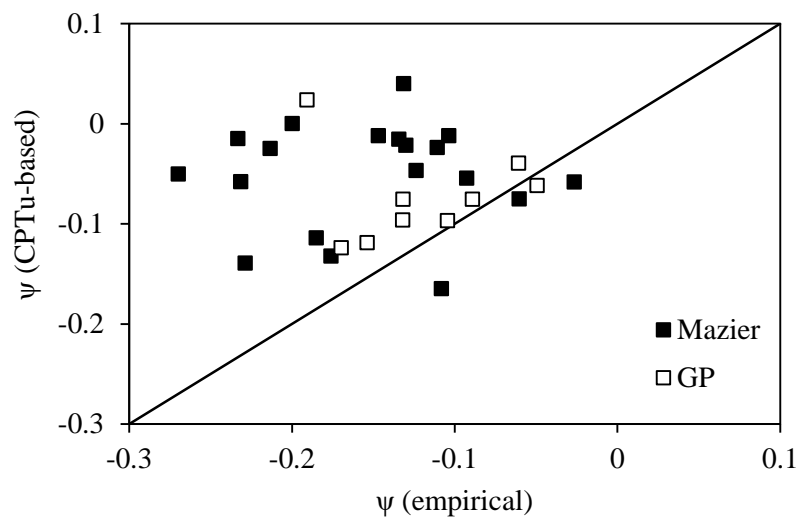
Figure 9.26 – Correlation between the estimated state parameter and the state parameter values averaged at +−25cm from the sampling depth obtained through CPTu-based correlations

9.5. CHAPTER SUMMARY

This Chapter addresses the physical and geomechanical characterisation of the undisturbed soil samples collected using the Mazier and GP samplers. The materials used in this work have variable properties, as they represent natural soils collected in heterogeneous profiles with sand-silt-clay interlayers and laminations. Each undisturbed sample tested under cyclic triaxial conditions was characterised in terms of the particle size distribution, with indices such as fines content (FC), mean grain size (D_{50}), coefficient of shape (C_C), and coefficient of uniformity (C_U), specific gravity (G_s), plasticity through Atterberg limits, void ratio limits (e_{max} and e_{min}), and shape parameters obtained using the Morphologi G3 (circularity, solidity, and aspect ratio). A set of undisturbed samples was opened and photographed, to document the soil structure and identify laminations and interlayers. Moreover, comparisons between the physical and mechanical properties of these soils were made against benchmark soils tested by other authors.

The CSL of undisturbed soils were estimated, based on an empirical correlation with e_{max}-e_{min}, proposed by Cubrinovski and Ishihara (2000). These results were compared with the CSL of reconstituted specimens, showing good agreement and validating the use of the estimated values of CS slope and intercept in the following analyses. Besides, the correlations between CS parameters and physical characteristics (e_{max}, e_{min}, FC, D_{50}, C_U, and shape parameters) follow the trends defined previously for the reconstituted soils tested and of data from other researchers.

The state parameters of the specimens tested under cyclic triaxial conditions were computed using the empirical correlation proposed by Cubrinovski and Ishihara (2000), and compared with the state parameter obtained from the CPTu-based correlation proposed by Robertson (2010). The state

parameter values obtained suggest that the specimens are denser than in the field, which might be due to the sampling process tends to densify the soil sample during collection, prior to testing in the laboratory. It was observed that the state parameters of GP specimens were closer to the empirical CPT determined values than the Mazier specimens, which confirms the better performance of the GP in the collection of high quality samples.

10. CYCLIC LIQUEFACTION BEHAVIOUR OF UNDISTURBED SAMPLES

10.1. INTRODUCTION

The aim of this Chapter is to assess the cyclic behaviour of the undisturbed samples collected using Mazier and Gel-Push samplers. The Chapter presents a detailed study of the liquefaction susceptibility of undisturbed specimens tested under cyclic triaxial conditions, and investigates the effects of fabric in liquefaction resistance and cyclic behaviour of different soils, by comparing the results of undisturbed specimens with the results of reconstituted specimens prepared with the same initial state (void ratio and confining pressure) and tested under the same conditions. The effect of fabric is also discussed based on the results of a set of cyclic direct simple shear tests.

The last part of the chapter analyses the comparison between field and laboratory results. Firstly, the cyclic resistance curves developed with CPTu-based correlations are compared with cyclic direct simple shear and cyclic triaxial tests performed in undisturbed specimens collected from the same depths. Secondly, the factors of safety against liquefaction (FS_{liq}) of the undisturbed specimens are determined, and compared with the respective FS_{liq} computed with CPTu data.

10.2. CYCLIC TRIAXIAL TESTS (CTX)

A total of 31 cyclic triaxial tests were performed in undisturbed samples, collected with the Mazier and Gel-Push samplers. The list of cyclic triaxial tests performed in undisturbed specimens is presented in Table 10.1. As described above, the specimens were collected from the four selected locations in the experimental site, S1, S2, NB1, and NB2, and are identified by the site, sampler, collection depth and position on the sampling tube, as detailed in section 6.5. The performance of cyclic triaxial tests in undisturbed specimens had two main objectives: study the cyclic behaviour of specimens in their natural structure and fabric, and compare the results with reconstituted specimens to assess the effect of different fabric on cyclic resistance and try to develop correlations between undisturbed and reconstituted specimens behaviour.

The sample preparation procedures were detailed in section 6.5.1, and consist on the extrusion of the sample from the sampling tube, measurement of the dimensions and weight, and careful placement on the triaxial cell. As the collection tubes were different, the Mazier specimens had around 86 mm diameter and 152 mm height, while the Gel-Push specimens had around 71 mm diameter and 142 mm height. The specimens diameters were defined by the diameter of the collection tube, so that the specimens would suffer as little disturbances as possible, and the heights were defined by the apparatus limitations, hence the ratio height/diameter of the Mazier specimens was lower than 2.

The confining pressures were selected according to the in situ stress state. However, during the execution of the tests, different considerations were made. The first three specimens tested were consolidated anisotropically, to better simulate the in situ confinement conditions. However, none of the specimens showed high axial deformation or increase in excess pore water pressure, so they were considered to not have liquefied. This was probably due to the clayey nature of the soils (inferred from the grain size curves and visual inspection) with a considerable percentage of fines content which could contribute for low generation of excess pore pressure and non-occurrence of liquefaction. In the end, the anisotropically consolidated tests were not considered for the following interpretations, as the specimens were mainly clays that did not liquefy and did not represent the soils that were the object of this study. After the performance of these three tests, the following specimens were isotropically consolidated, as it was found that isotropic consolidation replicates more closely the in situ conditions (Taylor, 2015). As discussed in the literature review chapter, there is no consensus on the selection of the confining stress for simulating field conditions. At first the specimens were consolidated isotropically to the vertical confining stress (σ'_v) as this pressure was more conservative. However, the last Mazier specimens and all GP specimens were confined to the in situ mean confining stress (p'_0), in an attempt to better simulate the in situ confinement.

The CSR adopted for each test was related to the CSR in the field (equation (2.76)), considering an earthquake magnitude of 7.5 and an average peak ground acceleration of 0.09g (due to a misinterpretation of the equipment software, the CSR_{tx} values considered were half the value that they would be for CSR_{field} calculated with a_{max}=0.20g, following the Eurocode 8 procedure defined in section 3.2.1, therefore, the actual a_{max} correspondent to the CSR_{tx} was 0.09g). In the case of Gel-Push specimens, the cyclic loading was performed in two stages: 30 cycles with a lower CSR value, and, if liquefaction did not occur, the CSR was increased to 1.5 times the initial value. However, the pore pressure increase during the first 30 cycles affected the CSR value of the second stage, as the vertical load is defined in the software beforehand and cannot be altered during the shear phase. Therefore, the second stage CSR is not always 1.5 times the initial value defined.

As for the loading stage, the majority of undisturbed specimens were sheared with a frequency of cycles of 1 Hz (1 cycle/s), except for S1_M25_I1 and NB2_F1_GP6_I3 that were sheared with a frequency of cycles of 0.1 Hz (1 cycle/10 s).

Two criteria were established to define liquefaction initiation: the pore pressure build up to 100%, which is translated in a pore pressure ratio of 1, and the single amplitude shear strain of 2.5% (that corresponds to a double amplitude shear strain of 5%). The results are presented in terms of cyclic resistance curves, that relate the cyclic stress ratio (CSR) and the number of cycles required to trigger liquefaction (N_{liq}). Contrary to what was observed in the reconstituted tests results, in which the two failure criteria gave similar results, in the undisturbed samples this was not verified. In all tests, the stress criterion (r_u=1) was reached first, so this was the criterion adopted for the development of the cyclic resistance curves. Besides, in some tests, the strain criterion was not meet, as specimens did not reach 5% double amplitude axial strain. The differences on N_{liq} obtained from the stress and strain criteria might be due to the density state and fabric of the specimens. As the undisturbed specimens have horizontal fabric, due to the layering and laminations, there is no guarantee that the pore pressure is constant throughout the entire specimen, as the pore pressure is only measured at the bottom and top of the specimens. Therefore, the pore pressure ratio of 1 might not be coincident with the complete loss of strength and large deformations. Other authors found similar results: for reconstituted specimens the number of cycles obtained with the two criteria was the same but for undisturbed specimens the number of cycles obtained with the two failure criteria was different, for both cyclic triaxial and simple shear tests (Taylor, 2015; Mele, 2020).

The tabulated results for all tests can be found in Table C.3 in Appendix C, that includes the test identification (Test ID), the void ratio after specimen preparation (e_0), at the beginning of consolidation (e_{i-1}) and after consolidation (e_i), the volumetric change during consolidation (ε_v), the confining pressure (p'_i), the shear wave velocity after consolidation (V_S), the state parameter (ψ), the frequency of cycles (Freq), the cyclic stress ratio (CSR), the number of cycles (N_{liq}) required to develop 5% axial strain in double amplitude ($\varepsilon_{a,DA}$) and required to develop 100% excess pore pressure ratio (r_u), and the cumulative dissipated energy until liquefaction (ΔW_{liq}).

From the set of tests in Table 10.1, not all were considered in the following analyses. Experimental laboratory work is often unpredictable, especially when dealing with natural soils, hence not all tests were carried out according to plan. As referred above, three Mazier specimens were tested under anisotropic conditions and did not liquefy. S1_M7_I1, NB1_F2_GP2.5_I3, and NB1_F5_GP4_I2 also did not liquefy in less than 1000 cycles, which was the limit defined in the software. Moreover, during the performance of S1_M14_I1 the acquisition of results failed and there is no record of the cyclic loading stage. As a result, these tests were not considered further in the definition of cyclic resistance curves or in the comparisons with reconstituted specimens presented in the following section.

Table 10.1 – List of cyclic triaxial tests performed with undisturbed specimens

Site	Test ID	Depth (m)	FC (%)	e_i	p'_i (kPa)	D_R (%)	ψ	Freq (Hz)	CSR $(q/2\sigma'_{h0})$
S1	S1_M2_I3	2.5	9.15	0.65	30	78	-0.185	1	0.13
	S1_M5_I2	5	21.50	0.64	25*	53	-0.108	1	0.09
	S1_M5_I4	5.5	10.56	0.50	50	98	-0.229	1	0.11
	S1_M6_I2	6	2.35	0.58	70	63	-0.093	1	0.16
	S1_M6_I3	6.5	6.31	0.66	45	42	-0.060	1	0.17
	S1_M7_I1	7	2.10	0.65	70	89	-0.176	1	0.13
	S1_M9_I1	9	27.61	0.56	150	95	-0.111	1	0.15
	S1_M11_I1	11	47.67	0.98	50*	-	-	1	0.08
	S1_M14_I1	14	17.44	0.60	75	79	-0.147	1	0.18
	S1_M15_I1	15	19.38	0.66	80	84	-0.134	1	0.21
	S1_M25_I1	25	17.30	0.61	200	-	-0.132	0.1	0.09
S2	S2_M6_I1_CTx	6	9.68	0.55	50	99	-0.233	1	0.13
	S2_M7_I1_CTx	7	39.85	0.70	55	77	-0.027	1	0.16
	S2_M7_I2_CTx	7.2	14.45	0.53	40	103	-0.270	1	0.15
	S2_M9_I1_CTx	9	28.58	0.63	65	86	-0.130	1	0.17
	S2_M11_I1_CTx3	11	17.72	0.65	50*	97	-0.232	1	0.17
	S2_M11_I2_CTx	11.5	9.37	0.74	100	77	-0.124	1	0.14
	S2_M12_I1_CTx7	12	12.46	0.61	110	100	-0.213	1	0.12
	S2_M13_I1_CTx	13	17.71	0.76	100	79	-0.104	1	0.14
	S2_M14_I1_CTx	14	8.03	0.72	75	94	-0.200	1	0.16
NB1	NB1_F2_GP2.5_I3	3	3.56	0.70	34	83	-0.191	1	0.11
	NB1_F2_GP3.5_I1	3.5	9.37	0.59	35	64	-0.132	1	0.12+0.18
	NB1_F4_GP4_I2	4.25	2.44	0.70	40	67	-0.132	1	0.12
	NB1_F5_GP4_I2	4.25	4.71	0.73	40	53	-0.089	1	0.14
	NB1_F1_GP4.5_I1	4.5	3.79	0.70	45	59	-0.105	1	0.11+0.21
	NB1_F5_GP5_I1	5	3.03	0.63	44	77	-0.154	1	0.12+0.29
	NB1_F5_GP5_I2	5.25	2.83	0.62	54	85	-0.170	1	0.32
NB2	NB2_F1_GP3_I4	3.75	32.10	0.74	35	64	-	1	0.11+0.173
	NB2_F2_GP4_I4	4.75	55.30	1.04	40	59	-	1	0.16+0.25
	NB2_F1_GP6_I2	6.25	4.96	0.72	49	52	-0.049	1	0.14
	NB2_F1_GP6_I3	6.5	2.00	0.66	50	56	-0.061	0.1	0.15+0.28

Note - specimens marked with a * were anisotropically consolidated

The analysis of the results of the Mazier undisturbed specimens, in terms of effect of specific parameters and soil properties, was difficult, as each specimen is basically a unique soil. Therefore, contrary to the analysis presented above for the reconstituted specimens, the evaluation of the influence of fines content, density, confining stress, structure, or fabric was challenging. Analysing the results of all the undisturbed specimens tested, there is no pattern of behaviour in the undisturbed specimens. The majority of specimens were dense to very dense, which is reflected on the high number of cycles required to trigger liquefaction. The specimens with lower fines content, which correspond to the less dense specimens, showed lower liquefaction resistance. While the majority of specimens showed a typical behaviour in terms of strain and excess pore pressure evolution, similar to the cyclic behaviour

illustrated in Figure 10.1, some specimens (e.g., S1_M5_I4, and S2_M6_I1) showed an initial compression during the first cycles, with the increase of axial strain in the same direction. This initial compression might be due to a rapid increase in excess pore pressure at the beginning of the shear stage, causing a readjustment of the particles and an initial compression of the specimen.

As for the liquefaction failure, as observed in the reconstituted tests, two different types of liquefaction failure were distinguished, flow liquefaction (FL) and cyclic mobility (CM). Figure 10.1 shows the example of test S2_M11_I2. It is observed that flow liquefaction occurs, as the specimen loses its strength and the deviatoric stress decreases. On the other hand, the stress criteria (r_u=1) is reached first, and the strain criteria is not reached, as $\varepsilon_{a,SA}$ never reaches 2.5%.
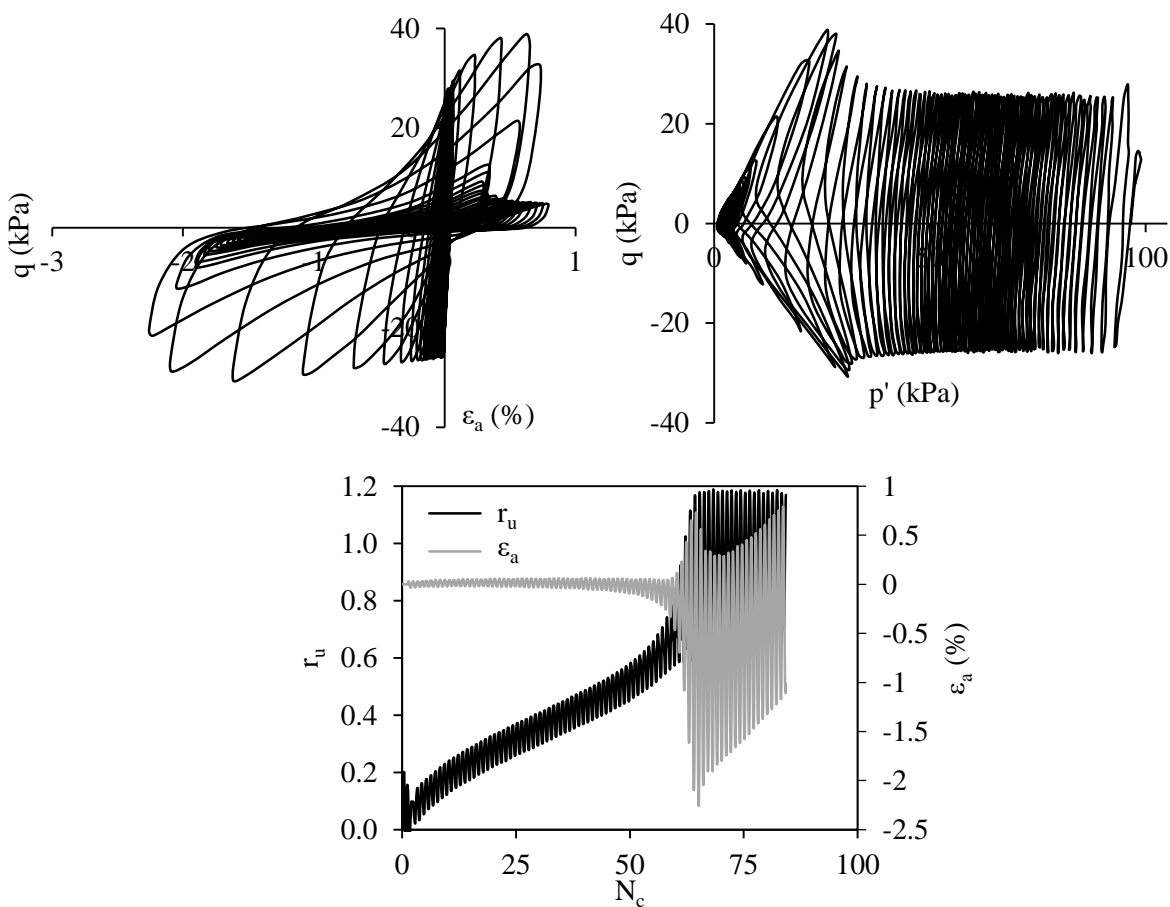
Figure 10.1 – Plot of cyclic triaxial test on a Mazier specimen (Test ID: S2_M11_I2, D_R=77%, FC=9.37%, p'_i=97 kPa, CSR=0.139)

Furthermore, most GP specimens were tested with a change in CSR. As observed in Figure 10.2, which displays an example of a GP specimen test, the first 30 cycles have low impact on the strain evolution and consequently on the dissipated energy accumulation. Therefore, and despite the increase in pore pressure, the author opted to "exclude" the first 30 cycles of load and recalculate a new CSR with the

respective deviatoric stress and mean effective stress (q and p' at that stage). The number of cycles considered for liquefaction was the number of cycles of the second stage of loading. These considerations were used in order to obtain a single point on the CSR-N_{liq} plot, as the cyclic resistance curves are defined by pairs of CSR and N_{liq}. It is important to mention that the first 30 cycles have influence on liquefaction behaviour, as will be discussed later when comparing individual undisturbed and reconstituted specimens sheared for different combinations of confining stress and CSR.
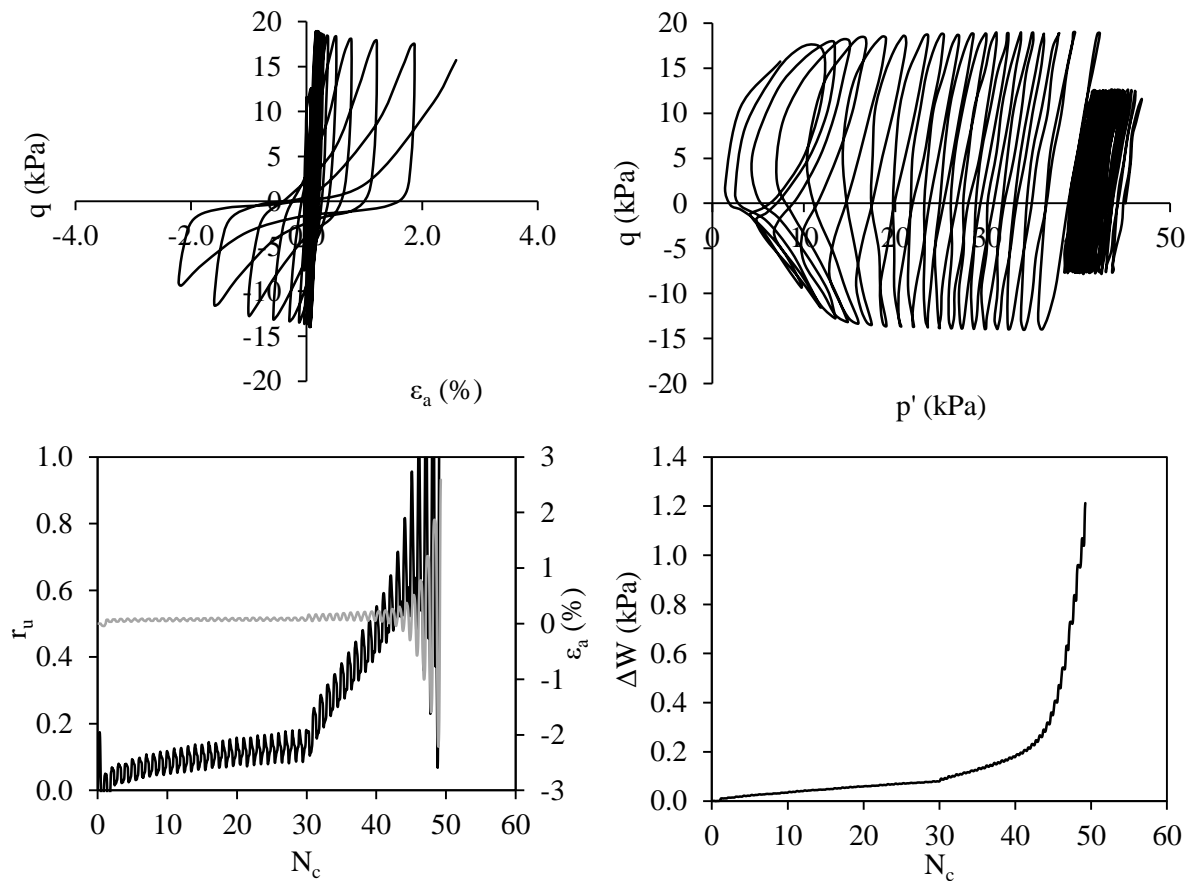
Figure 10.2 – Plot of cyclic triaxial test on a GP specimen (Test ID: NB1_F1_GP4.5_I1, D_R=59%, FC=3.79%, p'_i=45 kPa, CSR=0.11+0.21)

10.2.1. LIQUEFACTION RESISTANCE OF UNDISTURBED SPECIMENS

The undisturbed specimens collected are examples of the variety of soils found in the 4 experimental sites studied. As discussed before, each specimen is basically a unique soil, with the respective characterisation in terms of grain size, particle shape, and void ratio limits. As recognised from the analyses of the grain size curves from Figure 9.2 to Figure 9.4, all specimens have different particle sizes and fines content. Figure 10.3 presents the number of tests performed, organised in terms of fines content and relative density. It is important to note that the relative density might not correspond to the actual density of the undisturbed specimen, as it was obtained with e_{max} and e_{min} determined for the

homogeneous soil. However, it was not possible to assess the layered structure and the fabric of the undisturbed specimen, and separate the relative densities of fines and sand layers. Therefore, as e_{max} and e_{min} were determined with the same procedure for all specimens, the use of relative density allows for comparisons between soil specimens. The state parameter would be best to relate the behaviour of the soils, however, individual CSL were not determined and the use of estimated results might introduce more uncertainties.

It is observed that 10 specimens had less than 5% fines content, 9 had between 5 and 15% FC, and 12 had more than 15% FC. It is important to note that the specimens with low fines content were mainly collected with Gel-Push sampler, which is in accordance with the CPTu profiles, as GP specimens tested were collected at around 3-5 m at NB1 and 6 m at NB2, where the CPTu profile identified sands. Moreover, these results reflect the interlayering and laminations found in the S1 and S2 CPTu profiles, as specimens with higher fines content are probably specimens with more clay-silt-sand interlayers. Furthermore, no specimen was loose with relative density under 35%, 10 specimens had medium density (D_R between 35 and 65%), 9 were dense (D_R between 65 and 85%), and 11 were very dense (D_R between 85 and 100%). The number of tests considered in Figure 10.3b is 30 as void ratio limits were not measured in S1_M11_I1, hence it was not possible to compute its relative density. These results reflect the densification that might have occurred during the collection process of the Mazier samples, especially during the extrusion in the laboratory. On the other hand, GP specimens were generally less dense, which might be due to the use of a polymer solution that lubricated the sample, reduced penetration resistance and prevented friction during the extrusion process in the laboratory.
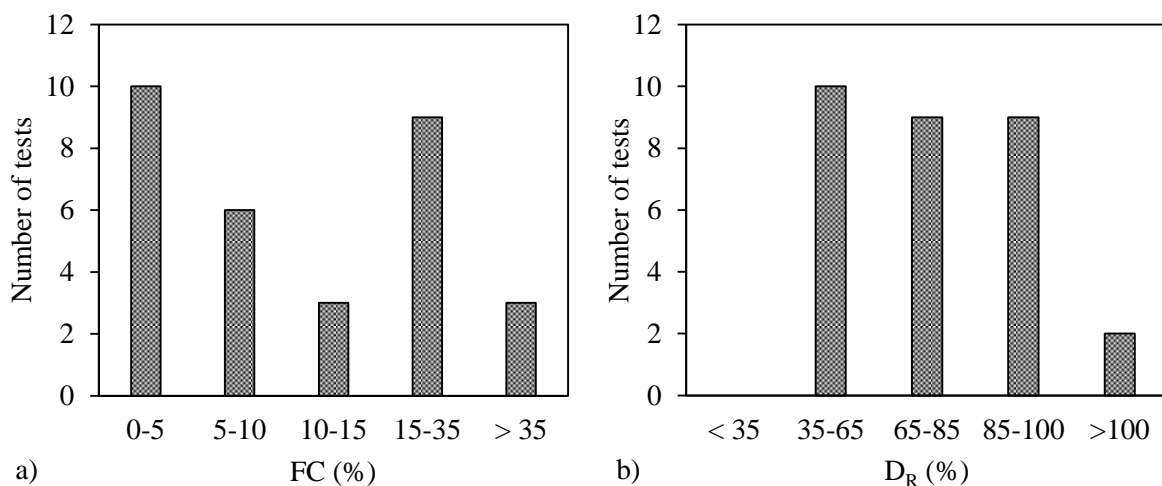
Figure 10.3 – Number of tests divided into categories: a) according to fines content; b) according to relative density

The results from undisturbed Mazier specimens are plotted in Figure 10.4. It is observed that the cyclic resistance curves seem to be grouped according to ranges of FC. The curve correspondent to lower FC (FC < 8%) is plotted in the middle, while the curve for specimens with intermediate fines content (8% < FC < 19%) is the lowest and the curve correspondent to FC > 19% is the highest. These tendencies agree with other works presented in the literature review, that stated that liquefaction resistance reduces with increase of fines content up to a threshold value and increases after this value is surpassed (Chang, 1990; Polito and Martin, 2001; Thevanayagam, 2007b; Huang and Chuang, 2011).

However, it is important to note that, as mentioned above, these results correspond to specimens of different soils, with different soil properties, relative densities and confining pressures (as observed in Figure 10.5, where the relative density of each specimens is identified). Nonetheless, the results seem to indicate that, in this case, the FC is the most prevalent factor that affects liquefaction behaviour, as specimens with different relative density seem to fit the same resistance curve depending on FC.
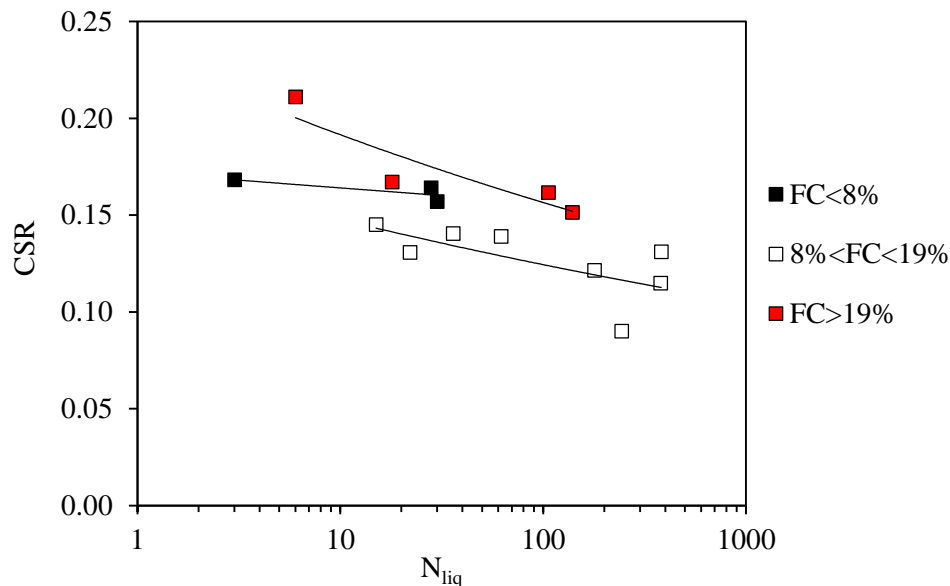
Figure 10.4 – Cyclic resistance curves of Mazier undisturbed specimens for different FC range
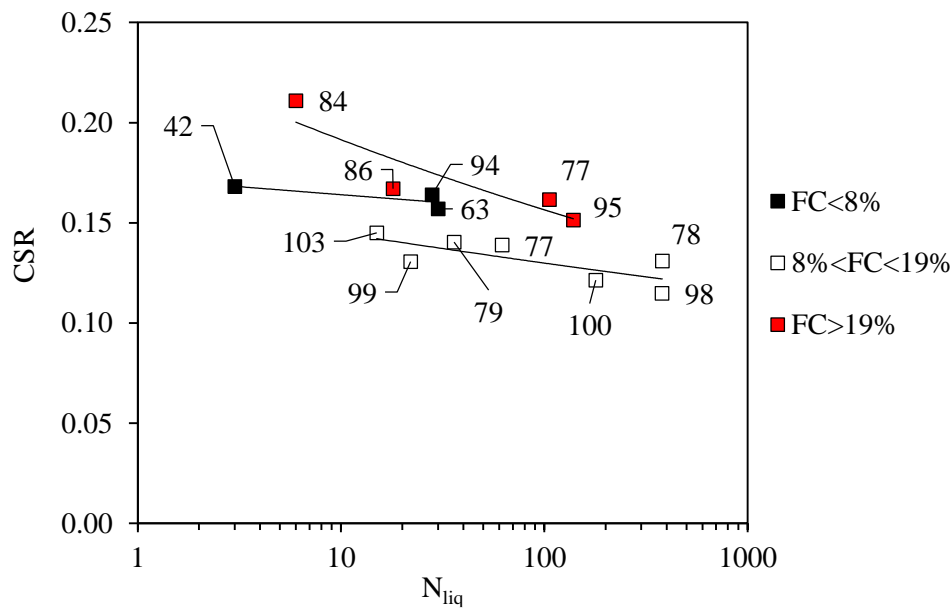
Figure 10.5 – Cyclic resistance curves of Mazier undisturbed specimens for different FC range with indication of D_R of each specimen

The results of cyclic triaxial tests in undisturbed GP specimens were also analysed in terms of cyclic liquefaction resistance. In this case, it was challenging to define clear resistance curves, as the results were sparse (Figure 10.6). The specimens have FC ranging between 2% and 9.37% and the confining pressures varied between 29 kPa and 49 kPa. On the other hand, the relative density of each specimen was different, which influenced the position of the results on the CSR-N_{liq} plane. The values of relative density of each specimen are reported in Figure 10.6, showing that, in general, denser specimens exhibit higher liquefaction resistance. However, there are two tests, namely NB1_F2_GP3.5_I1 and NB2_F1_GP6_I3, with 64% and 56% D_R respectively, that exhibit higher resistance than specimens with higher D_R. NB1_F2_GP3.5_I1 has the highest fines content (9.37%) which might increase its resistance and influence the comparisons with specimens with lower FC. On the other hand, NB2_F1_GP6_I3 was first loaded with an initial 50 cycles for CSR=0.15 and liquefied in the second stage of CSR at 13 cycles. According to Zhang et al. (2009), the cyclic preloading is responsible for the uniformisation of the sand pores and the enhanced interlocking of the particles, which might have improved the resistance of this specimen to liquefaction.
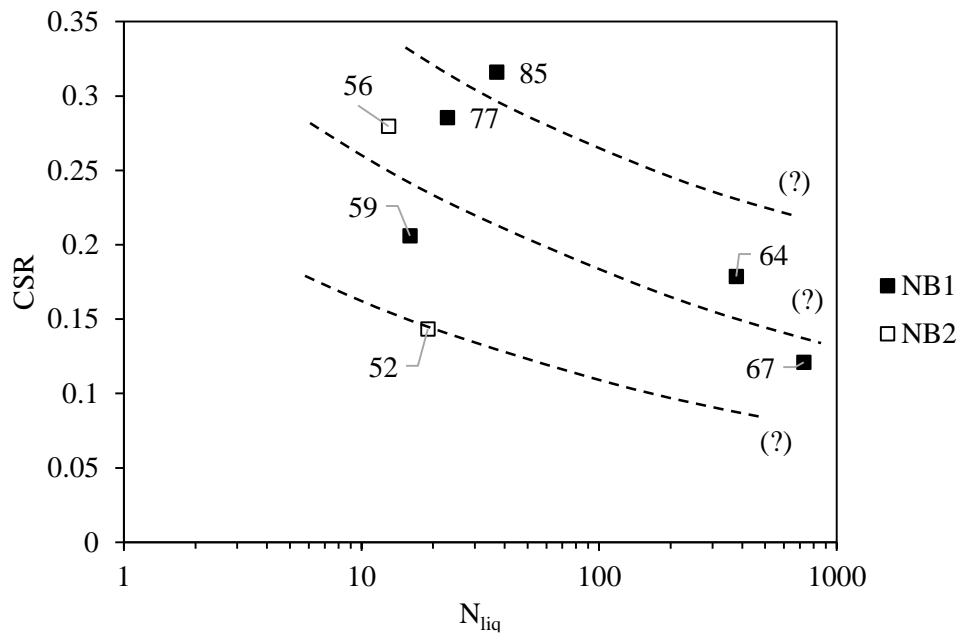
Figure 10.6 – CSR-N_{liq} plots of undisturbed GP specimens with indication of the relative densities of each specimen

10.2.2. EFFECT OF FABRIC – COMPARISON BETWEEN UNDISTURBED AND RECONSTITUTED SPECIMENS IN CTX

To study the effect of fabric, and since the materials from undisturbed specimens were all different, reconstituted specimens were prepared with each different material, to directly compare the cyclic behaviour results. As referred above, not all undisturbed specimens were considered, as not all the results were satisfactory and allowed comparisons. Therefore, a set of 28 tests was performed in reconstituted specimens, simulating the same conditions as the respective undisturbed specimens, as listed in Table 10.2.

After the performance of the cyclic triaxial test, the soil from each undisturbed specimen was mixed and homogenised, and used to recreate a reconstituted specimen with the same state and stress conditions (initial void ratio and water content, confining pressure, CSR). The reconstituted technique used to prepare the specimens was moist tamping, as the preparation of the same relative density was more practical and more controllable than with other preparation techniques. The test procedure is similar to that described in section 6.5.1. As the materials were reused, the reconstituted specimens were prepared in slightly smaller size than the undisturbed specimens to account for any loss of material: the Mazier specimens had around 70.5 mm diameter and 141.5 mm height, while the Gel-Push specimens had around 60.5 mm diameter and 121.5 mm height.

The tabulated results for all tests can be found in Table C.4 in Appendix C, which includes the test identification (Test ID), the void ratio after specimen preparation (e_0), at the beginning of consolidation

(e_{i-1}) and after consolidation (e_i), the volumetric change during consolidation (ε_v), the relative density (D_R), the confining pressure (p'_i), the shear wave velocity after consolidation (V_S), the frequency of cycles (Freq), the cyclic stress ratio (CSR), the number of cycles required to develop 5% axial strain in double amplitude ($\varepsilon_{a,DA}$), and required to develop 100% excess pore pressure ratio (r_u), the cumulative dissipated energy until liquefaction (ΔW_{liq}), and the type of liquefaction failure observed.

Table 10.2 – List of cyclic triaxial tests performed with reconstituted specimens with soils from the undisturbed specimens tested

Test ID	FC (%)	e_i	p'_i (kPa)	D_R (%)	ψ	Freq (Hz)	CSR ($q/2\sigma'_{h0}$)
S1_M2_R3	9.15	0.66	30	77	-0.183	0.1	0.14
S1_M5_R4	10.56	0.59	50	70	-0.135	0.1	0.13
S1_M6_R2	2.35	0.59	70	55	-0.075	0.1	0.17
S1_M6_R2_2	2.35	0.59	70	56	-0.078	0.1	0.16
S1_M6_R3	6.00	0.68	45	35	-0.043	0.1	0.18
S1_M7_R1	2.10	0.73	70	60	-0.094	0.1	0.14
S1_M15_R1	19.38	0.64	80	88	-0.153	0.1	0.23
S2_M6_R1	9.68	0.66	50	66	-0.122	0.1	0.14
S2_M7_R1	39.85	0.53	55	103	-0.196	0.1	0.18
S2_M9_R1	28.58	0.54	65	102	-0.222	0.1	0.31
S2_M11_R2	9.37	0.77	100	68	-0.089	0.1	0.14
S2_M12_R1	12.46	0.64	110	93	-0.181	0.1	0.13
S2_M13_R1	17.71	0.74	100	81	-0.115	0.1	0.17
S2_M14_R1	8.03	0.80	75	77	-0.118	0.1	0.18
NB1_F2_GP3.5_R1	9.37	0.64	35	49	-0.080	0.1	0.16
NB1_F2_GP3.5_R1_2	9.37	0.60	35	62	-0.126	0.1	0.11+0.19
NB1_F4_GP4_R2	2.44	0.70	40	65	-0.128	0.1	0.10
NB1_F4_GP4_R2_2	2.44	0.71	40	62	-0.118	0.1	0.12
NB1_F1_GP4.5_R1	3.79	0.71	45	56	-0.097	0.1	0.20
NB1_F1_GP4.5_R1_2	3.79	0.70	45	58	-0.104	0.1	0.11+0.18
NB1_F1_GP4.5_R1_3	3.79	0.75	45	43	-0.058	0.1	0.12+0.26
NB1_F5_GP5_R1	3.03	0.63	45	78	-0.158	0.1	0.18
NB1_F5_GP5_R1_2	3.03	0.63	45	77	-0.155	0.1	0.11+0.19
NB1_F5_GP5_R1_3	3.03	0.65	45	70	-0.149	0.1	0.29
NB1_F5_GP5_R2	2.83	0.60	55	91	-0.184	0.1	0.19
NB1_F5_GP5_R2_2	2.83	0.62	55	85	-0.186	0.1	0.32
NB2_F1_GP6_R2	4.96	0.67	50	69	-0.131	0.1	0.14
NB2_F1_GP6_R3	2.00	0.69	50	43	-0.058	0.1	0.14+0.27

The section of comparison between undisturbed and reconstituted specimens is divided into two parts. The first part compares the results of tests with a constant CSR throughout the entire loading stage. This includes all the Mazier specimens and two GP specimens. The second part refers to the GP specimens that were sheared with two distinct CSR. As mentioned before, the first 30 cycles were performed with a certain CSR and then CSR was increased to 1.5 times the initial value. These change in CSR was difficult to reproduce in the shear stage of the reconstituted specimens. For this reason, in some cases,

different combinations of confining pressure and CSR were applied, and more than one reconstituted specimen was tested. These results are compared and discussed in detail for each group of tests.

a) Constant CSR

The tests considered in this analysis include all the Mazier specimens and two GP specimens (NB1_F4_GP4_I2, and NB2_F1_GP6_I2). To assess the similarities between the pairs of tested specimens, Figure 10.7 presents the comparison between the shear wave velocities and void ratio of undisturbed and reconstituted specimens after consolidation (i.e. at the beginning of shear). It is observed that both V_S and e for undisturbed and reconstituted specimens are around the 1:1 line, showing that the pairs of specimens had approximately the same initial state conditions, which allows the comparison between cyclic liquefaction resistances. As the GP specimens had lower fines content and were more homogeneous, it was easier to simulate the same void ratio and replicate reconstituted specimens with the same shear wave velocity as the undisturbed specimens. Moreover, Figure 10.8 presents the comparison of the results of V_S normalised with the void ratio, using the void ratio function $F(e) = e^{-1.3}$ proposed by Lo Presti et al. (1995). The results show that the normalised Vs values are around the 1:1 line, thus confirming the feasibility of the comparisons between undisturbed and reconstituted specimens.
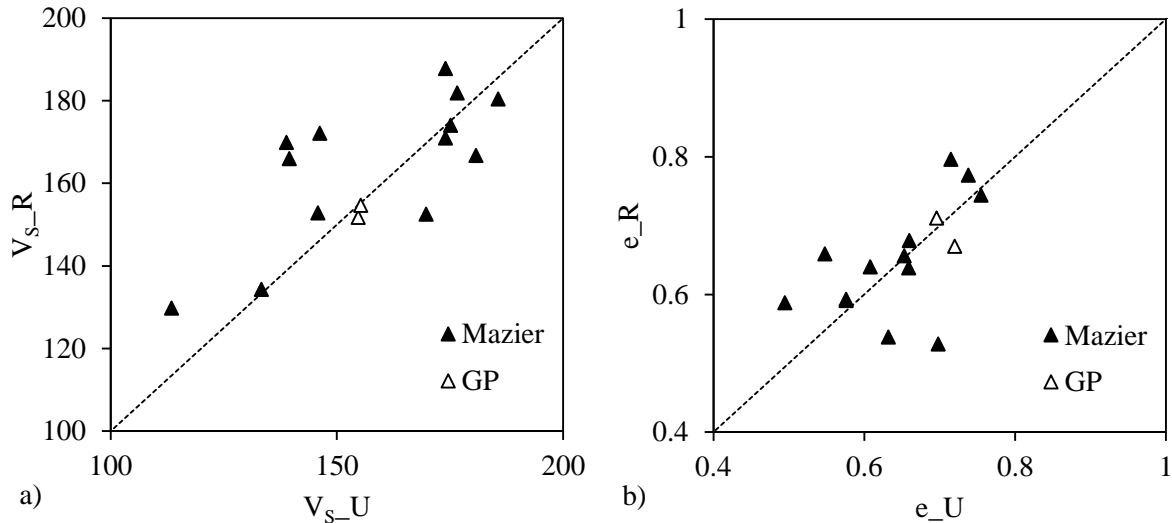
Figure 10.7 – Comparison between the a) shear wave velocity and the b) void ratio of undisturbed and reconstituted specimens after consolidation
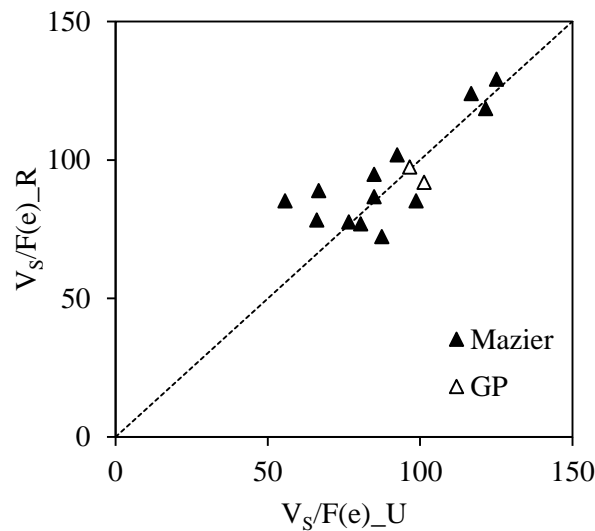
Figure 10.8 – Comparison between the shear wave velocity normalised by the void ratio function of undisturbed and reconstituted specimens

The number of cycles required to trigger liquefaction in undisturbed and reconstituted specimens is contrasted in Figure 10.9. The tests are grouped in terms of ranges of fines content, and the 1:1 line is also illustrated. Three tendencies are clearly distinguished: one line above the 1:1 line, indicating that these points correspond to reconstituted values higher than undisturbed values, and two lines below, indicating pairs of tests with reconstituted values lower than undisturbed values. These results show that, in general, when the soil had less than 6% FC, the reconstituted specimen exhibited higher cyclic resistance, while when the soil had more than 6% FC, the reconstituted specimen was less resistant than the correspondent undisturbed specimen. However, for soils with FC between 6% and 15% (orange squares), the results are grouped in two different trends. This might be explained since the points closer to the 1:1 line were specimens with a higher difference between void ratios. The void ratios of the reconstituted specimens were 10 to 20% higher than the void ratios of the undisturbed specimens. However, as the reconstituted specimens were looser, it was expected that the number of cycles required to liquefaction was lower, lowering the position of the trend line, which is not verified. The values of the number of cycles of undisturbed and reconstituted specimens are closer when the difference in voids ratio is higher. In terms of density, these results were not expected, however, the natural structure of undisturbed specimens might be responsible for this behaviour. The fines content of the undisturbed specimen is possibly related to the existence of layering and laminations, as a specimen with higher FC is expected to exhibit more layering. The layering configuration increases the resistance of undisturbed specimens, hence when the structure is altered due to homogenisation and reconstitution of the specimen, the resistance decreases. It was not possible to assess the type of layering present in each specimen, but a possible explanation for these results might be different levels of interlayering, despite

similar FC values (between 6 and 15%). On the other hand, there is one pair of tests with FC < 6% that showed N_{liq}_R lower than N_{liq}_U, contradicting the tendency of the results of FC < 6%. In this case, the reconstituted specimen was looser than the undisturbed specimen, with a void ratio 7% lower, which justifies the lower resistance of the reconstituted specimen.

These results suggest that the moist-tamping preparation procedure in clean sands with low FC might be non-conservative in the assessment of liquefaction susceptibility, as the reconstituted specimens were more resistant than the undisturbed specimens. On the other hand, for soils with moderate fines content (FC >6%), the equivalent reconstituted specimens might be conservative as their resistance to liquefaction was lower than the undisturbed specimen resistance. Therefore, it can be concluded that the effects of horizontal fabric in undisturbed specimens of the two types of soils must be carefully taken into account.
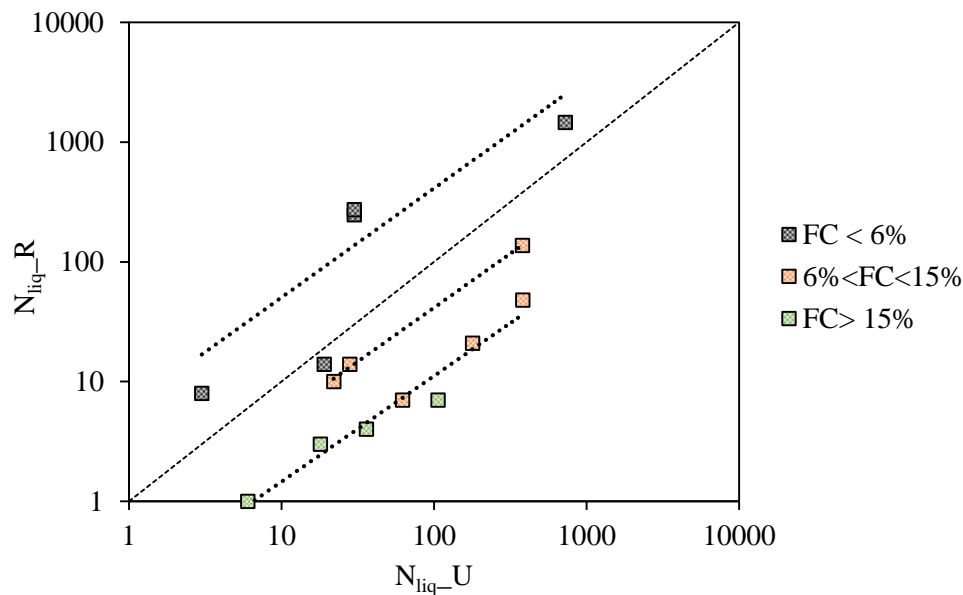
Figure 10.9 – Comparison between N_{liq} of undisturbed and reconstituted specimens

Additionally, Figure 10.10 presents the histograms of the number of tests and percentage of occurrence of each range of ratios N_{liq}_R/N_{liq}_U, according to fines content groups. As noticed above, there is a correlation between the ratio N_{liq}_R/N_{liq}_U and FC. For fines content higher than 15%, the ratios were always lower than 0.2, which means that N_{liq}_R was 20% or less the N_{liq}_U. On the other hand, for fines content lower than 6% the ratios were mainly higher than 2 (80% of occurrence), while for FC between 6% and 15%, the ratios were between 0.1 and 0.5. It is worth mentioning that the number of tests performed is not enough to make define conclusions. However, it was shown that, for FC higher than 6%, the reconstituted specimens exhibited lower resistance than undisturbed specimens, as specimens required less cycles to liquefy. The presence of fines content, a reflex of the presence of interlayers,

increased the resistance of the undisturbed specimen, hence for soils with FC higher than 6%, N_{liq}_U was higher than N_{liq}_R.
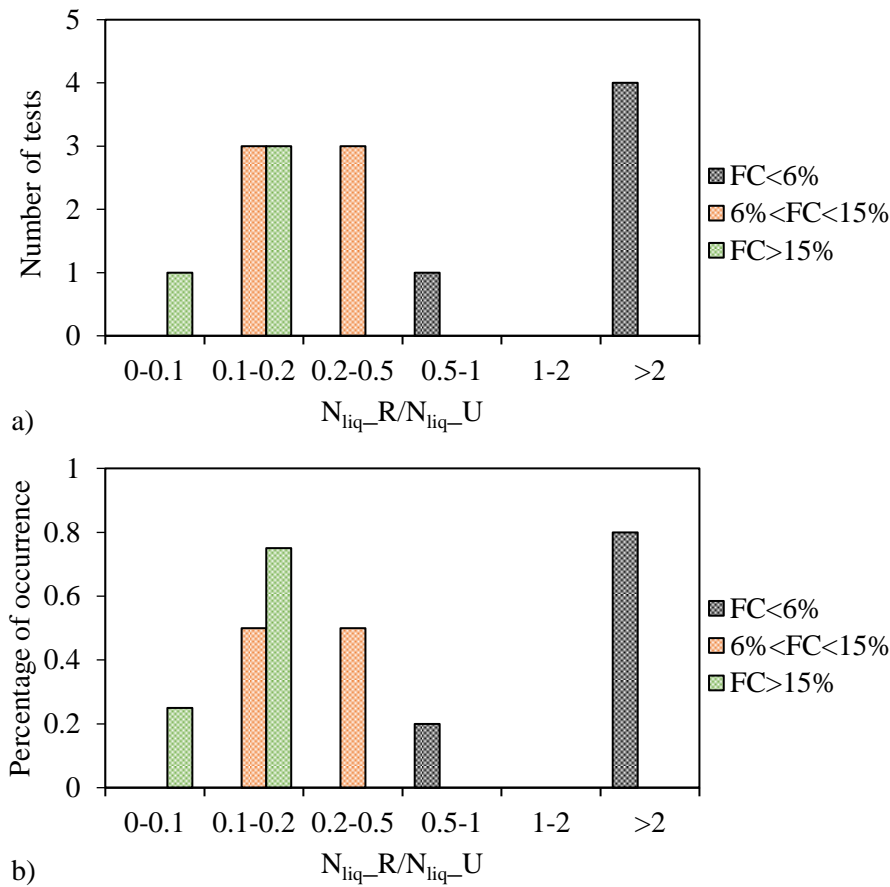
Figure 10.10 – Distribution of N_{liq}_R/N_{liq}_U according to FC in terms of: a) number of tests; b) percentage of occurrence

As outlined in the literature review, stratified specimens behave stiffer than uniform specimen at the same density (Yoshimine and Koike, 2005), this being relevant for moderate to high FC. Contradictory, in a previous work, Amini and Qi (2000) found that the liquefaction resistance of layered and uniform soils was not significantly different. The definition of the shape and position of the cyclic resistance curves for undisturbed specimens tested on the triaxial apparatus was challenging due to the varied composition of undisturbed specimens. Therefore, to evaluate the impact of soil fabric and structure on the cyclic soil response, a more detailed comparison of the cyclic behaviour of undisturbed and reconstituted specimens is performed, for each group of fines content selected above. To show the influence of fabric and structure on the specimens response, the cyclic tests compared were performed with specimens of the same soil type, very similar densities and applied CSR.

Figure 10.11 presents the cyclic behaviour comparison of effective stress path, stress-strain, and evolution of pore pressure ratio and axial strain with number of cycles for S1_M6_I3 and S1_M6_R3,

with D_R of 43% and 35%, respectively, and FC of 6%. The applied CSR were 0.17 and 0.18 for the undisturbed and reconstituted tests, respectively, and the confining pressure was 45 kPa. The moment when r_u reached 1, considered the stress criterion for liquefaction triggering, is marked on the different plots. The number of cycles to trigger liquefaction was higher in the reconstituted specimen, which was verified for the comparisons of specimens with FC < 6%. It is observed that the undisturbed specimen showed higher initial increase of strain, biased to the compression side, whereas the reconstituted specimen exhibited much lower strains. However, upon reaching r_u of 1, the reconstituted specimen developed very large strains, while the undisturbed specimen developed the same rate of strain even after liquefaction is reached. On the other hand, the undisturbed specimen developed large excess pore pressures at each cycle, while the rate of r_u increase was more constant in the reconstituted specimen. The failure mechanisms were also distinct, as the undisturbed specimen lost its strength entirely after liquefaction triggering, while the reconstituted specimen stress path followed the failure envelope.

Figure 10.11 – Comparison of undisturbed and reconstituted specimens cyclic response (FC=6%): a) stress-strain curves; b) effective stress path; c) pore pressure ratio; and d) axial strain with number of cycles

Figure 10.12 presents the cyclic behaviour comparison of effective stress path, stress-strain, and evolution of pore pressure ratio and axial strain with number of cycles for S2_M11_I2 and S2_M11_R2,

with D_R of 77% and 68%, respectively, and FC of 9.4%. The applied CSR was 0.14 for both tests, and the confining pressure was 100 kPa. The undisturbed specimen reached the liquefaction stress criteria in 62 cycles, while the reconstituted specimen only took 7 cycles to achieve r_u=1. The development of strain and r_u with number of cycles in the reconstituted specimen was faster than in the undisturbed specimen, showing an exponential increase in strain rate per cycle. The reconstituted specimen developed significant strains in both compression and extension, while the undisturbed specimen developed strains mainly to the extension side. In the undisturbed specimen, the strain criterion was not met, as specimens did not reach 5% double amplitude axial strain ($\varepsilon_{a,DA}$).

Figure 10.12 – Comparison of undisturbed and reconstituted specimens cyclic response (FC=9.4%): a) stress-strain curves; b) effective stress path; c) pore pressure ratio; and d) axial strain with number of cycles

Figure 10.13 presents the cyclic behaviour comparison of effective stress path, stress-strain, and evolution of pore pressure ratio and axial strain with number of cycles for S2_M13_I1 and S2_M13_R1, with D_R of 79% and 81%, respectively, and FC of 17.7%. The applied CSR were 0.14 and 0.17 for the undisturbed and reconstituted tests, respectively, and the confining pressure was 100 kPa. The observed behaviour was similar to the comparisons presented above for the soil with FC=9.4%. The reconstituted specimen reached liquefaction for lower number of cycles, with a rapid increase in excess pore pressure and an exponential increase in axial strain in both compression and extension directions. On the other

hand, the undisturbed specimen reached r_u of 1 for a higher number of cycles, with a constant rate of pore pressure ratio increase. Once liquefaction was reached, the axial strains developed to the extension side, but did not reach the strain criteria ($\varepsilon_{a,DA}$=5%).
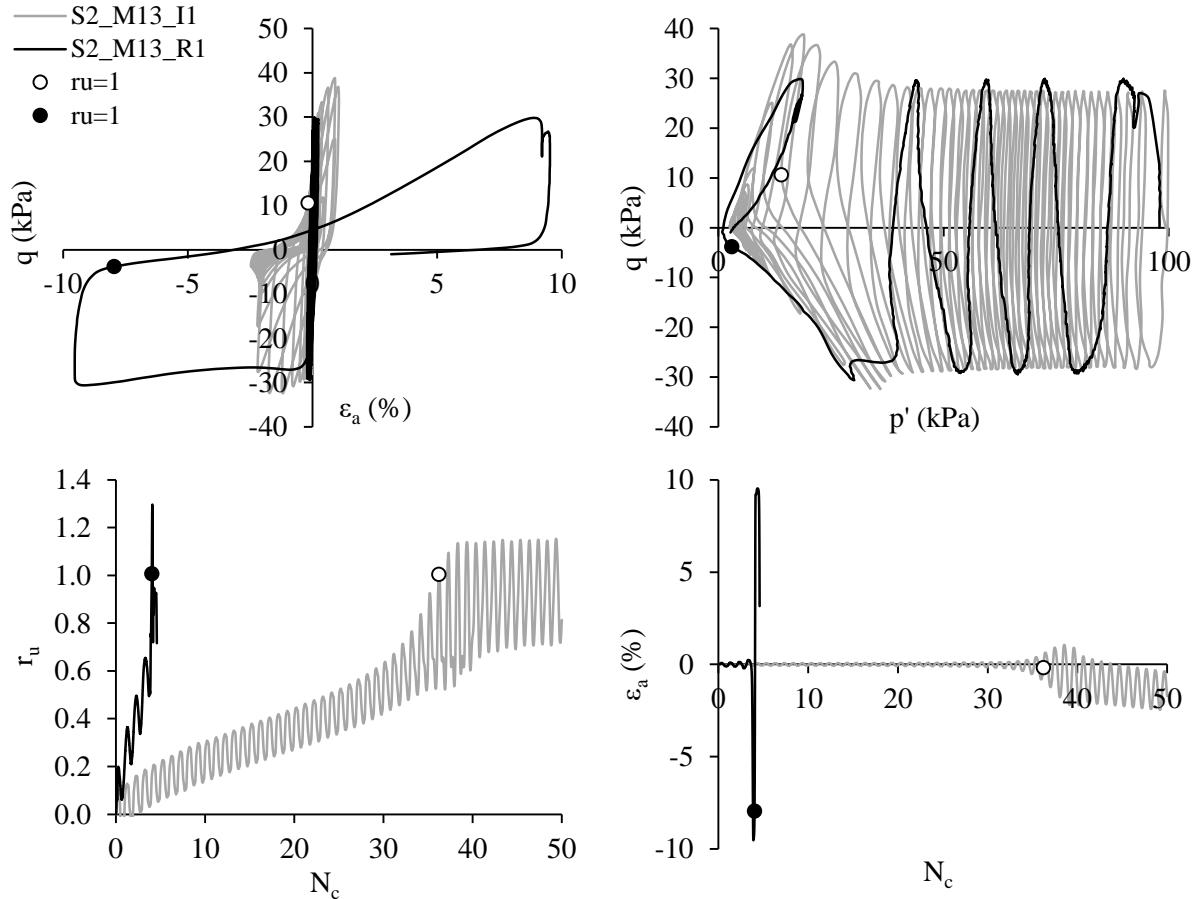
Figure 10.13 – Comparison of undisturbed and reconstituted specimens cyclic response (FC=17.7%): a) stress-strain curves; b) effective stress path; c) pore pressure ratio; and d) axial strain with number of cycles

The influence of fabric and structure on the cyclic behaviour of undisturbed and reconstituted specimens was distinguished according to the fines content. The specimens with lower fines content (FC < 6%) showed a different behaviour, as the reconstituted specimens exhibited higher cyclic resistance than the undisturbed specimens. These specimens were probably more homogeneous, with no presence of layers and laminations. For this reason, the reconstituted specimens prepared with MT might have been more resistant due to the compaction process that conferred a more stable structure. However, despite the rapid increase of excess pore pressure in the undisturbed specimens, the increase in strains was slower and more constrained. On the other hand, upon reaching liquefaction, the reconstituted specimens exhibited large strains in both compression and extension.

For fines content higher than 6%, the undisturbed specimens showed higher resistance than the reconstituted specimen. The effect that fines have on the structure of the specimen can justify these

results. The behaviour of homogeneous specimens with FC < 30% is sand-particle dominated, which means that the fines might be inactive and disperse in the sand-dominated matrix. However, the natural soil undisturbed specimens were obtained through successive depositions of sand and silt in the alluvial soil, forming a non-homogeneous structure with layers and lamination. In this case, the sand-dominated matrix concept does not apply and both materials are engaged in the load-transfer paths. On the other hand, in the reconstituted specimen the soil is homogenised, and mixed randomly. In this case, the soil matrix is dominated by the sand, and the fines might be inactive. The differences in soil structure are likely the reason for the distinct cyclic response in specimens with low to moderate FC (8–40%).

The response of undisturbed and reconstituted specimens in terms of strains and excess pore pressure was also distinct in specimens with more than 6% FC. The undisturbed specimens showed a more stable behaviour than the respective reconstituted specimen, with a more steady and constant increase in r_u and more constrained axial strains even after the liquefaction stress criterion is reached (r_u=1). The development of strains was slow and the specimens did not reached the strain criteria ($\varepsilon_{a,DA}$=5%). Besides, the evolution of strains is biased to the extension side. This might be due to the structure of the undisturbed specimens, with layers and laminations that provide a more stable response even beyond liquefaction triggering. On the other hand, the reconstituted specimens exhibited small strain development for initial loading cycles, but rapidly developed increasingly large strains with the exceedance of the strain criteria, in both compression and extension directions. The excess pore pressure ratio increases at a high rate each cycle, reaching the liquefaction stress criterion in a few cycles. The reconstituted specimen behaviour is more unstable, as the liquefaction causes a complete loss of particles contact, and the development of large strains.

Taylor (2015) compared undisturbed and MT specimens of Christchurch soils, and found no significant different between the cyclic resistance curves of GP natural samples and MT specimens, for specimens with either FC < 5% or FC > 40%, which was not expected. Natural samples were expected to have higher cyclic resistance than MT specimens. However, Taylor (2015) stated that ageing effects might have been reduced due to recent earthquakes, justifying those findings. On the other hand, Cappellaro (2019) analysed the effect of fines content and layering in CDSS tests. Cappellaro (2019) found that the global fines content did not affect the liquefaction resistance of layered specimens, which was mainly governed by the sand layers. Layered specimens were compared with specimens prepared with water sedimentation and did not show significant differences in terms of liquefaction resistance. However, these results correspond to specimens tested under CDSS, where the cyclic loading is applied parallel to the layering, while the results from the present work were obtained from cyclic triaxial tests, where the cyclic loading is applied perpendicular to the layering. Further CDSS tests should be performed in undisturbed specimens to assess differences between undisturbed and MT specimens.

b) Varying CSR

As mentioned above, the GP specimens were sheared with different CSR throughout the shear stage: a selected CSR was applied in the first 30 or 50 cycles and was then increased to 1.5 times the initial value. The CSR is applied to the specimen by means of a vertical stress, introduced in the software prior to the beginning of the shear stage. As the first 30 or 50 cycles induce an increase in the pore pressure of the specimen, the confining pressure (p') considered in the calculation of CSR at the beginning of the second loading stage is altered, hence changing the CSR value calculated at the beginning of the test. This uncertainty in the behaviour of the specimens hindered the simulation of the shear stage of undisturbed specimens in the reconstituted specimens' tests. Therefore, in some cases, the reconstituted specimen was repeated and tested with different combinations of confining pressure and CSR. The analysis of results is very particular for each specimen, so each undisturbed specimen was analysed separately, with the respective reconstituted specimens.

Figure 10.14 presents the comparison between the shear wave velocities and void ratio of undisturbed and reconstituted specimens after consolidation (i.e. at the beginning of shear). It is observed that the void ratios of undisturbed and reconstituted specimens are around the 1:1 line, showing that the pairs of specimens had similar initial state conditions, which allows the comparison between cyclic liquefaction resistances. The comparisons are supported by the results of Figure 10.15, which presents the shear wave velocity normalised by the void ratio function. However, the shear wave velocities (and consequently the small strain stiffness, G_{max}) in undisturbed specimens were slightly higher than in reconstituted specimens, which would reflect on a lower compressibility of GP specimens and consequently the GP specimens would exhibit higher cyclic resistance than reconstituted specimens, if sheared with similar loading conditions.
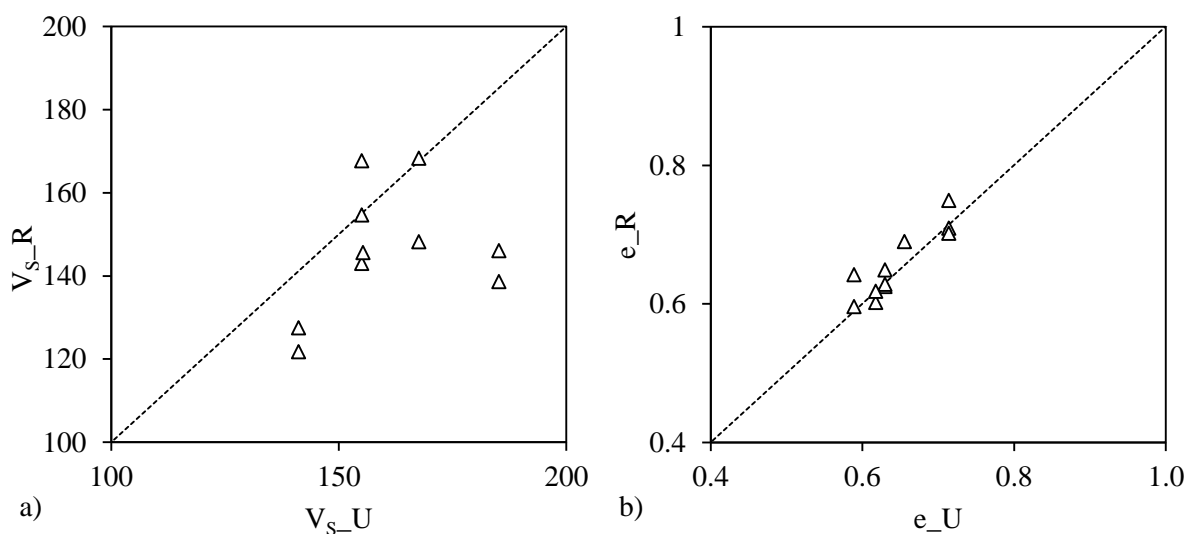
Figure 10.14 – Comparison between the a) shear wave velocity and the b) void ratio of undisturbed and reconstituted specimens after consolidation
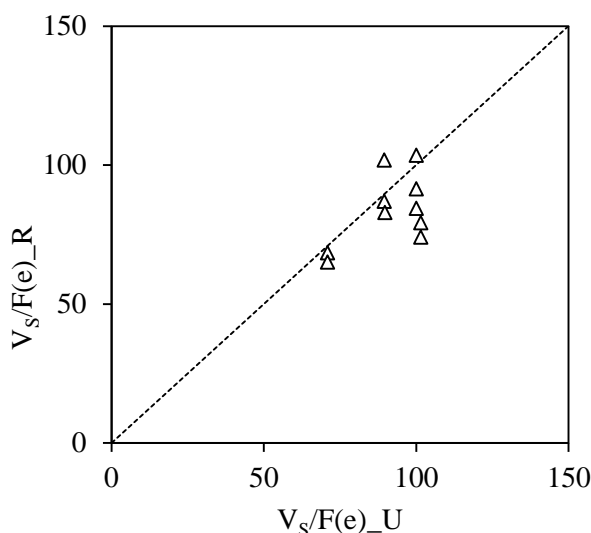
Figure 10.15 – Comparison between the shear wave velocity normalised by the void ratio function of undisturbed and reconstituted specimens

Figure 10.16 presents the cyclic behaviour comparison of effective stress path, stress-strain, and evolution of maximum pore pressure ratio and axial strain with number of cycles for NB1_F2_GP3.5_I1, NB1_F2_GP3.5_R1, and NB1_F2_GP3.5_R1_2, with D_R of 65%, 49%, and 62%, respectively, and FC of 9.4%. The undisturbed specimen was tested with an applied CSR of 0.12 that increased to 0.18 after 30 cycles. NB1_F2_GP3.5_R1 was tested at CSR=0.16, while NB1_F2_GP3.5_R1_2 was tested at CSR of 0.11, that increased to 0.19 after 30 cycles. All specimens were tested at p'=35 kPa. Both reconstituted specimens exhibited lower resistance than the undisturbed specimen, with an initial high strain in the compression direction and an exponential increase in strains

when approaching the zero effective stress condition. On the other hand, the undisturbed specimen exhibits a slow increase in strains, even after reaching the liquefaction stress criteria, and does not reach high strains with a maximum peak-to-peak axial strain of 1.2%. The first 30 cycles cause a higher increase of pore pressure on the reconstituted specimen than in the undisturbed specimen. It is interesting to note that comparing the two reconstituted specimens, NB1_F2_GP3.5_R1_2 liquefied at 33 cycles (excluding the first 30 cycles) while it took 24 cycles for specimen NB1_F2_GP3.5_R1 to reach liquefaction despite the lower CSR. This might be due to the slightly higher void ratio of NB1_F2_GP3.5_R1, which lowered its cyclic resistance.
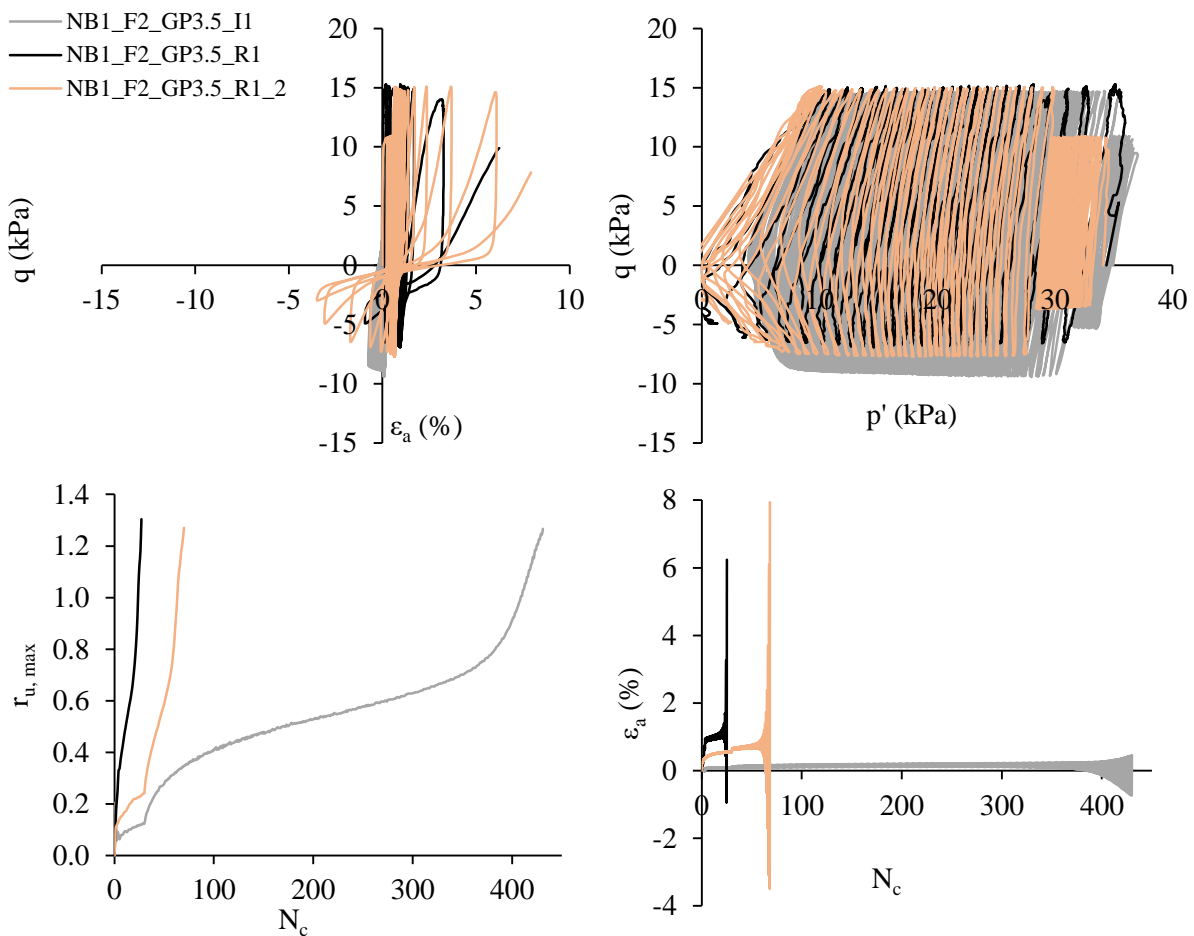
Figure 10.16 – Comparison of undisturbed and reconstituted specimens cyclic response (NB1_F2_GP3.5): a) stress-strain curves; b) effective stress path; c) maximum pore pressure ratio; and d) axial strain with number of cycles

Figure 10.17 presents the cyclic behaviour comparison of effective stress path, stress-strain, and evolution of maximum pore pressure ratio and axial strain with number of cycles for NB1_F1_GP4.5_I1, NB1_F1_GP4.5_R1, NB1_F1_GP4.5_R1_2, and NB1_F1_GP4.5_R1_3 with D_R of 54%, 56%, 58% and 43%, respectively, and FC of 3.8%. The undisturbed specimen was tested with an applied CSR of 0.11 that increased to 0.21 after 30 cycles. NB1_F1_GP4.5_R1 was tested at

CSR=0.20, NB1_F1_GP4.5_R1_2 was tested at CSR of 0.11, that increased to 0.18 after 30 cycles, and NB1_F1_GP4.5_R1_3 was tested at CSR of 0.12 for the first 30 cycles and 0.26 for the rest of the test. All specimens were tested at p'=45 kPa. The results show that small differences in loading might result in very distinct cyclic behaviour. While NB1_F1_GP4.5_R1_2 exhibited higher cyclic resistance than the undisturbed specimen, the other two reconstituted specimens were less resistant to liquefaction. Comparing the three reconstituted specimens with the undisturbed specimen, the following observations are made: NB1_F1_GP4.5_R1 was sheared at a constant value of CSR starting at the same initial confining pressure and exhibited lower resistance; NB1_F1_GP4.5_R1_2 exhibited higher pore pressure development in the first 30 cycles, but the rate of increase after those initial cycles was slower, and the specimen took more cycles (N_{liq}= 30+54) to achieve r_u=1, possibly due to the lower CSR (0.18); NB1_F1_GP4.5_R1_3 developed larger pore pressures during the first 30 cycles, achieving the stress criteria within three further cycles. In terms of strains, the reconstituted specimens exhibited similar tendencies, with initially low strains that developed into much larger strains upon loss of p'. On the other hand, the development of strain in the undisturbed specimen is at a lower rate and biased to the compression side.
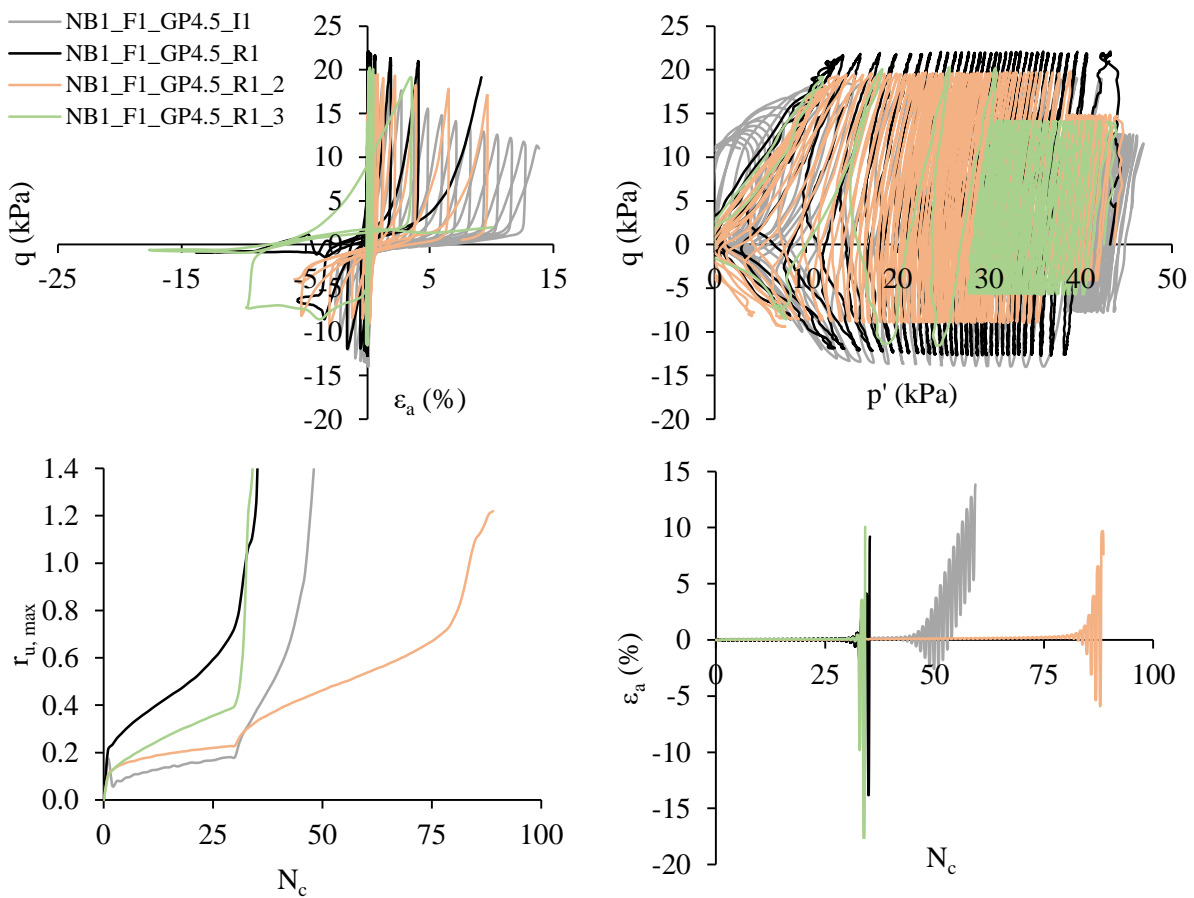
Figure 10.17 – Comparison of undisturbed and reconstituted specimens cyclic response (NB1_F1_GP4.5): a) stress-strain curves; b) effective stress path; c) maximum pore pressure ratio; and d) axial strain with number of cycles

Figure 10.18 presents the cyclic behaviour comparison of effective stress path, stress-strain, and evolution of maximum pore pressure ratio and axial strain with number of cycles for NB1_F5_GP5_I1, NB1_F5_GP5_R1, NB1_F5_GP5_R1_2, and NB1_F5_GP5_R1_3 with D_R of 77%, 78%, 77% and 70%, respectively, and FC of 3%. The undisturbed specimen was tested with an applied CSR of 0.12 and initial confining pressure of 45 kPa. However, a large increase in pore pressure after the first cycle took the CSR to 0.14 and p'=36 kPa. After 9 cycles, another jump in the pore pressure occurred and the specimen was tested at CSR=0.185 and p'=29 kPa for the rest of the initial 30 cycles. After 30 cycles, the CSR increased to 0.29 at p'=29 kPa. NB1_F5_GP5_R1 was tested at CSR=0.18 and p'=45 kPa, NB1_F5_GP5_R1_2 was tested at CSR of 0.11, that increased to 0.195 after 30 cycles, and NB1_F5_GP5_R1_3 was tested at CSR=0.29 with p'=29 kPa. The two reconstituted specimens that were tested with initial p'=45 kPa exhibited higher resistance than the undisturbed specimen, independently of being sheared with a constant CSR or a combination of two different CSR. However, it is worth mentioning that the specimen sheared first with 30 cycles at lower CSR exhibited much higher resistance than the reconstituted specimen tested at constant CSR. Apparently,

NB1_F5_GP5_R1_3 exhibited lower resistance (N_{liq}=26) than the undisturbed specimen (N_{liq}=30+23). However, if the first 30 cycles were excluded from the comparisons, the undisturbed specimen would have achieved liquefaction for lower number of cycles. The strains development is similar to the other cases, with the reconstituted specimens exhibiting initial small strains that increase exponentially upon loss of *p'*. The development of strain is slower in the undisturbed specimen, and biased to the extension side.
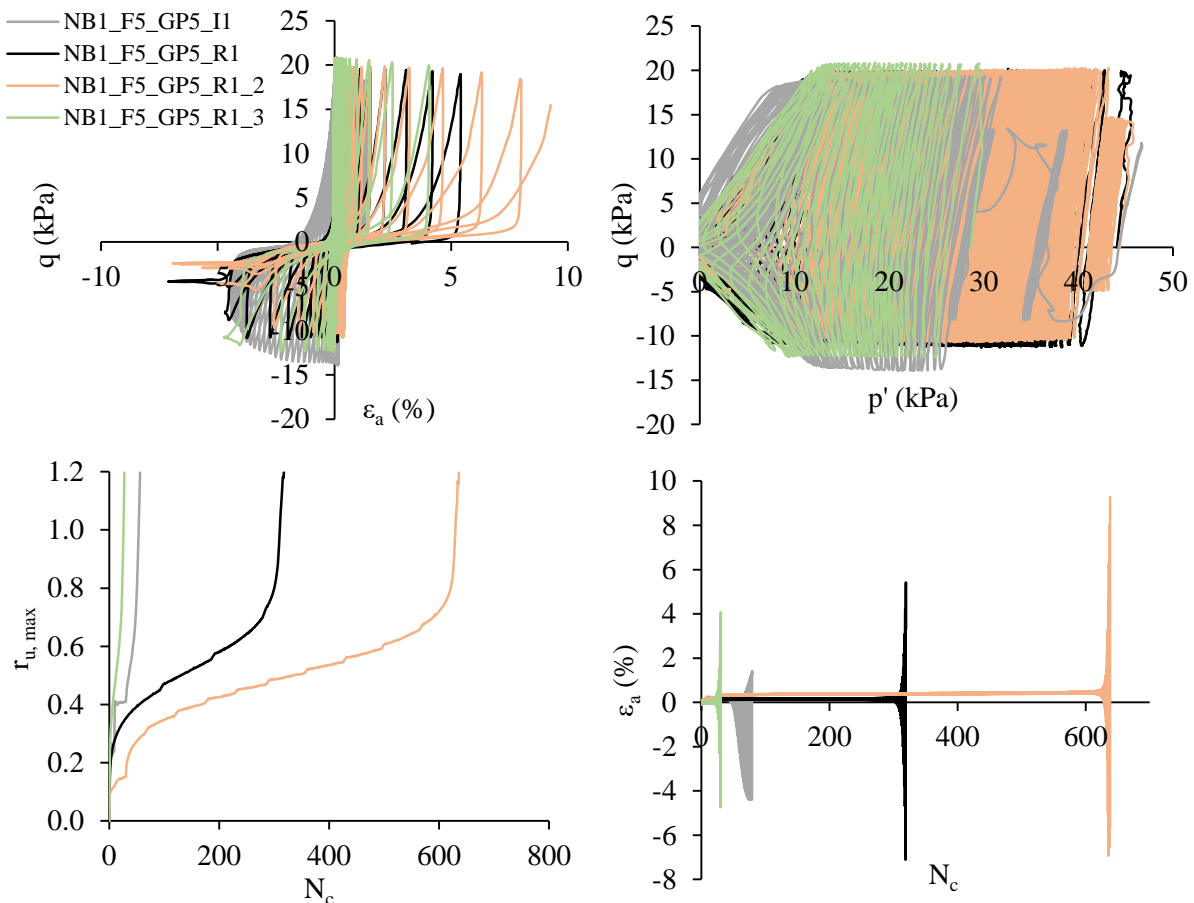
Figure 10.18 – Comparison of undisturbed and reconstituted specimens cyclic response (NB1_F5_GP5_1): a) stress-strain curves; b) effective stress path; c) maximum pore pressure ratio; and d) axial strain with number of cycles

Figure 10.19 presents the cyclic behaviour comparison of effective stress path, stress-strain, and evolution of maximum pore pressure ratio and axial strain with number of cycles for NB1_F5_GP5_I2, NB1_F5_GP5_R2, and NB1_F5_GP5_R2_2 with D_R of 85%, 90%, and 85%, respectively, and FC of 2.8%. The undisturbed specimen was tested with an applied CSR of 0.20 and initial confining pressure of 55 kPa. However, a large increase in pore pressure after the first cycle took the CSR to 0.315 and *p'*=34 kPa. The sudden pore pressure increase at the beginning of the undisturbed test lowered its resistance, and the specimen liquefied at 38 cycles. The two reconstituted specimens were tested at

constant CSR. NB1_F5_GP5_R2 was tested at CSR=0.186 and p'=55 kPa, and exhibited higher resistance than the undisturbed specimen. On the other hand, NB1_F5_GP5_R2_2 was tested at CSR=0.32 and p'=33 kPa and reached r_u=1 at lower number of cycles (N_{liq}=10) than the undisturbed specimen. The strains development is similar to the other cases, with the reconstituted specimens exhibiting initial small strains that increase exponentially upon loss of p', occurring to both extension and compression side. In the undisturbed specimen, the strains developed slower and were biased to the extension side.
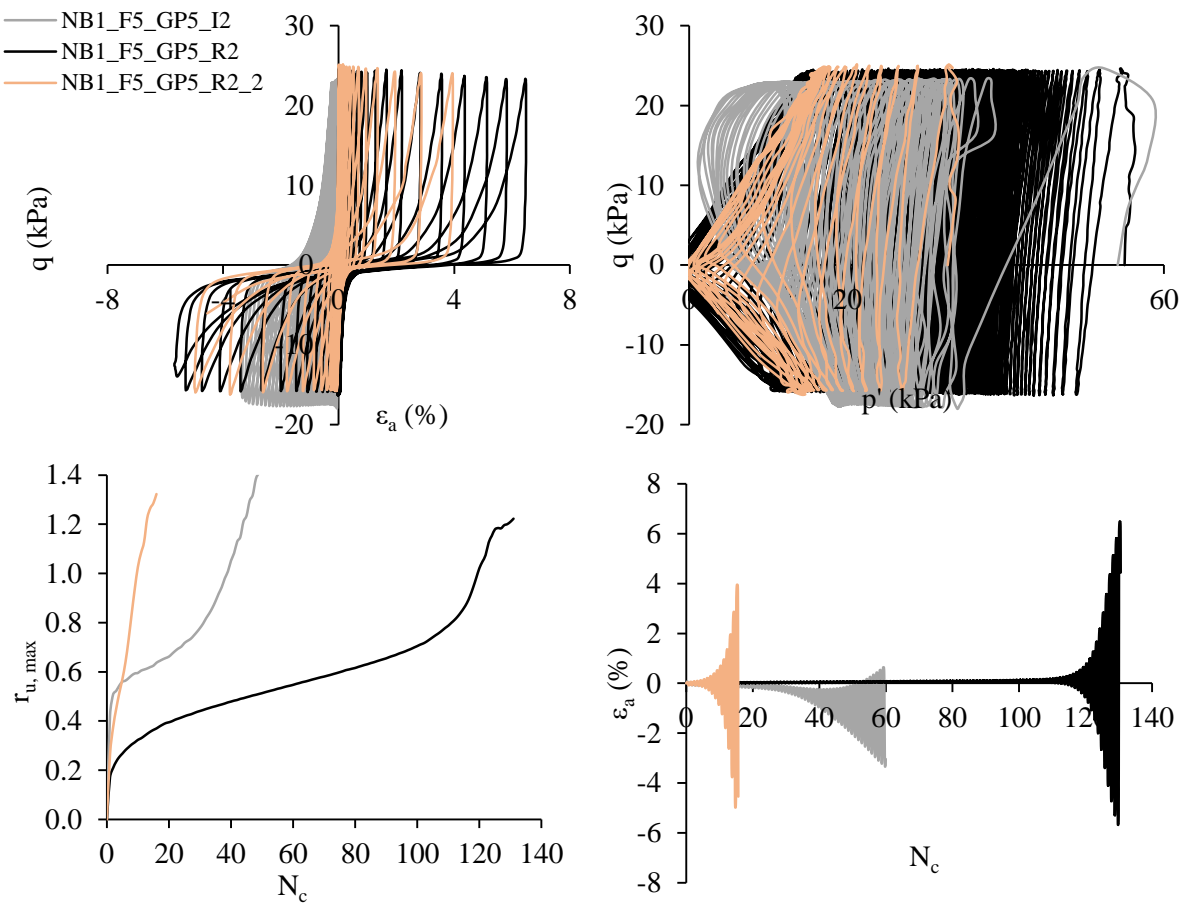
Figure 10.19 – Comparison of undisturbed and reconstituted specimens cyclic response (NB1_F5_GP5_2): a) stress-strain curves; b) effective stress path; c) maximum pore pressure ratio; and d) axial strain with number of cycles

Figure 10.20 presents the cyclic behaviour comparison of effective stress path, stress-strain, and evolution of maximum pore pressure ratio and axial strain with number of cycles for NB2_F1_GP6_I3, and NB2_F1_GP6_R3, with D_R of 56%, and 43%, respectively, and FC of 2.0%. The undisturbed specimen was tested with an applied CSR of 0.15 that increased to 0.28 after 50 cycles, while the reconstituted specimen was tested at CSR=0.14 that increased to 0.27 after 50 cycles. Both specimens were tested at p'=50 kPa. The loading conditions were similar, therefore the behaviour of the specimens

might be attributed to fabric and structure. The undisturbed specimen, despite the slightly higher density, exhibited lower N_{liq}. This results might be explained by the higher Vs/F(e) ratio of the reconstituted specimen, reflected on the lower compressibility and higher cyclic resistance of the reconstituted specimen. In this case, the moist-tamping procedure might have induced some additional fabric that increased the stability of the reconstituted specimen and consequently increased its resistance in relation to the undisturbed specimen. The strains development in the undisturbed specimen was steadier, while the reconstituted specimen exhibited an exponentially increasing rate of strains with successive cycles. Besides, the pore pressure developed in the first 50 cycles was higher in the reconstituted specimen. However, after the first 50 cycles of loading, the undisturbed specimens exhibited higher pore pressure development, and reached the stress criteria at 13 cycles, while the reconstituted specimen reached liquefaction at 19 cycles.
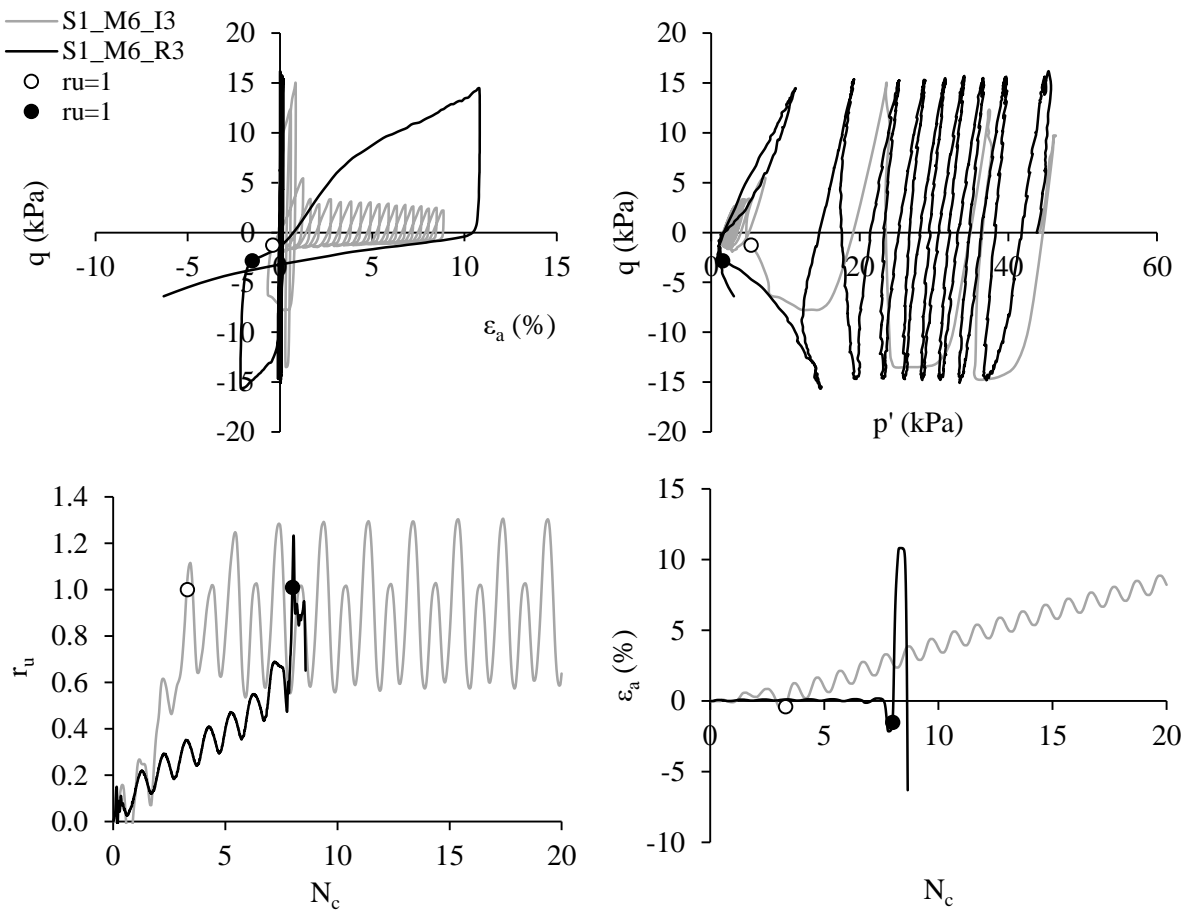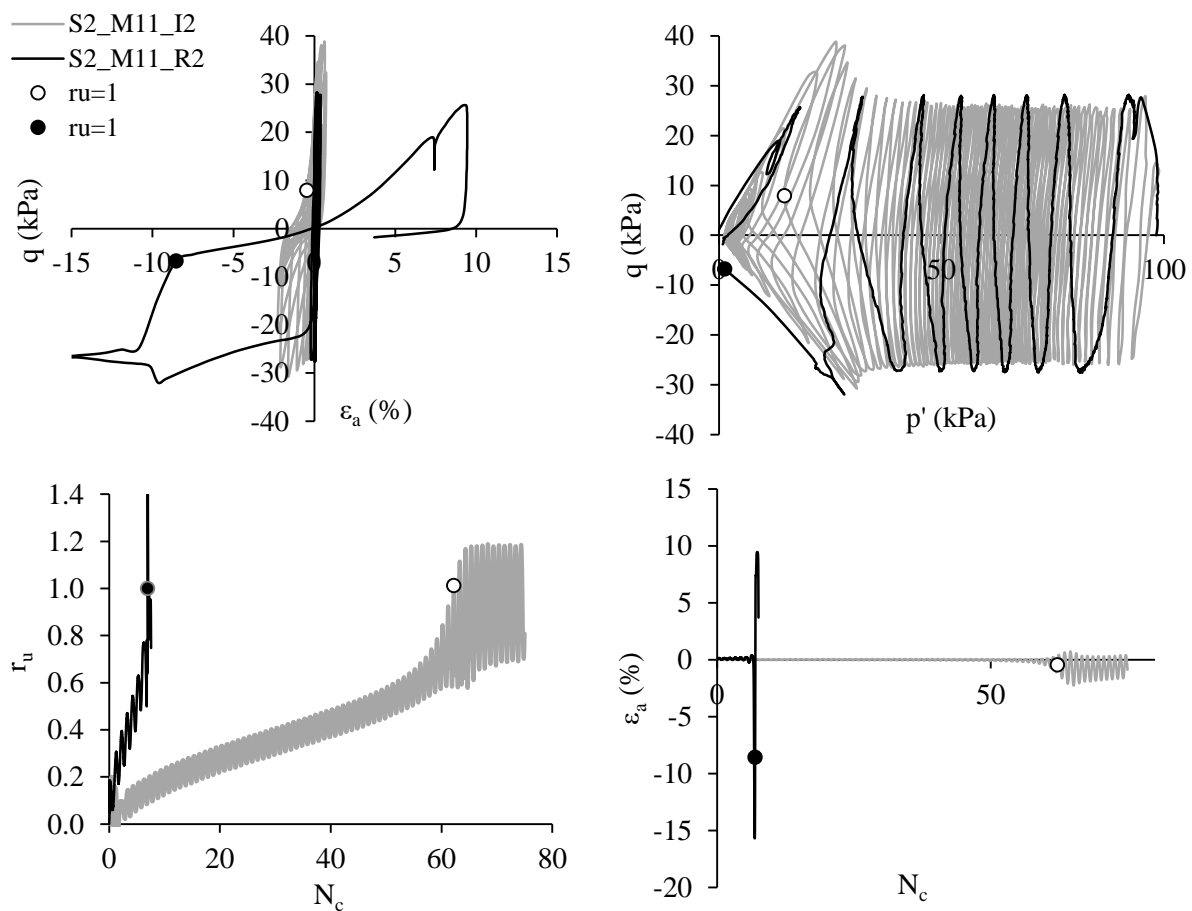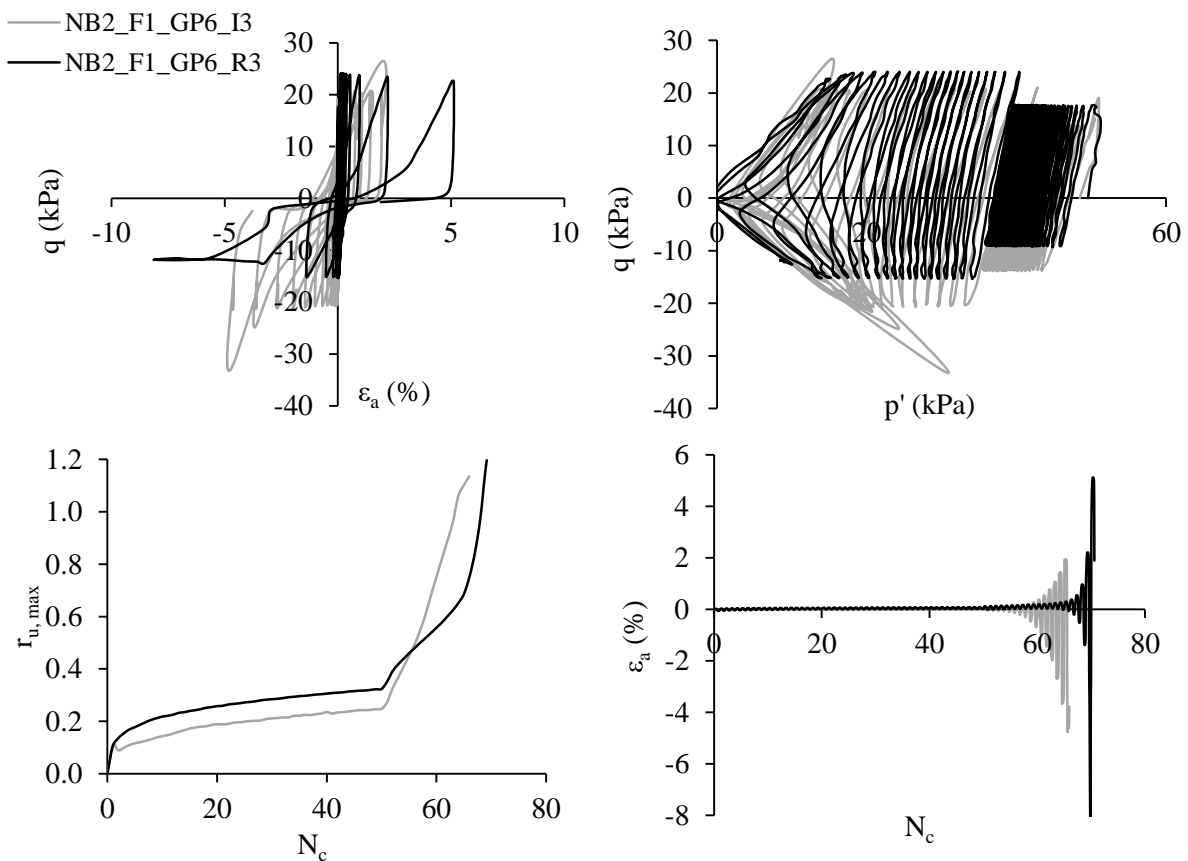

Figure 10.20 – Comparison of undisturbed and reconstituted specimens cyclic response (NB2_F1_GP6_3): a) stress-strain curves; b) effective stress path; c) maximum pore pressure ratio; and d) axial strain with number of cycles

The evaluation of fabric and structure influence on the GP specimens behaviour was not straightforward, as the loading conditions were not constant and affected the cyclic response. Despite this, the comparison of undisturbed and reconstituted specimens provided some interesting insights

about the differences in behaviour and influence of fabric and structure. When considering the comparison between the undisturbed specimen and the reconstituted specimen tested with the same applied CSR and confining pressure, the undisturbed specimens exhibited generally higher resistance than the reconstituted specimen. However, NB1_F1_GP6_I3 showed an opposite cyclic response, as the reconstituted specimen exhibited higher resistance. This was probably due to an additional fabric induced by the MT preparation procedure, that was reflected on the higher Vs/F(e) ratio, and consequently higher resistance, of the reconstituted specimen. The response of undisturbed and reconstituted specimens in terms of strains development was analogous to the observations in the Mazier specimens. The reconstituted specimens initially exhibited low strain development. However, upon reaching a certain number of cycles, as r_u increases, they exhibited an exponentially increasing rate of strains, that occurs to both compression and extension side. On the other hand, the undisturbed specimen exhibited, in general, a more stable behaviour, with a steady and constant increase in strains. Contrary to the observations of the Mazier specimens, some undisturbed GP specimens reached the strain criteria ($\varepsilon_{a,DA}$=5%) a few cycles after the stress criteria was reached. This might be due to the lower FC of GP specimens, reflecting on less layered specimens.

It is worth mentioning that the influence of the natural fabric in the behaviour found in cyclic triaxial tests might be different in cyclic simple shear tests, as, in the latter, the orientation of the layers and laminations is parallel to the loading direction.

10.2.3. INTERPRETATION OF CTX RESULTS THROUGH STATE PARAMETER

As mentioned above, for each undisturbed specimen tested under cyclic triaxial conditions, one pair of CSR-N_{liq} values was obtained, corresponding to the number of cycles required to trigger liquefaction for a selected CSR. Therefore, the determination of the cyclic resistance curve for each soil was not possible. However, the values of CRR$_{15}$ were computed with the equation from Figure 8.14, which relates CRR/CRR$_{15}$ with the number of cycles required to trigger liquefaction. Furthermore, the state parameter of each undisturbed specimens was computed using the critical state lines defined in 9.3. The state parameters were defined above in section 9.4.

The results of CRR$_{15}$ and respective state parameter were plotted together in Figure 10.21. It is observed that some results fit the trend defined by Jefferies and Been (2016) and agree with the reconstituted tests results, while other results do not agree with the defined trend. As mentioned above, the cyclic mobility is influenced by fabric and grain contact arrangements. These effects are more relevant in undisturbed specimens, as they present higher fines content, interlayers and laminations that, as discussed before, influence cyclic behaviour. The effects of fabric and structure might explain the deviations from the trend, which are less significant on the reconstituted specimens as they were

prepared with sands with low FC and without interlayers. Moreover, it is important to reflect on the uncertainty in the determination of state parameter of undisturbed specimen, as they were inferred from empirical relationships based on e_{max}-e_{min}.
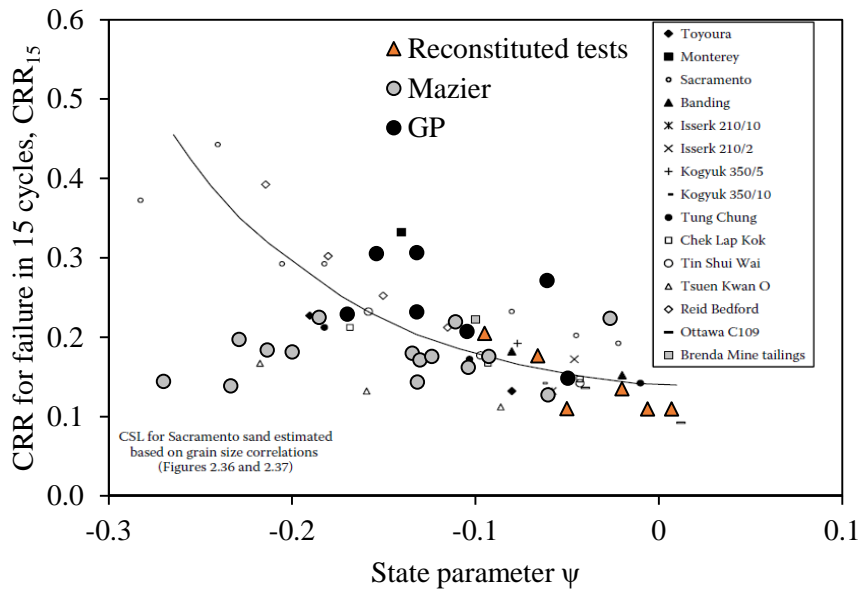
Figure 10.21 – CRR at 15 cycles as a function of state parameter of Mazier and GP specimens

10.2.4. PORE PRESSURE BUILD-UP IN CTX

The pore pressure build-up during the cyclic loading of a sand specimens tested under undrained conditions, is interconnected with the mechanisms of liquefaction. Therefore, in this section, the pore-pressure generation results of tests carried out in undisturbed tests are evaluated, and compared with the pore pressure build-up that occurred on the correspondent reconstituted specimen, prepared with MT to simulate the same initial conditions (void ratio and confining pressure). The pore pressure evolution with N_c/N_{liq} of Mazier undisturbed and respective reconstituted specimens are presented in Figure 10.22. It is observed that the pore pressure curves of undisturbed and reconstituted specimens are very similar, as the pairs of curves show good agreement. The results were also interpreted by using the equation proposed by Booker et al. (1976), and the parameter α was calibrated to provide the best fit with the actual test results, by means of the maximum R^2 value (defined in equation (8.1)). In terms of the α parameter, the best fitting values vary between 0.36 and 1.497, and deliver R^2 values of 0.87 in average. As each specimen is constituted by one type of soil, the value of α varies depending on the specimen.

As for the GP specimens, as in some cases the CSR changed in the middle of the loading stage, the pore pressure evolution curves do not fit the typical trend proposed by Booker et al. (1976). However, some conclusions can be drawn by the comparison of the pore pressure evolution curves (Figure 10.23). It is

observed that, for the specimens tested with change in CSR, the pore pressure ratio increased at a higher rate when CSR increased. The specimens of NB1_F2_GP3.5_I1, NB1_F4_GP4_I2, and NB1_F5_GP5_I1 soils showed similar pore pressure ratio evolution between undisturbed and reconstituted specimens. However, NB1_F5_GP5_I2 specimens showed a higher increase in pore pressure ratio at the beginning of shear, resulting in higher r_u–N_c/N_{liq} curves. On the other hand, when comparing the curves for NB1_F1_GP4.5_I1, NB2_F1_GP6_I2 and NB2_F1_GP6_I3, it was observed that the reconstituted specimens had a higher increase rate of r_u than the undisturbed specimens.

It is important to mention that the reproduction of the exact fabric and structure of the undisturbed specimens, especially when collected with high-quality equipment, is challenging. For that reason, it was very difficult to reproduce reconstituted GP specimens that simulated the same behaviour as the undisturbed specimens, as is observed in the results of Figure 10.23.
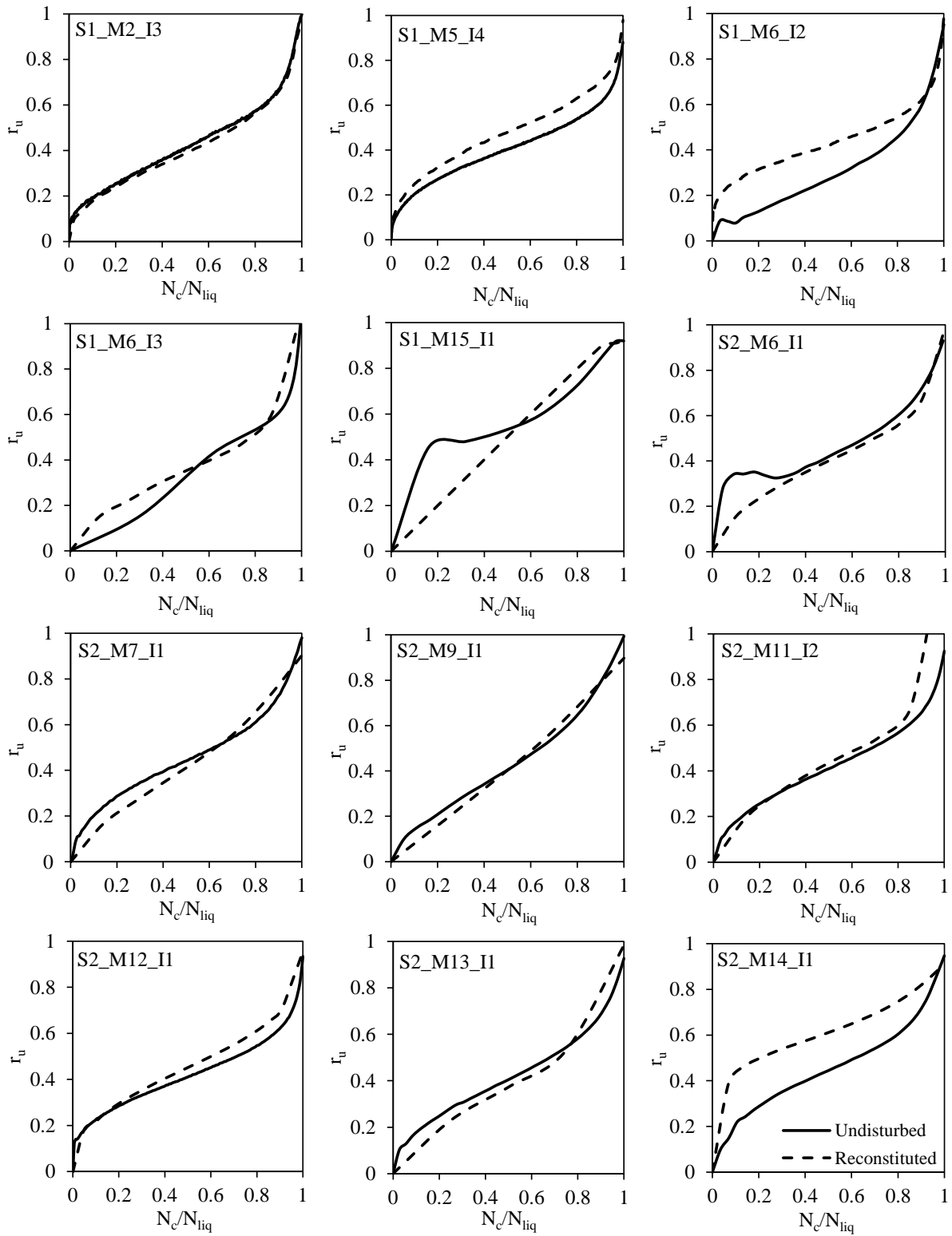
Figure 10.22 – Pore pressure ratio evolution with N_c/N_{liq} for undisturbed and reconstituted specimens collected with Mazier
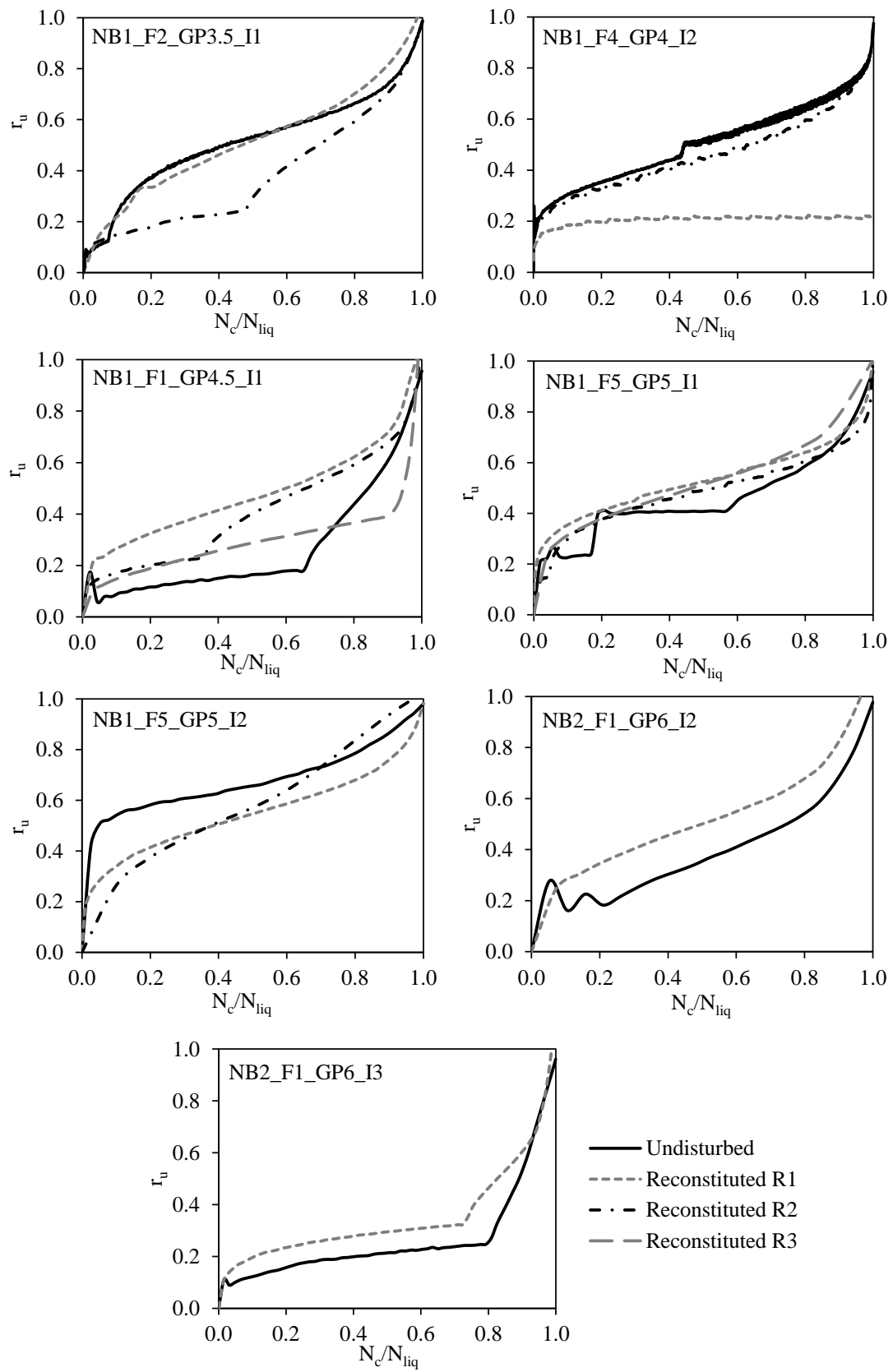
Figure 10.23 – Pore pressure ratio evolution with N_c/N_{liq} for GP tests

10.3. CYCLIC DIRECT SIMPLE SHEAR TESTS (CDSS)

The cyclic direct simple shear tests were performed in undisturbed specimens collected from Mazier samples that were opened in half to identify the internal structure of the specimens (refer to section 9.2.4). Each half of the specimen allowed the collection of a smaller undisturbed specimen, using a metallic ring with 63 mm of diameter and 24.8 mm of height. These specimens were collected in the opposite direction of sampling, as illustrated in Figure 6.20. As the size was suitable for the cyclic simple shear apparatus, the undisturbed specimens collected were tested under cyclic simple shear conditions.

The confining pressure was selected considering the corresponding triaxial test confining pressure at the same in situ depth. Since the triaxial confining stress was isotropic and in the simple shear the confining pressure is anisotropic, the vertical stress was calculated with equation (10.1), considering a K_0 of 0.5.

$$\sigma_v = \frac{3 \times p'}{2} \tag{10.1}$$

The loading waveform was sinusoidal with a frequency of 0.1 Hz. Similarly to the study of undisturbed specimens tested under triaxial conditions, after testing, the undisturbed specimens were homogenised and reconstituted for the same initial state conditions (similar void ratio, water content, and confining pressure). The cyclic resistance curves were obtained and the liquefaction failure criterion was the single amplitude shear strain of 3.75% (that corresponds to a double amplitude shear strain of 7.5%).

The effect of fabric on cyclic soil behaviour is discussed, by comparing the results of undisturbed and reconstituted specimens. The effect of water content is also addressed, as some specimens were not saturated and the different water contents might have an influence in the results. The undisturbed and reconstituted tests performed are presented in Table 10.3. The tabulated results are reported in Table C.7 in Appendix C, presenting the test identification (Test ID), the preparation method selected, the vertical stress (σ'_v), the void ratio after specimen preparation (e_0) and after consolidation (e_i), the initial and final water content (w_i and w_f, respectively), the state parameter (ψ), the cyclic stress ratio (CSR), the number of cycles (N_{liq}) required to develop 3.75% axial strain in single amplitude (γ_{SA}), and the cumulative dissipated energy until liquefaction (ΔW_{liq}).

Table 10.3 – List of cyclic direct simple shear tests performed with undisturbed and respective reconstituted specimens

Test ID	Method of sample preparation	σ_v (kPa)	Freq (Hz)	w_f (%)	e_i	CSR (τ/σ'_{v0})
S2_M12_I2	Undisturbed	165	0.1	16	0.58	0.24
S2_M12_I3_1	Undisturbed	165	0.1	27	0.75	0.16
S2_M12_I3_2	Undisturbed	165	0.1	27	0.77	0.20
S2_M13_I2	Undisturbed	150	0.1	23	0.71	0.27
S2_M13_I3_1	Undisturbed	150	0.1	24	0.64	0.18
S2_M13_I3_2	Undisturbed	150	0.1	26	0.72	0.22
S2_M14_I2	Undisturbed	112.5	0.1	19	0.56	0.22
S2_M14_I3	Undisturbed	112.5	0.1	24	0.63	0.32
S2_M12_R2_MT1	MT w=16%	165	0.1	13	0.53	0.24
S2_M12_R2_MT2	MT w=16%	165	0.1	14	0.55	0.15
S2_M12_R2_MT3	MT w=16%	165	0.1	13	0.58	0.20
S2_M12_R2_MT4	MT w=16%	165	0.1	13	0.59	0.24
S2_M12_R3_MT1	MT w=24.7%	165	0.1	22	0.76	0.16
S2_M12_R3_MT2	MT w=24.7%	165	0.1	22	0.75	0.20
S2_M13_R2_MT1	MT w=23%	150	0.1	21	0.71	0.27
S2_M13_R2_MT2	MT w=23%	150	0.1	21	0.69	0.20
S2_M13_R2_MT3	MT w=23%	150	0.1	20	0.71	0.21
S2_M13_R3_MT4	MT w=25%	150	0.1	21	0.70	0.20
S2_M13_R3_MT5	MT w=30%	145	0.1	23	0.71	0.20
S2_M14_R2_MT1	MT w=19%	112.5	0.1	17	0.69	0.19
S2_M14_R2_MT2	MT w=19%	112.5	0.1	16	0.62	0.24
S2_M14_R2_MT3	MT w=19%	112.5	0.1	16	0.61	0.15
S2_M14_R2_MT4	MT w=19%	112.5	0.1	16	0.60	0.29
S2_M14_R2_MT5	MT w=19%	112.5	0.1	17	0.63	0.28

10.3.1. EFFECT OF FABRIC – COMPARISON BETWEEN UNDISTURBED AND RECONSTITUTED SPECIMENS IN CDSS

The effect of fabric was assessed by comparing the cyclic direct simple shear tests results of undisturbed specimens with the corresponding reconstituted specimen. The reconstituted specimens were prepared with the moist tamping technique to produce specimens with similar void ratio and water content as the undisturbed specimens. The confining pressure was applied by gradually increasing the vertical stress, as the specimen was confined laterally by copper rings. The cyclic tests were performed with constant volume conditions, by fixing the sample height and measuring the variation of vertical stress.

Figure 10.24 shows the results for samples collected at 12 m depth. The filled symbols correspond to the results of tests performed in undisturbed samples (one from S2_M12_I2 and two from S2_M12_I3), while the open squares and triangles correspond to the reconstituted samples performed with S2_M12_R2 and S2_M12_R3, respectively. The confining pressure was always constant and equal to 165 kPa. The void ratio of S2_M12_I2 was smaller than S2_M12_I3, therefore, the reconstituted specimens tried to simulate that range of values. Observing the open squares results, two points are

located slightly above the other two, justified by a slightly lower void ratio and consequently higher relative density (around 0.54 for the upper points and 0.58 for the lower points).

Additionally, S2_M12_I2 and S2_M12_I3 had different water content. In this case, the effect of the water content is not detected on the cyclic resistance, which might be due to a combination of factors. The specimens with higher water content had higher void ratios, while the specimens with lower void ratio had lower water content. On the other hand, the small differences in fines content, that range between 6 and 10%, do not seem to influence the results.

It is possible to conclude that no clear distinction between the results was found and the undisturbed and reconstituted results seem to fall in the same curve, despite the differences in void ratio, water content and fines content of each specimen.
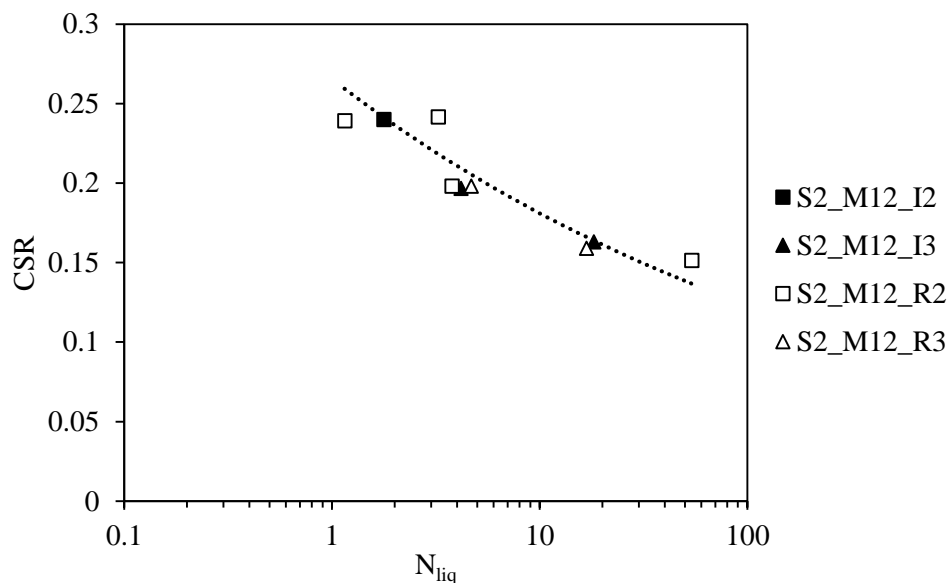
Figure 10.24 – Cyclic resistance curves for S2_M12

The results from the samples collected from 13 m depth are reported in Figure 10.25. There seems to be a difference in the undisturbed and reconstituted curves, being the undisturbed specimens more resistant (higher number of cycles to liquefy for the same CSR). As the reconstituted specimens were prepared to simulate the undisturbed specimens conditions, this result seems adequate, as the undisturbed specimens have a more stable structure, due to the fines layering, which is lost when the soil is homogenised. The water content of the undisturbed specimens is slightly higher than four of the reconstituted specimens, however, S2_M13_R3_MT5 has a water content similar to the undisturbed specimens and confirms the trend. The GSD curves were also similar, and both samples have around 11.5% fines content. In this case, there is no significant variation in void ratios, which facilitates the comparisons as there are less different factors to account for.
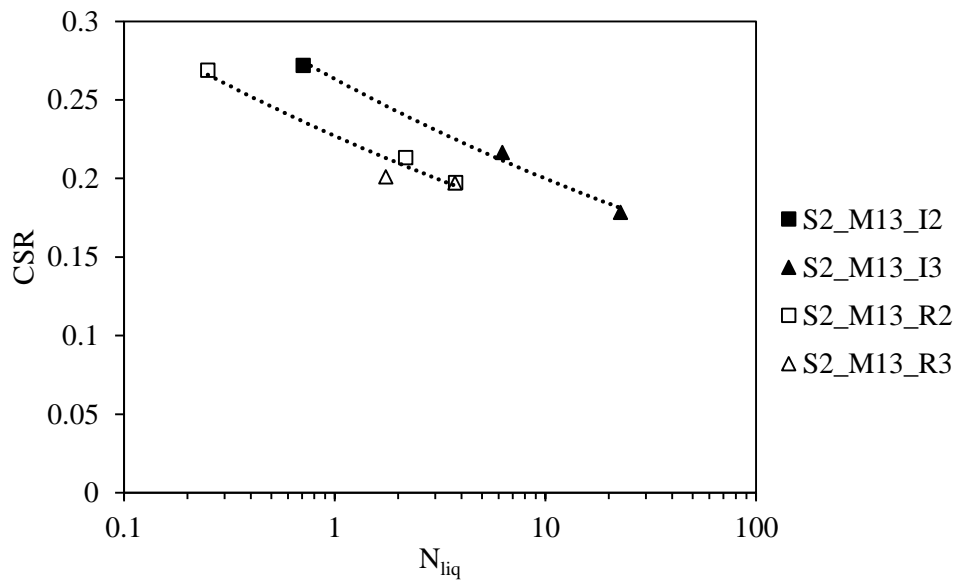
Figure 10.25 – Cyclic resistance curves for S2_M13

Figure 10.26 presents the results of soils collected at 14 m depth, with two undisturbed specimens tested. In this case, slight differences in the void ratio, in the reconstituted tests, show differences in resistance, as three specimens tested under different values of CSR required approximately the same number of cycles to trigger liquefaction. As expected, the specimen with a lower void ratio of 0.60 (higher density) is more resistant than the specimen with a higher void ratio of 0.69 (lower density). Moreover, the undisturbed specimens fall in the same cyclic resistance curve as the reconstituted specimens, although one having a lower void ratio (0.56) than the other (0.63). The differences in water content, which ranges from 16 to 25%, seem to not affect the results, as well as the differences of fines content (S2_M14_I2 has 8.7% FC while S2_M14_I3 has 25% FC). However, the number of tests performed in undisturbed specimens is insufficient for accurately evaluating the water content and fines content influence on the results.
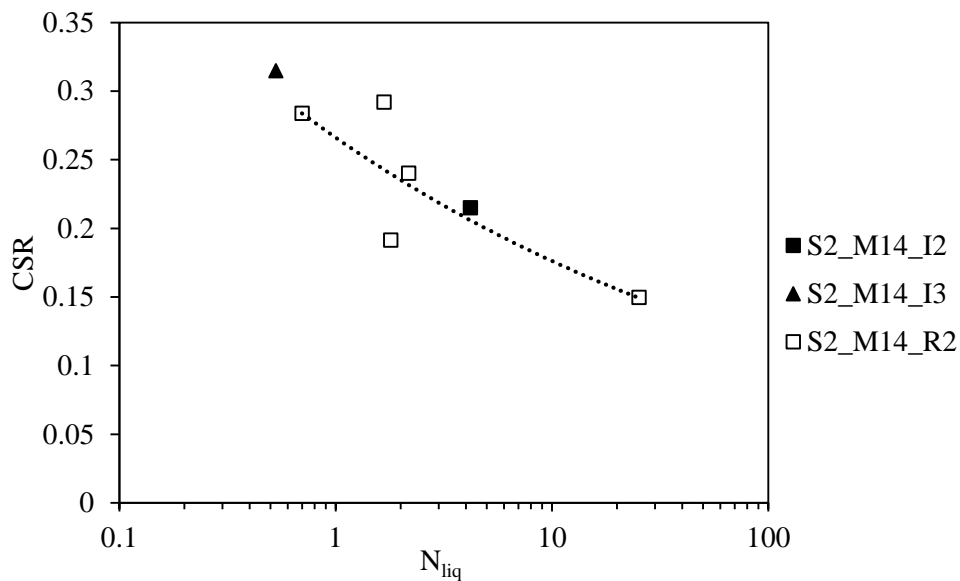
Figure 10.26 – Cyclic resistance curves for S2_M14

Although there are a variety of factors to consider when comparing the behaviour of undisturbed and reconstituted specimens, in this case some conclusions can be drawn. In the S2_M12 samples, the water content seems to not influence the results, however, the effect of water content might be suppressed by the difference in void ratios. The S2_M13 specimens were the most comparable as they had approximately the same void ratios and water content, and similar GSD curves, with the same percentage of fines. The results of this set of tests show that undisturbed specimens with more than 11% percentage of fines are more resistant to cyclic loading that reconstituted specimens.

10.4.   COMPARISON OF CSR-N$_{LIQ}$ CURVES OF LABORATORY TESTS WITH CPTU DATA

A soils resistance to liquefaction is often represented by the cyclic/liquefaction resistance curve, which relates the Cyclic Stress Ratio (CSR) with the number of cycles required for liquefaction to occur (N_{liq}). These curves might be obtained by cyclic laboratory tests in undrained conditions and are important parameters in the calibration of constitutive models.

In order to compare the CSR-N_{liq} obtained in the laboratory with the CPTu data, CSR-N_{liq} curves were determined based on q_{c1Ncs} from the CPTu results. The procedure to determine the cyclic resistance curves from CPTu data followed the simplified liquefaction triggering procedure of Boulanger and Idriss (2014), and is described in Cubrinovski et al. (2017). The approach can be summarised in 5 steps:

1 – The cyclic stress ratio (CSR) corresponding to 15 cycles (equivalent to the reference moment magnitude of 7.5) and effective overburden stress of $\sigma'_{v0} = 100$ kPa ($CSR_{Nc=15;\sigma'v=100kPa} = CRR_{M=7.5;\sigma'v=1}$) is obtained by equation (2.48).

2 – The magnitude scaling factor (MSF) is computed from equation (10.2) for a relevant range of magnitudes. MSF is related to q_{c1Ncs} through MSF_{max}, as described in equation (10.3).

$$MSF = 1 + (MSF_{max} - 1)\left(8.64\, exp\left(\frac{-M}{4}\right) - 1.325\right) \tag{10.2}$$

$$MSF_{max} = 1.09 + \left(\frac{q_{c1Ncs}}{180}\right)^3 \leq 2.2 \tag{10.3}$$

3 – To determine the CSR for different number of cycles, the $CRR_{M=7.5}$ must be multiplied by MSF:

$$CSR_{N_c;\sigma'_v=100kPa} = CRR_{M=7.5;\sigma'_v=1} \cdot MSF \tag{10.4}$$

4 – The number of cycles is associated to the magnitude, hence to MSF values, and is estimated using equation (10.5). The values of the exponent b were obtained using the MSF_{max}-b relationship proposed by Boulanger and Idriss (2014) (Figure 10.27).

$$N_c = \frac{15}{MSF^{1/b}} \tag{10.5}$$
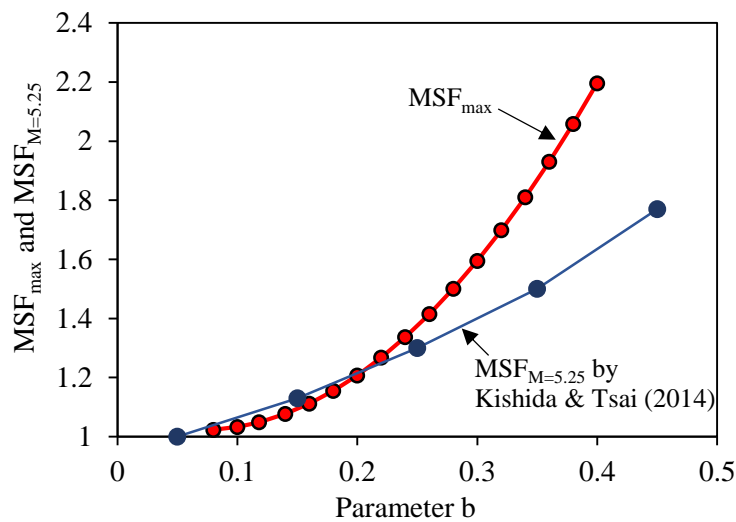
Figure 10.27 – Variation of MSF_{max} with parameter *b* (Boulanger and Idriss, 2014)

5 – The cyclic resistance curves are adjusted for the overburden stress effect, using the overburden stress correction factor K_σ, using equations (10.6) through (10.8):

$$\mathrm{CSR}_{\mathrm{N}_c;\sigma'_v} = \mathrm{CRR}_{\mathrm{N}c;\sigma'_v=100} \cdot K_\sigma \tag{10.6}$$

$$K_\sigma = 1 - C_\sigma \ln\left(\frac{\sigma'_v}{p_a}\right) \le 1.1 \tag{10.7}$$

$$C_\sigma = \frac{1}{37.3 - 8.27(q_{c1Ncs})^{0.264}} \le 0.3 \tag{10.8}$$

As referred throughout this work, there are several factors that affect the cyclic behaviour of soils, hence the cyclic resistance curve position varies according to fines content, relative density, sample preparation procedure, confining pressure, and fabric and structure. In this section, the comparisons between CPTu data and laboratory tests were made by comparing the cyclic resistance curves obtained in cyclic direct simple shear of undisturbed specimens (section 10.3.1) and the respective CPTu curve. These laboratory tests were selected as the specimens were undisturbed, and complete cyclic resistance curves were available, contrary to the results of triaxial tests on undisturbed specimens that only provide one value of CSR-N_{liq} for each sample. Nevertheless, the cyclic triaxial test results, represented by one point for each soil, were also compared with the CPTu-based cyclic resistance curve.

The three curves available correspond to three different soils, at 12 m, 13 m, and 14 m depth in soil profile S2, which q_{c1Ncs} values are around 74, 81, and 65, respectively. Table 10.4 presents the factors used to plot the cyclic resistance curves of the three layers. Moreover, the CSR$_{field}$ obtained is divided by 0.9, to account for the multidirectional shaking effect of earthquakes on the site that is not reproduced in the laboratory in unidirectional cyclic simple shear tests (Seed et al., 1975) (refer to equation (2.76)).

Table 10.4 – Parameters used to plot the cyclic resistance curves from CPTu data

Samples	Depth (m)	q_{c1Ncs}	MSF$_{max}$	b	σ'_v (kPa)	K_σ
S2_M12	12	74	1.159	0.181	165	0.96
S2_M13	13	81	1.181	0.19	150	0.96
S2_M14	14	65	1.137	0.172	112.5	0.99

Figure 10.28 to Figure 10.30 presents the results for S2_M12, S2_M13, and S2_M14 cyclic direct simple shear tests, respectively, plotted together with the cyclic resistance curve determined with the respective q_{c1Ncs} values. In order to compare the CSR-N_{liq} from field, cyclic direct simple shear, and cyclic triaxial tests, equation (2.76) was used to normalise all the results. The c_r was computed using the relationship by Ishihara et al. (1985) and considering K_0=0.5. As the results are normalised, it was expected that all points would be coincident and represented in the same cyclic resistance curve. However, this was not observed, as the results show the cyclic resistance curve of CDSS tests to be

higher than the curve determined by field data. On the other hand, the results from CTx tests showed good agreement with the cyclic resistance curve from the CPTu data.

There are some possible causes for these differences that are discussed herein in an attempt to explain the results. The saturation degree of the CDSS tests was considered a possible cause for the divergence in results. However, the undisturbed specimens had high water contents, which reflected on higher saturation degrees (between 75-100%). Considering the results of the effect of water content/saturation degree on the cyclic resistance of these soils (section 8.3.3), this factor was ruled out as a justification for the differences found between CDSS and field results. Therefore, the most probable cause of the observed differences in cyclic resistance is the orientation of the layering within the undisturbed specimens. The undisturbed specimens tested in CDSS were collected perpendicularly to the sampling direction, as explained in section 6.5.2, while the CTx specimens were collected vertically, following the same direction as sampling. The layering and laminations of the specimens tested in CDSS were perpendicular to the shear direction, which might have increased the resistance of the specimens tested under CDSS conditions.
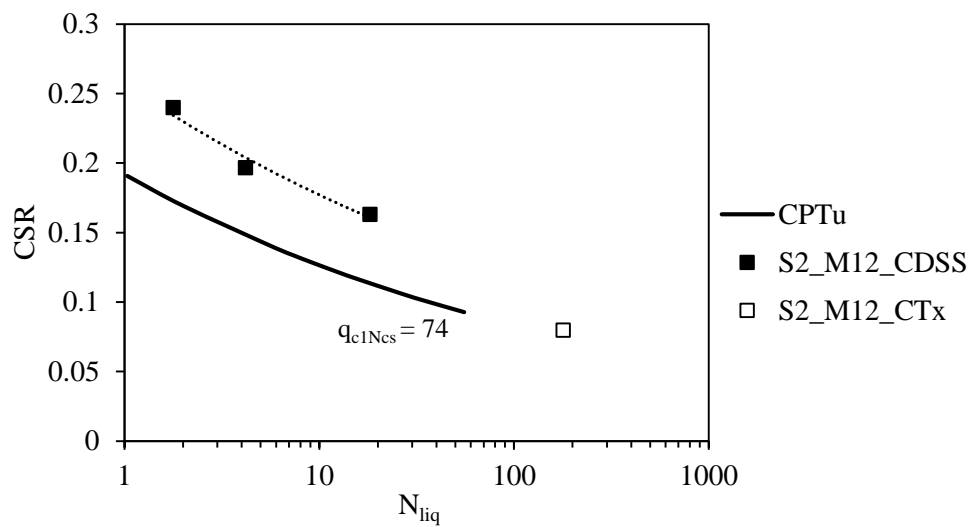
Figure 10.28 – Comparison of cyclic resistance curves from CPTu and laboratory data for S2_M12
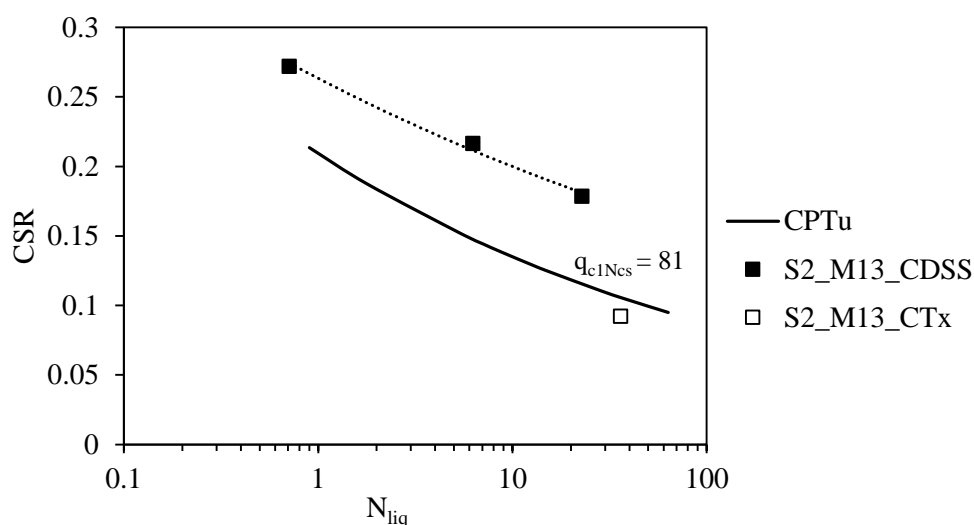
Figure 10.29 – Comparison of cyclic resistance curves from CPTu and laboratory data for S2_M13
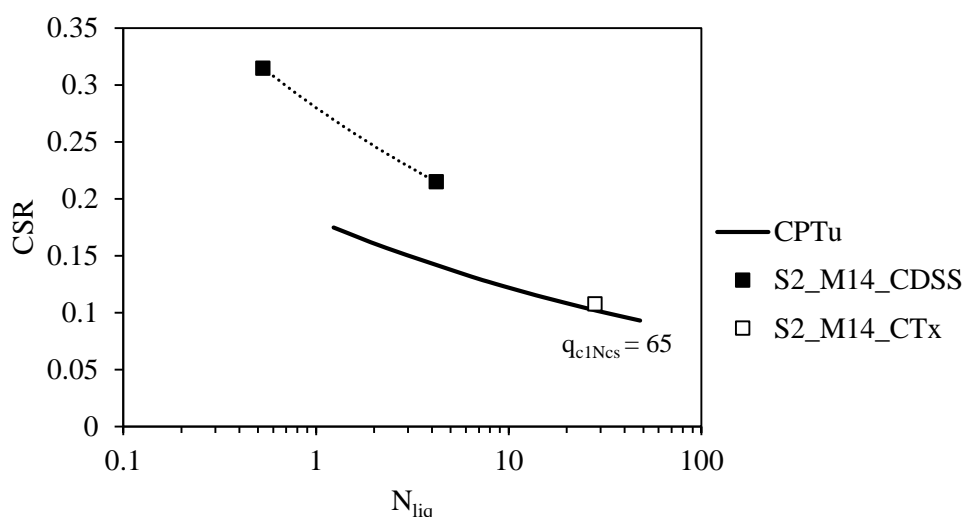
Figure 10.30 – Comparison of cyclic resistance curves from CPTu and laboratory data for S2_M14

10.5. ASSESSMENT OF THE FACTOR OF SAFETY AGAINST LIQUEFACTION IN THE LABORATORY

The factor of safety against liquefaction (FS$_{liq}$) is defined as the ratio between the soil resistance to liquefaction (CRR), and the cyclic loading (CSR), as expressed in equation (2.10). As stated in Chapter 2, the value of CRR$_{7.5}$ can be obtained from empirical correlations based on in situ tests results. Moreover, CRR may also be obtained from laboratory tests results and related to the applied CSR to compute the FS$_{liq}$ of each undisturbed specimen.

In this section, a procedure to determine the FS$_{liq}$ of the undisturbed specimens collected with Mazier and Gel-Push sampler is introduced and discussed. Since the applied CSR is already known, the next

step is to determine the CRR, which in this case is considered to be the value of the cyclic resistance curve corresponding to 15 cycles (CRR_{15}). As discussed above, for each depth, only one undisturbed specimen was collected and tested under cyclic triaxial conditions. Each specimen was tested with an applied CSR and liquefied in a certain number of cycles (N_{liq}). As one single point is not sufficient to define the cyclic resistance curve of that soil, a procedure was adopted to estimate the cyclic resistance curve of the undisturbed soils, based on the results of the reconstituted specimens prepared with the same soil and to the same initial conditions (i.e., with the same state parameter). This procedure involved the plotting of the CSR-N_{liq} results of the reconstituted specimen and the estimation of CRR_{15}_R from the equation on Figure 8.14, using the CSR/CRR_{15}−N_{liq} correlation proposed by Jefferies and Been (2016). At this stage, two points define the cyclic resistance curve of the reconstituted specimen, and a power law was fit to the two points (Figure 10.31a).

As the reconstituted specimen and undisturbed specimen have similar state parameters (the specimen had the same initial void ratio and confining pressure), the cyclic resistance curve of the undisturbed specimen was considered parallel to the reconstituted specimen. With that in mind, the cyclic resistance curve of the undisturbed specimen was determined, as well as the value of CRR_{15}_U, the CSR value for N_{liq}=15 (Figure 10.31b).
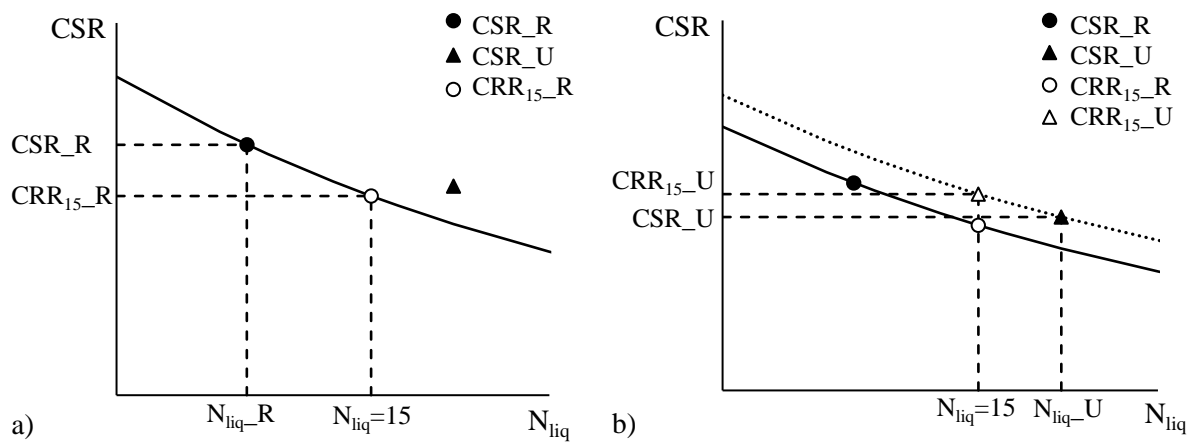
Figure 10.31 – Procedure to obtain CRR_{15} of undisturbed specimens

The FS_{liq} is computed by the ratio of the CRR_{15} and the applied CSR, as follows:

$$FS_{liq} = \frac{CRR_{15}\_U}{CSR\_U} \tag{10.9}$$

Following the procedure described above, the FS_{liq} of all undisturbed specimens tested under cyclic triaxial conditions were estimated. It is obvious that the factor of safety in the laboratory is higher than 1 for specimens that liquefied for more than 15 cycles and lower than 1 for specimens that liquefy in

under 15 cycles. Moreover, the FS_{liq} was related to N_{liq} for each test and the best fitting trend was obtained (Figure 10.32). Due to the procedure adopted to determine CRR_{15}, the equation of FS_{liq} (CRR_{15}/CSR) plotted against N_{liq} is actually the inverse of the equation defined in Figure 8.14 ($CRR/CRR_{15}-N_{liq}$).

$$FS_{liq} = 0.6391 N_{liq}^{0.1606}$$
$$R^2 = 0.9518$$
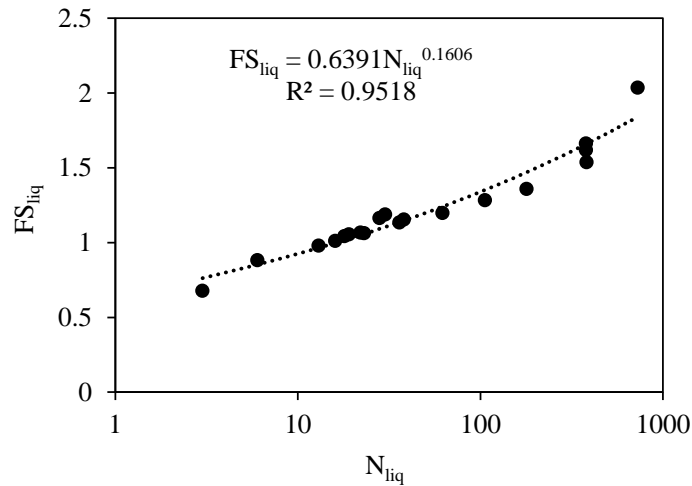
Figure 10.32 – Factor of safety against liquefaction related to N_{liq}

Moreover, the FS_{liq} determined in the laboratory tests was compared with the FS_{liq} determined based on the CPTu results. It is important to note that the FS_{liq} determined with the CPTu tests were recalculated using a peak ground acceleration correspondent to the average a_{max} (0.09g) determined with the CSR applied to the cyclic triaxial tests, after normalisation to the CSR_{field} as described in equation (2.76).

The comparisons between the FS_{liq} determined by the CPTu results (FS_{liq}_CPTu) and the FS_{liq} determined in the laboratory tests (FS_{liq}_lab) are illustrated in Figure 10.33. No clear correspondence between the results is perceived as, in some cases, the FS_{liq}_CPTu is higher than FS_{liq}_lab, while in other cases the opposite is observed. It is worth mentioning that direct comparisons between field and laboratory results were difficult, since the action imposed in the field was an average value of $a_{max}=0.09g$, and was not exactly the same as the applied CSR in the laboratory, which varied slightly according to the specimen tested.
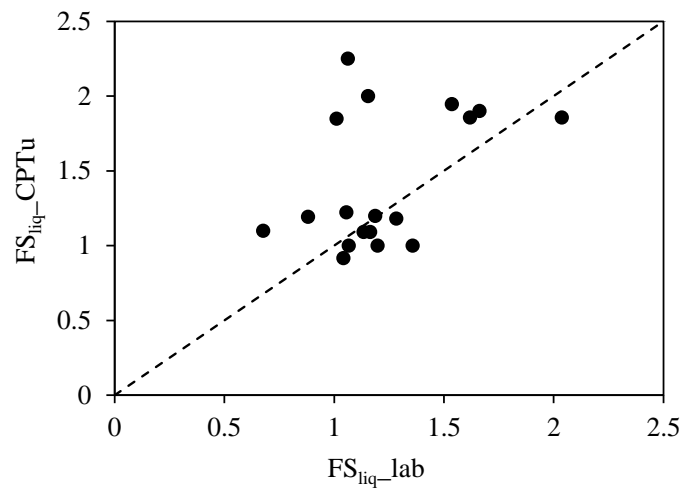
Figure 10.33 – Comparison between FS_{liq} obtained from CPTu and laboratory tests

Furthermore, the cyclic resistance ratios (CRR) determined with CPTu and CTx results are compared in Figure 10.34a. It is observed that the CRR_{15}_lab values are consistently higher than the CRR_{15}_CPTu. However, when the CRR_{15}_lab values are normalised to account for the differences between the cyclic shear conditions, according to equation (10.10), the results approximate the 1:1 line (Figure 10.34b). These results contribute to the reinforcement of the use of the proposals from Seed et al. (1975) and Ishihara et al. (1985), which stated that the CSR required to trigger liquefaction in the field was 10% less than that required in triaxial tests, and suggested c_r factor to account for the differences in cyclic conditions, respectively.

$$CRR_{15}\_lab^* = 0.9 \times \frac{1 + 2K_0}{3} \times CRR_{15}\_lab \qquad (10.10)$$
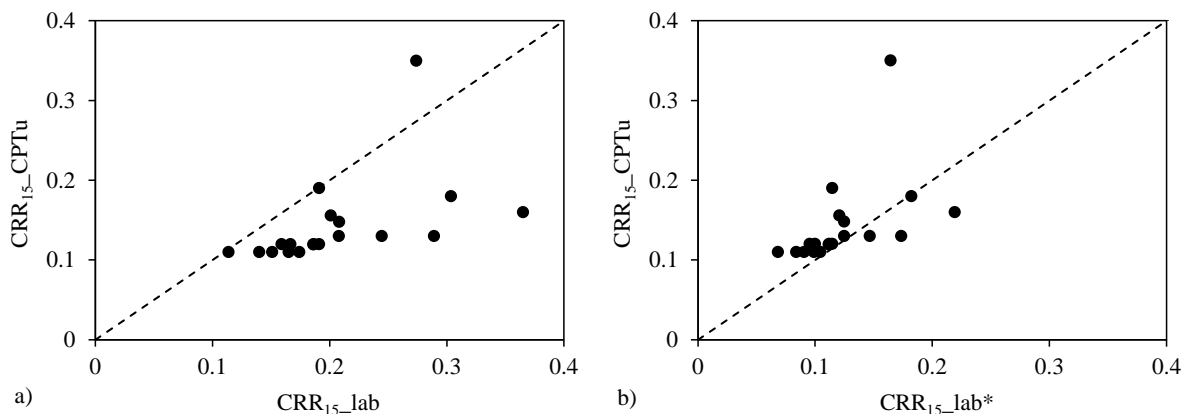
Figure 10.34 – Comparison between CRR_{15} obtained from CPTu and laboratory tests: a) without normalisation; b) with normalisation

10.6.   CHAPTER SUMMARY

This chapter presented the results of cyclic triaxial and cyclic direct simple shear tests performed on undisturbed samples collected with Mazier and Gel-Push samplers. The undisturbed specimens collected are examples of the variety of soils found in the 4 experimental sites studied, as each specimen is basically a unique soil, with different intrinsic properties. The specimens were in medium to very dense states, being the denser specimens the ones collected with the Mazier sampler.

Despite the specimens being composed of different soils, a tendency was found between the cyclic resistance curves of Mazier specimens and the soils fines content. Specimens with intermediate FC (8% < FC < 19%) showed the lowest cyclic resistance, while specimens with low FC (FC < 8%) exhibited intermediate resistance. On the other hand, the specimens with higher FC range (FC > 19%) exhibited the higher cyclic resistance. These tendencies agree with works from other researchers, that stated that liquefaction resistance reduces with increase of fines content up to a threshold value and increases after this value is surpassed (Chang, 1990; Polito and Martin, 2001; Thevanayagam, 2007b; Huang and Chuang, 2011; Gobbi, 2020).

The effect of fabric was assessed by comparing the results of undisturbed specimens and the respective reconstituted specimen, prepared with MT for the same initial state conditions. The cyclic triaxial tests performed with Mazier specimens tested at constant applied CSR enabled to distinguish three tendencies of the number of cycles required to trigger liquefaction in undisturbed and reconstituted specimens. The results showed that, in general, when the soil had less than 6% FC, the reconstituted specimen exhibited higher cyclic resistance, while when the soil had more than 6% FC, the reconstituted specimen was less resistant than the correspondent undisturbed specimen. As the tests compared were performed in specimens of the same soil type, with similar relative density and applied CSR, the differences were mainly attributed to fabric and structure. The presence of fines content, a reflex of the presence of interlayers, increased the resistance of the undisturbed specimen, hence for soils with FC higher than 6%, N_{liq}_U was higher than N_{liq}_R. Different conclusions were found by Taylor (2015), which found no distinction between the cyclic resistance curves of undisturbed and reconstituted specimens, regardless the presence of fines. However, the ageing effects might have been reduced due to recent earthquake activity in Christchurch, which might justify the similarities found between undisturbed and reconstituted specimens in Taylor's work.

Besides, the response of undisturbed and reconstituted specimens in terms of strains and excess pore pressure was also distinct, in both Mazier and GP collected specimens. The reconstituted specimens initially exhibited low strain development. However, upon reaching a certain number of cycles, as r_u increases, they exhibited an exponentially increasing rate of strains, that occurs to both compression and extension side. On the other hand, the undisturbed specimen exhibited a more stable behaviour,

with a steady and constant increase in strains, often biased to the extension side. This might be due to the structure of the undisturbed specimens, with layers and laminations that provide a more stable response even beyond liquefaction triggering.

Moreover, the pore pressure evolution curves with N_c/N_{liq} of Mazier undisturbed and respective reconstituted specimens were compared, and showed very similar curves. The α parameter of the Booker et al. (1976) model was calibrated to provide the best fit with the actual test results and its values varied between 0.36 and 1.497, and delivered R^2 values of 0.87 in average. This range of α values is due to the different soils that compose the undisturbed specimens.

The effect of fabric was also investigated with the performance of three sets of CDSS tests, for specimens collected with the Mazier sampler at three different depths, at S2. For two of the depths selected (12 m and 14 m), no distinction was made between the cyclic resistance curves of undisturbed and reconstituted specimens, and the specimens water content and fines content differences did not affect the position of the cyclic resistance curve. On the other hand, the undisturbed specimens collected at 13 m exhibited higher cyclic resistance than the respective reconstituted specimens. In this set of tests, the specimens had approximately the same void ratios and water content, and similar GSD curves, with the same percentage of fines, enabling a more clear interpretation of the results. The results of the set of specimens collected at 13 m were in agreement with the results found in the CTx tests with FC > 6%.

Additionally, the laboratory test data was compared with the field data from the CPTu tests. It was found that the cyclic resistance of CDSS tests was higher than the cyclic resistance determined using field data. This might be explained by the orientation of the layering in the undisturbed specimens tested under CDSS. The undisturbed specimens tested in CDSS were collected perpendicularly to the sampling direction, hence the layering and laminations were perpendicular to the shear direction, which might have increased the resistance of the specimens tested under CDSS conditions. On the other hand, the results from CTx tests showed good agreement with the cyclic resistance curve from the CPTu data.

Moreover, the factor of safety against liquefaction was computed for the laboratory cyclic triaxial tests and compared with the FS_{liq} obtained from the CPTu data, for an equivalent cyclic stress ratio. No clear correspondence between the results was perceived as, in some cases, the $FS_{liq\_}CPTu$ was higher than $FS_{liq\_}$lab, while in other cases the opposite was observed.

11. EVALUATION OF SOIL LIQUEFACTION USING AN ENERGY-BASED APPROACH

11.1. INTRODUCTION

In recent years, the energy-based approach has been increasingly used to assess liquefaction potential, as it represents a methodology with several advantages. The possibility of quantifying earthquakes in terms of energy, allows the comparison between a soil's energy capacity with the demand energy, and therefore compute the factor of safety against liquefaction. On the other hand, several researchers found the correlation between the cumulative strain dissipated energy and pore pressure build up to be unique, regardless the equipment used (cyclic triaxial, simple shear, or torsional shear tests) and the excitation applied (random or sinusoidal). Therefore, several models of pore pressure generation with dissipated energy have been proposed over the years (Berrill and Davis, 1985; Green et al., 2000; Kokusho, 2013; Millen et al., 2020).

This chapter is dedicated to the study of liquefaction results using an energy-based approach. At first, the procedure used to define the dissipated energy at liquefaction (ΔW_{liq}) for cyclic triaxial and cyclic direct simple shear tests is described and the effect that several parameters, such as confining pressure, cyclic conditions by means of different laboratory devices, relative density, sample preparation procedures, water content, and soil fabric, have on the normalised dissipated energy at liquefaction is investigated. Moreover, the soil's capacity to resist liquefaction is assessed by means of two equations proposed by Figueroa et al. (1994) and Baziar and Jafarian (2007) that allow to estimate the dissipated energy at liquefaction based on state and intrinsic soil parameters. The last part of the Chapter focuses on the study of the pore pressure build-up on cyclic triaxial tests and correlation with the dissipated energy during shear. The GMP model proposed by Green et al. (2000) is used to calibrate the parameter PEC to allow the best correlations between the model and the measured results, using data from reconstituted and undisturbed specimens.

11.2. ENERGY-BASED APPROACH IN CYCLIC LABORATORY TESTS

As mentioned in Chapter 2, when a soil is dynamically sheared, part of the energy is dissipated throughout the soil, and the other part is dissipated into the soil. The dissipated energy per unit volume of soil (ΔW) might be quantified by the area bounded by the stress-strain hysteresis loops. In typical results of cyclic laboratory tests, the area of the hysteresis loops in $q-\varepsilon_a$ or $\tau-\gamma$ planes, for cyclic triaxial and cyclic simple shear tests, respectively, increases as the soil is sheared until liquefaction. The dissipated energy per unit of volume was calculated for cyclic triaxial and cyclic direct simple shear using equations (2.65) and (2.66), respectively.

To better understand the relationship between the dissipated energy and liquefaction triggering, Figure 11.1 and Figure 11.2 present two examples of CTx and CDSS tests, respectively, where $r_u-N_c-\Delta W$ and $\varepsilon_a-N_c-\Delta W$ are plotted for CTx and $\gamma-N_c-\Delta W$ and $\sigma_v-N_c-\Delta W$ are plotted for CDSS. For the two cases, the results show that dissipated energy increases at a constant rate during the initial cycles, until liquefaction occurs and a sudden increase in ΔW is observed, which is explained by the rapid increase in the area of the hysteresis loops in the $q-\varepsilon_a$ or $\tau-\gamma$ graphs that occurs when liquefaction is triggered, as observed before (e.g. Figure 8.2). This sudden increase in dissipated energy causes a change in the slope of the $\Delta W-N_c$ curve, which might be identified as the point where liquefaction is triggered. In the following analyses, the values of ΔW at liquefaction triggering (ΔW_{liq}) were considered the point where the pore pressure ratio (r_u) reached 1 for cyclic triaxial tests, and the point where shear strain (γ) reached $\pm 3.75\%$ for cyclic direct simple shear tests, as these were the criteria used to determine the number of cycles required to trigger liquefaction in the previous chapters. It is important to note that most CDSS tests were performed in unsaturated specimens with constant volume conditions, where the pore pressure evolution is not measured. However, as discussed in section 6.6.2 and expressed in the ASTM D-6528-00 standard, the constant volume condition is achieved by maintaining the specimen height constant and changing the vertical stress. Since the pore pressure is zero throughout the shearing stage, the change in vertical stress is considered equal to the change in effective stress, hence equal to the change in pore water pressure if the specimen was saturated and tested in undrained conditions. However, as the specimens were not saturated, not all tests reached zero vertical stress. Therefore, the dissipated energy at liquefaction is defined by the shear strain criteria.
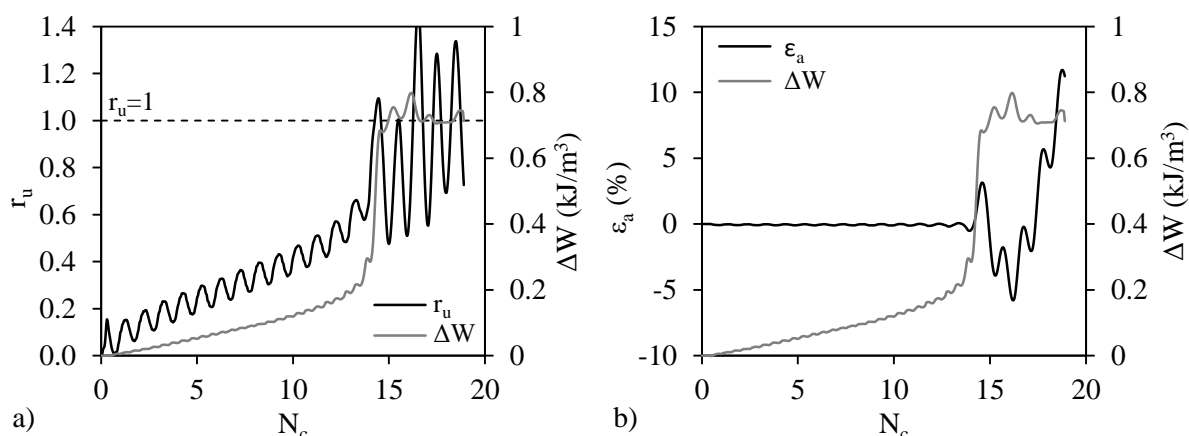
Figure 11.1 – Results of cyclic triaxial test NB1_MT_CTx6 in terms of: a) r_u–N_c–ΔW; and b) ε_a–N_c–ΔW
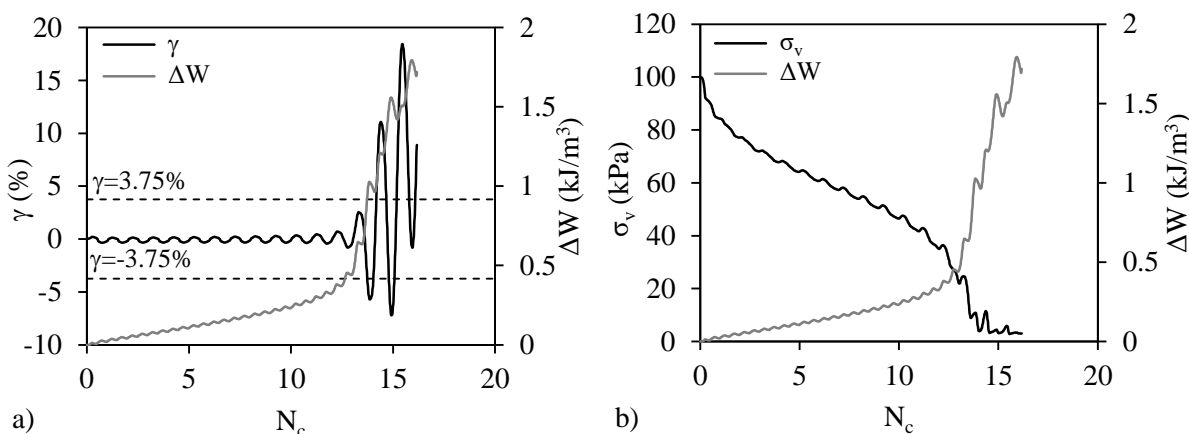
Figure 11.2 – Results of cyclic direct simple shear test NB1_MT_sat5 in terms of: a) γ–N_c–ΔW; and b) σ_v–N_c–ΔW

11.3. FACTORS AFFECTING ΔW_{LIQ}

As discussed in previous chapters, the behaviour of soils under cyclic loading is affected by several factors that depend on the material characteristics and the testing procedures chosen. Therefore, it is relevant to investigate the influence of those factors on the dissipated energy at liquefaction (ΔW_{liq}), which is addressed in the following sections.

11.3.1. EFFECT OF CONFINING PRESSURE ON ΔW_{LIQ}

The effect of confining pressure on ΔW_{liq} is examined first, as it is known to play an important role on the cyclic behaviour of soils. For this analysis, the CTx tests on NB1 sand are presented in Figure 11.3a. The specimens were prepared with MT to approximately the same relative density (50-60%) and consolidated with different confining pressures. A similar analyses was made for the CDSS tests (Figure 11.3b), with the results of tests performed on NB1 soil, prepared with MT, same relative density (50-

60%) and final water content of around 3.5%. As the CDSS specimens are not saturated, the dissipated energy presented is plotted against the total vertical stress (σ_v). Despite the differences in ΔW_{liq} for the same confining pressure, it is observed that ΔW_{liq} increases with the increase in confining pressure.
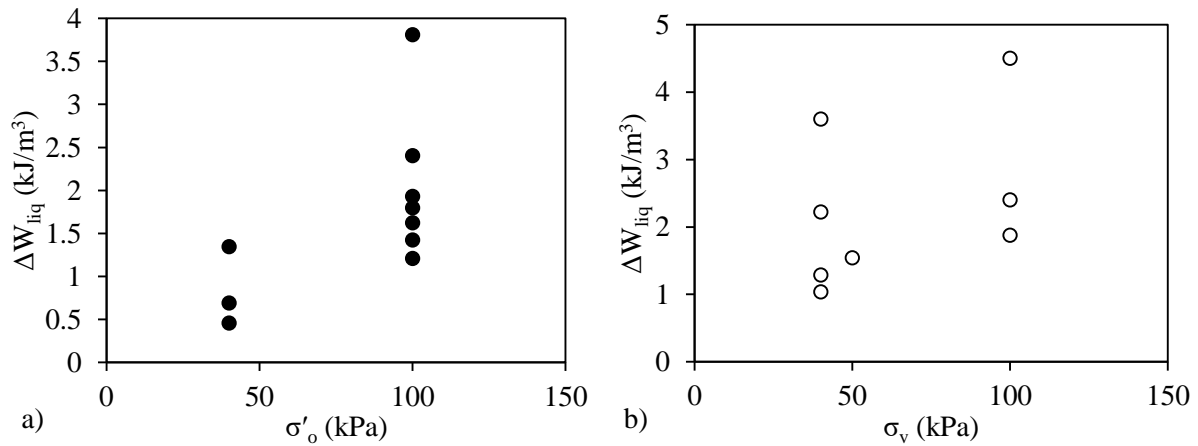
Figure 11.3 – Effect of confining pressure on ΔW_{liq} for: a) CTx tests; b) CDSS tests on NB1 sand

To eliminate the dependency of the dissipated energy at liquefaction on the confining pressure, the values of ΔW_{liq} were normalised by the initial confining stress. The CTx results were normalised by the initial effective mean stress (σ'_o) and the CDSS results were normalised by the initial vertical stress (σ_v). As discussed in Chapter 2, W_s is the dissipated energy (ΔW) normalised by the initial effective mean stress, therefore, the normalised dissipated energy at liquefaction is represented as $W_{s,liq}$, and will be considered in the following sections analyses.

11.3.2. EFFECT OF THE LABORATORY TEST ON $W_{S,LIQ}$

To analyse the effect of the laboratory device on the dissipated energy at liquefaction, two sets of tests performed on NB1 have been compared. The specimens were prepared with MT with similar conditions, and tested in different devices (cyclic triaxial and cyclic direct simple shear apparatus). The ΔW_{liq} of the CDSS tests was normalised with a mean stress (σ_m), so $W_{s,liq}$ could be directly compared with the CTx results. The mean stress is calculated using equation (11.1), in a process analogous to the use of c_r for correlating CSR$_{tx}$ with CSR$_{ss}$.

$$\sigma_m = \frac{\sigma_v(1 + 2K_0)}{3} \tag{11.1}$$

It is important to note that the criteria to define the dissipated energy at liquefaction were different, as the pore pressure evolution was not measured in CDSS tests. However, the CDSS tests selected had high degrees of saturation, and the dissipated energy defined by the two criteria gave similar results,

374

considering the decay of vertical stress in CDSS tests equivalent to the increase in excess pore water pressure in CTx. Figure 11.4a shows the pore pressure ratio evolution with W_s, for a selection of CTx and CDSS tests. To simplify the interpretation of results, only three tests performed in each device were selected. It is observed that the trend of pore pressure evolution is similar for both devices, regardless of the applied CSR and device used, which suggests that the relationship between r_u–W_s might be unique. However, these plots do not allow the clear identification of the dissipated energy at liquefaction. Therefore, to better understand the comparisons between the results, Figure 11.4b presents the results in the plot $W_{s,liq}$–D_R, comparing directly the dissipated energy at liquefaction from CTx and CDSS tests, in specimens with the same range of relative densities.
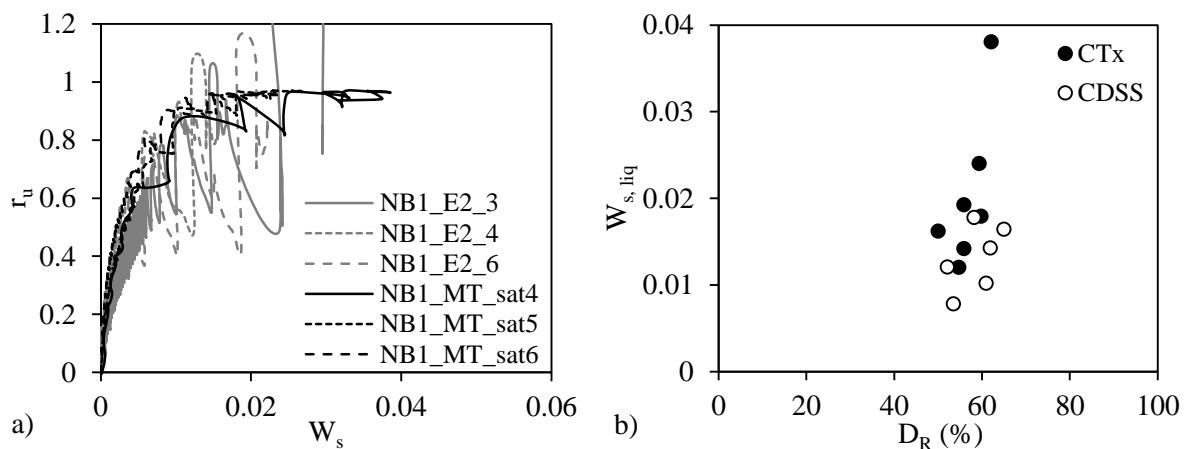
Figure 11.4 – Comparison between the results of CTx and CDSS tests on NB1 sand: a) W_s–r_u; b) D_R–$W_{s,liq}$

Despite the similarities found between the r_u–W_s plots of CTx and CDSS tests, the results of CDSS show lower values of normalised dissipated energy at liquefaction than the CTx tests. Moreover, most CDSS performed in this work were not saturated, so further comparisons with CTx might be misleading. Due to these differences between the tests performed with different devices, the results of CTx and CDSS tests will be analysed and discussed separately in the following sections.

11.3.3. EFFECT OF RELATIVE DENSITY ON $W_{S,LIQ}$

The effect of void ratio (or relative density) on liquefaction resistance was addressed in sections 8.2.1 and 8.3.1, for CTx and CDSS tests, respectively. It was clear that small differences in void ratio had low impact on the determination of the cyclic resistance curves, however, higher variations in e are reflected on the position of the CSR-N_{liq} curve, showing that liquefaction resistance decreases with decrease in relative density. The effect of relative density on the normalised dissipated energy at liquefaction was investigated by grouping the CTx and CDSS tests according to the specimens characteristics and testing conditions. The relative density is used herein since the dissipated energy is

normalized by the confining pressure, hence the differences in relative density reflect the differences in the specimen state. Besides, it is easier to understand and compare the results in terms of D_R than in terms of e.

The results of the CTx tests on NB1 are shown in Figure 11.5a, where NB1_MT are tests on specimens prepared with MT, $D_R = 25-35\%$, and $p'=100$ kPa; NB1_PL specimens were prepared with air pluviation, $D_R = 30-35\%$, and $p'=100$ kPa; NB1_E2 specimens were prepared with MT, $D_R = 50-60\%$, and $p'=100$ kPa; and NB1_C40 specimens were prepared with MT, $D_R = 55-60\%$, and $p'=40$ kPa (refer to Table 8.1). On the other hand, Figure 11.5b presents the results of CTx tests on S1_M2 and S1_M7. Observing the results of NB1, there seems to be a tendency of $W_{s,liq}$ to increase with the increase of D_R. It is worth mentioning that the tests were performed in different conditions, that will be analysed further in following sections, however, when comparing NB1_MT and NB1_E2, prepared with MT and $p'=100$ kPa, it is evident that $W_{s,liq}$ increases with increase of D_R. On the other hand, the results of S1_M2 and S1_M7 are very scattered, and no correlation between D_R and $W_{s,liq}$ was found. In S1_M7 specimens, despite the similar values of relative density, there is a group of tests with higher values of $W_{s,liq}$, that correspond to specimens that liquefied for a very high number of cycles. This discussion with be addressed later in this Chapter.
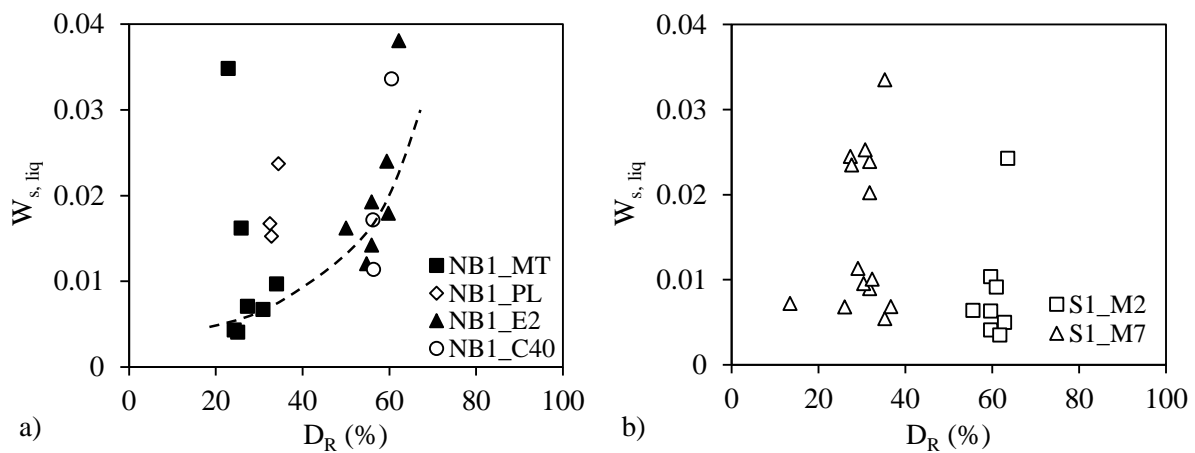
Figure 11.5 – Effect of relative density on $W_{s,liq}$ for CTx tests on: a) NB1 sand; b) S1 sands

The results of CDSS tests on NB1, S1_M2, and S1_M7 are reported in Figure 11.6. The NB1 specimens were grouped according to the water content, which effect on $W_{s,liq}$ will be addressed later. In this case, the relative density seems to play a role in the normalised dissipated energy at liquefaction, at least for NB1 specimens tested with 3.5% water content and for S1_M2 and S1_M7. The specimens prepared with S1_M2 and S1_M7 were also sheared with a final water content of 3.5%. The tendency of the results suggested that $W_{s,liq}$ increases with increase in D_R. As mentioned above in section 8.3.3, the resistance of specimens with 3.5% water content was higher than that of dry or saturated specimens,

due to suction effects. Therefore, it makes sense that, for these specimens, denser states require more energy to break the particles bonding. On the other hand, for dry and almost saturated specimens (with high water contents), it was not possible to trace a trend, due to the scattering of results.
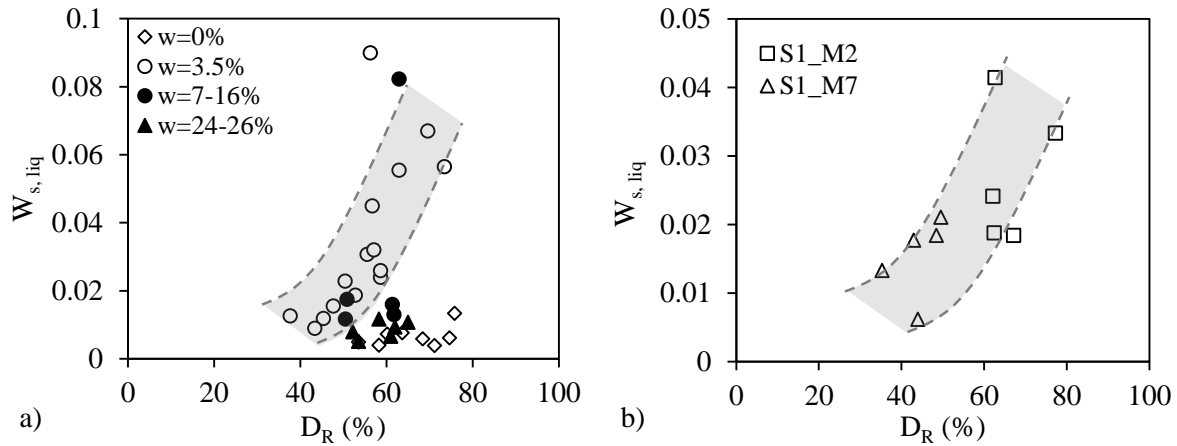
Figure 11.6 – Effect of relative density on $W_{s,liq}$ for CDSS tests on: a) NB1 sand; b) S1 sands

To sum up the results found, although the normalised dissipated energy at liquefaction might depend on the specimens relative density, a clear trend between $W_{s,liq}$ and D_R was not found. However, some results suggested that $W_{s,liq}$ increases with increase in D_R, as was also observed by Figueroa et al. (1994) and Baziar et al. (2011). This conclusion is more significant for CDSS results when considering the NB1 with 3.5% of water content and the S1_M2 and S1_M7 soils. However, despite being plotted in the same Figure, S1_M2 and S1_M7 had different fines content (9.2% and 2.1%, respectively) which might have interfered with $W_{s,liq}$ results.

11.3.4. EFFECT OF SAMPLE PREPARATION ON $W_{S,LIQ}$

As mentioned frequently in this research work, the sample preparation procedure plays a major role in cyclic behaviour of soil. The deposition process, soil moisture condition, and densification technique influence the particle arrangement and consequently, the soil resistance to cyclic loading. Although there are many studies on the influence of samples reconstitution methods on cyclic behaviour of soils, there are not many studies on the influence of the preparation technique on the dissipated energy at liquefaction. Therefore, this section addresses this issue, by comparing the results of specimens prepared with moist tamping (MT) and air pluviation (PL), tested in CTx and CDSS conditions.

The sample preparation influence in the dissipated energy at liquefaction was investigated by plotting $W_{s,liq}$ against D_R, as reported in Figure 11.7a and b, for CTx and CDSS devices, respectively. The CDSS

results suggest that the $W_{s,liq}$ of PL specimen is lower than that of MT specimens. However, the scatter of results did not allow to trace any trends.

It is curious to relate the results of the comparison between cyclic resistance curves (sections 8.2.2 and 8.3.4) with the results of $W_{s,liq}$ for both testing devices. The CSR-N_{liq} curves for CTx results showed that the sample preparation method did not influence the cyclic resistance of NB1 soil, in specimens with D_R=25−35%. On the other hand, the cyclic resistance curves for CDSS tests on NB1 with D_R=53−71%, showed that the MT specimens were more resistant than PL specimens, with higher number of cycles required to trigger liquefaction for the same applied CSR. These tendencies seem to be reproduced in the energy-based results, as $W_{s,liq}$ of CTx PL and MT specimens are scattered and inconclusive, while the CDSS PL specimens show lower $W_{s,liq}$ than MT specimens, analogous to the trends found when using the stress-based approach.
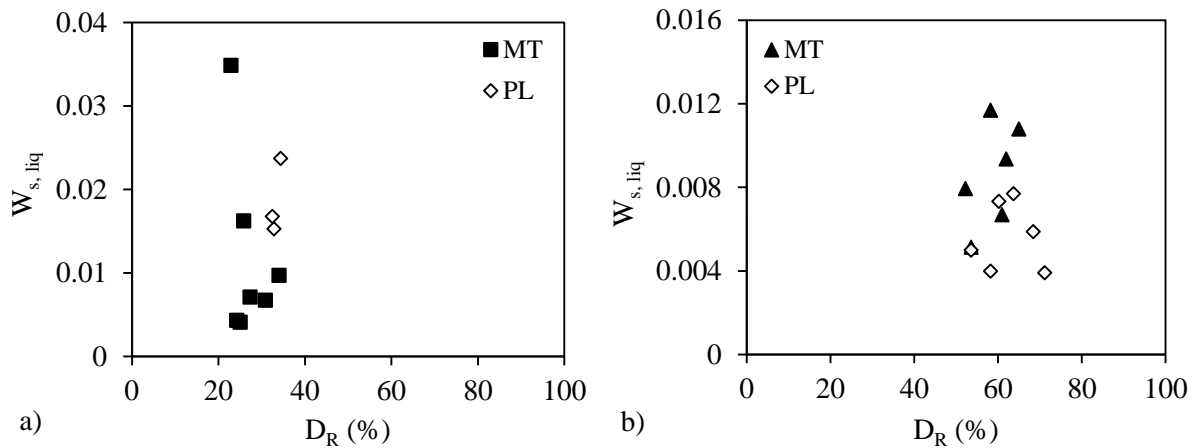
Figure 11.7 – Effect of sample preparation method on the $W_{s,liq}$ for: a) CTx tests; b) CDSS tests on NB1 sand

11.3.5. EFFECT OF WATER CONTENT ON $W_{S,LIQ}$

The results of CDSS tests performed on NB1 sand specimens with different water contents (i.e. different degrees of saturation) allowed the study of the effect of water content on liquefaction resistance, and it was observed that specimens with a low water content of around 3.5% showed higher resistance than dry or almost saturated specimens. In terms of dissipated energy at liquefaction, the results from NB1, S1_M2, and S1_M7 are presented in Figure 11.8, in the plot $W_{s,liq}$−w. An increase in $W_{s,liq}$ is observed for w=3.5%, as already predicted from the results of Figure 11.6a. On the other hand, dry and saturated specimens show similar values of $W_{s,liq}$, which is a positive proof of the advantage of using a simpler testing procedure as the CDSS for the purpose of evaluating the liquefaction susceptibility when compared with the more demanding CSS with specific methodologies of saturation and control of vertical stress to be constant.

From these results, it can be concluded that the matric suction effects due to partial saturation in MT specimens prepared with low water content influences cyclic liquefaction results, in both stress-based and energy-based approaches. The author realizes that there are other factors that might interfere with the conclusions, however, these results are important to understand the role of suction on the dissipated energy at liquefaction, in CDSS tests.
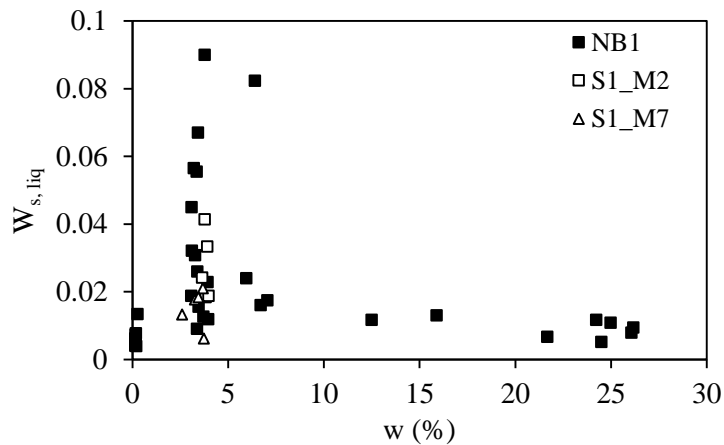
Figure 11.8 – Effect of water content on the $W_{s,liq}$ for CDSS tests

11.3.6. EFFECT OF NATURAL FABRIC ON $W_{s,LIQ}$

To assess the effect of fabric on the dissipated energy at liquefaction, the normalised dissipated energies at liquefaction of undisturbed and reconstituted tests were compared. Only the tests sheared with constant applied CSR were considered in this analyses, as the change in CSR hinders the direct comparisons and hence, might compromise the results found. Therefore, the tests performed with a change in CSR during shear (i.e., most GP specimens) were not included in this section. However, the detailed comparison of the r_u-W_s relationships of those tests is presented in following sections.

The normalised dissipated energy at liquefaction of undisturbed specimens ($W_{s,liq}$_U) is compared with the normalised dissipated energy at liquefaction of the respective reconstituted specimens ($W_{s,liq}$_R) in Figure 11.9, where tests were categorised according to the same FC ranges selected for the stress-based analysis. However, contrary to the results in terms of N_{liq}, no trends were found that relate $W_{s,liq}$ of undisturbed and reconstituted specimens based on FC ranges.
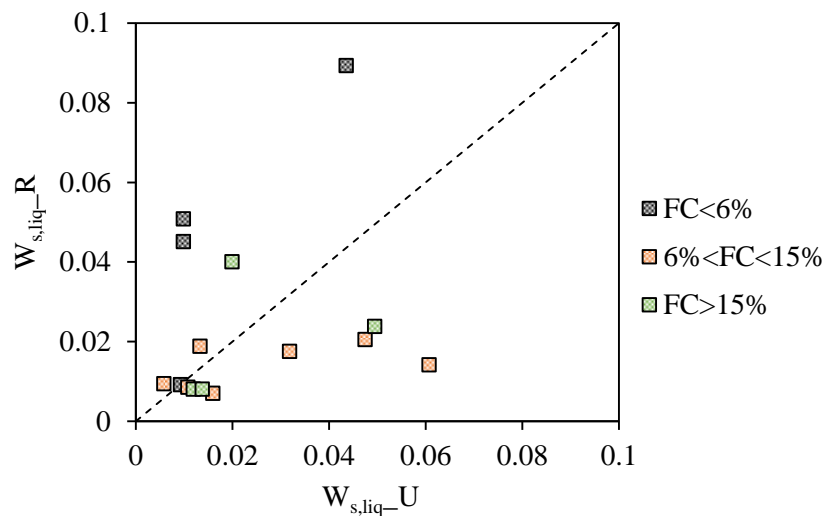
Figure 11.9 – Comparison between $W_{s,liq}$ of undisturbed and reconstituted specimens categorised according to FC range

On the other hand, the values of $W_{s,liq}$ seem to be influenced by the number of cycles required to trigger liquefaction (N_{liq}). The values of $W_{s,liq}$ and N_{liq} of undisturbed and reconstituted specimens are correlated in Figure 11.10, and suggest that $W_{s,liq}$ increases with increase in N_{liq}. The increase in $W_{s,liq}$ with N_{liq} was also found by Polito et al. (2013), when performing cyclic triaxial tests using different load shapes. The results found by Polito et al. (2013) are plotted in Figure 11.10b, and show good agreement with the results from this research, increasing confidence in the trends found.

Following this assumption, the $W_{s,liq}\_U$ and $W_{s,liq}\_R$ pairs were compared again in Figure 11.11, categorised according to the difference between N_{liq}_U and N_{liq}_R. When observing the pairs of tests with small differences between N_{liq} of undisturbed and reconstituted specimens, the results are close to the 1:1 line, which means that $W_{s,liq}\_U$ and $W_{s,liq}\_R$ values are similar. However, for higher differences between N_{liq}_U and N_{liq}_R, higher differences in $W_{s,liq}\_U$ and $W_{s,liq}\_R$ are observed. Moreover, the differences seem to be related to the magnitude of N_{liq} differences. For $N_{liq}\_U-N_{liq}\_R<0$, that is for pairs of tests where the reconstituted specimen liquefied for a higher number of cycles than the undisturbed specimen, the $W_{s,liq}\_R$ is also higher than $W_{s,liq}\_U$. These specimens correspond to clean sands, with low FC, hence the results show that for clean sands the reconstitution process was not conservative. On the other hand, for pairs of tests where the undisturbed specimen required more cycles to liquefy than the reconstituted specimen ($N_{liq}\_U-N_{liq}\_R>50$), the $W_{s,liq}\_U$ was higher than $W_{s,liq}\_R$. These specimens correspond to sands with fines. In this case, the presence of fines produces macro-fabric effects of reinforcement that disappear when the specimen is reconstituted. For sands with fines, the reconstitution process was, therefore, conservative.
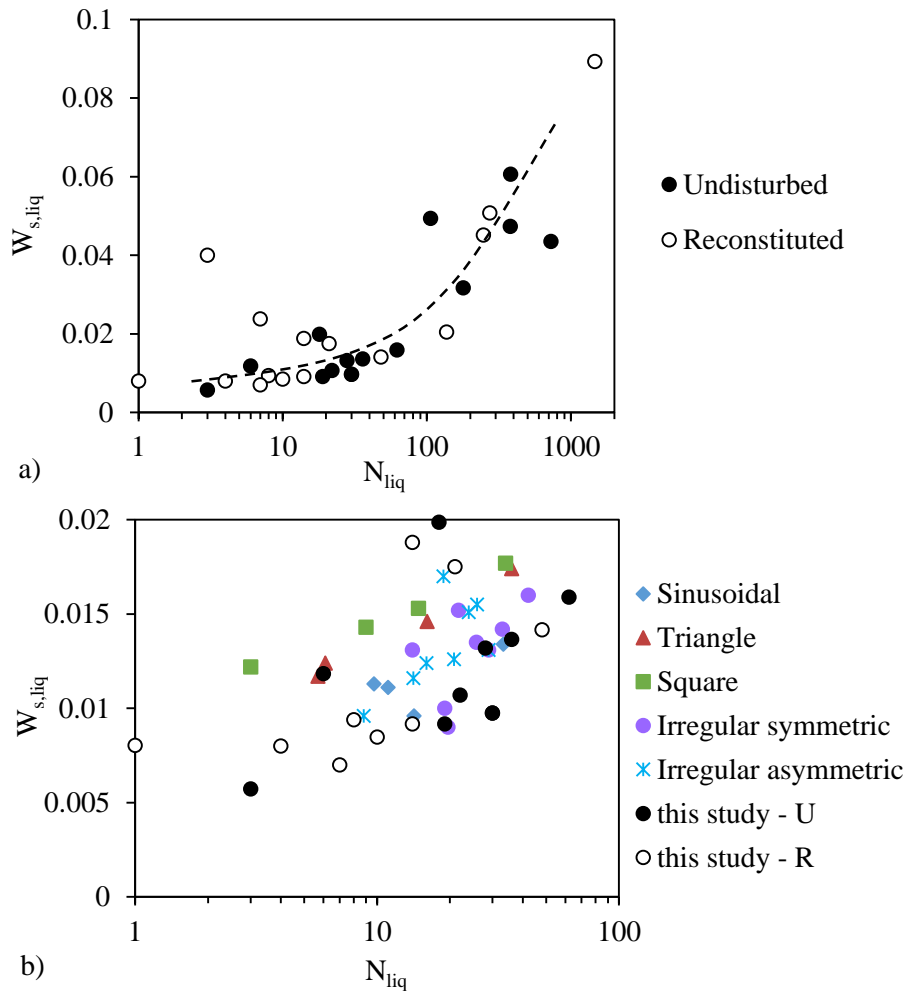
Figure 11.10 – Correlation between N_{liq} and $W_{s,liq}$: a) for undisturbed and reconstituted CTx specimens; b) comparison with data from Polito et al. (2013)
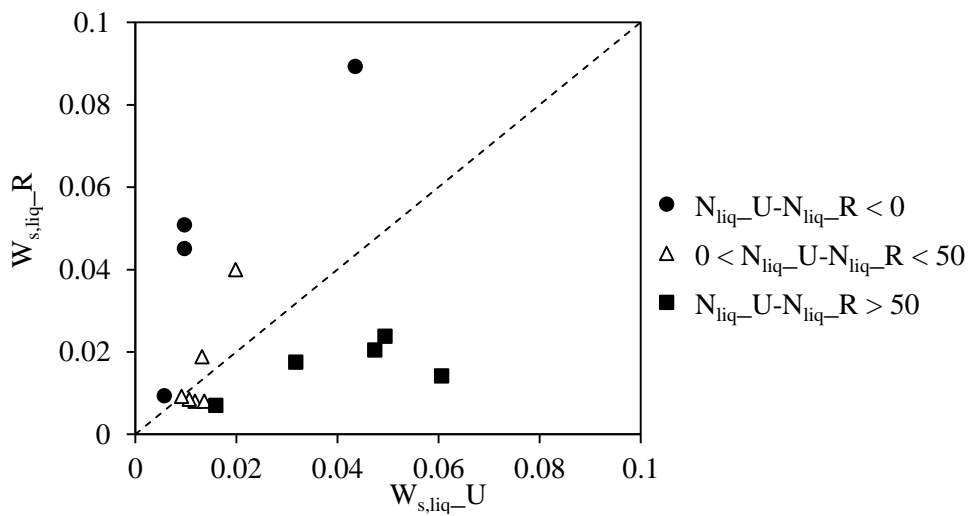
Figure 11.11 – Comparison between $W_{s,liq}$ of undisturbed and reconstituted specimens categorised according to $N_{liq\_U}-N_{liq\_R}$ range

11.4. ESTIMATION OF SOIL CAPACITY ENERGY

The factor of safety against liquefaction is computed as the ratio of the capacity to the demand. The demand imparted to the soil is often related to the earthquake magnitude, distance from site to the centre of energy release, and material damping. On the other hand, the soil capacity is the dissipated energy necessary to trigger liquefaction.

As observed in the previous sections, the normalised dissipated energy at liquefaction might be related to a variety of factors, such as confining pressure, relative density, water content, and fabric. Over the years, the influence of different factors on the dissipated energy at liquefaction has been studied, being the most important and impactful the state parameters (confining pressure and void ratio, through relative density, and more recently and fundamentally the state parameter) and the soil type, which includes the soils' intrinsic parameters (grain size, fines content, D_{50}, or C_U).

As referred in Chapter 2, researchers have studied the dissipated energy related to different factors. After performing several torsional shear tests in a hollow cylinder device, Figueroa et al. (1994) proposed an equation that relates the energy per unit volume required to trigger liquefaction (ΔW, in J/m^3)with the effective confining pressure (σ'_c, in kPa) and the specimens relative density (D_R, in %), as follows:

$$\log \Delta W = 2.002 + 0.00477\sigma'_c + 0.0116D_R \tag{11.2}$$

On the other hand, Baziar and Jafarian (2007) proposed a new multiple linear regression (MLR) method to establish a correlation between the dissipated energy required to reach liquefaction and the soils initial parameters. The soil capacity energy is related to five input parameters, namely the confining pressure (σ'_c, in kPa), relative density (D_R, in %), fines content (FC, in %), coefficient of uniformity (C_U) and mean grain size (D_{50}, in mm), and presented in equation (11.3).

$$\log \Delta W = 2.1028 + 0.004566\sigma'_c + 0.005685D_R + 0.001821FC - 0.02868C_U \\ + 2.0214D_{50} \tag{11.3}$$

The two equations differ in terms of the parameters used. While Figueroa et al. (1994) proposed a relationship based only on the initial state parameters (σ'_c and D_R), Baziar and Jafarian (2007) also included the fines content and grain size characteristics (C_U and D_{50}). It is interesting to note that the two equations constants are both around 2 and the coefficients associated with the σ'_c variable are similar (0.00477 and 0.004566). However, the relative importance of D_R is higher in equation (11.2), as the equation is composed of three terms. On the other hand, D_{50} is the parameter with higher relative importance in equation (11.3), and the other variables have low coefficients.

During the present research work, a large database of cyclic triaxial and direct simple shear tests performed on different soils, with different intrinsic parameters, confining pressures, and relative densities, was developed. To verify the accuracy of the estimations presented above, the logarithm of soil capacity measured in each test was compared with the logarithm of the capacity energy estimated using equations (11.2) and (11.3), from Figueroa et al. (1994) and Baziar and Jafarian (2007), respectively, in Figure 11.12. The 1:1 line is plotted, as well as two bounds that define the ±15% relationship between measured and estimated results, as suggested by Baziar and Jafarian (2007). It is observed that, despite the use of more intrinsic soil parameters in the equation from Baziar and Jafarian (2007), the equation from Figueroa et al. (1994) seems to estimate values closer to the measured results. These results might indicate that the parameters that have higher effect on soil capacity energy are the initial state parameters (σ'_c and D_R). The results contradict the findings of Baziar and Jafarian (2007), which stated that the MLR-based model yields a better performance than the Figueroa et al. (1994) model.
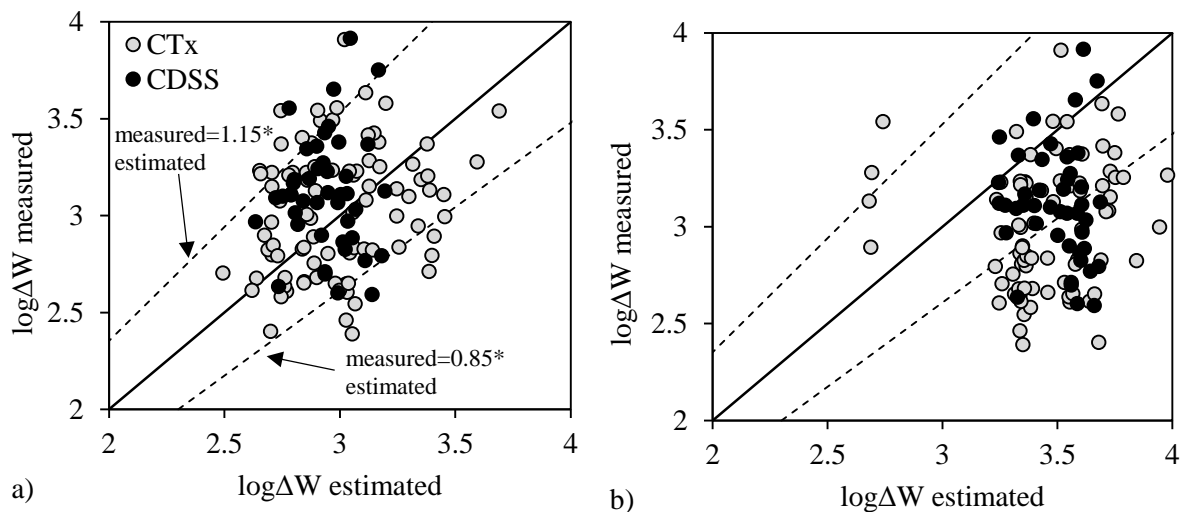
Figure 11.12 – Comparison between measured capacity of experimental results and the estimated capacity from: a) equation (11.2) from Figueroa et al. (1994); b) equation (11.3) from Baziar and Jafarian (2007)

From the results presented in Figure 11.12b, it is evident that equation (11.3) overestimated the results of capacity energy of the soils studied. Furthermore, the percentage error, defined by difference between the measured and estimated value divided by the measured value, was calculated for each test, for the two correlations studied (Figure 11.13). As expected, it is observed that the Figueroa et al. (1994) expression computes values of capacity energy closer to the measured values than the expression proposed by Baziar and Jafarian (2007), which is reflected on lower error.

Despite the better performance of the equation proposed by Figueroa et al. (1994), the results obtained in this work did not follow the 1:1 inclined line trend and are still very scattered. It was concluded that

these equations were not adequate to estimate the results obtained in this work. Nonetheless, these correlations are useful to compute the soil capacity energy, which is essential to assess the soil liquefaction susceptibility. Therefore, in a future work, it would be interesting to relate other parameters with the capacity energy, such as the shear wave velocity (small-strain shear modulus), or morphology parameters, and try to improve the correlations to obtain more accurate values of soil capacity.
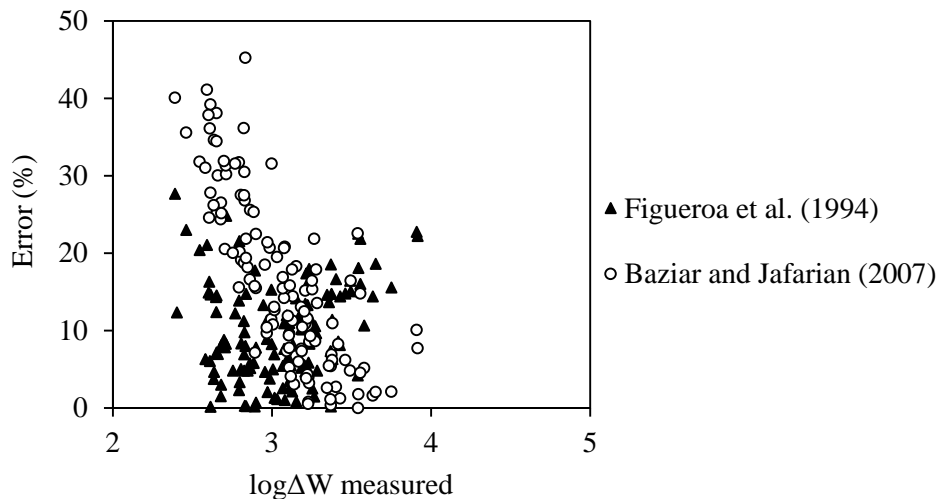
Figure 11.13 – Comparison in terms of error between the two correlations studied

11.5.   PORE PRESSURE BUILD-UP

The stress-based pore pressure model proposed by Booker et al. (1985) was investigated in sections 8.2.5 and 10.2.4, for the reconstituted and undisturbed results of cyclic triaxial tests, respectively. However, as discussed in Chapter 2, energy-based pore pressure generation models have been developed over the years, and correlations between r_u and W_s have been proposed, based on the assumption that there is a unique relationship between pore water pressure generation and the cumulative dissipated energy per unit volume of soil up to the onset of liquefaction.

In this section, the pore pressure generation is related to the normalised dissipated energy, using the GMP model proposed by Green et al. (2000) (equation (2.69)). The pore pressure ratio (r_u) was compared with the normalised dissipated energy (W_s), and the best values of PEC were determined using the R^2 equation (8.1) proposed by Polito et al. (2008), where Y_i is the r_u measured at the ith cycle ratio, $\overline{Y}$ is the average value of all r_u recorded during the test, and $\hat{Y}_i$ is the r_u predicted by equation (2.69) for the ith cycle ratio.

11.5.1. PORE PRESSURE BUILD-UP EVALUATION IN RECONSTITUTED SPECIMENS

Figure 11.14 to Figure 11.19 present the pore pressure ratio evolution with the normalised cumulative dissipated energy, for NB1, S1_M2, and S1_M7 soils, grouped according to the preparation technique used, relative density, and confining pressure (Table 8.1). The plot represents the maximum values of r_u for each cycle, to allow the calculation of R^2 and a better comparison between the estimated and measured results. Contrary to what was expected, the r_u-W_s curves of specimens of the same material, prepared for the same initial conditions, are not convergent and do not follow the same trend.

However, care should be taken when analysing these results. The specimens that show different behaviour, namely NB1_MT_CTx5, NB1_MT_CTx7, NB1_E2_1, NB1_E2_2, NB1_E2_5_REP, NB1_C40_3, S1_M2_CTx2, S1_M7_CTx1, S1_M7_CTx4, S1_M7_CTx5, S1_M7_CTx8, S1_M7_CTx10, and S1_M7_CTx12, liquefied for a number of cycles higher than 100 cycles. Therefore, the specimens were more resistant and the initial hysteresis loops might not correspond to the real specimen deformation, but rather to the system compliance, as the axial deformations are measured with external LVDT. The dissipated energy accumulation increase may be hindered by the lack of precision of the initial axial deformation measurements, and hence the evolution of r_u with W_s fall out of the expected trends. To solve these issues, internal instrumentation is recommended in more resistant specimens, as it is the only way to assess the real specimen deformations.
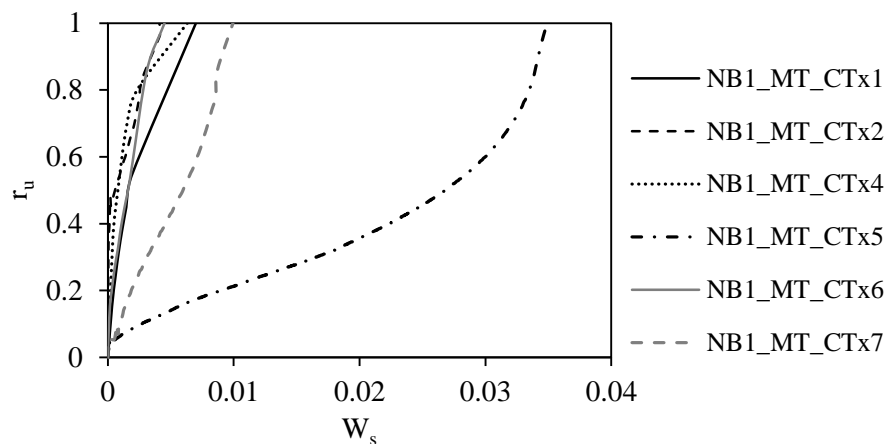
Figure 11.14 – Pore pressure ratio evolution with W_s for NB1_MT tests
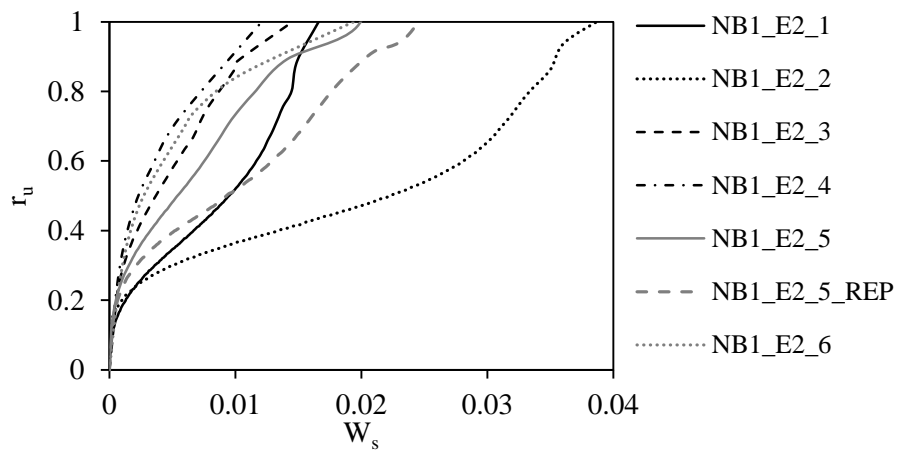
Figure 11.15 – Pore pressure ratio evolution with W_s for NB1_E2 tests
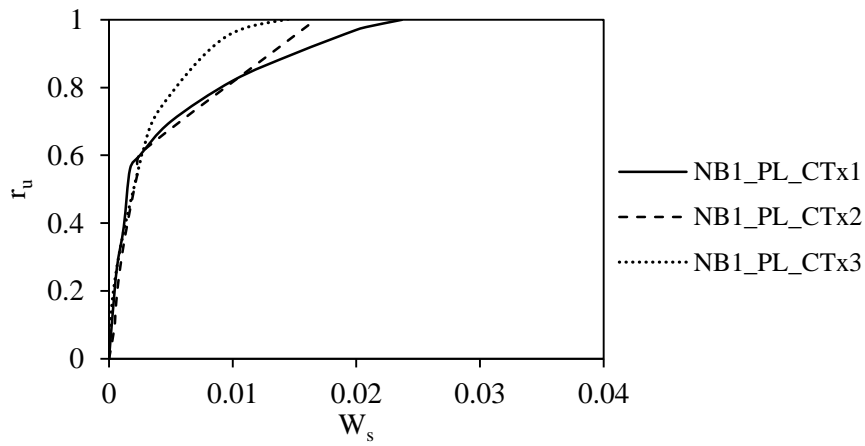
Figure 11.16 – Pore pressure ratio evolution with W_s for NB1_PL tests
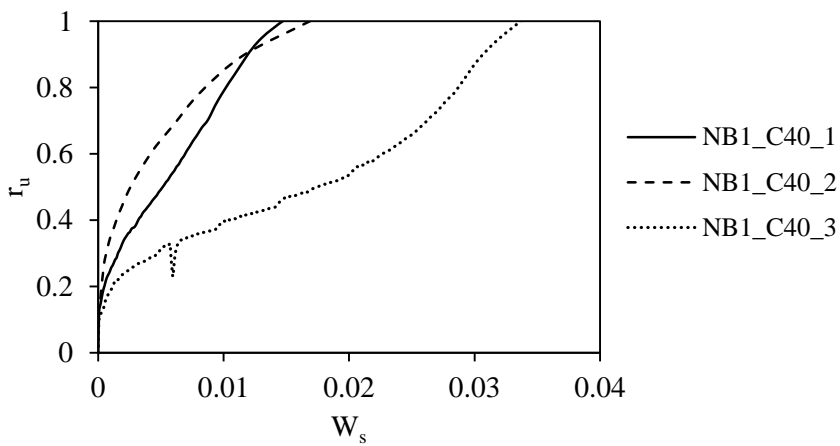
Figure 11.17 – Pore pressure ratio evolution with W_s for NB1_C40 tests
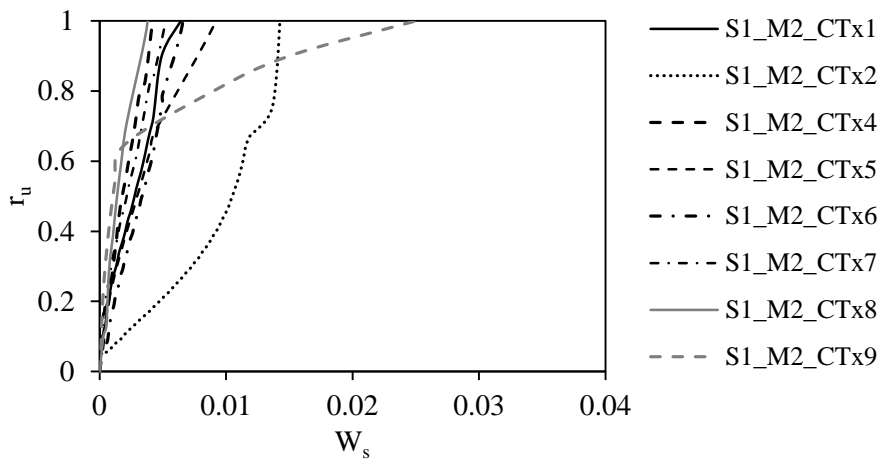
Figure 11.18 – Pore pressure ratio evolution with W_s for S1_M2 tests
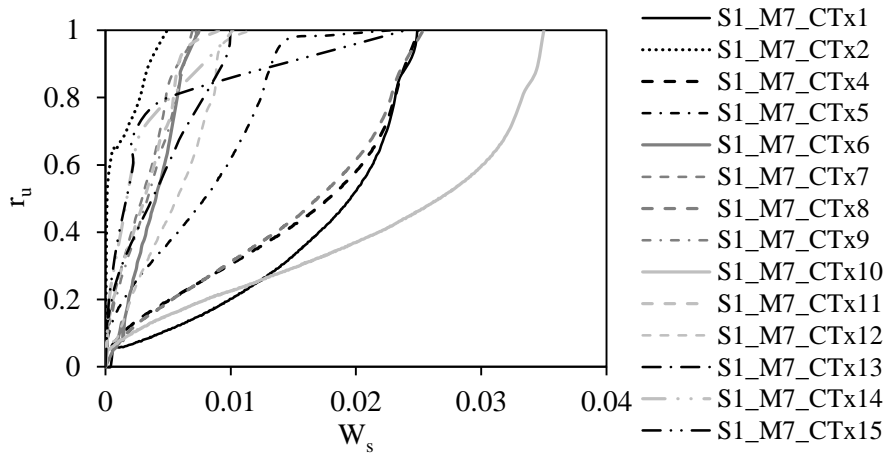
Figure 11.19 – Pore pressure ratio evolution with W_s for S1_M7 tests

Moreover, to analyse the effect of the isotropic confining pressure, Figure 11.20 shows the $r_u - W_s$ relationship of two pairs of specimens prepared with the same void ratio and sheared at the same CSR, but confined with 40 kPa and 100 kPa. The results suggest that the $r_u - W_s$ relationship is practically independent of the confining pressure.
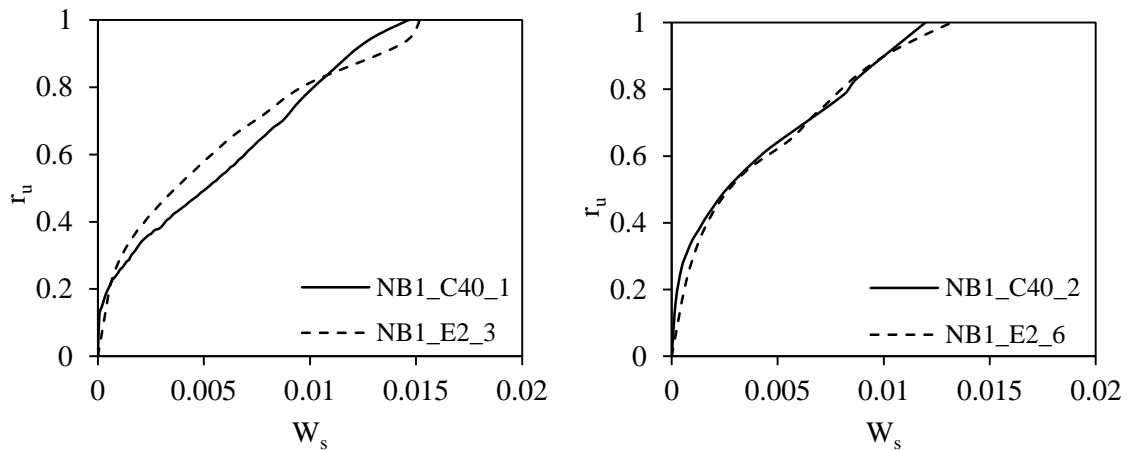
Figure 11.20 – Influence of isotropic confining pressure on the evolution of pore pressure ratio with the normalised accumulation of dissipated energy

For each test, the value of PEC was computed to return the highest value of R^2. The values of PEC ranged between 0.0035 and 0.02, for the specimens that liquefied for under 100 cycles. Figure 11.21 presents the histogram of the percentage of occurrence of each range of R^2 values, showing that more than 80% of tests showed R^2 higher than 0.80, and 60% showed R^2 higher than 0.90, evidencing the good performance of equation (2.69) in modelling the pore pressure generation over these range of soils. Moreover, the boundary values of PEC were used to compute de estimated r_u for each type of soil, and the r_u–W_s estimated curves are integrated in Figure 11.22, together with the r_u–W_s curves of all specimens. A good correlation between the estimated and measured curves was observed. It was not possible to define a single value of PEC that best fits all the results, however, it is worth noting that the average PEC values range within a small interval (0.0035−0.02).
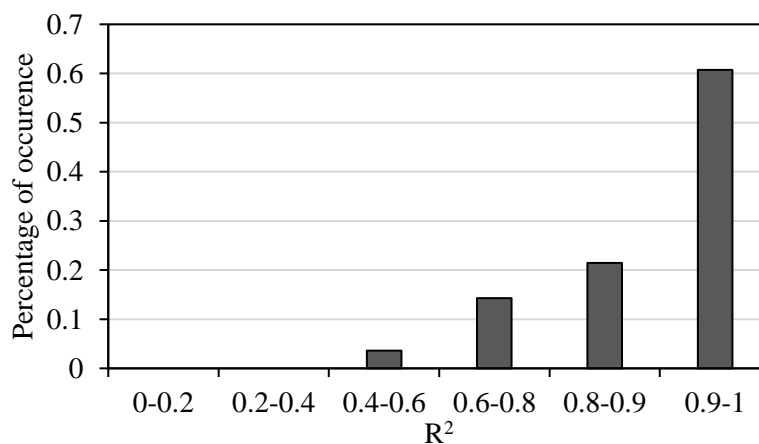
Figure 11.21 – Histogram of R^2 values for Green et al. (2000) model fit to data from cyclic triaxial tests
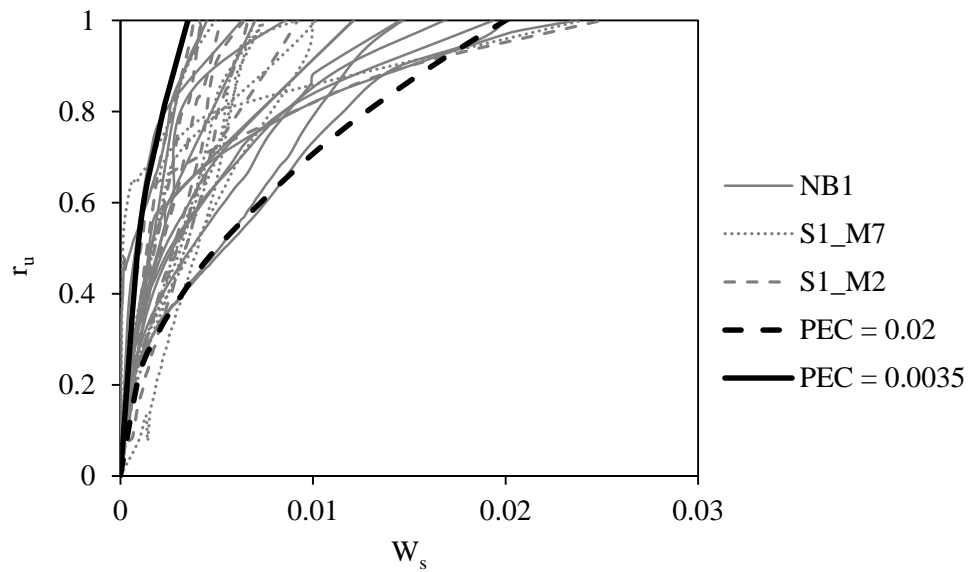
Figure 11.22 – Boundaries of PEC values for NB1, S1_M2 and S1_M7 specimens in r_u–W_s plane

Azeiteiro et al. (2017) collected the laboratory test results obtained for other sands reported in the literature. The characteristics of each soil and test conditions applied are described in Azeiteiro et al. (2017) and presented in Table 11.1, together with a summary of NB1 sand properties. The r_u–$\Delta W/\sigma'_o$ curves of the Toyoura, Fujian, Reid Bedford, Futtsu beach, and Hostun sands are compared with the experimental results of this work in Figure 11.23, showing that the results obtained are well framed within other benchmark sands. It is observed that the r_u–$\Delta W/\sigma'_o$ relationship depends on the soil type and on the test conditions. Therefore, for the liquefaction assessment of a specific site through the energy-based method, it is important to test representative samples of the soil deposits, preferably undisturbed high-quality samples.

Table 11.1 – Material properties and test conditions of literature sands used for comparison

Sand	Material properties				Test conditions		Apparatus
	e_{max}	e_{min}	C_U	D_{50} (mm)	e_0	σ'_0 (kPa)	
Toyoura	0.98	0.6	1.7	0.17	0.79 - 0.83	294	Torsional shear
Fujian	0.86	0.55	1.6	0.4	0.65	150	Triaxial
Reid Bedford	0.85	0.58	0.57	0.26	0.7	124	Torsional shear
Futtsu beach	1.08	0.68	1.9	0.19	0.80, 0.88, 0.96	98	Triaxial
Hostun	1	0.66	1.4	0.33	0.83	80	Triaxial
NB1	0.85	0.59	2.16	0.45	0.69 - 0.78	40, 100	Triaxial
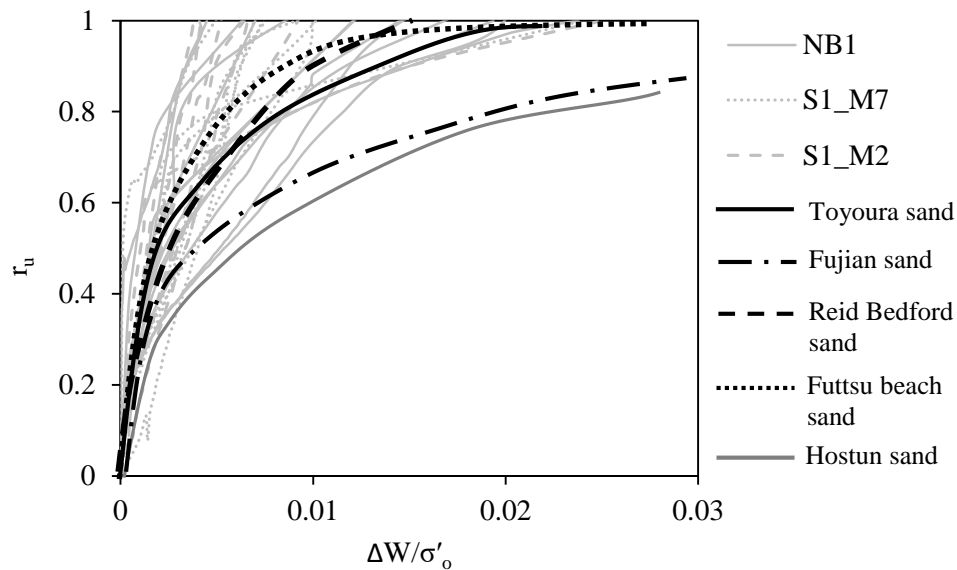
Figure 11.23 – Comparison of r_u–$\Delta W/\sigma'_o$ curves of benchmark sand with the experimental results of this work

11.5.2. PORE PRESSURE BUILD-UP EVALUATION IN UNDISTURBED SPECIMENS

Following the procedures defined above, the pore pressure ratio evolution with the normalised dissipated energy of the undisturbed specimens and respective reconstituted specimens tested under cyclic triaxial conditions are discussed in this section. The results of the Mazier specimens are presented in Figure 11.24. Contrary to the observations of the stress-based pore pressure build-up, the relationships between r_u and W_s are distinct for undisturbed and reconstituted specimens. It is important to state that the undisturbed specimens that showed a higher dissipated energy at liquefaction than the respective reconstituted specimen, correspond to tests that liquefied for a number of cycles considerably higher than the reconstituted specimens. As explained above, for these specimens the hysteretic loops may be hindered by the lack of precision of the initial axial deformation measurements.

The results were interpreted by using the GMP model proposed by Green et al. (2000), and the parameter PEC was calibrated to provide the best fit with the actual test results, by means of the maximum R^2 value. In terms of the PEC parameter, the best fitting values vary between 0.0092 and 0.102, and between 0.0064 and 0.107 for undisturbed and reconstituted specimens, respectively, and deliver R^2 values of 0.91 and 0.89 in average, for undisturbed and reconstituted specimens respectively. As each specimen is constituted by one type of soil, the value of PEC varies depending on the specimen.

As for the GP specimens, the pore pressure ratios are plotted against the normalised dissipated energy for undisturbed and reconstituted tests, in Figure 11.25. Some interesting conclusions can be drawn, when the results are related to the cyclic behaviour described in section 10.2.2. The $W_{s,liq}$ of NB1_F2_GP3.5_I1 undisturbed specimen was higher than the $W_{s,liq}$ of the two reconstituted specimens.

The undisturbed specimen required a higher number of cycles to trigger liquefaction and the pore pressure evolution rate was lower, hence the higher accumulation of energy during shear, until liquefaction. Despite the differences in cyclic behaviour of the two reconstituted specimens, they showed a similar behaviour in terms of W_s. On the other hand, the NB1_F4_GP4_I2 undisturbed specimen liquefied for a lower number of cycles than the respective reconstituted specimens, and its dissipated energy at liquefaction was also lower. The analysis of the pore pressure build-up of NB1_F1_GP4.5 specimens showed that the r_u-W_s evolution of the four specimens is not very different. However, the undisturbed specimen showed the lower dissipated energy at liquefaction, despite being liquefied for an intermediate number of cycles. NB1_F5_GP5_I1 undisturbed specimen showed a pore pressure ratio development similar to NB1_F5_GP5_R1_3, but slightly lower. As referred before, these two specimens reached liquefaction for a similar number of cycles (N_{liq}=26 for NB1_F5_GP5_R1_3 and N_{liq}=30+23 for NB1_F5_GP5_I1). The other two reconstituted specimens required more cycles to liquefy and consequently, the dissipated energy at liquefaction was also higher. Similar conclusions are made for the NB1_F5_GP5_I2 soil. The undisturbed and reconstituted specimen that liquefied for lower N_{liq} showed lower $W_{s,liq}$. The NB2_F1_GP6_I2 undisturbed specimen showed higher dissipated energy throughout the shear stage and also took more cycles to reach liquefaction. On the contrary, the NB1_F1_FP6_I3 undisturbed specimen reached liquefaction for a lower N_{liq} than the reconstituted specimen but its $W_{s,liq}$ was higher. This might be due to the slower ε_a increase rate in the undisturbed specimen, that increases the area of the hysteresis loops until liquefaction occurs, reflecting on higher cumulative dissipated energy. These results support the assumption that $W_{s,liq}$ is related to N_{liq}, as proposed in section 11.3.6.
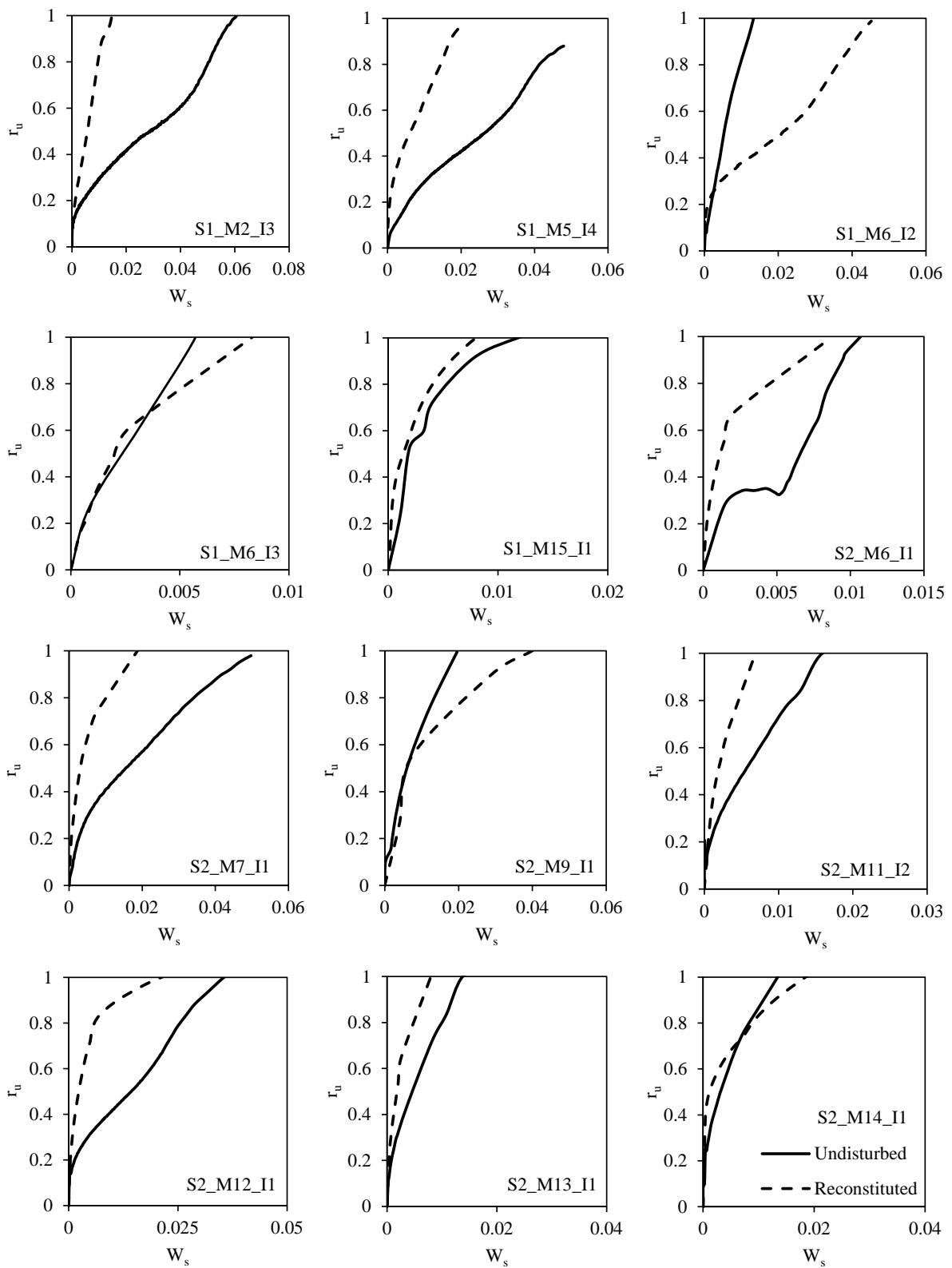
Figure 11.24 – Pore pressure ratio evolution with W_s for Mazier tests
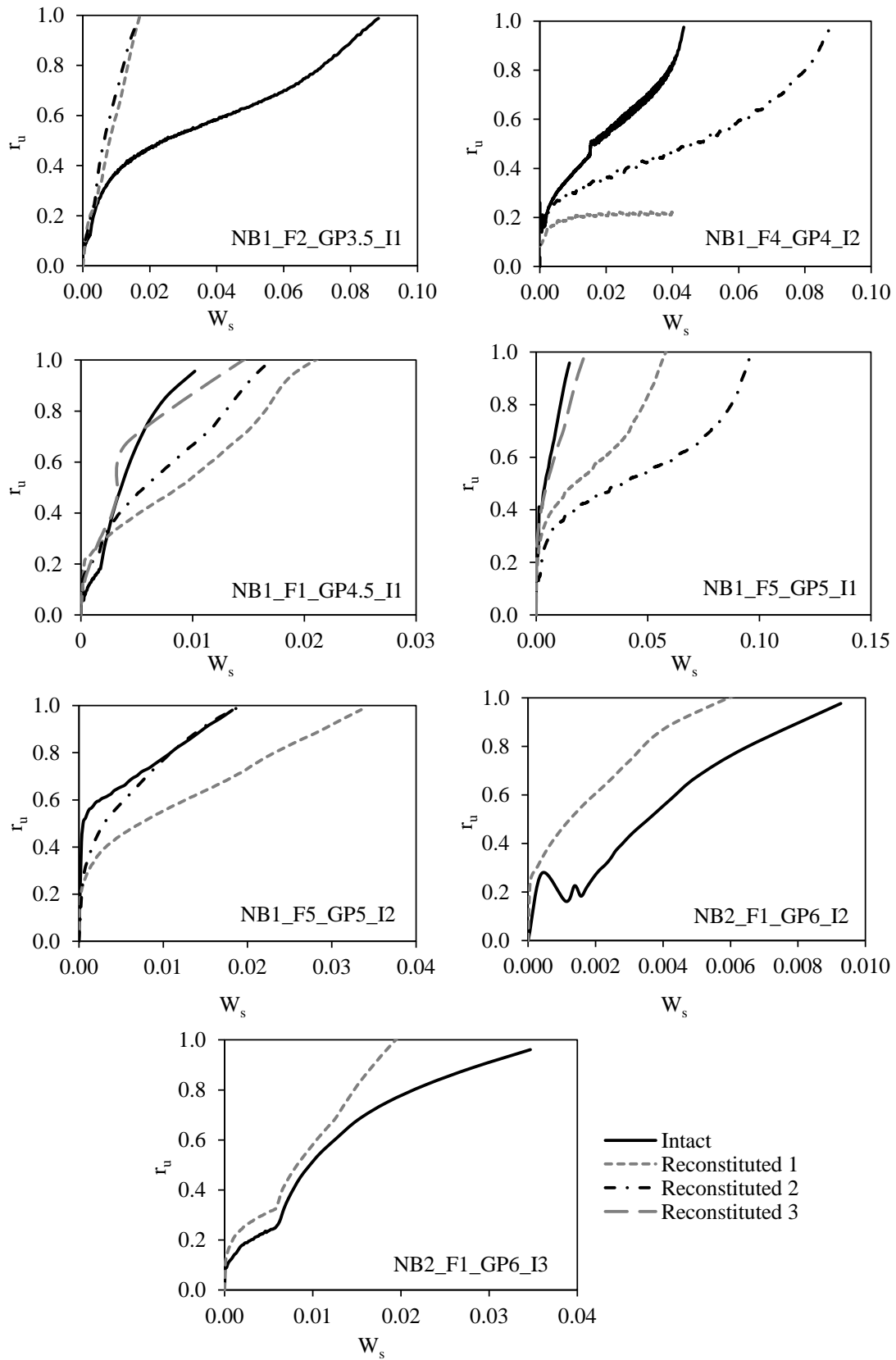
Figure 11.25 – Pore pressure ratio evolution with W_s for GP tests

11.6.   CHAPTER SUMMARY

This Chapter presented the analysis of the liquefaction results of cyclic triaxial and direct simple shear tests, by means of the energy-based approach. The energy-based approach considered in the present work was based on the dissipated energy per unit volume of soil (ΔW), which corresponds to the area of the hysteresis loops in $q-\varepsilon_a$ or $\tau-\gamma$ planes, for cyclic triaxial and cyclic simple shear tests, respectively. Moreover, the definition of the dissipated energy at liquefaction (i.e., the ΔW required to trigger liquefaction, ΔW_{liq}) was considered the point where the pore pressure ratio (r_u) reached 1 for cyclic triaxial tests, and the point where shear strain (γ) reached $\pm 3.75\%$ for cyclic direct simple shear tests. Having determined the values of dissipated energy at liquefaction for all tests performed, the effect of several factors on ΔW_{liq} was investigated.

The first factor evaluated was the confining pressure, and it was observed that, despite the differences in ΔW_{liq} for the same confining pressure, ΔW_{liq} increased with the increase in confining pressure. Therefore, to eliminate the dependence of the dissipated energy at liquefaction on the confining pressure, the values of ΔW_{liq} were normalised by the initial confining stress in the following analyses.

The comparison between the results of cyclic triaxial and cyclic direct simple shear tests indicated that the pore pressure development was similar in tests performed with both devices. However, the results of CDSS showed lower values of normalised dissipated energy at liquefaction than the CTx tests.

As for the effect of relative density, there seemed to be a tendency of $W_{s,liq}$ to increase with the increase of D_R, in both CTx and CDSS tests.

The effect of sample preparation was assessed by comparing specimens prepared with moist tamping and dry air pluviation. The results were inconclusive, as there was a lot of scatter in the plots. However, the CDSS results suggest that the $W_{s,liq}$ of PL specimens was lower than that of MT specimens.

The effect of water content on $W_{s,liq}$ was analysed for the CDSS tests. Specimens with $w=3.5\%$ showed higher $W_{s,liq}$ than dried specimens and specimens with higher water contents, emphasising the role of the matric suction effects due to partial saturation in MT specimens prepared with low water content. On the other hand, dry and almost saturated specimens showed similar values of $W_{s,liq}$.

The effect of natural fabric was assessed by comparing the results of undisturbed and reconstituted specimens. It was found that $W_{s,liq}$ increased with increase in N_{liq}, which motivated the investigation of the N_{liq}_U-N_{liq}_R influence on the relationship between $W_{s,liq}\_U$ and $W_{s,liq}\_R$. For specimens with N_{liq}_U-$N_{liq}\_R<0$, that is for pairs of tests where the reconstituted specimen liquefied for a higher number of cycles than the undisturbed specimen, the $W_{s,liq}\_R$ was higher than $W_{s,liq}\_U$. These were clean sand specimens and it was observed that the reconstitution is not conservative. On the other hand, for pairs of tests where the undisturbed specimen required more cycles to liquefy than the reconstituted specimen

(N_{liq}_U-N_{liq}_R>50), the $W_{s,liq}$_U was higher than $W_{s,liq}$_R. These were sands with fines, where the fines reinforce the specimen fabric that is destroyed when reconstituted. For pairs of tests with small differences between N_{liq} of undisturbed and reconstituted specimens (less than 50 cycles), the $W_{s,liq}$_U and $W_{s,liq}$_R values were similar.

The soil capacity energy was evaluated by comparing the measured results with the estimated values using two known expressions (Figueroa et al., 1994, and Baziar and Jafarian, 2007). It was concluded that, despite the use of more intrinsic soil parameters in the equation from Baziar and Jafarian (2007), the equation from Figueroa et al. (1994) seems to estimate values closer to the measured results.

Moreover, the pore pressure generation was related to the normalised dissipated energy, using the GMP model proposed by Green et al. (2000), in reconstituted and undisturbed specimens. The reconstituted tests results showed that, excluding some tests that required many loading cycles to reach liquefaction, the r_u–W_s curves are relatively convergent. The values of PEC that best fit the r_u–W_s curves measured were ranged between 0.0035 and 0.02, with R^2 values higher than 0.80.

As for the pore pressure build-up evaluation in undisturbed specimens, the comparison between Mazier undisturbed and reconstituted specimens showed distinct relationships between r_u and W_s. In terms of the PEC parameter, the best fitting values varied between 0.0092 and 0.102, and between 0.0064 and 0.107 for undisturbed and reconstituted specimens, respectively, and delivered R^2 values of 0.91 and 0.89 in average. On the other hand, the results of GP specimens support the assumption that $W_{s,liq}$ is related to N_{liq}, as once again higher $W_{s,liq}$ values are associated with higher N_{liq}.

PART IV - SUMMARY AND CONCLUSIONS

12. CONCLUSIONS

12.1. CONCLUDING REMARKS

This work presented an in-depth study of the behaviour of soils that compose the LTV experimental site, through the performance and analysis of several field and laboratory tests. After the selection of the experimental site, under the protocol defined in the work packages of H2020 EU project "LIQUEFACT", an extensive experimental campaign was carried out, including the performance of different field tests and the collection of soil samples using three different samplers. The analysis of the field tests results allowed the characterisation of the experimental site soil profiles and liquefaction susceptibility assessment, by comparing and contrasting different in situ testing techniques. The quality of the samples was evaluated, emphasising the more relevant and recommended procedures to preserve the samples integrity during the entire sampling process, transportation conditions and extrusion of the specimens to be tested. The extensive laboratory experimental programme, including over 200 cyclic triaxial and cyclic direct simple shear tests, contributed to characterise the physical and geomechanical properties of young Holocene alluvial soils prone to liquefaction, and to a better understanding of the factors that affect the cyclic liquefaction behaviour of those materials, the behaviour of high quality undisturbed specimens and the correlations between the laboratory results of undisturbed and reconstituted specimens.

The following sections present the main findings and conclusions of this research. The partial conclusions of each Chapter are presented at the end of each respective Chapter, and the most relevant findings/conclusions are summarised here.

12.1.1. LIQUEFACTION SUSCEPTIBILITY FROM FIELD TESTS

The liquefaction susceptibility of the experimental site was assessed by the performance of different field tests, including standard penetration tests (SPT), cone penetration tests (CPTu), flat dilatometer tests (DMT) and measurement of shear wave velocities (with SDMT and SCPTu equipment). Besides, high quality samples were collected from the four experimental site locations, using Mazier, Gel-Push, and Dames and Moore samplers.

The variety of in situ tests performed at the experimental site allowed a detailed analyses and comparison of different liquefaction assessment methodologies, which is rare when dealing with the

design of low to moderate risk projects, as they involve high costs and are very time consuming. The investigated experimental sites were constituted by very heterogeneous soil profiles, with interbedded sand-silt-clay layers. However, despite the heterogeneity of the soil profiles, in some locations, homogeneous layers of sand were found at different depths and thick potentially liquefiable layers were identified, concluding that the experimental site had significant areas prone to liquefaction, as generalised in Viana da Fonseca et al. (2019b). From a qualitative perspective, the results suggest that S1 and NB2 present very high risk of liquefaction, while S2 and NB1 present high liquefaction risk. On the other hand, the LSN values predict moderate expression of liquefaction in S1, NB1 and NB2, with some structural damage, and minor expression of liquefaction in S2.

The use of different field tests for the assessment of liquefaction susceptibility was beneficial, especially when complemented with laboratory analyses of grain size distribution and Atterberg limits. Nevertheless, some discrepancies were found in the SPT and V_S measurements, particularly in the identification of soil interlayers. The SPT was not able to detect small interbedded layers, while the CPTu allowed for the definition of more detailed continuous soil profiles, being the most accurate in situ test to identify small interlayers. The liquefaction analyses based on in situ V_S were also not successful in the discretisation of the interbedded layers, which was expected, providing values of LPI lower than the other tests. Despite not being adequate to distinguish the layering of sandy to clayey soils, the measurements of the in situ V_S were crucial for a comprehensive sample quality assessment.

The use of different methodologies to evaluate liquefaction potential based on CPTu results was discussed, highlighting the importance of consistency when using a certain CPTu-based liquefaction assessment method. Therefore, the implementation of the logic tree approach (Lai et al., 2020), which attributes a weight to each method and computes a weighted average of the results to obtain a representative value, should be careful as it may contradict the coherence of the analyses.

Based on the results of the four experimental sites and 33 additional CPTu tests, a new chart relating LPI and LSN_{20} values was proposed and might be used to assess liquefaction severity and damage. The suggested boundaries define three severity damage categories: low to minor for LPI lower than 5 and LSN_{20} lower than 5; moderate for LPI between 5 and 15 and LSN_{20} between 5 and 25; and major to severe for LPI higher than 15 and LSN_{20} higher than 25.

12.1.2. SAMPLE QUALITY ASSESSMENT

At the experimental site, samples were collected using Mazier, Gel-Push and Dames and Moore samplers. The three samplers proved to be competent in retrieving soil samples of most soil types collected. However, the D&M and the GP samplers collected samples of higher quality than the Mazier sampler, due to their improved characteristics. The D&M smooth brass liner of smaller length minimized friction between the tube walls and reduced disturbances in the soil during penetration and

extrusion in the laboratory. Besides, the neoprene skirt seal prevented the sample from falling during the tube extraction from the borehole. In the GP sampler, the presence of the gel polymer allowed for a smoother extrusion of the soil samples from the metallic liner, reducing the friction during the extraction process and preserving the sample integrity. The Mazier sampling procedure presented the following disadvantages:

- It involved rotation with water injection, which can generate disturbances on the samples, due to wash out of the finer particles;
- The liners were made of PVC and required a more carefully extrusion process, in order to not damage the sample as a consequence of the flexibility of the tube;
- The internal PVC tube surface was not smooth, causing some surface damages when extruding samples of fine soil, as the soil was dragged through the surface while the PVC tube was removed.

The quality of the samples collected with three samplers was assessed based on visual inspection, the comparison of in situ and laboratory measured shear wave velocities, the measurement of volume changes during reconsolidation, and the comparison between in situ correlations and laboratory measured soil density.

The visual inspection of samples is crucial to determine the preliminary state of the soil samples and to select the most adequate samples for extensive laboratory testing. This is ideally done by X-ray or tomographic processes, which were not accessible at the time of this work. It is advised to record and photograph the specimens as they are extruded from the sampling tube, as well as labelling them for future reference.

The methods based on volume changes during reconsolidation method and the comparison between in situ and laboratory D_R values were not appropriate for the materials tested in this work (granular materials with the presence of fines and interlayers). While the volume changes during reconsolidation method is often used for clayey soils, the D_R-CPT correlations have large uncertainties, particularly for the analysis of heterogeneous soil profiles.

On the other hand, the method based on the in situ measurements of the shear wave velocities was the most adequate for assessing sample quality. It is important to mention that the in situ tests need to be performed with precision and care, preferably by direct measurements from downhole logging (e.g. SDMT or SCPTu). As downhole logging measures of V_S are usually performed every 0.50 m or 1 m, they might be misleading when analysing a smaller specimen from a particular depth. Therefore, it is recommended that CPTu testing is performed close to the sampling borehole, to improve the results interpretation. Moreover, in the present work, the CPT-V_S correlation proposed by Robertson (2009) computed results that agreed well with the direct measurements. The shear wave velocities measured

in the laboratory with bender elements implemented in the triaxial cell proved to be more accurate than the "bench" test results, as the specimens were submitted to the same confining stresses as in the field and were fully saturated, providing a cleaner wave signal and facilitating the interpretation of results. The normalisation of both field and laboratory V_S with void ratio function and mean effective stress improved the comparisons and is highly recommended for a more accurate comparison of results.

A ponderation of various methods, considering a Specimen Quality Index (Taylor, 2015), with weights reflecting the precision and amount of confidence in each method, was used for assessing the global quality of samples. Most specimens were classified as being of good to excellent quality.

12.1.3. PHYSICAL AND GEOMECHANICAL CHARACTERISATION OF STUDIED SOILS

One of the objectives of the FCT project LIQ2PROEARTH and this PhD thesis, as part of that, was to characterise the different soils collected in four experimental sites located in the Lower Tagus Valley. Therefore, the experimental laboratory work was focused on the undisturbed samples collected at the four pilot sites and on reconstituted tests on the NB1 soil. Physical identification included the particle size distribution, with indices such as fines content (FC), mean grain size (D_{50}), coefficient of shape (C_C), and coefficient of uniformity (C_U), specific gravity (G_s), plasticity through Atterberg limits, void ratio limits (e_{max} and e_{min}), and shape parameters (circularity, solidity, and aspect ratio).

The tested specimens presented a variety of physical characteristics, which were in accordance with the heterogeneous soil profiles found in the in situ testing results. Some specimens were opened vertically and thin layers of finer soil interbedded with sand were identified, confirming the heterogeneity of the undisturbed specimens tested. The material properties were compared with sands previously studied by FEUP geotechnical group CONSTRUCT-GEO and framed within benchmark soils studied by Cubrinovski and Ishihara (2002), Cho et al. (2006), Altuhafi et al. (2013), and Altuhafi et al. (2016) showing good agreement with the benchmark soils, in terms of void ratio limits correlations with fines content, D_{50}, and shape parameters.

The critical state lines of four soils were determined based on the results of drained compression triaxial tests and the critical state parameters of the other undisturbed soils were determined using the empirical correlations with e_{max} and e_{min} proposed by Cubrinovski and Ishihara (2000). The critical state line parameters of all the undisturbed specimens tested were compared with benchmark sands and framed within the previous results in terms of void ratio, grain size characteristics, and shape factors, showing that the results fit well with the trends defined for other soils. Moreover, the comparison between the estimated CSL determined with the empirical correlations and those obtained using reconstituted specimens showed good agreement. This supports the use of empirical CSL to determine the state parameters of undisturbed soils like these, when it is not possible to determine the CSL with triaxial compression tests data. Besides, the correlations between CS parameters and physical characteristics

(e_{max}, e_{min}, FC, D_{50}, C_U, and shape parameters) follow the trends defined previously for the reconstituted soils tested and of data from other researchers.

12.1.4. FACTORS AFFECTING THE CYCLIC BEHAVIOUR OF RECONSTITUTED SPECIMENS

The experimental programme involved an extensive number of cyclic triaxial and cyclic direct simple shear tests on reconstituted specimens of selected sandy soils from the pilot sites (S1_M2, S1_M7, and NB1), with a variety of state parameters and loading conditions. This allowed for the investigation of the effects of several factors on cyclic stress-strain behaviour and liquefaction resistance of the three sands. The main findings may be summarised as follows:

- **State parameters**: Slight changes in void ratio did not affect the location of the cyclic resistance curves. However, as expected, when considering higher changes in void ratio, the liquefaction resistance increases with increase in D_R. The confining pressure variation range was small (40 – 100kPa), so major conclusions were difficult to make. However, in the CTx tests analyses, the increase in p'_i lowered the cyclic resistance curve, while in CDSS tests different values of p'_i (from 40 kPa to 100kPa) had no influence in the position of the cyclic resistance curve. It was concluded that specimens with lower state parameter (ψ) exhibited higher resistance, as they were located on the dense side of the CSL.

- **Frequency**: As expected, changes in frequency from 1 Hz to 0.1 Hz did not influence the location of the cyclic resistance curve.

- **Sample preparation method**: For CTx tests no difference was observed in the cyclic resistance curve of moist tamping (MT) and air pluviation (PL) specimens, contradicting the expected trends found by several other authors. However, despite the similarity of the cyclic resistance curves, the behaviour during shearing was found to be different. On the other hand, the cyclic resistance curves obtained by CDSS tests on MT and PL specimens showed that PL specimens had lower liquefaction resistance than MT specimens. The CRR_{15} increased from 0.083 on PL specimens to 0.112 on MT specimens (+35%).

- **Boundary conditions**: For S1_M7 specimens, it was found that the flexible membrane specimens had higher resistance than specimens tested with rigid boundary. The secant shear modulus, G_{sec}, was higher for specimens confined with flexible membrane. However, once liquefaction occurs, the flexible membrane specimens showed higher levels of deformation. On the other hand, the pore pressure evolution was faster on the specimens confined with rigid rings, which supports the assumption that the rigid boundary specimens had lower cyclic resistance.

- **Water content**: Higher cyclic resistance was observed for specimen with lower water content, which might be related to the matric suction effects due to partial saturation during specimen

preparation. However, the water retention curve of the soil should be performed to confirm these effects.

- **Layering**: The effect of layering in liquefaction behaviour was investigated for two pairs of tests. When the layered and mixed specimens were prepared to the same target void ratio, the liquefaction behaviour of the two specimens was similar, confirming what was observed by Cappellaro (2019). On the other hand, when the specimens were prepared with the same compaction effort, and consequently the initial void ratio of the fines and sand layers were different, the layered specimens exhibited higher resistance.

- **Laboratory devices**: Two trends were observed when comparing the results of tests performed with CTx and CDSS devices: when the CTx and CSS tests were both performed with saturated specimens under isotropic conditions, the results showed a good correspondence between CSR_{ss} and CSR_{tx}; when the CDSS tests were anisotropically consolidated, they showed lower resistance than CTx tests. However, after the normalisation of CTx results with c_r, the cyclic resistance curves were similar. Moreover, the value of c_r was found to decrease with increasing number of cycles to trigger liquefaction.

12.1.5. EVALUATION OF CYCLIC BEHAVIOUR OF UNDISTURBED SPECIMENS

The undisturbed specimens collected represented the variety of soils found in the 4 experimental sites studied, as each specimen was basically a unique soil, with different intrinsic properties. The study of the cyclic behaviour of undisturbed specimens allowed for the identification of pattern behaviours related to some soil properties. Despite the specimens being composed of different soils, a tendency was found between the cyclic resistance curves of Mazier specimens and the soils fines content. Specimens with intermediate FC (8% < FC < 19%) showed the lowest cyclic resistance, while specimens with low FC (FC < 8%) exhibited intermediate resistance. On the other hand, the specimens with higher FC range (FC > 19%) exhibited the higher cyclic resistance. These tendencies suggest that liquefaction resistance reduces with increase of fines content up to a threshold value and increases after this value is surpassed, confirming what was observed by other researchers (Chang, 1990; Polito and Martin, 2001; Thevanayagam, 2007b; Huang and Chuang, 2011; Cappellaro, 2019; Gobbi, 2020).

The comparison between the results of undisturbed specimens and the respective reconstituted specimen, prepared with MT for the same initial state conditions, enabled the study of the effect of fabric on the cyclic behaviour and liquefaction resistance of the soils studied. The results of CTx tests performed on Mazier specimens showed that, in general, when the soil had less than 6% FC, the reconstituted specimen exhibited higher cyclic resistance, while when the soil had more than 6% FC, the reconstituted specimen was less resistant than the correspondent undisturbed specimen. As the tests compared were performed in specimens of the same soil type, with state parameters and applied CSR, the differences were mainly attributed to fabric and structure. The presence of fines, a reflex of the

presence of interlayers, increased the resistance of the undisturbed specimen, hence for soils with FC higher than 6%, N_{liq}_U was higher than N_{liq}_R.

The response of undisturbed and reconstituted specimens in terms of strains and excess pore pressure was also distinct. The undisturbed specimens exhibited a more stable behaviour, with a steady and constant increase in strains, often biased to the extension side, while the reconstituted specimens exhibited an exponentially increasing rate of strains, which occurs to both compression and extension side. This might be due to the structure of the undisturbed specimens, with layers and laminations that provide a more stable response even beyond liquefaction triggering.

The effect of fabric was also investigated with the performance of three sets of CDSS tests, for specimens collected with the Mazier sampler at three different depths, at S2. The undisturbed specimens collected at 13 m exhibited higher cyclic resistance than the respective reconstituted specimens, which was in agreement with the results found in the CTx tests with FC > 6%.

12.1.6. COMPARISON BETWEEN LABORATORY AND FIELD DATA

The comparison between laboratory and field data was performed in four parts: comparison between the V_S and D_R determined in the laboratory and in the field (already addressed in the sample quality assessment section), comparison between the state parameters obtained in the laboratory with the state parameter obtained using an empirical correlation with CPTu data, comparison between cyclic resistance curves determined in the laboratory and CSR-N_{liq} curves estimated with CPTu data, and comparison between the factor of safety against liquefaction obtained in the laboratory and using CPTu data.

The state parameters of undisturbed laboratory specimens were generally lower than the state parameter estimated with the CPTu-based correlation, suggesting that the laboratory specimens were denser than the soil in the field. It is worth to note there are significant uncertainties associated with both the empirical CSL relationship and the field-based relationship that might compromise these conclusions. Nevertheless, the state parameters of GP specimens were closer to the empirical CPT determined values than the Mazier specimens, which reveals the better performance of the GP in the collection of high quality samples.

The cyclic resistance of CDSS tests was higher than the cyclic resistance determined using field data. This was explained by the orientation of the layering in the undisturbed specimens tested under CDSS. The undisturbed specimens tested in CDSS were collected perpendicularly to the sampling direction, hence the layering and laminations were perpendicular to the shear direction, which might have increased the resistance of the specimens tested under CDSS conditions. On the other hand, the results from CTx tests showed good agreement with the cyclic resistance curve from the CPTu data.

Moreover, the factor of safety against liquefaction was computed for the laboratory cyclic triaxial tests and compared with the FS_{liq} obtained from the CPTu data, for an equivalent cyclic stress ratio. No clear correspondence between the results was perceived as, in some cases, the $FS_{liq\_}$CPTu was higher than $FS_{liq\_}$lab, while in other cases the opposite was observed. However, a correlation between the FS_{liq} and number of cycles required to trigger liquefaction (N_{liq}) was found.

12.1.7. ENERGY-BASED APPROACH

The liquefaction results presented in this work were analysed using an energy-based approach. This analysis was based on the evidence that, when a soil is cyclically sheared, part of the energy is dissipated throughout the soil, and the other part is dissipated into the soil. The accumulated dissipated energy might be related to the cumulative area limited by stress-strain hysteresis loops in the plot of $q-\varepsilon_a$ or $\tau-\gamma$, facilitating the determination of the dissipated energy required to trigger liquefaction and its developments towards the full process.

Therefore, the influence of several factors, which depend on the material characteristics and the testing procedures, on the dissipated energy at liquefaction (ΔW_{liq}) was investigated, and the following conclusions were drawn:

- **Confining pressure**: The ΔW_{liq} increased with the increase in confining pressure. To eliminate this dependence on the confining pressure, the values of ΔW_{liq} were normalised by the initial confining stress ($W_{s,liq}= \Delta W_{liq}/\sigma'_c$).

- **Laboratory device**: The pore pressure development was similar in CTx and CDSS tests. However, the results of CDSS showed lower $W_{s,liq}$ than the CTx tests.

- **Relative density**: There seemed to be a tendency of $W_{s,liq}$ to increase with the increase of D_R, in both CTx and CDSS tests.

- **Sample preparation technique**: The results were inconclusive, as there was a lot of scatter in the plots. However, the CDSS results suggested that the $W_{s,liq}$ of PL specimens was lower than that of MT specimens.

- **Water content**: Specimens moulded with moisture content of 3.5% showed higher $W_{s,liq}$ than dry specimens and specimens with higher water contents, emphasising the role of the matric suction effects due to partial saturation in MT specimens prepared with low water content. Dry and saturated specimens showed similar values of $W_{s,liq}$.

- **Fabric**: It was found that $W_{s,liq}$ increased with increase in N_{liq}. For pairs of tests where the reconstituted specimen liquefied for a higher number of cycles than the undisturbed specimen, the $W_{s,liq\_}$R was higher than $W_{s,liq\_}$U. For pairs of tests where the undisturbed specimen required more cycles to liquefy than the reconstituted specimen ($N_{liq\_}$U-$N_{liq\_}$R>50), the $W_{s,liq\_}$U was higher than $W_{s,liq\_}$R. Moreover, for pairs of tests with small differences between N_{liq} of

undisturbed and reconstituted specimens, the $W_{s,liq}\_U$ and $W_{s,liq}\_R$ values were similar. The results of GP specimens support the assumption that $W_{s,liq}$ is related to N_{liq}, as the higher $W_{s,liq}$ values are associated with higher N_{liq}.

Two known expressions by Figueroa et al. (1994) and Baziar and Jafarian (2007) were applied to the experimental data of this study to compute the estimated soil capacity energy. After comparing the measured results with the estimated values, it was concluded that the equation from Figueroa et al. (1994) was more promising, as the estimated $\log\varDelta W$ values were closer to the measured values than when using the Baziar and Jafarian (2007) equation. However, both equations were considered inadequate to estimate the results obtained in this work, as the results were very sparse.

12.1.8. Pore Pressure generation models

Earthquake-induced soil liquefaction is a phenomenon typically associated with the increase in pore water pressure, therefore, the study of pore pressure generation models has been developed in an attempt to find ways to predict soil liquefaction. This work addressed two pore pressure generation models, the stress-based model suggested by Booker et al. (1976) and the energy-based model proposed by Green et al. (2000).

As for the stress-based approach, the pore pressure generation was related to N_c/N_{liq}. It was found that the r_u–N_c/N_{liq} curves of reconstituted specimens grouped according to similar initial state parameters were relatively convergent. Moreover, the r_u–N_c/N_{liq} curves of undisturbed and respective reconstituted Mazier specimens also showed good agreement. The Booker et al. (1976) model was calibrated to best fit the undrained cyclic triaxial results, and the α values that provided the best estimation of pore pressure evolution with N_{liq} were ranged between 0.25 and 1.18 (with averages between 0.53 and 0.78) for the reconstituted specimens of case study soils and between 0.36 and 1.497 for the undisturbed Mazier and GP specimens.

As for the energy-based approach, the reconstituted tests results showed that, excluding some tests that required many loading cycles to reach liquefaction, the r_u–W_s curves are relatively convergent, however, the comparison between Mazier undisturbed and reconstituted specimens showed distinct relationships between r_u and W_s. The GMP model (Green et al., 2000) was calibrated to best fit the undrained cyclic triaxial results and high values of R^2 were found, reflecting the good performance of the model in the estimation of the r_u–W_s behaviour.

12.2. FUTURE WORKS

The most important conclusions of the present work were summarised in the previous section. However, much work still needs be done, in the journey to fully understand the mechanisms of cyclic liquefaction resistance. This section outlines some recommendations for future works.

- It was observed that the use of laboratory-measured fines content and plasticity had a huge influence on the identification of the critical liquefiable layers and soil behaviour from in situ tests, especially for SPT tests. Therefore, the effects of fines content and plasticity on SPT and CPTu resistances should be investigated further.

- The D_R-CPTu correlations should be revised and improved, to decrease the uncertainties of the estimated values, particularly when it concerns soils with fines. This could be attempted by performing calibration chamber tests.

- Several specimens collected with the three samplers (Mazier, Gel-Push, and Dames and Moore) were not yet tested. It would be interesting to test more undisturbed specimens from the experimental site, to deepen the knowledge on the cyclic behaviour of natural soils and to solidify the tendencies discussed in this work.

- Some monotonic tests should be performed in undisturbed specimens collected near the specimens tested under cyclic triaxial conditions. This would allow the definition of more accurate critical state lines of undisturbed soils and consequently a better determination of the specimen's state parameters. A more accurate knowledge of the state parameter of the soils is crucial for the understanding of the liquefaction behaviour of undisturbed soils.

- Cyclic direct simple shear tests should be performed in undisturbed specimens collected in the same direction as sampling, to evaluate the cyclic behaviour of the natural soil when tested under loading conditions that better simulate the field conditions.

- Reconstituted specimens prepared with other sample preparation methods, such as air pluviation or wet sedimentation, should be performed, to better simulate the fabric of the undisturbed specimens and to improve the comparisons between undisturbed and reconstituted specimens.

- It would be interesting to integrate other soil parameters in the estimation of the soil capacity energy, such as the shape parameters, the small-strain shear modulus, or the state parameter.

- The next step of the work would be the numerical simulation of the laboratory tests (cyclic triaxial and cyclic simple shear) at the element level and the calibration of the parameters that define the soil behaviour.

REFERENCES

Altuhafi, F., O'Sullivan, C., and Cavarretta, I. (2013). Analysis of an image-based method to quantify the size and shape of sand particles. Journal of Geotechnical and Geoenvironmental Engineering, 139(8): 1290–1307.

Altuhafi, F.N., Coop, M.R., and Georgiannou, V.N. (2016). Effect of particle shape on the mechanical behavior of natural sands. Journal of Geotechnical and Geoenvironmental Engineering, 142(12): 04016071.

Amini, F. and Qi, G.Z. (2000). Liquefaction testing of stratified silty sands. Journal of Geotechnical and Geoenvironmental Engineering, 126(3): 208–217.

Amoroso, S. (2014). Prediction of the shear wave velocity V_S from CPT and DMT at research sites. Frontiers of Structural and Civil Engineering, 8(1): 83-92 doi: 10.1007/s11709-013-0234-6

Andresen, A., and Kolstad, P. (1979). The NGI 54mm samplers for undisturbed sampling of clays and representative sampling for coarser materials. In Proceedings of the International Symposium on Soil Sampling. Singapore, pp. 13-21.

Andrus R.D., and II Stokoe K.H. (2000). Liquefaction resistance of soils from shear-wave velocity. Journal of Geotechnical and Geoenvironmental Engineering, 126(11): 1015–1025.

Arthur, J.R.F., Chua, K.S., Dunstan, T., and Rodriguez, J.I. (1980). Principal stress rotation: A missing parameter. Journal of Geotechnical Engineering, ASCE, 106(GT4): 419–433.

ASTM International (2000). D6528-00 – Standard Test Method for Consolidated Undrained Direct Simple shear Testing of Cohesive Soils.

ASTM International (2015). D6519-15 – Standard Practice for Sampling of Soil Using the Hydraulically Operated Stationary Piston Sampler.

ASTM International (2017). D2487-17 – Standard Practice for Classification of Soils for Engineering Purposes (Unifed Soil Classification System).

Atkinson, J. (2007). The Mechanics of Soils and Foundations, Second Edition, London: CRC Press, https://doi.org/10.1201/9781315273549

Azeiteiro, R.J., Coelho, P.A., Taborda, D.M., and Grazina, J.C. (2017). Energy-based evaluation of liquefaction potential under non-uniform cyclic loading. Soil Dynamics and Earthquake Engineering, 92: 650–665.

Baldi, G., Bellotti, R., Ghionna, N., Jamiolkowski, M., and Pasqualini, E. (1986). Interpretation of CPT's and CPTU's, 2nd part, drained penetration of sands. In 4th International Geotechnical Seminar, Singapore.

Baligh, M.M., Azzouz, A.S., Chin, C.-T. (1987). Disturbances due to ideal tube sampling. Journal of Geotechnical Engineering, ASCE, 113(7): 739–757.

Baziar, M.H., and Jafarian, Y. (2007). Assessment of liquefaction triggering using strain energy concept and ANN model: capacity energy. Soil Dynamics and Earthquake Engineering, 27(12): 1056-1072.

Baziar, M.H., Jafarian, Y., Shahnazari, H., Movahed, V., and Amin Tutunchian, M. (2011). Prediction of strain energy-based liquefaction resistance of sand–silt mixtures: An evolutionary approach. Computers & Geosciences, 37: 1883–1893.

Been, K. and Jefferies, M.G. (1985). A state parameter for sands. Géotechnique, 35(2): 99–112.

Been, K., Jefferies, M.G., and Hachey, J. (1991). The critical state of sands. Géotechnique, 41(3): 365–381.

Bedin, J., Schnaid, F., Viana da Fonseca, A., and Costa-Filho, L. (2012). Gold tailings liquefaction using critical state soil mechanics concepts. Géotechnique, 62(3): 263–267.

Benahmed, N., Canou, J., and Dupla, J.-C. (2015). Liquefaction properties and initial structure of a loose sand. In Proceedings of 6th International Conference on Earthquake Geotechnical Engineering, Christchurch, New Zealand, 1-4 November 2015.

Berrill, J.B., and Davis, R.O. (1985). Energy Dissipation and Seismic Liquefaction of Sands: Revised Model. Soils and Foundations, 25(2): 106–118.

Booker, J.R., Rahman, M.S., and Seed H.B. (1976). GADFLEA – A Computer Program for the Analysis of Pore Pressure Generation and Dissipation During Cyclic or Earthquake Loading. EERC 76-24. University of California, Berkeley.

Boulanger, R.W. (2003a). High overburden stress effects in liquefaction analyses, Journal of Geotechnical and Geoenvironmental Engineering, ASCE,n129(12): 1071–082.

Boulanger, R.W. (2003b) Relating Kα to relative state parameter index. Journal of Geotechnical and Geoenvironmental Engineering, ASCE 129(8): 770–73.

Boulanger, R. W. (2012). Liquefaction in the 2011 Great East Japan Earthquake: Lessons for U.S. Practice. Proceedings of the International Symposium on Engineering Lessons Learned from the 2011 Great East Japan Earthquake, March. Tokyo, Japan.

Boulanger, R.W., and Idriss, I.M. (2008). Evaluating the potential for liquefaction or cyclic failure of silts and clays. Report UCD/CGM-04/01, Center for Geotechnical Modeling, University of California, Davis. 129 pp.

Boulanger, R.W., and Idriss, I.M. (2014). CPT and SPT based liquefaction triggering procedures. Report No. UCD/CGM-14/01. Center for Geotechnical Modeling, Department of Civil and Environmental Engineering, University of California, Davis. 134 pp.

Boulanger, R.W., and Idriss, I.M. (2016). CPT-based liquefaction triggering procedure. Journal of Geotechnical and Geoenvironmental Engineering, ASCE, 142(2):04015065. doi:10.1061/(ASCE)GT.1943-5606.0001388

Boulanger, R.W., and DeJong, J.T. (2018). Inverse filtering procedure to correct cone penetration data for thin-layer and transition effects. In Proceedings of the 4th International Symposium on Cone Penetration Testing (CPT'18), Delft, The Netherlands.

Bray, J.D., and Sancio, R.B. (2006). Assessment of the Liquefaction Susceptibility of Fine- Grained Soils. Journal of Geotechnical and Geoenvironmental Engineering, 132(9): 1165–1177. doi:10.1061/(ASCE)1090-0241(2006)132:9(1165)

Bui, M., Clayton, C.R.I., and Priest, J. (2010). The universal void ratio functions for small strain shear modulus. In Proceedings of 5th International Conference on Recent Advances in Geotechnical Earthquake Engineering and Soil Dynamics, San Diego, California, Section 1a, paper No 1.24a.

Cabral, J., Moniz, C., Batlló, J., Figueiredo, P., Carvalho, J., Matias, L., Teves-Costa, P., Dias, R., and Simão, N. (2013). The 1909 Benavente (Portugal) earthquake: search for the source. Natural Hazards. 69(2):1211–1227. doi:10.1007/s11069-011-0062-8.

Cappellaro, c. (2019). The influence of fines content, fabric and layered structure on the undrained cyclic behaviour of Christchurch sand soils. Ph.D. dissertation, University of Canterbury, New Zealand.

Carrera, A. (2008). Mechanical behaviour of Stava tailings. Ph.D. dissertation, Politecnico di Torino, Torino, Italy.

Carrera, A., Coop, M.R., and Lancellotta, R. (2011). Influence of grading on the mechanical behaviour of Stava tailings. Géotechnique, 61(11): 935–946.

Carvalho, A., Zonno, G., Franceschina, G., Bilé Serra, J., and Campos Costa, A. (2008). Earthquake shaking scenarios for the metropolitan area of Lisbon, 28(5): 347–364.

Casagrande, A. (1936). Characteristic of cohesionless soils affecting the stability of slope and earth fill. Journal of the Boston Society of Civil Engineering, 13–32.

Castro, G. (1969). Liquefaction of sands. Harvard Soil Mechanics Series No. 81, Harvard University, Cambridge, Massachusetts.

Castro, G., and Poulos, S.J. (1977). Factors Affecting Liquefaction and Cyclic Mobility. Journal of the Geotechnical Engineering Division, 103(GT6): 501–516.

Cetin, K.O. (2000). Reliability-based assessment of seismic soil liquefaction initiation hazard. Ph.D. dissertation, University of California, Berkeley.

Cetin, K.O., Seed, R.B., Moss, R.E.S., Der Kiureghian, A., Tokimatsu, K., Harder, L.F., Jr., and Kayen, R.E. (2000). Field case histories for SPT-based in situ liquefaction potential evaluation. Geotechnical Engineering Research Report No. UCB/GT-2000/09, Department of Civil and Environmental Engineering, University of California, Berkeley.

Cetin, K.O., Seed, R.B., Der Kiureghian, A.K., Tokimatsu, K., Harder Jr., L.F., Kayen, R.E., and Moss, R.E.S. (2004). Standard penetration test-based probabilistic and deterministic assessment of seismic soil liquefaction potential. Journal of Geotechnical and Geoenvironmental Engineering, 130(12):1314–1340.

Chang, N.Y. (1990). Influence of Fines Content and Plasticity on Earthquake-induced Soil Liquefaction. Contract No. DACW3988-C-0078, US Army WES, MS.

Chang, N,Y., Hsieh, N.P., Samuelson, D.L., and Horita, M. (1982). Effect of Frequency on Liquefaction Potential of Saturated Monterey No. O Sand. Computational Methods and Experimental Measurements. Springer, Berlin, Heidelberg, 433-446.

Chester, D.K. (2001). The 1755 Lisbon earthquake. Progress in Physical Geography, 25(3): 363–383.

Cho, G.-C., Jake, D., and Santamarina, J. C. (2006). Particle shape effects on packing density, stiffness, and strength: Natural and crushed sands. Journal of Geotechnical and Geoenvironmental Engineering, 132(5): 591–602.

Chu, J., and Lo, S.C.R. (1993). On the measurement of critical state parameters of dense granular soils. Geotechnical Testing Journal, 16(1): 27–35.

Chung, R.M., Yokel, F.Y., Wechsler, H. (1984). Pore pressure buildup in resonant column tests. Journal of the Geotechnical Engineering Division, ASCE, 110(2): 247–261.

Coop, M.R. (2005). On the mechanics of reconstituted and natural sands. In Deformation Characteristics of Geomaterials, Vol. 2 – Di Benedetto et al (eds), Taylor & Francis Group, London

Cubrinovski, M. (1993). A constitutive model for sandy soils based on a stress dependent density parameter. Dr. Eng. Thesis, University of Tokyo.

Cubrinovski, M., and Ishihara, K. (1999). Empirical correlation between SPT Nvalue and relative density for sandy soils. Soils and Foundations, 39(5): 67–71.

Cubrinovski, M., and Ishihara, K. (2000). Flow potential of sandy soils with different grain compositions. Soils and Foundations, 40(4): 103–119.

Cubrinovski, M., and Ishihara, K. (2002). Maximum and minimum void ratio characteristics of sands. Soils and Foundations, 42(6): 65–78.

Cubrinovski, M., and Rees, S. (2008). Effects of fines on undrained behavior of sands. In Proccedings of Geotechnical Earthquake Engineering and Soil Dynamics IV, Sacramento, California. https://doi.org/10.1061/40975(318)91

Cubrinovski, M., Rees, S., and Bowman, E. (2010). Effects of non-plastic fines on liquefaction resistance of sandy soils. In Ansal, A., editor, Earthquake Engineering in Europe. Geotechnical, Geological, and Earthquake Engineering 17, London & New York. Springer.

Cubrinovski, M., Bradley, B.A., Wotherspoon, L., Green, R., Bray, J.D., Wood, C., Pender, M., Allen, J., Bradshaw, A.S., Rix, G., Taylor, M.L., Robinson, K., Henderson, D., Giorgini, S., Ma, K., Winkley, A., and Zupan, J. (2011). Geotechnical aspects of the 22 February 2011 Christchurch earthquake. Bulletin of the New Zealand Society for Earthquake Engineering, 44(4): 205–226.

Cubrinovski, M., McMaunus, K., Anderson, K. (2016). Earthquake geotechnical engineering practice. Module 3: Identification, assessment and mitigation of liquefaction hazards. NZGS Guidelines, ISBN: 978-0-947497-50-7.

Cubrinovski, M., Rhodes, A., Ntritsos, N., Van Ballegooy, S. (2017). System response of liquefiable deposits. Proceedings of the 3rd International Conference on Performance-based Design in Earthquake Geotechnical Engineering, Vancouver, 16-19 July 2017.

Dabeet, A. (2014). Discrete Element Modeling of Direct Simple Shear Response of Granular Soils and Model Validation Using Laboratory Tests. PhD Thesis. University of British Columbia.

Davis, R.O., and Berrill, J.B. (1982). Energy Dissipation and Seismic Liquefaction in Sands. Earthquake Engineering and Structural Dynamics, 10: 59–68.

De Alba, P., Seed, H.B., and Chan, C.K. (1976). Sand liquefaction in large-scale simple shear tests. American Society of Civil Engineers, Journal of the Geotechnical Engineering Division, 102(9): 909–927.

De Alba, P., Baldwin, K., Janoo, V., Roe, G., and Celikkol, B. (1984). Elastic-wave velocities and liquefaction potential. Geotechnical Testing Journal, 7(2): 77–87.

DeGennaro, V., Canou, J., Dupla, J.C., and Benahmed, N. (2004). Influence of loading path on the undrained behaviour of medium loose sand. Canadian Geotechnical Journal, 41: 166–180.

Dobry, R., Stokoe II, K.H., Ladd, R.S., and Youd, T.L. (1981). Liquefaction susceptibility from S-wave velocity. In Proceedings of In Situ Tests to Evaluate Liquefaction Susceptibility, ASCE National Convention, St. Louis, Mo.

Dobry, R., Ladd, R.S., Yokel, F.Y., Chung, R.M., and Powell, D. (1982). Prediction of pore water pressure build-up and liquefaction of sands during earthquakes by the cyclic strain method. National Bureau of Standards Building Science Series, Rep. No. 138.

Dyvik, R., Berre, T., Lacasse, S., and Raadim, B. (1987). Comparison of truly undrained and constant volume direct simple shear tests. Géotechnique, 37(1): 3–10.

EN ISO 22476-1:2012 Geotechnical investigation and testing -- Field testing - Part 1: Electrical cone and piezocone penetration test.

EN ISO 22476-3:2005 Geotechnical investigation and testing -- Field testing - Part 3: Standard penetration test.

EN ISO 22476-11:2017 Geotechnical investigation and testing -- Field testing - Part 11: Flat dilatometer test.

Ferrão C., Bezzeghoud M., Caldeira B., and Borges J.F. (2016). The Seismicity of Portugal and Its Adjacent Atlantic Region from 1300 to 2014: Maximum Observed Intensity (MOI) Map. Seismological Research Letters, 87(3): 743-750.

Ferreira, C. (2009). The use of seismic wave velocities in the measurement of stiffness of a residual soil. PhD Thesis, FEUP, Portugal.

Ferreira, C., Viana da Fonseca, A., and Nash, D.F.T. (2011). Shear wave velocities for sample quality assessment on a residual soil. Soils and Foundations, 51(4): 683–692. doi:10.3208/sandf.51.683

Ferreira, C., Viana da Fonseca, A., Saldanha, S., Ramos, C., Amoroso, S., and Minarelli, L. (2018). Estimated versus measured V_S profiles and V_{S30} at a pilot site in the Lower Tagus Valley, Portugal. Proceedings of the 16th European Conference on Earthquake Engineering, Thessaloniki, 18-21 june 2018, ID: 10591.

Figueroa, J.L., Saada, A.S., Liang, L., and Dahisaria, N.M. (1994). Evaluation of soil liquefaction by energy principles. Journal of Geotechnical Engineering, ASCE, 120(9): 1554–1569.

Finn, W.D.L., Pickering, D., and Bransby, P.L. (1971). Sand liquefaction in triaxial and simple shear tests. Journal of Soil Mechanics and Foundations Division, ASCE, 97(SM4): 639–59.

Finn, W., Vaid, Y., and Bhatia, S.K. (1978). Constant Volume Cyclic Simple Shear Testing. Second International Conference on Microzonation for Safer Construction: Research and Applications. San Francisco, California, 839–851.

Fioravante, V., Giretti, D., Abate, G., Aversa, S., Boldini, D., Capilleri, P.P., Cavallaro, A., Chamlagain, D., Crespellani, T., Dezi, F., Facciorusso, J., Ghinelli, A., Grasso, S., Lanzo, G., Madiai, C., Massimino, M.R., Maugeri, M., Pagliaroli, A., Rainieri, C., Tropeano, G., Santucci De Magistris, F., Sica, S., Silvestri, F., and Vannucchi, G. (2013). Earthquake Geotechnical Engineering Aspects of the 2012 Emilia-Romagna Earthquake (Italy). In Proceedings of the 7th International Conference on Case Histories in Geotechnical Engineering, Paper EQ-5, 34 pp.

Frost, J.D., and Park, J.Y. (2003). A Critical Assessment of the Moist Tamping Technique. Geotechnical Testing Journal, ASTM, 26(1): 57–70.

Fukushima, S., and Tatsuoka, F. (1984). Strength and deformation characteristics of saturated sand at extremely low pressures. Soils and Foundations, 24(4): 30–48.

Ghionna, V.N., and Porcino, D. (2006). Liquefaction resistance of undisturbed and reconstituted samples of a natural coarse sand from undrained cyclic triaxial tests. Journal of Geotechnical and Geoenvironmental Engineering, ASCE, 132(2): 194–202.

Giannakogiorgos, A., Papathanassiou, G., Vautherin, E. (2015). Quantitative assessment of liquefaction potential in selected areas in Christchurch, New Zealand. In Proceedings of 6th International Conference on Earthquake Geotechnical Engineering, Christchurch, New Zealand, 1-4 November 2015.

Gobbi, S. (2020). Characterisation of liquefaction parameters for saturated soil under dynamic loading using laboratory tests and calibration of constitutive laws by numerical modelling. Ph.D. dissertation, University of Paris-Est, France.

Green, R.A. (2001). Energy-based evaluation and remediation of liquefiable soils. PhD Thesis, Virginia Polytechnic Institute State University, Blacksburg, VA. 393 pp.

Green, R.A., Mitchell, J.K., and Polito C.P. (2000). An Energy-Based Excess Pore Pressure Generation Model for Cohesionless Soils. In Proceedings of Developments in Theoretical Geomechanics – The John Booker Memorial Symposium D.W. Smith and J.P. Carter, eds., Balkema Publishers, Rotterdam, The Netherlands, 383–390.

Green, R., Cubrinovski, M., Cox, B., Wood, C. M., Wotherspoon, L., Bradley, B. A., and Maurer, B. (2014). Select liquefaction case histories from the 2010-2011 Canterbury earthquake sequence. Earthquake Spectra, 30(1): 131–153.

Gutenberg, B., and Richter, C.F. (1956). Magnitude and Energy of Earthquakes. Annali di Geofisica, 9: 1–15.

Harder Jr, L.F., and Boulanger, R. (1997). Application of Kσ and Kα correction factors. In Proceedings of NCEER Workshop on Evaluation of Liquefaction Resistance of Soils, T.L. Youd and I.M. Idriss, eds., Technical Report NCEER-97-0022, National Center for Eathquake Engineering Research, SUNY, Buffalo, NY, 167–190.

Hardin, B.O. (1978). The nature of stress-strain behaviour of soils. Proceedings of the Earthquake Engineering and Soil Dynamics Conference, ASCE. Pasadena, California, 1: 3–39.

Hardin, B.O., and Richart, F.E.Jr. (1963). Elastic wave velocities in granular soils. Journal of Soil Mechanics and Foundation Division, ASCE, 89(1): 33–65.

Hardin, B.O., and Black, W.L. (1969). Closure to: Vibration modulus of normally consolidated clays. Journal of Soil Mechanics and Foundation Division, ASCE, 95(6): 1531–1537.

Hardin, B.O., and Drnevich, V.P. (1972). Shear modulus and damping in soils: Design equations and curves. Journal of Soil Mechanics and Foundations Division, ASCE, 98(7): 667–692.

Hardin, B.O., and Blandford, G.E. (1989). Elasticity of articulate materials. Journal of Geotechnical Engineering, ASCE, 115(6): 788–805.

Høeg, K., Dyvik, R., and Sandbækken, G. (2000). Strength of undisturbed versus reconstituted silt and silty sand specimens. Journal of Geotechnical and Geoenvironmental Engineering, 126(7): 606–617.

Huang, A.B., and Chuang, S.Y. (2011). Correlating Cyclic Strength with fines contents through state parameters. Soils and Foundations, 51(6): 991–1001.

Huang, A.B., Tai, Y.Y., Lee, W., and Ishihara, K. (2008). Sampling and field characterisation of the silty sand in Central and Southern Taiwan. In 3rd International Conference on Site Characterisation (ISC-3), 1457–1463, Taipei. Taylor & Francis.

Hynes, M.E., and Olsen, R. (1999). Influence of confining stress on liquefaction resistance. Physics and Mechanics of Soil Liquefaction, Lade and Yamamuro, eds., Balkema, Rotterdam, Netherlands, 145–152.

Idriss, I. M. (1999). An update to the Seed-Idriss simplified procedure for evaluating liquefaction potential. In Proceedings of the TRB Workshop on New Approaches to Liquefaction, Federal Highway Administration, Washington DC

Idriss, I.M., and Boulanger, R.W. (2004). Semi-empirical procedures for evaluating liquefaction potential during earthquakes. In Proceedings of the 11th International Conference on Soil Dynamics and Earthquake Engineering, and 3rd International Conference on Earthquake Geotechnical Engineering, D. Doolin et al., eds., Stallion Press, 1: 32–56.

Idriss, I.M., and Boulanger, R.W. (2006). Semi-empirical procedures for evaluating liquefaction potential during earthquakes. Soil Dynamics and Earthquake Engineering, 26: 115-130.

Idriss, I.M., and Boulanger, R. W. (2008). Soil Liquefaction during Earthquakes. Monograph MNO-12. Earthquake Engineering Research Institute, Oakland, CA.

Idriss, I.M., and Boulanger, R.W. (2010). SPT-based liquefaction triggering procedures. ReportUCD/CGM-10/02, Department of Civil and Environmental Engineering, University of California, Davis, CA, 259 pp.

Ishihara, K. (1985). Stability of natural deposits during earthquakes. Proceedings of 11th International Conference On Soil Mechanics and Foundation Engineering, San Francisco, 1: 321–376.

Ishihara, K. (1993). Liquefaction and flow failure during earthquakes. Géotechnique, 43(3): 351–415.

Ishihara, K. (1996). Soil behaviour in Earthquake Geotechnics. Oxford University Press, New York.

Ishihara, K., and Towhata, I. (1983). Sand response to cyclic rotation of principal stress directions as induced by wave loads. Soils and Foundations, 23(4): 11–26.

Ishihara, K., Silver, M., and Kitagawa, H. (1978). Cyclic strengths of undisturbed sands obtained by large diameter sampling. Soils and Foundations, 18(4):61–76.

Ishihara, K., Yamazaki, H., and Haga, K. (1985). Liquefaction of k0-consolidated sand under cyclic rotation of principal stress direction with lateral constraint. Soils and Foundations, 25(4): 63–74.

Ishihara, K., Harada, K., Lee, W., Chan, C., and Safiullah, A. (2016). Post-liquefaction settlement analyses based on the volume change characteristics of undisturbed and reconstituted samples. Soils and Foundations, 56(3): 533–546. doi:10.1016/J.SANDF.2016.04.019.

ISO 17892-3:2015, Geotechnical investigation and testing – Laboratory testing of soil - Part 3: Determination of particle density

ISO 17892-4:2016, Geotechnical investigation and testing - Laboratory testing of soil - Part 4: Determination of particle size distribution

ISO 17892-5:2017, Geotechnical investigation and testing - Laboratory testing of soil - Part 5: Incremental loading oedometer test

ISO 17892-9:2018, Geotechnical investigation and testing – Laboratory testing of soil - Part 9: Consolidated triaxial compression tests on water saturated soils

ISO 17892-12:2018, Geotechnical investigation and testing – Laboratory testing of soil - Part 12: Determination of liquid and plastic limits

Iwasaki, T., Tatsuoka, F., Tokida, K., and Yasuda, S. (1978a). A practical method for assessing soil liquefaction potential based on case studies at various sites in Japan. In Proceedings of 2nd International Conference on Microzonation, National Science Foundation, Washington, DC.

Iwasaki, T., Tatsuoka, F., and Takagi, Y. (1978b). Shear moduli of sands under cyclic torsional shear loading. Soils and Foundations, 18(1): 39–56.

Iwasaki, T., Tokida, K., Tatsuoka, F., Watanabe, S., Yasuda, S., Sato, H. (1982). Microzonation for soil liquefaction potential using simplified methods. In Proceedings of 3rd international conference on microzonation, Seattle, 3: 1319–1330.

Jaky, J. (1948). Pressure in soils. In Proceedings of 2nd International Conference on Soil Mechanics and Foundation Engineering, 1: 103–107.

Jamiolkowski, M., Leroueil, S., Lo Presti, D.C.F. (1991). Design parameters from theory to practice. Theme Lecture. Proceedings of Geo-Coast'91, Yokohama, 2: 877–917.

Jamiolkowski, M., Lo Presti, D., and Manaserro, M. (2001). Evaluation of the relative density and shear strength of sands from CPT and DMT. In Soil Behavior and Soft Ground Construction, GSP 119, pages 201–238, Reston, Virginia. ASCE.

Jefferies, M., and Davies, M.P. (1993). Use of CPTU to estimate equivalent SPT N60. Geotechnical Testing Journal, 16(4): 458–468. doi:10.1520/GTJ10286J.

Jefferies, M. and Been, K. (2006). Soil Liquefaction: A Critical State Approach. First Edition. CRC Press Taylor & Francis Group.

Jefferies, M. and Been, K. (2016). Soil Liquefaction: A Critical State Approach. Second Edition. CRC Press Taylor & Francis Group.

Jefferies, M., Shuttle, D., and Been, K. (2015). Principal stress rotation as cause of cyclic mobility. Geotechnical Research, 2(2): 66–96.

Japanese Geotechnical Society (JGS) 0161-2009. Test method for minimum and maximum densities of sands

Jorge, C. (1993). Zonamento do Potencial de Liquefação- Tentativa de aplicação a Portugal. MSc Dissertation, University Nova de Lisboa. in portuguese

Jorge, C. and Vieira, A.M. (1997). Liquefaction potential assessment – application to the Portuguese territory and to the town of Setúbal. Seismic Behaviour of Ground and Geotechnical Structures, Sêco e Pinto (ed.): 33–43.

Kayen, R., Moss, R.E.S., Thompson, E.M., Seed, R.B., Cetin, K.O., Der Kiureghian, A., Tanaka, Y., Tokimatsu, K. (2013). Shear-wave velocity-based probabilistic and deterministic assessment of seismic soil liquefaction potential. Journal of Geotechnical and Geoenvironment Engineering, ASCE, 139(3): 407–419. https://doi.org/10.1061/(ASCE)GT.1943-5606.0000743

Kokusho, T. (2013). Liquefaction potential evaluations: energy-based method versus stress-based method. Canadian Geotechnical Journal, 50: 1088–99.

Kokusho, T. (2017). Innovative Earthquake Soil Dynamics. CRC Press/Balkema. Taylor & Francis Group, London, UK.

Kokusho, T., and Kojima, T. (2002). Mechanism for postliquefaction water film generation in layered sand. Journal of Geotechnical and Geoenvironmental Engineering, 128(2): 129–137.

Kramer, S.L. (1996). Geotechnical Earthquake Engineering, Prentice Hall, Inc., Upper Saddle, New Jersey, USA.

Kwan, W.S., and El Mohtar, C.E. (2018). A review on sand sample reconstitution methods and procedures for undrained simple shear test. International Journal of Geotechnical Engineering, 1-9. doi: 10.1080/19386362.2018.1461988

Ladd, R.S. (1974). Specimen Preparation and Liquefaction of Sands. J. Soil Mechanics Foundation Division, ASCE, 100(GT10): 1180–1184.

Ladd, R.S. (1978). Preparing test specimens using undercompaction. Geotechnical Testing Journal, 1(1):16–23.

Lade, P.V. and Yamamuro, J.A. (1997). Effects of nonplastic fines on static liquefaction of sands. Canadian Geotechnical Journal, 34: 918–928, 1997.

Lade, P.V. and Yamamuro, J.A. (2011). Evaluation of static liquefaction potential of silty sand slopes. Canadian Geotechnical Journal, 48(2): 247–264.

Lade, P.V., Liggio, C.D. Jr., Yamamuro, J.A. (1998). Effects of non-plastic fines on minimum and maximum void ratios of sand. Geotechnical Testing Journal, 21(4), 336–347.

Lai, C.G., Bozzoni, F., Conca, D., Famà, A., Özcebe, A.G., Zuccolo, E., Meisina, C., Bonì, R., Bordoni, M., Cosentini, R.M., Martelli, L., Poggi, V., Viana da Fonseca, A., Ferreira, C., Rios, S., Cordeiro, D., Ramos, C., Molina-Gómez, F., Coelho, C., Logar, J., Maček, M., Oblak, A., Ozcep, F., Bozbey, I., Oztoprak, S., Sargin, S., Aysal, N., Oser, C., Kelesoglu, M.K. (2020). Technical guidelines for the assessment of earthquake induced liquefaction hazard at urban scale. Bulletin of Earthquake Engineering. doi:10.1007/s10518-020-00951-8

Lee, K.L., and Fitton, J.A. (1969). Factors affecting the cyclic loading strength of soil. Vibration Effects of Earthquakes on Soils and Foundations, 450: 71–95. doi: 10.1520/STP33637S

Lee, K.L., and Albaisa, A. (1974). Earthquake induced settlements in saturated sands. Journal of the Geotechnical Engineering Division, 100(4): 387–406.

Lee, J.-S., and Santamarina, J. C. (2005). Bender Elements: Performance and Signal Interpretation. Journal of Geotechnical and Geoenvironmental Engineering, 131(9):1063–1070. doi:10.1061/(ASCE)1090-0241(2005)131:9(1063)

Lee, D.-H., Ku, C.-S., and Yuan, H. (2003). A study of liquefaction risk potential at Yuanlin, Taiwan. Engineering Geology, 71(1–2): 97–117.

Lee, W., Ishihara, K., and Chen, C.-C. (2012). Liquefaction of silty sand – preliminary studies from recent Taiwan, New Zealand and Japan earthquakes. In International Symposium on Engineering Lessons Learned from the 2011 Great East Japan Earthquake, Tokyo.

Li, X.S., and Wang, Y. (1998). Linear representation of steady-state line for sand. Journal of Geotechnical and Geoenvironmental Engineering, ASCE, 124(12):1215–1217.

Liao, S.S.C., and Whitman, R.V. (1986). A Catalog of Liquefaction and Non-Liquefaction Occurrences during Earthquakes. Research Report. Cambridge: Department of Civil Engineering, Massachusetts Institute of Technology.

Lo Presti, D.C.F. (1995). General report: Measurement of shear deformation of geomaterials in the laboratory. Pre-failure Deformation of Geomaterials. Shibuya, Mitachi & Miura (eds). Balkema, Rotterdam, pp. 1067-1088.

Lunne, T., Berre, T., and Strandvik, S. (1997). Sample disturbance effects in soft low plastic Norwegian clay. Recent Developments in Soil and Pavement Mechanics, Almeida (ed.). Balkema, Rotterdam, pp. 81–102.

Marchetti, S. (1980). In Situ Tests by Flat Dilatometer. Journal of the Geotechnical Engineering Division ASCE, 106(3): 299–321.

Marchetti, S. (2016). Incorporating the Stress history parameter KD of DMT into the liquefaction correlations in clean uncemented sands. Journal of Geotechnical and Geoenvironmental Engineering, 142(2): 04015072.

Marchetti, D., and Marchetti, S. (2016). Flat Dilatometer (DMT). Some recent advances. Procedia Engineering, 158: 428–433.

Marchetti, S., Monaco, P., Totani, G., Marchetti, D. (2008). In situ tests by seismic dilatometer (SDMT). In: Laier JE, Crapps DK, Hussein MH (eds) From Research to Practice in Geotechnical Engineering, ASCE, Geotechnical Special Publication, 180: 292–311.

Markham, C.S., Bray, J.D., Riemer, M.F., and Cubrinovski, M. (2016). Characterisation of Shallow Soils in the Central Business District of Christchurch, New Zealand. Geotechnical Testing Journal, 39(6): 20150244. doi:10.1520/GTJ20150244

Martin, G.R., Finn, W.D.L., and Seed, H.B. (1975). Fundamentals of liquefaction under cyclic loading. Journal of the Geotechnical Engineering Division, 101(5): 423–438.

Maurer, B.W., Green, R.A., Cubrinovski, M., and Bradley, B.A. (2014). Evaluation of the liquefaction potential index for assessing liquefaction hazard in Christchurch, New Zealand. Journal of Geotechnical and Geoenvironmental Engineering, 140(7):04014032.

Mayne, P. 2007. Cone Penetration Testing – A synthesis of highway practice. NCHRP Synthesis 268, Transportation Research Board, Washington, D.C.

Mayne, P.W., Coop, M.R., Springman, S., Huang, A-B., and Zornberg, J. (2009). State-of-the-Art Paper (SOA-1): GeoMaterial Behavior and Testing. In Proceedings of the 17th International Conference on Soil Mechanics and Geotechnical Engineering, (ICSMGE, Alexandria, Egypt), Millpress/IOS Press Rotterdam: 2777–2872.

Mazzocchi, G. (2016). Risk Assessment of Soil Liquefaction across Southern Europe. MSc Dissertation, Universitá Degli Studi di Pavia, Italy.

Mele, L. (2020). Experimental and theoretical investigation on cyclic liquefaction mechanisms and on the effects of some mitigation measures. PhD Thesis, University of Napoli, Italy.

Mele, L., Tan Tian, J., Lirer, S., Flora, A., and Koseki, J. (2019). Liquefaction resistance of unsaturated sands: experimental evidence and theoretical interpretation. Géotechnique, 69(6): 541–553.

Millen, M., Rios, S., Quintero, J., and Viana da Fonseca, A. (2020). Prediction of time of liquefaction using kinetic and strain energy. Soil Dynamics and Earthquake Engineering, 128: 105898. Doi: 10.1016/j.soildyn.2019.105898

Miura, K., Maeda, K., Furukawa, M., and Toki, S. (1997). Physical characteristics of sands with different primary properties. Soils and Foundations, 37(3): 53–64.

Molina-Goméz, F., Viana da Fonseca, A., Ferreira, C., Ramos, C. (2018). Getting high-quality samples for liquefaction testing in Portugal. Research report – LIQ2PROEARTH – PTDC/ECM-GEO/1780/2014, Porto, Portugal.

Molina-Gómez, F., Ferreira, C., Ramos, C., and Viana da Fonseca, A. (2020a). Performance of Gel-Push sampling in liquefiable soils. Géotechnique Letters, 10: 1-6. doi: 10.1680/jgele.19.00073

Molina-Goméz, F., Viana da Fonseca, A., Ferreira, C., Ramos, C., and Cordeiro, D.(2020b). Novel sampling techniques for collecting high-quality samples: Portuguese experience in liquefiable soils. In Proceedings of the 6th International Conference on Geotechnical and Geophysical Site Characterisation, ISC-6, Budapest, Hungary.

Mori, K. and Sakai, K. (2016). The GP sampler: a new innovation in core sampling. In Geotechnical and geophysical site characterisation (eds B. Lehane, H. Acosta-Martínez, and R. Kelly), vol. 5, pp. 99–124. Sydney, NSW, Australia.

Moss, R.E.S. (2003) CPT-based probabilistic assessment of seismic soil liquefaction initiation. PhD Thesis, University of California at Berkeley, Berkeley, CA.

Moss, R.E.S., Seed, R.B., Kayen, R.E., Stewart, J.P., Der Kiureghian, A., Cetin, K.O. (2006). CPT-based probabilistic and deterministic assessment of in situ seismic soil liquefaction potential. Journal of Geotechnical and Geoenvironmental Engineering, ASCE, 132(8): 1032–1051.

Mulilis, J.P., Seed, H.B., Chan, C.K., Mitchell, J.K., and Arulanandan, K. (1977). Effects of sample preparation on sand liquefaction. American Society of Civil Engineers, Journal of the Geotechnical Engineering Division, 103(2): 91–108.

National Academies of Sciences, Engineering, and Medicine (NASEM, 2016). State of the Art and Practice in the Assessment of Earthquake-Induced Soil Liquefaction and Its Consequences. Washington, DC: The National Academies Press. doi: 1017226/23474

National Research Council (NRC, 1985). Liquefaction of soils during earthquakes. National Academy Press.

Nemat-Nasser, S., and Shokooh, A. (1977). A Unified Approach to Densification and Liquefaction of Cohesionless Sand. Technical Report No. 77-10-3. Evanston, IL: Earthquake Research and Engineering Laboratory, Department of Civil Engineering. 44 pp.

Nicholson, P.G., Seed, R.B., and Anwar, H.A. (1993). Elimination of membrane compliance in undrained triaxial testing. I. Measurement and evaluation. Canadian Geotechnical Journal, 30: 727–738.

NP EN 1997-1 (2010). Eurocódigo 7 – Projeto geotécnico – Parte 1: Regras gerais

NP EN 1998-1 (2010). Eurocódigo 8 – Projeto de estruturas para resistência aos sismos – Parte 1: Regras gerais, ações sísmicas e regras para edifícios

NP EN 1998-5 (2010). Eurocódigo 8 – Projeto de estruturas para resistência aos sismos – Parte 5: Fundações, estruturas de suporte e aspetos geotécnicos

Oda, M. (1972). Initial fabrics and their relations to mechanical properties of granular materials. Soils and Foundations, 12(1): 17–36.

Osterberg, J.O. (1973). An improved hydraulic piston sampler. In 8th international conference on soil mechanics and foundation engineering (pp. 317–321). Moscow.

Papathanassiou, G. (2008). LPI-based approach for calibrating the severity of liquefaction-induced failures and for assessing the probability of liquefaction surface evidence. Engineering Geology, 96(1–2): 94–104.

Papathanassiou, G., Mantovani, A., Tarabusi, G., Rapti, D., Caputo, R. (2015). Assessment of liquefaction potential for two liquefaction prone areas considering the May 20, 2012 Emilia (Italy) earthquake. Engineering Geology, 189:1–16. https://doi.org/10.1016/j.enggeo.2015.02.002

Peacock, W.H., and Seed, H.B. (1968). Sand liquefaction under cyclic loading simple shear conditions. Journal of the Soil Mechanics and Foundations Division, Proc. ASCE, 94(SM3): 689–708.

Pillai, V., and Stewart, R. (1994). Evaluation of liquefaction potential of foundation soils at Duncan Dam. Canadian Geotechnical Journal, 31(6): 939–950.

Pinto, A. (2014). Abordagem à problemática da amostragem em solos granulares com envelhecimento natural através de ondas sísmicas. MSc dissertation, FEUP, in Portuguese.

Plewes, H., Pillai, V., Morgan, M., and Kilpatrick, B. (1994). In situ sampling, density measurements, and testing of foundation soils at Duncan Dam. Canadian Geotechnical Journal, 31(6): 919–926.

Polito, C.P. (1999). The effect of non-plastic and plastic fines on the liquefaction of sandy soils. PhD Thesis, Virginia Polytechnic Institute State University, Blacksburg, VA. 274 pp.

Polito, C.P., and Martin II, J.R. (2001). Effects of Nonplastic Fines on the Liquefaction Resistance of Sands. Journal of Geotechnical and Geoenvironmental Engineering, ASCE, 127(5): 408–415.

Polito, C.P., Green, R.A., Lee, J. (2008). Pore pressure generation models in sands and silty soils during cyclic loading. Journal of Geotechnical and Geoenvironmental Engineering, 134(10): 1490–500.

Polito, C.P., Green, R.A., Dillon, E., and Sohn, C. (2013). Effect of load shape on relationship between dissipated energy and residual excess pore pressure generation in cyclic triaxial tests. Canadian Geotechnical Journal, 50: 1118–1128.

Poulos, S.J. (1981). The steady state of deformation. Journal of the Geotechnical Engineering Division, ASCE, 107(GT5): 553–562.

Poulos, S.J., Castro, G., and France, J.W. (1985). Liquefaction evaluation procedure. Journal of Geotechnical Engineering, 111(6): 772–792.

Qadimi, A., and Coop, M.R. (2007). The undrained cyclic behaviour of a carbonate sand. Géotechnique, 57(9): 739–750. doi: 10.1680/geot.2007.57.9.739

Rahman, M.M., Lo, S., and Gnanendran, C. (2008). On equivalent granular void ratio and steady state behaviour of loose sand with fines. Canadian Geotechnical Journal, 45(10): 1439–1456.

Ramos, C., Ferreira, C., Molina-Gómez, F., and Viana da Fonseca, A. (2019). Critical State Lines of Portuguese liquefiable sands. In Proceedings of the 7th International Symposium on Deformation Characteristics of Geomaterials (IS-Glasgow 2019). E3S Web Conferences, 92: 06003.

Ramos, C., Ferreira, C., Molina-Gómez, F., and Viana da Fonseca, A. (2020). Enhanced liquefaction susceptibility evaluation of Lisbon sands by CPTu and SPT tests with laboratory GSD and plasticity. In Proceedings of the 6th International Conference on Geotechnical and Geophysical Site Characterisation, ISC-6, Budapest, Hungary.

Ramos, C., Viana da Fonseca, A., and Ferreira, C. (2021). CPTu-based cyclic liquefaction assessment of young Holocene soil profiles considering different approaches. Soils and Rocks (under revision)

Rascol, E. (2009). Cyclic Properties of Sand: Dynamic Behaviour for Seismic Applications. PhD Thesis, École Polytechnique Fédérale de Lausanne, Switzerland.

Rauch, A.F., Duffy, M., and Stokoe, II, K.H. (2000). Laboratory correlation of liquefaction resistance with shear wave velocity. ASCE Geotechnical Special Publication, 110: 66–80.

Reyno, A., Airey, D., and Taiebat, H. (2005). Influence of height and boundary conditions in simple shear tests. In Proceedings of the Frontiers in Offshore Geotechnics: ISFOG 2005, Perth, Australia, pp. 1101–1107.

Reynolds, O. (1885). On the dilation of media composed of rigid particles in contact with experimental illustrations. Philosophical Magazine, 20(127): 469–481.

Riemer, M.F., and Seed, R.B. (1997). Factors affecting apparent position of steady-state line. Journal of Geotechnical and Geoenvironmental Engineering, 123(3): 281–288.

Riemer, M.F., Seed, R.B., Nicholson, P.G., and Jong, H.L. (1990). Steady state testing of loose sands: limiting minimum density. Journal of the Geotechnical Engineering, 116(2): 332–337.

Robertson, P.K. (1990). Soil classification using cone penetration test. Canadian Geotechnical Journal, 27:151–158.

Robertson, P.K. (1994). Suggested terminology for liquefaction. In Proceedings of the 47th Canadian Geotechnical Conference, Halifax, N.S. CGS. Sept. pp. 277–286.

Robertson, P.K. (2009). Interpretation of cone penetration tests: a unified approach. Canadian Geotechnical Journal, 46(11): 1337–1355.

Robertson, P.K. (2010). Estimating in-situ state parameter and friction angle in sandy soils from the CPT. In Proceedings of the 2nd International Symposium on Cone Penetration Testing, CPT'10, Huntington Beach, CA, USA.

Robertson, P.K. (2012). Interpretation of in-situ tests – some insight. Mitchell Lecture in Proceedings of the 4th International Conference on Geotechnical and Geophysical Site Characterisation, ISC-4, pp. 3-24, Porto de Galinhas, Brazil.

Robertson, P.K. (2016). Cone penetration test (CPT)-based soil behaviour type (SBT) classification system – an update. Canadian Geotechnical Journal, 53(12):1910-1927.

Robertson, P.K., and Fear, C.E. (1995). Liquefaction of sands and its evaluation. In IS Tokyo '95, Proceedings of the 1st International Conference on Earthquake Geotechnical Engineering. Nov. Edited by K. Ishihara. A.A. Balkema, Amsterdam.

Robertson, P.K., and Wride, C.E. (1998). Evaluating cyclic liquefaction potential using the cone penetration test. Canadian Geotechnical Journal, 35(3): 442–459.

Robertson, P.K., and Cabal, K.L. (2010). Estimating soil unit weight from CPT. 2nd International Symposium on Cone Penetration Testing, Huntington Beach, CA, USA, May 2010.

Robertson, P.K., and Cabal, K.L. (2015). Guide to Cone Penetration Testing for Geotechnical Engineering, 6th edition, Gregg Drilling & Testing, 133 pp.

Robertson, P.K., Woeller, D.J., and Finn, W. D.L. (1992). Seismic cone penetration test for evaluating liquefaction potential under cyclic loading. Canadian Geotechnical Journal, 29(4):686–695.

Roscoe, K.H., Schofield, A.N. and Wroth, C.P. (1958). On the Yielding of Soils. Géotechnique, 8(1): 22–53.

Saldanha, A. (2017). Microzonamento de Suscetibilidade à liquefação. Aplicação a um caso de estudo na região da Grande Lisboa. MSc dissertation, FEUP, in Portuguese.

Salgado, R., Mitchell, J.K., and Jamiolkowski, M. (1997). Cavity expansion and penetration resistance in sands, Journal of Geotechnical and Geoenvironmental Engineering, ASCE, 123(4): 344–54.

Santamarina, J.C., Klein, K.A., and Fam, M.A. (2001). Soils and Waves: particulate materials behaviour, characterisation and process monitoring, Wiley, New York.

Schofield, A., and Wroth, P. (1968). Critical State Soil Mechanics. McGraw-Hill, London, U.K.

Seed, H.B. (1983). Earthquake-resistant design of earth dams. In Proceedings of Symposium of Seismic Design of Embankments and Caverns, ASCE, 41–64.

Seed, H.B., and Lee, K.L. (1966). Liquefaction of saturated sands during cyclic loading. Journal of Soil Mechanics and Foundations Division, ASCE, 92(6): 105–134.

Seed, H.B., and Idriss, I.M. (1971). Simplified procedure for evaluating soil liquefaction potential. Journal of the Geotechnical Engineering Division, ASCE, 97(9): 1249–1273.

Seed, H.B., and Peacock, W.H. (1971). Test procedure for measuring soil liquefaction characteristics. Journal of Soil Mechanics and Foundation Engineering, ASCE, 97(SM8): 1099–1119.

Seed, H.B., and Idriss, I.M. (1982). Ground motions and soil liquefaction during earthquakes. Earthquake Engineering Research Institute Monograph.

Seed, R.B., and Harder, L.F., Jr. (1990). SPT-based analysis of cyclic pore pressure generation and undrained residual strength. In Proceedings of H. B. Seed Memorial Symposium, BiTech Publishers, 2: 351–376.

Seed, H.B., Martin, P.P., and Lysmer, J. (1975). The generation and dissipation of pore water pressures during soil liquefaction. Rep. No. EERC 75-26, University of California.

Seed, H.B., Idriss, I.M., and Arango, I. (1983). Evaluation of liquefaction potential using field performance data. Journal of Geotechnical Engineering, 109(3): 458–482.

Seed, R.B., Cetin, K.O., Moss, R.E.S., Kammerer, A., Wu, J., Pestana, J., Riemer, M., Sancio, R.B., Bray, J.D., Kayen, R.E. and Francis, A. (2003). Recent advances in soil liquefaction engineering: A unified and consistent framework. In Proceedings of the 26th Annual Los Angeles Geotechnical Spring Seminar, Long Beach, CA.

Sharma S.S., Ramsey, N., Lee, F., and Bhattarai, B.N. (2017). Challenges in assessing the shear strength of offshore sediments using simple shear tests. In Proceedings of the Geotechnical Frontiers 2017: Geotechnical Materials, Modelling and Testing, Orlando, Florida, 327-336.

Silva V., Crowley H., Varum H., and Pinho R. (2014). Seismic hazard and risk assessment of Portugal. Second Proceedings of European Conference on Earthquake Engineering and Seismology, Istanbul, Turkey.

Silver, M.L., Tatsuoka, F., Phukunnhaphan, A., and Avramidis, A. (1980). Cyclic undrained strength of sand by triaxial test and simple shear test. In Proceedings of the 7th World Conference on Earthquake Engineering, 3: 281–288.

Skempton, A.W. (1954). The pore-pressure coefficients A and B. Géotechnique, 4(4): 143–147.

Sladen, J.A., and Handford, G. (1987). A potential systematic error in laboratory testing of very loose sands. Canadian Geotechnical Journal, 24(3): 462–466.

Sladen, J.A., D'Hollander, R.D., and Krahn, J. (1985). The liquefaction of sands, a collapse surface approach. Canadian Geotechnical Journal, 22(4): 564–578.

Soares, M. (2014). Evaluation of soil liquefaction potential based on laboratory data – Major factors and limit boundaries. PhD Thesis, FEUP, Portugal.

Soares, M., and Viana da Fonseca, A. (2016). Factors affecting steady state locus in triaxial tests. Geotechnical Testing Journal, 39(6): 1056–1078.

Sonmez, H. (2003). Modification to the liquefaction potential index and liquefaction susceptibility mapping for a liquefaction-prone area (Inegol-Turkey). Environmental Geology, 44(7): 862–871.

Sousa, M.L., and Campos Costa, A. (2009). Ground motion scenarios consistent with probabilistic seismic hazard disaggregation analysis. Application to Mainland Portugal. Bulletin of Earthquake Engineering, 7: 127–147.

Stark, T.D., and Olson, S.M. (1995). Liquefaction resistance using CPT and field case histories. Journal of Geotechnical Engineering, ASCE, 121(12): 856–869. doi: 10.1061/(ASCE)0733-9410(1995)121:12(856)

Stringer, M., Taylor, M.L., and Cubrinovski, M. (2015). Advanced soil sampling of silty sands in Christchurch. Research Report 2015-06, Civil & Natural Resources Engineering, University of Canterbury, Australia.

Suzuki, Y., Tokimatsu, K., Koyamada, K., Taya, Y., and Kubota, Y. (1995). Field correlation of soil liquefaction based on CPT data. In Proceedings of the International Symposium on Cone Penetration Testing, CPT'95, Lingköping, Sweden, Vol. 2, pp. 583–588.

Tatsuoka, F., Ochi, K., Fujii, S., and Okamoto, M. (1986). Cyclic undrained triaxial and torsional shear strength of sands for different sample preparation methods. Soils and Foundations, 26(3): 23–41.

Taylor, D.W. (1948). Fundamentals of Soil Mechanics. Wiley, New York, pp. 700.

Taylor, M.L. (2015). The Geotechnical Characterisation of Christchurch Sands for Advanced Soil Modelling. PhD Thesis. University of Canterbury, Christchurch, New Zealand.

Taylor, M.L., Cubrinovski, M., and Haycock, I. (2012). Application of new 'Gel-push' sampling procedure to obtain high quality laboratory test data for advanced geotechnical analyses. In 2012 New Zealand Society for Earthquake Engineering Conference, Christchurch, New Zealand.

Terzaghi, K., Peck, R.B., and Mesri, G. (1996). Soil Mechanics in Engineering Practice. John Wiley & Sons, New York.

Teves-Costa, P., and Batlló, J. (2011). The 23 April 1909 Benavente earthquake (Portugal): macroseismic field revision. Journal of Seismology, 15(1): 59–70. doi: 10.1007/s10950-010-9207-6

Thevanayagam, S. (1998). Effect of fines and confining stress on undrained shear strength of silty sands. Journal of Geotechnical and Geoenvironmental Engineering, 124(6): 479–491.

Thevanayagam, S. (2007a). Intergrain contact density indices for granular mixes - I: Framework. Earthquake Engineering and Engineering Vibration, 6 (2): 123–134.

Thevanayagam, S. (2007b). Intergrain contact density indices for granular mixes - II: liquefaction resistance. Earthquake Engineering and Engineering Vibration, 6 (2): 135–146.

Thevanayagam, S., Wang, C.C., and Ravishankar, K. (1996). Determination of post-liquefaction strength: steady state vs residual strength. Uncertainty in the geological environment: From theory to practice, Proc. Uncertainty '96, Schackelford et al., eds., Geotechnical Special Publication, 58(2): 1210–1224.

Thevanayagam, S., Shenthan, T., Mohan, S., and Liang, J. (2002). Undrained fragility of sands, silty sands and silt. Journal of Geotechnical and Geoenvironmental Engineering, 128(10): 849–859.

Tokimatsu, K., and Uchida, A. (1990). Correlation between liquefaction resistance and shear wave velocity. Soils and Foundations, 30(2): 33–42.

Tonkin and Taylor (2013). Liquefaction Vulnerability Study. Report for Earthquake Commission, T&T ref. 52020.0200/v1.0.

Toprak, S., and Holzer, T.L. (2003). Liquefaction potential index: Field assessment. Journal of Geotechnical and Geoenvironmental Engineering, 129(4): 315–322.

Torres-Cruz, L.A. (2019). Limit void ratios and steady-state line of non-plastic soils. Geotechnical Engineering, 172(3): 283–295.

Torres-Cruz, L.A., and Santamarina, J.C. (2020). The critical state line of nonplastic tailings. Canadian Geotechnical Journal, 57(10): 1508–1517.

Towhata, I., and Ishihara, K. (1985). Shear work and pore water pressure in undrained shear. Soils and Foundations, 25(3): 73–85.

Townsend, F.C. (1978). A review of factors affecting cyclic triaxial tests. Dynamic Geotechncal Testing, ASTM STP 654: 356–383.

Tran, D.T.Q., Fredlund, D.G., and Chan, D.H. (2016). Improvements to the calculation of actual evaporation from bare soil surfaces. Canadian Geotechnical Journal, 53: 118-133.

Tsuchida, H. (1970). Prediction and countermeasure against the liquefaction in sand deposits. Seminar in the Port and Harbor Research Institute.

USGS (2020a). USGS Denver Library Photographic Collection. Available at https://library.usgs.gov/photo/#/?terms=niigata; accessed 2 July 2020.

USGS (2020b). El Salvador Landslide. Available at https://www.usgs.gov/media/images/el-salvador-landslide; accessed 2 July 2020.

Vaid, Y.P., and Negussey, D. (1984). Relative density of pluviated sand samples. Soils and Foundations, 24(2): 101–105.

Vaid, Y.P., Chern, J.C. (1985). Cyclic and Monotonic Undrained Response of Saturated Sands. In V. Khosla ed., Advances in the art of testing soils under cyclic conditions, ASCE, New York, pp. 120–147.

Vaid, Y.P., and Sivathayalan, S. (1996). Static and cyclic liquefaction potential of Fraser Delta sand in simple shear and triaxial tests. Canadian Geotechnical Journal, 33(2): 281–289.

Vaid, Y.P., and Sivathayalan, S. (2000). Fundamental factors affecting liquefaction susceptibility of sands. Canadian Geotechnical Journal, 37: 592–606.

Vaid, Y.P., Sivathayalan, S., and Stedman, D. (1999). Influence of Specimen-Reconstituting Method on the Undrained Response of Sand. Geotechnical Testing Journal, 22(3): 187–195.

Vasquez-Herrera, A., and Dobry, R. (1989). The behaviour of undrained contractive sand and its effects on seismic liquefaction flow failure of earth structures. Contract No. 86-003. Dept. of the Army, US. Army Corps of Engineers, Washington, D.C.

Verdugo, R., and Ishihara, K. (1996). The steady state of sandy soils. Soils and Foundations, 36(2): 81–91.

Viana da Fonseca, A., Ferreira, C., and Fahey, M. (2009). A Framework Interpreting Bender Element Tests, Combining Time-Domain and Frequency-Domain Methods. Geotechnical Testing Journal, 32(2): 100974. doi: 10.1520/GTJ100974

Viana da Fonseca, A., Coop, M.R., Fahey, M., and Consoli, N.C. (2011). The interpretation of conventional and non-conventional laboratory tests for challenging geotechnical problems. In Proceedings of the International Symposium on Deformation Characteristics of Geomaterials, Seoul, Korea.

Viana da Fonseca, A., and Pineda, J. (2017). Getting high-quality samples in 'sensitive' soils for advanced laboratory tests. Innovative Infrastructure Solutions, 2(34): 1–42. doi:10.1007/s41062-017-0086-3

Viana da Fonseca, A., Ferreira, C., Ramos, C., Molina-Gómez, F. (2019a). The geotechnical test site in the greater Lisbon area for liquefaction characterisation and sample quality control of cohesionless soils. AIMS Geosciences, 5(2): 325–343. doi: 10.3934/geosci.2019.2.325

Viana da Fonseca, A., Ferreira, C., Coelho, C., Quintero, J., Rios, S., Millen, M., Cordeiro, D. (2019b). Microzonation of the Lisbon Area in Portugal. Methodology for assessment of earthquake-induced risk of soil liquefaction at the four European testing sites (microzonation). Deliverable D 2.7 of the European H2020 LIQUEFACT research project, chpt. 3, pp. 51-126 (www.liquefact.eu: July 2019).

Vis, G.-J., Kasse, C., and Vandenberghe J. (2008). Late Pleistocene and Holocene paleogeography of the Lower Tagus Valley (Portugal): effects of relative sea level, valley morphology and sediment supply. Quaternary Science Reviews, 27: 1682–1709.

Vis, G.-J., Kasse, C., Kroon, D., Vandenberghe, J., Jung, S., Lebreiro, S., and Rodrigues, T. (2016). Time-integrated 3D approach of late Quaternary sediment-depocenter migration in the Tagus depositional system: From river valley to abyssal plain. Earth-Science Review, 153:192-211.

Wair, B.R., DeJong, J.T., Shantz, T. (2012). Guidelines for Estimation of Shear Wave Velocity Profiles. PEER 808 Report 2012/08. Pacific Earthquake Engineering Research Center.

Wang, W. (1979). Some findings in soil liquefaction. Water Conservancy and Hydroelectric Power Scientific Research Institute, Beijing, China.

Wang, J.J.-H., Moran, K., and Baxter, C.D.P. (2006). Correlation between cyclic resistance ratios of intact and reconstituted offshore saturated sands and silts with the same shear wave velocity. Journal of Geotechnical and Geoenvironmental Engineering, ASCE, 132(12): 1574–1580.

Wichtmann, T., and Triantafyllidis, T. (2004). Influence of a cyclic and dynamic loading history on dynamic properties of dry sand, part I: cyclic and dynamic torsional prestraining. Soil Dynamics and Earthquake Engineering, 24(2): 127–147.

Wong, R.K.S., and Arthur, J.R.F. (1986). Sand sheared by stresses with cyclic variation in direction. Géotechnique, 36(2): 215–226.

Wotherspoon, L.M., Orense, R.P., Green, R.A., Bradley, B.A., Cox, B.R., Wood, C.M. (2015). Assessment of liquefaction evaluation procedures and severity index frameworks at Christchurch strong motion stations. Soil Dynamics and Earthquake Engineering, 79(Part B): 335–346. https ://doi.org/10.1016/j.soild yn.2015.03.022

Wroth, C.P., and Bassett, R.H. (1965). A stress-strain relationship for the shearing behaviour of a sand. Géotechnique, 15(1): 32–56.

Wu, J., Kammerer, A.M., Riemer, M.F., Seed, R.B., and Pestana, J.M. (2004). Laboratory study of liquefaction triggering criteria. 13th World Conference on Earthquake Engineering, Vancouver, Canada.

Yamada, S., Takamori, T., and Sato, K. (2010). Effects on reliquefaction resistance produced by changes in anisotropy during liquefaction. Soils and foundations, 50(1): 9–25.

Yoshimi, Y., Takahashi, K., and Hosaka, Y. (1989). Evaluation of liquefaction resistance of clean sands based on high quality undisturbed samples. Soils and Foundations, 29(1):93–104.

Yoshimi, Y., Tokimatsu, K., Kaneko, O., and Makihara, Y. (1984). Undrained cylic shear strength of a dense Niigata sand. Soils and Foundations, 24(4): 131–145.

Yoshimine, M., and Koike, R. (2005). Liquefaction of clean sand with stratified structure due to segregation of particle size. Soils and Foundations, 45(4): 89–98.

Yoshimine, M., Nishizaki, H., Amano, K., Hosono, Y. (2006). Flow deformation of liquified sand under constant shear load and its application to analysis of flow slide of infinite slope. Soil Dynamics and Earthquake Engineering, 26: 253–264.

Youd, T.L. (1973). Factors controlling maximum and minimum densities in sands. Evaluation of Relative Density and Its Role in Geotechnical Projects Involving Cohesionless Soils, ASTM STP 523, American Society for Testing and Materials, pp. 98–112.

Youd, T.L. (1977). Packing changes and liquefaction susceptibility. Journal of the Geotechnical Engineering Division, 103(GT8): 918–922.

Youd, T.L., Idriss, I.M., Andrus, R.D., Arango, I., Castro, G., Christian, J.T., Dobry, R., Finn, W.D.L., Harder, L.F., Hynes, M.E., Ishihara, K., Koester, J.P., Liao, S.C.C., Marcuson, W.F. III., Martin, G.R., Mitchell, J.K., Moriwaki, Y., Power, M.S., Robertson, P.K., Seed, R.B., and Stokoe, K.H. II. (2001). Liquefaction resistance of soils: Summary report from the 1996 NCEER and 1998 NCEER/NSF Workshops on Evaluation of Liquefaction Resistance of Soils. Journal of Geotechnical and Geoenvironmental Engineering, 127:817–833.

Zhang, G., Robertson, P.K., Brachman, R.W.I. (2002). Estimating liquefaction-induced ground settlements from CPT for level ground. Canadian Geotechnical Journal, 39: 1168–1180.

Zhang, Zd., Luan, Mt., Jin, D., Guo, Y., and Nie, Y. (2009). Experimental study on the effect of cyclic preloading on the resistance to liquefaction of saturated loose sand under wave loading. Journal of Shanghai Jiaotong University (Science), 14: 398–403. https://doi.org/10.1007/s12204-009-0398-3

Zhou, T.-G., and Chen, T.-M. (2007). Laboratory investigation on assessing liquefaction resistance of sandy soils by shear wave velocity. Journal of Geotechnical and Geoenvironmental Engineering, 133(8): 959–972.

APPENDIX A

CYCLIC DIRECT SIMPLE SHEAR TEST: EQUIPMENT DESCRIPTION, SAMPLE PREPARATION, AND PROBLEMS ENCOUNTERED

This Appendix constitutes a Manual for the complete performance of direct simple shear tests in the cyclic simple shear equipment from LabGeo in FEUP. It includes the preparation of the specimen, the use of the software, and the disassembling of the specimen after the test. As the apparatus is relatively new at LabGEO, these descriptions can be helpful to guide new users. Moreover, it describes the problems encountered, the reasons, results, and solutions found for those problems (when possible).

A.1. DESCRIPTION OF THE EQUIPMENT PARTS

The apparatus is composed of four main components: the simple shear device, the Air Pressure Controller (APC), an electronic volume measuring apparatus and a computer connected to the internet with the GEOsys software installed.

As for the simple shear device, it is composed of a robust chamber equipped with connections to plug the cell-pressure, back and pore pressure and LVDTs. The main equipment dimensions are 570 mm x 1500 mm x 1300 mm and it weights approximately 320 kg. The load cell has a maximum force capacity of 5 kN (vertical force) and 4 kN (horizontal force).

The Air Pressure Controller (APC) has three automated pressure channels, that measure and control air pressure. It can be controlled manually or through the software installed on a computer. The front of the equipment shows the control panel, where the pressures can be monitored and in the rear-side are the pneumatic input and outputs and the electrical connections, mainly three output pressures, analogue channels and an Ethernet connection.

Figure A.1 – APC a) front; b) back
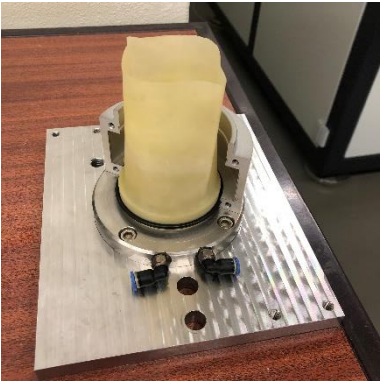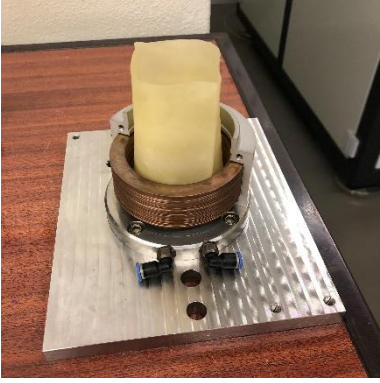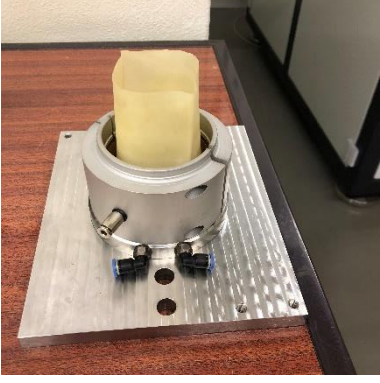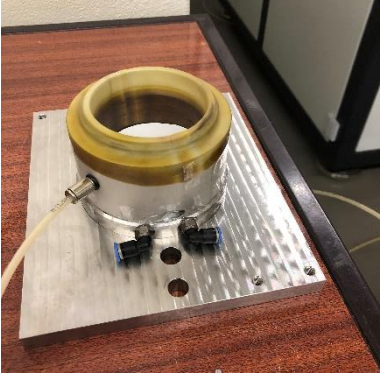
The Electronic Volume Measuring Apparatus is used to measure the variation in volume of liquid quantities under pressure. The burette has a capacity for 100 ml and is composed of a burette inside a protecting tube. The air pressure from the APC goes to the volume measuring apparatus and supplies water pressure to the interior of the specimen.
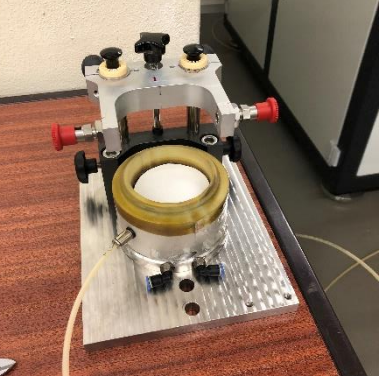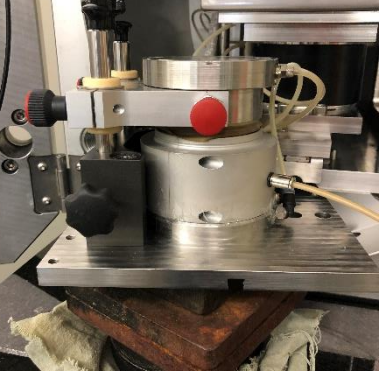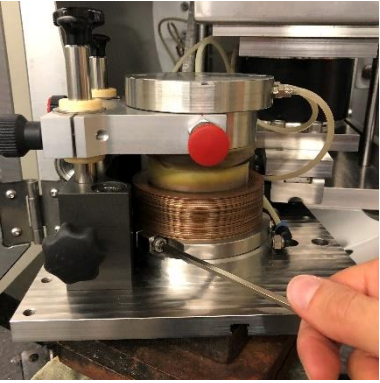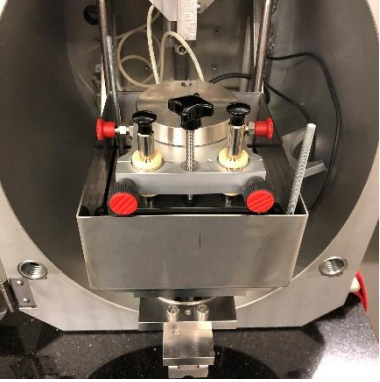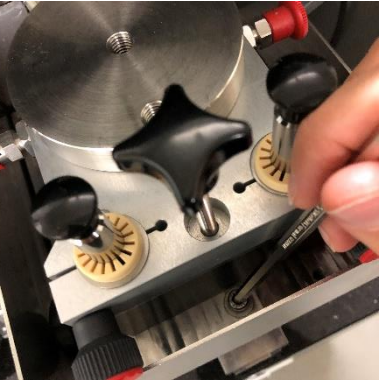
Figure A.2 – Volume Measuring Apparatus
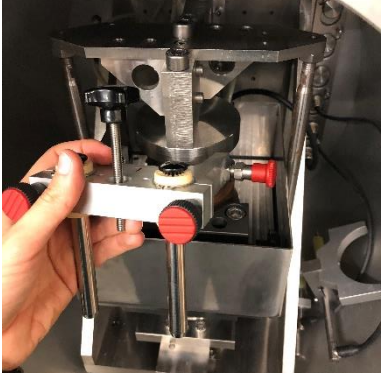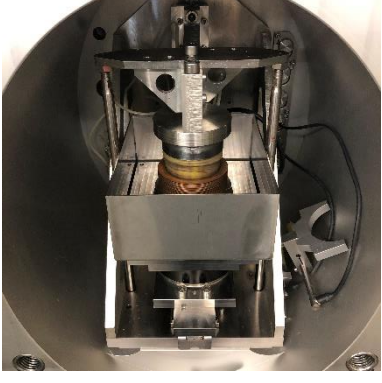
A.2. DESCRIPTION OF SAMPLE PREPARATION WITH AND WITHOUT RINGS

The following instructions detail the procedures to prepare a specimen for direct simple shear test.

	First, place the membrane around the pedestal and secure it with an o-ring. Place one half of the mould around the pedestal. Be careful to place the mould in a direction where the screws can be easily assessed when everything is assembled.
	Place the copper rings inside the mould, around the membrane
	Place the second half of the mould and screw with 4 screws.
	Place the top o-ring on the top of the mould and suck the membrane with vacuum applied to the interior of the mould. Use transparent tape to seal the mould. Place a paper filter at the bottom of the pedestal, above the porous stone. Measure the height (mean of three measures).

	Prepare your specimen with the desired method.
	Measure the height that is left (mean of three measurements) to assess the specimen's actual height. Place a paper filter on top of the specimen. Attach the support piece in the predefined holes on the base plate.
	Secure the top cap in the supporting piece and lower it until touching the top of the specimen.
	Assemble the membrane and the top o-ring. Connect the back-pressure tubes to the bottom of the pedestal.

	Turn off the vacuum (at this stage, the vaccum can be applied to the interior of the sample) and unscrew the mould. When the mould is taken off, a bottom piece is inserted to secure the rings in place.
	Screw the bottom piece that maintains the rings in place.
	Place everything inside the bathtub.
	Tighten the two screws to fix the bottom plate to the bathtub.

	Push everything to the inside of the chamber and fix the horizontal brake piece (on the back of the equipment).
	In the software, drive the horizontal displacement to the zero position. Lower the vertical piston until it touches the top cap. Screw the 3 top screws, to fix the top cap to the vertical piston (the longer screw fits in the middle hole).
	Remove the supporting piece.
	The specimen is ready to start the test.

Close the chamber door and control the test procedures on the software program.
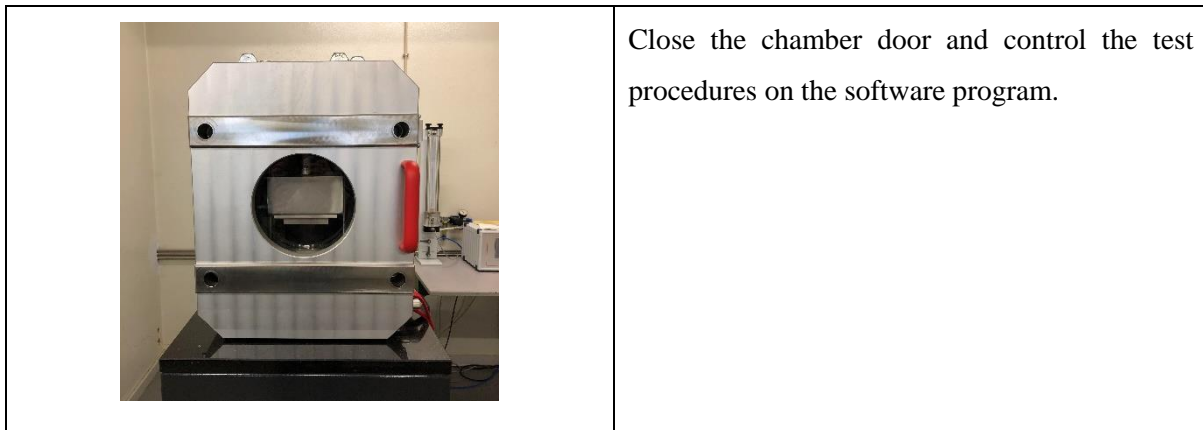
To prepare specimens without confinement by copper rings, a rubber component was made to aid the moulding procedure. To prepare a specimen with no rings, place the rubber part on the inside of the mould. Then, the preparation procedure is the same as explained for the assembling with rings.

Figure A.3– Adaptation of the mould to prepare specimens without rings

A.3. HOW TO CONNECT THE EQUIPMENT

First, turn the APC ON (in the switch on the back of the equipment box), wait until the monitor presents the measured pressures for the three channels and increase the pressure supplier to around 7 bar. The device is turned on by rotating the main switch. When the device is ON, a loud sound is heard and a green light appears.

Figure A.4 – Main switch on the device

A.4. GEOSYS SOFTWARE

The software is installed in a fixed computer and an Ethernet connection is required. The program opens when clicking on the GEOsys icon on the Desktop. Once opened, an interface language bar appears to select the language and after clicking "Ok" the program starts.
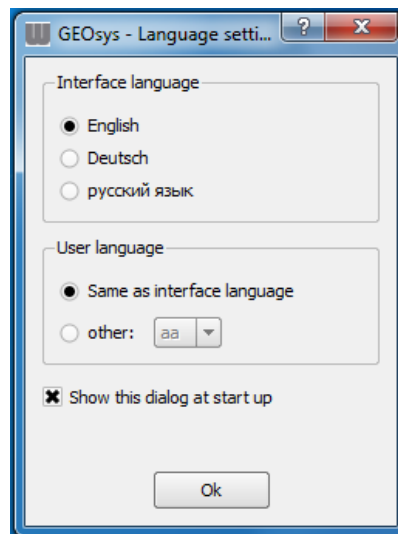
Figure A.5 – Language interface

The APC and shear device need to be connected to the software. Click on the "Connect" icon , wait until it is on and then click on the "Turn On" icon .

Note – It is important to select the correct test procedure file at the beginning of the test. The files are "Test-procedure-03082018.proc.gs" if the cyclic simple shear is going to be performed with constant vertical stress, and "Test-procedure-03082018_hconst.proc.gs.proc.gs" if the cyclic simple shear is going to be performed with constant height. The test procedure is selected in the "Test Procedure" tab, by clicking the button "New" and selecting the respective file.

At this stage, the manual controls can be used, allowing the control of every channel. In the tab "4-Manual Controls", select the channel and click "All commands". A window opens where the secondary channel, command and parameters are selected and the "Execute" starts the command. The most used commands are "ramp", that moves the selected channel to the desired value at a constant rate, or the "Manual positioning", that allows the control of the rate and values.
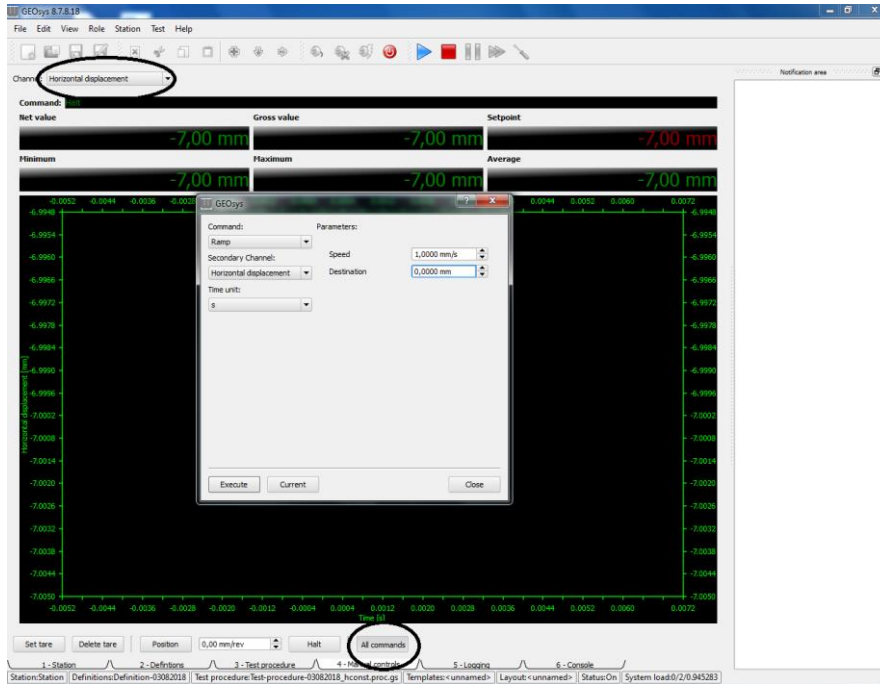
Figure A.6 – "4-Manual Commands" tab example

To start a test procedure, click the icon "Start/Continue test" ▶. A window appears where the user can define the sample geometry and description.
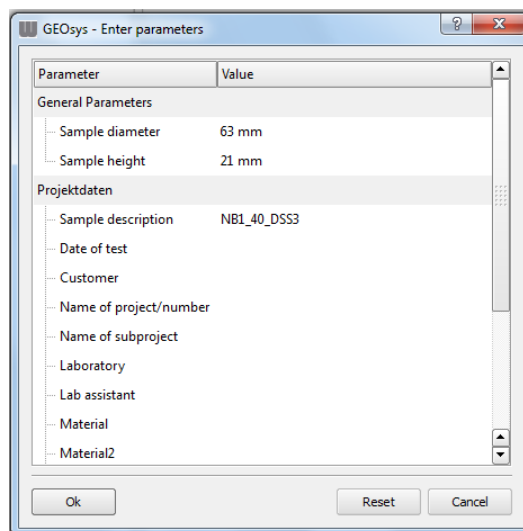
Figure A.7 – Definition of the initial parameters

After selecting the initial parameters, the program will ask the user to continue or pause the test procedure. Click "Continue test" and then save the data file in the chosen location.
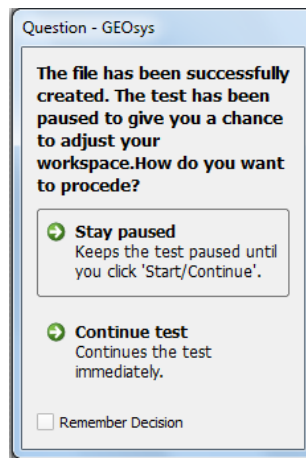
Figure A.8 – Continue test or remain paused window

After saving the data file, a window appears to select the initial cell pressure. If the test is a direct simple shear with no cell pressure, click "Ok" and ensure that the CP valve attached to the cell chamber is closed (so that no air pressure goes inside the chamber).
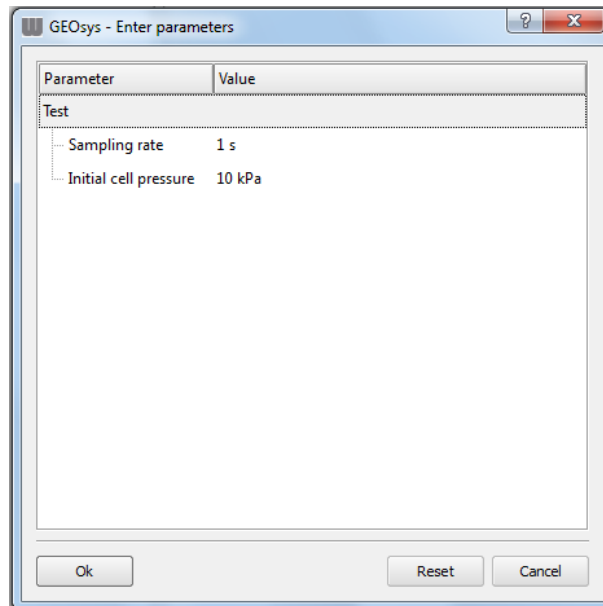
Figure A.9 – Definition of the initial stress window

In this stage, the specimen is already inside the chamber and the vertical piston was fixed to the top cap. Click "continue" in all the messages that appear on the right side of the program window and then click "Done". The cell pressure will increase until the selected value. The test stage window opens and by

clicking on the roll-up, the different stages of the test procedure are shown. By choosing each stage, the selected stage will be activated.
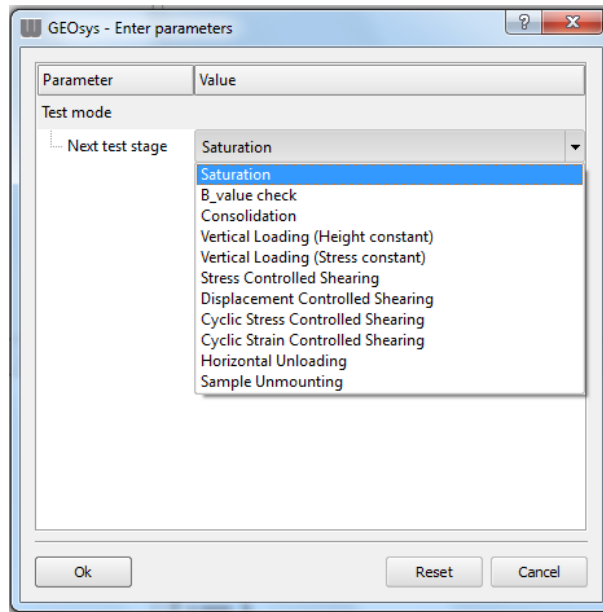
Figure A.10 – Test modes window

To perform a direct simple shear, the test stages used are the "Saturation", where the vertical stress parameters will be inserted and the "Cyclic Stress Controlled Shearing" to perform the cyclic shear phase so these two test stages are explained in detail above.

The "Saturation" test stage is the ideal stage to input the pressure conditions required. The user can define the speed of loading, the back pressure, the cell pressure, the vertical stress, the deviatoric stress, maximum deformation and sampling rate. The deviatoric stress is the differential stress between vertical and cell pressure and the maximum deformation defines the limit for maximum deformation in horizontal and vertical directions. The sampling rate is rate of recording data. In case of a dry test, select the desired vertical stress and insert CP = 10 kPa, BP = 5 kPa, and deviatoric stress = 0 kPa as default values.
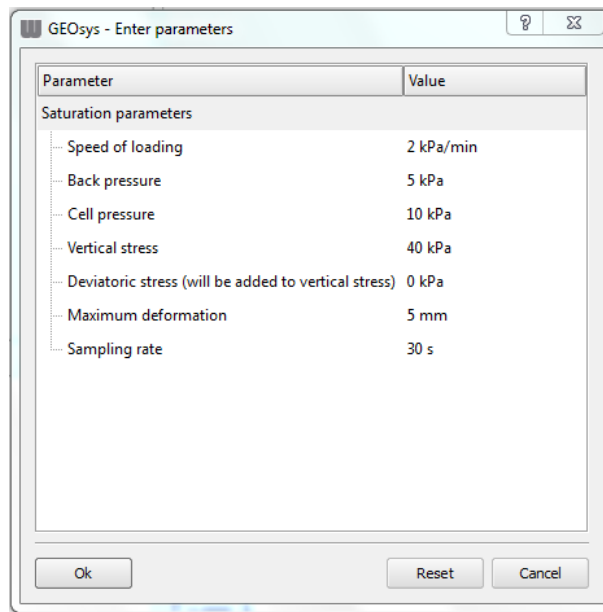
Figure A.11 – Saturation stage parameters window

The cyclic loading can be performed controlling the stress or the strain. The maximum and minimum horizontal stresses or the strain amplitude are input, as well as the frequency of cycles, the number of cycles, the horizontal displacement/load limit and the sampling rate. Note that the sampling rate depends on the frequency, so a representative number of points per cycle are recorded.
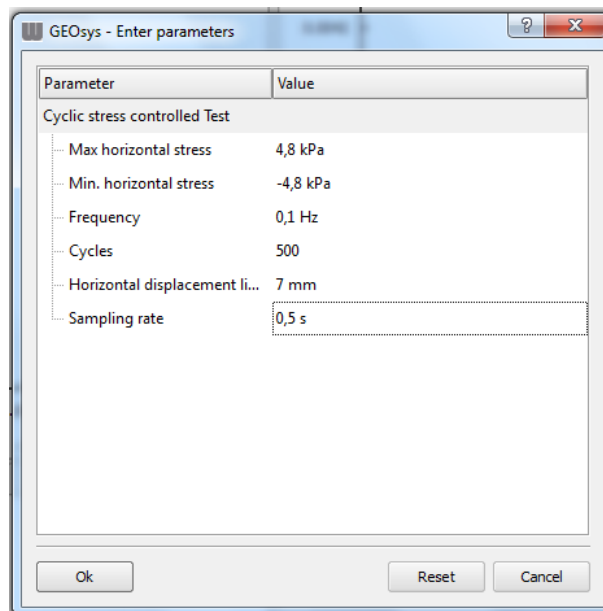
Figure A.12 – Cyclic stress controlled stage window

The software allows the monitoring of all channels and the presentation of the measurements can be shown as channel, single value, or diagram comparing the evolution of different channels. In the "6 - Console" tab, click the "New View" icon and then the "Modify" icon to select the pretended measurement. To draw a diagram, select the Diagram option and then select the File corresponding to the current test procedure stage. Then select the channels for each axis and click "Add". The tabs in the Console monitoring can be organised according to the user preferences.
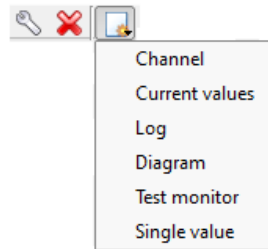
Figure A.13 – Types of monitoring windows
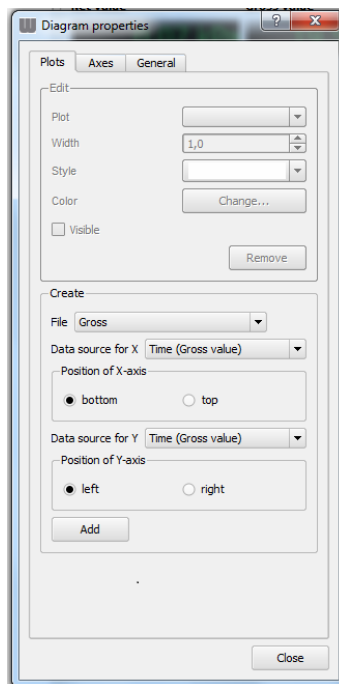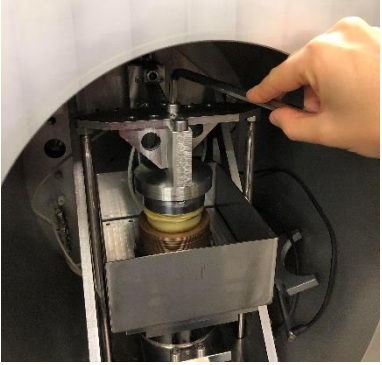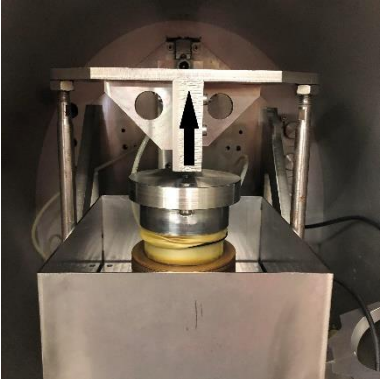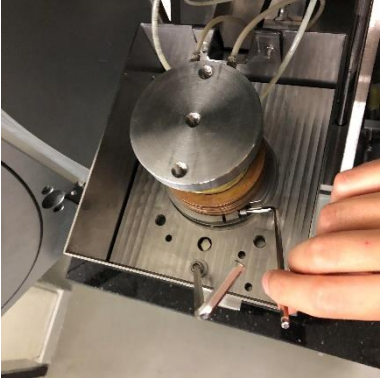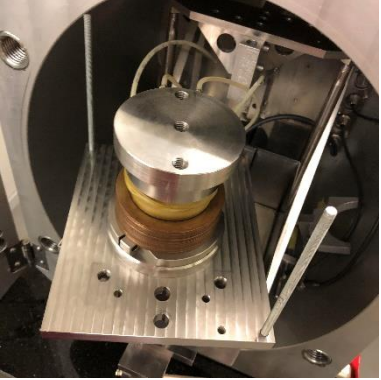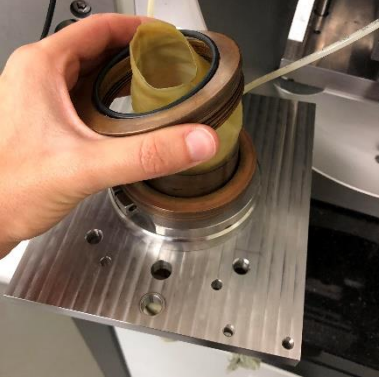
Figure A.14 – Diagram properties window

A.5. HOW TO DISASSEMBLE A TEST

	Once the test is finish, click the "Stop Test" icon, ■. Set the horizontal displacement to zero. Take off the screws attaching the vertical piston to the top cap.
	In the software, move the vertical piston up (Vertical displacement command) until there is space enough to remove the base pedestal without damaging the specimen.
	Disconnect the horizontal piston and push the base plate to the front, to unplug it from the horizontal piston.
	Take of the screws that fix the bottom part to the bathtub and the base supporting the rings.

	Remove the base plate from the interior of the bathtub.
	Take off the top cap carefully.
	Take off the top o-ring and the rings from around the membrane.
	Carefully put your specimen in a recipient to be weighted.

A.6. HOW TO EXPORT FILES FROM GEOSYS

The ASCII Export in GEOzip is used to transform and transfer the files from the software. The measuring data will be saved by the GEOsys as a file with the extension *.txt. The first step is to open

GEOzip ![icon] and open the chosen file (menu dialog File > Open). After opening the file, all items of the container file will appear in a table. The desired files to extract are the *.txt with the name of the procedure phase. Extract the file and save as "Excel Workbook". When opening the excel file, a message error will appear as the files are not in the correct numeric format. In the "Advanced Text Import Settings" select the decimal separator as a full stop and the thousands separator as comma. Save the file in "Excel Workbook" extension.
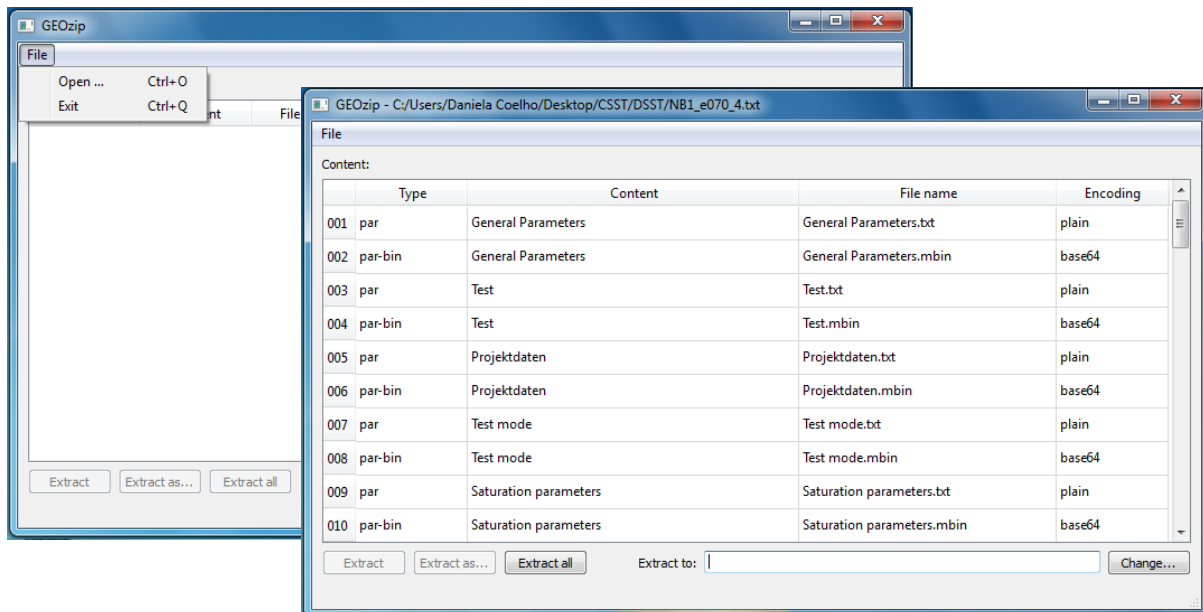
Figure A.15 – Extracting Data from GEOzip
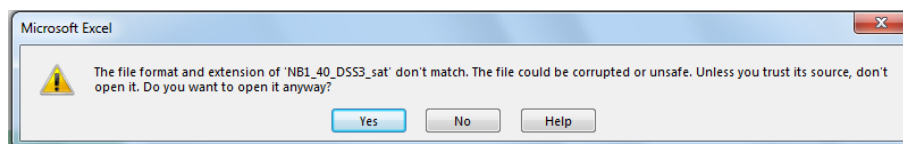
Figure A.16 – Microsoft Excel error message
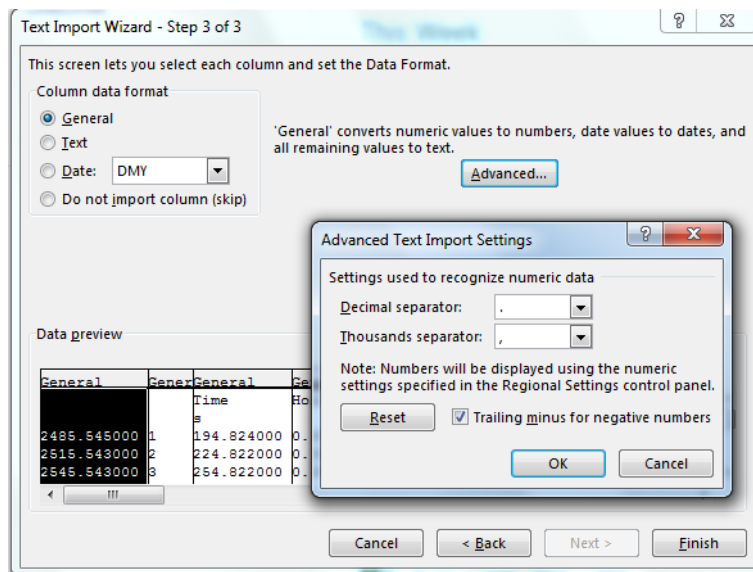
Figure A.17 – Changing numeric data settings in Excel

A.7. PROBLEMS ENCOUNTERED DURING THIS WORK AND SOLUTIONS FOUND

The cyclic simple shear equipment was supposed to allow the performance of cyclic simple shear tests, without confinement of rings, as it allowed the control of cell and back pressure, and the measurement of pore pressures. The initial trials were performed with a procedure similar to the triaxial test: sample preparation; increase of CP and BP to 20 kPa and 10 kPa, respectively; percolation of CO_2 and de-aired water; saturation until CP of 310 kPa and BP of 300 kPa; consolidation with increase of CP. Some trials were performed on sand specimens, however, when the vertical stress was increased for the anisotropic consolidation, the specimen settled a lot and would lose its cylinder shape (Figure A.18). The actual vertical stress was hard to determine as the cell pressure affects the vertical stress but it is not possible to quantify how.

Figure A.18 – Shape of the specimen after applying the vertical stress

Another problem encountered was the leakage of air to the inside of the specimen. All the connections to the inside of the specimen were fixed, but the leakage still occurred. It was found out that the leakage was a problem of the air confinement, as the rubber membrane allowed the penetration of the confinement air, hence the volume during consolidation never stabilised, as air was flowing to the interior of the specimen. The load cell it placed under the sample and it is not submersible, so it was not possible to fill the cell chamber with water. To fix this problem, the solution was to construct a "bathtub" (Figure A.19), in order to submerge the specimen in water, so the pressures were applied through the air to the water and simulate an immerged condition. The placement of the "bathtub" caused other problems, such as: i) impossibility of placing the external LVDTs as they would not fit in the interior of the cell chamber; ii) due to height constraints, the specimen preparation set for samples with 70 mm diameter did not fit the inside of the chamber with the bathtub; iii) all the connection of top and bottom with the exterior of the chamber would not fit the inside of the bathtub. However, these issues were solved as: i) the actuator measures and registers the vertical and horizontal displacements and it is accurate; ii) a specimen preparation set for samples with 63 mm diameter was ordered; iii) all the connections were changed.

Figure A.19 – "Bathtub"

As mentioned above, the control of the pressures was very difficult. The use of the "bathtub", and consequently the confinement of the specimen with water, brought other challenge. As the saturation of the specimen began, the vertical displacement lost control, lift the vertical piston, and disconnect from the top of the sample (Figure A.20).
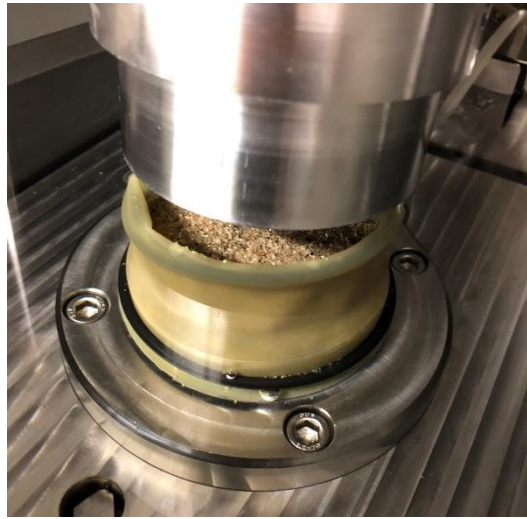
Figure A.20 – Top cap separation from the sample

More than 50 tests were performed to detect and solve these anomalies, but no solution was found. Therefore, it was decided to perform tests without cell and back-pressures, on unsaturated soil samples. The test procedures for these tests were described in Chapter 6. As it was not possible to perform tests with flexible membrane, the tests were performed with rigid boundary (copper rings). However, for direct simple shear tests, the loading stage is performed with constant height. Therefore, a new test procedure was created by the author, to maintain the height constant during the cyclic loading stage.

In the final part of the thesis, an attempt was made to perform direct simple shear tests with saturated specimens. To guarantee that the problems described above did not occur, a careful procedure was developed, and it was possible to saturate (flood) the specimens without compromising the test results.

The procedure was defined by the following steps:

- Sample preparation as described above;
- Application of the pretended vertical stress
- Application of a 10 kPa pressure in the cell, by air
- Percolation of CO_2 and percolation of de-aired water with 2 kPa back-pressure from the top to the bottom of the specimen (this procedure allowed to reach high values of saturation degree)
- Removal of the cell pressure
- Cyclic shear procedure with constant height

In a last attempt to perform a test with constant vertical stress during shear, one specimen was prepared following the same procedures described in the last paragraph. However, the cyclic loading was performed with constant vertical stress. Figure A.21 presents the results of tangential stress, shear strain, axial strain, and pore pressure with number of cycles. It is observed that at each new increase in

tangential stress, the specimen densified (increase in axial strain) and then stabilised, with no increase in pore water pressure and nor development of significant shear strains. As the vertical stress was set to be maintained constant, the specimen would densify to support that pressure, and the higher density would increase the sample resistance to that tangential stress. It was concluded that the control of the vertical stress during shear with confinement with rings is not possible in these conditions.
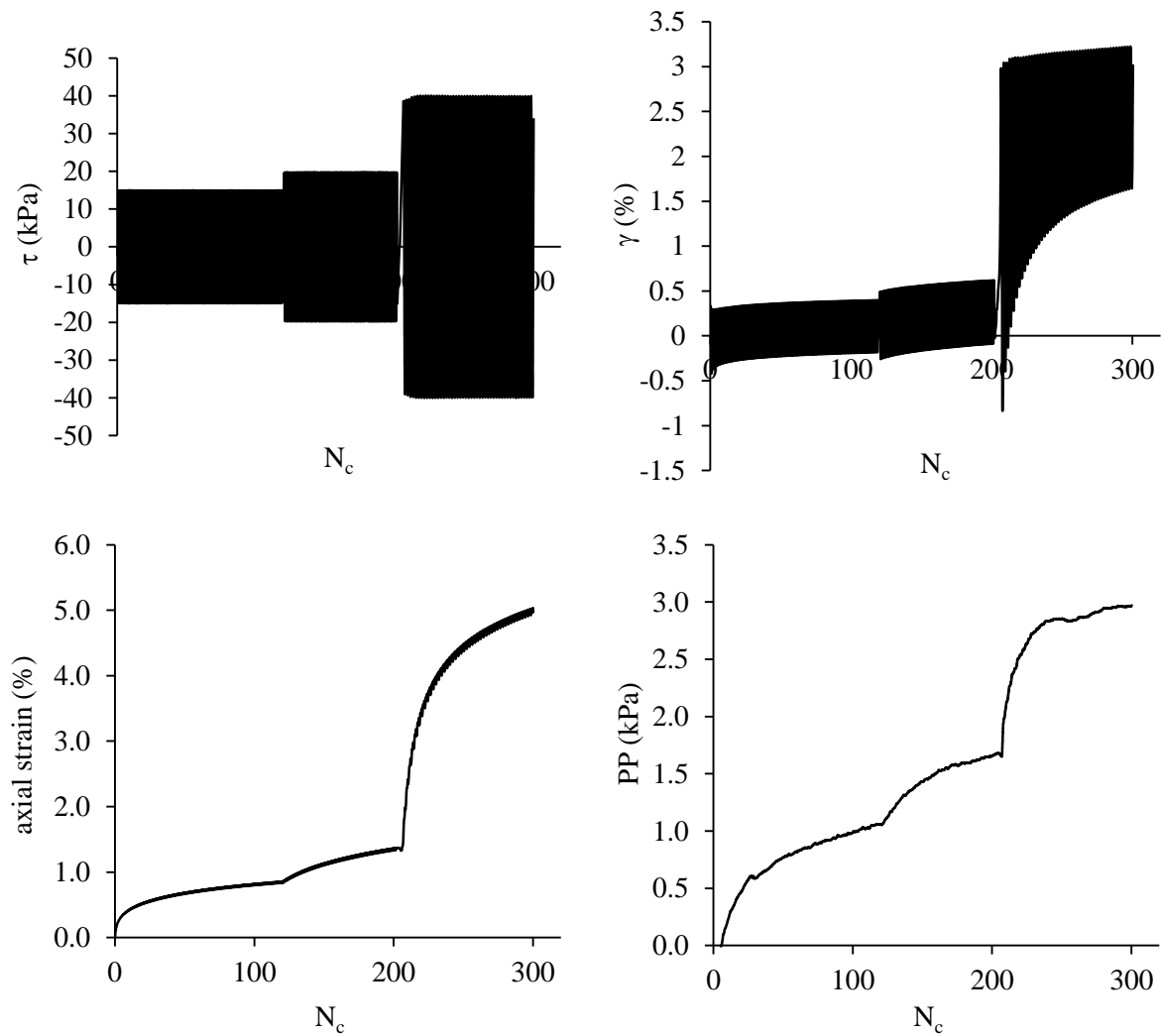
Figure A.21 – Cyclic simple shear test results for loading at constant vertical stress

APPENDIX B

MATERIAL PROPERTIES OF SPT SOIL SAMPLES, UNDISTURBED SOIL SAMPLES, AND BENCHMARK SOILS

Due to the large data set of laboratory tests performed in this work, the results of the material properties of all soils studied were summarised in this Appendix. The material properties of soils collected with the SPT tube are provided, including fines content (FC), specific gravity (G_s), mean grain size (D_{50}), Atterberg limits (w_L and w_P), plasticity index (PI). Moreover, the materials properties of soils collected with Mazier and Gel-Push samplers are also tabulated, presenting the void ratio limits (e_{max} and e_{min}), fines content (FC), specific gravity (G_s), mean grain size (D_{50}), coefficient of shape and coefficient of uniformity (C_C and C_U), and shape parameters.

This Appendix also includes the material properties of benchmark sands used for comparisons with soils from this study. The data was collected from Cho et al. (2006) and Altuhafi et al. (2016).

Besides, this Appendix presents the tabulated results of the estimated critical state parameters of specimens collected with Mazier and Gel-Push samplers, obtained with empirical correlations with emax-emin (Cubrinovski and Ishihara, 2002). Moreover, the estimated critical state parameters are correlated with the void ratio limits, and grain size characteristics, such as D_{50}, C_U, and FC. The effect of shape parameters (circularity, solidity, aspect ratio, and SAGI) is also analysed for the estimated CS parameters.

B.1. TABULATED VALUES OF MATERIAL PROPERTIES OF SPT AND UNDISTURBED SPECIMENS SOILS

Table B.1 – Material properties of soil samples collected with SPT at S1

Sample	Depth (m)	FC (%)	G	D_{50} (mm)	w_L (%)	w_P (%)	PI (%)
S1	1.5	91.8	2.73	0.004	52	25	27
S1	2.5	10.17	2.63	0.5	-	-	-
S1	3.5	-	2.67	-	37	19	18
S1	4.5	22.5	2.63	0.27	-	-	-
S1	5.5	4.72	2.65	0.59	-	-	-
S1	6.5	1.6	2.62	0.6	-	-	-
S1	7.5	6.85	2.63	0.55	-	-	-
S1	8.5	79.3	2.70	0.005	77	37	40
S1	9.5	69.4	2.68	0.01	46	25	21
S1	10.5	16.2	-	0.22	-	-	-
S1	11.5	13.59	2.65	0.3	-	-	-
S1	12.5	54.6	2.68	0.045	32	19	13
S1	13.5	10.6	-	0.23	-	-	-
S1	14.5	13.2	2.70	0.15	-	-	-
S1	15.5	12.4	2.70	0.2	-	-	-
S1	16.5	20.3	2.69	0.19	-	-	-
S1	17.5	53.3	2.69	0.063	31	20	11
S1	18.5	60.6	2.70	0.04	35	20	15
S1	19.5	18.02	2.70	0.15	-	-	-
S1	20.5	13.5	2.69	0.15	-	-	-
S1	21.5	86.62	2.72	0.006	60	31	29
S1	22.5	83.73	2.71	0.0095	43	21	22
S1	23.5	62.02	2.71	0.0043	36	20	16
S1	24.5	95.8	-	0.0075	50	27	23
S1	25.5	69.2	2.66	0.014	70	32	38

Table B.2– Material properties of soil samples collected with SPT at S2

Sample	Depth (m)	FC (%)	G	D_{50} (mm)	w_L (%)	w_P (%)	PI (%)
S2	1.5	99.35	-	0.0013	-	-	-
S2	2.5	99.87	-	0.0024	-	-	-
S2	3.5	99.79	2.76	0.0036	67	32	35
S2	4.5	99.12	-	0.0028	-	-	-
S2	5.5	48.39	2.67	0.09	27	15	12
S2	6.5	63.94	-	0.007	-	-	-
S2	7.5	23.78	-	0.15	-	-	-
S2	8.5	33.05	-	0.2	-	-	-
S2	11.5	15.69	-	0.28	-	-	-
S2	14.5	10.71	2.684	0.27	-	-	-
S2	15.5	61.4	2.703	0.055	33	20	13
S2	16.5	85.18	2.708	0.029	36	20	16
S2	17.5	85.68	2.703	0.018	42	24	18
S2	18.5	97.4	2.698	0.007	50	26	24
S2	19.5	94.9	2.691	0.007	51	26	25
S2	20.5	97.06	2.755	0.012	43	23	20
S2	21.5	83.17	2.702	0.032	38	24	14
S2	22.5	90.31	2.692	0.018	43	24	19
S2	23.5	94.38	2.699	0.0085	52	25	27
S2	24.5	78.08	2.723	0.017	44	22	22
S2	25.5	90.47	2.688	0.0068	50	24	26

Table B.3 – Material properties of soils collected with Mazier and Gel-Push samplers, tested under triaxial conditions

Name	Depth (m)	Packing		FC (%)	G_s	Gradation			Shape parameters			
		e_{max}	e_{min}			D_{50}	C_C	C_U	Circularity	Solidity	Aspect ratio	SAGI
S1_M2_I3	2.5	0.940	0.571	9.2	2.651	0.33	1.01	3.76	0.885	0.963	0.741	10.1
S1_M5_I2	5.0	0.819	0.489	21.5	2.687	0.27	-	-	-	-	-	-
S1_M5_I4	5.5	0.819	0.489	10.6	2.615	0.45	2.73	9.17	0.869	0.949	0.730	12.2
S1_M6_I2	6.0	0.713	0.494	2.4	2.629	0.70	0.99	2.80	0.880	0.973	0.719	9.7
S1_M6_I3	6.5	0.762	0.523	6.0	2.626	0.60	1.01	3.04	0.880	0.968	0.792	10.4
S1_M7_I1	7.0	0.902	0.613	2.1	2.643	0.40	0.89	1.81	0.889	0.967	0.707	9.3
S1_M9_I1	9.0	1.119	0.528	27.6	2.660	0.28	15.43	233.33	-	-	-	-
S1_M11_I1	11.0	-	-	47.7	2.675	0.11	-	-	-	-	-	-
S1_M14_I1	14.0	0.920	0.517	17.4	2.632	0.40	56.94	294.12	-	-	-	-
S1_M15_I1	15.0	1.094	0.579	19.4	2.670	0.28	22.06	113.33	0.861	0.945	0.745	13.2
S1_M25_I1	25.0	-	-	17.3	2.664	0.19	25.57	55.00	-	-	-	-
S2_M6_I1	6.0	0.877	0.546	9.7	2.639	0.40	2.34	6.40	0.883	0.955	0.731	10.7
S2_M7_I1	7.0	1.197	0.545	39.9	2.692	0.28	1.14	350.00	0.869	0.947	0.773	12.6
S2_M7_I2	7.2	0.934	0.543	14.5	2.692	-	-	-	-	-	-	-
S2_M9_I1	9.0	1.117	0.551	28.6	2.630	0.30	24.50	450.00	0.867	0.947	0.767	12.7
S2_M11_I1	11.0	1.136	0.636	17.7	2.666	0.23	17.30	92.50	-	-	-	-
S2_M11_I2	11.5	1.039	0.646	9.4	2.620	0.26	1.19	3.20	0.872	0.948	0.748	12.1
S2_M12_I1	12.0	1.022	0.610	12.5	2.678	0.30	10.81	37.00	0.885	0.957	0.747	10.5
S2_M13_I1	13.0	1.139	0.651	17.7	2.675	0.25	4.80	30.00	0.872	0.949	0.743	12.0
S2_M14_I1	14.0	1.160	0.688	8.0	2.660	0.20	1.11	2.10	0.877	0.950	0.724	11.5
NB1_F2_GP2.5_I3	3.0	0.958	0.644	3.6	2.660	0.36	1.05	2.22	-	-	-	-
NB1_F2_GP3.5_I1	3.8	0.805	0.470	9.4	2.636	0.43	2.21	6.38	0.890	0.961	0.738	9.8
NB1_F4_GP4_I2	4.3	0.884	0.603	2.4	2.667	0.45	0.86	2.26	0.895	0.961	0.717	9.3
NB1_F5_GP4_I2	4.8	0.897	0.572	4.7	2.601	0.32	1.02	2.06	-	-	-	-
NB1_F1_GP4.5_I1	4.8	0.883	0.572	3.8	2.637	0.38	1.05	2.15	0.902	0.962	0.736	8.8
NB1_F5_GP5_I1	5.4	0.840	0.566	3.0	2.630	0.50	0.95	2.38	0.887	0.957	0.752	10.4
NB1_F5_GP5_I2	5.6	0.851	0.576	2.8	2.635	0.58	1.02	2.32	0.900	0.964	0.745	8.9
NB2_F1_GP3_I4	3.7	1.153	0.501	32.1	2.646	0.29	3.71	330.00	-	-	-	-
NB2_F2_GP4_I4	4.8	1.583	0.658	55.3	2.689	0.07	7.62	82.00	-	-	-	-
NB2_F1_GP6_I2	6.3	0.876	0.578	5.0	2.640	0.50	1.00	2.68	0.894	0.958	0.719	9.6
NB2_F1_GP6_I3	6.5	0.803	0.541	2.0	2.623	0.60	1.28	2.75	0.886	0.962	0.717	9.9
NB1	4-5	0.846	0.590	2.9	2.640	0.45	0.90	2.16	0.886	0.956	0.724	10.4

B.2. TABLES OF BENCHMARK SANDS USED IN THE MATERIAL PROPERTIES COMPARISONS OF THE SOILS FROM THIS STUDY, DATA FROM ALTUHAFI ET AL. (2016) AND CHO ET AL. (2006)

Table B.4 – Material properties of benchmark soils from Altuhafi et al. (2016)

Sand type	Packing		Shape properties			SAGI	CS parameters		
	e_{min}	e_{max}	AR	Solidity	Circularity		ϕ'_{cs}	λ_{ln}	Γ
Badger sand	0.490	0.690	0.810	0.980	0.930	5.5	28.4	0.010	0.697
Ottawa	0.502	0.742	0.797	0.974	0.918	7.0	27	0.024	0.802
Albany sand	0.505	0.804	0.760	0.949	0.903	9.7	31	-	-
M31	0.528	0.870	0.755	0.946	0.899	10.2	31	0.011	0.795
Monterey	0.550	0.860	0.749	0.954	0.891	10.9	32	0.013	0.910
Nevada	0.570	0.850	0.772	0.927	0.909	10.8	31	0.026	1.040
Ticino	0.574	0.990	0.732	0.951	0.879	11.3	33	0.053	1.050
HRS	0.526	0.870	0.705	0.933	0.892	11.3	32	0.008	0.839
Toyoura	0.605	0.977	0.743	0.934	0.894	11.3	31	0.021	0.941
FBS-NE34	0.540	0.865	0.731	0.933	0.889	11.7	31	0.030	0.980
FRS	0.627	0.995	0.723	0.939	0.882	11.8	35	0.029	1.110
Longstone	0.614	0.995	0.724	0.921	0.892	12.2	33	0.007	0.893
Thanet	0.659	0.808	0.742	0.911	0.900	12.4	32	0.056	1.156
Stava	0.615	1.068	0.729	0.925	0.881	12.9	35	0.009	0.987
Osorio	0.570	0.850	0.699	0.926	0.876	13.0	37	0.017	0.900
Hostun	0.656	1.000	0.723	0.935	0.869	13.1	35.7	0.020	0.892
Aio sand	0.582	0.958	0.718	0.947	0.857	13.2	40.6	0.015	-

Table B.5 – Material properties of benchmark soils from Cho et al. (2006)

Sand type	FC (%)	Gradation		Packing		CS parameters		References
		D_{50} (mm)	C_U	e_{max}	e_{min}	λ	Γ	
Chiba #3	3	0.17	2.00	1.271	0.839	0.085	1.265	R1
Chiba #18	18	0.15	4.00	1.307	0.685	0.09	1.12	R1
Fraser River	0	0.30	1.90	1.13	0.78	0.067	1.11	R2
Hostun RF	0	0.32	1.80	1	0.655	0.069	0.969	R3
Monterey #0	0	0.38	1.60	0.86	0.53	0.039	0.905	R4
Monterey #16	16	1.30	1.30	0.71	0.49	0.023	0.73	R5
Ottawa #20/30 sand	0	0.72	1.20	0.742	0.502	0.047	0.802	R2
Nevada	0	0.15	1.80	0.85	0.57	0.071	1.04	R2
Ticino	0	0.58	1.50	0.99	0.574	0.053	1.05	R2
Kogyuk 350	0	0.35	1.70	0.783	0.523	0.014	0.784	R6
Kogyuk 350	2	0.35	1.80	0.829	0.47	0.065	0.845	R6
Kogyuk 350	5	0.36	2.00	0.866	0.487	0.105	0.925	R6
Kogyuk 350	10	0.34	2.30	0.927	0.465	0.175	1.056	R6
Sydney	0	0.30	1.50	0.855	0.565	0.073	0.969	R7
Toyoura	0	0.17	1.70	0.977	0.597	0.06	1.048	R1

References: R1 – Ishihara (1993); R2 – Cho et al. (2006); R3 – Thevanayagam et al. (1996); R4 – Riemer et al. (1990); R5 – Riemer and Seed (1997); R6 – Been and Jefferies (1985); R7 – Chu and Lo (1993)

B.3. ESTIMATED CRITICAL STATE PARAMETERS OF SPECIMENS COLLECTED WITH MAZIER AND GEL-PUSH SAMPLERS AND CORRELATIONS WITH MATERIAL PROPERTIES

Table B.6– Estimated critical state parameters of specimens collected with Mazier and Gel-Push samplers

Name	Depth (m)	Estimated CS parameters	
		λ	Γ
S1_M2_I3	2.5	0.102	0.989
S1_M5_I2	5.0	0.093	0.881
S1_M5_I4	5.5	0.093	0.881
S1_M6_I2	6.0	0.065	0.788
S1_M6_I3	6.5	0.070	0.837
S1_M7_I1	7.0	0.082	0.973
S1_M9_I1	9.0	0.158	1.014
S1_M11_I1	11.0	-	-
S1_M14_I1	14.0	0.111	0.955
S1_M15_I1	15.0	0.139	1.057
S1_M25_I1	25.0	0.174	1.141
S2_M6_I1	6.0	0.093	0.939
S2_M7_I1	7.0	0.173	1.026
S2_M7_I2	7.2	0.108	0.974
S2_M9_I1	9.0	0.152	1.036
S2_M11_I1	11.0	0.135	1.111
S2_M11_I2	11.5	0.108	1.078
S2_M12_I1	12.0	0.113	1.052
S2_M13_I1	13.0	0.132	1.123
S2_M14_I1	14.0	0.128	1.155
NB1_F2_GP2.5_I3	3.0	0.089	1.024
NB1_F2_GP3.5_I1	3.8	0.094	0.866
NB1_F4_GP4_I2	4.3	0.080	0.956
NB1_F5_GP4_I2	4.8	0.091	0.960
NB1_F1_GP4.5_I1	4.8	0.088	0.950
NB1_F5_GP5_I1	5.4	0.079	0.913
NB1_F5_GP5_I2	5.6	0.079	0.924
NB2_F1_GP3_I4	3.7	0.173	0.982
NB2_F2_GP4_I4	4.8	0.241	0.986
NB2_F1_GP6_I2	6.3	0.085	0.945
NB2_F1_GP6_I3	6.5	0.076	0.877
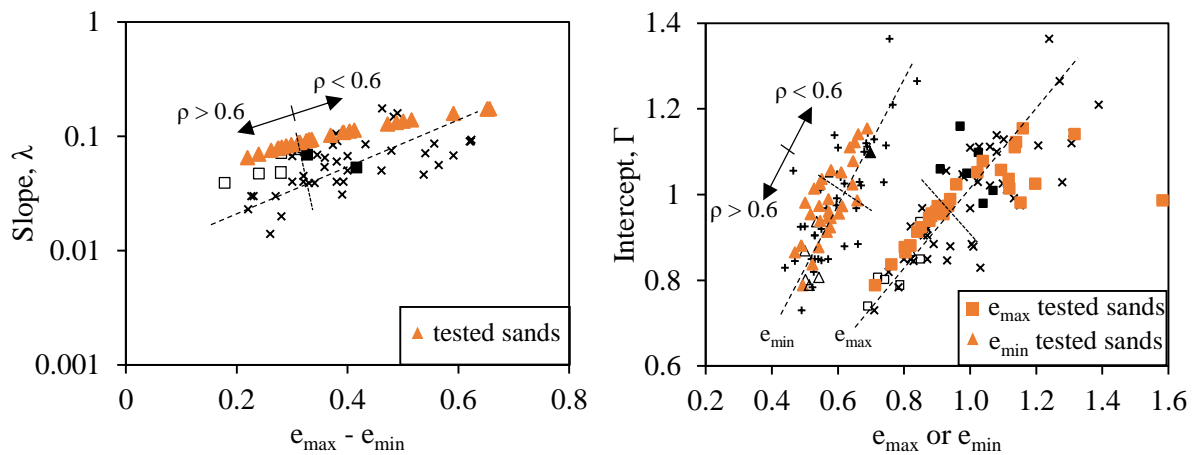
Figure B.1– Correlations between estimated CS parameters and void ratio limits (data compiled by Cho et al. (2006) and completed with present data)
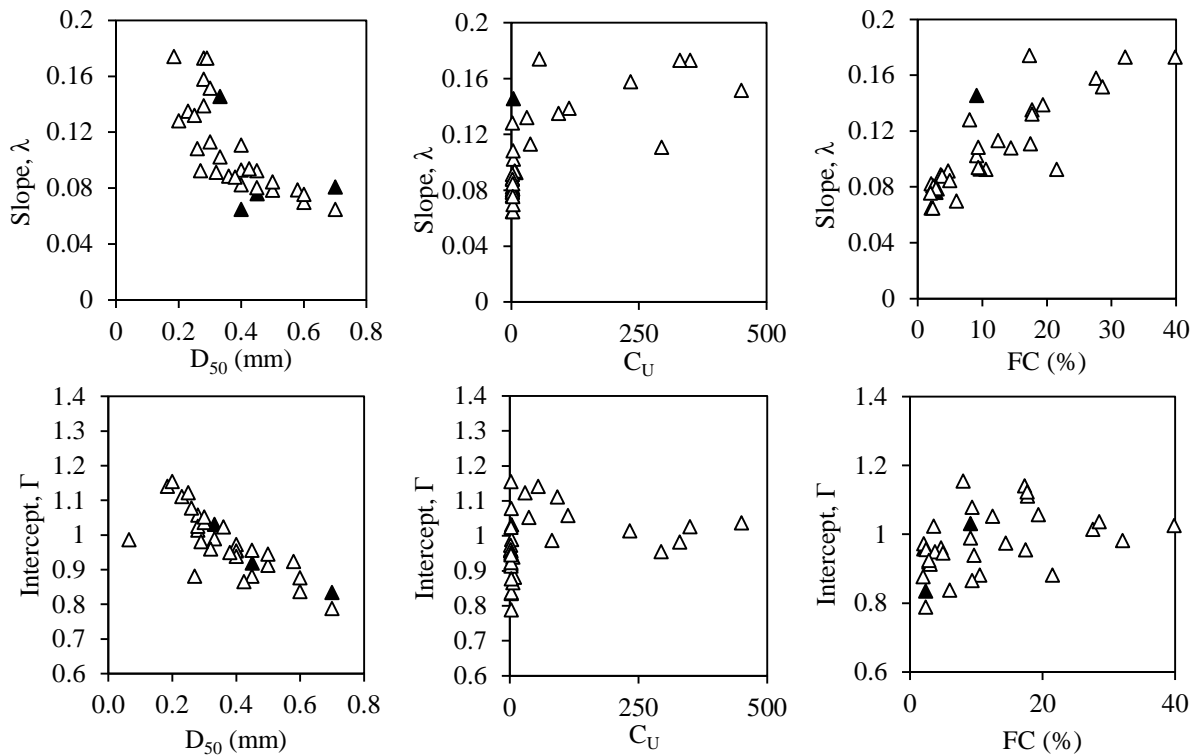
Figure B.2 – Correlations between grain size and critical state parameters (filled triangles represent the results of CSL determined from triaxial tests, empty triangles are the estimated CS parameters)
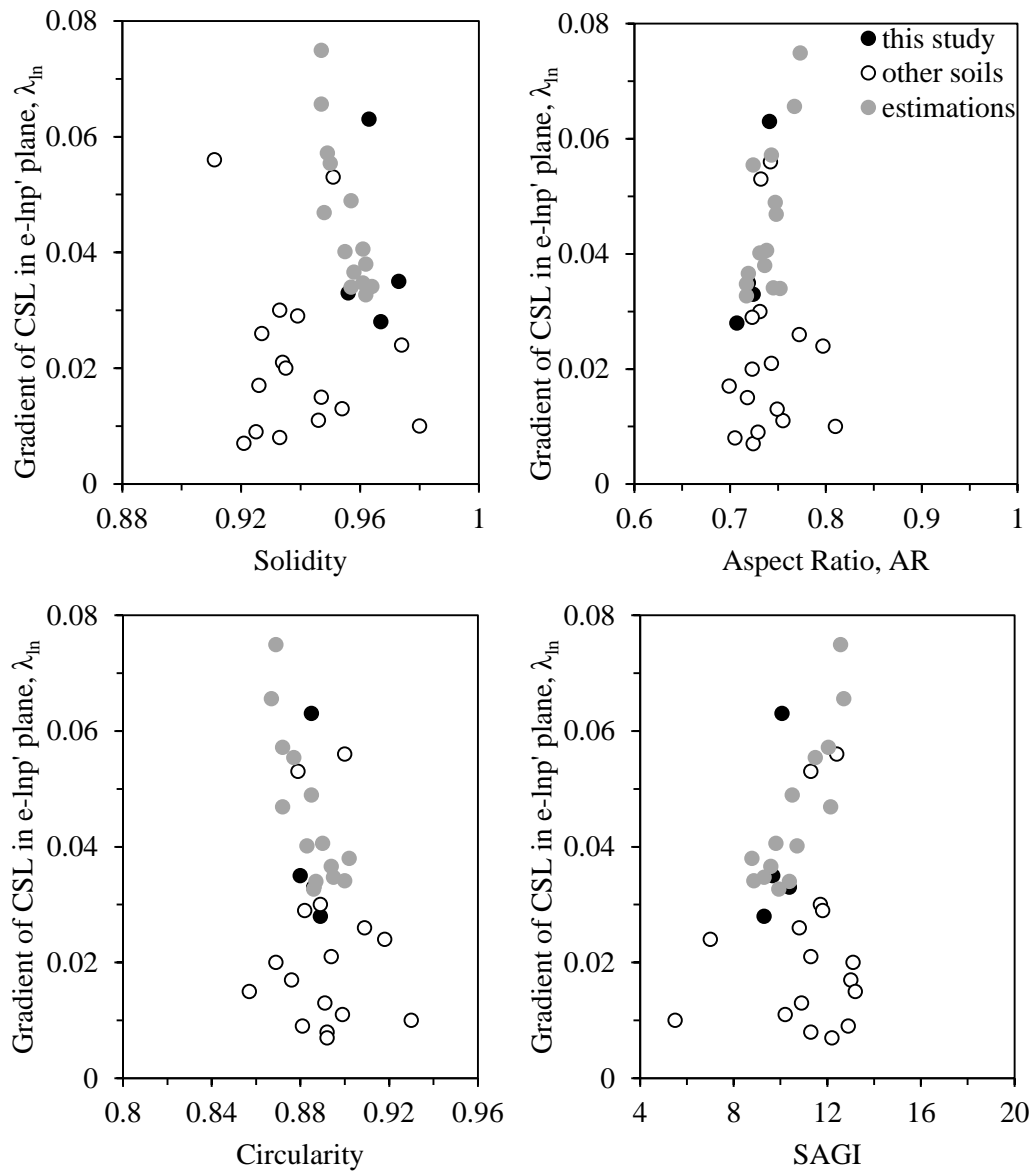
Figure B.3 – Effect of shape parameters and SAGI on the CSL slope (empty symbols represent the soils from Altuhafi et al. (2016), black dots represent the results of CSL determined from triaxial tests, grey dots represent the estimated CS parameter)
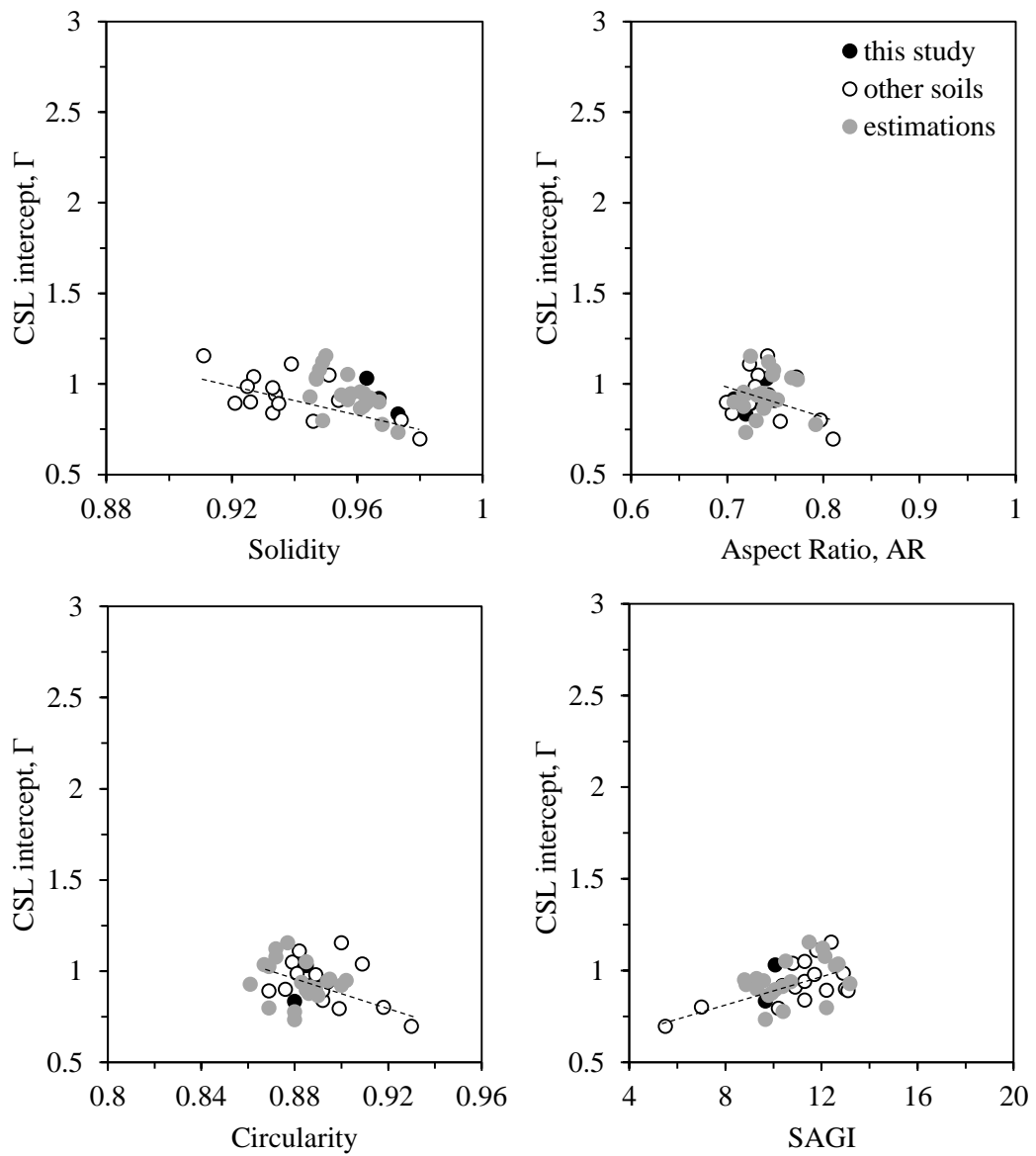
Figure B.4 – Effect of shape parameters and SAGI on the CSL intercept (empty symbols represent the soils from Altuhafi et al. (2016), black dots represent the results of CSL determined from triaxial tests, grey dots represent the estimated CS parameter)

APPENDIX C

TABULATED RESULTS OF LABORATORY TESTS

Due to the large data set of laboratory tests performed in this work, the extensive results were organised and indexed to this Appendix. The following tables present the results of monotonic triaxial tests, cyclic triaxial tests performed with undisturbed and reconstituted specimens, and cyclic direct simple shear tests performed with undisturbed and reconstituted specimens.

The monotonic triaxial tests table provides the summary of each test stage, giving the void ratio after assembling (e_0), the void ratio at the end of saturation (e_{i-1}), the void ratio after consolidation (e_i), the volumetric strain during consolidation and during shear (ε_v), the applied mean effective stress (p'_i), the shear wave velocity after consolidation (V_S), the void ratio at the end of shear (e_f), the mean effective stress (p'_f), and deviatoric stress (q_f) at the end of shear, the peak values of p' and q.

The cyclic triaxial tests tables provide the void ratio after specimen preparation (e_0), at the beginning of consolidation (e_{i-1}) and after consolidation (e_i), the volumetric change during consolidation (ε_v), the relative density (D_R), the confining pressure (p'_i), the shear wave velocity after consolidation (V_S), the state parameter (ψ), the frequency of cycles (Freq), the cyclic stress ratio (CSR), the number of cycles (N_{liq}) required to develop 5% axial strain in double amplitude ($\varepsilon_{a,DA}$) and required to develop 100% excess pore pressure ratio (r_u), and the cumulative dissipated energy at liquefaction (ΔW_{liq}), and the type of liquefaction failure.

The cyclic direct simple shear tests tables include the preparation method selected, the vertical stress (σ_v), the void ratio after specimen preparation (e_0) and after consolidation (e_i), the initial and final water content (w_i and w_f, respectively), the state parameter (ψ), the cyclic stress ratio (CSR), the number of cycles (N_{liq}) required to develop 3.75% axial strain in single amplitude (γ_{SA}), and the cumulative dissipated energy at liquefaction (ΔW_{liq}).

Table C.1 – Monotonic triaxial test results for reconstituted specimens of S1 and NB1 soils

Test ID	After assembling	Percolation + saturation		Consolidation					Shear				Values used for
	e_0	e_{i-1}	ε_v	e_i	p'_i	V_S	ε_v	e_f	p'_f	q_f	p'_{peak}	q_{peak}	
			%		kPa	m/s	%		kPa	kPa	kPa	kPa	
S1_M2_R3_STxD1	0.926	0.85	1.37	0.82	50	133	4.11	0.75	90	119	-	-	CSL
S1_M2_R3_STxD2	0.897	0.831	4.46	0.75	200	219	5.08	0.66	365	499	-	-	CSL
S1_M2_R3_STxD3	0.987	0.81	4.65	0.72	400	254	6.14	0.62	738	1013	-	-	CSL
S1_M6_STxD1	0.847	0.746	1.51	0.72	70	142	3.26	0.66	126	166	-	-	CSL
S1_M6_STxD2	0.86	0.758	4.13	0.68	398	239	4.98	0.60	729	987	-	-	CSL
S1_M6_STxD3	0.86	0.754	2.63	0.71	200	198	3.62	0.64	358	474	-	-	CSL
S1_M7_STxD1	0.959	0.91	2.31	0.86	200	223	3.33	0.80	360	480	-	-	CSL
S1_M7_STxD2	1.005	0.92	3.09	0.86	401	257	5.05	0.76	717	955	-	-	CSL
S1_M7_STxD3	1.01	0.911	1.18	0.89	70	164	2.58	0.84	125	163	-	-	CSL
S1_M7_STxD4	0.952	0.89	0.1	0.89	20	109	1.93	0.85	32	37	-	-	CSL
NB1_MT_STx1	0.848	0.773	3.16	0.71	649	337	5.71	0.62	1170	1563	1179	1590	CSL grain crushing
NB1_MT_STx2	0.845	0.787	0.18	0.78	46	-	0.05	0.78	79	99	85	118	CSL
NB1_MT_STx3	0.845	0.776	0.18	0.77	19	118	0.61	0.76	36	47	38	51	did not reach CSL
NB1_MT_STx4	0.825	0.792	0.42	0.78	44	-	0.19	0.78	77	95	86	119	CSL
NB1_MT_STx5	0.857	0.796	0.12	0.79	19	120	1.29	0.77	32	36	34	43	did not reach CSL
NB1_MT_STx6	0.887	0.822	3.96	0.75	650	-	7.82	0.61	1166	1546	1193	1626	CSL grain crushing
NB1_MT_STx7	0.823	0.782	1.61	0.76	198	236	1.91	0.73	340	419	371	507	CSL
NB1_MT_STx8	0.815	0.769	0.42	0.76	45	-	-0.65	0.77	74	88	82	108	CSL
NB1_PL_STx1	0.852	0.789	0.67	0.78	46	-	-0.19	0.78	82	112	88	126	CSL
NB1_PL_STx2	0.763	0.76	1.65	0.73	200	-	0.32	0.73	344	431	383	544	CSL
NB1_PL_STx3	0.85	0.79	2.84	0.73	395	291	3.85	0.67	691	887	740	1034	CSL grain crushing
NB1_PL_STx4	0.847	0.81	0.63	0.80	43	-	-0.01	0.80	80	102	89	125	outlier
NB1_PL_STx5	0.868	0.8	0.14	0.80	20	130	-0.17	0.80	32	37	36	48	CSL
NB1_PL_STx6	0.86	0.78	3.49	0.71	667	344	5.9	0.61	1190	1548	1288	1808	CSL grain crushing

Table C.2 – Cyclic triaxial test results for reconstituted specimens of S1 and NB1 soils

Test ID	After assembling e_0	Percolation + saturation e_{i-1}	ε_v %	Consolidation e_i	D_R %	p'_i kPa	V_S m/s	ψ	Freq Hz	CSR $q/2\sigma'_c$	Shear N_{liq} r_u=100%	N_{liq} $\varepsilon_{a,DA}$=5%	ΔW_{liq} r_u=100%	ΔW_{liq} $\varepsilon_{a,DA}$=5%	Type of liquefaction failure
NB1_MT_CTx1	0.849	0.796	1.06	0.776	27	100	172	0.01	0.1	0.13	7	7	0.71	0.75	FL
NB1_MT_CTx2	0.870	0.807	1.28	0.780	25	100	170	0.01	1.0	0.12	32	32	0.41	0.46	FL
NB1_MT_CTx3	0.839	0.788	1.63	0.760	34	100	170	-0.01	1.0	0.04	-	-	-	-	-
NB1_MT_CTx4	0.844	0.789	1.2	0.767	31	100	172	0.00	1.0	0.13	4	4	0.67	0.57	FL
NB1_MT_CTx5	0.866	0.809	1.17	0.788	23	100	175	0.02	1.0	0.05	1072	1073	3.48	3.59	FL
NB1_MT_CTx6	0.858	0.807	1.23	0.784	24	100	175	0.02	1.0	0.11	14	14	0.43	0.66	FL
NB1_MT_CTx7	0.811	0.774	0.85	0.759	34	100	170	-0.01	1.0	0.08	132	132	0.97	1.24	FL
NB1_MT_CTx8	0.848	0.800	1.08	0.780	26	100	163	0.01	0.1	0.17	1	1.2	1.62	1.50	FL
NB1_PL_CTx1	0.860	0.780	1.18	0.758	34	100	176	-0.01	0.1	0.13	4	4	2.37	1.62	FL
NB1_PL_CTx2	0.837	0.784	1.17	0.763	32	100	182	0.00	0.1	0.11	18	18	1.68	1.22	FL
NB1_PL_CTx3	0.850	0.784	1.24	0.762	33	100	178	-0.01	0.1	0.10	26	26	1.53	0.75	FL
NB1_E2_1	0.752	0.730	0.65	0.718	50	100	195	-0.05	1.0	0.11	172	173	1.62	2.36	CM
NB1_E2_2	0.722	0.697	0.55	0.687	62	100	193	-0.08	1.0	0.13	281	282	3.81	5.14	CM
NB1_E2_3	0.739	0.714	0.59	0.703	56	100	196	-0.06	0.1	0.16	30	31	1.42	2.29	CM
NB1_E2_4	0.738	0.716	0.54	0.706	55	100	197	-0.06	0.1	0.19	9	10	1.21	2.48	CM
NB1_E2_5	0.743	0.713	0.6	0.703	56	100	196	-0.06	0.1	0.14	71	71	1.93	2.10	CM
NB1_E2_5_REP	0.723	0.704	0.57	0.694	59	100	193	-0.07	0.1	0.14	128	130	2.40	3.46	CM
NB1_E2_6	0.735	0.703	0.57	0.693	60	100	188	-0.07	0.1	0.21	8	9	1.79	3.43	CM
NB1_C40_1	0.746	0.706	0.2	0.702	56	40	162	-0.09	0.1	0.16	65	66	0.69	1.08	CM
NB1_C40_2	0.728	0.705	0.2	0.702	56	40	162	-0.10	0.1	0.21	16	17	0.46	1.16	CM
NB1_C40_3	0.717	0.695	0.2	0.691	60	40	168	-0.11	0.1	0.14	296	298	1.35	1.78	CM
S1_M2_CTxR1	0.763	0.737	1.13	0.720	60	70	-	-0.04	1	0.09	43	43	0.44	0.59	FL
S1_M2_CTxR2	0.782	0.744	1.34	0.720	60	70	-	-0.04	1	0.09	107	107	0.73	0.78	FL
S1_M2_CTxR3	0.759	0.712	1.1	0.690	68	70	-	-0.07	1	0.04	-	-	-	-	-
S1_M2_CTxR4	0.784	0.737	1.23	0.720	60	70	-	-0.04	1	0.09	18	17	0.29	0.43	FL
S1_M2_CTxR5	0.796	0.737	1.24	0.715	61	70	149	-0.05	0.1	0.09	35	35	0.64	0.69	FL
S1_M2_CTxR6	0.849	0.761	1.36	0.735	56	70	149	-0.03	1	0.08	67	67	0.45	0.50	FL
S1_M2_CTxR7	0.777	0.724	0.85	0.708	63	70	151	-0.05	1	0.10	34	34	0.35	0.55	FL
S1_M2_CTxR8	0.768	0.730	1.04	0.712	62	70	-	-0.05	1	0.12	10	10	0.25	0.52	FL
S1_M2_CTxR9	0.767	0.723	1	0.705	64	70	138	-0.06	0.1	0.16	2.8	3	1.70	1.10	FL
S1_M7_CTxR1	0.842	0.824	0.68	0.81	32	70	171	-0.03	1	0.09	336	337	1.42	1.47	FL
S1_M7_CTxR2	0.838	0.806	0.57	0.80	35	70	165	-0.04	1	0.11	17	17	0.38	0.58	FL
S1_M7_CTxR3	0.833	0.790	0.55	0.78	42	70	176	-0.06	1	0.04	-	-	-	-	-
S1_M7_CTxR4	0.833	0.822	0.59	0.81	32	70	177	-0.03	1	0.07	342	343	1.67	1.76	CM
S1_M7_CTxR5	0.870	0.835	0.72	0.82	27	70	-	-0.01	0.1	0.07	286	284	1.71	1.08	FL
S1_M7_CTxR6	0.955	0.880	0.86	0.86	13	70	157	0.03	1	0.08	70	69	0.51	0.48	FL
S1_M7_CTxR7	0.890	0.839	0.66	0.83	26	70	159	-0.01	1	0.10	47	47	0.48	0.46	FL
S1_M7_CTxR8	0.866	0.827	0.76	0.81	31	100	171	-0.01	1	0.06	945	946	2.53	2.48	FL
S1_M7_CTxR9	0.858	0.806	0.53	0.80	37	70	-	-0.04	1	0.13	44	45	0.48	0.93	CM
S1_M7_CTxR10	0.847	0.810	0.5	0.80	35	70	157	-0.04	1	0.08	607	609	2.35	2.54	CM
S1_M7_CTxR11	0.862	0.823	0.62	0.81	32	70	177	-0.03	1	0.11	40	40	0.63	0.60	CM
S1_M7_CTxR12	0.868	0.828	0.55	0.82	29	70	160	-0.02	1	0.09	119	119	0.79	0.77	CM
S1_M7_CTxR13	0.859	0.825	0.59	0.81	30	70	150	-0.02	0.1	0.13	38	39	0.67	0.95	CM
S1_M7_CTxR14	0.850	0.817	0.48	0.81	32	70	150	-0.03	0.1	0.19	5	5	0.71	0.94	FL
S1_M7_CTxR15	0.864	0.833	0.56	0.82	28	70	167	-0.02	0.1	0.16	6	6	1.65	1.42	FL

Note: FL - Flow liquefaction; CM - Cyclic mobility

Table C.3 – Cyclic triaxial test results for undisturbed specimens

Test ID	After assembling e₀	Percolation + saturation e_{i-1}	Consolidation ε_v (%)	e_i	D_R (%)	p'_i (kPa)	ψ	V_S (m/s)	Shear Freq (Hz)	CSR q/2σ'_c	N_liq r_u=100%	N_liq ε_a,DA=5%	ΔW_liq r_u=100%	ΔW_liq ε_a,DA=5%	Type of liquefaction failure
S1_M2_I3	0.6925	0.661	0.42	0.65	78	28.0	-0.185	133	1	0.131	381	*	1.70	1.96	CM
S1_M5_I2	0.7638	0.664	0.74	0.64	53	24.3 **	-0.108	-	1	0.089	-	-	-	-	no liq
S1_M5_I4	0.52	0.509	0.89	0.50	98	49.6	-0.229	139	1	0.115	379	*	2.35	-	CM
S1_M6_I2	0.604	0.593	1.07	0.58	63	70.0	-0.093	174	1	0.157	30	47	0.68	0.93	FL
S1_M6_I3	0.7136	0.675	0.78	0.66	42	44.3	-0.060	113	1	0.168	3	6.5	0.25	0.33	FL
S1_M7_I1	0.6244	0.658	0.77	0.65	89	69.1	-0.176	183	1	0.131	-	-	-	-	no liq
S1_M9_I1	0.725	0.593	1.89	0.56	95	149.8	-0.111	-	1	0.151	139	141	9.47	11.89	CM
S1_M11_I1	1.2456	1.1	5.43	0.98	-	66.6 **	-	-	1	0.082	-	-	-	-	no liq
S1_M14_I1	0.653	0.638	2.03	0.60	79	75.0	-0.147	-	1	0.175	-	-	-	-	no results recorded
S1_M15_I1	0.7101	0.693	1.99	0.66	84	74.7	-0.134	170	1	0.211	6	8	0.88	1.93	FL
S1_M25_I1	0.735	0.663	3.69	0.61	-	199.3	-0.132	226	0.1	0.090	243	243	7.42	7.65	CM
S2_M6_I1	0.553	0.563	0.98	0.55	99	48.2	-0.233	146	1	0.131	22	95	0.52	1.15	CM
S2_M7_I1	0.790	0.744	2.65	0.70	77	54.1	-0.027	139	1	0.162	106	*	2.67	-	CM
S2_M7_I2	0.619	0.546	0.91	0.53	103	37.4	-0.270	144	1	0.145	15	*	0.46	-	CM
S2_M9_I1	0.739	0.709	4.46	0.63	86	63.4	-0.130	146	1	0.167	18	*	1.26	-	CM
S2_M11_I1	0.6346	0.68	1.6	0.65	97	66.0 **	-0.232	-	1	0.165	-	-	-	-	no liq
S2_M11_I2	0.799	0.772	1.92	0.74	77	96.7	-0.124	186	1	0.139	62	65	1.54	2.88	CM
S2_M12_I1	0.646	0.642	2.04	0.61	100	109.4	-0.213	177	1	0.121	179	*	3.47	-	CM
S2_M13_I1	0.738	0.795	2.29	0.76	79	99.3	-0.104	175	1	0.140	36	*	1.36	-	CM
S2_M14_I1	0.59	0.744	0.96	0.72	94	75.1	-0.200	181	1	0.164	28	31	0.99	2.50	CM
NB1_F2_GP2.5_I3	0.75	0.704	0.32	0.70	83	33.7	-0.191	197	1	0.11	-	-	-	-	no liq
NB1_F2_GP3.5_I1	0.5739	0.597	0.54	0.59	64	34.9	-0.132	141	1	0.12÷0.18	30+378	*	3.10	-	CM
NB1_F4_GP4_I2	0.7315	0.703	0.41	0.70	67	39.6	-0.132	155	1	0.12	726	746	1.72	2.66	CM
NB1_F5_GP4_I2	0.6767	0.730	0.33	0.73	53	40.0	-0.089	160	1	0.14	-	-	-	-	no liq
NB1_F1_GP4.5_I1	0.7435	0.723	0.47	0.70	59	45.1	-0.105	155	1	0.11+0.21	30+16	30+19	0.48	1.21	FL
NB1_F5_GP5_I1	0.6378	0.638	0.53	0.63	77	44.4	-0.154	185	1	0.12+0.29	30+23	30+30	0.67	1.77	CM
NB1_F5_GP5_I2	0.6022	0.630	0.77	0.62	85	54.2	-0.170	168	1	0.32	37	53	1.00	3.36	CM
NB2_F1_GP3_I4	0.76	0.752	0.71	0.74	64	35.0	-	144	1	0.11+0.17	30+321	*	2.79	-	CM
NB2_F2_GP4_I4	1.11	1.076	1.56	1.04	59	40.0	-	120	1	0.16+0.25	30+615	*	13.97	-	CM
NB2_F1_GP6_I2	0.753	0.735	0.84	0.72	52	49.1	-0.049	155	1	0.14	19	21	0.45	0.86	FL
NB2_F1_GP6_I3	0.688	0.668	0.73	0.66	56	50.0	-0.061	155	0.1	0.15+0.28	50+13	50+14	1.79	2.12	CM

Note: * - Did not reach ε_a,DA=5%; ** - Anisotropically consolidated; FL - Flow liquefaction; CM - Cyclic mobility

Table C.4 – Cyclic triaxial test results for reconstituted specimens of undisturbed specimens soil

Test ID	After assembling e_0	Percolation + saturation e_{i-1}	Consolidation ε_v %	Consolidation e_i	Consolidation D_R %	Consolidation p'_i kPa	Consolidation V_S m/s	Freq Hz	CSR $q/2\sigma'_c$	Shear N_{liq} r_u=100%	Shear N_{liq} $\varepsilon_{a,DA}$=5%	Shear ΔW_{liq} r_u=100%	Shear ΔW_{liq} $\varepsilon_{a,DA}$=5%	Type of liquefaction failure
S1_M2_R3	0.690	0.658	0.153	0.656	77	28.5	134	0.1	0.142	48	49	0.40	0.55	CM
S1_M5_R4	0.607	0.595	0.457	0.588	70	50.8	170	0.1	0.127	137	138	1.04	1.55	CM
S1_M6_R2	0.636	0.599	0.361	0.593	55	69.3	171	0.1	0.169	247	249	3.13	3.98	CM
S1_M6_R2_2	0.610	0.597	0.389	0.591	56	70.9	188	0.1	0.163	273	276	3.60	5.21	CM
S1_M6_R3	0.710	0.684	0.364	0.678	35	43.9	130	0.1	0.181	8	8	0.41	0.42	FL
S1_M7_R1	0.754	0.734	0.354	0.730	60	68.8	181	0.1	0.142	1249	1251	8.13	9.00	CM
S1_M15_R1	0.770	0.704	3.691	0.639	88	77.9	153	0.1	0.233	1	1	0.63	0.63	FL
S2_M6_R1	0.692	0.670	0.656	0.659	66	48.5	153	0.1	0.140	10	10	0.41	0.61	CM
S2_M7_R1	0.680	0.596	4.031	0.528	103	54.1	166	0.1	0.180	7	7	1.29	1.65	FL
S2_M9_R1	0.794	0.622	4.668	0.538	102	40.2	172	0.1	0.305	3	2	1.61	1.54	FL
S2_M11_R2	0.833	0.809	1.931	0.773	68	98.3	180	0.1	0.142	7	7	0.69	0.69	FL
S2_M12_R1	0.705	0.667	1.572	0.640	93	108.3	182	0.1	0.132	21	21	1.90	2.42	CM
S2_M13_R1	0.860	0.814	3.705	0.744	81	98.0	174	0.1	0.168	4	4	0.78	0.78	FL
S2_M14_R1	0.830	0.809	0.689	0.796	77	73.3	167	0.1	0.178	14	16	1.38	3.38	CM
NB1_F2_GP3.5_R1	0.683	0.647	0.250	0.642	49	34.4	122	0.1	0.1615	24	24	0.62	0.70	FL
NB1_F2_GP3.5_R1_2	0.629	0.598	0.130	0.596	62	34.1	128	0.1	0.107+0.188	30+33	30+36	0.57	0.95	FL
NB1_F4_GP4_R2	0.744	0.702	0.170	0.700	65	39.4	149	0.1	0.102	-	-	-	-	no liq
NB1_F4_GP4_R2_2	0.774	0.716	0.250	0.711	62	39.2	152	0.1	0.1207	1466	1470	3.50	3.82	CM
NB1_F1_GP4.5_R1	0.752	0.713	0.250	0.709	56	43.3	143	0.1	0.201	33	34	1.02	1.42	CM
NB1_F1_GP4.5_R1_2	0.739	0.706	0.260	0.702	58	43.7	138	0.1	0.109+0.181	30+54	30+56	0.78	1.17	CM
NB1_F1_GP4.5_R1_3	0.791	0.756	0.390	0.749	43	42.6	148	0.1	0.117+0.257	30+3	30+3	0.93	1.51	FL
NB1_F5_GP5_R1	0.667	0.629	0.220	0.625	78	44.1	146	0.1	0.178	311	317	2.61	3.56	CM
NB1_F5_GP5_R1_2	0.667	0.632	0.220	0.628	77	44.4	155	0.1	0.11+0.1946	30+600	30+604	4.31	4.96	CM
NB1_F5_GP5_R1_3	0.681	0.651	0.110	0.649	70	28.6	146	0.1	0.29	26	30	0.64	1.49	CM
NB1_F5_GP5_R2	0.641	0.611	0.300	0.602	91	55.0	168	0.1	0.186	119	125	1.85	3.06	CM
NB1_F5_GP5_R2_2	0.654	0.621	0.170	0.618	85	32.7	139	0.1	0.317	10	14	0.67	1.75	CM
NB2_F1_GP6_R2	0.707	0.680	0.440	0.670	69	48.9	155	0.1	0.1404	14	14	0.45	0.41	FL
NB2_F1_GP6_R3	0.722	0.697	0.390	0.690	43	49.6	168	0.1	0.137+0.265	50+19	50+20	1.19	1.73	CM

Table C.5 – Cyclic simple shear test results for reconstituted specimens of NB1 soil

Test ID	Preparation method	σ_v kPa	e_0	e_i	w_i %	w_f %	ψ	CSR τ/σ_v	N_{liq} $\gamma_{SA}=3.75\%$	N_{liq} $r_u=0.95$	ΔW_{liq} $\gamma_{SA}=3.75\%$
NB1_070_MT1	MT	100	0.76	0.66	5.1	3.2	-0.11	0.20	13.0	14.0	5.65
NB1_070_MT2	MT	100	0.79	0.70	5.2	3.1	-0.07	0.15	66.2	65.5	4.50
NB1_070_MT3	MT	100	0.81	0.71	5.1	3.1	-0.06	0.21	2.0	4.0	1.88
NB1_070_MT4	MT	100	0.81	0.70	5.2	6.0	-0.07	0.18	7.0	10.0	2.40
NB1_080_MT1	MT	100	0.84	0.73	5.1	4.0	-0.04	0.15	5.3	6.0	1.19
NB1_080_MT2	MT	100	0.82	0.72	5.0	3.9	-0.05	0.12	58.8	61.6	2.29
NB1_080_MT3	MT	100	0.87	0.75	5.1	3.7	-0.02	0.13	6.8	8.0	1.26
NB1_080_MT4	MT	100	0.83	0.72	5.1	3.5	-0.04	0.16	4.8	5.0	1.56
NB1_080_MT5	MT	100	0.87	0.74	5.0	3.4	-0.03	0.16	1.8	2.6	0.90
NB1_MT_w10	MT	100	0.77	0.69	9.9	6.7	-0.08	0.15	5.2	7.0	1.60
NB1_MT_w10_2	MT	100	0.81	0.72	10.0	7.1	-0.05	0.13	14.2	16.0	1.75
NB1_MT_w10_3	MT	100	0.74	0.69	9.9	6.4	-0.08	0.10	407.0	403.6	8.23
NB1_MT_sat1	MT	100	0.81	0.72	4.9	12.5	-0.05	0.17	3.2	3.6	1.17
NB1_MT_sat2	MT	100	0.77	0.69	5.1	15.9	-0.08	0.15	5.8	6.6	1.30
NB1_MT_sat3	MT	100	0.76	0.68	5.0	25.0	-0.09	0.13	9.3	10.1	1.08
NB1_MT_sat4	MT	100	0.79	0.70	5.1	24.2	-0.07	0.15	3.8	4.1	1.17
NB1_MT_sat5	MT	100	0.78	0.69	5.3	26.2	-0.08	0.11	13.8	14.0	0.94
NB1_MT_sat6	MT	100	0.81	0.71	5.2	26.1	-0.05	0.09	29.2	29.6	0.79
NB1_MT_sat7	MT	100	0.77	0.71	5.2	24.5	-0.06	0.07	190.3	190.0	0.51
NB1_MT_sat8	MT	100	0.77	0.69	5.1	21.7	-0.08	0.08	321.0	319.0	0.67
NB1_50_1	MT	50	0.78	0.70	5.2	3.3	-0.09	0.15	24.0	22.0	1.54
NB1_40_1	MT	40	0.75	0.69	5.2	3.4	-0.11	0.15	27.0	14.0	2.22
NB1_40_2	MT	40	0.75	0.67	5.2	3.4	-0.13	0.20	17.9	8.6	2.68
NB1_40_3	MT	40	0.79	0.70	5.3	3.8	-0.10	0.12	192.0	167.0	3.60
NB1_40_4	MT	40	0.77	0.70	5.0	3.1	-0.10	0.17	11.5	9.3	1.28
NB1_40_5	MT	40	0.78	0.70	5.1	3.4	-0.10	0.19	5.8	3.6	1.04
NB1_100_PL1	PL	100	0.78	0.65	0.2	0.3	-0.12	0.15	5.2	5.5	1.34
NB1_100_PL2	PL	100	0.88	0.69	0.1	0.2	-0.08	0.12	3.2	3.5	0.73
NB1_100_PL3	PL	100	0.79	0.66	0.2	0.2	-0.11	0.08	254.0	254.0	0.62
NB1_100_PL4	PL	100	0.85	0.67	0.1	0.2	-0.10	0.10	5.3	6.0	0.59
NB1_100_PL5	PL	100	0.83	0.68	0.1	0.2	-0.08	0.12	0.8	2.5	0.77
NB1_100_PL6	PL	100	0.94	0.71	0.1	0.2	-0.06	0.10	4.2	6.0	0.50
NB1_100_PL7	PL	100	0.91	0.70	0.1	0.2	-0.07	0.08	7.2	9.6	0.40
NB1_100_PL8	PL	100	0.78	0.66	0.1	0.2	-0.10	0.06	184.3	186.0	0.39
Test_layers1	MT	100	0.79/0.78	0.66	5.6/5.2	26.1	-	0.12	6.2	6.6	0.59
Test_mixture1	MT	100	0.77	0.68	5.4	23.3	-	0.12	6.2	6.6	0.75
Test_layers2	MT	100	1.31/0.69	0.73	5.6/5.0	25.4	-	0.11	15.9	16.5	1.07
Test_mix2	MT	100	0.98	0.71	5.1	22.1	-	0.11	7.2	7.5	0.61

Table C.6 – Cyclic simple shear test results for reconstituted specimens of S1 soils

Test ID	Preparation method	σ_v	e_0	e_i	w_i	w_f	ψ	CSR	N_{liq}	N_{liq}	ΔW_{liq}
		kPa			%	%		τ/σ_v	γ_{SA}=3.75%	r_u=0.95	γ_{SA}=3.75%
S1_M2_1	MT	70	0.76	0.66	5.2	3.9	-0.11	0.15	35.0	31.0	2.33
S1_M2_2	MT	70	0.81	0.69	5.1	3.8	-0.07	0.17	7.0	7.0	1.29
S1_M2_3	MT	70	0.81	0.71	5.1	3.8	-0.05	0.12	140.0	138.0	2.90
S1_M2_4	MT	70	0.81	0.71	5.2	3.7	-0.05	0.19	7.0		1.69
S1_M2_5	MT	70	0.84	0.71	5.2	4.0	-0.05	0.21	2.0	2.0	1.32
S1_M7_1	MT	70	0.83	0.76	5.0	3.7	-0.08	0.15	10.0	9.5	1.47
S1_M7_2	MT	70	0.90	0.80	5.0	2.6	-0.04	0.12	12.0	-	0.93
S1_M7_3	MT	70	0.87	0.78	5.0	3.3	-0.06	0.19	2.7	3.6	1.24
S1_M7_4	MT	70	0.88	0.76	5.2	3.4	-0.08	0.17	4.0	3.5	1.29
S1_M7_5	MT	70	0.91	0.80	5.1	3.3	-0.04	0.08	-		-
S1_M7_6	MT	70	0.88	0.78	5.1	3.7	-0.06	0.10	35.2	34.0	0.43
S1_M2_L1	MT	70	0.71	0.71	5.0	27.0	-0.05	0.16	6.1	6.4	-
S1_M2_L2	MT	70	0.70	0.70	5.6	26.0	-0.06	0.22	1.5	1.9	-
S1_M2_L3	MT	70	0.69	0.69	5.3	27.1	-0.07	0.09	36.2	3.6	-
S1_M7_L1	MT	70	0.80	0.82	4.8	31.0	-0.02	0.27	1.5	2.5	-
S1_M7_L2	MT	70	0.80	0.81	5.0	30.8	-0.03	0.16	12.5	12.5	-
S1_M7_L3	MT	70	0.80	0.80	5.2	31.0	-0.03	0.09	163.3	163.5	-

Table C.7 – Cyclic direct simple shear test results for undisturbed and respective reconstituted specimens

Test ID	Preparation method	σ_v	e_0	e_i	w_i	w_f	CSR	N_{liq}	ΔW_{liq}
		kPa			%	%	τ/σ_v	γ_{SA}=3.75%	γ_{SA}=3.75%
S2_M12_l2	Undisturbed	165	0.674	0.579	16.1	16.1	0.24	1.8	3.83
S2_M12_l3_1	Undisturbed	165	0.847	0.750	27.6	26.6	0.16	18.2	7.07
S2_M12_l3_2	Undisturbed	165	0.868	0.774	30.6	27.4	0.20	4.2	5.07
S2_M13_l2	Undisturbed	150	0.796	0.711	23.0	23.0	0.27	0.7	1.91
S2_M13_l3_1	Undisturbed	150	0.717	0.639	27.4	24.1	0.18	22.8	9.88
S2_M13_l3_2	Undisturbed	150	0.811	0.720	26.9	26.1	0.22	6.3	5.87
S2_M14_l2	Undisturbed	112.5	0.642	0.564	19.0	19.2	0.22	4.2	2.52
S2_M14_l3	Undisturbed	112.5	0.712	0.628	25.2	24.5	0.32	0.5	1.06
S2_M12_R2_MT1	MT	165	0.669	0.530	16.1	13.4	0.24	3.3	4.68
S2_M12_R2_MT2	MT	165	0.647	0.547	15.9	14.5	0.15	54.0	8.83
S2_M12_R2_MT3	MT	165	0.676	0.577	15.9	12.9	0.20	3.8	3.71
S2_M12_R2_MT4	MT	165	0.704	0.589	16.3	13.4	0.24	1.2	3.30
S2_M12_R3_MT1	MT	165	0.886	0.758	24.7	21.5	0.16	16.8	6.28
S2_M12_R3_MT2	MT	165	0.887	0.751	24.7	21.9	0.20	4.7	4.36
S2_M13_R2_MT1	MT	150	0.910	0.707	22.9	21.0	0.27	0.3	1.23
S2_M13_R2_MT2	MT	150	0.820	0.691	23.0	20.8	0.20	3.8	2.96
S2_M13_R2_MT3	MT	150	0.815	0.705	23.0	20.1	0.21	2.2	3.55
S2_M13_R3_MT4	MT	150	0.810	0.701	25.3	20.9	0.20	3.7	3.67
S2_M13_R3_MT5	MT	145	0.840	0.710	30.0	23.0	0.20	1.8	2.21
S2_M14_R2_MT1	MT	112.5	0.775	0.688	19.2	16.6	0.19	1.8	1.63
S2_M14_R2_MT2	MT	112.5	0.708	0.623	19.2	15.9	0.24	2.2	3.04
S2_M14_R2_MT3	MT	112.5	0.685	0.614	19.2	16.4	0.15	25.3	4.62
S2_M14_R2_MT4	MT	112.5	0.688	0.603	18.9	16.0	0.29	1.7	3.32
S2_M14_R2_MT5	MT	112.5	0.706	0.631	18.9	16.8	0.28	0.70	1.99